NASA Conference Publication 3163
Part 1

Tenth Workshop for Computational Fluid Dynamic Applications in Rocket Propulsion

Compiled by
R. W. Williams
George C. Marshall Space Flight Center
Marshall Space Flight Center, Alabama

Proceedings of a workshop held at
NASA George C. Marshall Space Flight Center
Huntsville, Alabama
April 28–30, 1992

NASA
National Aeronautics and
Space Administration
Office of Management
Scientific and Technical
Information Program
1992

TABLE OF CONTENTS

PRECEDING PAGE BLANK NOT FILMED

TABLE OF CONTENTS (Continued)

TABLE OF CONTENTS (Continued)

TABLE OF CONTENTS (Continued)

TABLE OF CONTENTS (Continued)

George C. Marshall Space Flight Center
Science and Engineering Directorate

Propulsion Laboratory

National Aeronautics and
Space Administration

TECHNOLOGY TEST BED
REVIEW

N92-32279

H.V. McConnaughey
April 28, 1992

AGENDA

- o WHAT IS TTB?
- o TTB OBJECTIVES
- o TTB MAJOR ACCOMPLISHMENTS
- o SOME CFD CHALLENGES
- o FUTURE PLANS

SSME TECHNOLOGY TEST BED HISTORY

PLANNING INITIATED IN 1982

MOTIVATION: SSME PROGRAM BENEFITS (CHARACTERIZATION OF ENGINE INTERNAL OPERATING ENVIRONMENTS AND ASSESSMENT OF PROTOTYPE HARDWARE)

OAST PROPULSION TECHNOLOGY SYSTEM-LEVEL VALIDATION

SITE: SATURN S1-C STAGE TEST STAND AT MSFC

FACILITY MODIFICATIONS: 1984 - 1988

TESTING INITIATED: FALL, 1988

TTB OBJECTIVES

- o ASSESS PROPULSION TECHNOLOGY ADVANCES IN AN ENGINE SYSTEMS ENVIRONMENT
- o ENHANCE THE PROCESS FOR IMPLEMENTATION OF TECHNOLOGY INTO EMERGING AND OPERATIONAL PROGRAMS
- o PROVIDE SYSTEM TEST CAPABILITY FOR EVALUATION OF PROTOTYPE HARDWARE
- o SUPPORT NASA PROGRAMS WITH ANOMALY RESOLUTION ON AN AS-NEEDED BASIS
- o DEVELOP AND MAINTAIN IN-HOUSE, HANDS-ON ROCKET PROPULSION HARDWARE AND TEST EXPERIENCE/CAPABILITY AT MSFC

TTB MAJOR ACCOMPLISHMENTS

- 31 SSME TESTS CONDUCTED/ ~3000 SECONDS CUMULATIVE TEST TIME
- EVALUATION OF A MODIFIED SSME
- ENGINE 3001 (HIGHLY INSTRUMENTED SSME) ENVIRONMENT CHARACTERIZATION
- DEMONSTRATION OF SSME ADVANCED DEVELOPMENT CONCEPTS
- SUPPORT OF SHUTTLE FLIGHT AND DEVELOPMENT INVESTIGATIONS
- ASSESSMENT OF ADVANCED PROPULSION TECHNOLOGY CONCEPTS
- NUMEROUS IMPROVEMENTS DERIVED FROM IN-HOUSE, HANDS-ON INVOLVEMENT

TTB ACTIVITES TO DATE

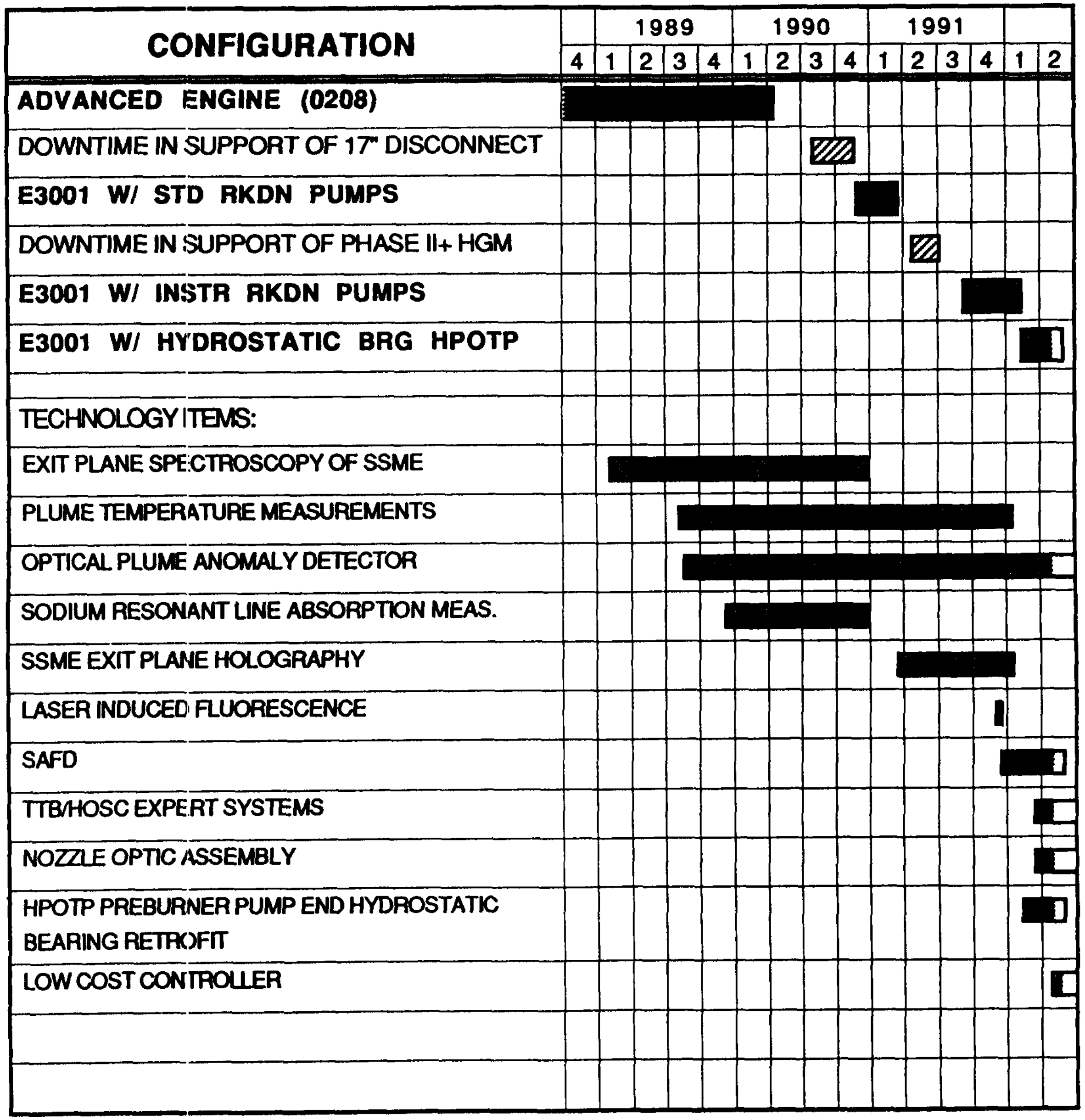

TTB CONTRIBUTIONS TO SSME

ACCOMPLISHMENT: LARGE THROAT SSME CHARACTERIZATION

SYSTEM PERFORMANCE DEFINED

MORE BENIGN ENVIRONMENT DEMONSTRATED

STABLE COMBUSTION DEMONSTRATED

TURBOMACHINERY REDESIGN REQUIREMENTS IDENTIFIED

ENGINE: 0208

BENEFIT: EARLY ASSESSMENT OF PROPOSED SSME IMPROVEMENTS

PERFORMANCE OF ASSESSMENT WAS FREE FROM USUAL DEVELOPMENT PRESSURES AND WAS ACCOMPLISHED WITHOUT INTERFERENCE TO SSC

IMPACT: TTB RESULTS FORMED THE BASIS FOR ADVANCED FAB LTMCC BASELINE

STABLE COMBUSTION WITHOUT BAFFLES OR ACOUSTIC CAVITIES IS APPLICABLE TO FUTURE DESIGNS

TTB CONTRIBUTIONS TO SSME

ACCOMPLISHMENT: PHASE II SSME INTERNAL ENVIRONMENT CHARACTERIZATION

~ 630 TTB-UNIQUE ENGINE MEASUREMENTS

DEFINES INTEGRATION PARAMETERS FOR ALTERNATE COMPONENTS (e.g., ATDs)

∞

ENGINE: 3001

BENEFIT: INCREASED UNDERSTANDING OF OPERATING ENVIRONMENT

BASELINE DATA FOR COMPARISON WITH ATDs AND PHASE II+ POWERHEAD

CALIBRATION AND IMPROVEMENT OF POWER BALANCE MODEL, DIGITAL TRANSIENT MODEL, AND ADVANCED ANALYTICAL MODELS

IMPACT: TO BE FULLY REALIZED. EXAMPLES: SIGNIFICANT DEFICIENCIES IN SSME POWER BALANCE MODEL HAVE BEEN DISCOVERED. HAVE MADE NEW DISCOVERIES ABOUT TURBOPUMP OPERATION.

George C. Marshall Space Flight Center
Science and Engineering Directorate

Propulsion Laboratory

MAJOR IMPACTS OF 3001 TESTING

NASA
National Aeronautics and
Space Administration

- ACQUISITION OF HERETOFORE UNMEASURED SSME HOT-FIRE DATA - COMPLETE MAPPING OF ENGINE OPERATION FOR RANGE OF MIXTURE RATIO, POWER LEVEL, PUMP INLET (NPSP), F7 ORIFICE AND REPRESS CONDITIONS

  MAJOR FLOWRATES
  INSTRUMENTED TURBOPUMPS
  OTHER Ps, Ts, STRAINS, etc.

  ~ 630 MEASUREMENTS IN TOTAL

- CALIBRATION AND IMPROVEMENT OF MODELS

  POWER BALANCE MODEL
  1-D TURBOPUMP MODELS
  CFD MODELS
  THERMAL MODELS
  STRUCTURAL MODELS
  STRESS MODELS

- NUMEROUS LESSONS LEARNED

  INSTRUMENTATION DESIGN AND IMPLEMENTATION
  TEST OPERATION EFFICIENCY ENHANCEMENTS

MAJOR IMPACTS OF 3001 TESTING

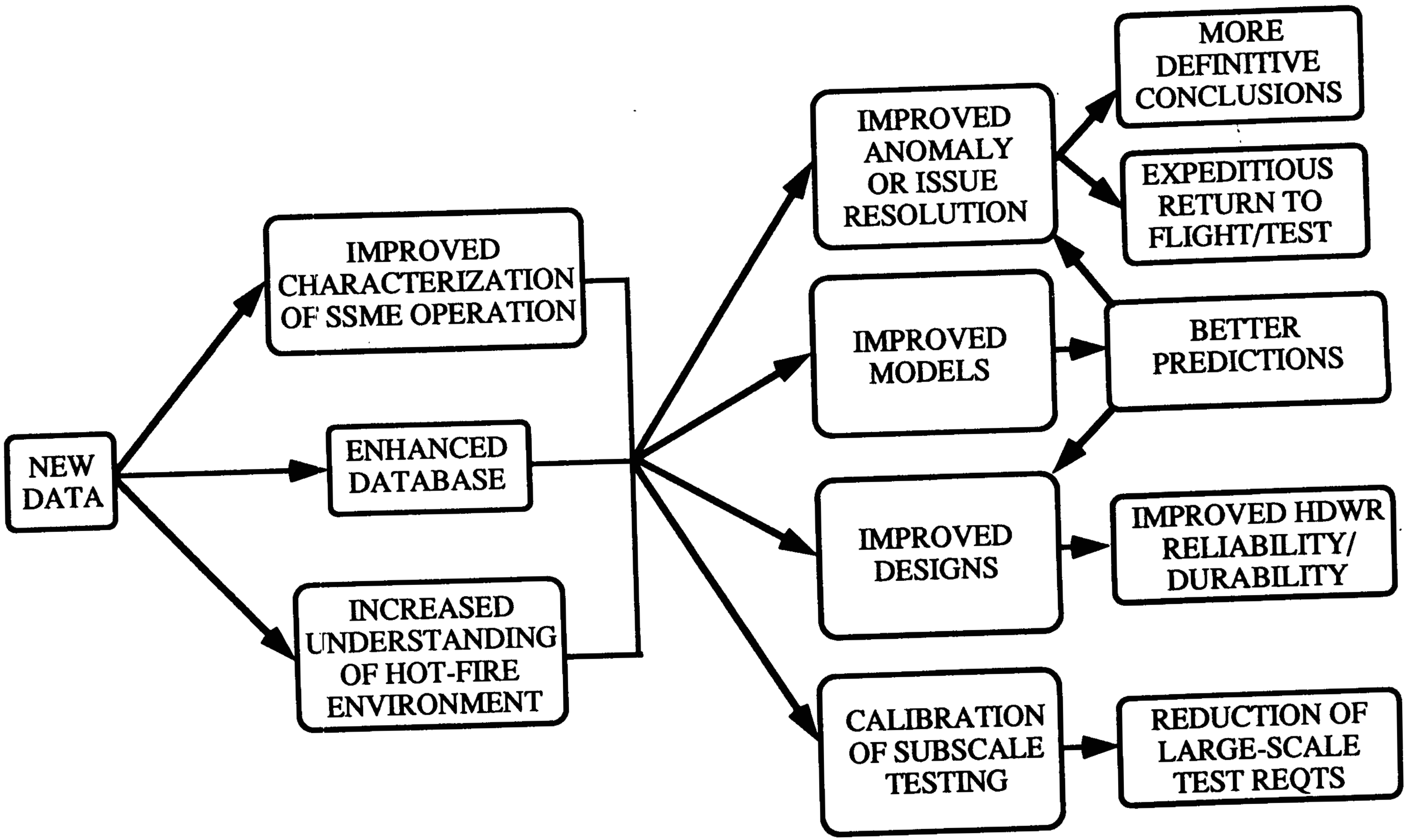

SOME CHALLENGES TO CFD

- o COMPARE HOT-FIRE PREDICTIONS WITH 3001 DATA

  - UTILIZE DATA TO CALIBRATE/IMPROVE MODELS
  - UTILIZE MODELS (+ KNOWLEDGE OF FLUID MECHANICS, etc.) TO EXPLAIN DATA

- o TAKE AN ACTIVE ROLE AND ENCOURAGE CONCURRENT ENGINEERING IN THE DESIGN PROCESS

  - PLACEMENT OF SENSORS IN INSTRUMENTED TEST ARTICLES
  - HARDWARE DESIGN (EARLY INVOLVEMENT, TIMELY INPUT)

- o EXAMPLES ...

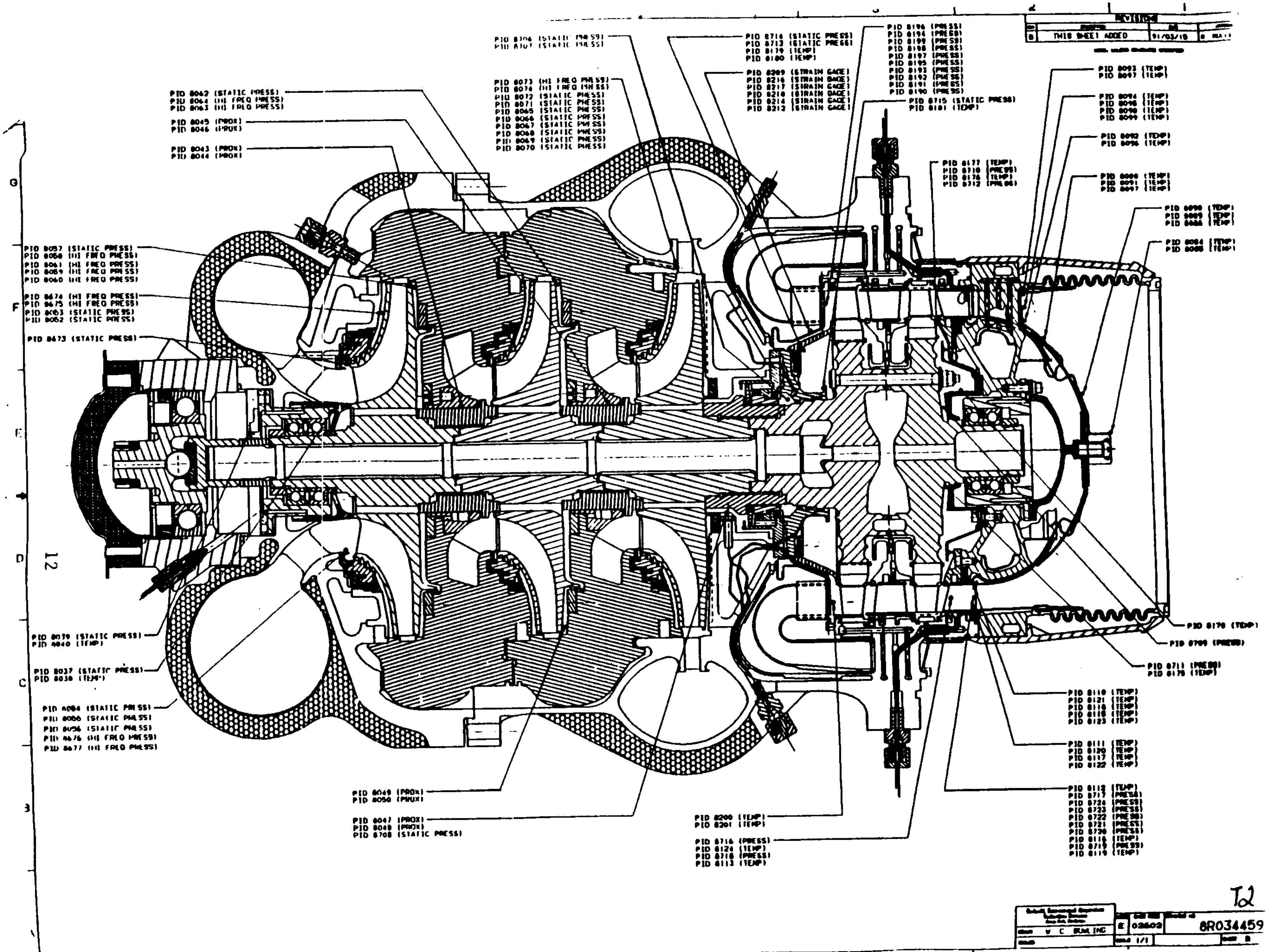

THIS SHEET ADDED 91/03/19
PID 8706 (STATIC PRESS)
PID 8707 (STATIC PRESS)
PID 8062 (STATIC PRESS)
PID 8064 (HI FREQ PRESS)
PID 8063 (HI FREQ PRESS)
PID 8045 (PROX)
PID 8046 (PROX)
PID 8043 (PROX)
PID 8044 (PROX)
PID 8073 (HI FREQ PRESS)
PID 8074 (HI FREQ PRESS)
PID 8072 (STATIC PRESS)
PID 8071 (STATIC PRESS)
PID 8065 (STATIC PRESS)
PID 8066 (STATIC PRESS)
PID 8067 (STATIC PRESS)
PID 8068 (STATIC PRESS)
PID 8069 (STATIC PRESS)
PID 8070 (STATIC PRESS)
PID 8716 (STATIC PRESS)
PID 8713 (STATIC PRESS)
PID 8179 (TEMP)
PID 8180 (TEMP)
PID 8209 (STRAIN GAGE)
PID 8216 (STRAIN GAGE)
PID 8217 (STRAIN GAGE)
PID 8218 (STRAIN GAGE)
PID 8214 (STRAIN GAGE)
PID 8212 (STRAIN GAGE)
PID 8196 (PRESS)
PID 8194 (PRESS)
PID 8199 (PRESS)
PID 8198 (PRESS)
PID 8197 (PRESS)
PID 8195 (PRESS)
PID 8193 (PRESS)
PID 8192 (PRESS)
PID 8191 (PRESS)
PID 8190 (PRESS)
PID 8715 (STATIC PRESS)
PID 8181 (TEMP)
PID 8177 (TEMP)
PID 8710 (PRESS)
PID 8176 (TEMP)
PID 8712 (PRESS)
PID 8093 (TEMP)
PID 8097 (TEMP)
PID 8094 (TEMP)
PID 8098 (TEMP)
PID 8099 (TEMP)
PID 8092 (TEMP)
PID 8096 (TEMP)
PID 8057 (STATIC PRESS)
PID 8058 (HI FREQ PRESS)
PID 8061 (HI FREQ PRESS)
PID 8059 (HI FREQ PRESS)
PID 8060 (HI FREQ PRESS)
PID 8674 (HI FREQ PRESS)
PID 8675 (HI FREQ PRESS)
PID 8063 (STATIC PRESS)
PID 8052 (STATIC PRESS)
PID 8673 (STATIC PRESS)
PID 8079 (STATIC PRESS)
PID 8040 (TEMP)
PID 8037 (STATIC PRESS)
PID 8038 (TEMP)
PID 8084 (STATIC PRESS)
PID 8086 (STATIC PRESS)
PID 8676 (HI FREQ PRESS)
PID 8677 (HI FREQ PRESS)
PID 8049 (PROX)
PID 8050 (PROX)
PID 8047 (PROX)
PID 8048 (PROX)
PID 8708 (STATIC PRESS)
PID 8200 (TEMP)
PID 8201 (TEMP)
PID 8716 (PRESS)
PID 8124 (TEMP)
PID 8718 (PRESS)
PID 8113 (TEMP)
PID 8178 (TEMP)
PID 8709 (PRESS)
PID 8711 (PRESS)
PID 8175 (TEMP)
PID 8110 (TEMP)
PID 8111 (TEMP)
PID 8112 (TEMP)
PID 8717 (PRESS)
PID 8119 (TEMP)
W C BUHLING
E 02602
8R034459
1/1
T2

HPFTP 2ND DISC AFT CAVITY AVERAGE TEMPERATURE 109% VS. 100% P.L.

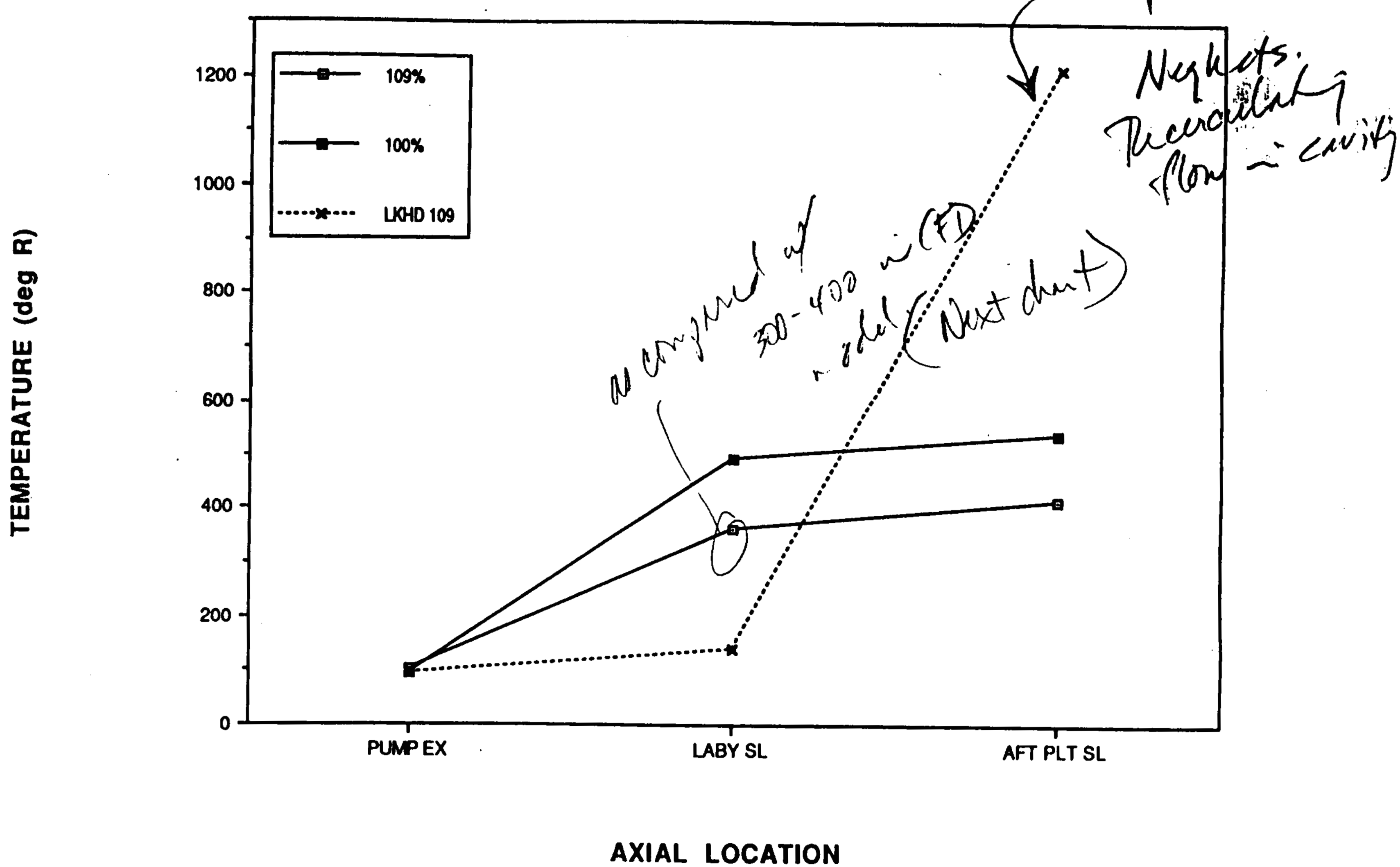

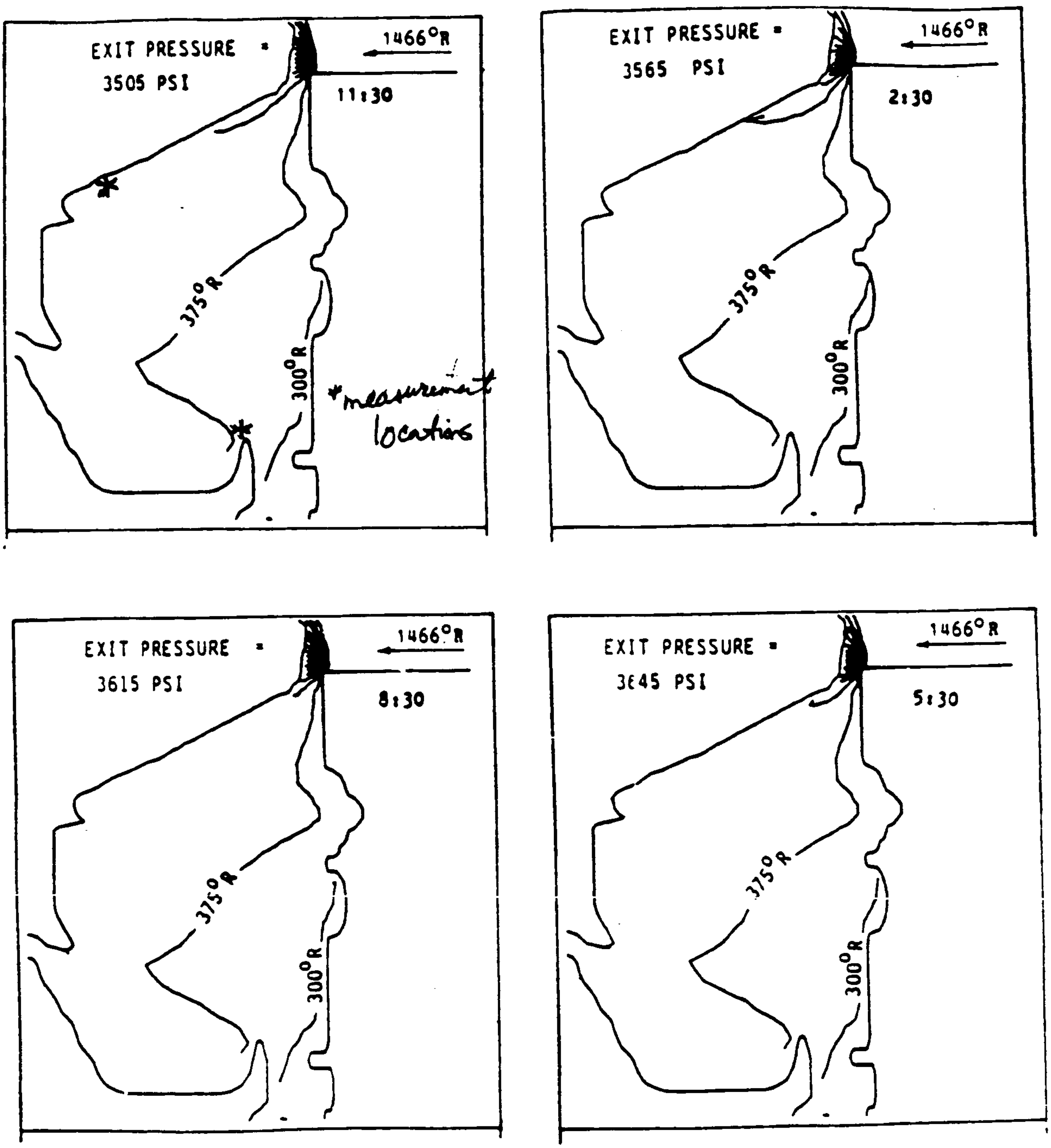

Three-dimensional basecase results: temperature.

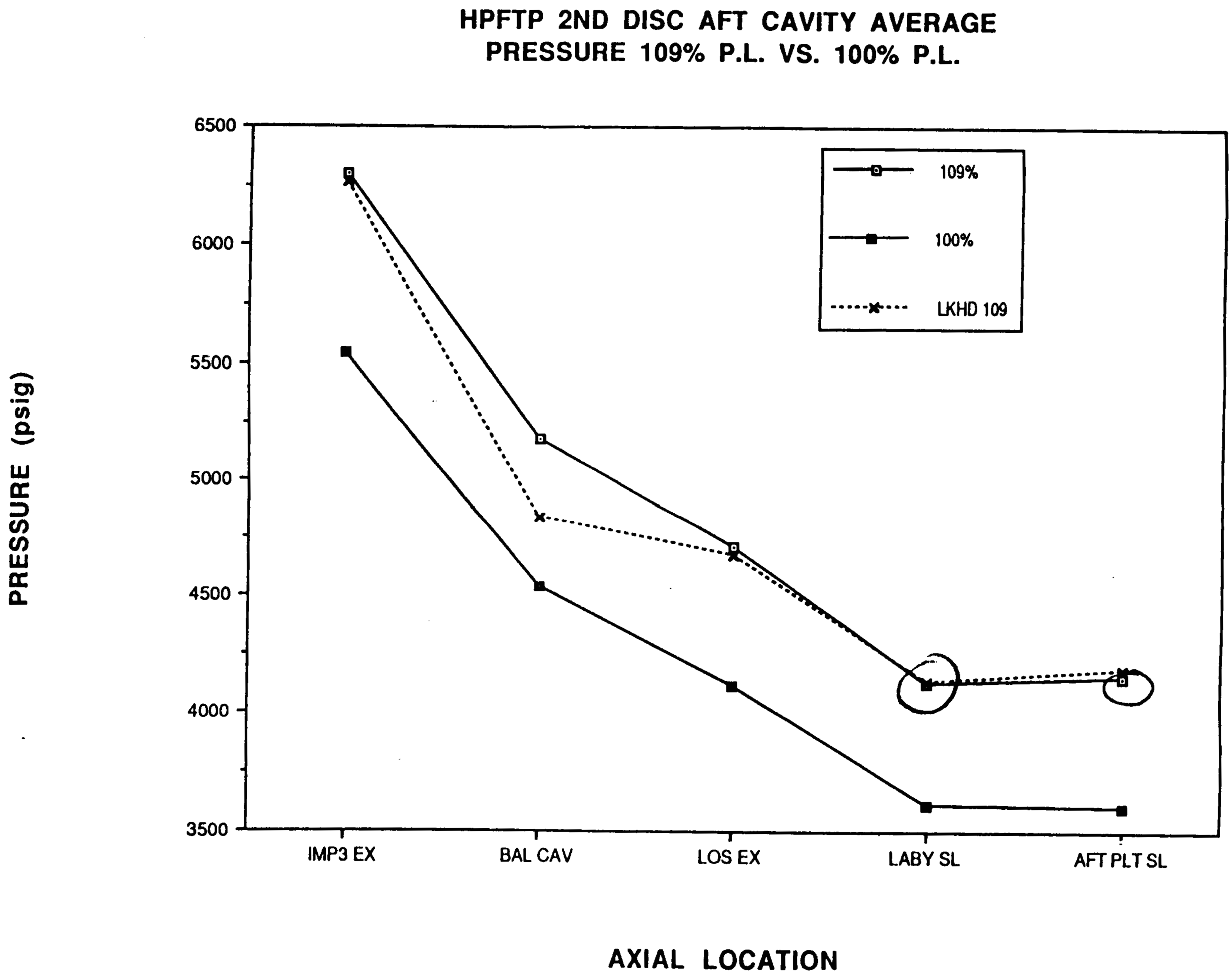
HPFTP 2ND DISC AFT CAVITY AVERAGE
PRESSURE 109% P.L. VS. 100% P.L.
6500
6000
5500
5000
4500
4000
3500
PRESSURE (psig)
109%
100%
LKHD 109
IMP3 EX
BAL CAV
LOS EX
LABY SL
AFT PLT SL
AXIAL LOCATION

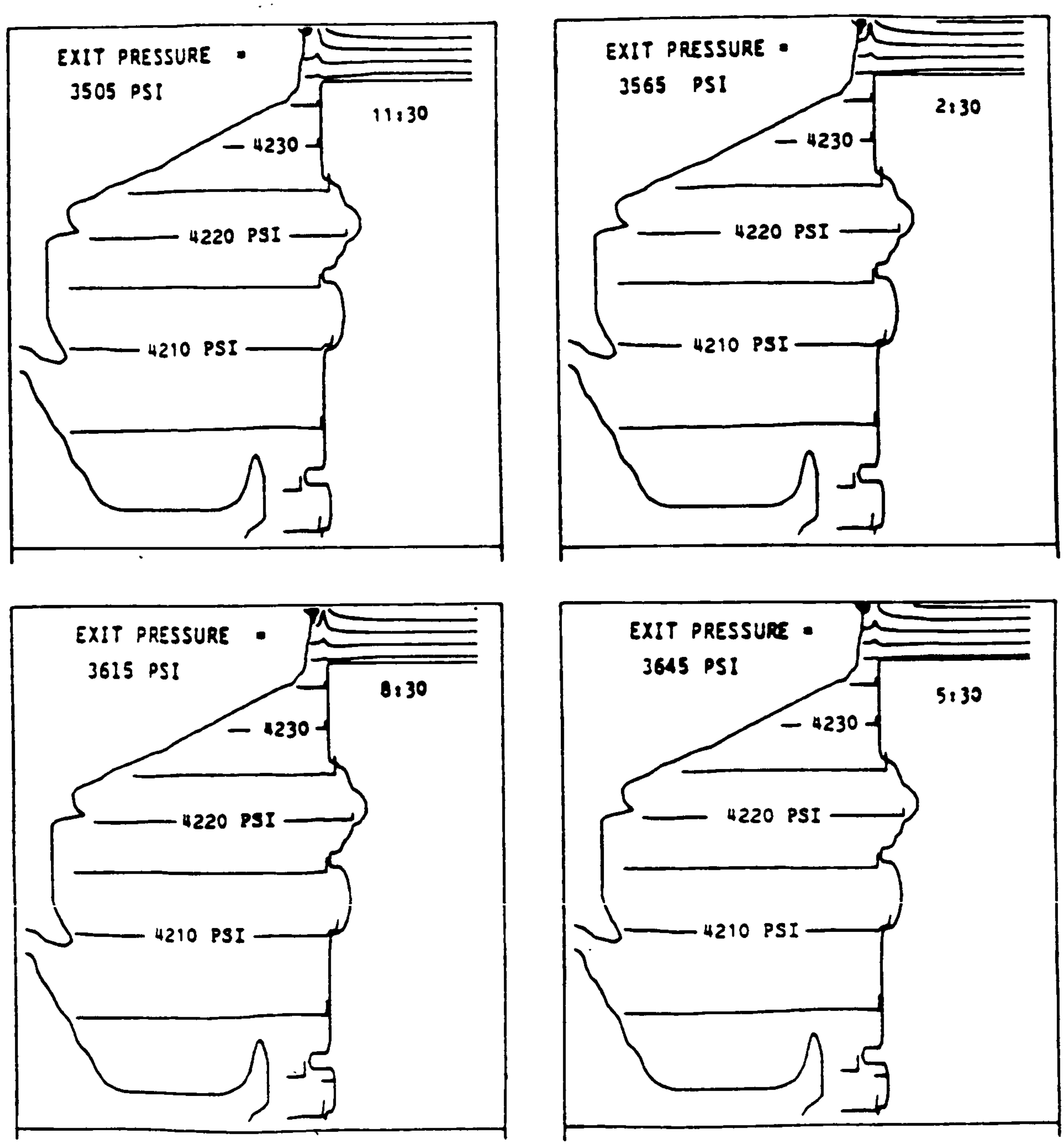

Three-dimensional basecase results: static pressure.

HPFTP INLET DOME AND STRUTS TEMPs

100% POWERLEVEL
t = 5 sec
TEST 801-023
(801-022)

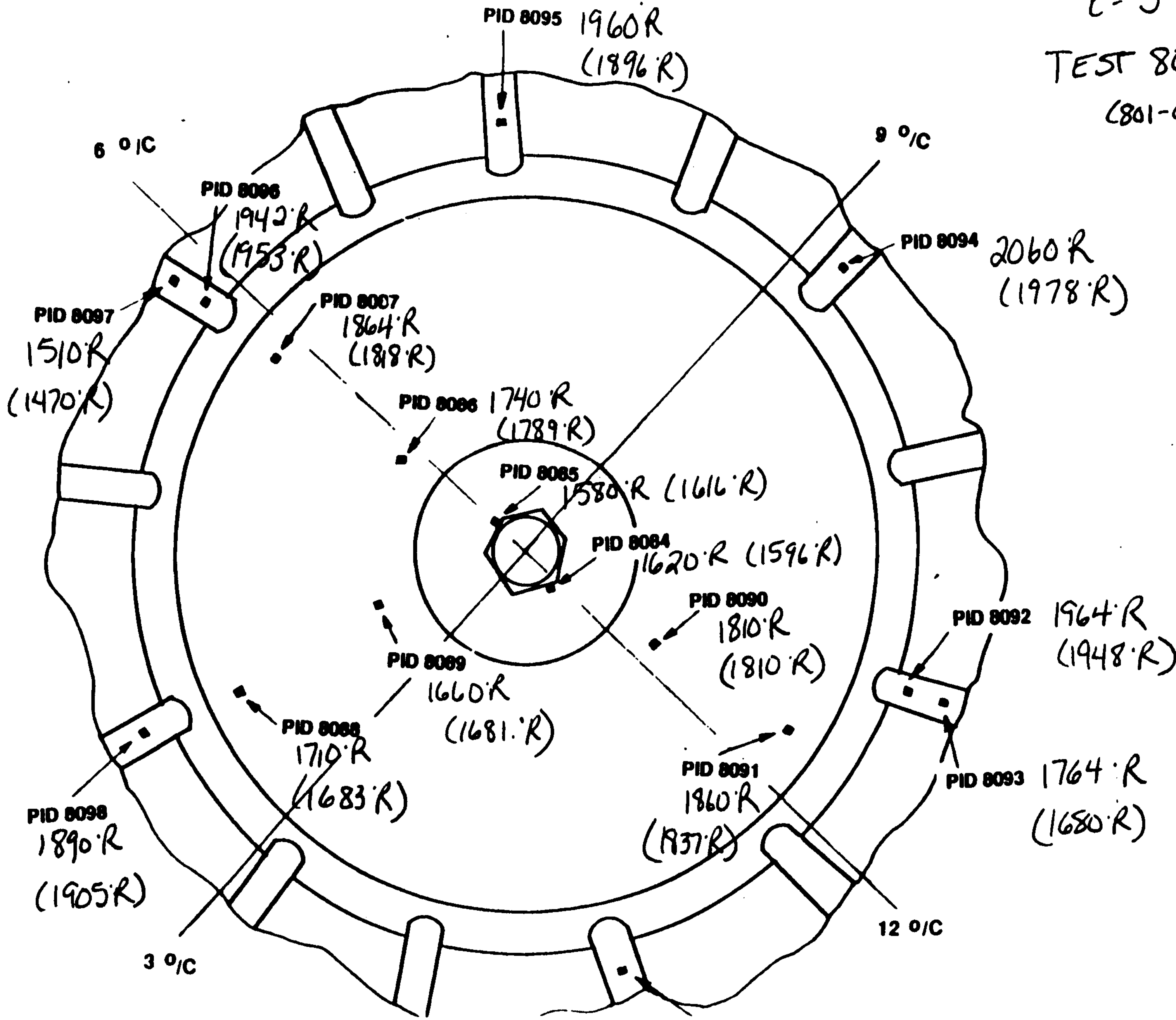

HPFTP 1st NOZZLE TEMPERATURES

100% POWER LEVEL

t= 5 sec

TEST 801-023

(801-022)

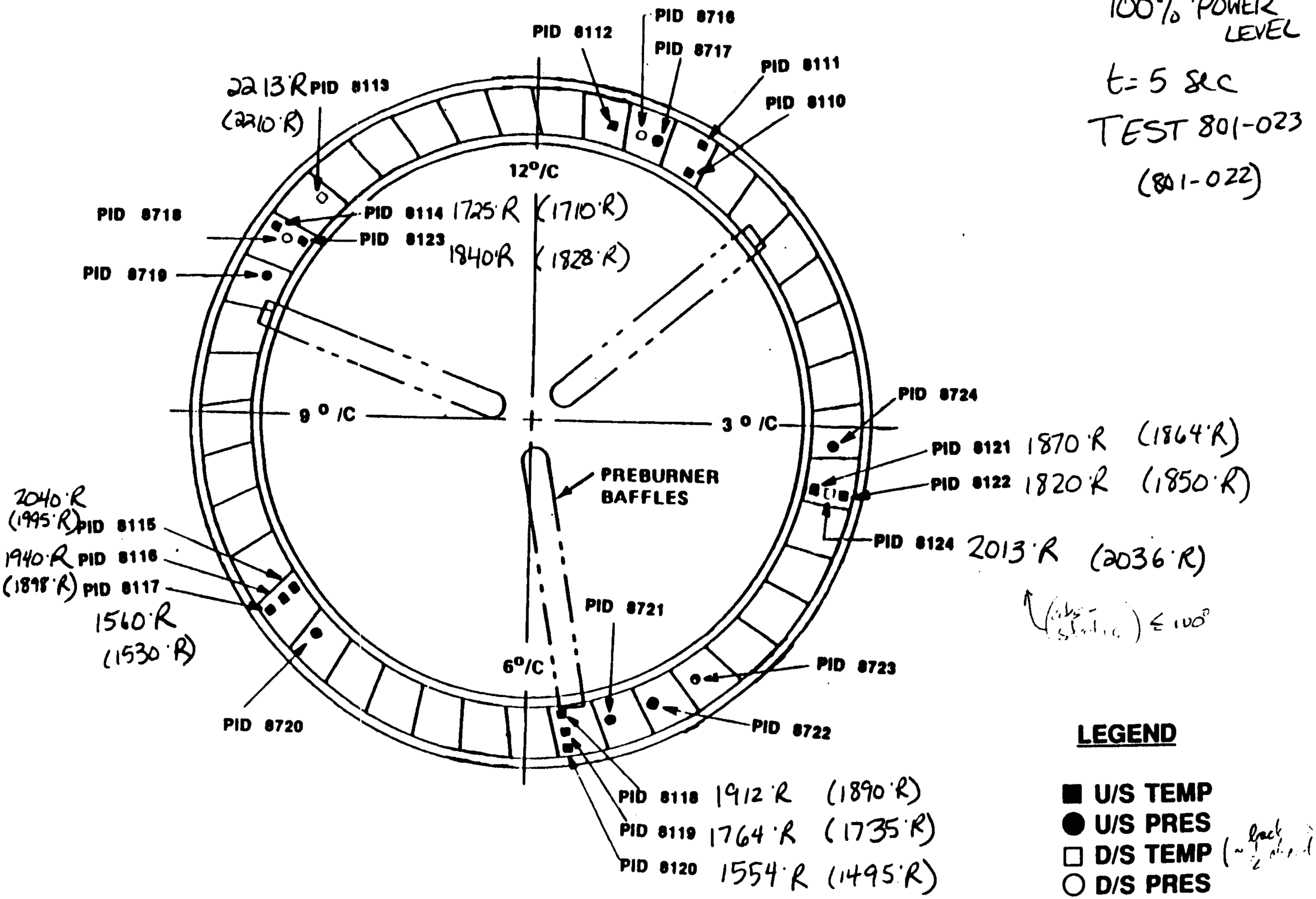

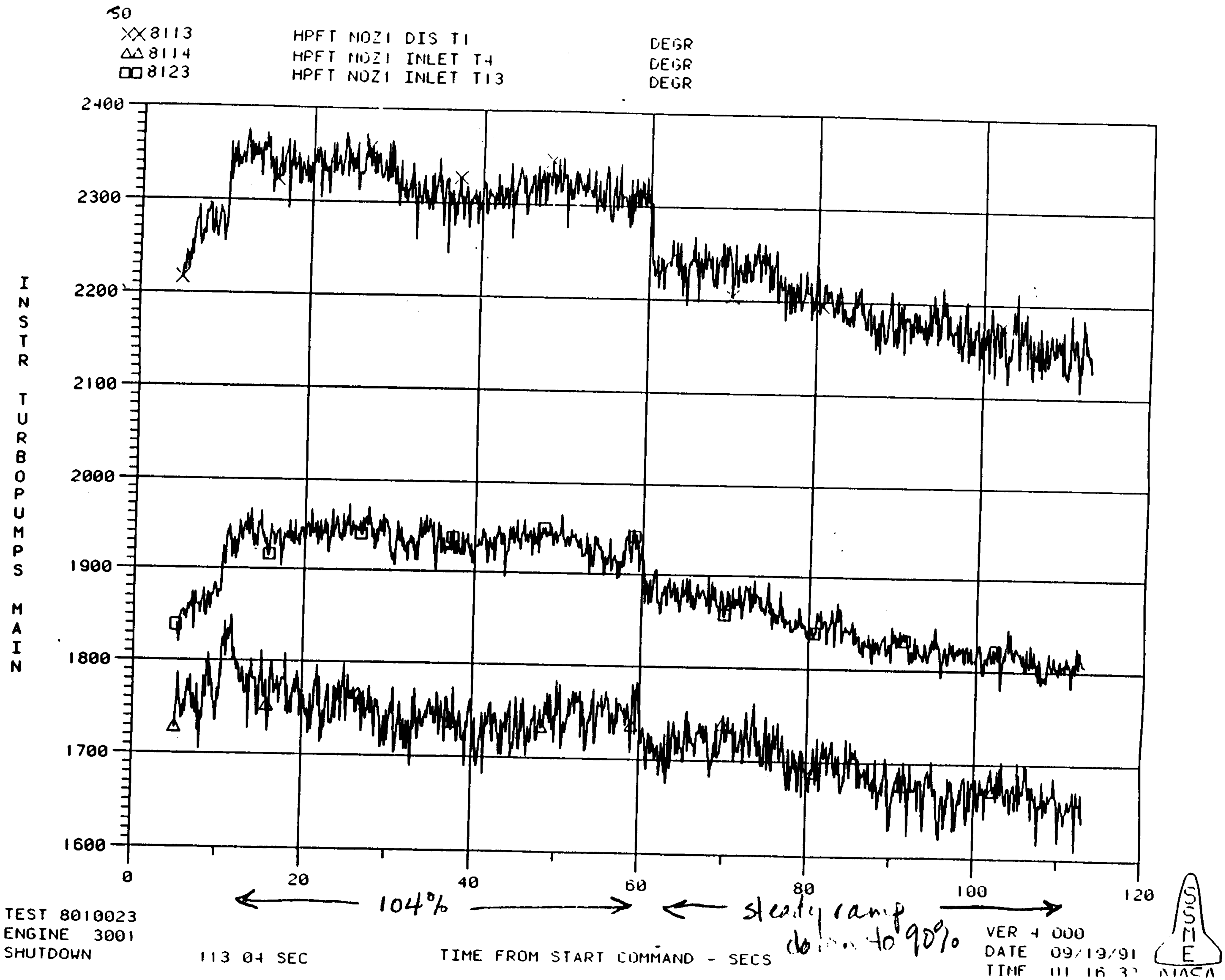

50
8113 HPFT NOZ1 DIS T1 DEGR
8114 HPFT NOZ1 INLET T4 DEGR
8123 HPFT NOZ1 INLET T13 DEGR
INSTR TURBOPUMPS MAIN
2400
2300
2200
2100
2000
1900
1800
1700
1600
0
20
40
60
80
100
120
104%
steady ramp down to 90%
TEST 8010023
ENGINE 3001
SHUTDOWN
113 04 SEC
TIME FROM START COMMAND - SECS
VER 4 000
DATE 09/19/91
SSME

Nozzle Wall Static Pressure

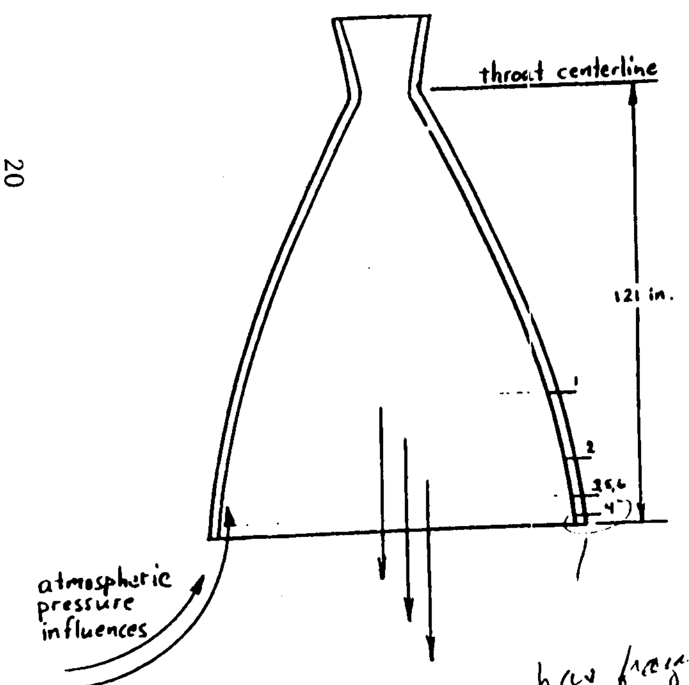

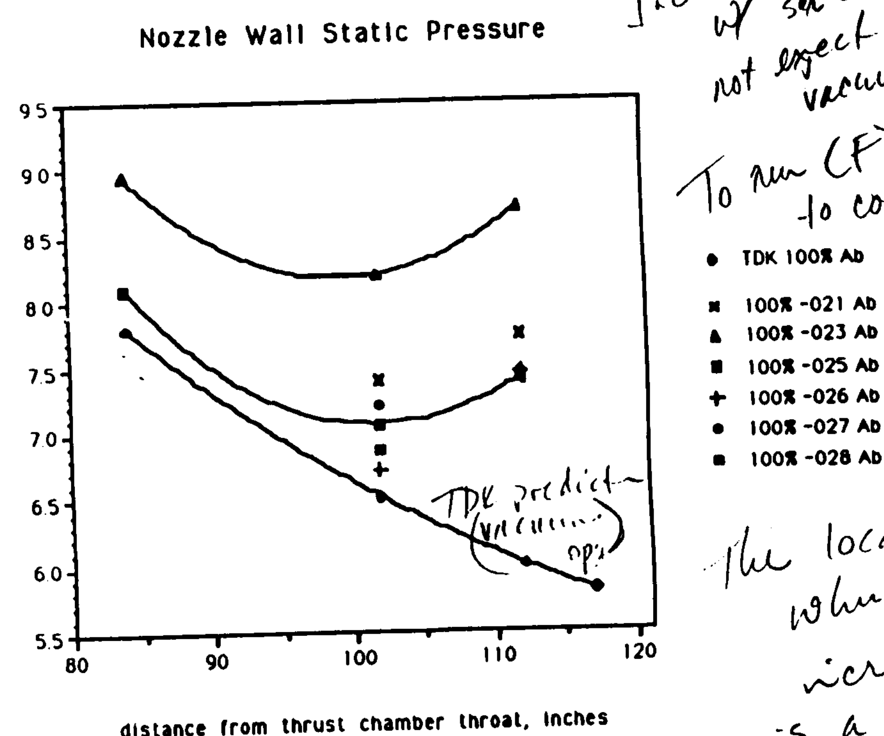

Per Klaus: Increase associated w/ sea level. not expected at vacuum cond.

To run CFD calcs to compare

The location where P increases is a surprise. It is farther upstream than expected

have fragm... during test. No data ...

2/26/92HJD11

3001 LESSONS LEARNED (CONT.)
DESIGN AND OPERATIONS

- ENGINE DESIGN/TESTING

  INSTRUMENTATION:

  - GLASS BRAIDED TYPE THERMOCOUPLE WIRE SHOULD BE REPLACED BY TEFLON COATED T/C WIRE TO AVOID UNRAVELING OF COATING DUE TO NORMAL FIELD OPERATION. (i.e. RUBBING WIRES DURING PUMP INSTALLATION)

  - ADDITIONAL EFFORT SHOULD BE MADE ON INSTRUMENTATION PLACEMENT TO AVOID LOCATIONAL EFFECTS WHICH MISREPRESENT THE DESIRED DATA: (i.e. ELBOWS, STAGNATION AND RECIRCULATION REGIONS)

  - EFFORT SHOULD BE MADE TO EQUALIZE SENSE LINE VOLUMES ON BOTH HIGH AND LOW SIDE OF DELTA PRESSURE TRANSDUCERS WHERE ACCURATE TRANSIENT DATA IS REQUIRED

  - PRESSURE SENSE LINES REQUIRED TO MEASURE HOT GAS ENVIRONMENTS AND THAT ARE ROUTED " NEAR " COOLANT CIRCUITS SHOULD BE CONSIDERED FOR PURGING DURING TESTING TO PREVENT ICING.

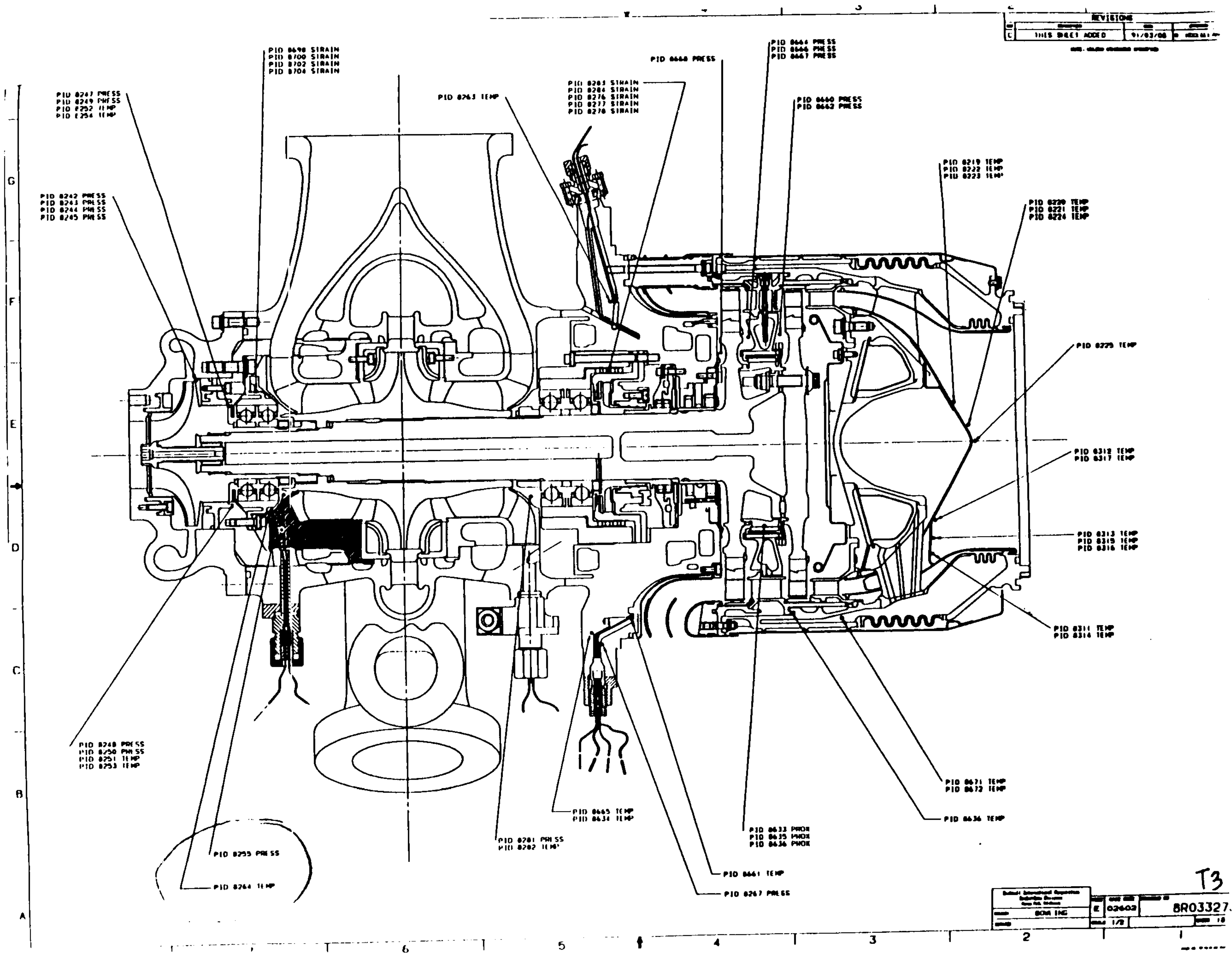
REVISIONS
THIS SHEET ADDED
PID 8698 STRAIN
PID 8700 STRAIN
PID 8702 STRAIN
PID 8704 STRAIN
PID 8247 PRESS
PID 8249 PRESS
PID 8252 TEMP
PID 8254 TEMP
PID 8242 PRESS
PID 8243 PRESS
PID 8244 PRESS
PID 8245 PRESS
PID 8263 TEMP
PID 8283 STRAIN
PID 8284 STRAIN
PID 8276 STRAIN
PID 8277 STRAIN
PID 8278 STRAIN
PID 8668 PRESS
PID 8664 PRESS
PID 8666 PRESS
PID 8667 PRESS
PID 8660 PRESS
PID 8662 PRESS
PID 8219 TEMP
PID 8222 TEMP
PID 8223 TEMP
PID 8220 TEMP
PID 8221 TEMP
PID 8224 TEMP
PID 8225 TEMP
PID 8312 TEMP
PID 8317 TEMP
PID 8313 TEMP
PID 8315 TEMP
PID 8316 TEMP
PID 8311 TEMP
PID 8314 TEMP
PID 8248 PRESS
PID 8250 PRESS
PID 8251 TEMP
PID 8253 TEMP
PID 8671 TEMP
PID 8672 TEMP
PID 8636 TEMP
PID 8665 TEMP
PID 8634 TEMP
PID 8633 PROX
PID 8635 PROX
PID 8636 PROX
PID 8281 PRESS
PID 8282 TEMP
PID 8255 PRESS
PID 8661 TEMP
PID 8267 PRESS
PID 8264 TEMP
T3
BOEING
E
02602
8R03327
1/2
G
F
E
D
C
B
A
7
6
5
4
3
2
1

HPOP PREBURNER PUMP BEARING COOLANT FLOW TEMPERATURE 109% VS. 100% P.L.

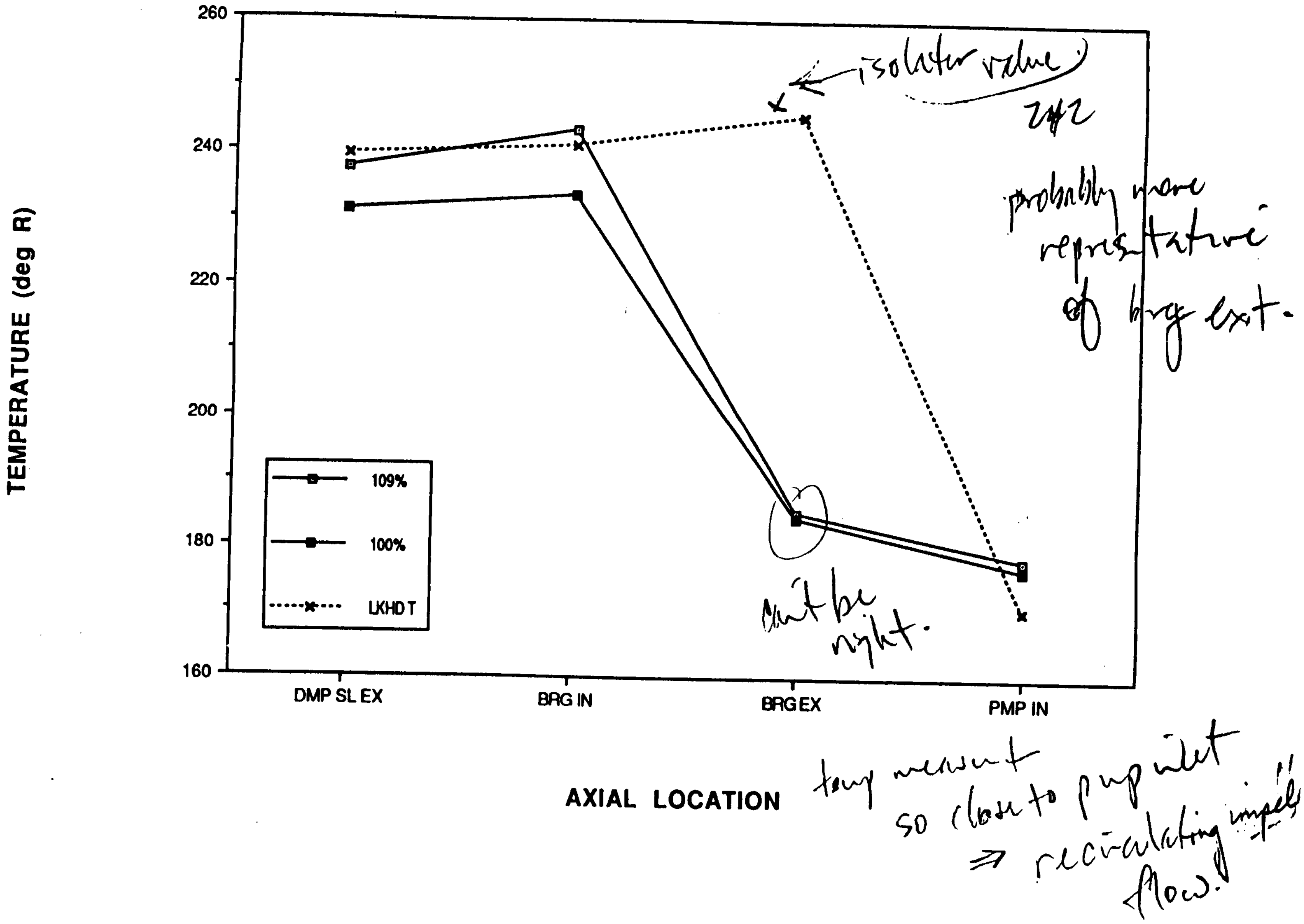

FUTURE PLANS

CONTINUATION OF PHASE II ENVIRONMENT CHARACTERIZATION
- o INSTRUMENTED RKDN TURBOPUMPS
- o P&W ALTERNATE TURBOPUMPS

CONTINUATION OF TECHNOLOGY ITEM INTEGRATION AND EVALUATION
- o HEALTH MONITORING SYSTEMS
- o TURBOMACHINERY
- o COMBUSTION DEVICES
- o INSTRUMENTATION
- o CONTROLLER

CHARACTERIZATION OF FUTURE PROPULSION SYSTEM DESIGNS
- o SSME PROTOTYPE BLOCK II (PHASE II+ POWERHEAD, ATDs, LTMCC)
- o SSME PRODUCIBILITY IMPROVEMENTS
- o HLLV STME PROTOTYPE

TTB SCHEDULE

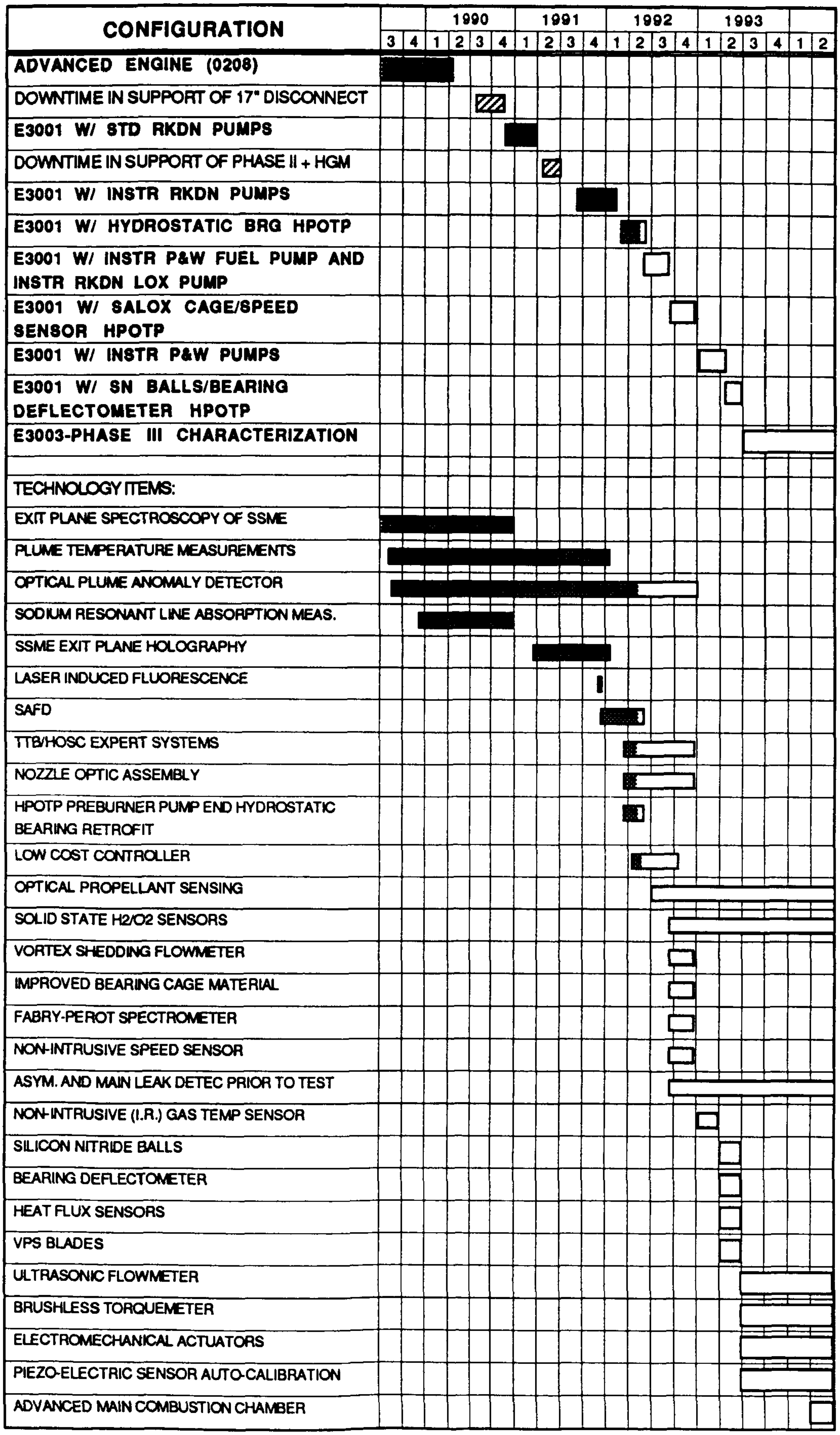

SUMMARY

TECHNOLOGY TEST BED HAS PROVEN TO BE EFFECTIVE IN CHARACTERIZING PROPULSION SYSTEM DESIGNS

TECHNOLOGY TEST BED HAS PROVIDED VALUABLE HOT-FIRE DATA FOR INCREASED UNDERSTANDING OF THE INTERNAL OPERATING ENVIRONMENT OF THE SSME AND FOR CALIBRATION OF SSME MODELS

TECHNOLOGY TEST BED HAS ENHANCED SHUTTLE DEVELOPMENT TESTING AND ANOMALY RESOLUTION

TECHNOLOGY TEST BED HAS PROVIDED A VALUABLE PLATFORM FOR ASSESSMENT OF ADVANCED PROPULSION TECHNOLOGIES

TECHNOLOGY TEST BED FUTURE PLANS INCLUDE CHARACTERIZATION OF FORTHCOMING PROPULSION SYSTEM DESIGNS AND EVALUATION OF EMERGING PROPULSION TECHNOLOGIES

ADVANCED SOLID ROCKET MOTOR PROJECT STATUS

Tenth Workshop for Computational Fluid Dynamics (CFD) Applications in Rocket Propulsion

28 April 1992

Keith Coates
EE 71
MSFC

N92-32280

15/4/10

OUTLINE

- Project Objectives
- Team
- Locations
- Motor Design
- Schedule
- Technical Issues

PROJECT OBJECTIVES

- **Improve System Safety and Reliability**
  - Design Features
  - Enhanced Quality
  - Reproducibility
- **Improve Shuttle Payload Performance: 12,000 lb**
- **Optimize Program Cost**
- **Promote Competitive SRM Industry**
  - Construct and Operate Government Owned Manufacturing and Test Installations

ASRM PROJECT TEAM

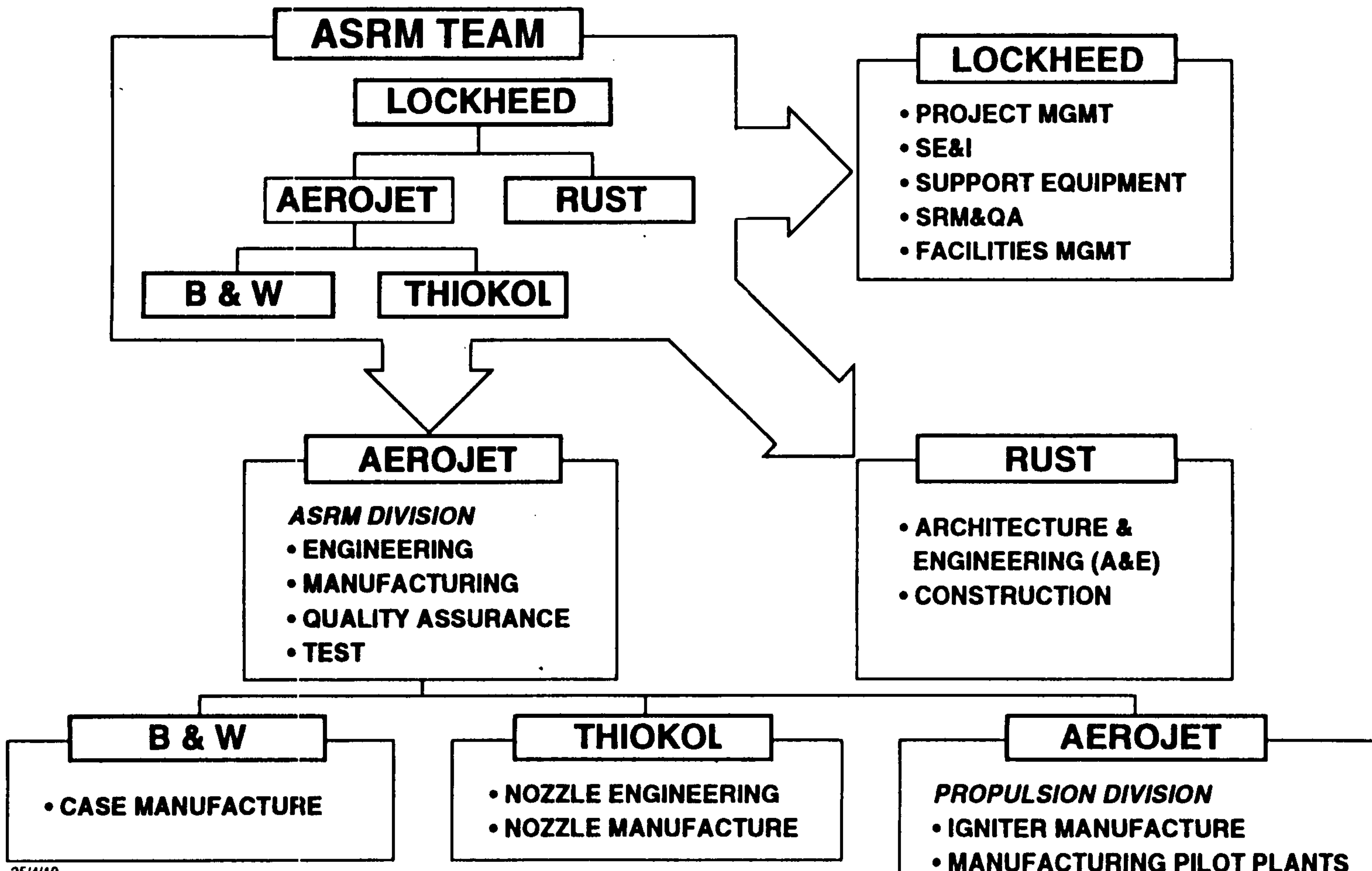

ASRM 3074.01

ASRM PROJECT TEAM LOCATIONS

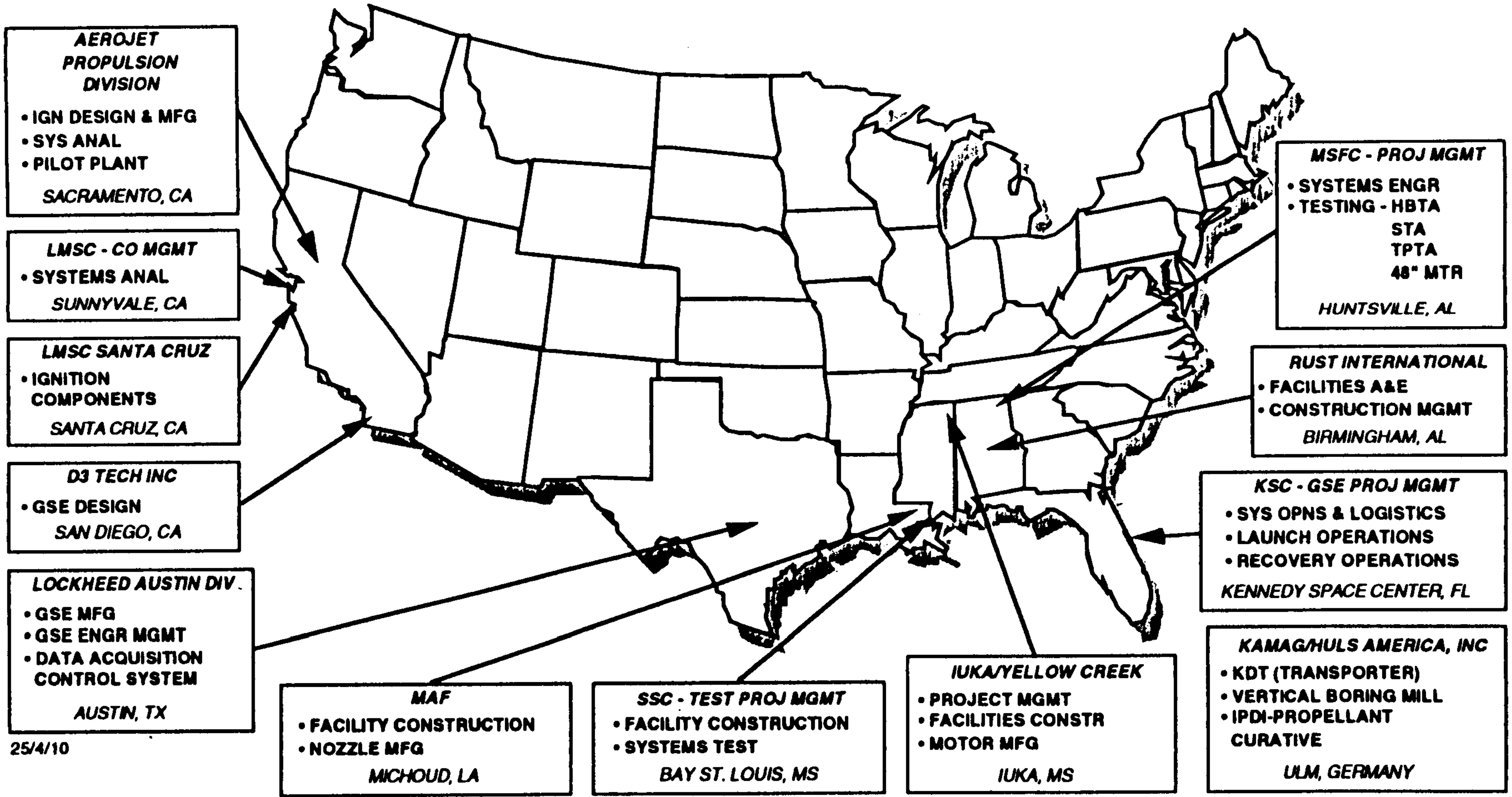

25/4/10

ASRM 3074.02

ASRM MOTOR DESIGN HIGHLIGHTS

INSULATION
- Uses RSRM J-Seal Design at Field Joint
- Castable Inhibitor-to-Stress Relief Flap Joint Location Minimizes Potential for Jetting Into Sidewall Insulation
- Asbestos Free Formulation

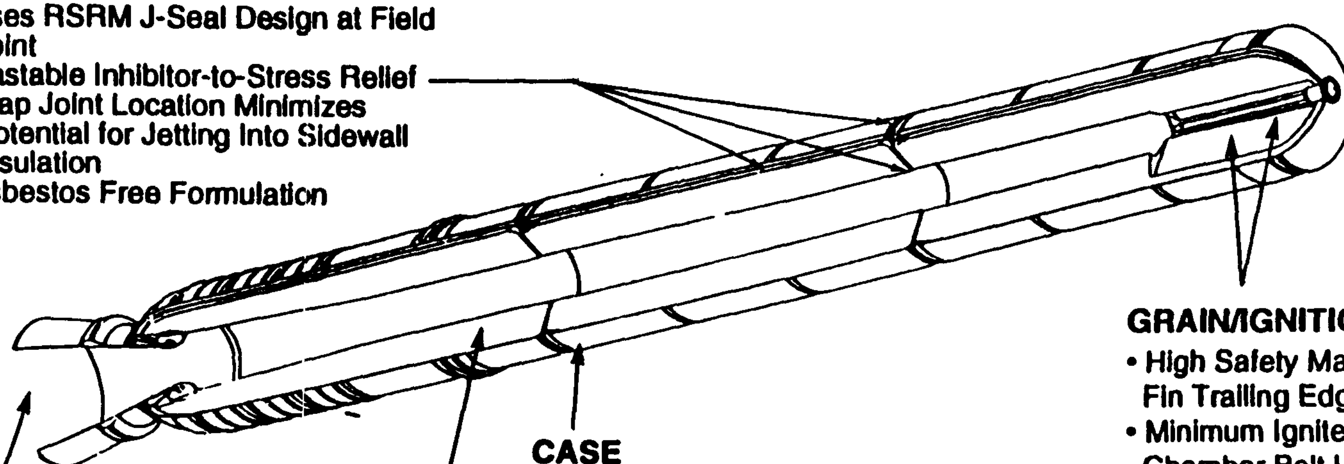

GRAIN/IGNITION
- High Safety Margin In Forward Fin Trailing Edge
- Minimum Igniter Chamber Bolt Leak Paths
- Expendable Carbon Filament Chamber
- TBI Initiator Eliminates S&A Device Leak Paths

CASE
- Two Field Joints
- High Fracture Toughness
- High Stress Corrosion Resistance
- Welded Factory Joints
- Integral Stiffeners and ET Attach Ring In Aft Segment Eliminates Failure Points Experienced With Bolt-On Stiffeners and Ring

NOZZLE
- Minimum Joints and inlet/throat rings
- Improved process ablative materials
- Eliminates flexseal cowl and boot assembly

PROPELLANT
- Industry Proven HTPB Propellant with over 60M lbs Successfully Produced
- Formulated and Proven for Continuous Mix Process
- Positive Margins

ASRM DESIGN PARAMETERS

■ Diameter/Length, in	150/1,513.43
■ Average Thrust Vacuum, lbf; Web time	2,654,776
■ Delivered Isp Vacuum, sec	268.1
■ Area Ratio, (Ae/At)	7.48
■ Motor Weight, lb	1,351,092
■ Propellant Weight, lb	1,209,589
■ Motor Propellant Mass Fraction, (Wp/Wt)	0.895
■ Inert Weight , lb	141,503
❑ Metal Case Weight/Number of Segments, lb	98,553/3
❑ Single Nozzle Weight, lb	18,800
■ Solid Propellant Type	HTPB
■ Average Chamber Pressure, psia; Action Time	612
■ Burn Rate at 625 psia, in/sec	0.350
■ Action Time, sec	130.9
■ Thrust Vector Control	Flexible Bearing
■ Recovery/Reuse	Yes

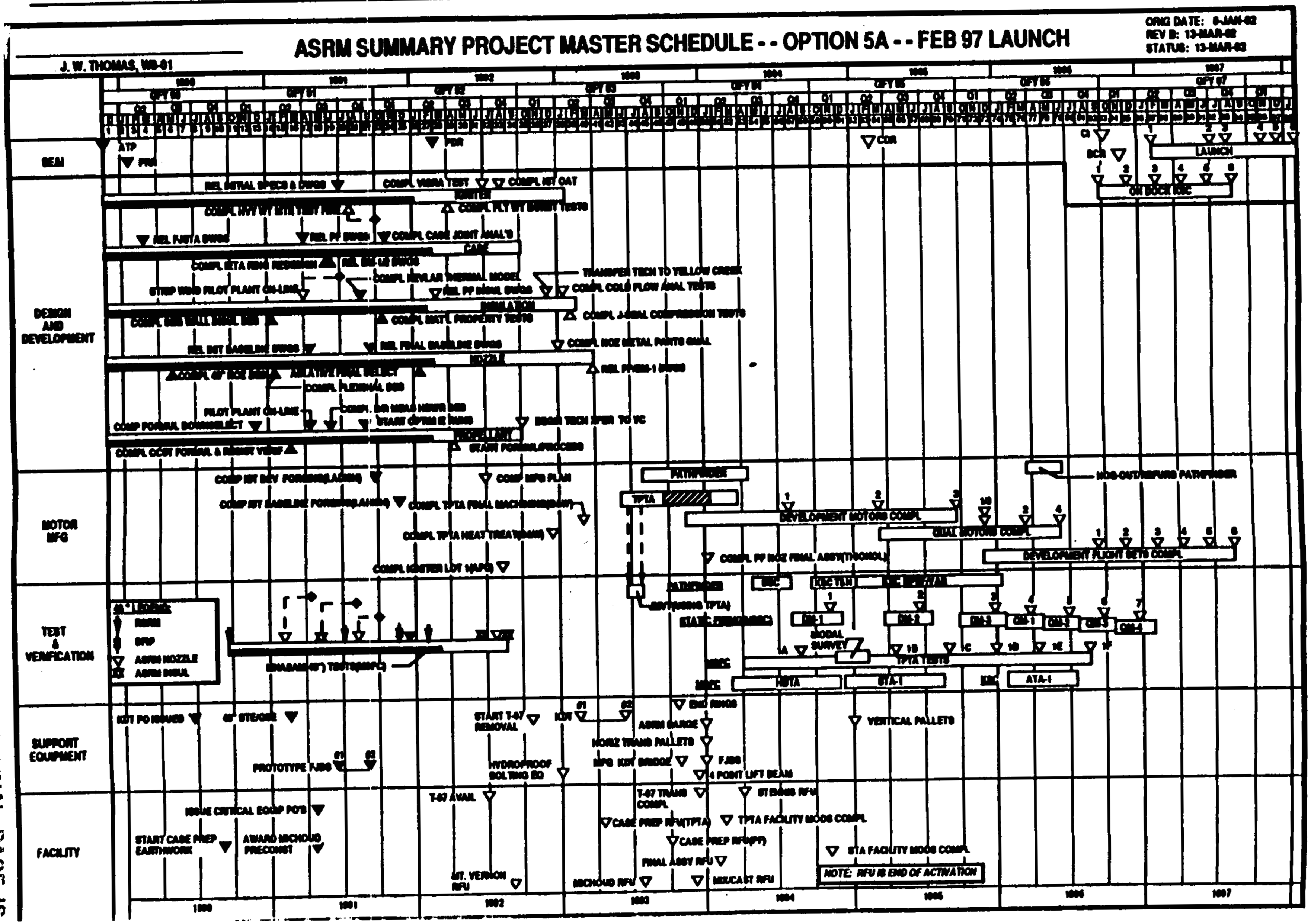

ORIGINAL PAGE IS OF POOR QUALITY

YELLOW CREEK

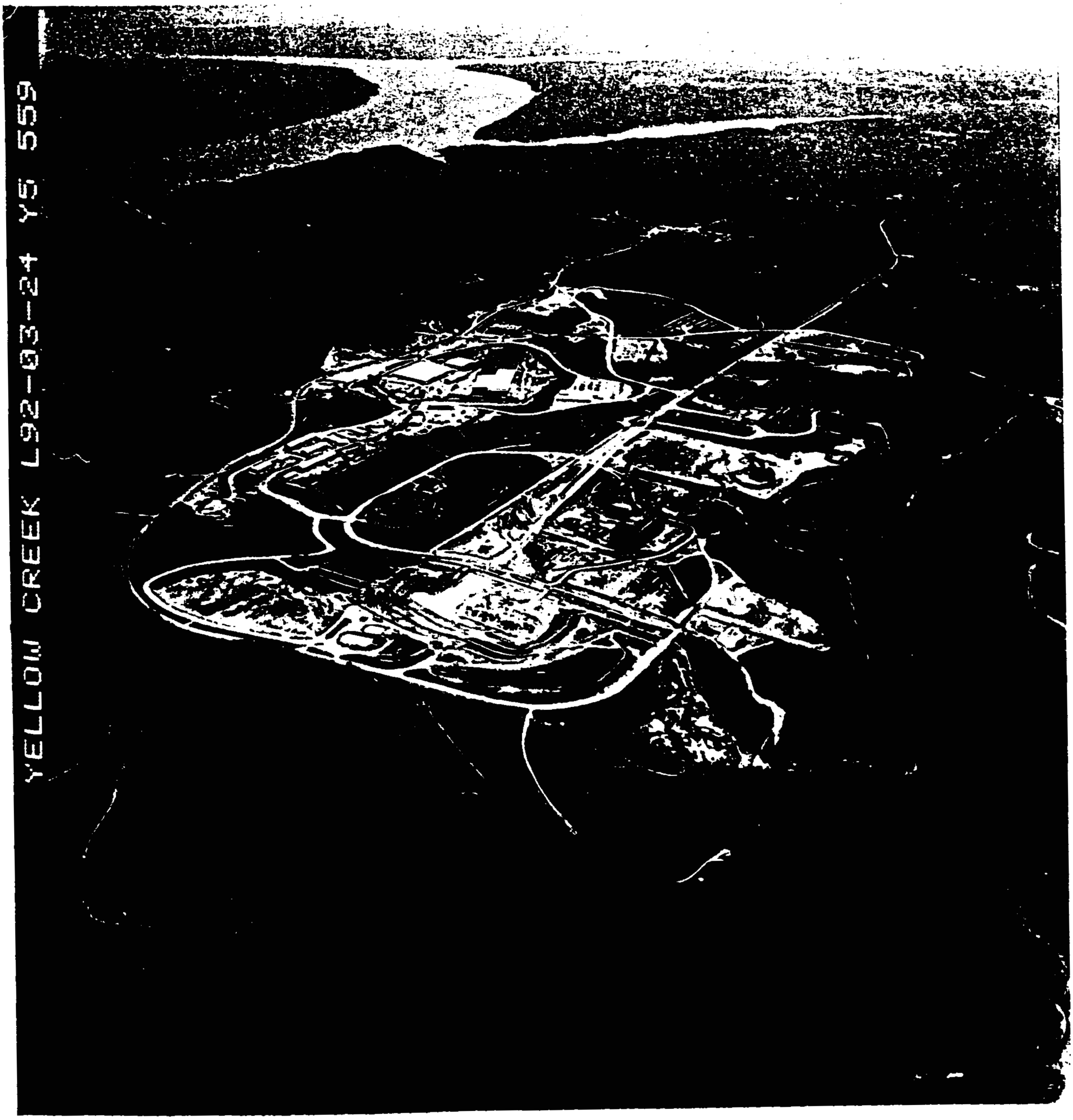

ORIGINAL PAGE IS
OF POOR QUALITY

CASE PREP BUILDING

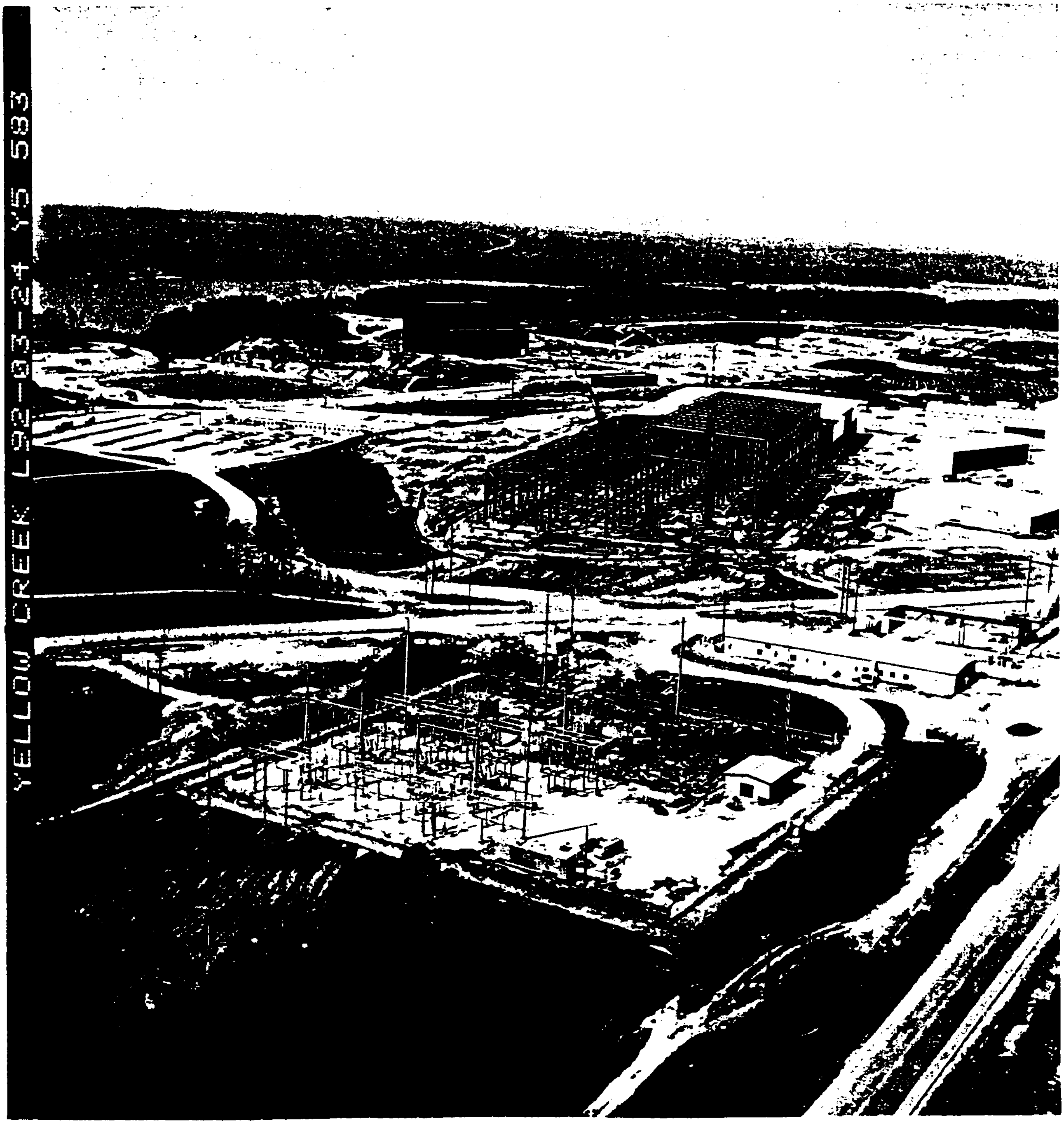

CASE PREP AUTOCLAVE
ON-SITE FABRICATION AT YELLOW CREEK

MICHOUD PILING AND PERIMETER WALL

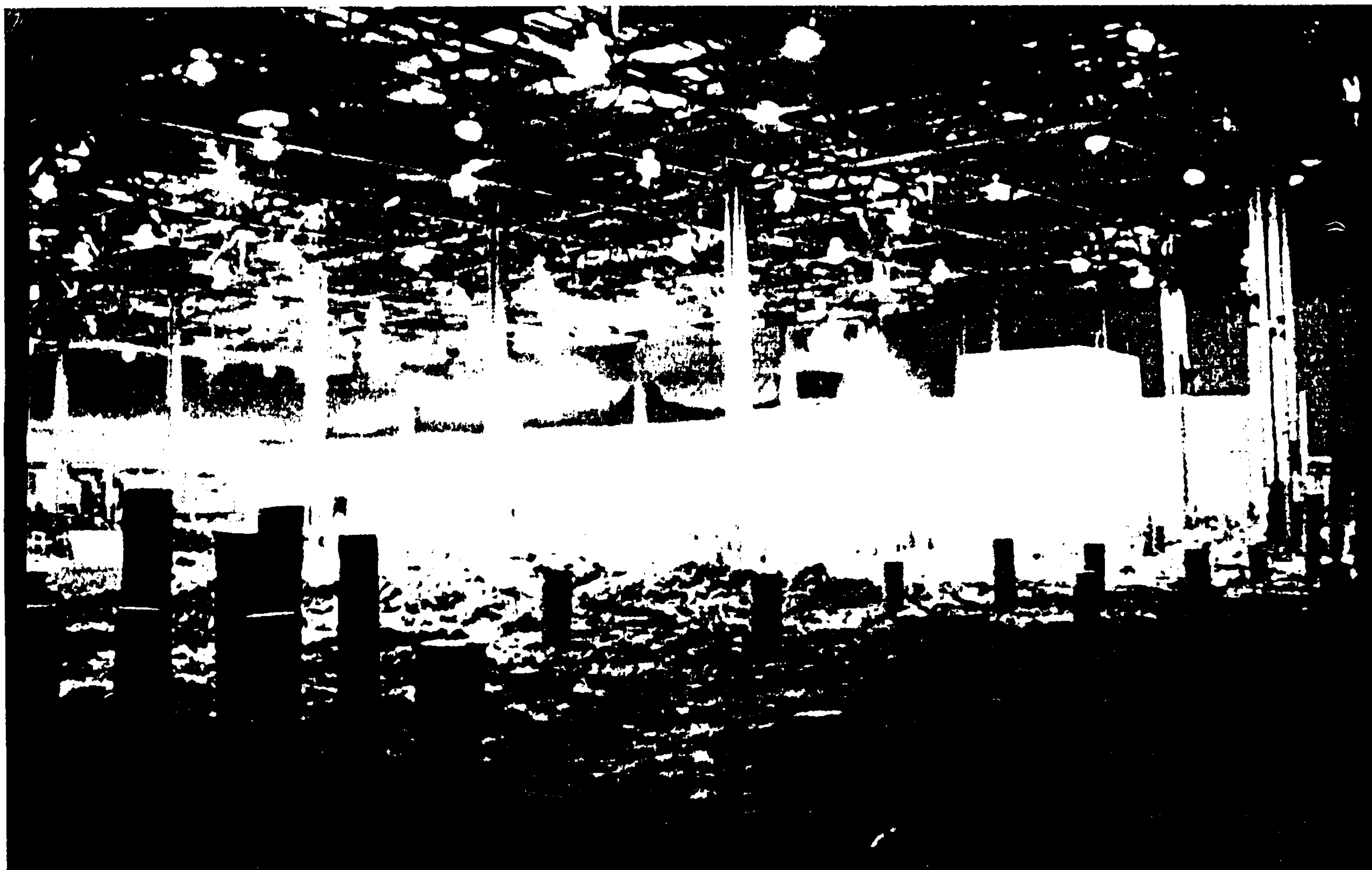

ORIGINAL PAGE IS
OF POOR QUALITY

VERTICAL BORING MILL (VBM)

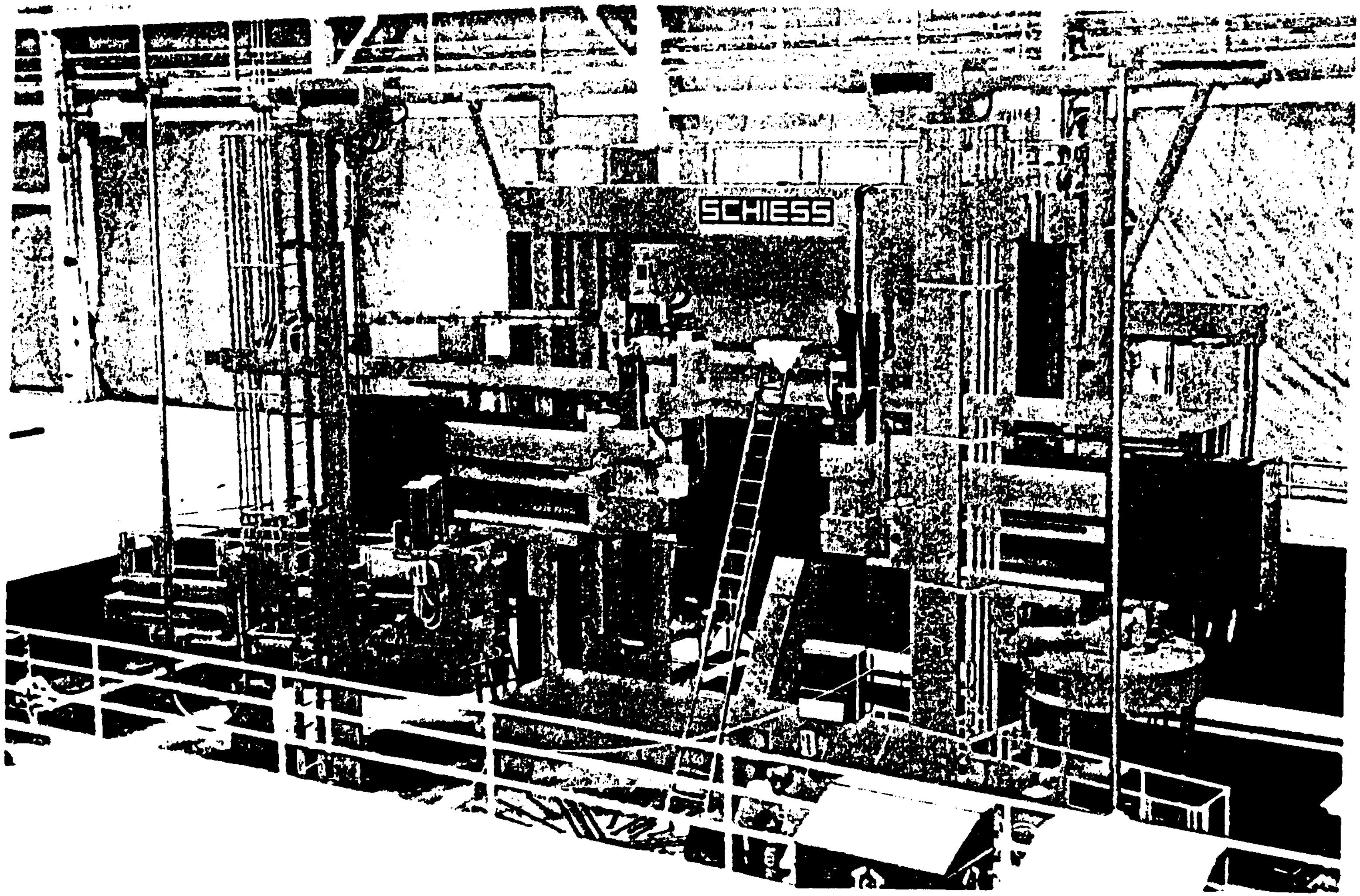

ORIGINAL PAGE IS
OF POOR QUALITY

HEAT TREAT/CHILLER BUILDING

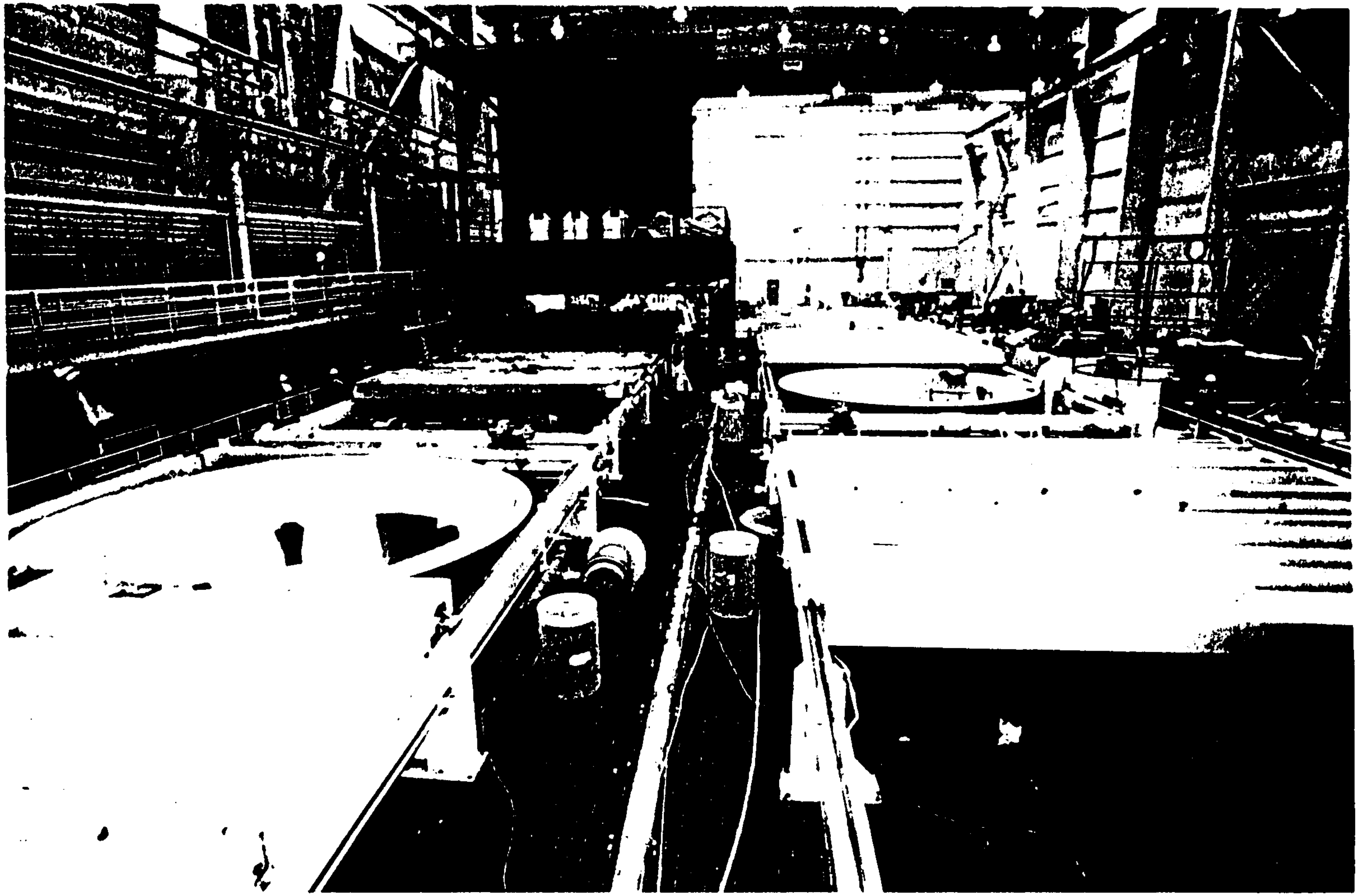

SSC ASRM TEST SITE

ASRM TECHNICAL TOP 5
March 27, 1992

1. Mix/Cast Construction, Outfitting & Process Verification
2. Soluble Casting Mandrels
3. Integration Effects; P_c Dot; Loads; Recovery; Overpressure; Moldlines
4. Low-Density Nozzle Ablatives Performance
5. Forward-Facing Cast Inhibitor

SOLUBLE CORE DESIGN

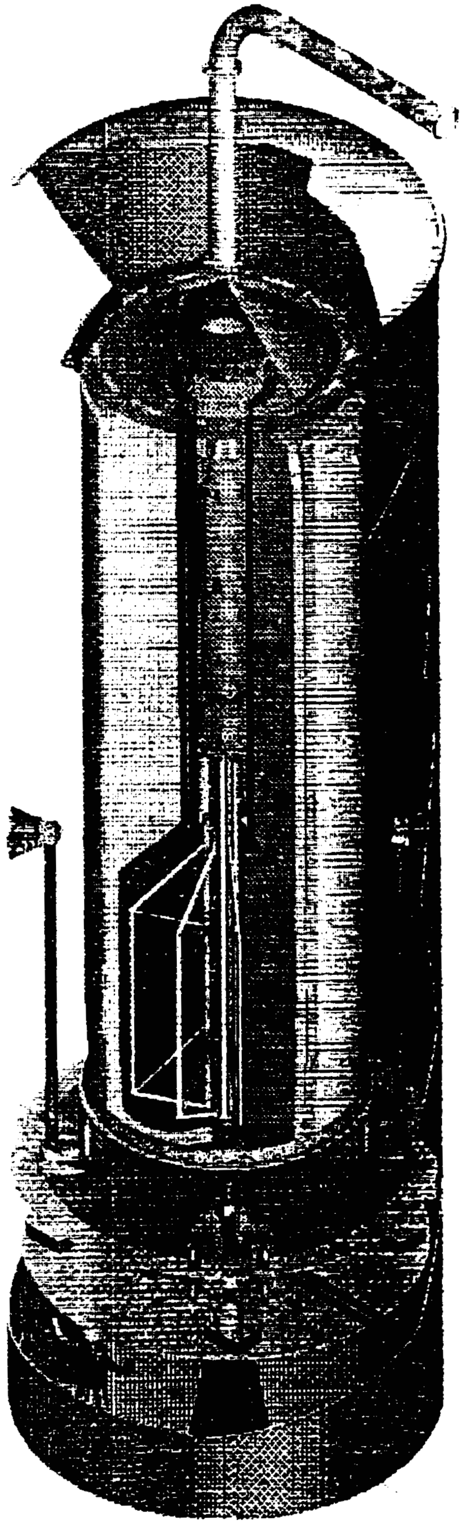

SPACE TRANSPORTATION MAIN ENGINE

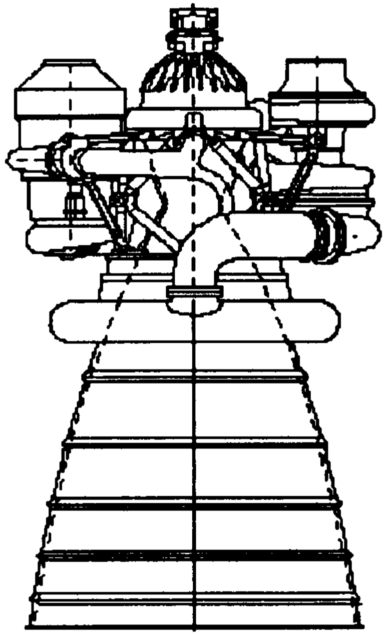

APRIL 28, 1992

Jan C. Monk
Chief Engineer
Space Transportation Main Engine
Marshall Space Flight Center

PRECEDING PAGE BLANK NOT FILMED

N92-32281

STME DEFINITION

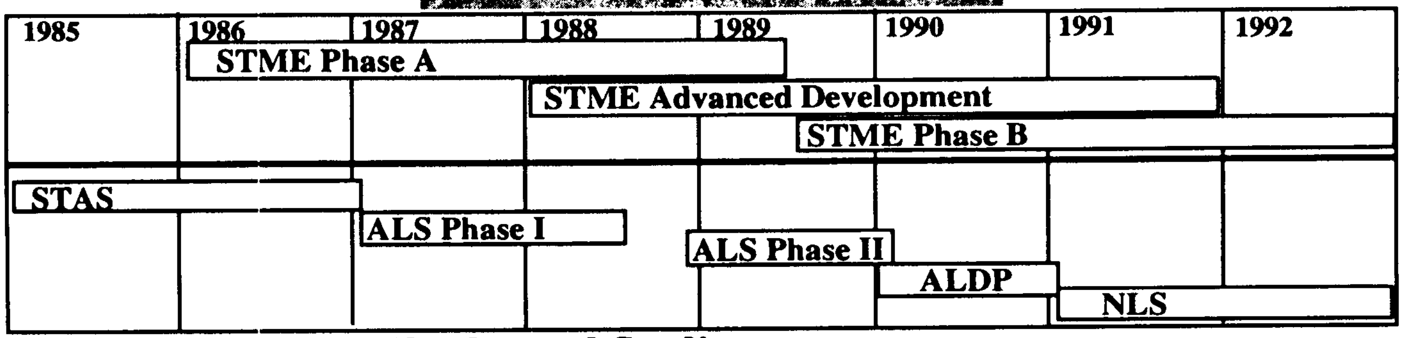

- **Over 7500 STME Trades and Studies**
  - Engine System Level Trades
  - Engine Component Level Trades
  - Manufacturing Studies
  - Assembly Facilities Studies
  - Test Facilities Studies
  - Overhaul Facilities Studies
- **STME Design Concept Formed in Total System Context**
  - Interactive Engine/Vehicle/Operability Trades
  - Broad range of Vehicles and Missions
  - QFD established Strategic Quality Characteristics, Pugh Concept Selection
  - National Consensus Cycle Decision
- **Design Effort Supported by Extensive Data Base**
  - ADP Hardware
  - Lessons Learned: SSME, J-2, LR87, F-100, F-119, etc.

DESIGN PHILOSOPHY

- ROBUST DESIGN
- DESIGN FOR OPERABILITY
- DESIGN FOR RELIABILITY
- DESIGN FOR LOW COST

ROBUST DESIGN

- **ACHIEVABLE REQUIREMENTS**
  - Mission Life - 10
  - Chamber Pressure - 2250 psia
  - Weight - 9100 pounds
- **SERIES TURBINES**
  - Enhances benign system response to fuel turbopump failures
- **DESIGN MARGINS**
  - Design based on internal operating environment worst case plus development margin
- **REDUCED INTERNAL ENVIRONMENTS TO ASSURE ROBUST PROCESSES**
  - No sheet metal liners, no overlays, no platings
- **NEAR NET SHAPE PROCESSES**
  - Minimum number of welds, capable processes, reduced process steps

MAXIMUM DESIGN CONDITION

- MDC = NOMINAL PARAMETER VALUE
  + RSS OF PREDICTED COMPONENT VARIATIONS
  + THRUST/MR CALIBRATION ERRORS
  + FLIGHT EFFECTS
  + DEVELOPMENT MARGIN

FUEL PUMP DISCHARGE PRESSURE

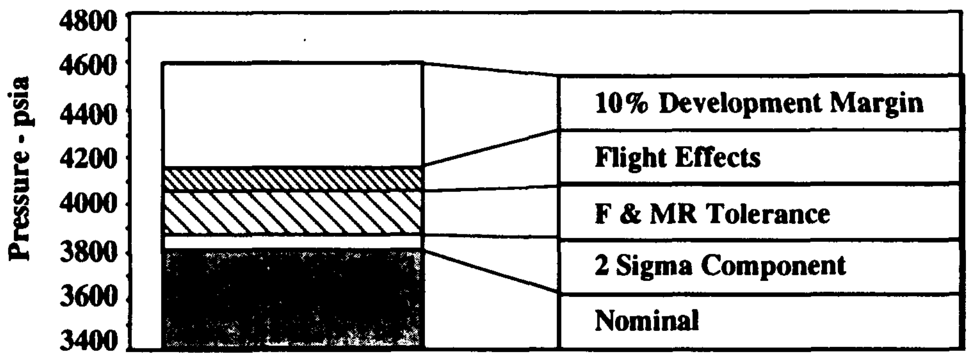

CASTINGS VS MACHINED AND WELDED FORGINGS

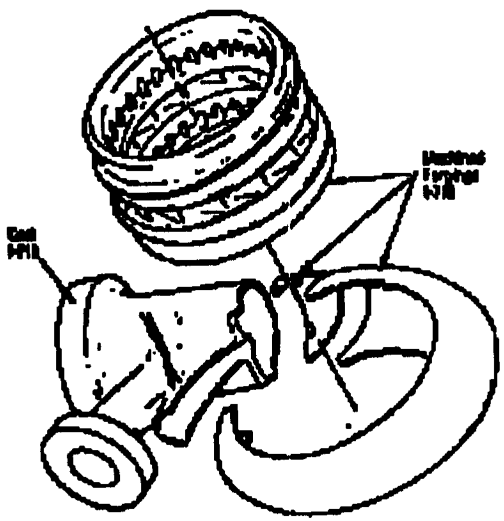

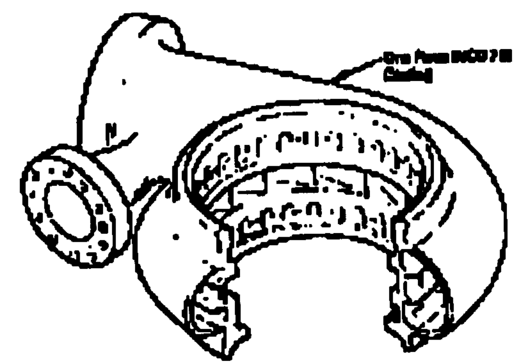

- Material costs $ 15,182
- Machine and welding 440,824

Total cost $456,006

SSME Turbopump Volute

I-718 cast $14,527*
Machining 20,700

Total cost $35,227

IR&D Cast Volute

* Based on vendor quote for 6 parts

OPERABILITY CONSIDERATIONS

- **TANK-HEAD START**
  - No start valve or ducting
- **ELECTROMECHANICAL ACTUATORS**
  - Simplify pre-launch checkout
  - No pneumatics or hydraulics
- **COMMONALITY FACILITATES INVENTORY AND ON-PAD REPLACEMENT**
  - Electromechanical actuators/seals/fastners
- **REDUCTION OF POTENTIAL LEAK PATHS**
  - Proven joint and seal designs
  - Reduced number of joints
- **SIMPLE COMPONENT INSTALLATION**
  - No stretch bolt joints
- **AUTOMATED PRE-LAUNCH CONTROLS CHECKOUT**
- **MINIMUM FLIGHT-CRITICAL INSTRUMENTATION**

HIGH RELIABILITY DESIGN PHILOSOPHY

- **DESIGN FOR RELIABILITY IS AN INTEGRAL PART OF THE STME DESIGN PROCESS**
  - Concurrent engineering
  - Design to reliability goals
  - reliability lessons learned
  - Bottoms-up failure modes and effects analysis
  - Tops-down fault tree analysis
  - Reliability tracking
  - New manufacturing techniques
  - Reliability demonstration program
  - Development margin

ENGINE RELIABILITY ENHANCEMENT

- **NON-INTRUSIVE OXIDIZER HEAT EXCHANGER (FOR TANK PRESSURIZATION)**
- **SIMPLE SAFETY MONITORING APPROACH. SAFE ENGINE SHUTDOWN TRIGGERED BY ABNORMAL VALUES OF:**
  - Chamber pressure
  - Interpropellant seal purge pressure
  - Gas generator temperature
- **MECHANICALLY LINKED GAS GENERATOR VALVES (TO PREVENT GG MIXTURE RATIO EXCURSIONS)**
- **PRUDENT USE OF REDUNDANCY IN CONTROL SYSTEM**
  - Dual EMA motors and resolvers
  - Duplex / triplex controller electronics
  - Dual power source

LOW COST DESIGN PHILOSOPHY

- **DESIGN-TO-COST IS AN INTEGRAL PART OF THE STME DESIGN PROCESS**
  - New manufacturing techniques
  - Advanced Development Programs used to investigate low cost ideas
  - Suppliers integral part of design effort
  - Customer (Government) integral part of design effort
  - Costs continually estimated and tracked
  - Cost drivers identified and worked
  - Trade studies used to select lowest cost concepts
  - Zero RID'S
  - Zero MR'S

ENGINE SYSTEM REQUIREMENTS

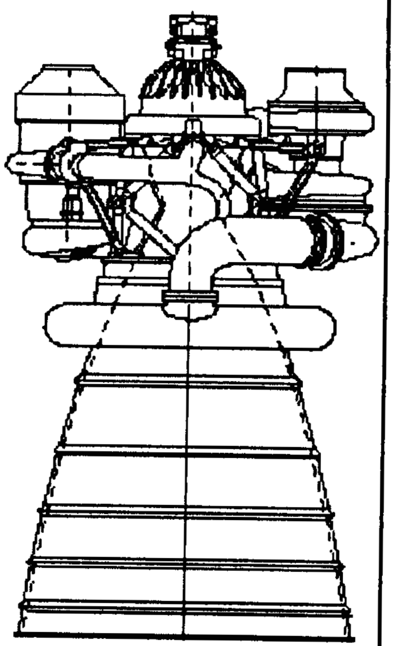

Dual Thrust (Step)	
Normal Thrust (100%):	**650,000 lbf**
Minimum Thrust (70%):	**455,000 lbf**
Mixture Ratio:	**6.0**
Specific Impulse (100%):	**428.5 sec.**
Specific Impulse (70%):	**427.3 sec.**
Chamber Pressure:	**2250 psia**
Dry Weight:	**9100 lbm**
Area Ratio:	**45:1**
Length:	**160 inches**
Nozzle Diameter:	**96 inches**
Design Life:	**10 missions**
Verified Reliability:	**0.995**
500th Unit Cost Goal:	**$5.3M**

STME COMPARISONS

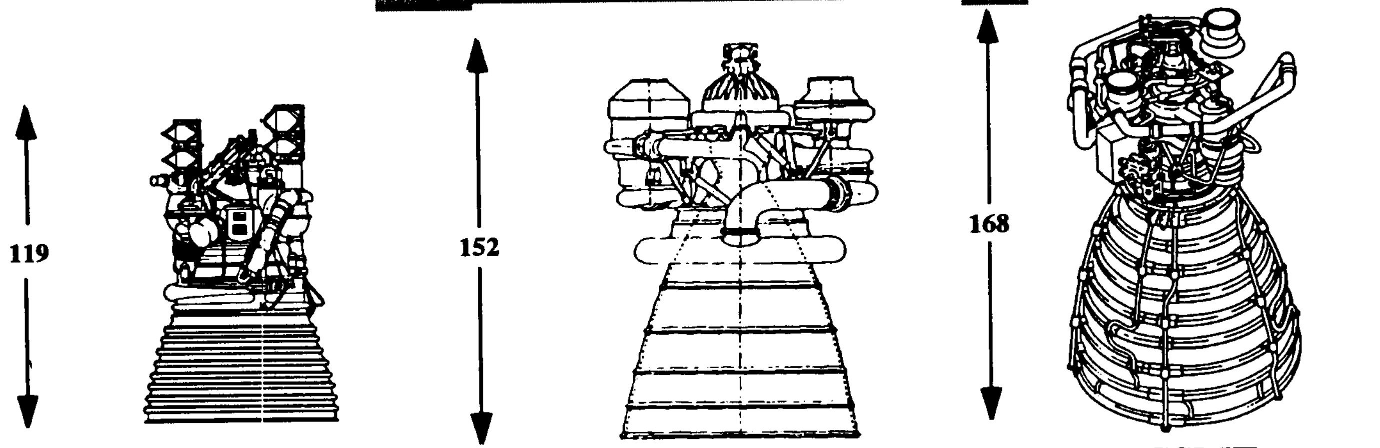

J-2
Gas Generator

STME
Gas Generator

SSME
Staged Combustion

	J-2	STME	SSME
Thrust (klbf-vac)	225	650	489
Chamber Pressure (psia)	700	2250	3130
Fuel Pump Power Density	30	35	100
Thrust-to-weight Ratio	68	67	70
Specific Impulse (vac)	425	428	452
Mixture Ratio	5.5	6.0	6.0
	27:1	45:1	77:1

STME SCHEMATIC

Rated Conditions

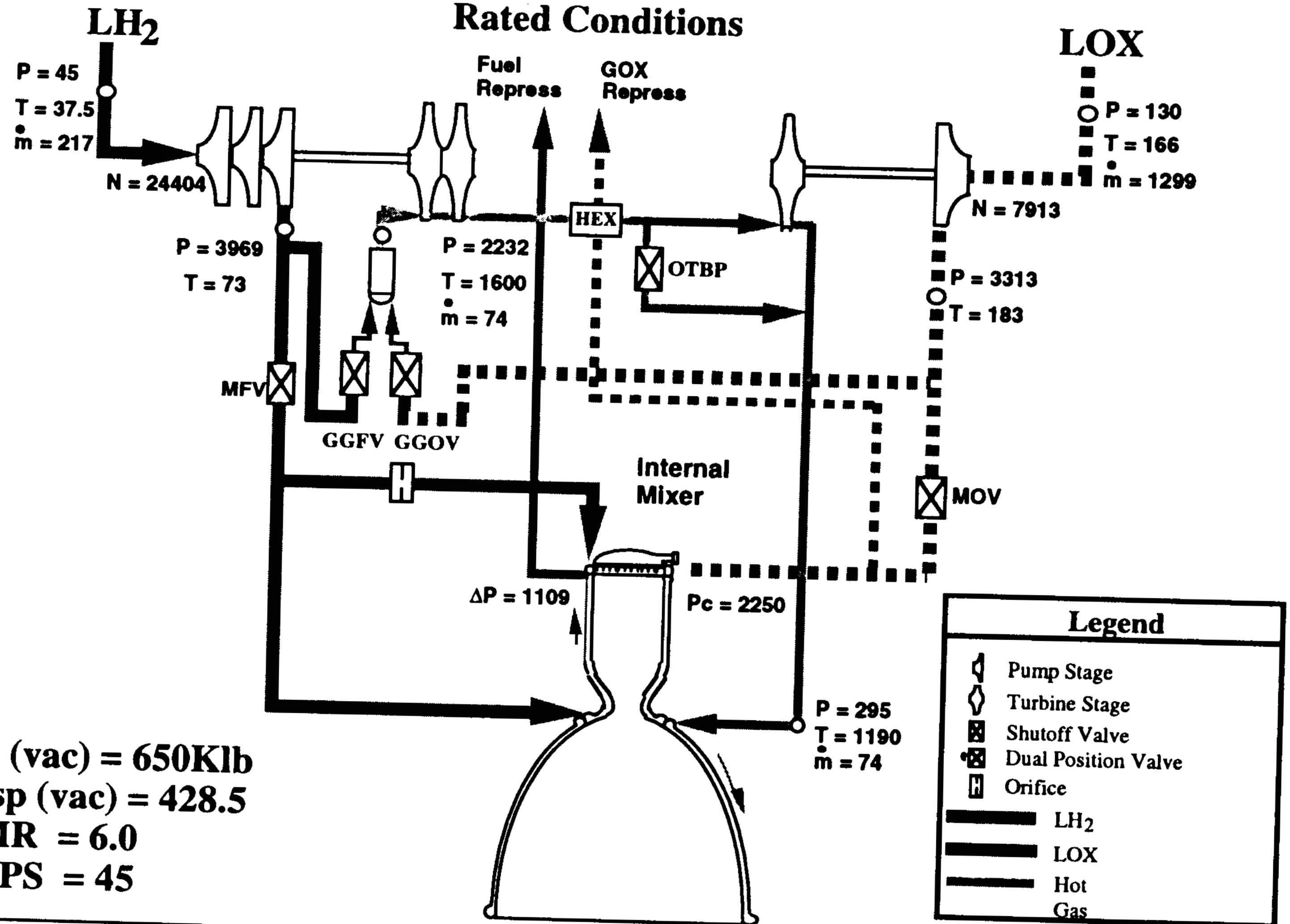

F (vac) = 650Klb
Isp (vac) = 428.5
MR = 6.0
EPS = 45

STME SIDE VIEW

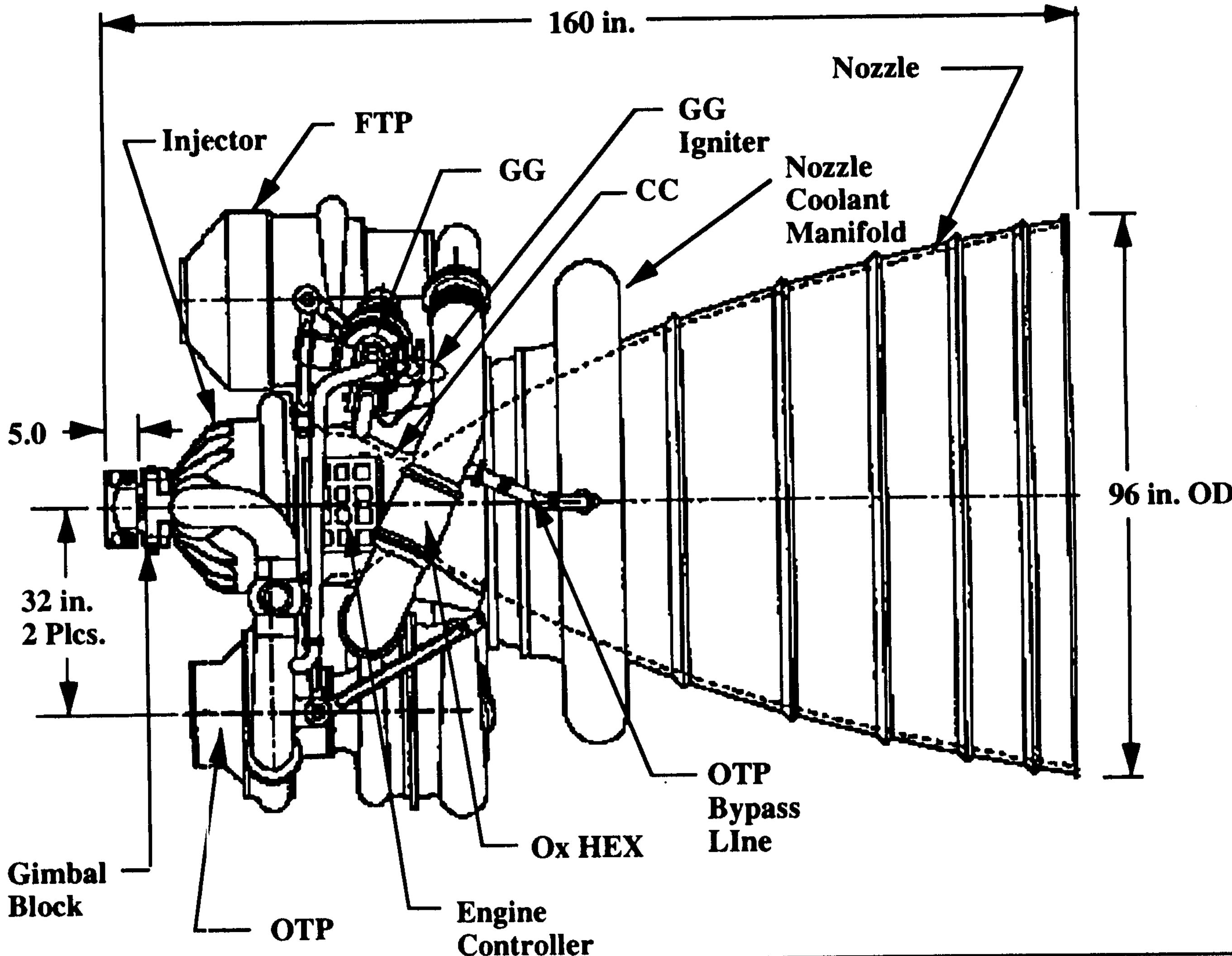

STME TOP VIEW

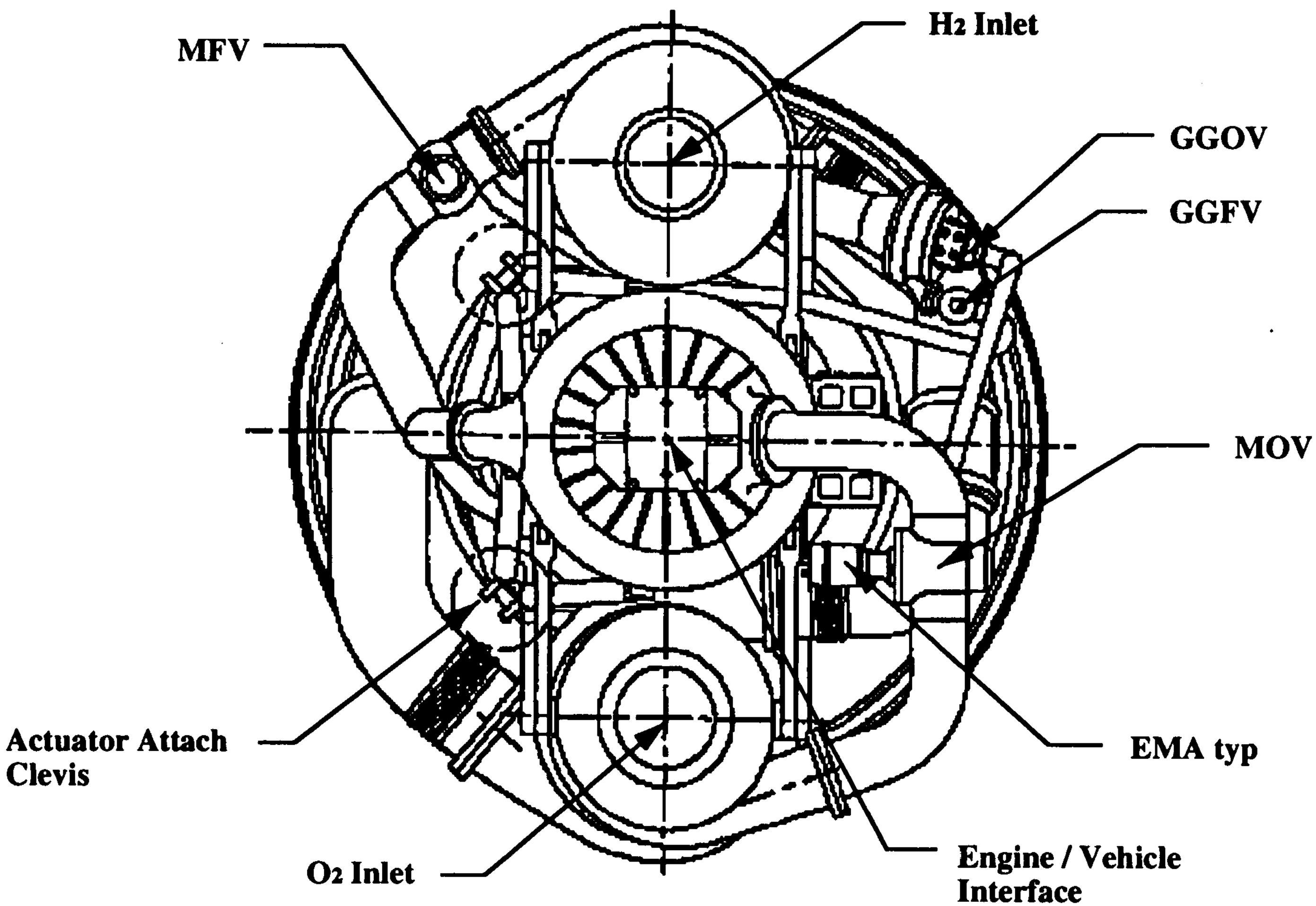

MAJOR ENGINE COMPONENTS

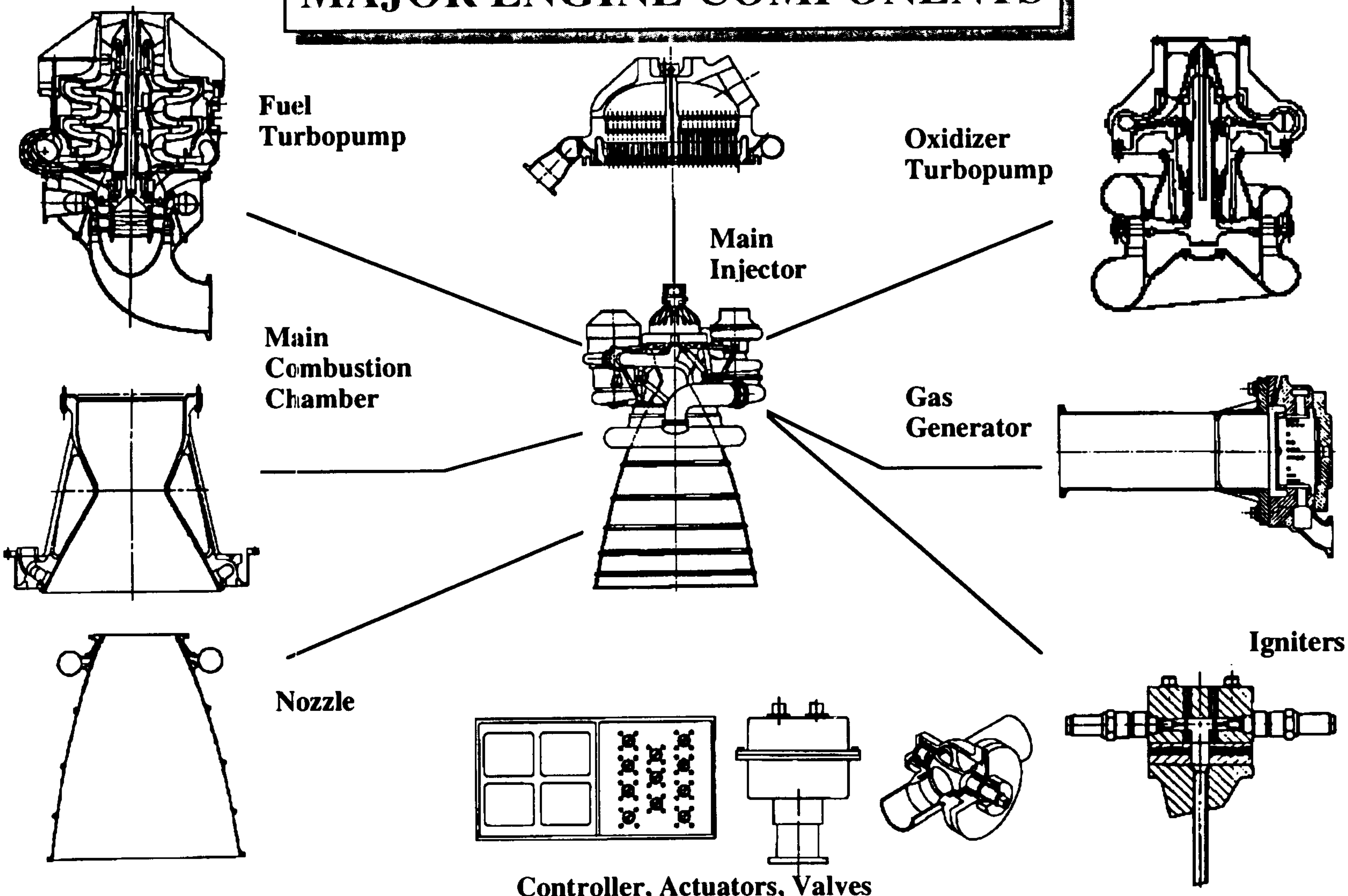

FUEL TURBOPUMP

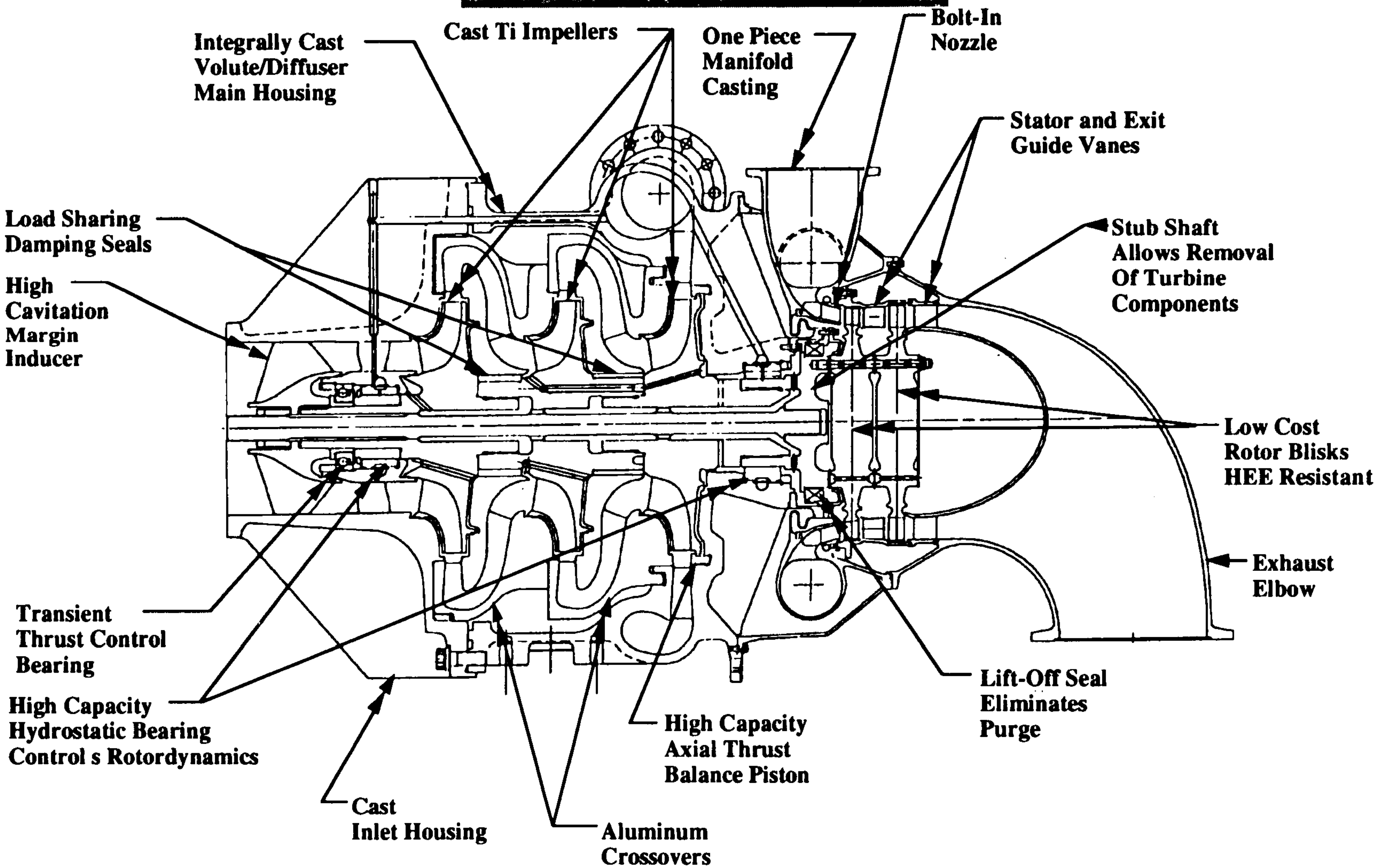

FUEL TURBOPUMP

BASELINE DESIGN FEATURES
- CAST HOUSINGS
- INTEGRALLY BLADED TURBINE
- CAST PUMP IMPELLERS
- HYDROSTATIC BEARINGS

OPTIONAL FEATURES
- LOW COST MACHINED IMPELLERS
- BACKUP DESIGNS FOR TURBINE AND BEARINGS

DEVELOPMENT STATUS
- FABRICATION PROCESSES IN TRIAL
- HYDROSTATIC BEARING RIG TESTING UNDERWAY
- SUPPLIERS ON CONCURRENT ENGINEERING TEAM

92 PLANS
- CONTINUED FAB DEVELOPMENT
- HYDROSTATIC BEARING TESTING

**LEAD: STPT-ROCKETDYNE/CANOGA PARK CA,
AEROJET/SACRAMENTO CA**

FUEL TURBOPUMP COMPARISON

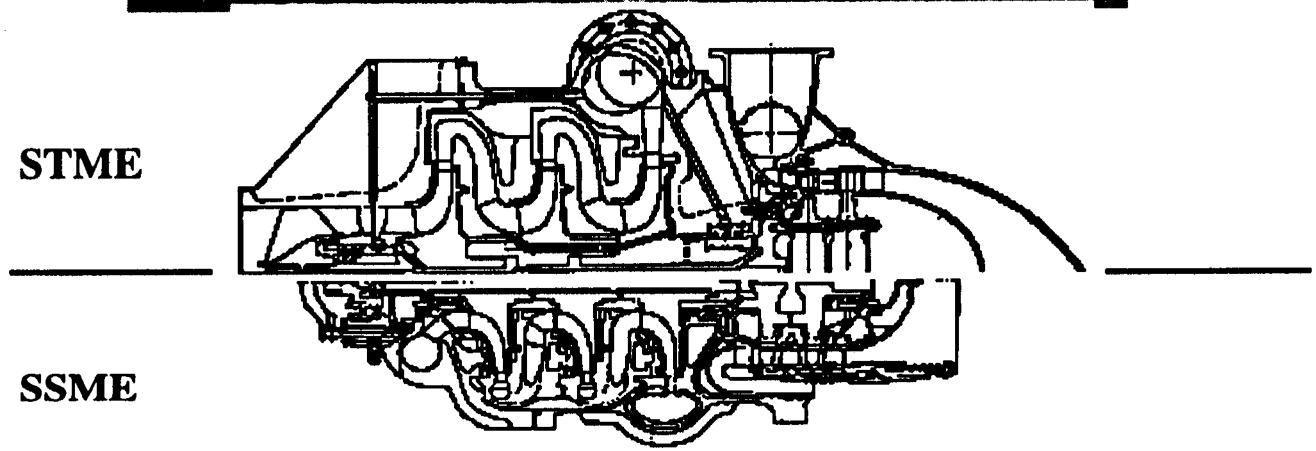

Discriminators	SSME	STME
Number of parts	198	60
Number of weld counts	801	1
Weld overlays	Yes	No
Sheet Metal Liners	Yes	No
Cost (TFU)	$4.1M	$ 1.02M
Discharge Pressure	6320 psia	3969 psia
Turbine Inlet Temperature	1860 deg R	1600 deg R
Speed	35180 rpm	23000 rpm
Weight	771 lbs	1877 lbs

LOX TURBOPUMP

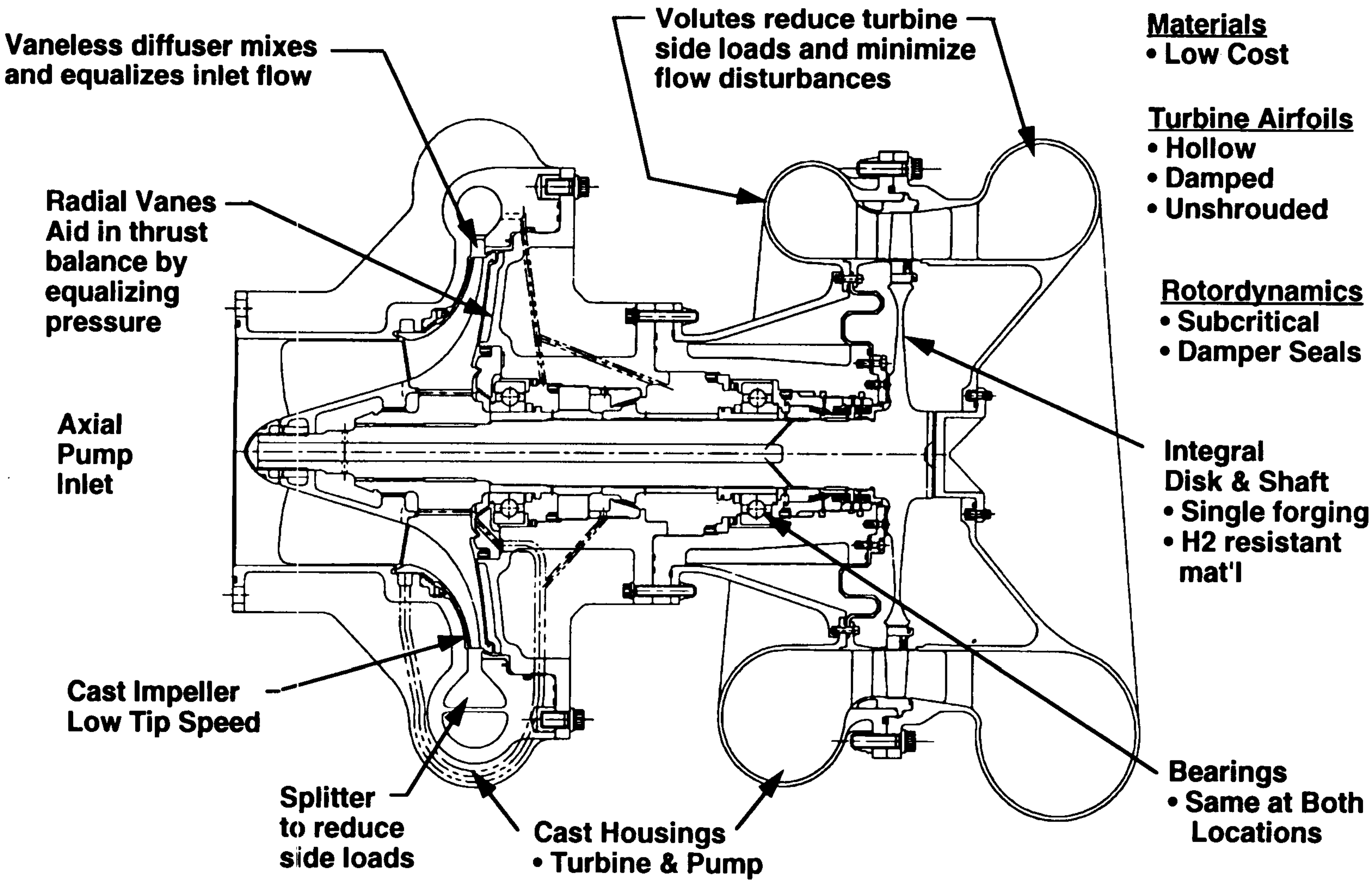

Materials
- Low Cost

Turbine Airfoils
- Hollow
- Damped
- Unshrouded

Rotordynamics
- Subcritical
- Damper Seals

LOX TURBOPUMP

BASELINE DESIGN FEATURES
- CAST HOUSINGS
- SUB-CRITICAL SPEED DESIGN
- CAST PUMP IMPELLORS
- SINGLE PIECE FORGED DISK/SHAFT

OPTIONAL FEATURES
- LOW COST MACHINED IMPELLORS
- BACKUP DESIGNS FOR SHAFT AND BEARINGS

DEVELOPMENT STATUS
- FABRICATION PROCESSES IN TRIAL
- SPIN RIG INSTRUMENTATION UNDERWAY
- SUPPLIERS ON CONCURRENT ENGINEERING TEAM

92 PLANS
- CONTINUED FAB DEVELOPMENT
- SPIN TESTING OF IMPELLER

LEAD: STPT-PRATT & WHITNEY/WEST PALMBEACH FL

LOX TURBOPUMP COMPARISON

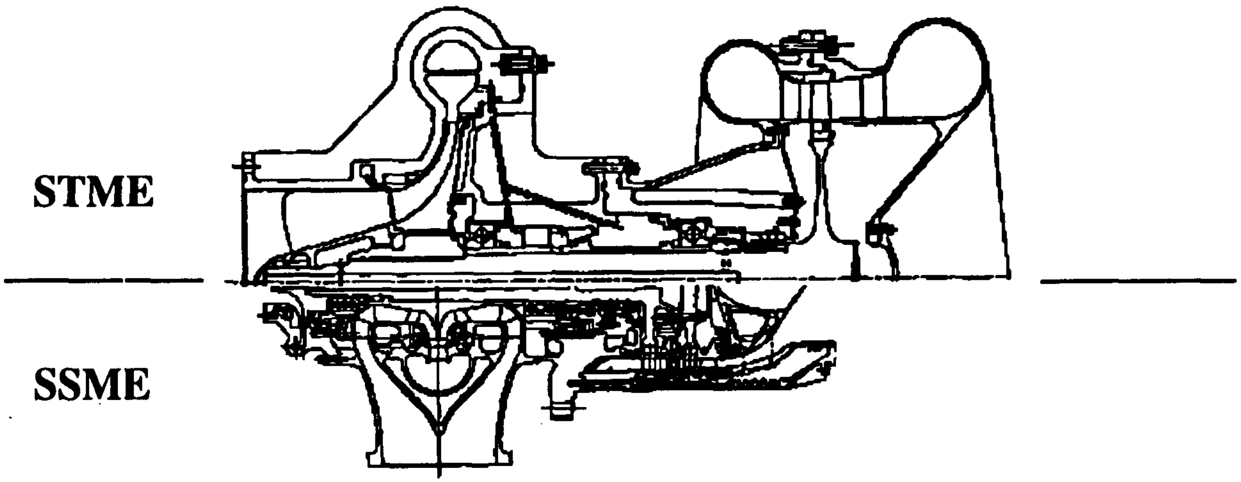

Discriminators	SSME	STME
Number of parts	153	87
Number of weld counts	128	0
Weld overlays	Yes	No
Disk gold plating	Yes	No
Cost (TFU)	5.16M	1.38M
Discharge Pressure	4360/7340 psia	3313 psia
Turbine Inlet Temperature	1510 deg R	1190 deg R
Speed	28200 rpm	7913 rpm
Weight	570 lbs	1712 lbs

MAIN INJECTOR

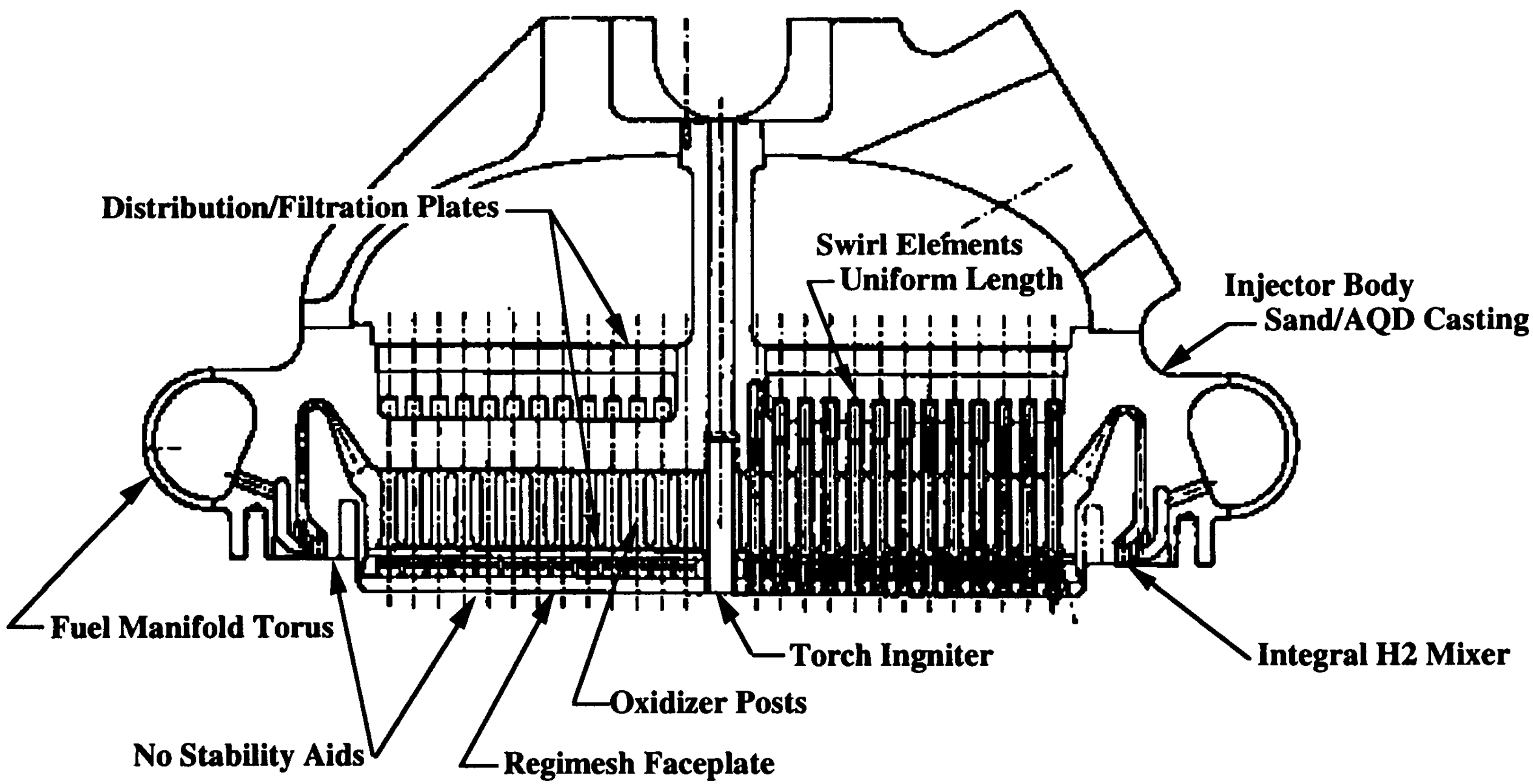

MAIN INJECTOR

BASELINE DESIGN FEATURES
- TWO MAJOR COMPONENTS (DOME AND BODY)
- BRAZED IN ELEMENTS
- 100 % INSPECTIBLE

OPTIONAL FEATURES
- ELEMENTS INTEGRAL TO BODY (SINGLE PIECE)

DEVELOPMENT STATUS
- FABRICATION PROCESSES IN TRIAL DEVELOPMENT
- 40K SUBSCALE AND UNIELEMENT TESTING INITIATED
- SUPPLIERS ON CONCURRENT ENGINEERING TEAM
- FIRST FULL SCALE TEST INJECTOR DELIVERED

92 PLANS
- PATTERN OPTIMIZATION
- 40K TEST FOR PERFORMANCE VERIFICATION
- 1ST FULL SCALE TEST (STABILITY DATA)

LEAD: STPT-AEROJET/SACRAMENTO CA

INJECTOR COMPARISON

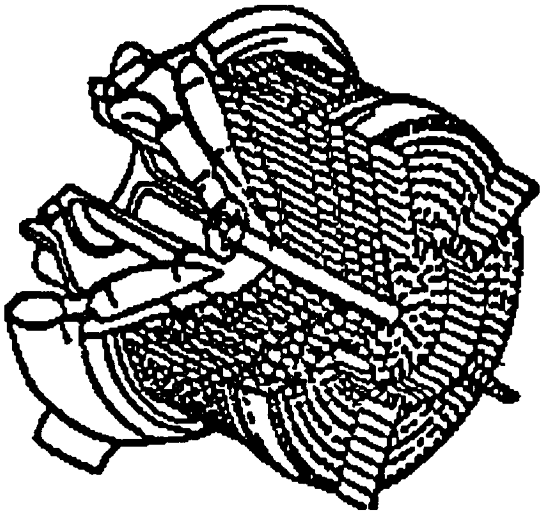

SSME

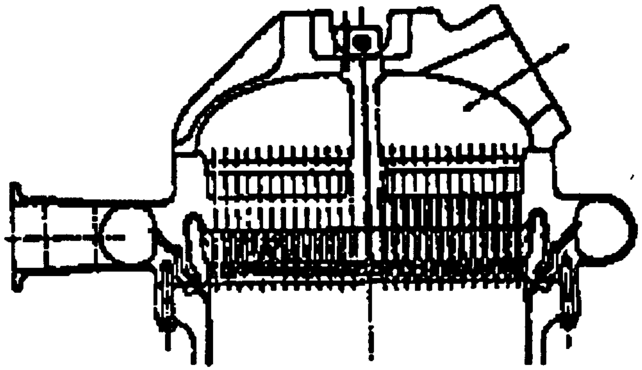

STME

Discriminators	SSME	STME
Number of parts	>3200	2213
Number of processes	170	151
Number of welds	>360	13
Number of inspections	90	58
Cost (TFU)	2.71M	0.88M
Chamber Pressure	3126 psia	2250 psia
Weight	394 lbs	1339 lbs

COMBUSTION CHAMBER

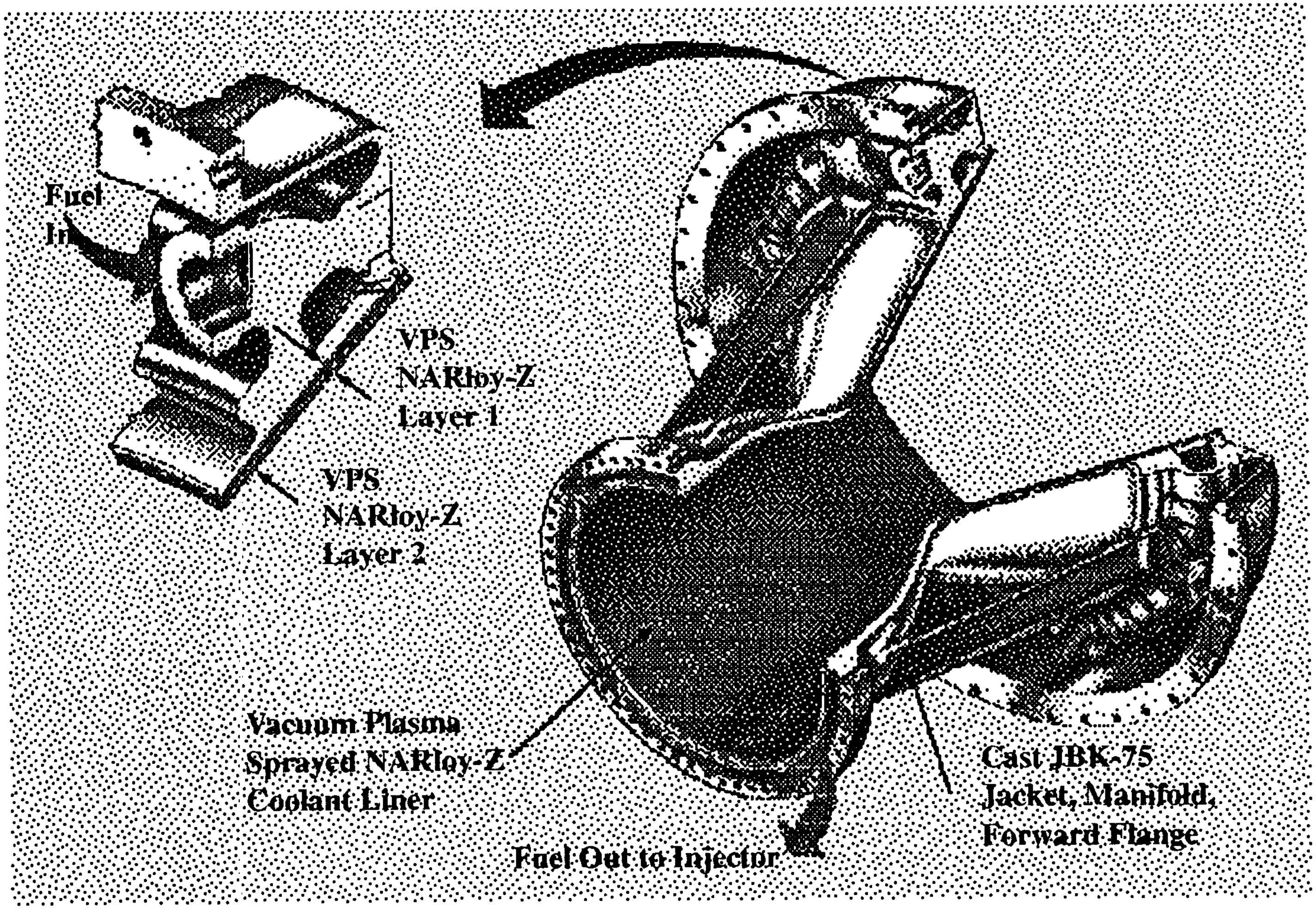

COMBUSTION CHAMBER

BASELINE DESIGN FEATURES
- CAST STRUCTURAL JACKET AND MANIFOLD
- VACUUM PLASMA SPRAY NARLOY Z LINER

OPTIONAL PROCESSES
- LIQUID INTERFACE DIFFUSION BOND ASSY
- PLATELET LINER

DEVELOPMENT STATUS
- FABRICATION PROCESSES IN TRIAL
- 1ST FAB DEVELOPMENT JACKET CAST @ PCC -PORTLAND, OR
- 1ST LIDB CHAMBER FAB COMPLETE
- VPS SPRAY TESTS UNDERWAY

92 PLANS
- LIDB CHAMBER HOT FIRE TEST WITH LSI
- CONTINUE CASTING AND VPS DEVELOPMENT

LEAD: STPT-ROCKETDYNE/CANOGA

COMBUSTION CHAMBER COMPARISON

SSME

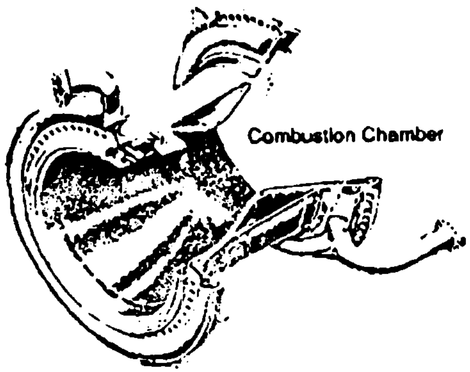

STME

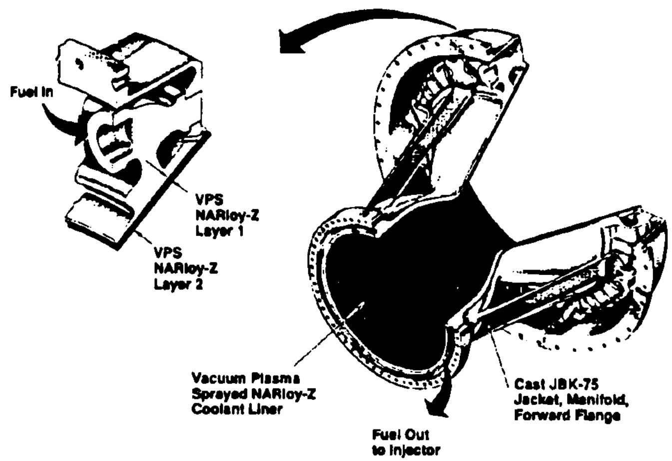

Discriminators	SSME	STME
Number of parts	60	6
Number of welds	96 (incl. overlays)	4
Coating operations	7 (plating)	2 (vps)
Cost	4300K	800K
Chamber Pressure	3126 psia (104%)	2250 psia
Weight	466 lbs	1834 lbs

NOZZLE

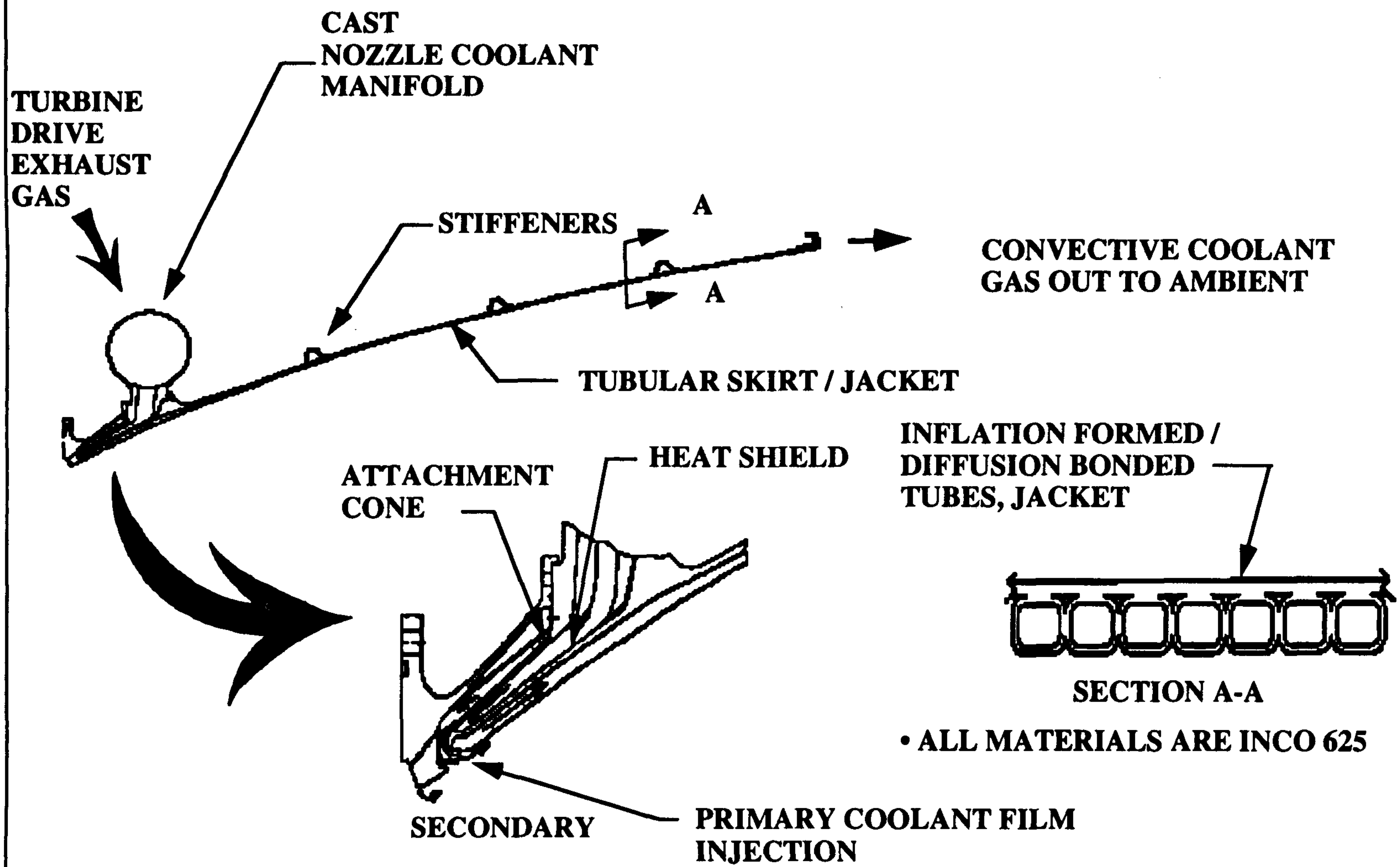

• ALL MATERIALS ARE INCO 625

NOZZLE

DESIGN FEATURES
- ALL COMPONENTS MADE OF SAME ALLOY
- TUBULAR SKIRT/JACKET - NO WELDS
- BOLT TO CHAMBER
- CAST MANIFOLDS

DEVELOPMENT STATUS
- FABRICATION PROCESSES IN TRIAL
- BASELINE TO BE SELECTED EARLY 92
- SUBSCALE NOZZLE IN FABRICATION

92 PLANS
- SUBSCALE NOZZLE HOT FIRE TESTING
- DESIGN UPDATE AND CONTINUED FAB DEVELOPMENT

LEAD: STPT-PRATT & WHITNEY/W. PALM BEACH FL

NOZZLE COMPARISON

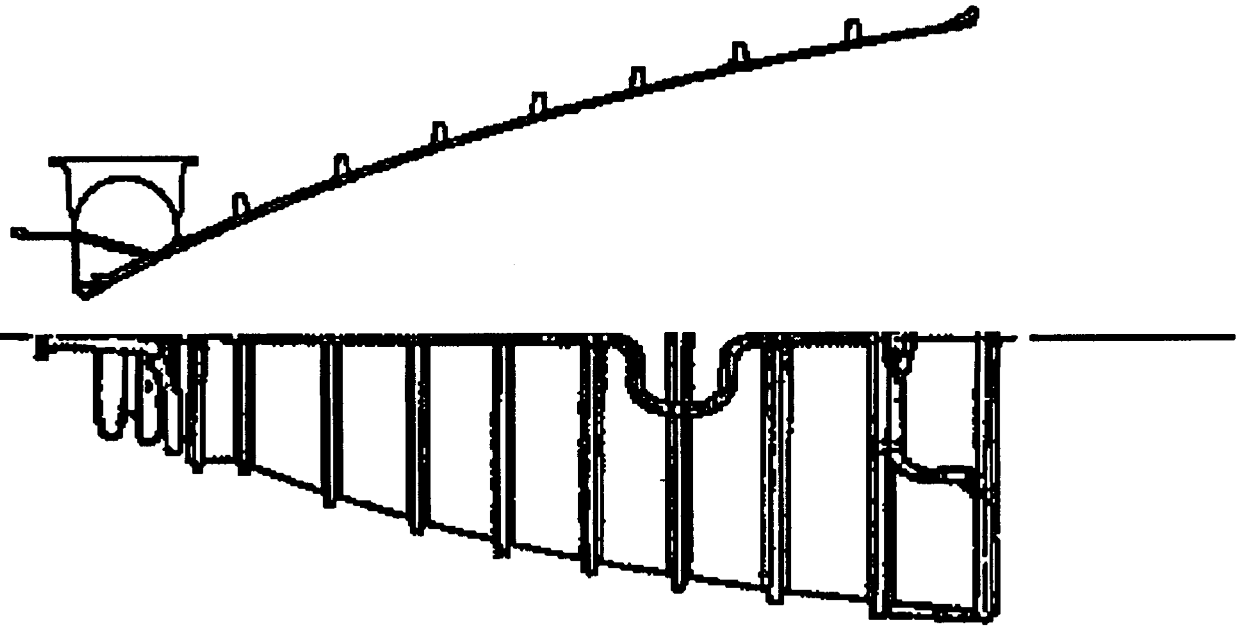

Discriminators	SSME	STME
Number of parts	1600	611
Number of weld counts	113	33
Number of processes	520	207
Number of inspections	633	34
Cost (TFU)	5.6M	1.56M
Weight	1328 lbs	1945 lbs

GAS GENERATOR

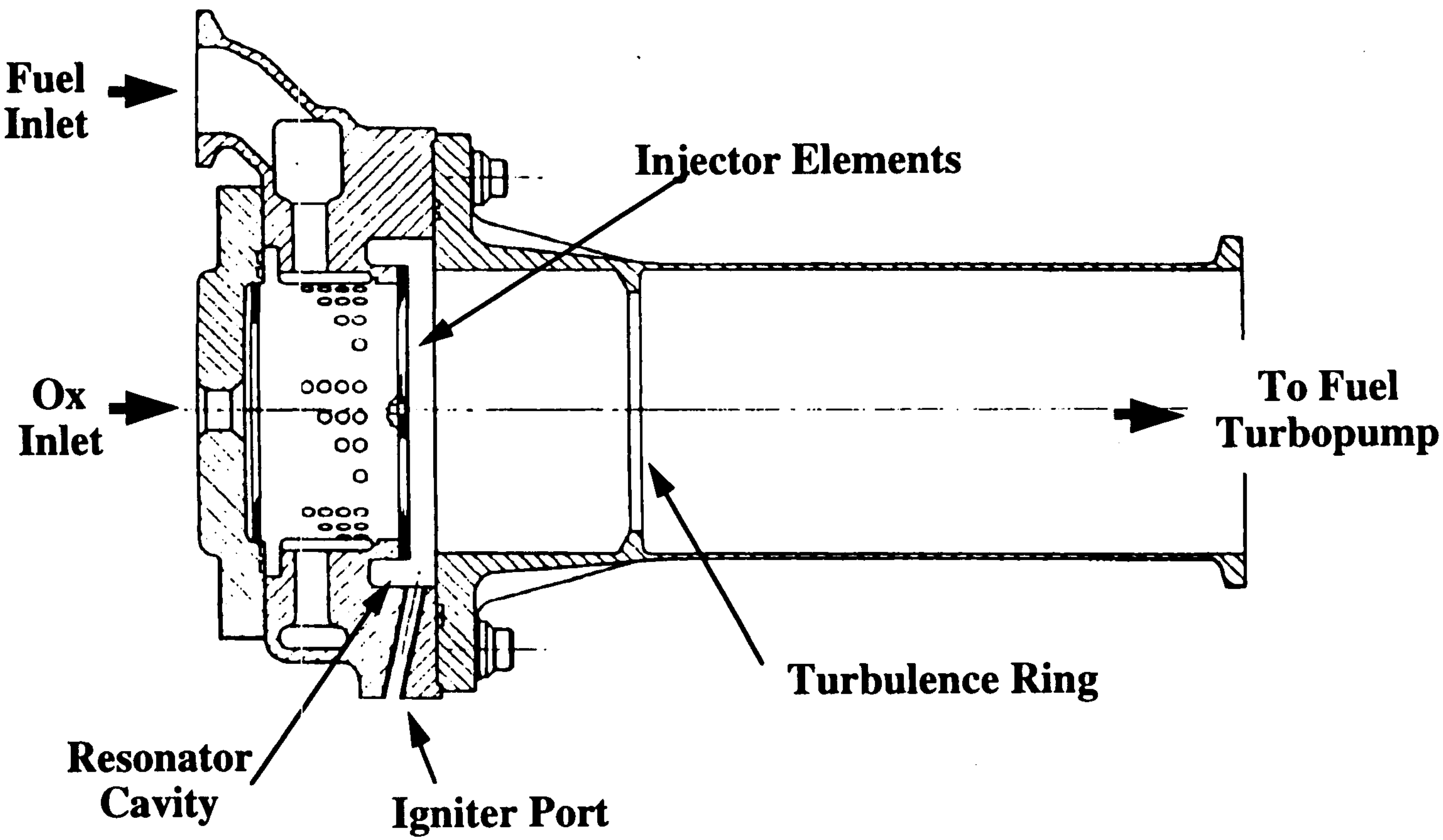

GAS GENERATOR

DESIGN FEATURES
- UNCOOLED CHAMBER
- OPERATING PRESSURE SAME AS MAIN CHAMBER

DEVELOPMENT STATUS
- WORKHORSE GAS GENERATOR TESTED
- DESIGN OPTIONS IDENTIFIED

92 PLANS
- IGNITER DESIGN • CONCEPTUAL GAS GENERATOR DESIGN

LEAD: STPT-AEROJET/SACRAMENTO CA

GAS GENERATOR/PREBURNER COMPARISON

STME

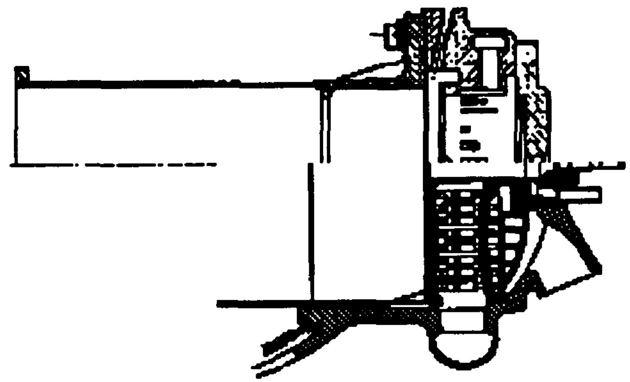

SSME

Discriminators	SSME*	STME
Number of parts	591	70
Number of weld counts	20	5
Weld overlays	2	0
Sheet Metal Liners	2	0
Cost (TFU)	1.17	243 K
Discharge Pressure	5460 PSIA	2205 PSIA
Turbine Inlet Temperature	1900 R	1600 R
Weight	143 LBS	111 LBS

* Fuel Preburner Only

SPACE TRANSPORTATION PROPULSION TEAM (STPT)

Senior Executive Council

- "Board of Directors"
- Delegates Authority to team
- Establishment of Policy
- Provision of Overall Guidance
- Final Resolution for Team Conflicts
- One Senior Executive from each Company

Team Program Office (TPO)

- **Project Director is Final Authority**
- **Overall Program Management Responsibility**
- **Principal Director from each Company**

Aerojet Propulsion Division
ALS/STME Program

- **Thrust Chamber Assembly (L)**
- **Control System (L)**
- **Injector (L)**
- **Gas Generator**
- **Igniter**
- **Engine Systems D&D**
- **Fuel Turbopump (Turbine)**
- **System Components**

Pratt & Whitney Space Propulsion & Systems
ALS/STME Program

- **Engine Systems D&D (L)**
- **Oxidizer Turbopump (L)**
- **Nozzle (L)**
- **Engine Systems Assy & Test**
- **Control Systems**
- **System Components**

Rocketdyne Division
ALS/STME Program

- **Fuel Turbopump Assy (L)**
- **Main Combustion Chamber (L)**
- **Engine System D&D**
- **Engine Systems Test**
- **Control Systems**
- **System Components**

SPACE TRANSPORTATION MAIN ENGINE PARTICIPANTS

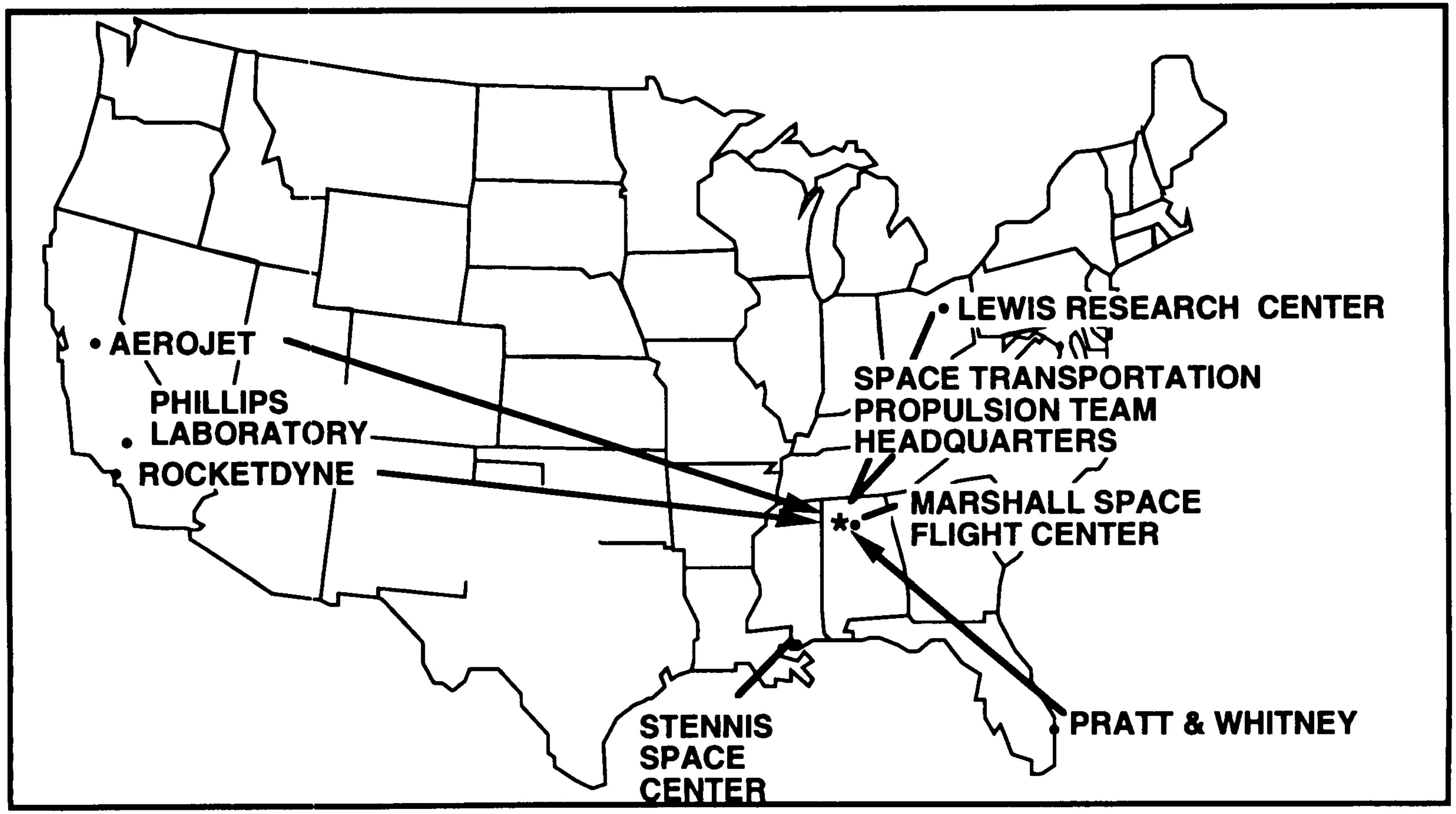

PROGRAM STATUS

THRUST LEVEL INCREASED TO 650K
- REQUIRED TO SUPPORT 20K VEHICLE
- DESIGNS BEING REVISED TO REFLECT INCREASE

FULL SCALE DEVELOPMENT
- REQUEST FOR PROPOSALS IN PREPARATION
- SCHEDULE FOR RELEASE - JUNE 1992
- FIRST ENGINE SYSTEM TEST - MAY 1996

SUMMARY

- **STME IS PROCESS FOCUSED**
- **PRODUCT OF INTEGRATED SYSTEMS PROCESS**
- **INNOVATIVE APPROACH TO PROJECT**
- **DEFINITION MATURE**
- **BENEFITS**
  - Robust Propulsion
  - Legacy of New Process

N92-32282

THE IMPACT OF TIME STEP DEFINITION ON CODE CONVERGENCE AND ROBUSTNESS

S.Venkateswaran, J. M. Weiss and C. L. Merkle
Propulsion Engineering Research Center
The Department of Mechanical Engineering
The Pennsylvania State University
University Park, PA 16802

A large fraction of the Navier-Stokes codes in use today are based on the so-called 'time-marching' procedures, wherein the unsteady form of the governing equations are solved in time. For compressible flows, these methods perform very well in the transonic and supersonic flow regimes and have been applied to solving a wide variety of problems. There are, however, several disadvantages associated with these methods. It is well known that at low Mach numbers, the convergence of these schemes deteriorate dramatically. The reason for the behaviour is the wide disparity in the eigenvalues of the system at low speeds. Furthermore, highly viscous regions of the flow and the presence of strong source terms also introduce convergence difficulties. These again are due to the very disparate time scales involved in these processes.

Preconditioning offers a means of controlling the time-step size for a wide variety of flow situations. Originally, preconditioning methods were developed as a means of circumventing the disparity in the eigenvalues at low Mach numbers. Essentially, this involves altering the time derivative of the equations of motion such that the acoustic speed is scaled down to the level of the fluid velocity. This 'inviscid' preconditioning enables Mach number-independent convergence to be obtained. We have also extended the preconditioning approach to handling very viscous flows. Here, the acoustic speed is altered such that the local CFL number is approximately the same order as the viscous time step. This enables excellent convergence rates to be maintained over a wide range of Reynolds numbers. We are currently investigating extending this approach to various source terms of interest---particularly related to reacting flowfields.

We have implemented preconditioning for multi-species reacting flows in two independent codes---an implicit (ADI) code developed in-house and the RPLUS code (developed at NASA-Lewis Research Center). The RPLUS code has been modified to work on a 4-stage Runge-Kutta scheme. The performance of both the codes have been tested and show that preconditioning can improve convergence by a factor of two to a hundred depending on the problem. Our efforts are currently focussed on evaluating the effect of chemical sources and on assessing how preconditioning may be applied to improve convergence and robustness in the calculation of reacting flows.

The Impact of Time-Step Definition on Code Convergence and Robustness

S. Venkateswaran

Jonathan M. Weiss

Charles L. Merkle

Propulsion Engineering Research Center

The Pennsylvania State University

University Park, PA 16802

85

Problems Associated with Conventional Codes

- Convergence is poor at low Mach Numbers.
  — e.g., the combustion zone in rocket engines.
- Convergence is poor in viscous regions.
  — e.g., boundary layers, recirculation zones, etc.
- Large source terms induce instabilities.
  — e.g., combustion, turbulence, axisymmetry, etc.
- High aspect ratio grids cause poor convergence.
  — in regions where strong local grid stretching is used.

Time-Step Definition in Conventional Codes

- Eigenvalues of Jacobian A define inviscid time-step.
  - Eigenvalues are u+c, u-c, u, u, u, etc.

$$CFL_\lambda = \frac{\lambda \Delta t}{\Delta x}$$

- In viscous regions, a viscous time-step is defined.

$$VNN = \frac{\nu \Delta t}{\Delta s^2}$$

- Time step is fixed based on CFL and VNN conditions.

- Variable time stepping is normally used.

Problems with Conventional Definition

- At low Mach numbers, $CFL_{u+c} \gg CFL_u$.
  - Acoustic wave speeds dominate over particle convection speed.
- In viscous regions, $VNN \gg CFL$.
  - Diffusion time scales are much larger than wave speeds for acoustic and particle convection.
- For high aspect ratio cells, $CFL_{v+c} \gg CFL_{u+c}$.
  - Wave speeds are much higher in the direction normal to the flow direction.
- Source terms introduce additional time scales.

C-2

Preconditioning the Equations of Motion

- Alter the time derivative by multiplying with a preconditioning matrix Γ.

$$\Gamma \frac{\partial Q_v}{\partial t} + \frac{\partial E}{\partial x} + \frac{\partial F}{\partial y} = H + \frac{\partial E_v}{\partial x} + \frac{\partial F_v}{\partial y}$$

— $Q_v = (P, \ u, \ v, \ T, \ Y_1, \ Y_2, \ . \ . \ . \ )$

- Steady state solution remains unaltered.

- Eigenvalues of $\Gamma^{-1} A$ now define CFL number.

Choosing the Preconditioning Matrix

- Define Γ so that the acoustic speeds are altered.
- At low Mach numbers, keep acoustic speeds of the same order as fluid velocities.
- In viscous regions, alter acoustic speed so that the inviscid time-step is of the same order as the viscous time-step.
- Scale acoustic speed in a similar manner to account for large source terms.
- Extend philosophy to high aspect ratio grid cells.

Example of Preconditioning

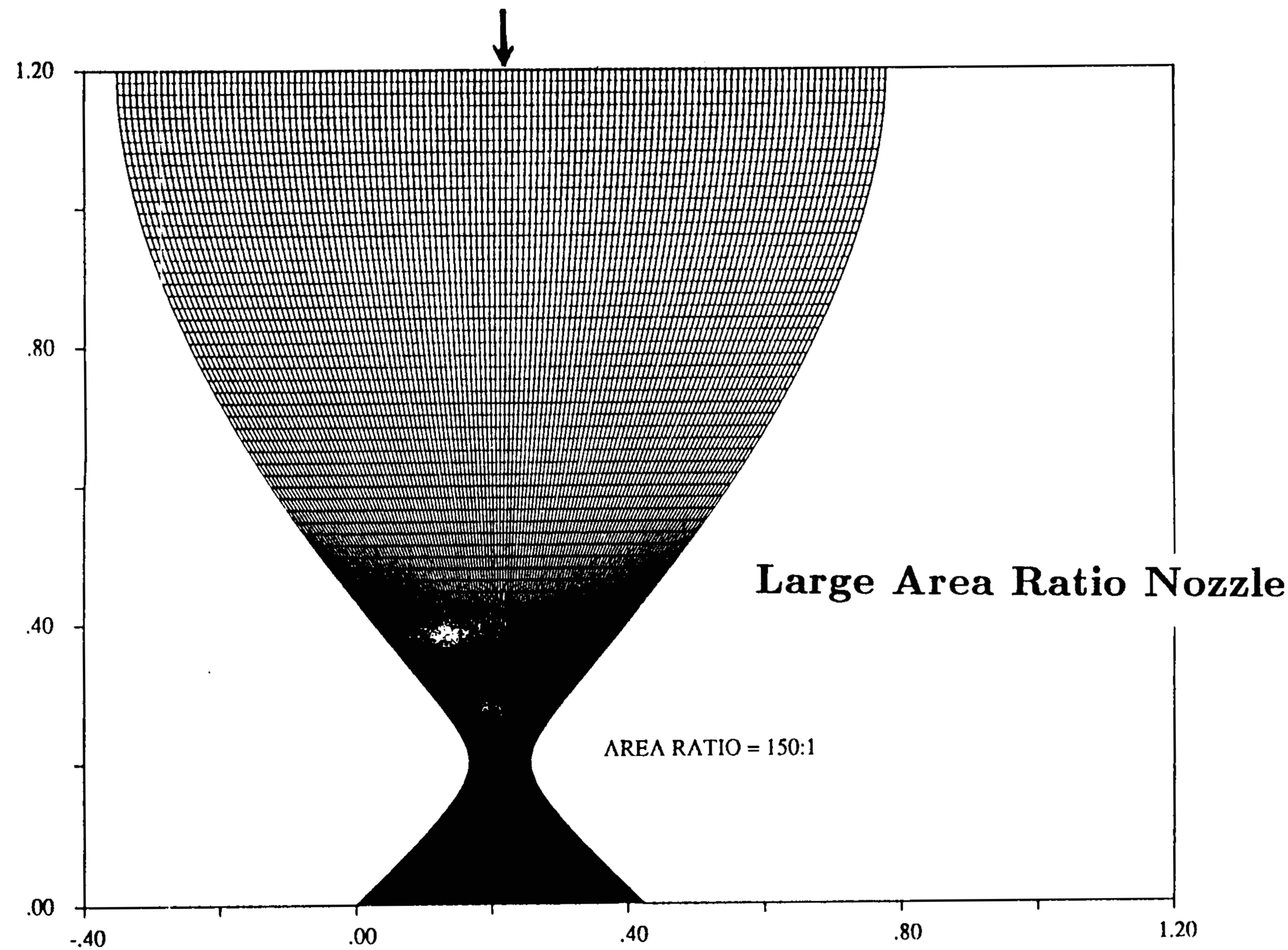

Comparison of Convegence

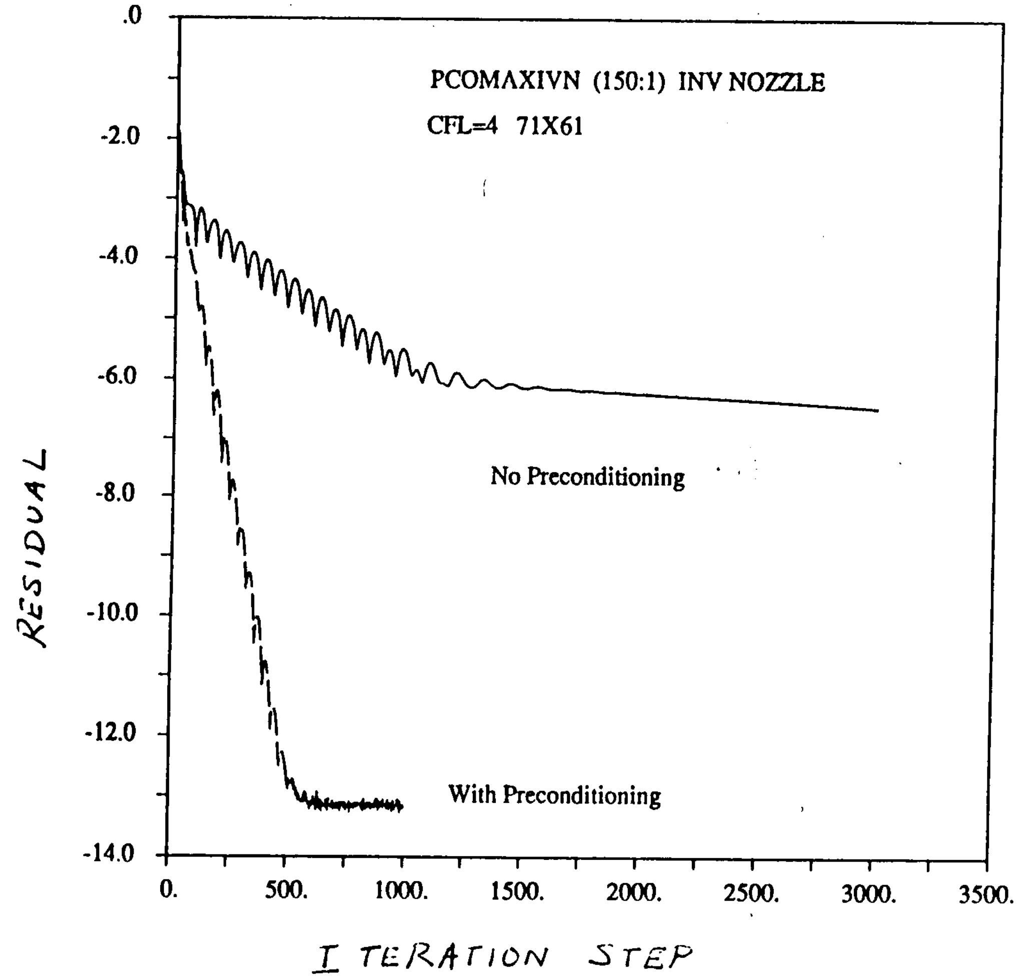

Comparison of Solutions

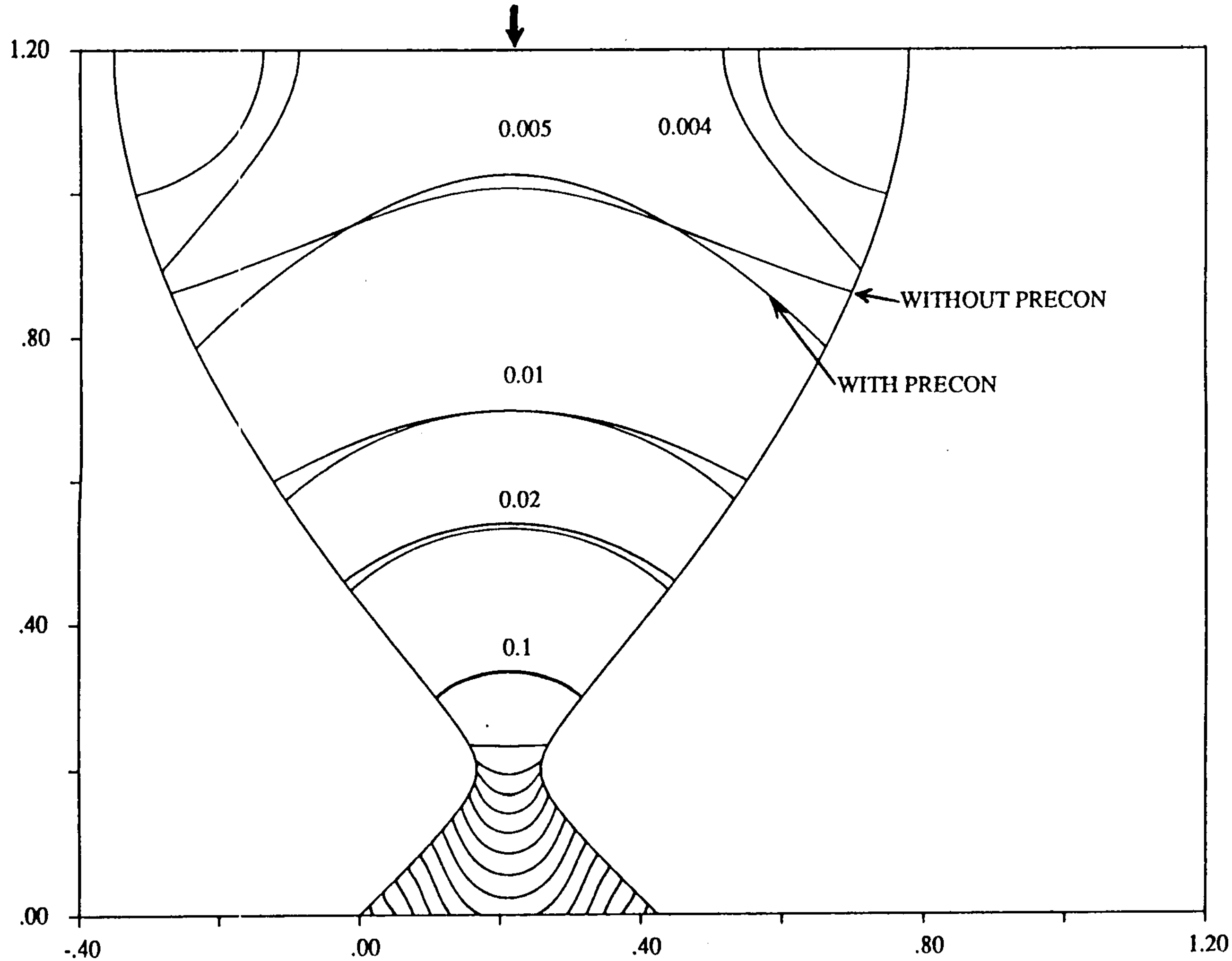

Implementation of Preconditioning

- Incorporate preconditioning in implicit, reacting flow code.
  - Euler Implicit/ADI Algorithm
  - Two D/Axisymmetric Code
  - Multi-Component Species Transport
  - Multi-Step Finite Rate Chemistry
- Incorporate preconditioning into RPLUS code.
  - Developed at NASA-Lewis Research Center.
  - Multi-Stage Explicit Runge-Kutta (RPLUS/RK)

Preconditioning in the RPLUS Code

- Modified Runge-Kutta Stage:

$$\Delta Q_v = -\alpha_k \Delta t \; \Gamma^{-1} \; \left(\frac{\partial E}{\partial x} + \frac{\partial F}{\partial y} - H - \frac{\partial E_v}{\partial x} - \frac{\partial F_v}{\partial y}\right)$$

- Time-Step definition altered using the new eigenvalues of the system.

Convergence of RPLUS/RK

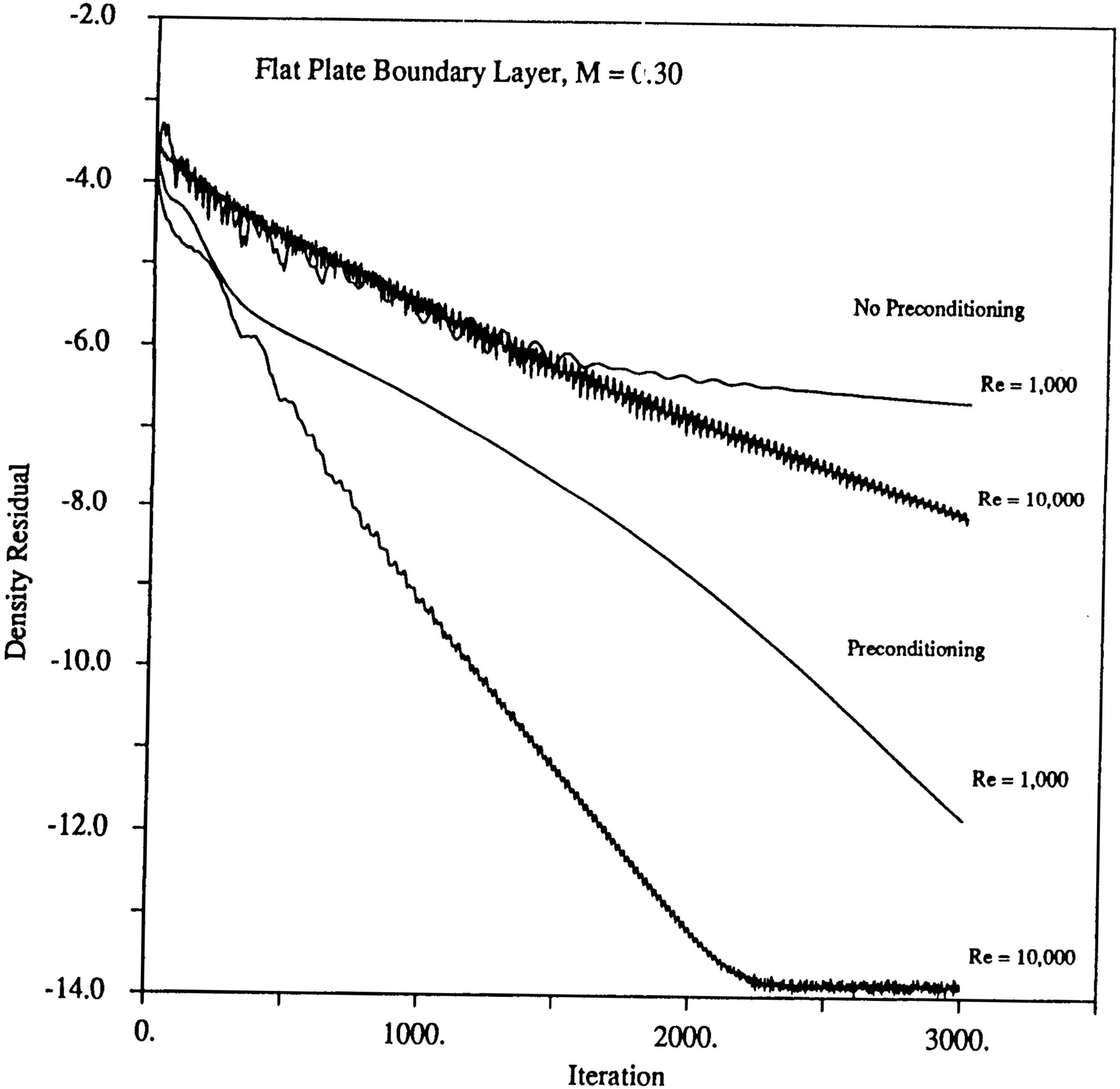

26 Apr 92 20:27:28

Convergence of RPLUS/RK

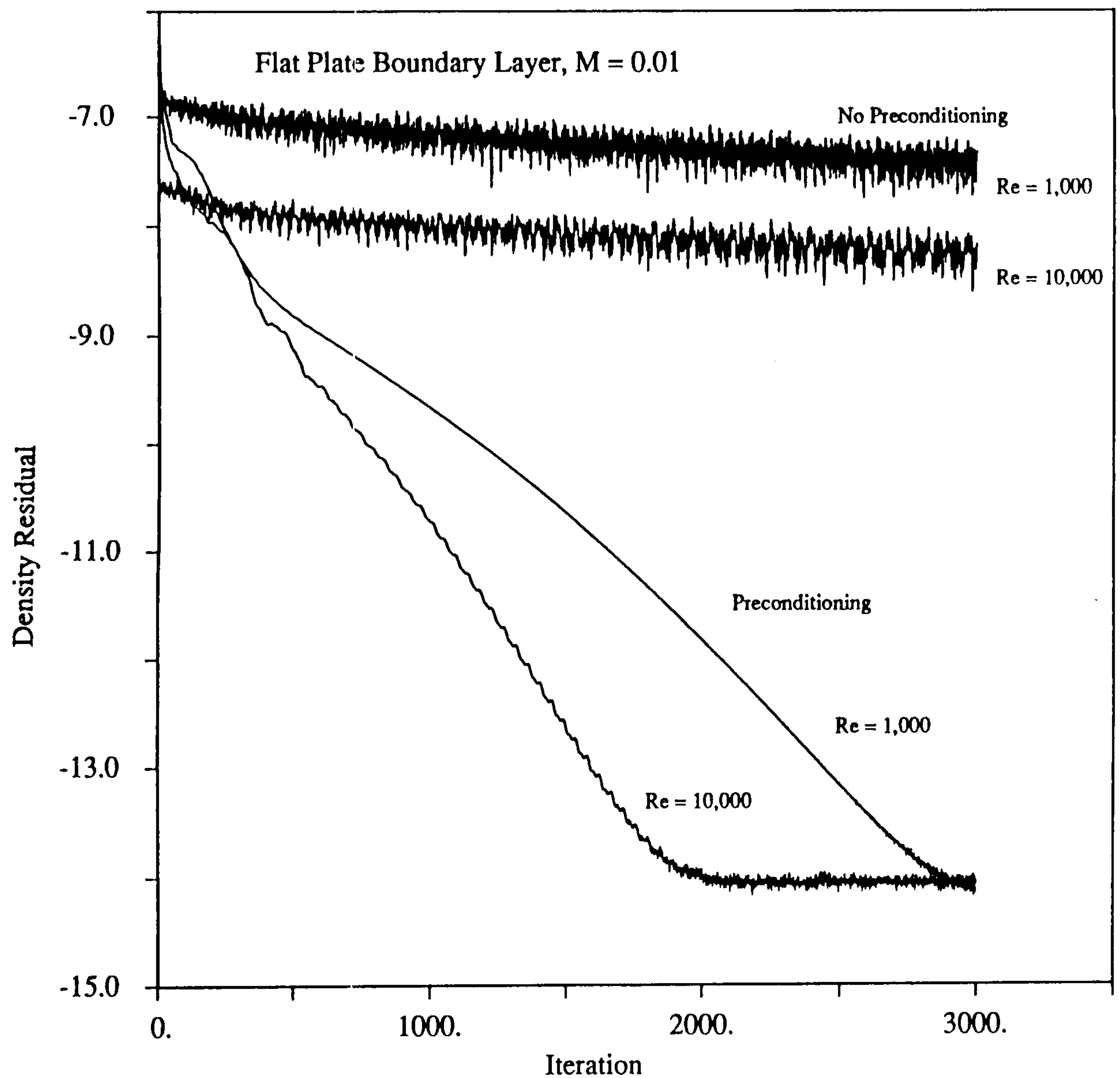

26 Apr 92 20:19:34

Computation of Reacting Shear Layer

Grid Geometry

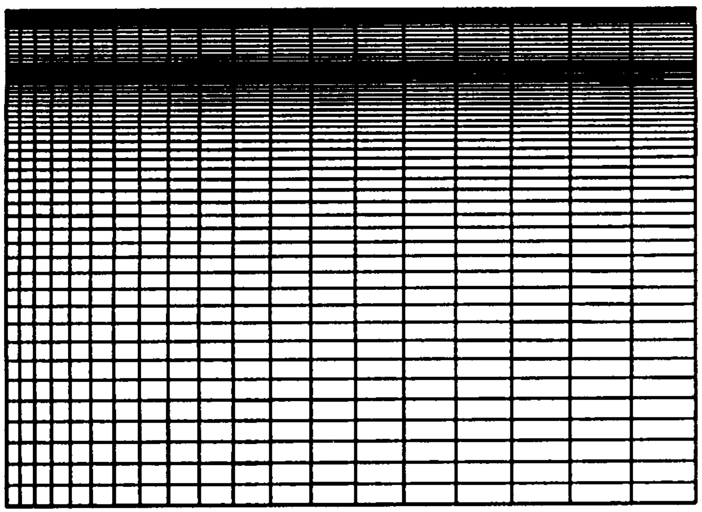

H_2O Mass Fraction

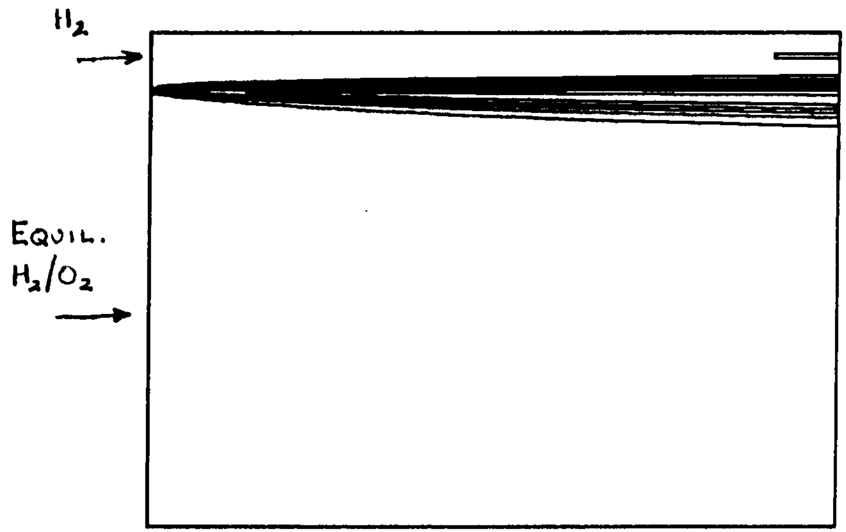

Convergence of RPLUS/RK

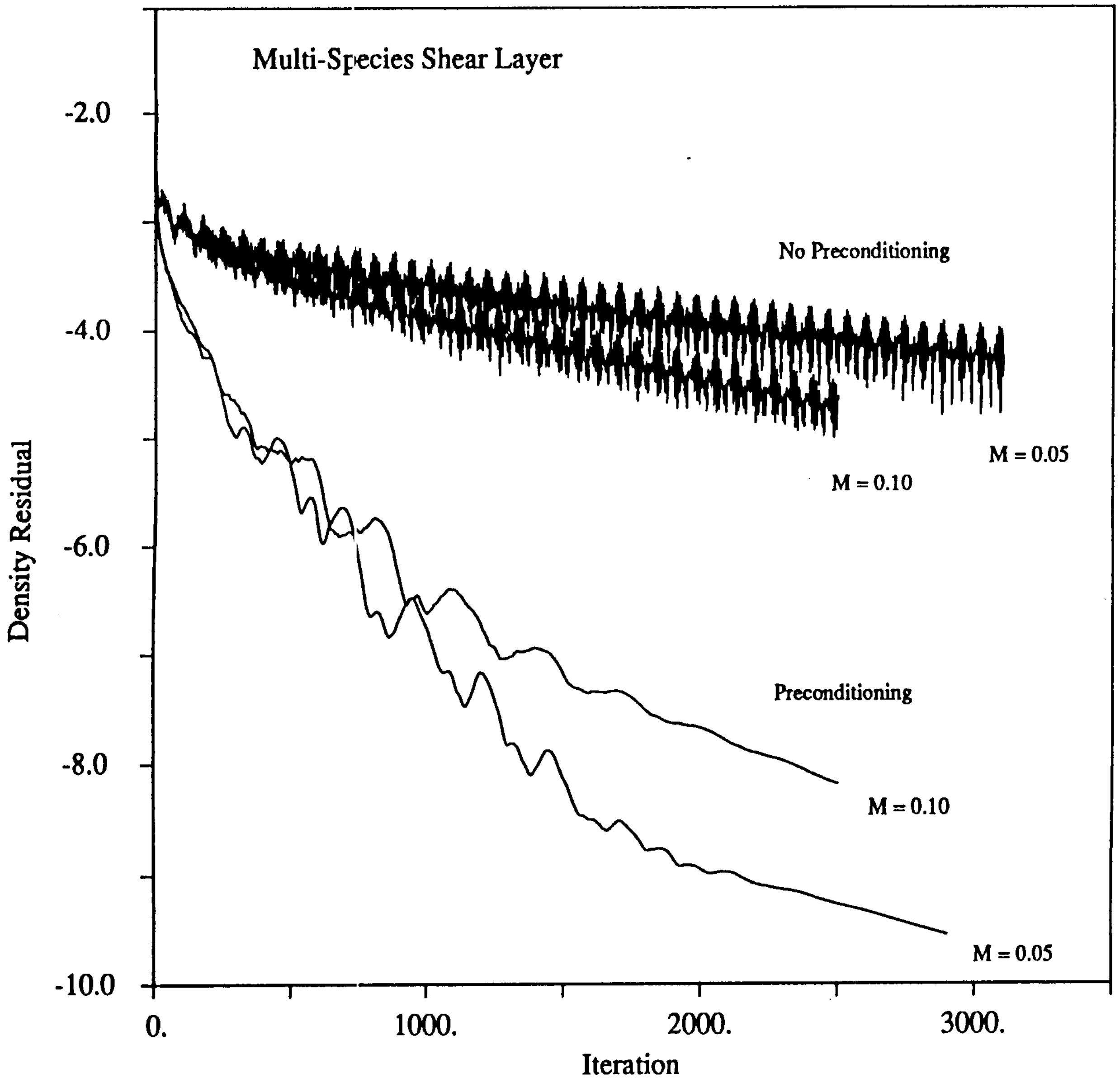

26 Apr 92 20:38:56

Convergence of RPLUS/RK

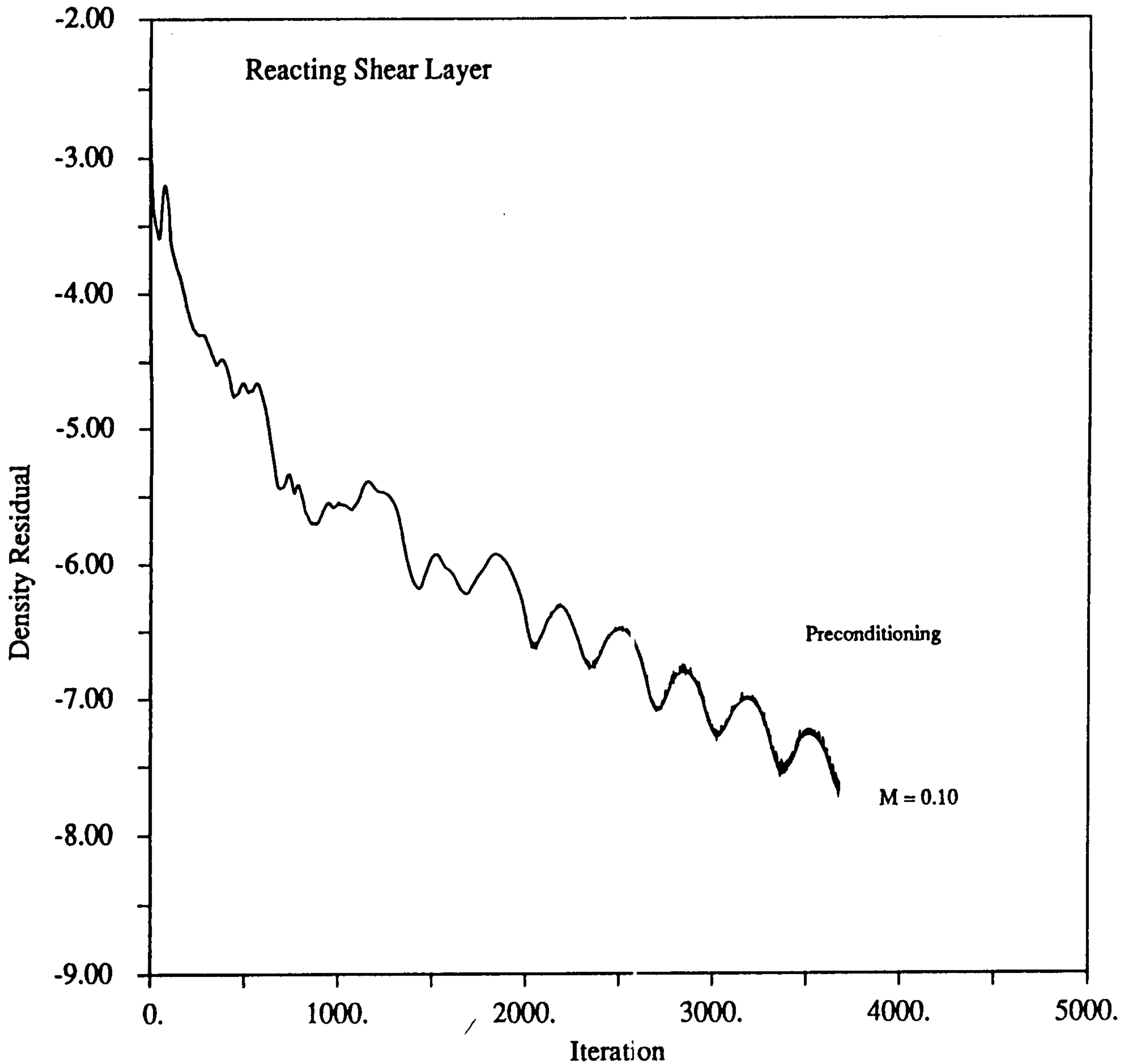

26 Apr 92 20:50:14

Convergence of Implicit-ADI

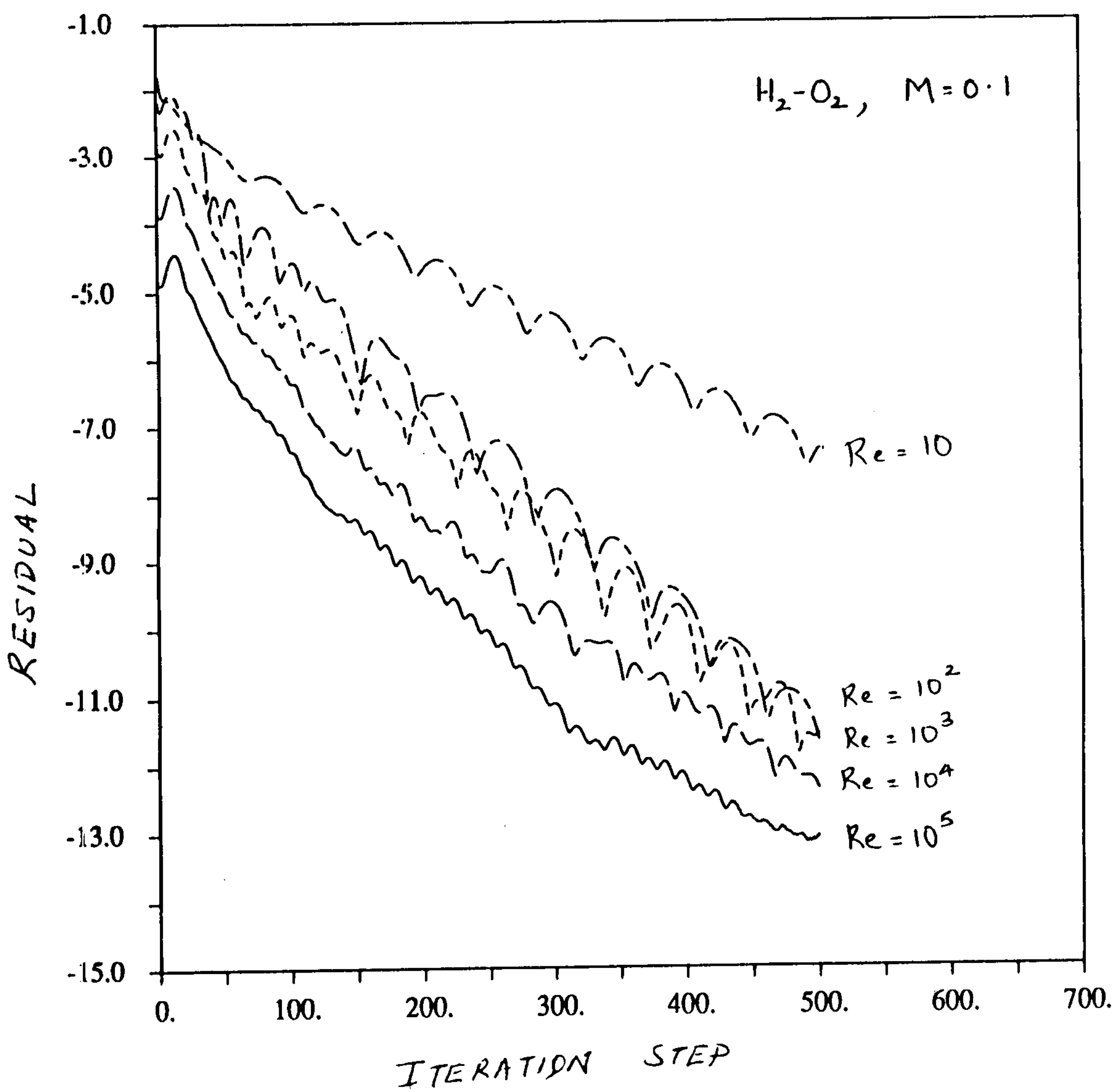

Convergence of Implicit ADI

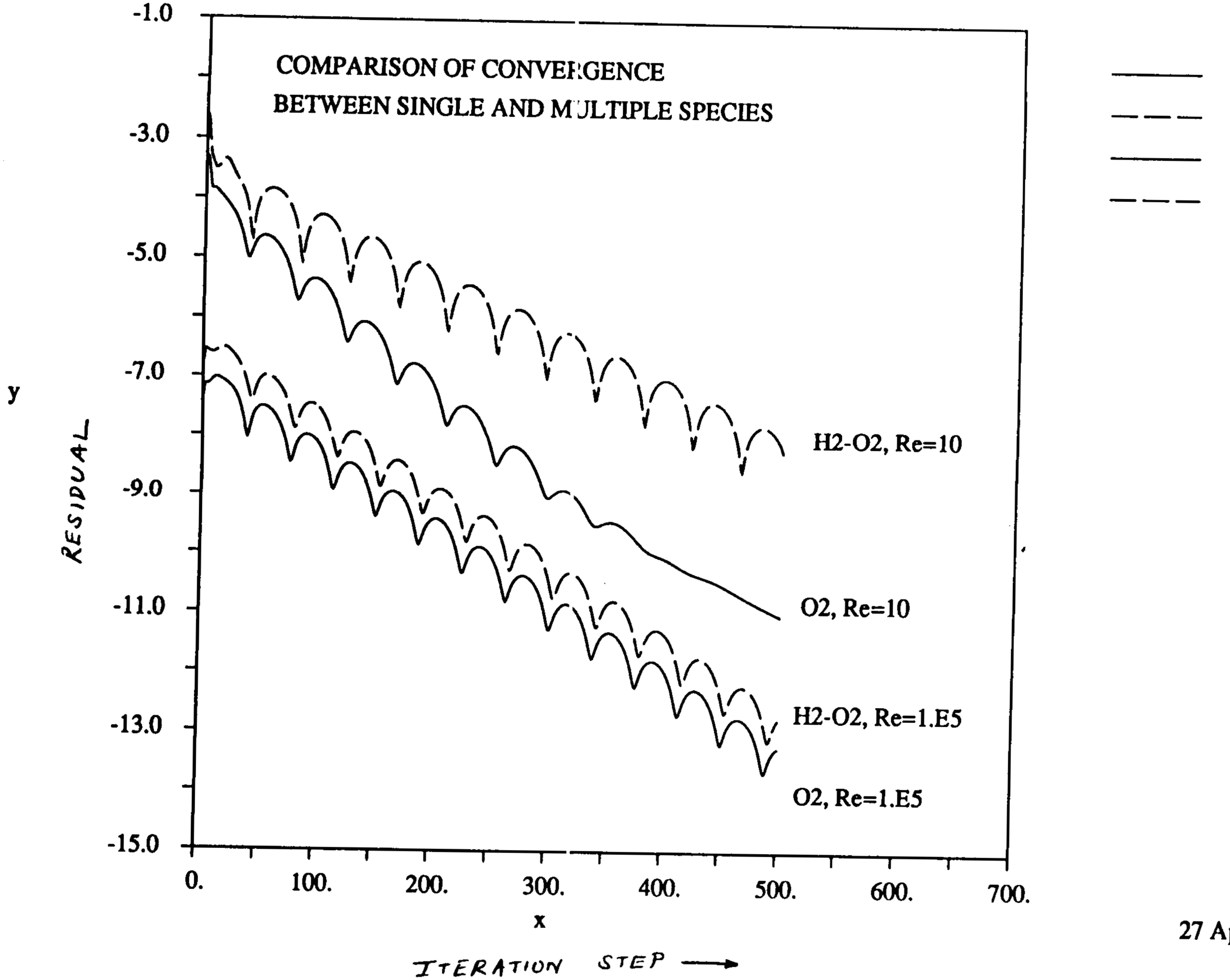

27 Apr 92 10:25:26

Definition of Time-Step

$$\Delta t = \frac{CFL\Delta x}{\lambda}$$

- Based on the maximum eigenvalue:

$$\lambda = \ Max\ (\ u + c,\ \ v + c\ )$$

- Based on an average eigenvalue:

$$\lambda = \sqrt{(u + c)^2 + (v + c)^2}$$

$$\lambda = 1/2(\ u + c\ \ +\ \ v + c\ )$$

- Based on the eigenvalue in the direction of flow:

$$\lambda = u + c$$

2D Convergence

Maximum Eigenvalue

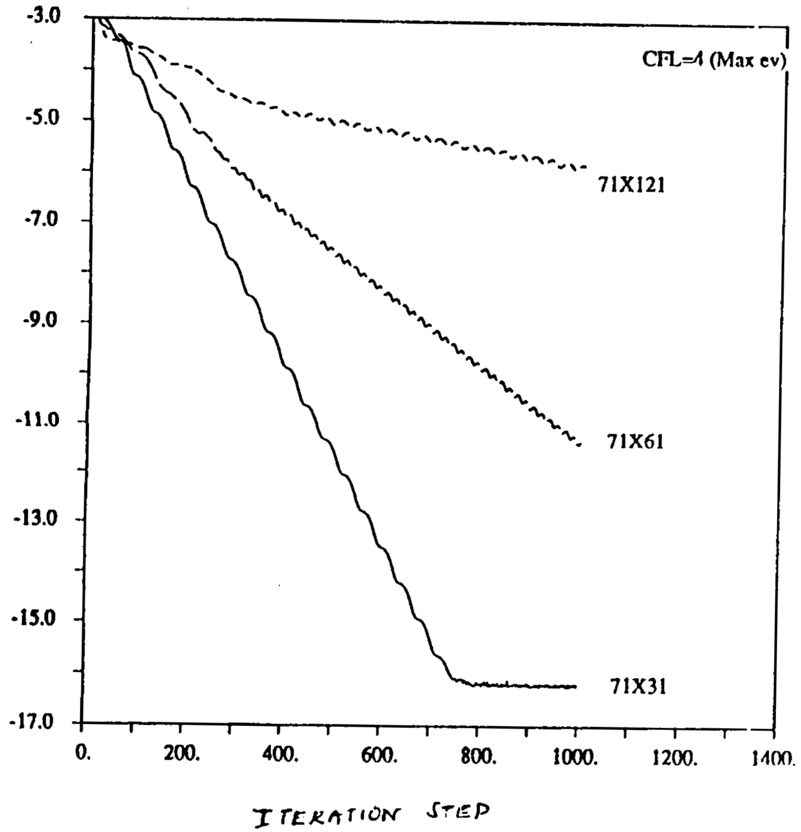

X-Eigenvalue

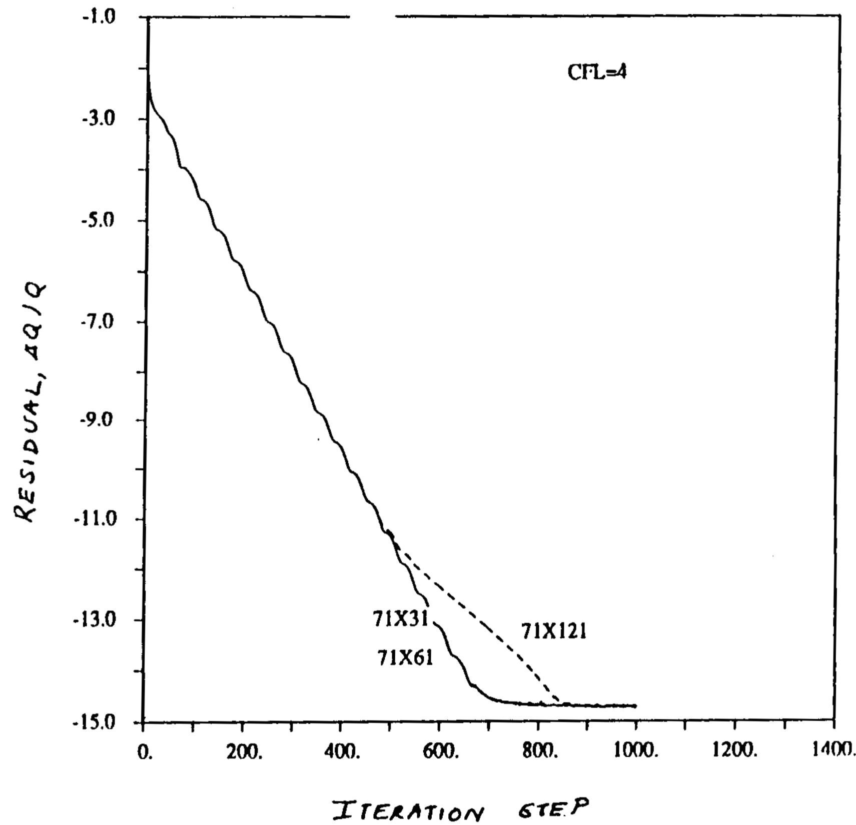

Axisymmetric Convergence

Maximum Eigenvalue

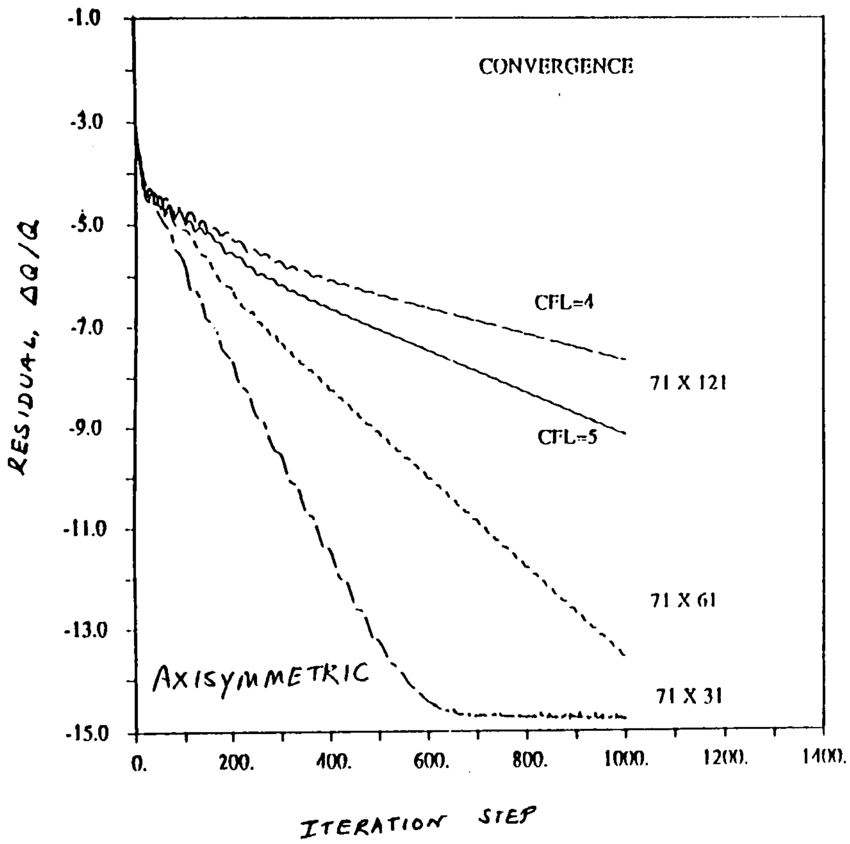

X-Eigenvalue

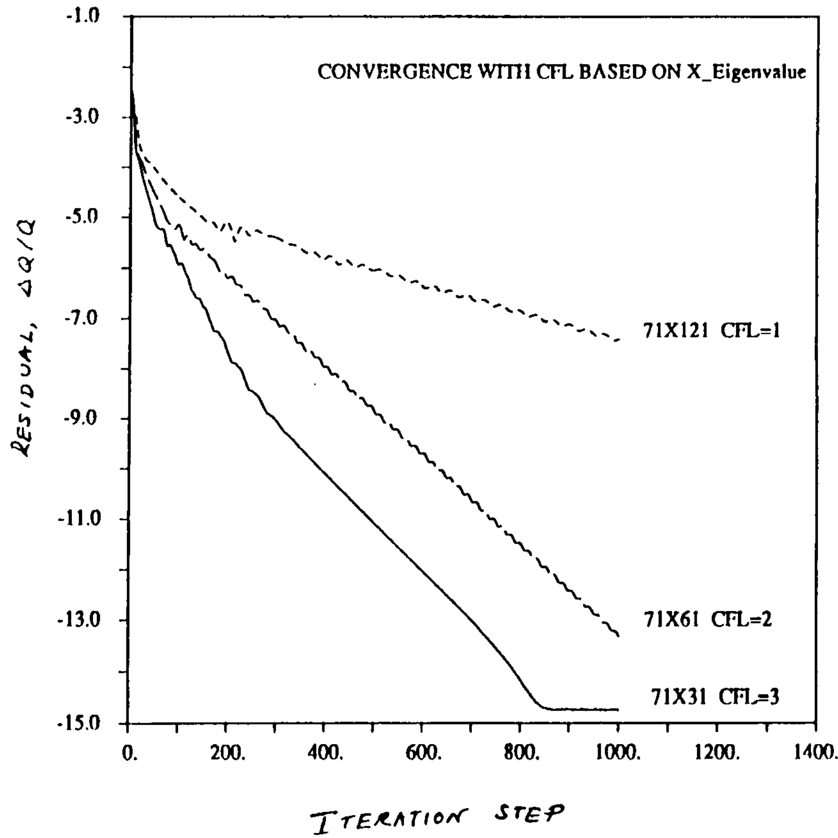

Convergence Based on X-Eigenvalue

Axisymmetric

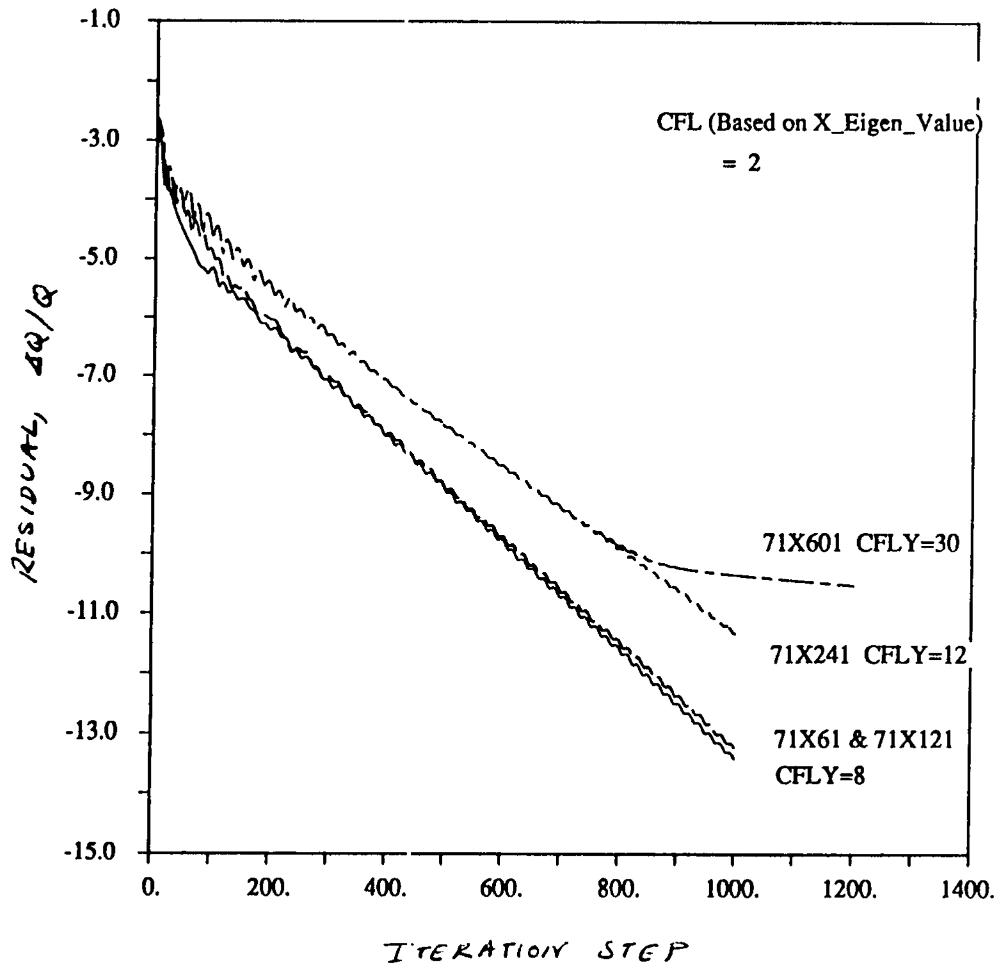

Time Step Definition

- Important to use proper eigenvalue in CFL.
  - u+c
  - Max(u+c,v+c)
  - $\sqrt{(u+c)^2+(v+c)^2}$
- Preliminary results for H-grids show:
  - best choice is u+c
  - control convergence with grid refinement
  - control convergence in near wall region
- Additional work needed to generalize

Conclusions

- The definition of time-step has a profound impact on the performance of time-marching codes.

- Preconditioning is a powerful method of controlling the time-step.
  - Low Mach number preconditioning or characteristic time-stepping has been used widely.
  - Preconditioning has been successfully extended to viscous dominated flows.
  - Similar extensions are currently being investigated for combustion and other sources of interest.

- Time-step should be defined based on the eigenvalue in the direction of flow.
  - Important when the grid aspect ratio is very high.

107

N92-32283

Development of CFD Code Evaluation Criteria and a Procedure for Assessing Predictive Capability and Performance

S.J. Lin, D.C. Chan, M.M. Sindir, and S.L. Barson
Rockwell International, Rocketdyne Division
Canoga Park, California

Careful validation of Computational Fluid Dynamic codes is essential if they are to be used as engineering design tools. Validation must be carried out in a systematic manner to ensure that all code aspects as they apply to the application of interest are understood and, to the greatest extent possible, quantified.

A study is being conducted in which a general code validation procedure is defined and demonstrated. A four phase validation procedure is defined in which a series of validation test cases are computed and compared with available analytical solutions and test data. The procedure is demonstrated using the REACT CFD code to compute validation cases for each of the four phases. For phase 4, the application of interest, the SSME high pressure fuel turbopump impeller flowfield is computed.

PRECEDING PAGE BLANK NOT FILMED

DEVELOPMENT OF CFD CODE EVALUATION CRITERIA AND PROCEDURE FOR ASSESSING PREDICTIVE CAPABILITY AND PERFORMANCE

S.J. Lin, D.C. Chan, M.M. Sindir, and S.L. Barson
Rockwell International, Rocketdyne Division

110

Workshop for Computational Fluid Dynamic Applications in Rocket Propulsion

April 28-30, 1992
NASA Marshall Space Flight Center

Rockwell International
Rocketdyne Division

CFD 92-030-001/D2/SLB

DEVELOPMENT OF CODE EVALUATION CRITERIA AND A PROCEDURE

- **TASK OBJECTIVES**
  - PROVIDE CODE EVALUATION CRITERIA, CLASSIFICATION SCHEME, NUMERICAL ERROR ASSESSMENT TECHNIQUES, AND A PROCEDURE FOR COMPREHENSIVE CODE EVALUATION AND CERTIFICATION
  - ENSURE INTEGRITY, ACCURACY, AND APPLICABILITY OF CFD CODES
  - PROVIDE PROCEDURES AND GUIDELINES FOR CFD SOFTWARE QUALITY CONTROL
  - DEMONSTRATE CODE EVALUATION PROCEDURE USING 2-D AND 3-D BENCHMARK EXPERIMENTS.

- **PRESENTATION FOCUS**
  - CODE VALIDATION PROCEDURE
  - DEMONSTRATION OF PROCEDURE

THOUGHTS ON VALIDATION

- GENERAL VALIDATION PROCEDURE FOR ALL APPLICATIONS IS POSSIBLE
- NO GENERAL AND ABSOLUTE VALIDATION POSSIBLE FOR ALL CASES
- QUANTITATIVE VALIDATION ONLY MEANINGFUL WITHIN A LIMITED CLASS OF APPLICATIONS
- LEVEL OF VALIDATION DEPENDS ON FINAL APPLICATION
- VALIDATION PROCESS MUST BE REALISTICALLY ACHIEVABLE

FOUR PHASE CODE VALIDATION PROCEDURE DEFINED

PHASE 1 UNIT PROBLEM	PHASE 2 BENCHMARK CASES	PHASE 3 SIMPLIFIED PARTIAL FLOWPATH	PHASE 4 ACTUAL HARDWARE
• SINGLE FLOW FEATURE • ANALYTIC SOLUTION OR HIGH FIDELITY COMPUTATIONAL SOLUTION (DNS) AVAILABLE	• MORE THAN ONE FLOW FEATURE • SIMPLE FLOW PHYSICS • BENCHMARK EXPERIMENT DATA	• MULTIPLE RELEVANT FLOW FEATURES • ACTUAL FLOW PHYSICS • HIGH QUALITY TEST DATA	• COMPLETE FLOW PHYSICS • HARDWARE TEST DATA

INCREASING GEOMETRIC AND FLOW COMPLEXITY →

• RUN UNIT PROBLEMS • VERIFY INTEGRITY • ASSESS ACCURACY, CONVERGENCE, AND FUNCTIONALITY	• RUN BENCHMARK CASES • ASSESS PHYSICAL MODELS • ESTABLISH GRID DISTRIBUTION REQUIREMENTS	• RUN SIMPLIFIED PARTIAL FLOWPATH • ASSESS AGREEMENT WITH DATA • ESTABLISH GRID DISTRIBUTION REQUIREMENTS	• RUN ACTUAL CONFIGURATION • COMPARE WITH TEST DATA

DECREASING DATA AVAILABILITY AND ACCURACY →

Rockwell International
Rocketdyne Division

CFD 92-030-004/D2/SLB

DECREASING NUMBER OF CASES REQUIRED FOR LATTER VALIDATION PHASES

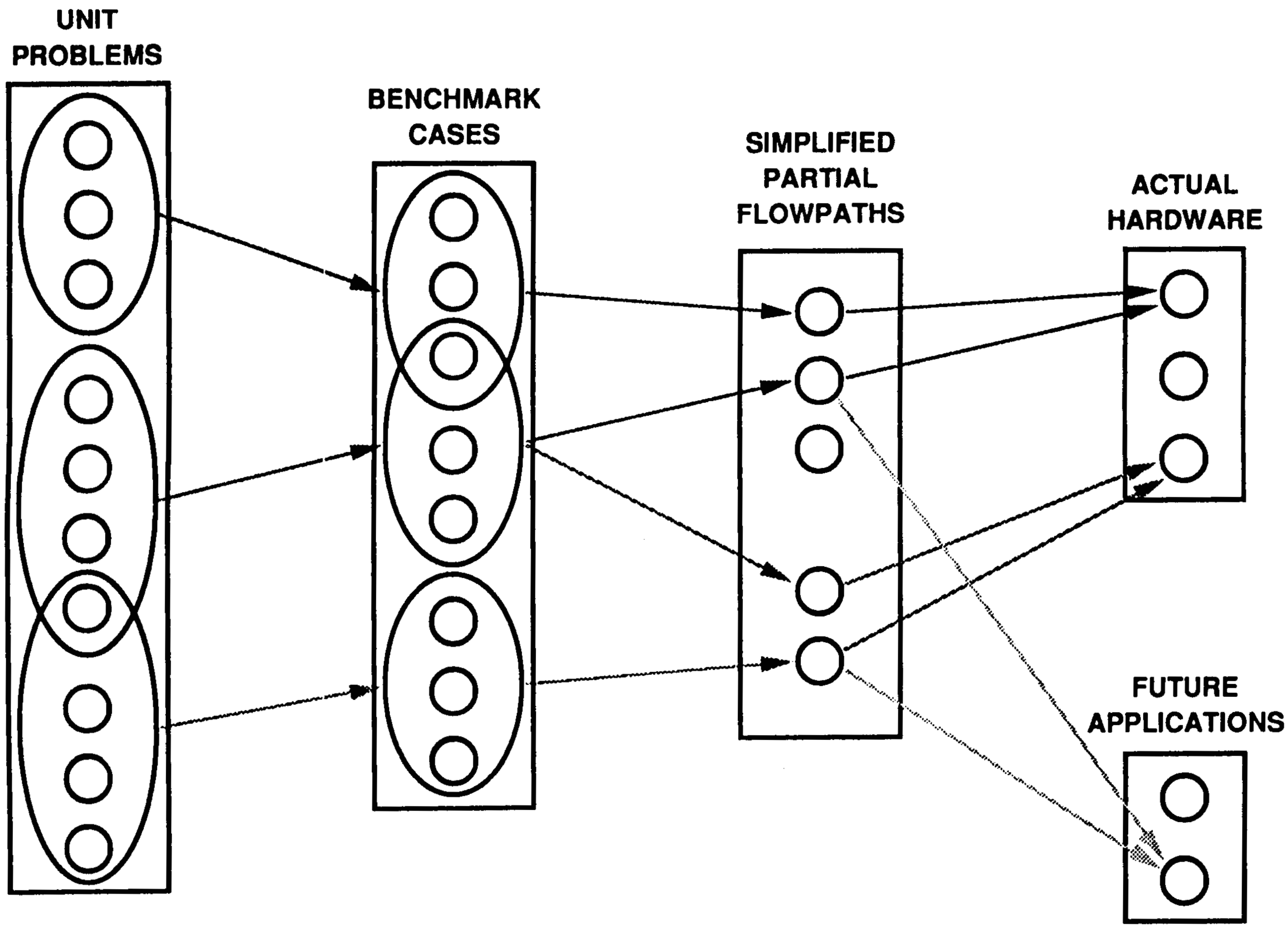

Rockwell International
Rocketdyne Division

CFD 92-030-005/D2/SLB

PROBLEM OF INTEREST SUCCESSIVELY DECOMPOSED INTO LESS COMPLEX CASES

EXAMPLE: SSME HPFTP IMPELLER

PHASE 1
UNIT PROBLEMS

- flat plate
- straight duct
- diffuser
- sudden contraction (lam.)
- backward facing step (lam.)
- driven cavity
- rotating concentric cylinders (Taylor-Couette flow)

PHASE 2
BENCHMARK CASES

- square duct with 90° bend
- S-shaped duct
- backward facing step (turb.)
- orifice flow (turb.)
- flow around confined bluff bodies
- 2-D turbine cascade
- rotating disk

PHASE 3
SIMPLIFIED FLOWPATHS

- 3-D turbine blade cascade
- rotating curved duct

PHASE 4
ACTUAL HARDWARE

- SSME HPFTP impeller (2 sets partial blades)

Rockwell International
Rocketdyne Division

CFD 92-030-008/D2/SLB

REACT* CODE DESCRIPTION

- CO-DEVELOPED BY ROCKETDYNE/UNIVERSITY OF LONDON
- 2-D/3-D, STEADY STATE OR TRANSIENT, FULL NAVIER-STOKES
- MULTI-ZONE FINITE-VOLUME IN GENERALIZED COORDINATES
- PRESSURE-VELOCITY COUPLING THROUGH "SIMPLE" AND "PISO"
- STONE'S STRONGLY IMPLICIT AND CONJUGATE GRADIENT SOLVERS
- VARIOUS 2-EQUATION TURBULENCE MODELS
- CONJUGATE FLUID-SOLID HEAT TRANSFER CAPABILITY
- MULTI-SPECIES CAPABILITY
- PRIMARY USE FOR TURBOMACHINERY APPLICATIONS

* Rocketdyne Elliptic Analysis Code for Turbomachinery

Rockwell International
Rocketdyne Division

CFD 92-030-007/02/SLB

UNIT PROBLEMS COMPUTED FOR PHASE 1
DUCT FLOW

Verify Single Zone and Multizone Convergence

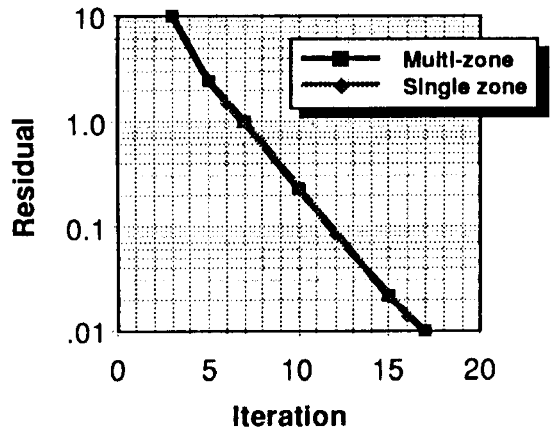

Establish Multizone Grid Matching Requirements

Non-smooth Interface

Smooth Interface

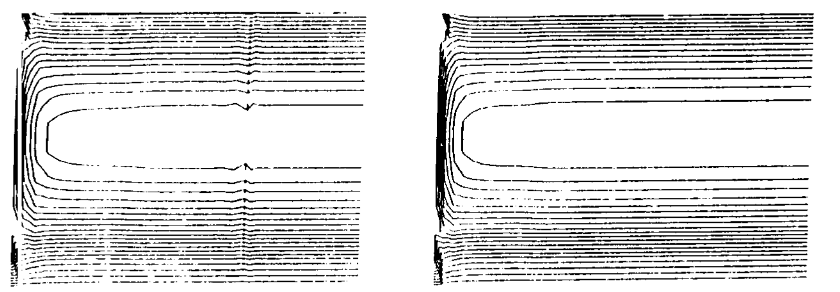

Refined Grid Computations Approach Exact Solution

Coarse Grid

Fine Grid

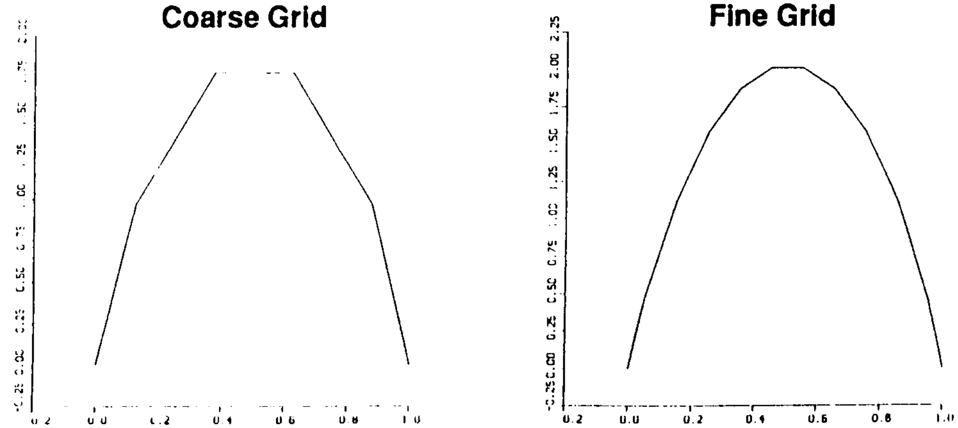

Rockwell International
Rocketdyne Division

CFD 92-030-008/D2/SLB

BENCHMARK CASES COMPUTED FOR PHASE 2
CURVED DUCT FLOW

90° Bend With Square Cross Section

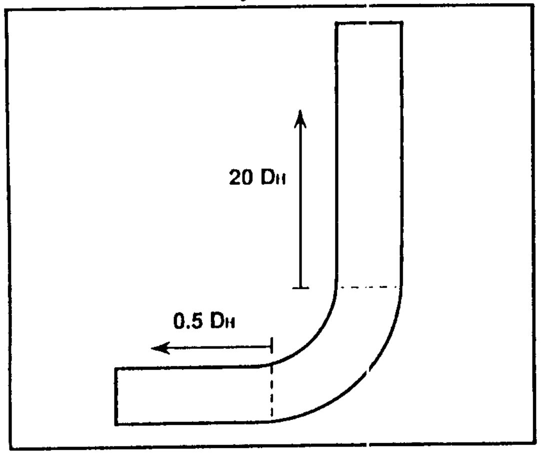

Refined Grid Yields Improved Agreement With Experimental Data

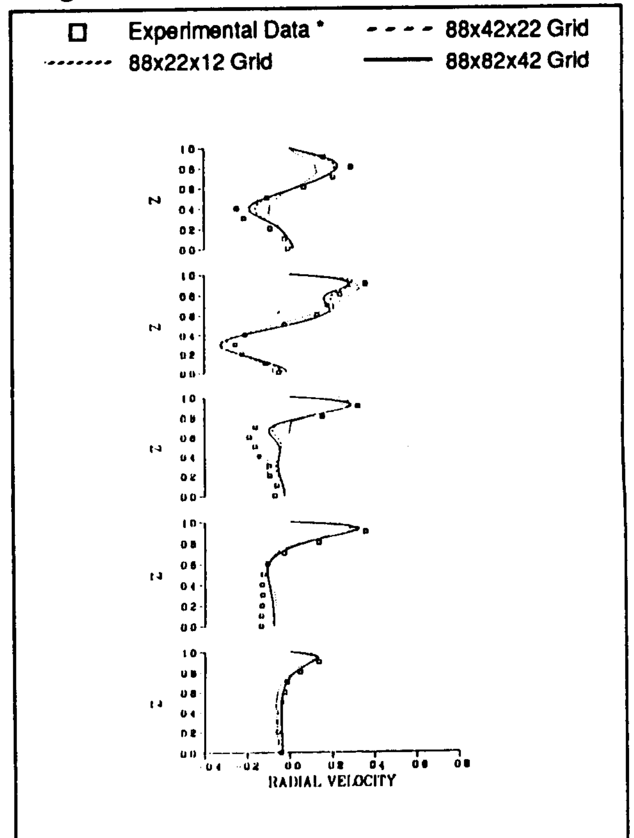

Velocity Profiles At 77.5° Location

Secondary Flow Features Captured

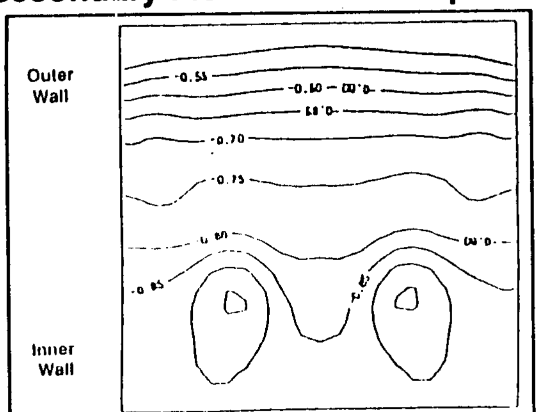

Pressure Contours

* A.M.K. Taylor, J.H. Whitelaw, And M. Yianneskis, "Measurements of Laminar and Turbulent Flow in a Curved Duct with Thin Inlet Boundary Layers," NASA Contractor Report 3367

Rockwell International
Rocketdyne Division

CFD 92-030-009/D2/SLB

PARTIAL FLOWPATH COMPUTED FOR PHASE 3
HPFTP FIRST STAGE TURBINE CASCADE

SSME HPFTP First Stage Stator
Multizone O-H Grid

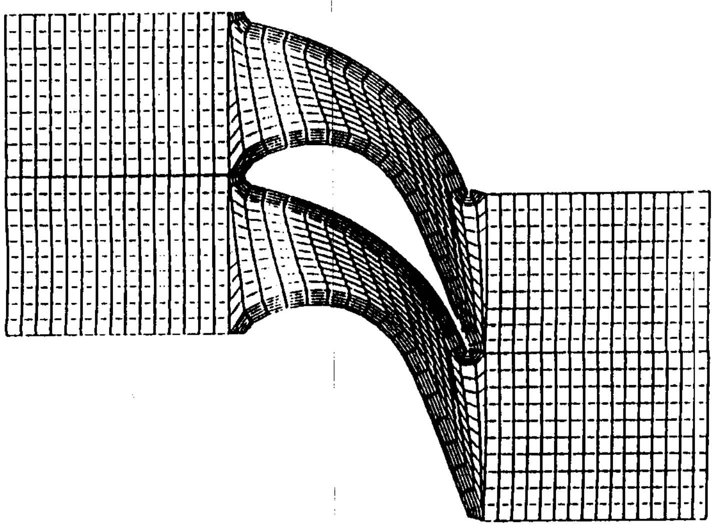

Static Pressure At Stator Mid-section
Fine Grid Solution

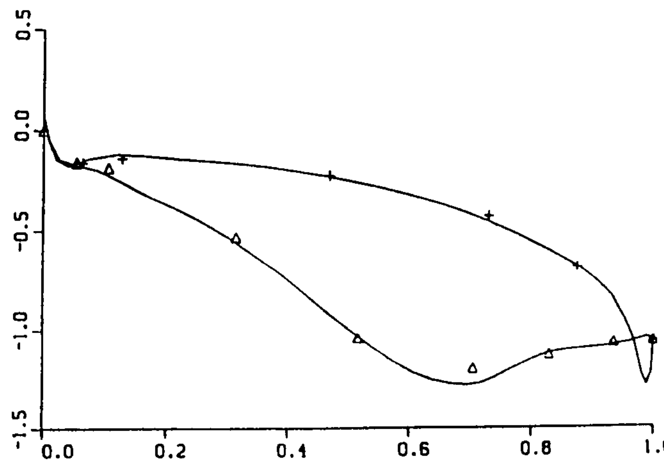

- STUDY EFFECTS OF SINGLE ZONE H GRID AND MULTIZONE O-H GRID
- PERFORM COARSE AND FINE GRID COMPUTATIONS ON EACH AND COMPARE WITH TEST DATA

Rockwell International
Rocketdyne Division

CFD 92-030-010/D2/SLB

COMPUTATIONS ON ACTUAL HARDWARE CONFIGURATION IN PROGRESS FOR PHASE 4

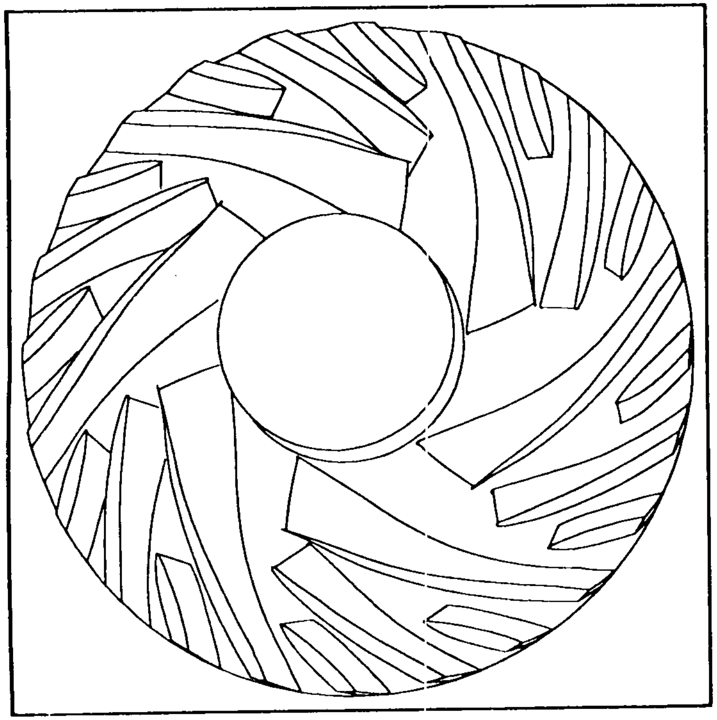

- **PROBLEM FEATURES**
  - HIGHLY THREE-DIMENSIONAL
  - TWO SETS OF PARTIAL BLADES
  - STRONG CURVATURE
  - HIGH ROTATIONAL SPEEDS
  - TURBULENT FLOW
- **MODELING APPROACH**
  - 3-D MULTIZONE MODEL
  - k-ε TURBULENCE MODEL
- **STATUS AND PLANS**
  - COARSE GRID SOLUTION COMPLETED WITH ASSUMED INLET CONDITION
  - TWO FINE GRID COMPUTATIONS PLANNED
    - ASSUMED INLET CONDITION
    - INLET CONDITION FROM TEST DATA
  - DATA ACQUISITION IN PROGRESS
    - INLET FLOW DATA NOW AVAILABLE
    - OUTLET DATA AVAILABLE SOON

Rockwell International
Rocketdyne Division

CFD 92-030-011/D2/SLB

SUMMARY

- **GENERAL VALIDATION PROCEDURE DEFINED FOR ALL APPLICATIONS**
  - FOUR PHASE PROCEDURE OUTLINED
  - QUANTITATIVE VALIDATION ONLY MEANINGFUL WITHIN LIMITED CLASS OF APPLICATIONS
  - CRITERIA BEING DEFINED

- **REALISTIC VALIDATION PROCEDURE DEMONSTRATED ON ACTUAL HARDWARE**
  - SSME HPFTP IMPELLER
  - DATA ACQUISITION IN PROGRESS
  - FINAL COMPUTATIONS AND DATA COMPARISONS TO FOLLOW

Rockwell International
Rocketdyne Division

CFD 92-030-012/D2/SLB

N92-32284

COMPARISON BETWEEN THE PISO ALGORITHM AND PRECONDITIONING METHODS FOR COMPRESSIBLE FLOW

Charles L. Merkle, Philip E. O. Buelow and S. Venkateswaran
Propulsion Engineering Research Center
The Department of Mechanical Engineering
The Pennsylvania State University
University Park, PA 16802.

Two widely used family of algorithms, pressure-based and density-based methods, have been developed for CFD problems over the years. Pressure-based methods (such as SIMPLE and PISO) use a Poisson-like equation for updating pressure instead of the continuity equation, while density-based methods use the continuity equation to update density (an equation of state is used to provide density in pressure based schemes and pressure in density based schemes). Pressure-based methods were developed originally for incompressible flows at low Reynolds numbers and were then extended to high Reynolds numbers and compressible applications. On the other hand, density based methods were originally developed for transonic flows and have been extended down to low Mach numbers through the use of preconditioning techniques. Both methods have enjoyed considerable success in solving complex flowfields, though the relative effectiveness of the schemes has long been argued. Generally, pressure-based methods are more robust while density-based schemes are more temperamental but provide more accurate solutions.

In the present paper, we compare these two very different approaches to solving the Navier-Stokes equations in order to gain an understanding of their similarities and differences. Specifically, we consider the PISO scheme as a representative pressure-based method and contrast it with a recently developed preconditioning scheme. To facilitate the comparison, we write both schemes in a vector formulation. Our findings indicate that the PISO scheme is very closely related to the philosophy of the preconditioning scheme. In particular, preconditioning causes the density-based scheme to appear pressure-based at low speeds but to remain density-based at high speeds. Furthermore, both schemes alter the sonic speed so that the equations stay well conditioned in the limit of low Mach numbers.

We also compare the relative performance of the PISO algorithm with an Euler implicit algorithm that is employed to solve the preconditioned equations by means of a vector stability analysis. The results of the stability analysis indicate that the PISO algorithm, which is a multi-step (one predictor step followed by several corrector steps), uncoupled (i.e., sequential) solution procedure, is conditionally stable. Good convergence is promised at low CFL numbers, while at high CFL numbers, both low wave number and high wave number instabilities are present. The high wave number instability appears to be 'compressible' in origin, arising from the treatment of the equation of state. The low wave number instability is 'incompressible' in origin since it is present when the incompressible limit of the equations are examined. An important finding, in this regard, is that the overall scheme may be unstable even when the individual predictor and corrector stages are themselves stable. In contrast, the Euler implicit algorithm shows unconditional stability. It should be noted, however, that multi-dimenisional solution of the equations demands the use of approximate factorization which limits CFL numbers to about 10. Thus, the two algorithms still remain quite competetive in solving practical flow problems.

PRECEDING PAGE BLANK NOT FILMED

The Relationship Between Pressure- and Density-Based Algorithms

Charles L. Merkle, Sankaran Venkateswaran
and Philip E. O. Buelow
The Pennsylvania State University
Propulsion Engineering Research Center
Department of Mechanical Engineering

Presented at

Computational Fluid Dynamics Workshop
Marshall Space Flight Center
April 28-30,1992

Introduction

Compare Pressure-Based and Density-Based Methods

Pressure-Based

- SIMPLE, MAC,PISO etc.
- Replace Continuity by Poisson Equation
- Solve by Sequential Procedure

Density-Based

- ADI, LU, Lax-Wendroff
- Solve Continuity Directly
- Solve by Simultaneous, Coupled Procedure

Express in Common Vector Form for Comparison

Development of Pressure Poisson Relation

Use Continuity with Source:

$$\nabla \bullet \mathbf{V} = D$$

Discretize Momentum:

$$\frac{u^{n+1} - u^n}{\Delta t} + \left(\frac{\partial u^2}{\partial x} + \frac{\partial uv}{\partial y} + \frac{\partial p}{\partial x} \right)^* = 0$$

$$\frac{v^{n+1} - v^n}{\Delta t} + \left(\frac{\partial uv}{\partial x} + \frac{\partial v^2}{\partial y} + \frac{\partial p}{\partial y} \right)^* = 0$$

Take Divergence of Momentum and Combine with Continuity:

$$\nabla^2 p^* + \sigma^* + \frac{1}{\Delta t}\left(\nabla \bullet \mathbf{V}\right)^{n+1} - \frac{1}{\Delta t}\left(\nabla \bullet \mathbf{V}\right)^{n} = 0 \qquad \text{where:} \qquad \sigma = \frac{\partial^2 u^2}{\partial x^2} + 2\frac{\partial^2 uv}{\partial x \partial y} + \frac{\partial^2 v^2}{\partial y^2}$$

Solution of Poisson Equation

Solve by Point Jacobi with OverRelaxation:

- Express as Equivalent Time Marching

$$\frac{4\Delta t}{\omega \Delta x^2}\frac{\partial p^{n+1}}{\partial t} = \nabla^2 p^* + \sigma^* - \frac{1}{\Delta t}\left(\nabla \bullet \mathbf{V}\right)^n \qquad \text{where:} \quad \left(\nabla \bullet \mathbf{V}\right)^{n+1} = 0$$

By Comparison of Equations:

$$\frac{4\Delta t}{\omega \Delta x^2}\frac{\partial p^{n+1}}{\partial t} = \frac{1}{\Delta t}\left(\nabla \bullet \mathbf{V}\right)^{n+1} = \frac{1}{\Delta t}D^{n-1}$$

Hence the Equivatent Equation Can Be Written

$$\frac{4\Delta t^2}{\omega \Delta x^2}\frac{1}{\Delta t}\left[\frac{\partial p^{n+1}}{\partial t} - \frac{\partial p^n}{\partial t}\right] = \nabla^2 p^* + \sigma^*$$

Poisson Method is Hyperbolic if $\frac{1}{\Delta t}D^n$ Is Retained

Poisson Method is Parabolic i f $\frac{1}{\Delta t}D^n$ Is Dropped

Poisson Equation in Compressible PISO Method

Continuity Equation:

$$\frac{\rho^{**}-\rho^{n}}{\Delta t}+\left(\frac{\partial \rho u}{\partial x}+\frac{\partial \rho v}{\partial y}\right)^{**}=0$$

Or, Using Perfect Gas Relation

$$\rho^{**}=p^{**}/RT^{*}$$

$$\frac{p^{**}-p^{n}}{RT^{n}\Delta t}+\left(\frac{\partial \rho u}{\partial x}+\frac{\partial \rho v}{\partial y}\right)^{**}=0$$

Momentum Equations:

$$\frac{\rho^{**}u^{**}-\rho^{n}u^{n}}{\Delta t}+\left(\frac{\partial u^{2}}{\partial x}+\frac{\partial uv}{\partial y}\right)^{*}+\frac{\partial p}{\partial x}^{**}=0$$

$$\frac{\rho^{**}v^{**}-\rho^{n}v^{n}}{\Delta t}+\left(\frac{\partial uv}{\partial x}+\frac{\partial v^{2}}{\partial y}\right)^{*}+\frac{\partial p}{\partial y}^{**}=0$$

Combine from Divergence of Momentum

Characteristic Speed in PISO Poisson Equation

- Combined Continuity and Momentum Equations

$$\frac{p^{**}-p^{n}}{RT^{n}\Delta t^{2}}+\frac{1}{\Delta t}\left(\frac{\partial\rho u}{\partial x}+\frac{\partial\rho v}{\partial y}\right)^{n}-\sigma^{*}-\nabla^{2}p^{**}=0$$

- Replace Divergence with Density Derivative

$$\frac{p^{**}-2p^{n}+p^{n-1}}{RT^{n}\Delta t^{2}}=\nabla^{2}p^{**}+\sigma^{*}$$

- PISO Poisson Equation is Hyperbolic
  - Characteristic Speeds Are the Acoustic Speeds
- LowMach Number Convergence Requires:
  - Multiple Sweeps of Continuity Equation
  - Re-scaling of Time Derivative--Preconditioning

Equations of Motion

$$\frac{\partial Q}{\partial t}+\frac{\partial E}{\partial x}+\frac{\partial F}{\partial y}=L_v(Q_v)$$

where

$$Q=(\rho,\rho u,\rho v,e)^T$$

$$E=(\rho u,\rho u^2+p,\rho uv,eu+pu)^T \quad (2)$$

$$F=(\rho v,\rho uv,\rho v^2+p,ev+pv)^T$$

$$L_v(Q_v)=\frac{\partial}{\partial x}R_{xx}\frac{\partial}{\partial x}Q_v+\frac{\partial}{\partial x}R_{xy}\frac{\partial}{\partial y}Q_v+\frac{\partial}{\partial y}R_{yx}\frac{\partial}{\partial x}Q_v+\frac{\partial}{\partial y}R_{yy}\frac{\partial}{\partial y}Q_v$$

Formulation of PISO Algorithm

Split Flux Vectors:

$$E = E_L + E_N$$

$$E_L = (\rho u, p, 0, 0)^T$$

ρu

$$E_N = (0, \rho u^2, \rho u v, (e+p)u)^T$$

eu

Use Predictor-Corrector Procedure:

$$\left\{ I_c + I_m \left[\Gamma + \Delta t \left(\frac{\partial}{\partial x} A_N{}^n + \frac{\partial}{\partial y} B_N{}^n - L_v \right) \right] \right\} \Delta Q^* = -\Delta t \, I_m \left[\frac{\partial E}{\partial x} + \frac{\partial F}{\partial y} - L_v(Q_v) \right]^n$$

$$\left\{ \Gamma + \left[\frac{\partial}{\partial x} A_L{}^* + \frac{\partial}{\partial y} B_L{}^* \right] \right\} \Delta Q^{**} + I_e \left(\frac{\partial}{\partial x} A_N{}^* + \frac{\partial}{\partial y} B_N{}^* - L_v \right) \Delta Q^{**}$$

$$= -\Delta t \left\{ \frac{\partial}{\partial x} A_L{}^* Q_v{}^* + \frac{\partial}{\partial y} B_L{}^* Q_v{}^* \right\} + I_e \left(\frac{\partial}{\partial x} A_N{}^* Q_v{}^* + \frac{\partial}{\partial y} B_N{}^* Q_v{}^* - L_v(Q_v{}^*) \right)$$

Stability Analysis

Represent Disturbance Growth by Amplification Matrix

$$Q^{n+1} = GQ^{n}$$

Result Provides Four Amplification Factors

Plot Maximum of These Four

For PISO Scheme,

$$Q^{*} = G^{*}Q^{n}, \quad Q^{**} = G^{**}Q^{*}, \quad Q^{n+1} = G^{***}Q^{**}$$

$$G = G^{***}G^{**}G^{*}$$

DENSITY-BASED STABILITY RESULTS

EULER IMPLICIT ALGORITHM

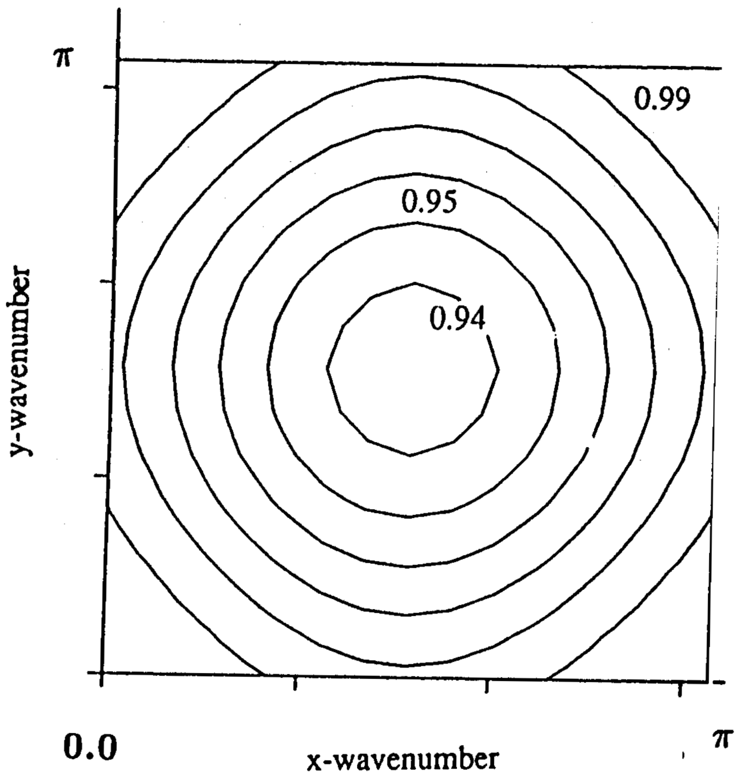

CFL=1, M=0.3

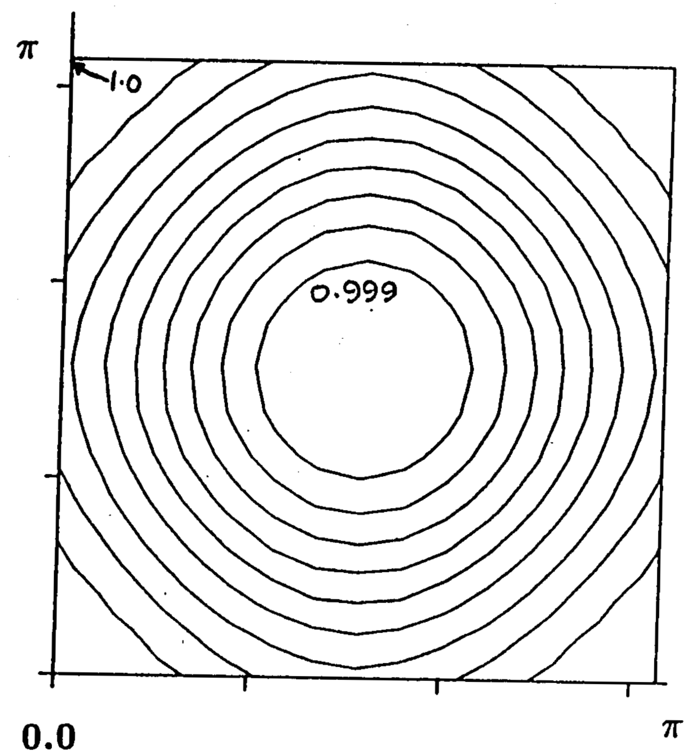

CFL=1, M=0.03

MACH NUMBER EFFECT FOR PISO SCHEME

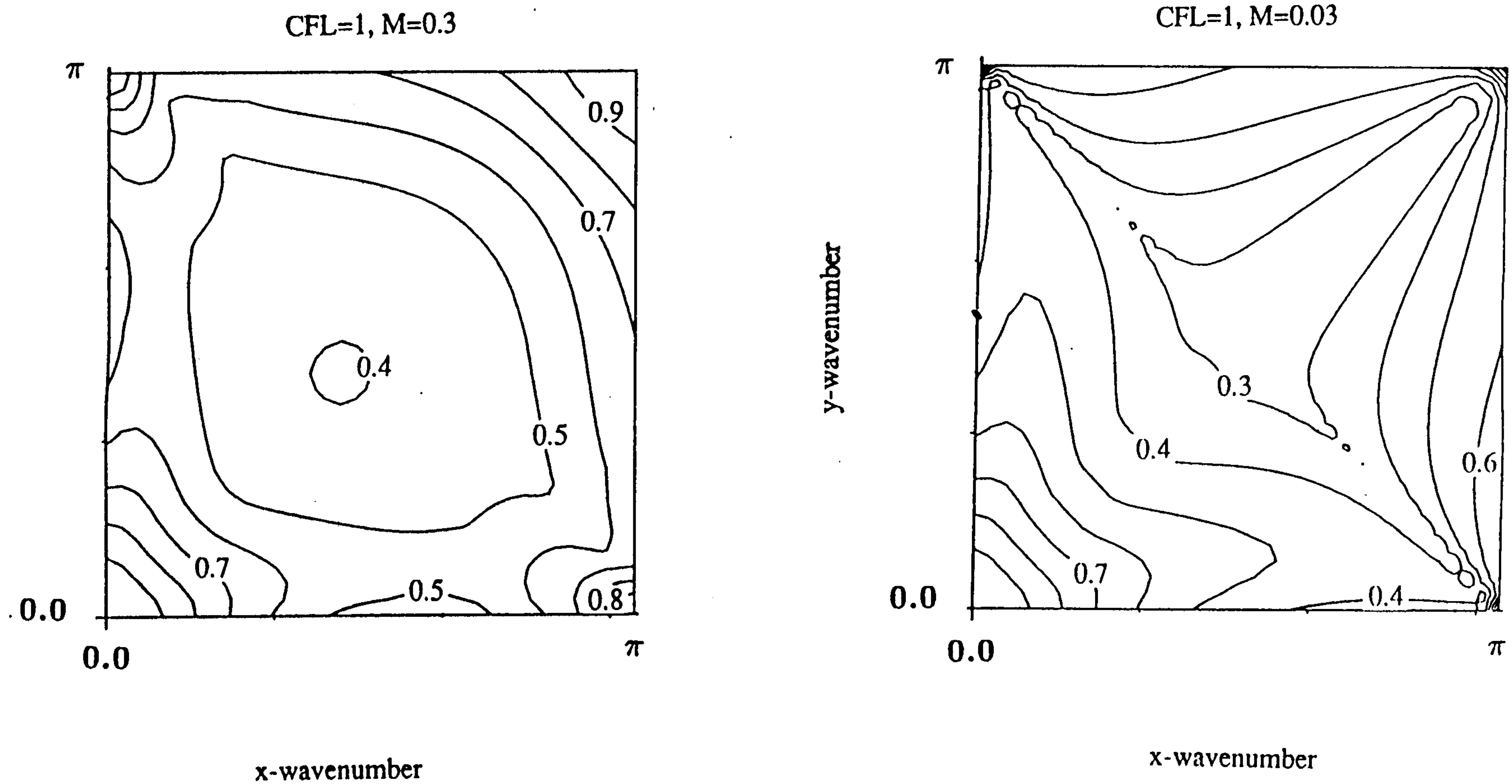

TIME DERIVA' IVE EFFECT ON PISO SCHEME

CFL=5, M=0.3

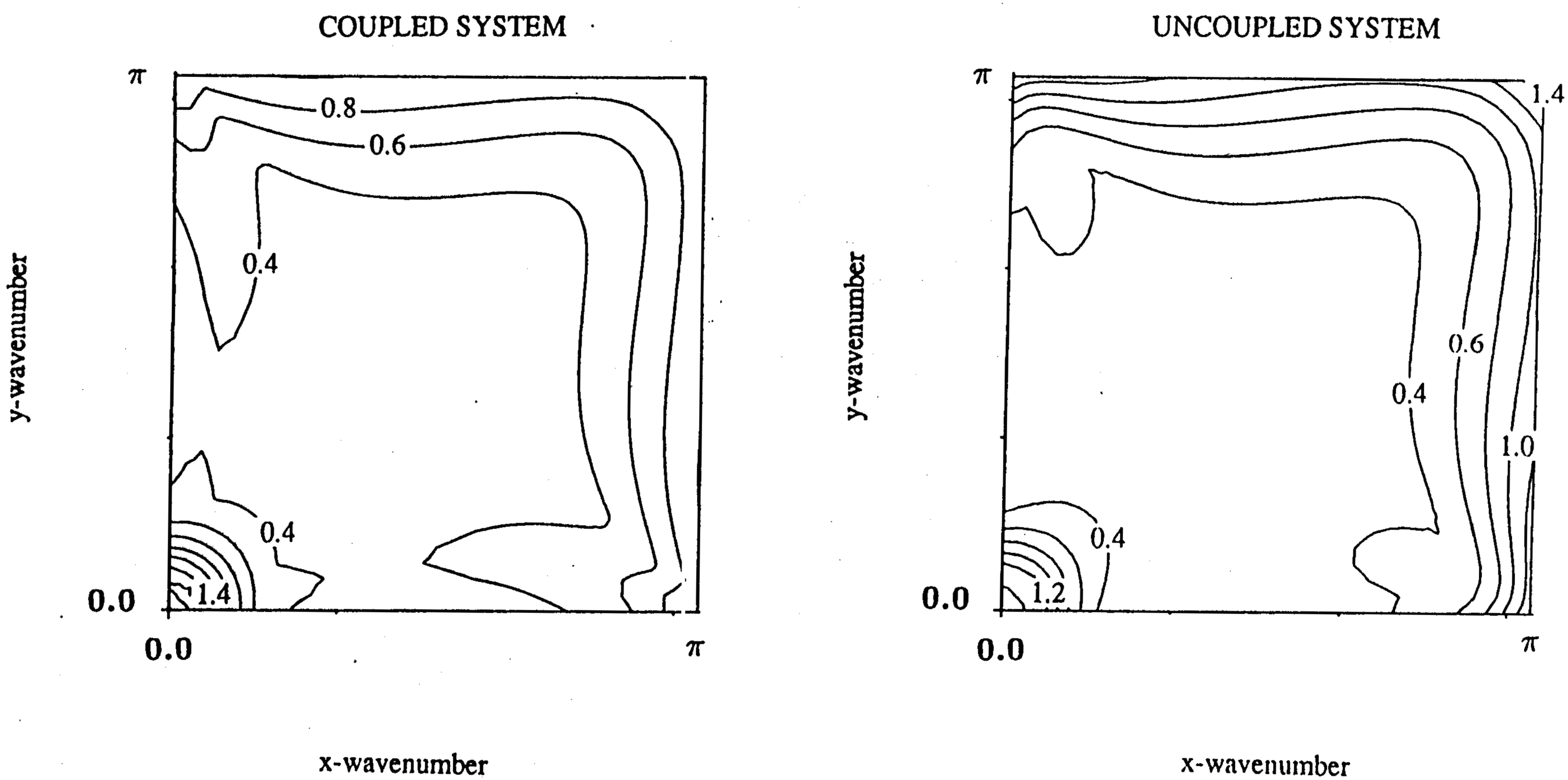

Comparison of Convergence

PISO: 1-D Incompressible

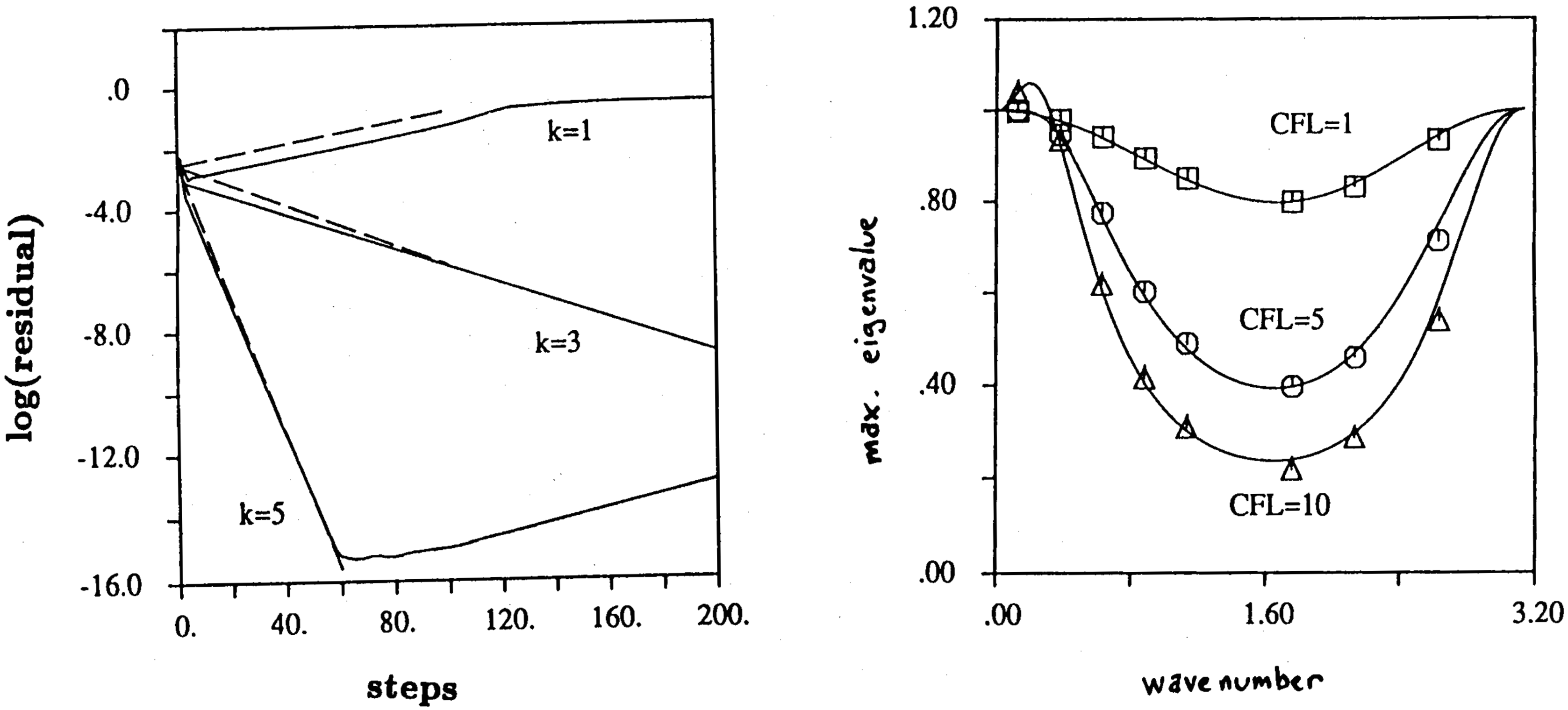

Compariso n of Convergence

inflo v/outflow B.C.'s

137

Euler Implicit

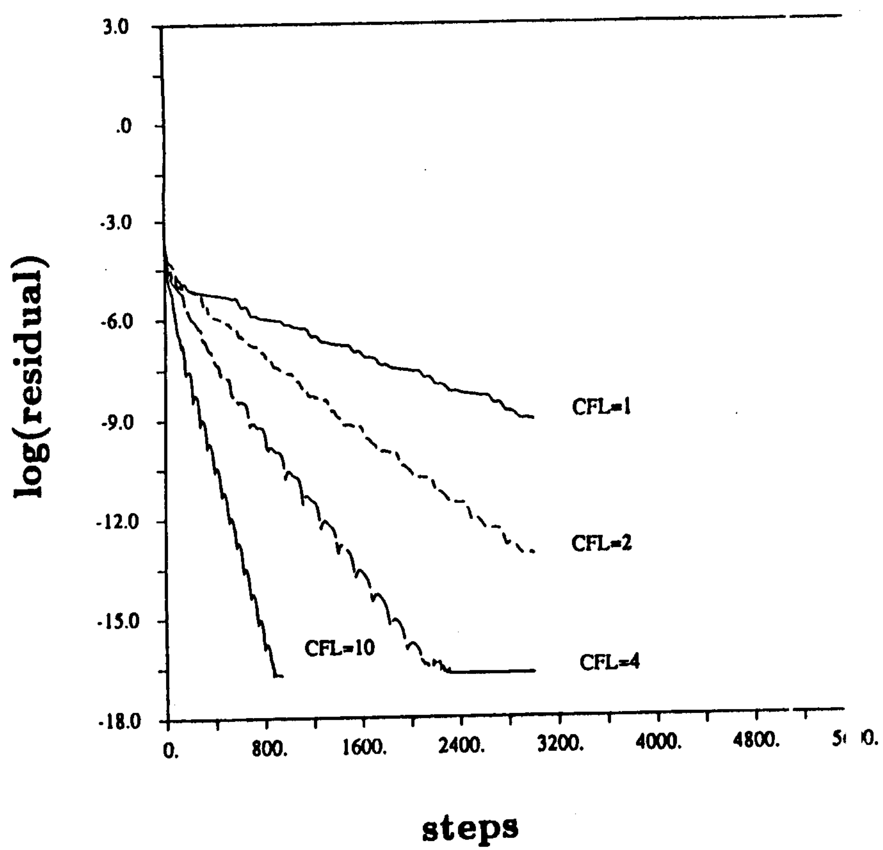

PISO

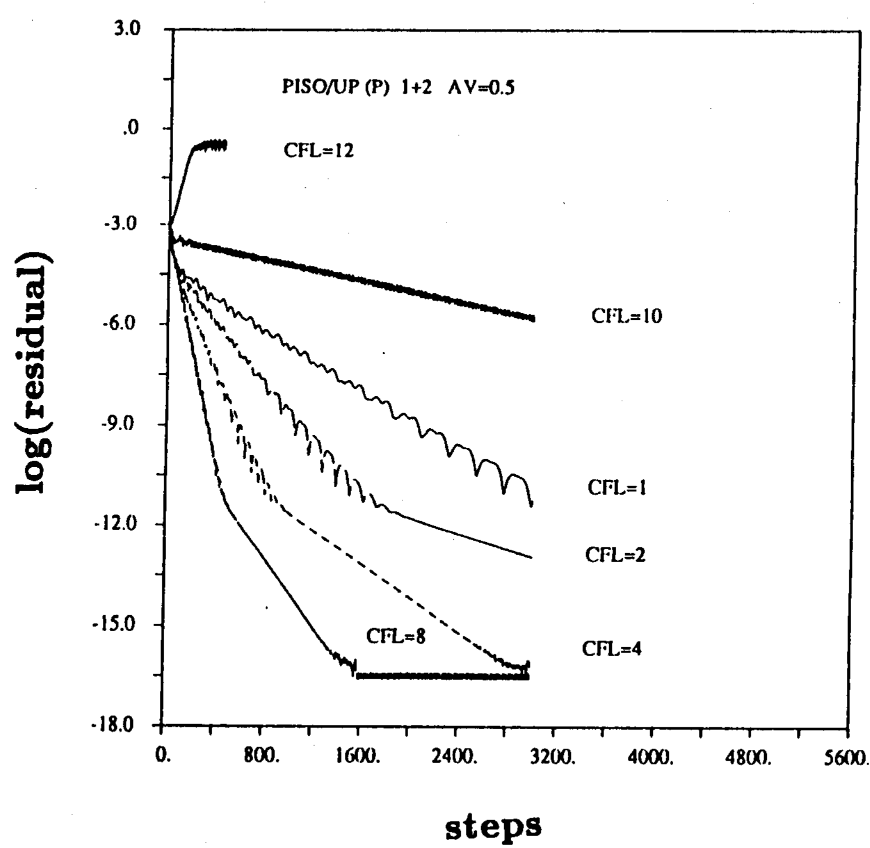

PISO: Fully Implicit

CFL = 1

M = 0.3

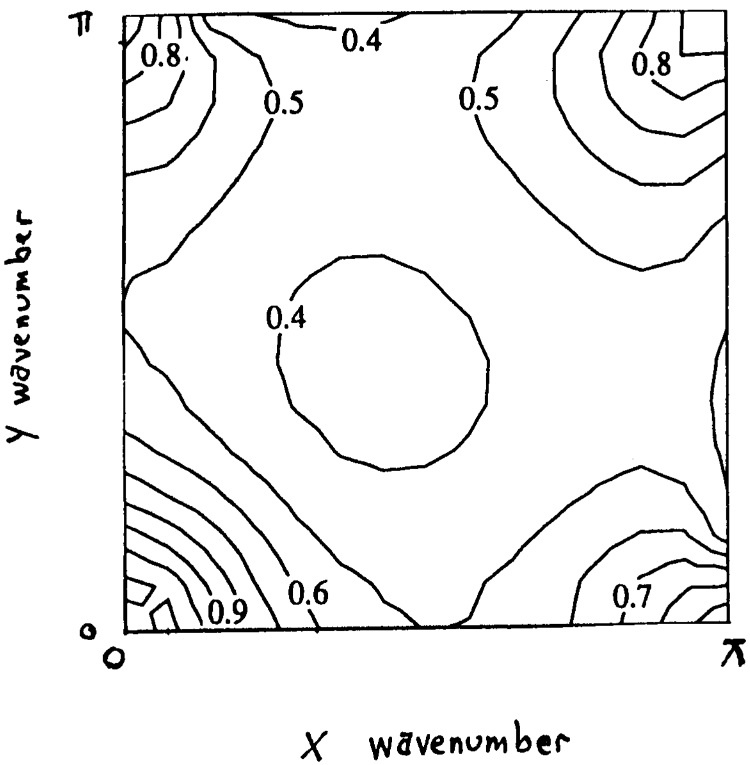

M = 0.03

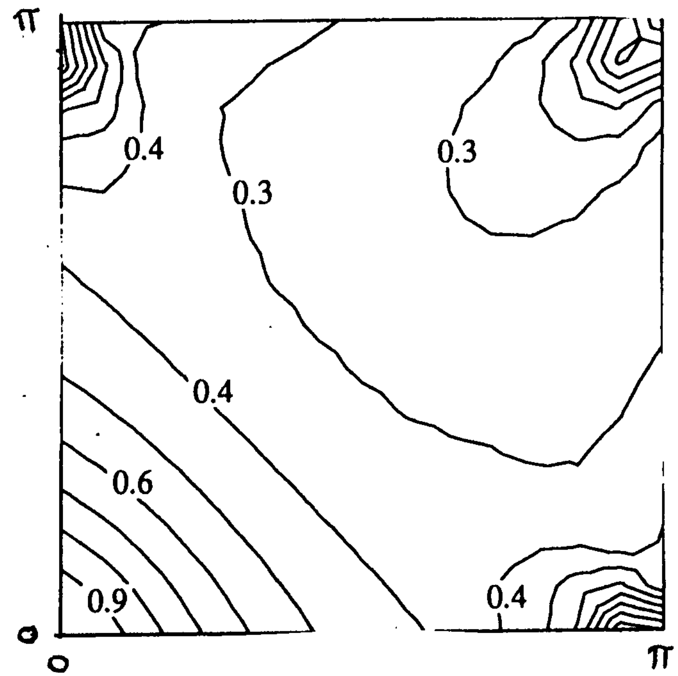

PISO: ADI

CFL = 1

M = 0.3 **M = 0.03**

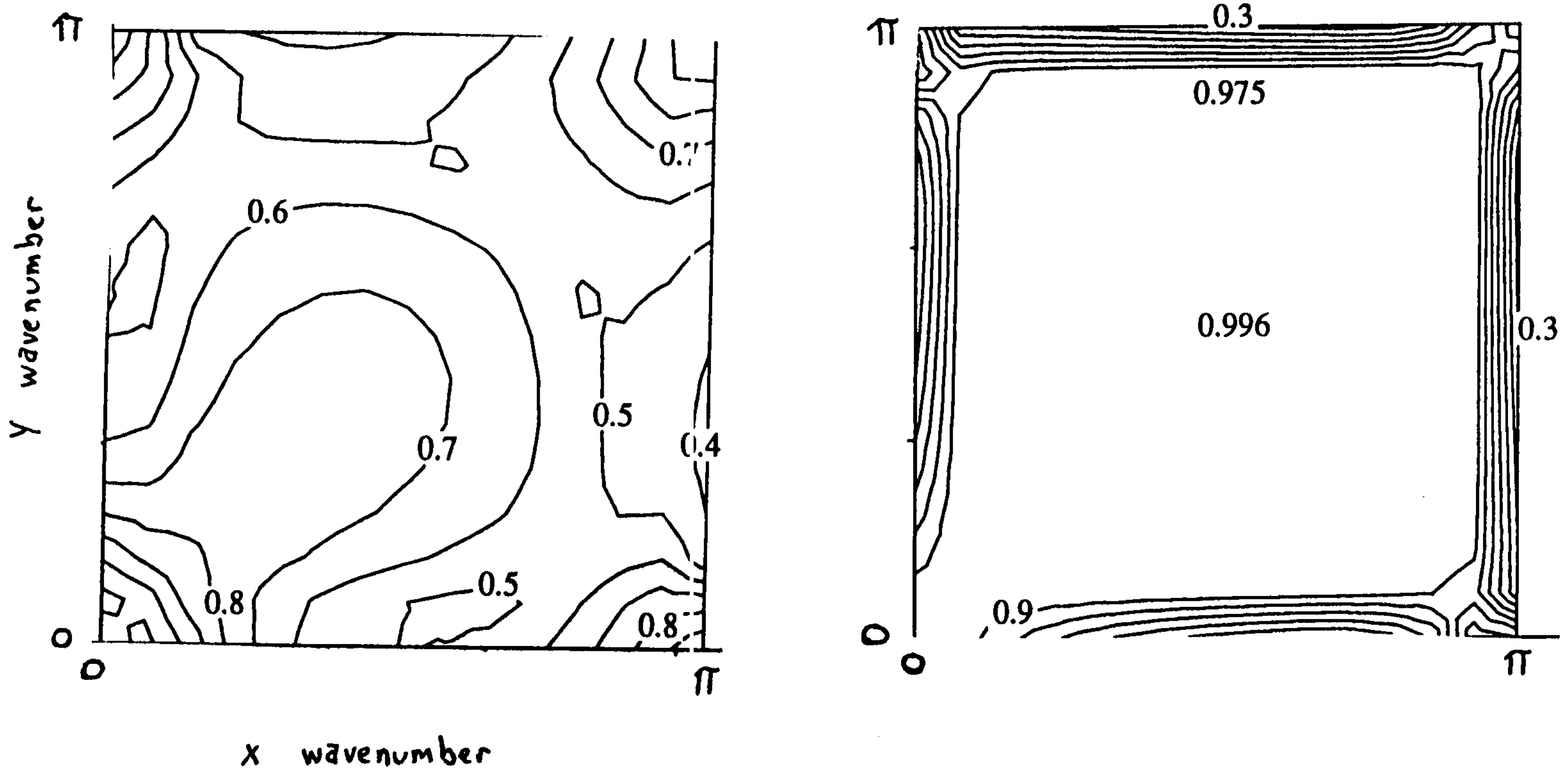

PISO: ADI with Poisson Time Scaling

CFL = 1

M = 0.3 **M = 0.03**

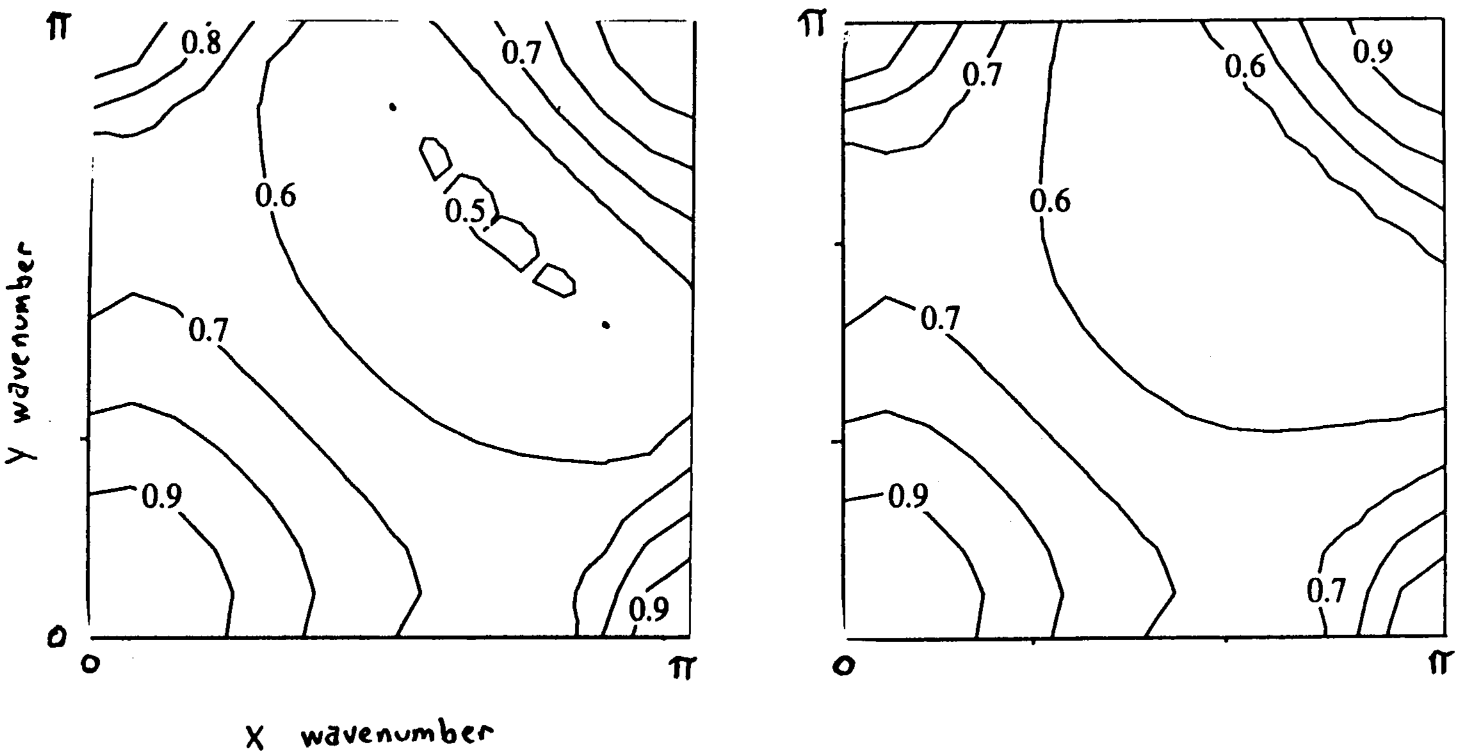

PISO: Gauss Seidel (1 sweep)

CFL = 1

M = 0.3 **M = 0.03**

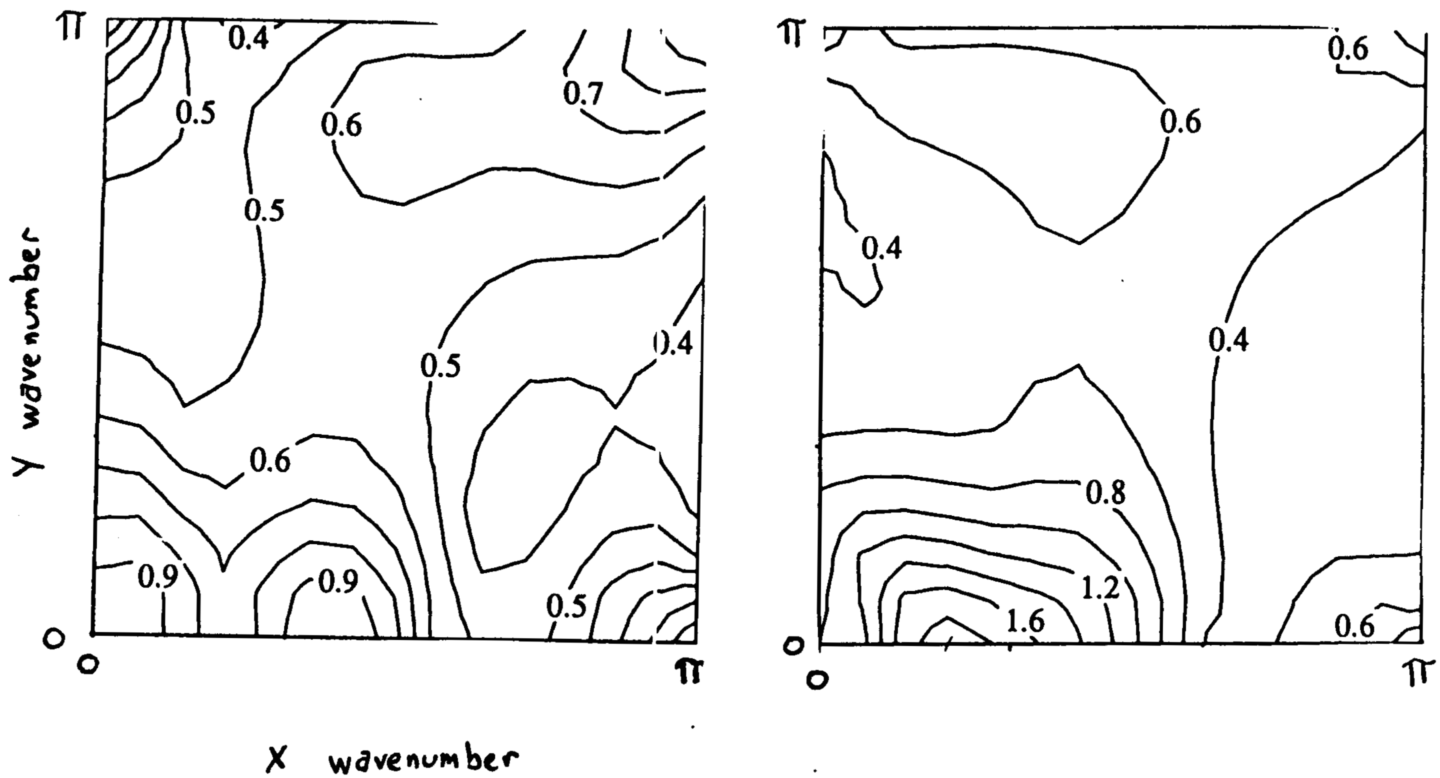

PISO: Gauss Seidel (10 sweeps)

CFL = 1

M = 0.3 **M = 0.03**

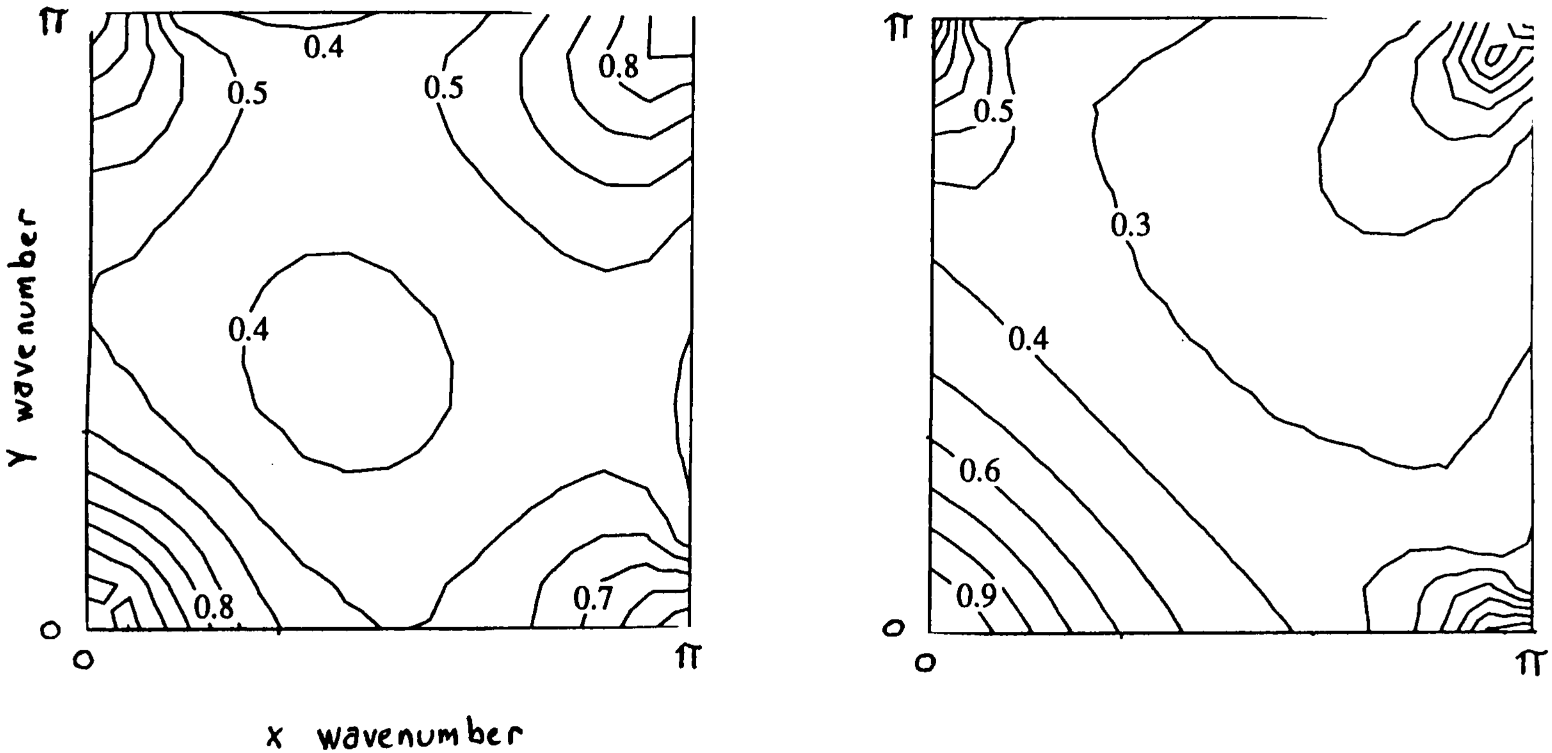

PISO: Gauss Seidel (1 sweep)

No time deriv. in Poisson

CFL = 1

M = 0.3 **M = 0.03**

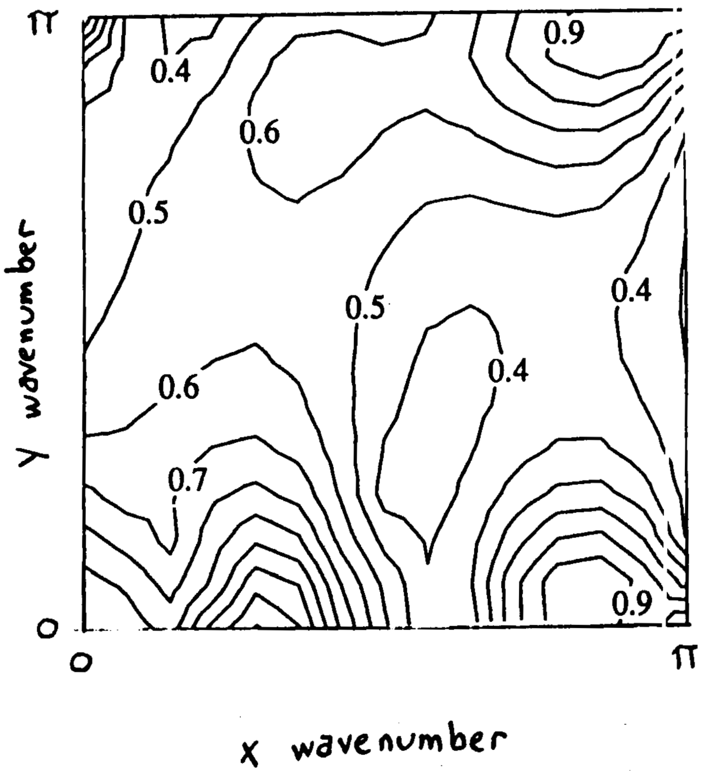

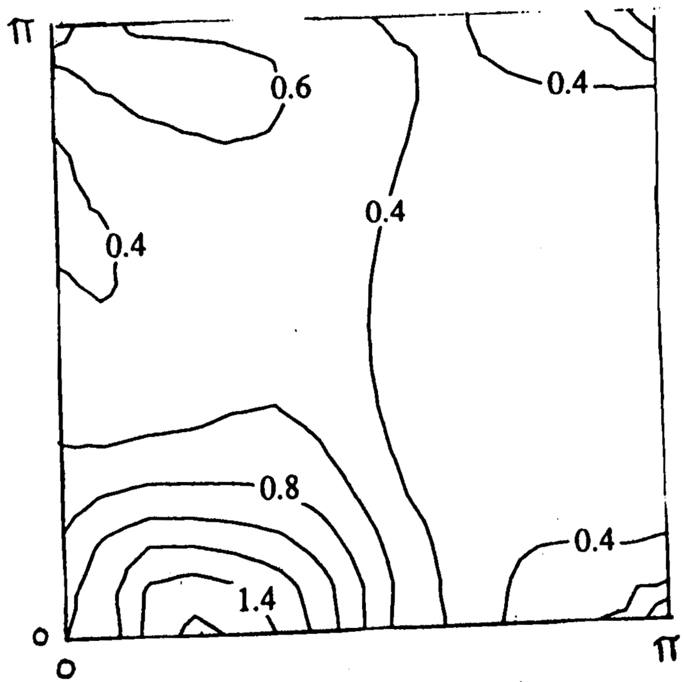

PISO: Gauss Seidel (10 sweeps)

No time deriv. in Poisson

CFL = 1

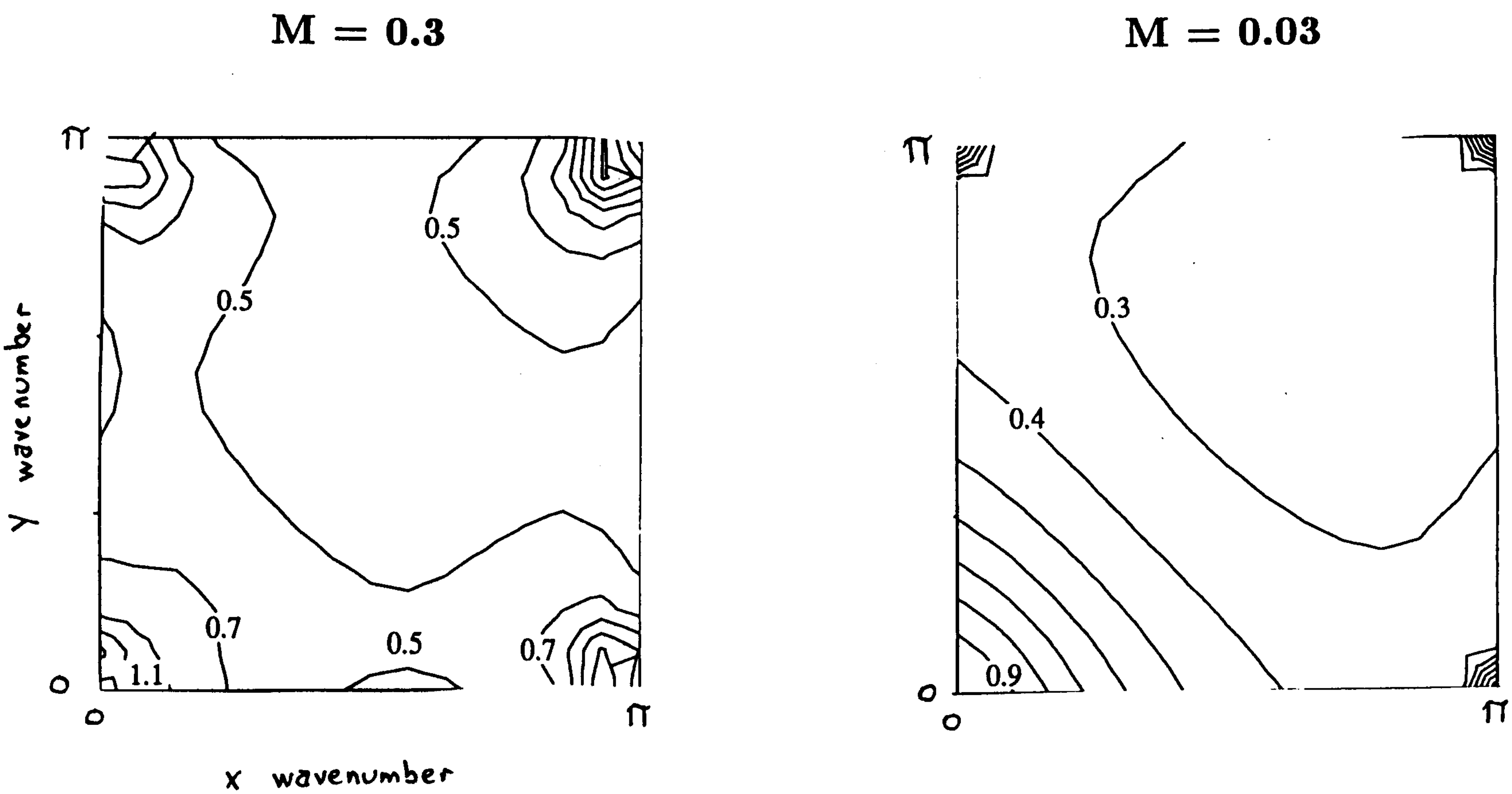

Summary

- Differences in Pressure- and Density-Based Methods.
  - Upwind Direction
  - Choice of Solution Variables
  - Coupled vs. Uncoupled Equations
- Pressure-Based Methods for Incompressible Flows Are Hyperbolic
  - Not Parabolic
- Pressure-Based Methods for Compressible Flow are Hyperbolic
  - Characteristics of Poisson Equation are Stiff
  - Time-step Control is Needed for Convergence
  - Can be Offset by Multiple Sweeps of the Poisson Equation

Summary (Contd.)

- Vector Form of Pressure-Based Method Facilitates Comparison
- PISO Vector Stability Analysis Indicates:
  - — Conditionally Stable
  - — Low Wave Number Instability (Incompressible)
  - — High Wave Number Instability (Compressible)
- Code Convergence Verifies Stability Predictions
- Approximate Factorization of Poisson Equation
  - — Low Mach Number Stiffness
  - — Mitigate by Scaling Time Step
  - — Circumvented by Gauss-Seidel

N92-3?285

A Comparison of Artificial Compressibility and Fractional Step Methods for Incompressible Flow Computations

Daniel C. Chan
Department of Aerospace Engineering, University of Southern California,
Los Angeles, California
and
Rocketdyne Division, Rockwell International Corporation
Armen Darian and Munir Sindir
Rocketdyne Division, Rockwell International Corporation
Canoga Park, California

We have applied and compared the efficiency and accuracy of two commonly used numerical methods for the solution of Navier-Stokes equations. The artificial compressibility method, postulated by Chorin, augments the continuity equation with a transient pressure term and allows one to solve the modified equations as a coupled system. Due to its implicit nature, one can have the luxury of taking a large temporal integration step in the expenses of higher memory requirement and larger operation counts per step. Meanwhile, the fractional step method, developed independently by Chorin and Temam, splits the Navier-Stokes equations into a sequence of differential operators and integrates them in multiple steps. The memory requirement and operation count per time step are low, however, the restriction on the size of time marching step is more severe.

To explore the strength and weakness of these two methods, we used them for the computation of a two-dimensional driven cavity flow with Reynolds number of 100 and 1000, respectively. Three grid sizes, 41x41, 81x81 and 161x161 were used. The computations were considered converged after the L_2-norm of the change of the dependent variables in two consecutive time steps has fallen below 10^{-5}. Same programming style is applied to the development of these codes. All computations were performed on the NASA-Marshall Convex C240 computer with double precision arithmetic.

In summary, we find that the artificial compressibility method requires twice as much memory per grid points and is less efficient for grid resolution below 81x81. Fractional step method, on the other hand, is more efficient in both memory requirement and computational speed for coarse grid computations, however, due to its explicit nature, its convergence rate deteriorates dramatically for fine grid computations

A COMPARISON OF FRACTIONAL STEP AND ARTIFICIAL COMPRESSIBILTY METHODS

BY:

DANIEL C. CHAN
ARMEN DARIAN
MUNIR M. SINDIR

CFD TECHNOLOGY CENTER
ROCKETDYNE DIVISION
ROCKWELL INTERNATIONAL

PRESENTED AT NASA MARSHALL SPACE FLIGHT CENTER
TENTH WORKSHOP FOR COMPUTATIONAL FLUID
DYNAMIC APPLICATIONS IN ROCKET PROPULSION

APRIL 28-30, 1992

Rockwell International
Rocketdyne Division

CFD-92/030/001/D2/AD

AGENDA

- MOTIVATION
- APPROACH
- TEST CASE DESCRIPTION
- RESULTS

Rockwell International
Rocketdyne Division

CFD-92-030-009/D2/AD

MOTIVATION

- **EXPLORE AN ALTERNATIVE NAVIER-STOKES SOLVER FOR ENGINEERING APPLICATIONS**
  - INTERNAL, INCOMPRESSIBLE FLOWS
- **IDENTIFY THE STRENGTH AND WEAKNESS**
  - LEVEL OF EXPERTISE REQUIRED
  - ACCURACY
  - SPEED

151

APPROACH

- **COUPLED METHOD**
  - EXTENSION OF COMPRESSIBLE FLOW FORMULATION
  - HIGHLY IMPLICIT
  - ELEGANT MATHEMATICAL FORMULATION
- **ITERATIVE METHOD**
  - LESS IMPLICIT
  - LONGER TRACK RECORD
  - LESS COMPLICATED TO FORMULATE

GOVERNING EQUATIONS FOR ARTIFICAL COMPRESSIBILITY METHOD

$$\frac{\partial \vec{q}}{\partial t}+\frac{\partial \vec{F}}{\partial x}+\frac{\partial \vec{G}}{\partial y}-\frac{1}{\mathrm{Re}}[D]\nabla^2\vec{q}=0$$

$$\vec{q}=\begin{bmatrix}\frac{p}{a^2}\\ u\\ v\end{bmatrix} \qquad \vec{F}=\begin{bmatrix}u^2\\ u^2+p\\ uv\end{bmatrix}$$

$$\vec{G}=\begin{bmatrix}v\\ uv\\ v^2+p\end{bmatrix} \qquad [D]=\begin{bmatrix}0&0&0\\0&1&0\\0&0&1\end{bmatrix}$$

Rockwell International
Rocketdyne Division

NUMERICS

- SECOND ORDER CENTRAL DIFFERENCING FOR ALL SPATIAL DERIVITIVES
- IMPLICIT TEMPORAL INTEGRATION IS NEEDED TO OVERCOME STIFFNESS
- APPROXIMATE FACTORIZATION IN DELTA FORM PLUS SECOND ORDER IMPLICIT AND FOURTH ORDER EXPLICIT DAMPING

Rockwell International
Rocketdyne Division

CFD-92-029-004/D2/AD

BOUNDARY CONDITIONS

- **VELOCITY**
  - NO-SLIP ALONG SOLID WALLS
- **PRESSURE**
  - NEUMANN CONDITION DERIVED FROM MOMENTUM EQUATIONS
- **EXPLICIT IMPLEMENTATION**

FRACTIONAL STEP METHOD

- INTEGRATE DIFFERENTIAL OPERATORS IN A SEQUENCE OF STEPS

$$\frac{\hat{u}_i - u_i^n}{\Delta t} = L(u_i) - N(u_i)$$

$$\frac{u_i^{n+1} - \hat{u}_i^n}{\Delta t} = -\frac{\delta\phi}{\delta x_i} \quad \text{where} \quad \frac{\delta\phi}{\delta x_i} \sim \frac{\delta P}{\delta x_i} - L(u_i)$$

CONTINUITY REQUIRES

$$\frac{1}{\Delta t}\frac{\delta \hat{u}_i^n}{\delta x_i} = -\frac{\delta^2 \phi}{\delta x_i \delta x_i}$$

Rockwell International
Rocketdyne Division

FRACTIONAL STEP METHOD (CONT'D)

- **VARIOUS MULTI-STEP METHODS CAN BE INCORPORATED TO ACHIEVE DESIRED TEMPORAL ACCURACY AND STABILITY**
  - FULLY IMPLICIT, LEAP-FROG, CRANK-NICOLSON, RUNGE-KUTTA
- **BOUNDARY CONDITION**
  - NO-SLIP ALONG WALL
  - GREEN'S THEOREM REQUIRES:

$$\int \frac{\partial \phi}{\partial n} ds = \int \vec{u} \cdot \vec{n} ds \Rightarrow \frac{\partial \phi}{\partial n} = 0$$

Rockwell International
Rocketdyne Division

A COMPARISON OF THE TWO METHODS

	ARTIFICIAL COMPRESSIBILITY	FRACTIONAL STEP
TIME INTEGRATION	FULLY IMPLICIT (NEWTON'S LINEARIZATION)	CONVECTION: EXPLICIT DIFFUSION: IMPLICIT PRESSURE: IMPLICIT
SPATIAL DISCRETIZATION	CENTRAL DIFFERENCING	CONVECTION: LINEAR UPWIND DIFFUSION: CENTRAL PRESSURE: CENTRAL
GRID ARRANGEMENT	COLLOCATION POINTS	FINITE VOLUME NON-STAGGERED
ARTIFICIAL DAMPING	4TH ORDER EXPLICIT; 2ND ORDER IMPLICIT FOR ALL EQUATIONS	NON-LINEAR, EXPLICIT 4TH AND 2ND ORDER FOR PRESSURE STEP
BOUNDARY CONDITION	EXPLICIT	EXPLICIT ON V IMPLICIT ON ϕ
ACCURACY	2ND ORDER	2ND ORDER
MEMORY	30 WORDS/POINT	20 WORDS/POINT
ADJUSTABLE CONSTANTS	$a^2, \Delta t, \varepsilon_i, \varepsilon_e$	Δt

COMPUTATIONAL MODEL FOR THE FRACTIONAL STEP METHOD

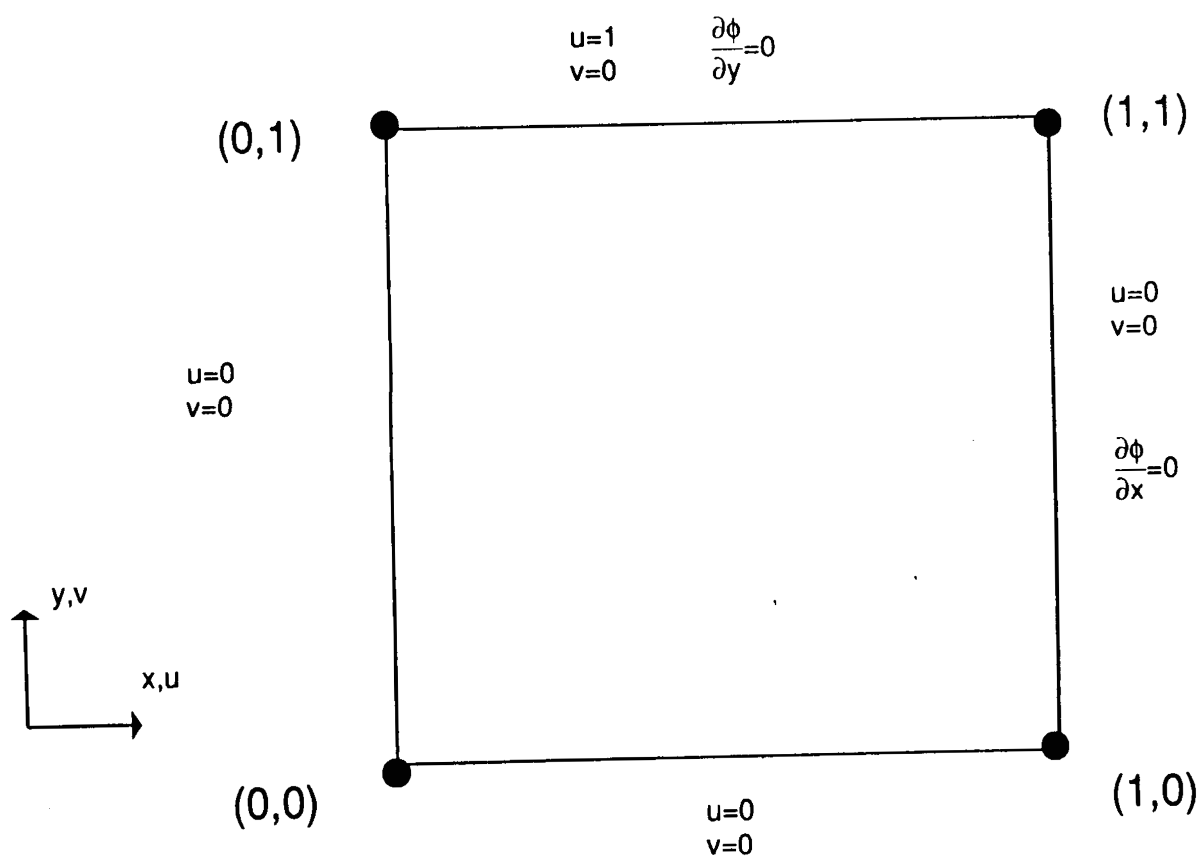

Rockwell International
Rocketdyne Division

CFD-92-029-006/D2/AD

COMPUTATIONAL MODEL FOR THE ARTIFICIAL COMPRESSIBILTY METHOD

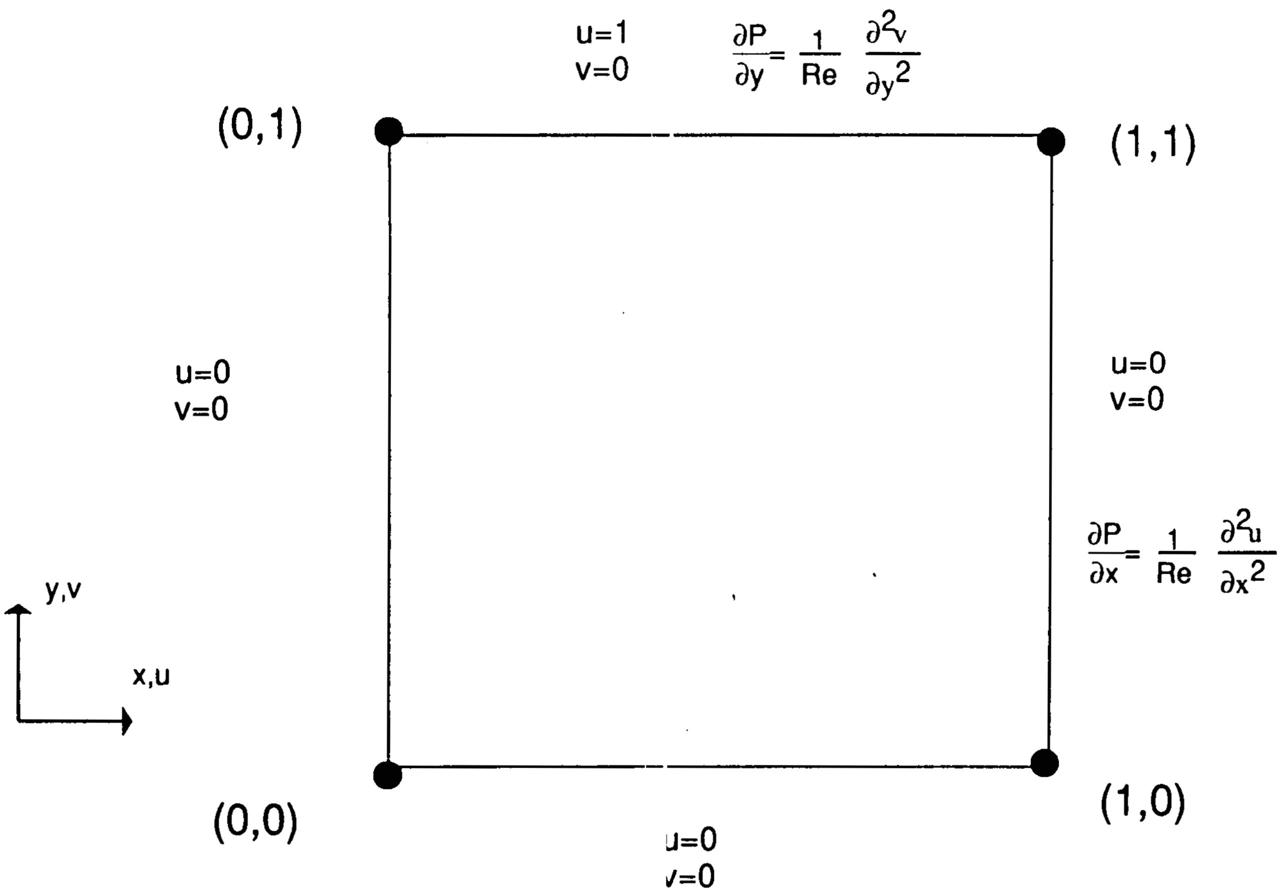

METHOD OF COMPARISON

- **CONSISTENT PROGRAMMING STYLE**
  - ONE DEVELOPER
  - NO EXPLICIT VECTORIZATION
- **USE ONE COMPUTER WITH SAME COMPILATION OPTION**
  - CONVEX C-240
  - fc -02 -pd8
- **MAINTAIN CONSTANT ΔT AT EACH GRID POINT**
- **'OPTIMIZE' INPUT PARAMETERS WITH 41x41 GRID RESOLUTION**
- **ε_i AND ε_e FIXED AT 0.2 AND 0.1, RESPECTIVELY**
- **a=1**

PARAMETERS TO COMPARE

- RANGE OF OPERATION
- CPU TIME REQUIREMENT AS A FUNCTION OF GRID POINTS USED
- REYNOLDS NUMBER DEPENDENCY
- ACCURACY

CONVERGENCE HISTORY FOR 41 x 41 GRID, Re=100

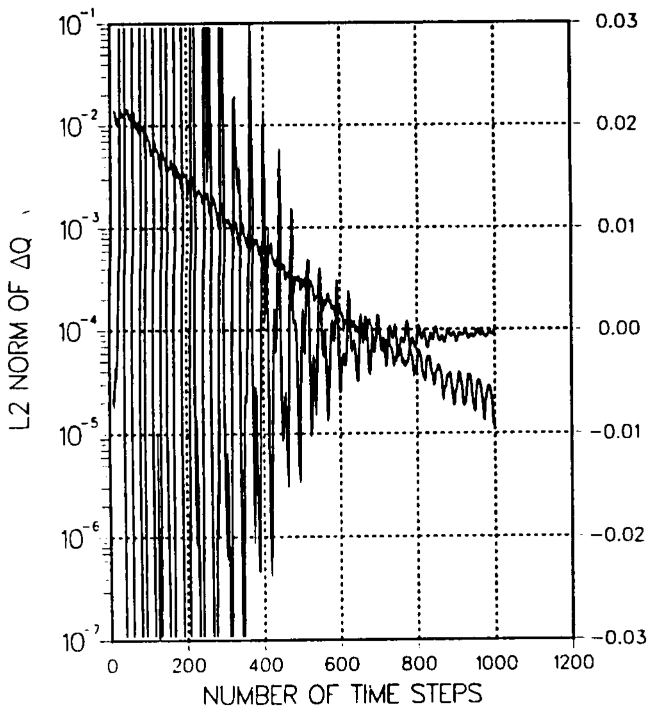

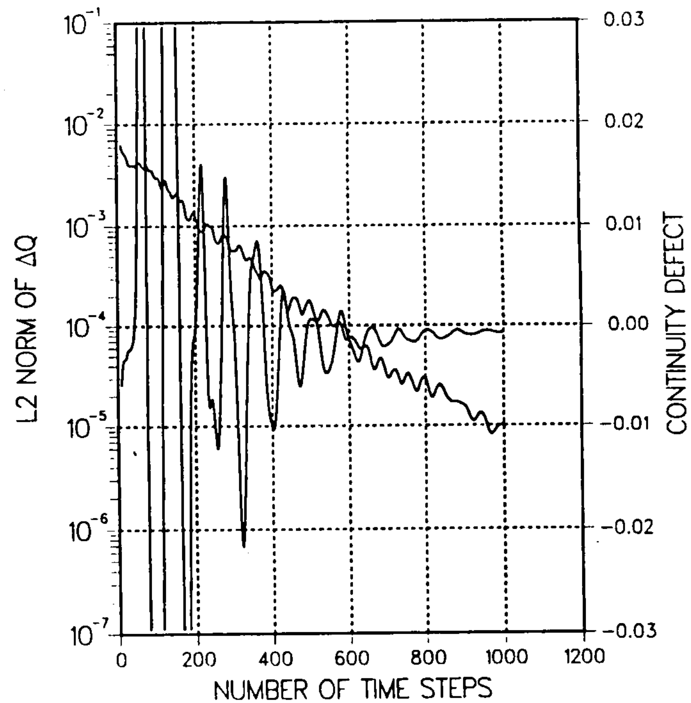

Rockwell International
Rocketdyne Division

CFD-92-030-013/D2/AD

CONVERGENCE HISTORY FOR 41 x 41 GRID, Re=100

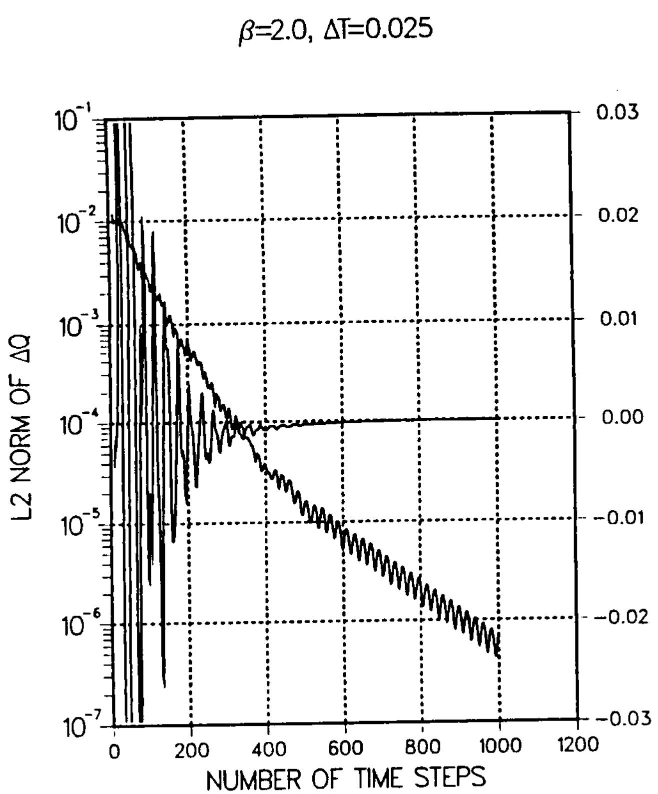

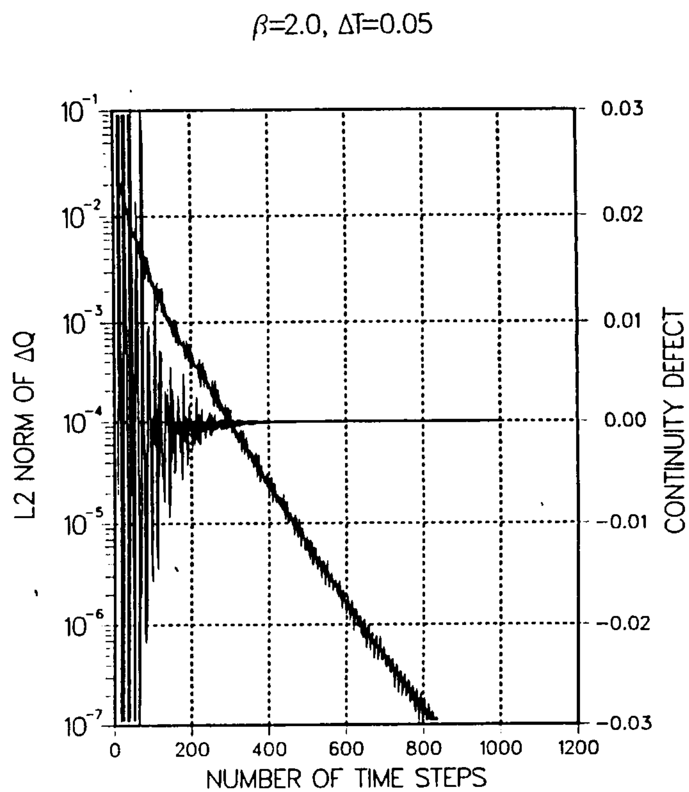

Rockwell International
Rocketdyne Division

CFD-92-030-014/D2/AD

CONVERGENCE HISTORY FOR 41 x 41 GRID, Re=100

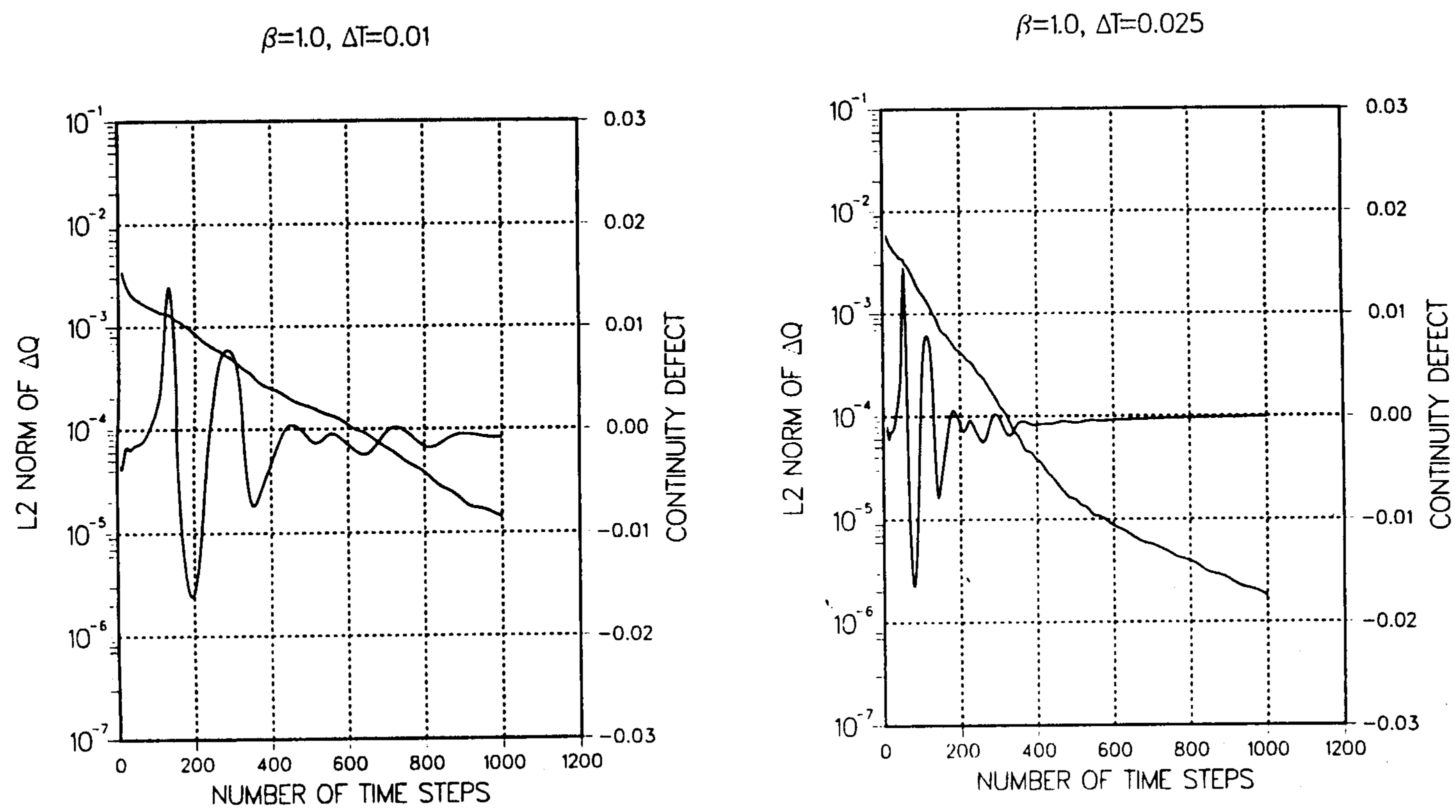

Rockwell International
Rocketdyne Division

CFD-92-030-015/D2/AD

CONVERGENCE HISTORY FOR 41 x 41 GRID, Re=100

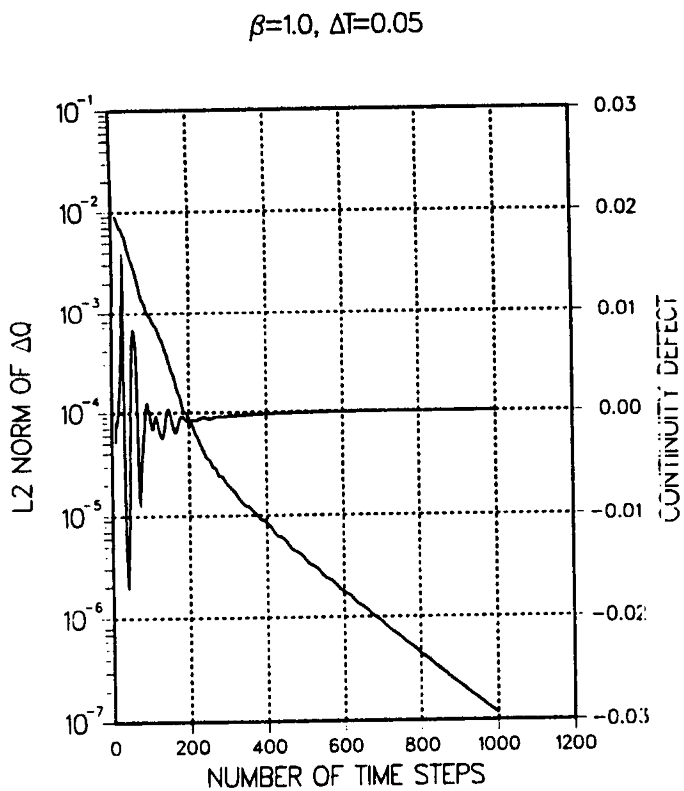

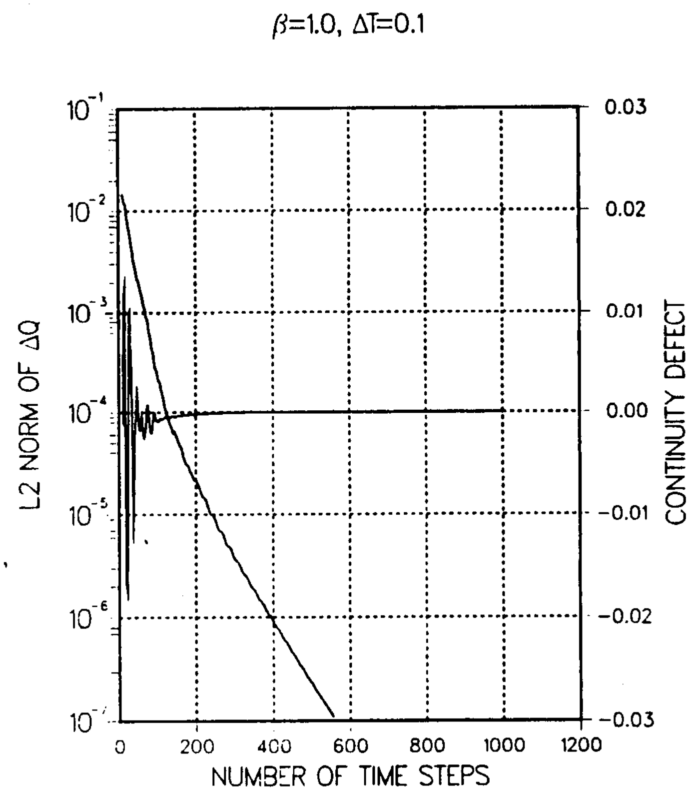

CONVERGENCE HISTORY FOR 81 x 81 GRID, Re=1000

AC METHOD
ΔT=0.05

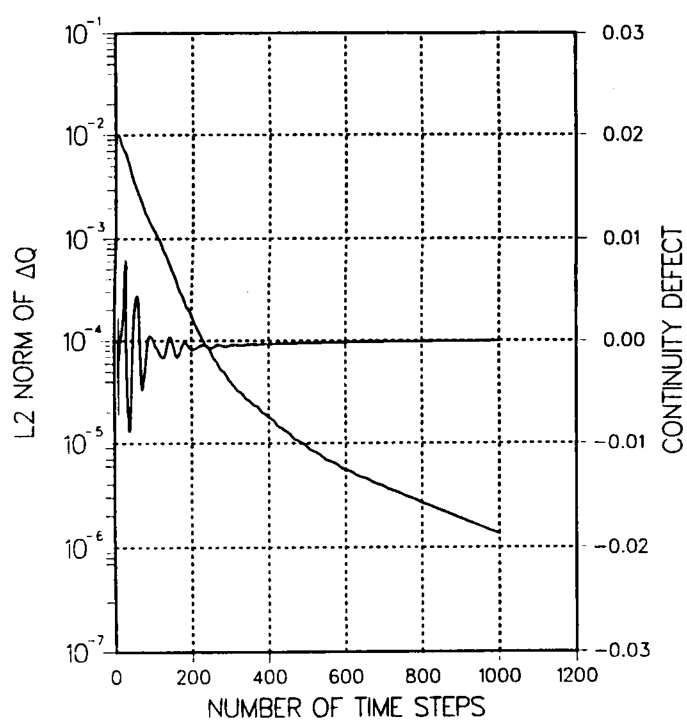

FS METHOD
ΔT=0.004

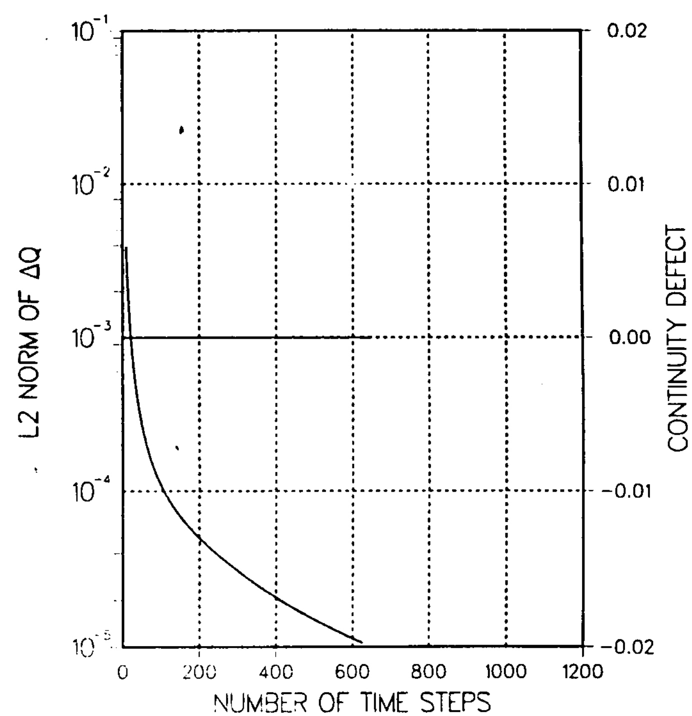

COMPUTATIONAL REQUIREMENT

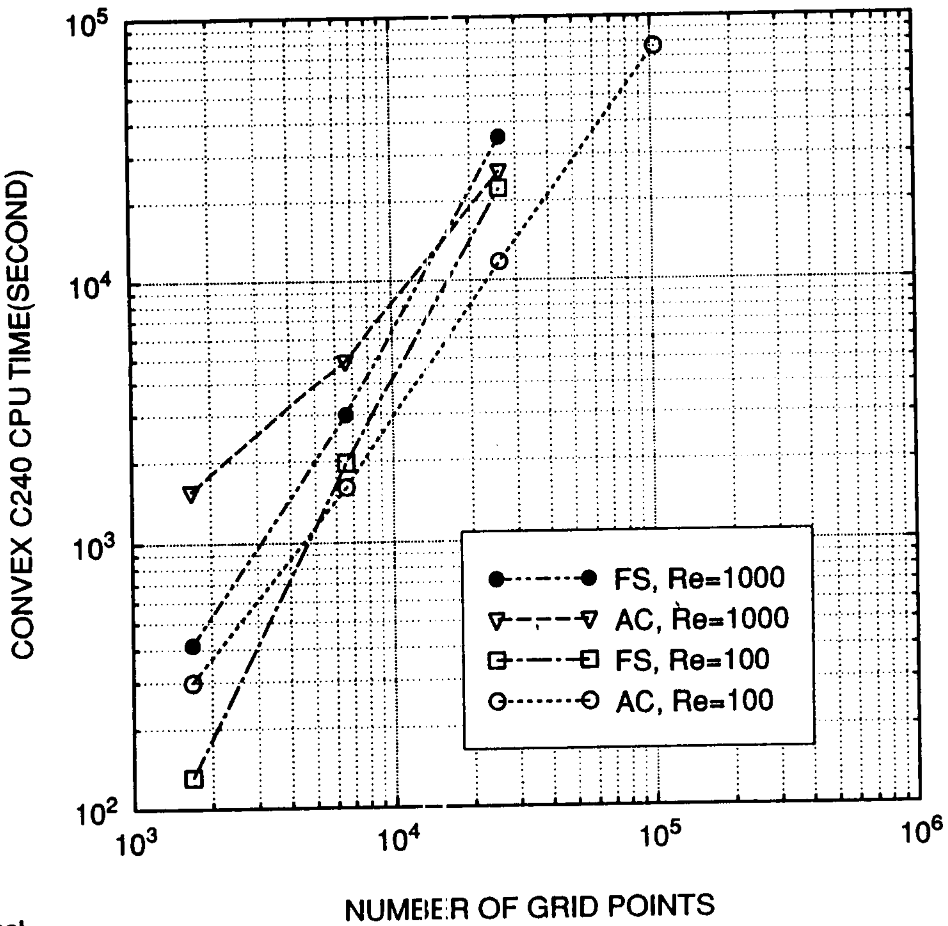

Rockwell International
Rocketdyne Division

CFD-92-030-021/D2/AD

EFFECT OF TIME STEP ON CONVERGENCE RATE

Re=100, 41X41 GRID

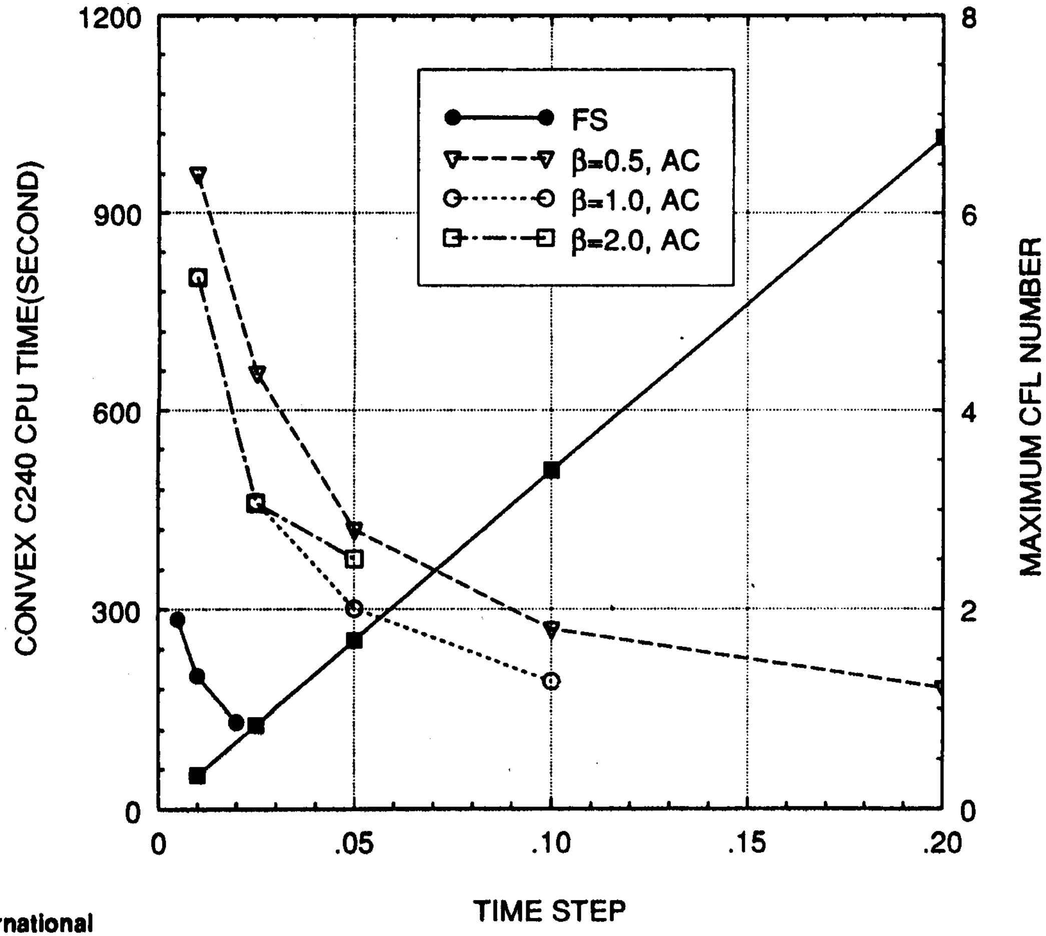

Rockwell International
Rocketdyne Division

CFD-92-030-020/D2/AD

VELOCITY PROFILES ALONG THE GEOMETRIC CENTERLINES OF A DRIVEN CAVITY FLOW
Re=100

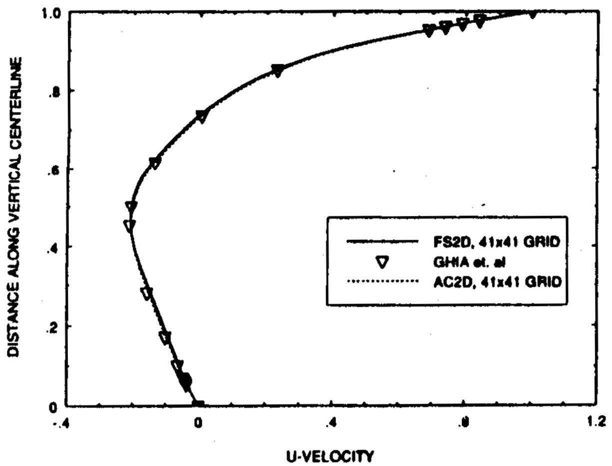

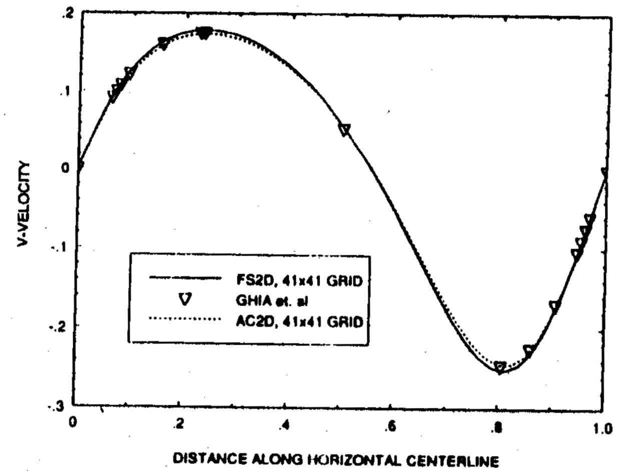

Rockwell International
Rocketdyne Division

CFD-92-030-018/D2/AD

VELOCITY PROFILES ALONG THE GEOMETRIC CENTERLINES OF A DRIVEN CAVITY FLOW Re=1000

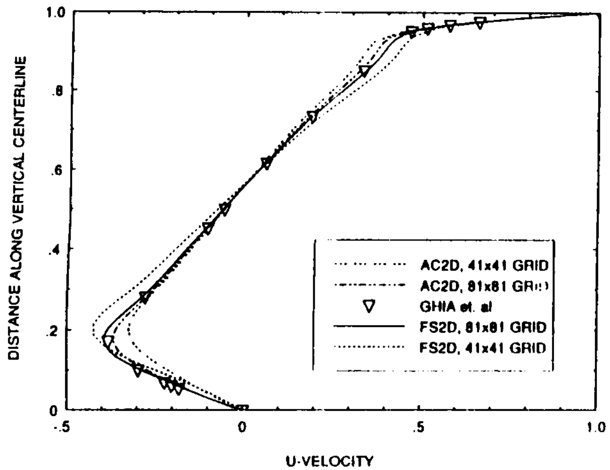

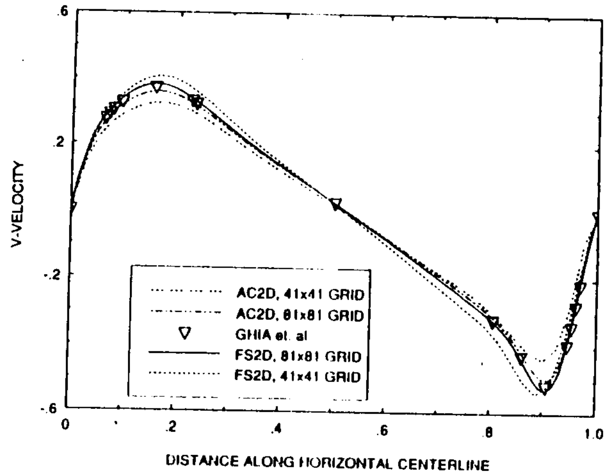

Rockwell International
Rocketdyne Division

CFD-92-030-019/D2/AD

SUMMARY OF RESULTS

- **APPROXIMATE FACTORIZATION/ARTIFICIAL COMPRESSIBILITY METHOD**
  - MEMORY INTENSIVE
  - SENSITIVE TO REYNOLDS NUMBER
  - REQUIRES MORE USER INTERACTIONS

- **FRACTIONAL STEP METHOD**
  - MEMORY EFFICIENCY
  - SENSITIVE TO TIME STEP USED
  - COMPUTING INTENSIVE FOR FINE GRID

N92-32286

Submitted for the CFD Workshop -- 1992

A Status of the Activities of the NASA/MSFC Pump Stage Technology Team

R. Garcia, R. Williams, and Y. Dakhoul

The Consortium for Computational Fluid Dynamics (CFD) Application in Propulsion Technology was established to aid the transfer of CFD related advancements among academia, government agencies, and industry. The specific goals of the Consortium are to develop CFD methodologies necessary to solve propulsion problems, to validate these methodologies, and to apply these methodologies in the design process. To accomplish these goals, a team of experts in various related fields has been formed, a schedule of activities necessary to meet the goals has been generated, and funding for the activities has been obtained from NASA. During the past year (3/91-3/92) the team's activities have focused on preliminary code validation and on the design of an advanced impeller. Six codes were used to calculate the flow in a Rocketdyne 0.3 flow coefficient inducer and the results were compared to L2F data available for the inducer. This activity identified shortcomings in the experimental data sets and in the analytical solutions which must be surmounted in any future team activity. The design of the advanced impeller relied heavily on CFD results to obtain an optimized geometry. The optimized geometry has been analyzed using four different codes and at design and off-design conditions. Activities for the next year include the optimization of a tandem blade impeller design, benchmark of CFD codes for diffuser and volute flows, the collection of L2F data for "state-of-the-art" impeller and inducer, and the verification of the advanced pump team impeller design in a water rig.

PRECEDING PAGE BLANK NOT FILMED

A Summary of the Activities of the NASA/MSFC

Pump Stage Technology Team

R. Garcia
NASA, Marshall Space Flight Center

R. Williams
NASA, Marshall Space Flight Center

Y. Dakhoul
Sverdrup Technologies

Presented:
CFD Applications Workshop
MSFC, April 28–30, 1992

National Aeronautics and Space Administration

A Summary of the Activities of the NASA/MSFC Pump Stage Technology Team

Overview

- Structure/objectives
- Approach
- Validation data
- CFD Analysis:
  - Benchmark activity
  - Advanced hardware
- Summary/conclusions

National Aeronautics and
Space Administration

A Summary of the Activities of the NASA/MSFC Pump Stage Technology Team

Structure/Objectives

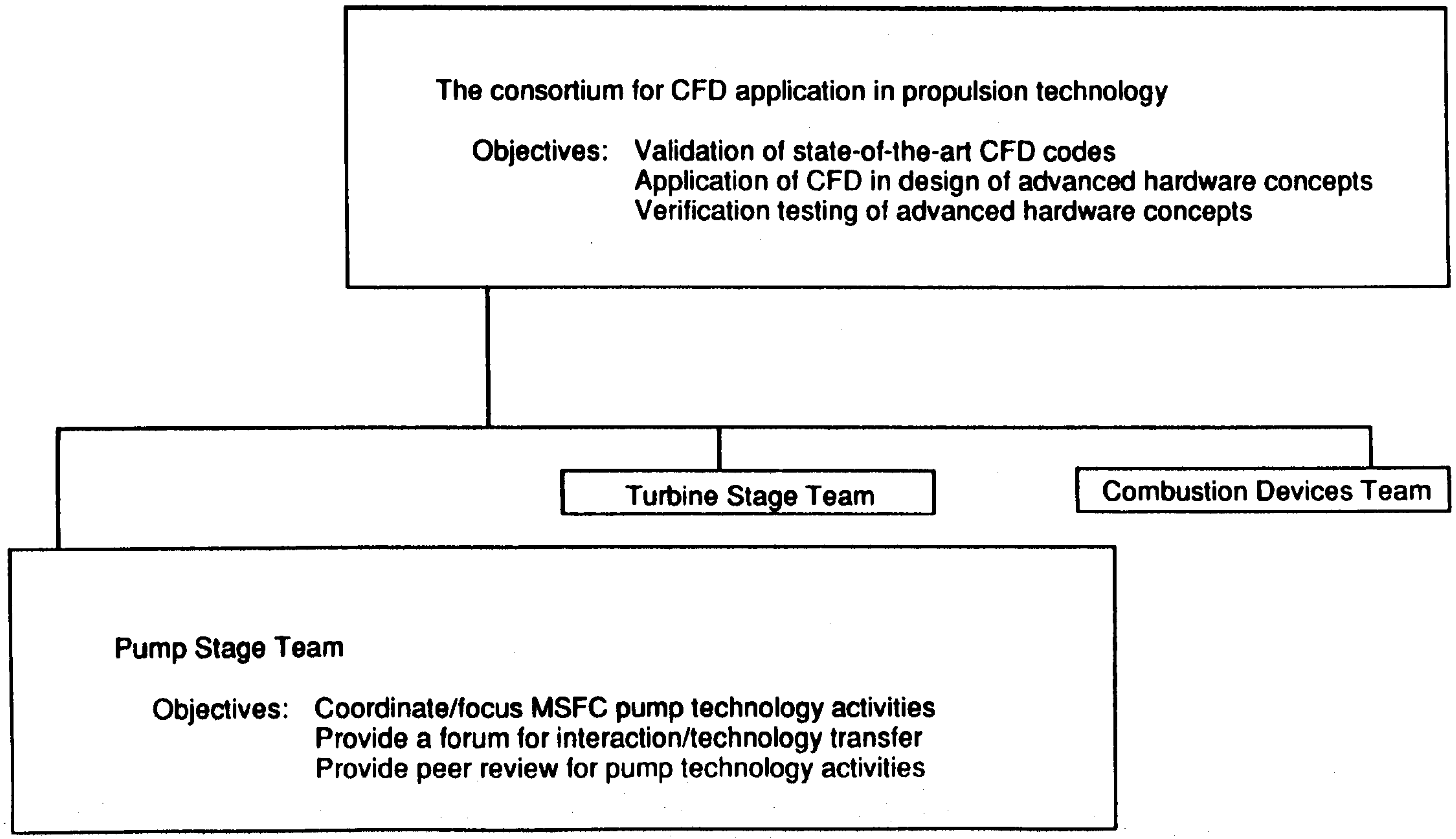

NASA
National Aeronautics and Space Administration

A Summary of the Activities of the NASA/MSFC Pump Stage Technology Team

Approach

- Assemble a team of experts
  - Team members from academia, industry, and government agencies
- Implement a plan to coordinate pump team activities
  - Set milestone dates consistent with rocket engine development requirements
- Hold quarterly meetings to:
  - Critique activities
  - Raise unexpected/new issues and requirements
  - Maintain focus on the deliverable product and on the schedule

National Aeronautics and Space Administration

A Summary of the Activities of the NASA/MSFC Pump Stage Technology Team

Pump Team Members

Consortium for CFD Application In Propulsion Technology Pump Stage Technology Team

- NASA Marshall Space Flight Center (MSFC)
- NASA Ames Research Center (ARC)
- NASA Lewis Research Center (LeRC)
- David Taylor Research Center
- Rocketdyne (RDYN)
- Pratt & Whitney (P&W)
- Aerojet
- Ingersoll-Rand
- Computational Fluid Dynamics (CFD) Research Corporation
- SECA
- Scientific Research Associates (SRA)
- The University of Alabama in Huntsville (UAH)
- Pennsylvania State University (PSU)
- University of Cincinnati
- Virginia Polytechnic Institute
- California Institute of Technology

PUMP DESIGN TECHNOLOGY

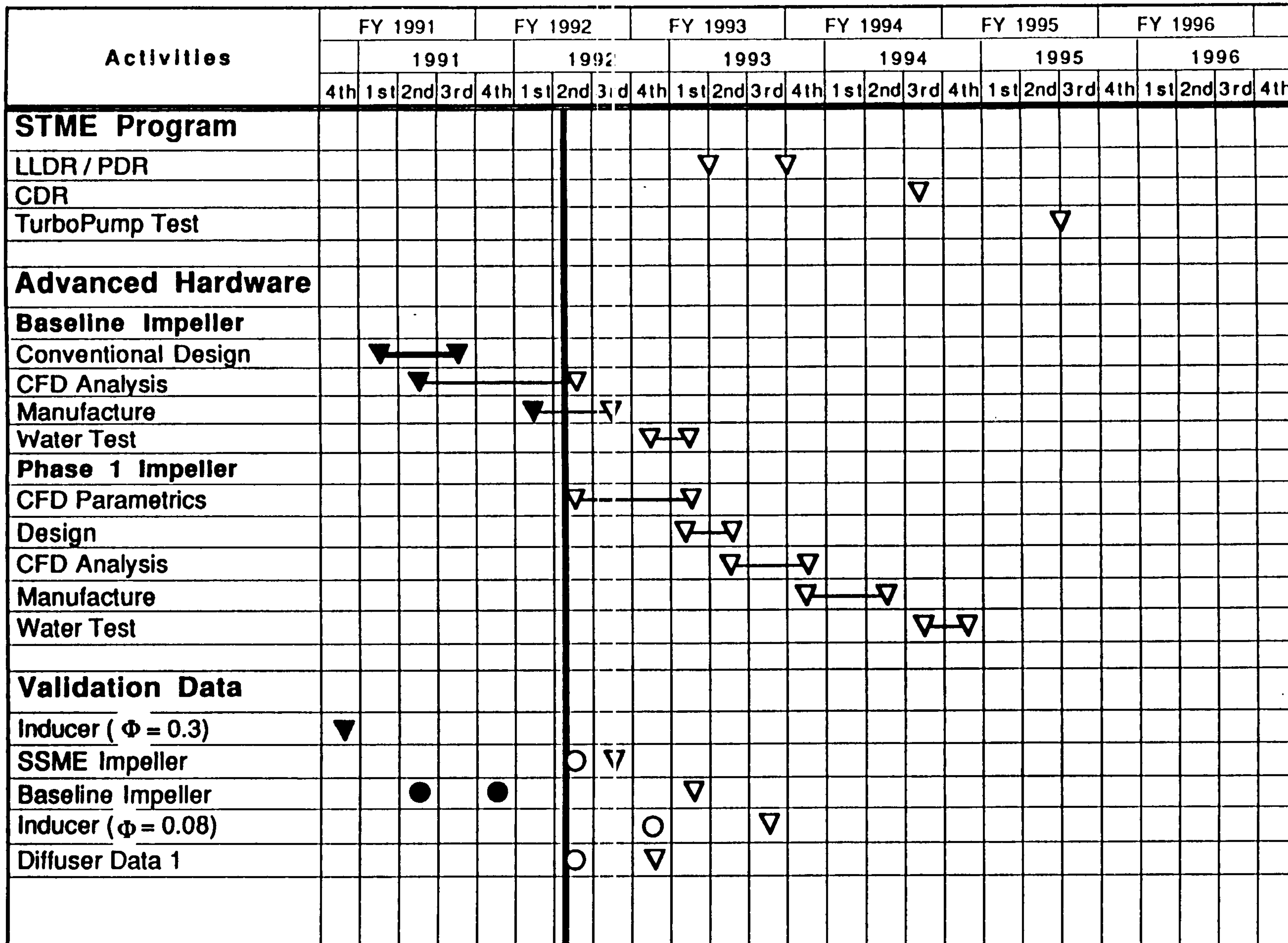

Sunday, April 26, 1992

PUMP DESIGN TECHNOLOGY

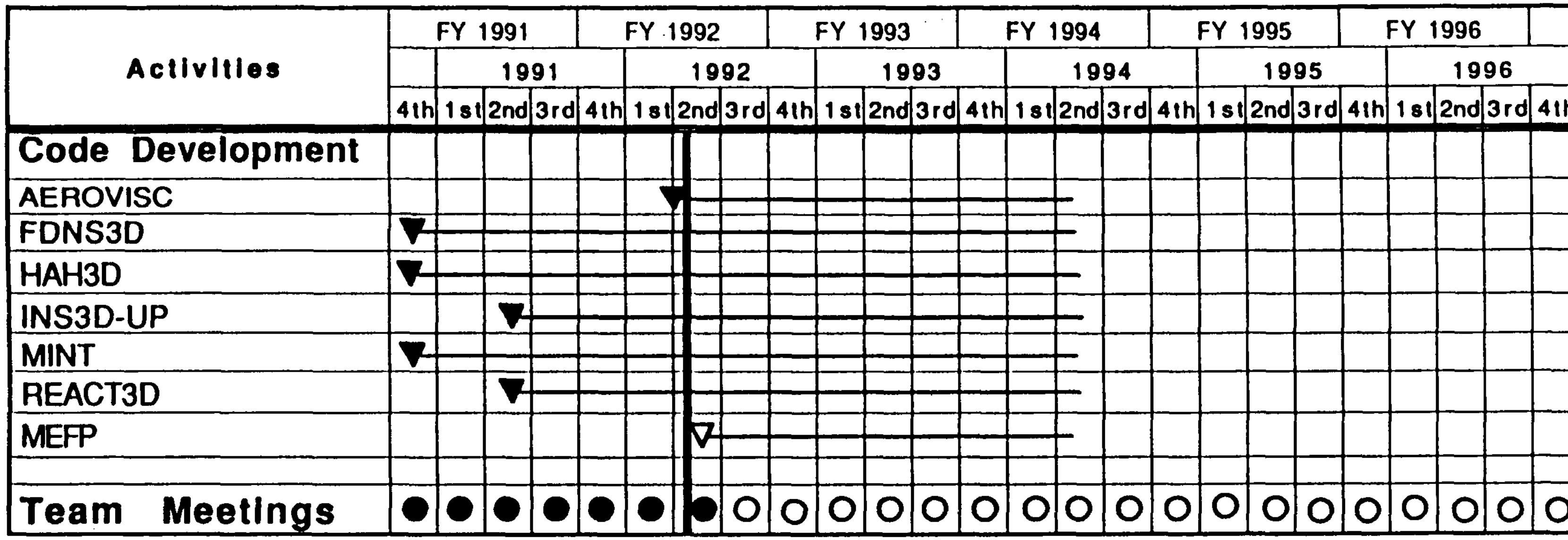

Sunday, April 26, 1992

CFD Code Verification Inducer
Data Planes and Geometry Definition

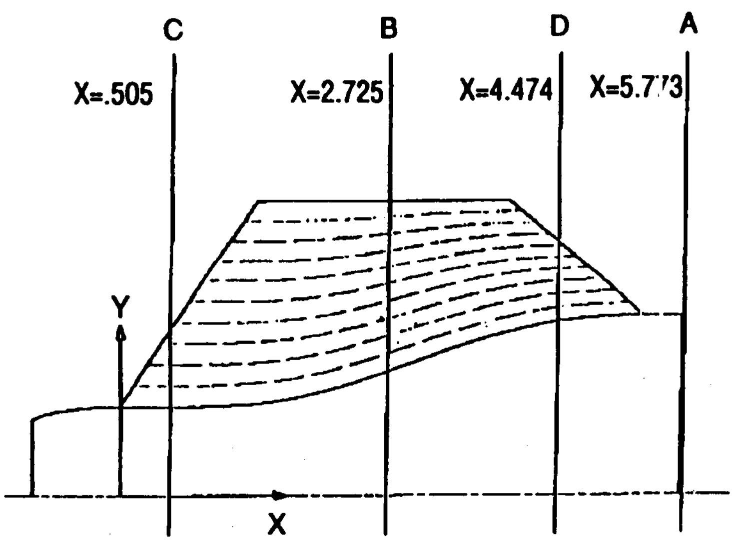

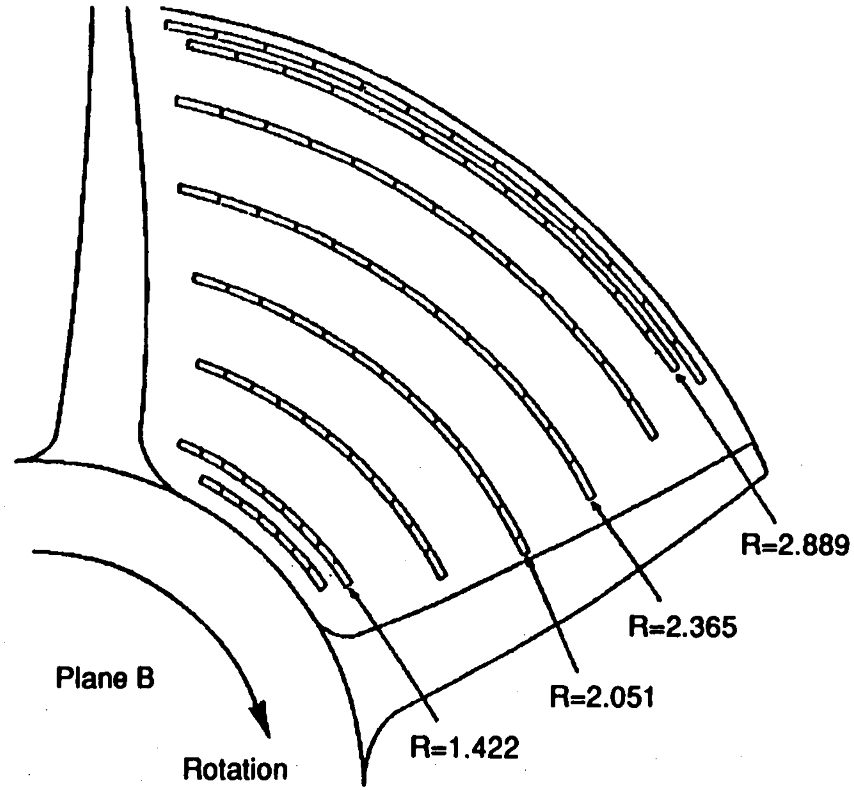

Pump CFD Code Validation Tests SMSME HPFTP Impeller

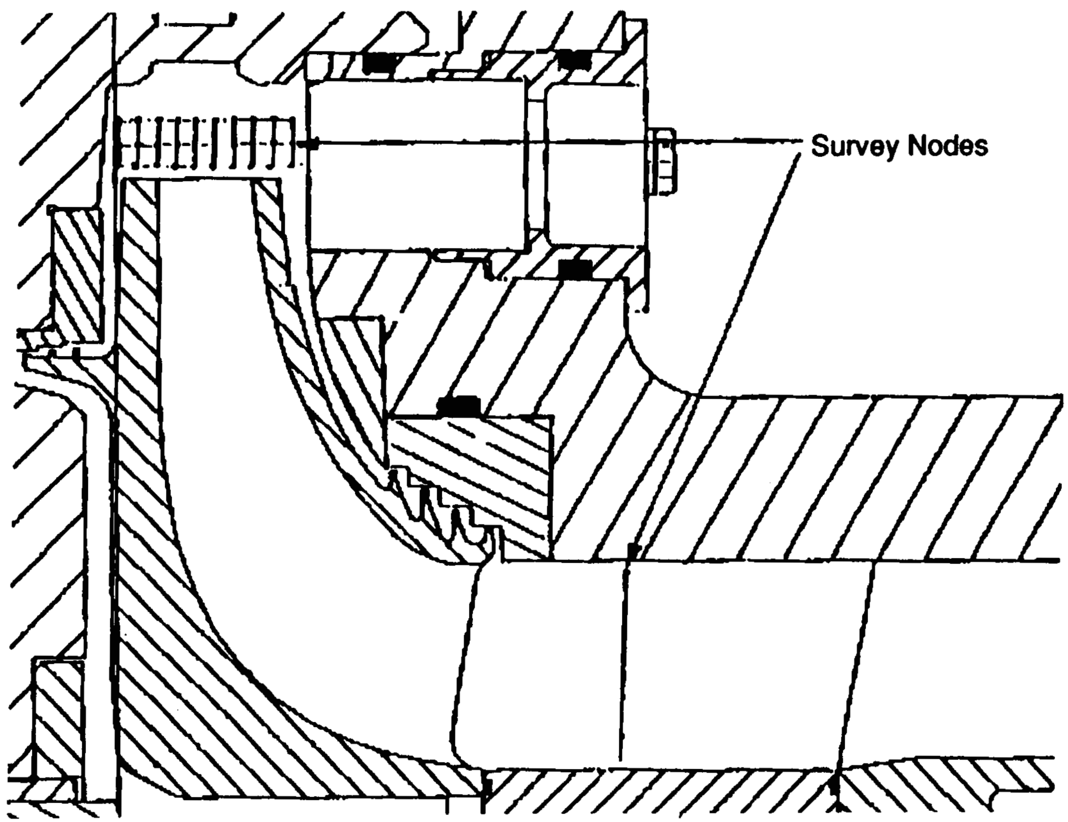

ORIGINAL PAGE IS
OF POOR QUALITY

A Summary of the Activities of the NASA/MSFC Pump Stage Technology Team

CFD Analysis

- Advanced hardware development
  - Conventionally designed advanced impeller optimized using CFD
    - Impeller design to satisfy STME fuel pump requirements with two stages
    - CFD study of 15 parameters: b_2, β_2, axial length, total wrap angle, and discharge wrap angle difference (hub-to-tip)
    - Viability of CFD parametrics demonstrated
    - Baseline and optimized geometry analyzed by five team members
    - All solutions show higher efficiency and reduced impeller discharge flow distortion
    - Off-design analysis under way
    - Impeller being manufactured; performance to be verified in water rig in the fall of 1992
  - Tandem blade impeller concept
    - Concept has potential for increased head coefficient and efficiency
    - CFD parametric study to begin in May 1992
    - Study to include position of blade split, blade clocking, and chordwise spacing
    - Final configuration to rely entirely on results of parametric study
    - Impeller will be sized to satisfy STME fuel pump requirements

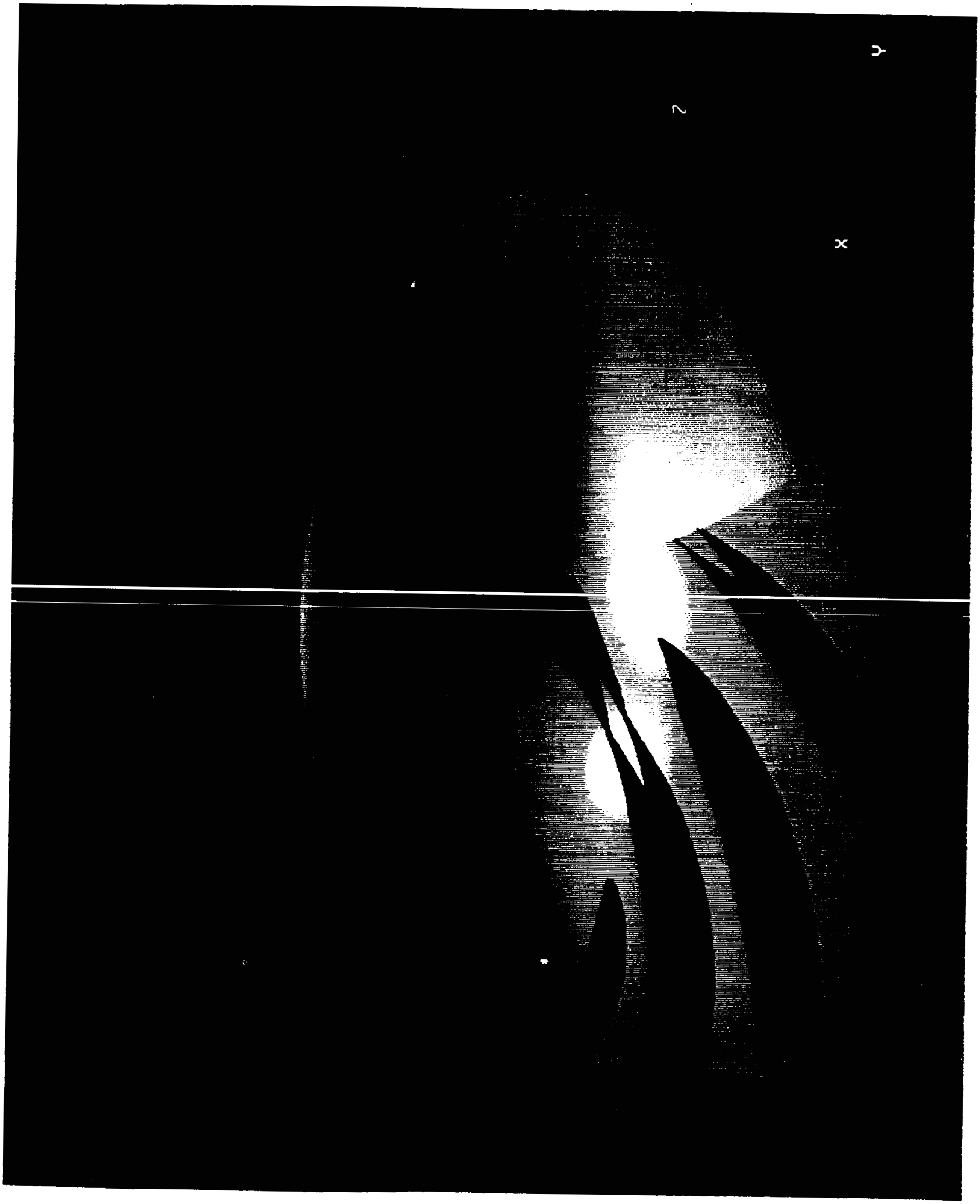

ORIGINAL PAGE IS
OF POOR QUALITY

Cases Postprocessed:

Organization	Inlet Shroud	Exit Walls	Flows
Ames	Fixed	Slip	80%, 100%, 120%
(204 X 33 X 52)			
Lewis	Fixed	Rotating	100%
(73 X 23 X 30)			
Rocketdyne	Rotating	Rotating	100%
(122 X 24 X 30)			
SECA: Case 1	Fixed	Fixed	100%
Case 2	Fixed	Slip	100%
Case 3	Rotating	Fixed	100%
Case 4	Rotating	Rotating	100%
Case 5	Rotating	Slip	100%
(103 X 23 X 30)			
SRA	Fixed	Slip	100%
(121 X 26 X 51)			

OPTIMIZED IMPELLER: INLET CM VS. R

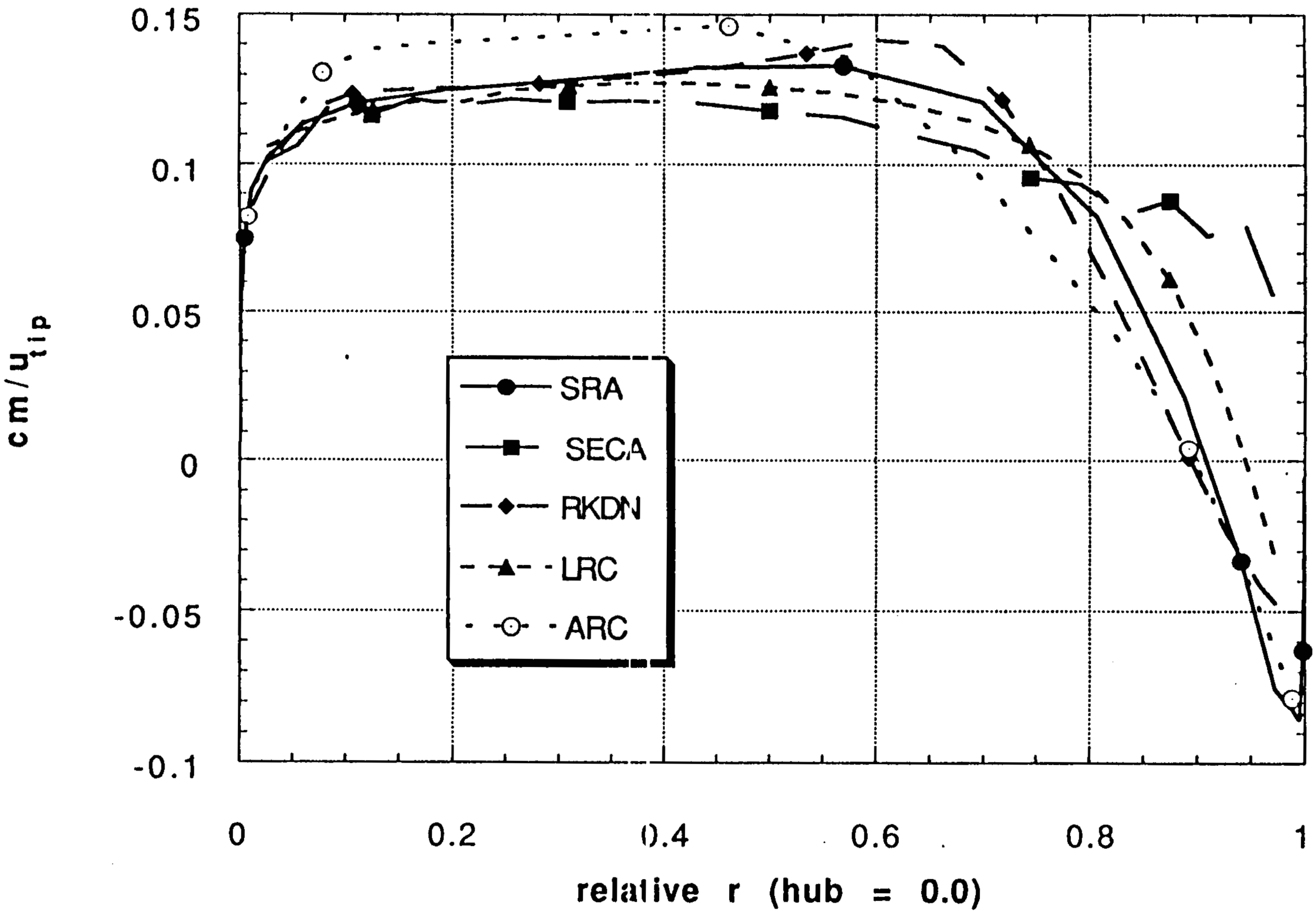

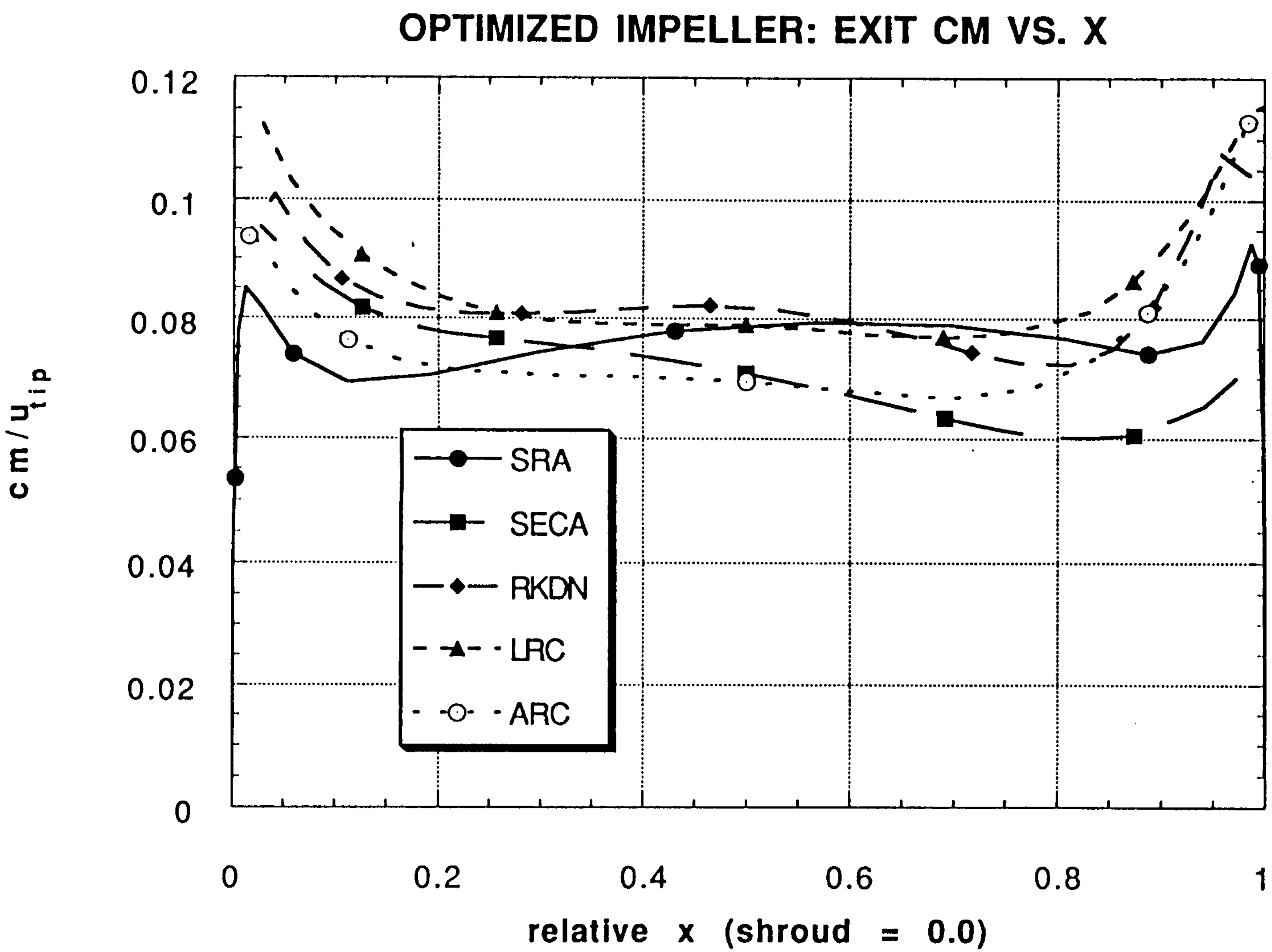
OPTIMIZED IMPELLER: EXIT CM VS. X
0.12
0.1
0.08
0.06
0.04
0.02
0
0
0.2
0.4
0.6
0.8
1
cm/u_tip
relative x (shroud = 0.0)
SRA
SECA
RKDN
LRC
ARC

OPTIMIZED IMPELLER: EXIT CM BLADE-TO-BLADE NEAR THE SHROUD

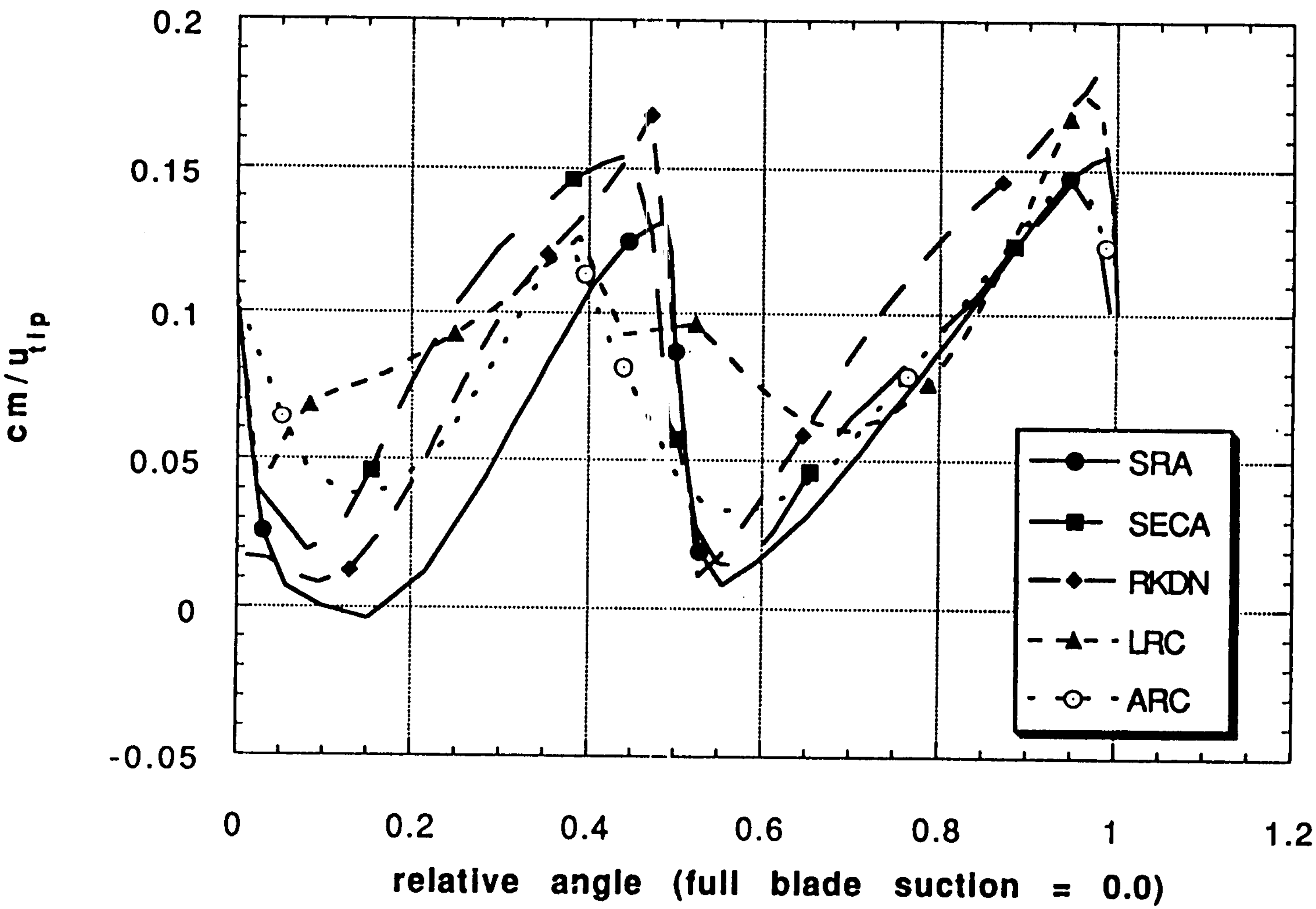

OPTIMIZED IMPELLER: EXIT CM BLADE-TO-BLADE
NEAR THE HUB

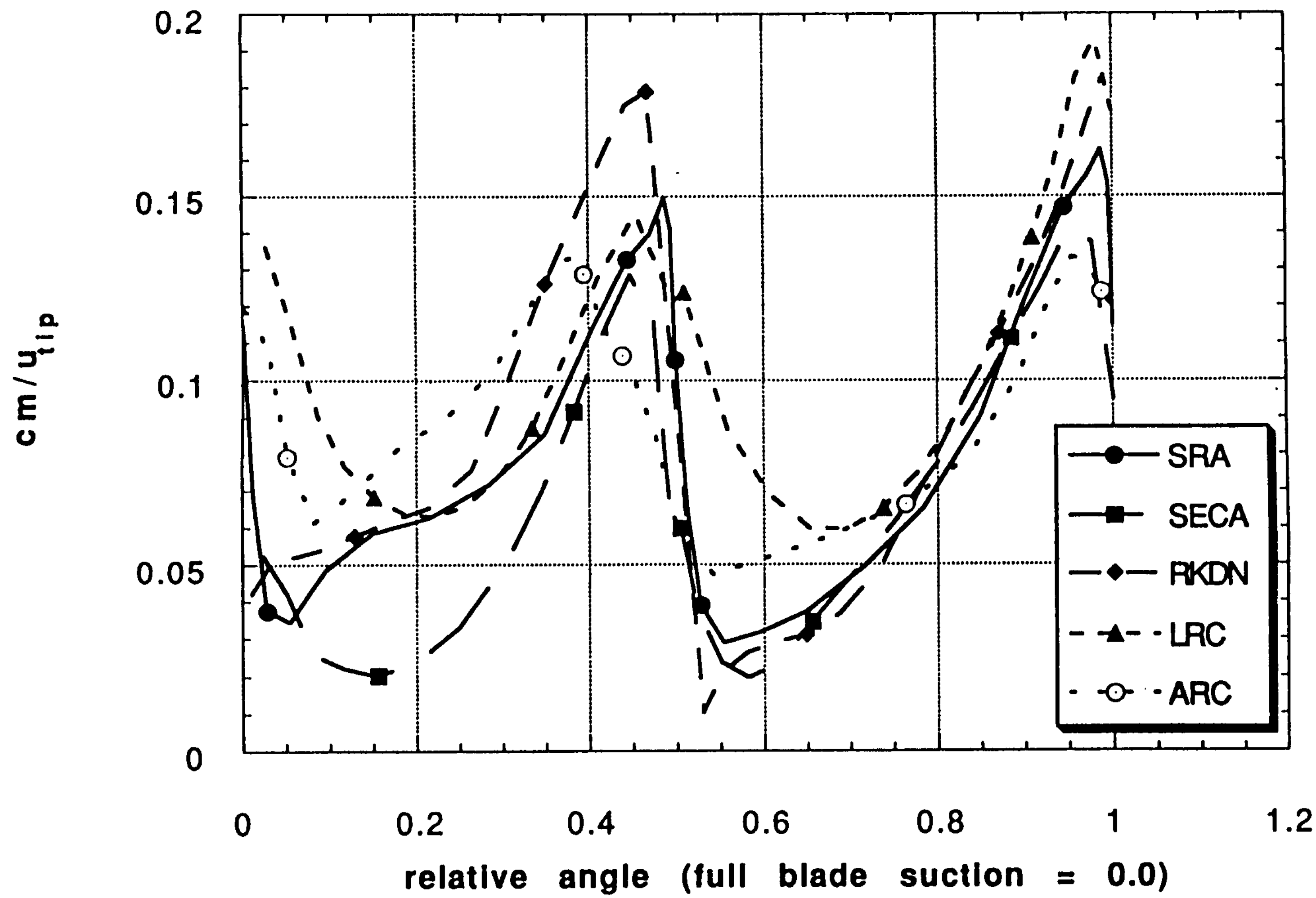

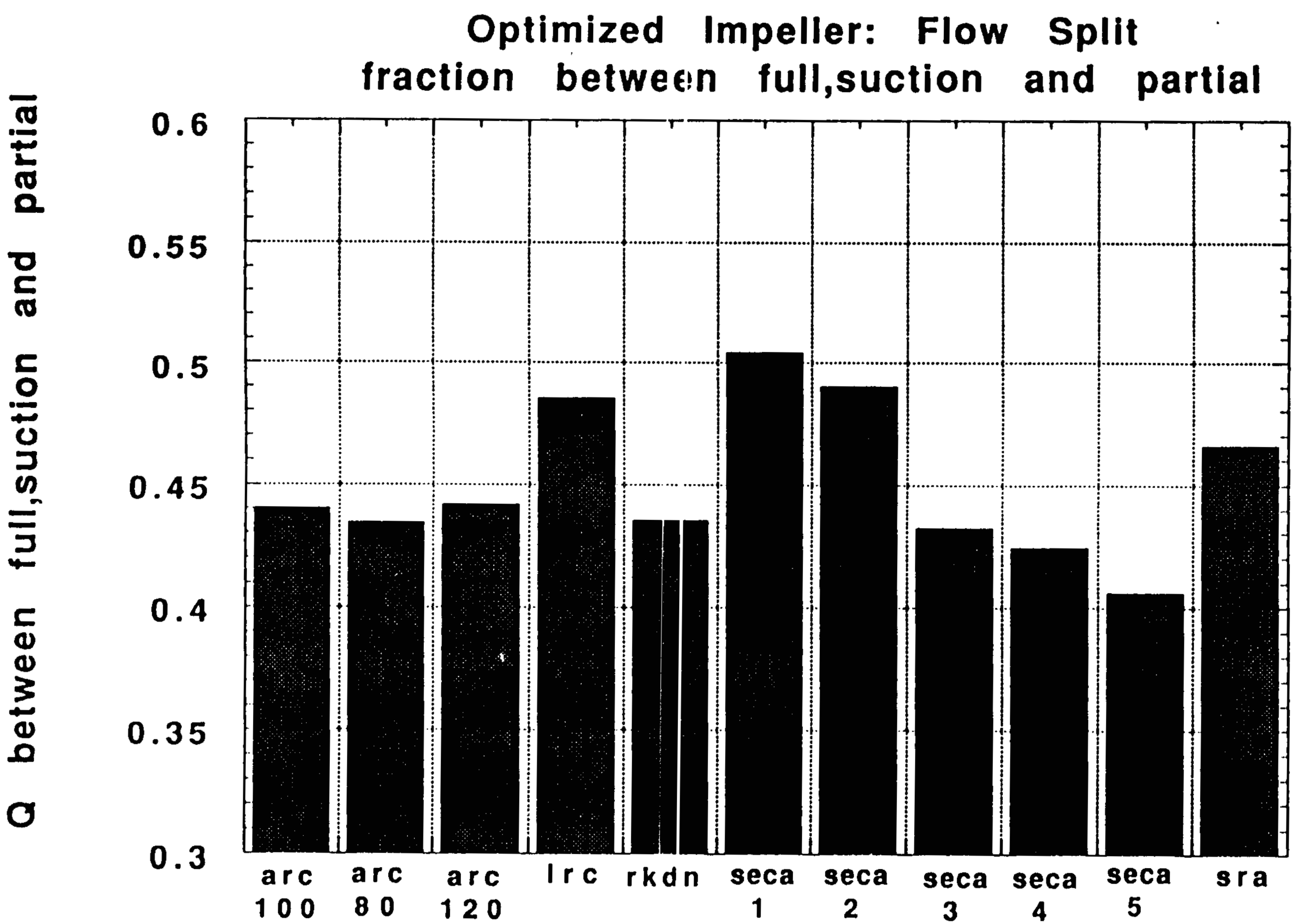
Optimized Impeller: Flow Split
fraction between full,suction and partial
Q between full,suction and partial
0.6
0.55
0.5
0.45
0.4
0.35
0.3
arc 100
arc 80
arc 120
lrc
rkdn
seca 1
seca 2
seca 3
seca 4
seca 5
sra

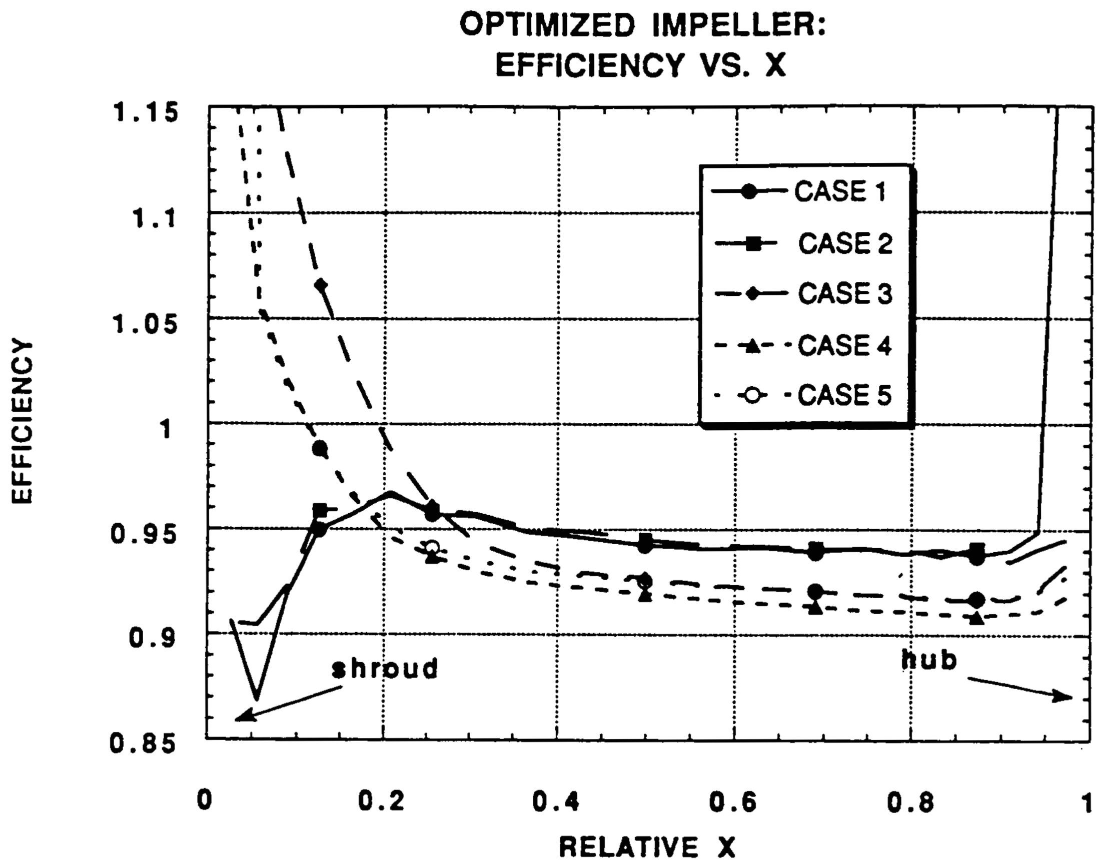
OPTIMIZED IMPELLER:
EFFICIENCY VS. X
EFFICIENCY
1.15
1.1
1.05
1
0.95
0.9
0.85
0
0.2
0.4
0.6
0.8
1
RELATIVE X
CASE 1
CASE 2
CASE 3
CASE 4
CASE 5
shroud
hub

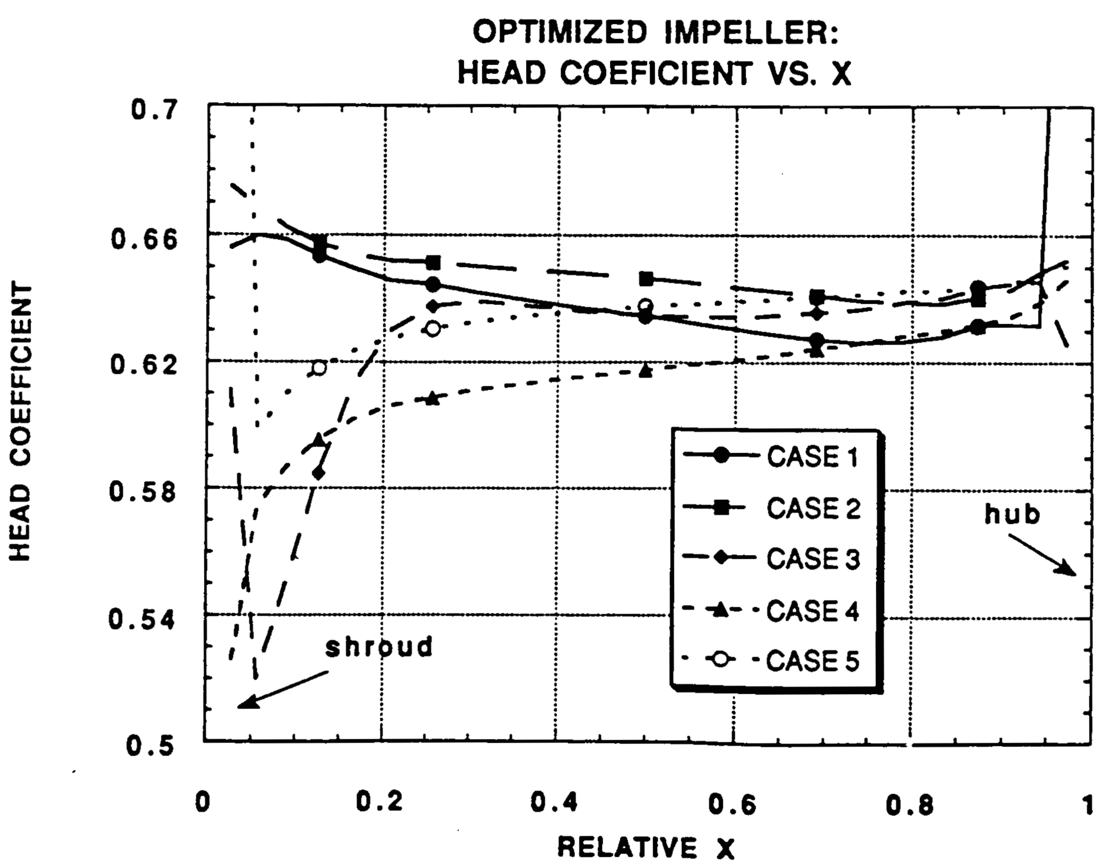
OPTIMIZED IMPELLER:
HEAD COEFICIENT VS. X
HEAD COEFFICIENT
0.7
0.66
0.62
0.58
0.54
0.5
0
0.2
0.4
0.6
0.8
1
RELATIVE X
CASE 1
CASE 2
CASE 3
CASE 4
CASE 5
hub
shroud

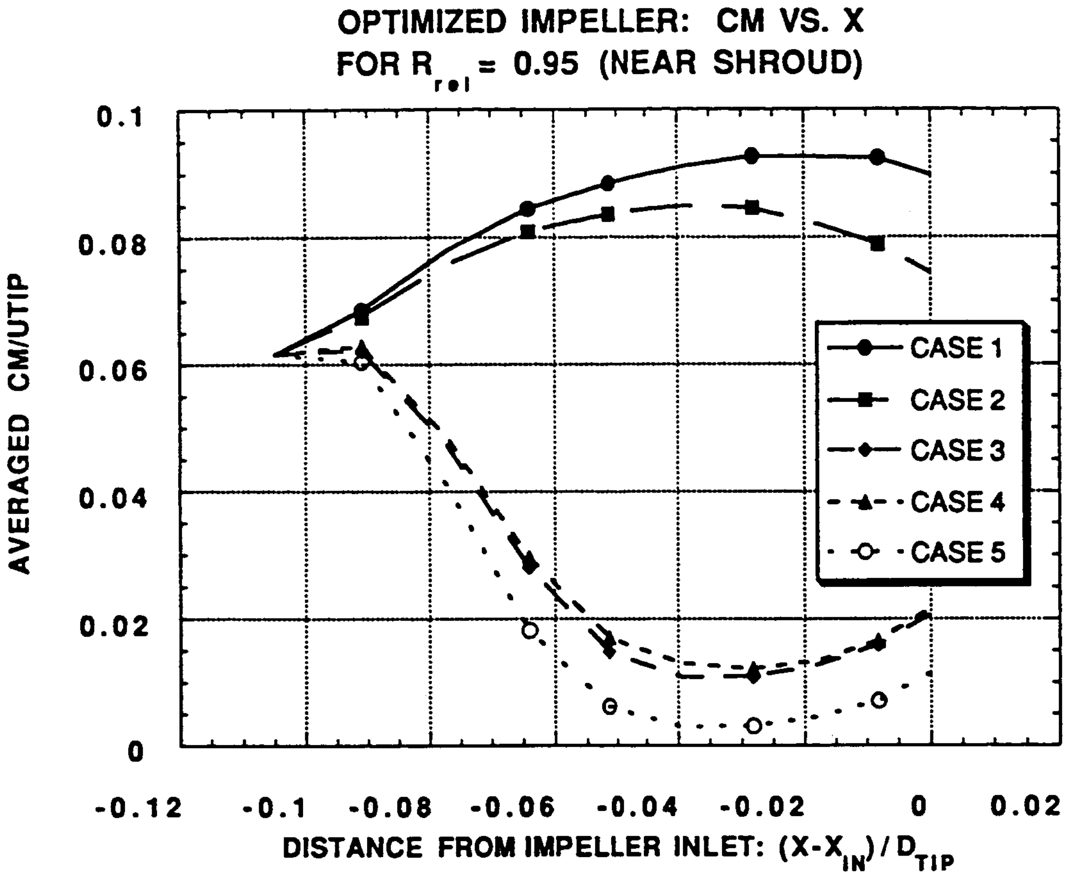

OPTIMIZED IMPELLER: CM VS. X
FOR R_{rel} = 0.95 (NEAR SHROUD)
AVERAGED CM/UTIP
DISTANCE FROM IMPELLER INLET: $(X-X_{IN})/D_{TIP}$
CASE 1
CASE 2
CASE 3
CASE 4
CASE 5

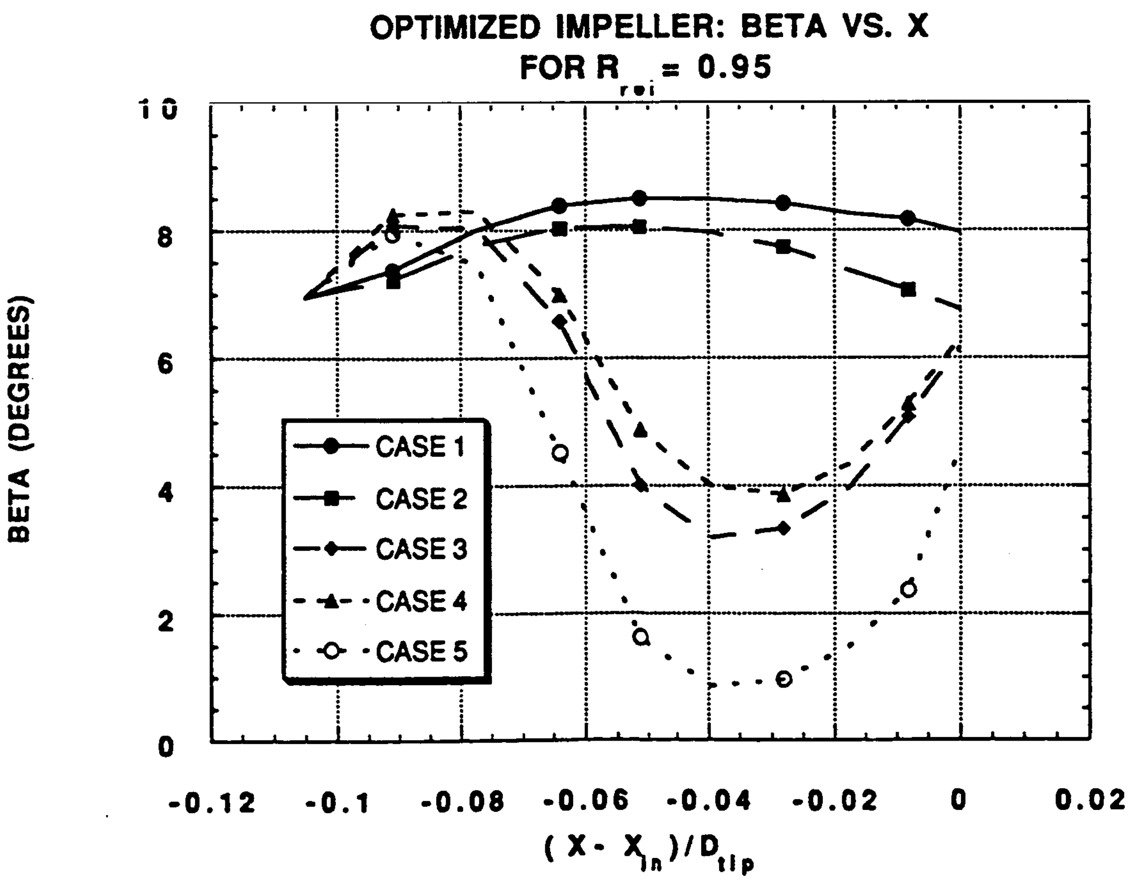

OPTIMIZED IMPELLER: BETA VS. X
FOR R_{rel} = 0.95
BETA (DEGREES)
$(X-X_{in})/D_{tip}$
CASE 1
CASE 2
CASE 3
CASE 4
CASE 5

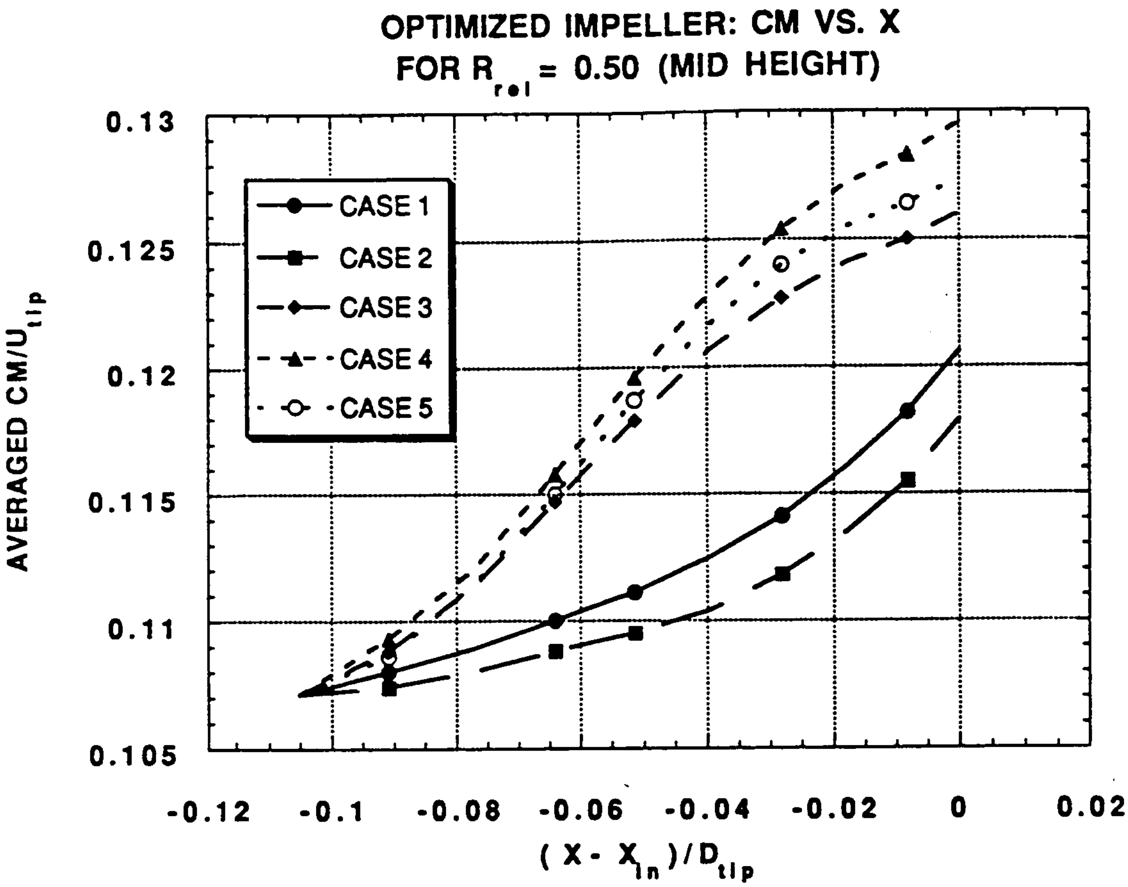
OPTIMIZED IMPELLER: CM VS. X
FOR R rel = 0.50 (MID HEIGHT)
AVERAGED CM/U tip
(X - X in)/D tip
CASE 1
CASE 2
CASE 3
CASE 4
CASE 5
0.13
0.125
0.12
0.115
0.11
0.105
-0.12
-0.1
-0.08
-0.06
-0.04
-0.02
0
0.02

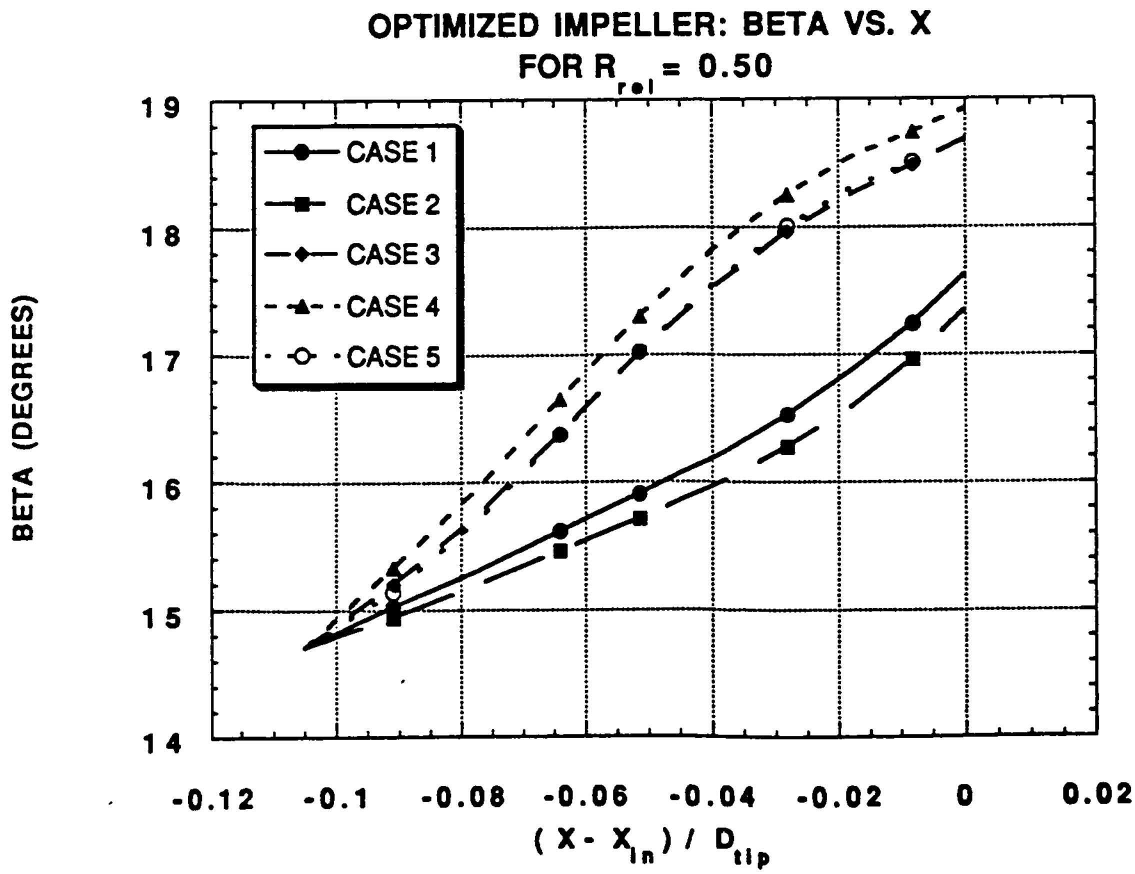
OPTIMIZED IMPELLER: BETA VS. X
FOR R rel = 0.50
BETA (DEGREES)
(X - X in) / D tip
CASE 1
CASE 2
CASE 3
CASE 4
CASE 5
19
18
17
16
15
14
-0.12
-0.1
-0.08
-0.06
-0.04
-0.02
0
0.02

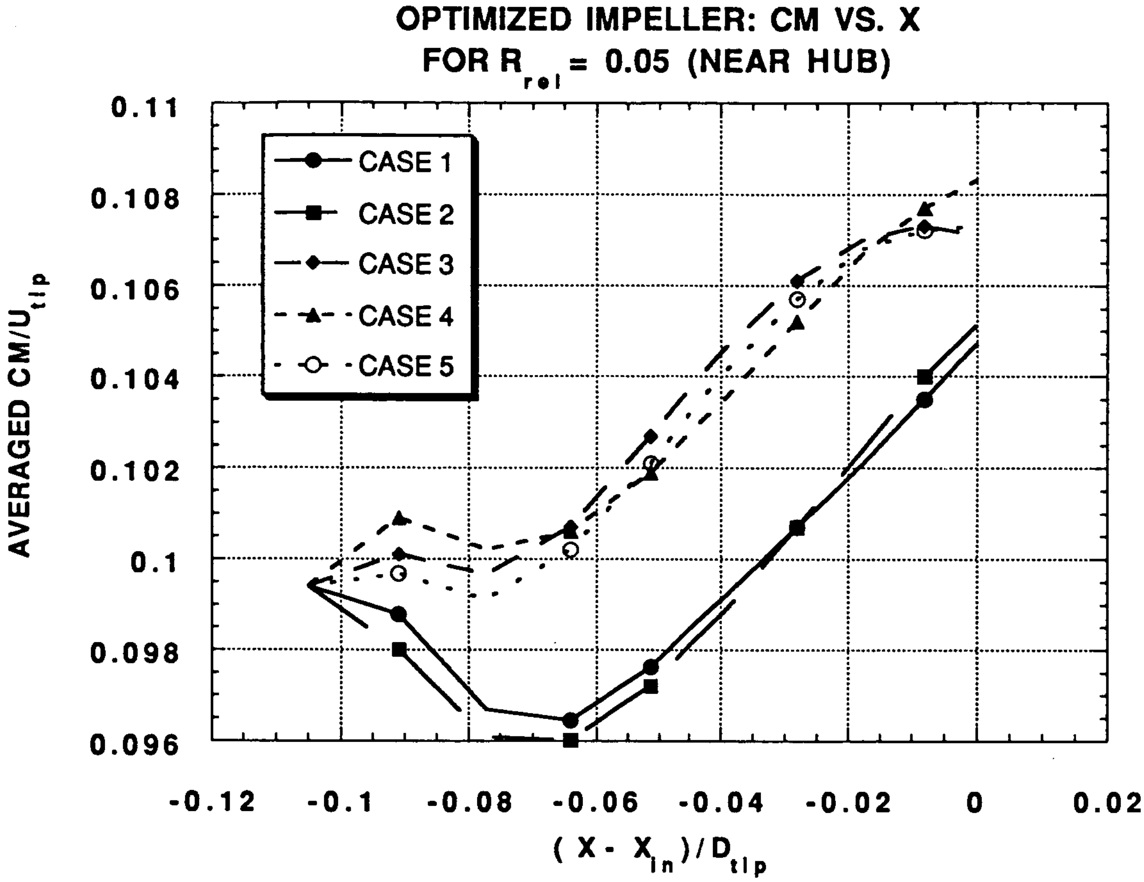
OPTIMIZED IMPELLER: CM VS. X
FOR R_{rel} = 0.05 (NEAR HUB)
AVERAGED CM/U_{tip}
0.11
0.108
0.106
0.104
0.102
0.1
0.098
0.096
CASE 1
CASE 2
CASE 3
CASE 4
CASE 5
-0.12
-0.1
-0.08
-0.06
-0.04
-0.02
0
0.02
$(X - X_{in})/D_{tip}$

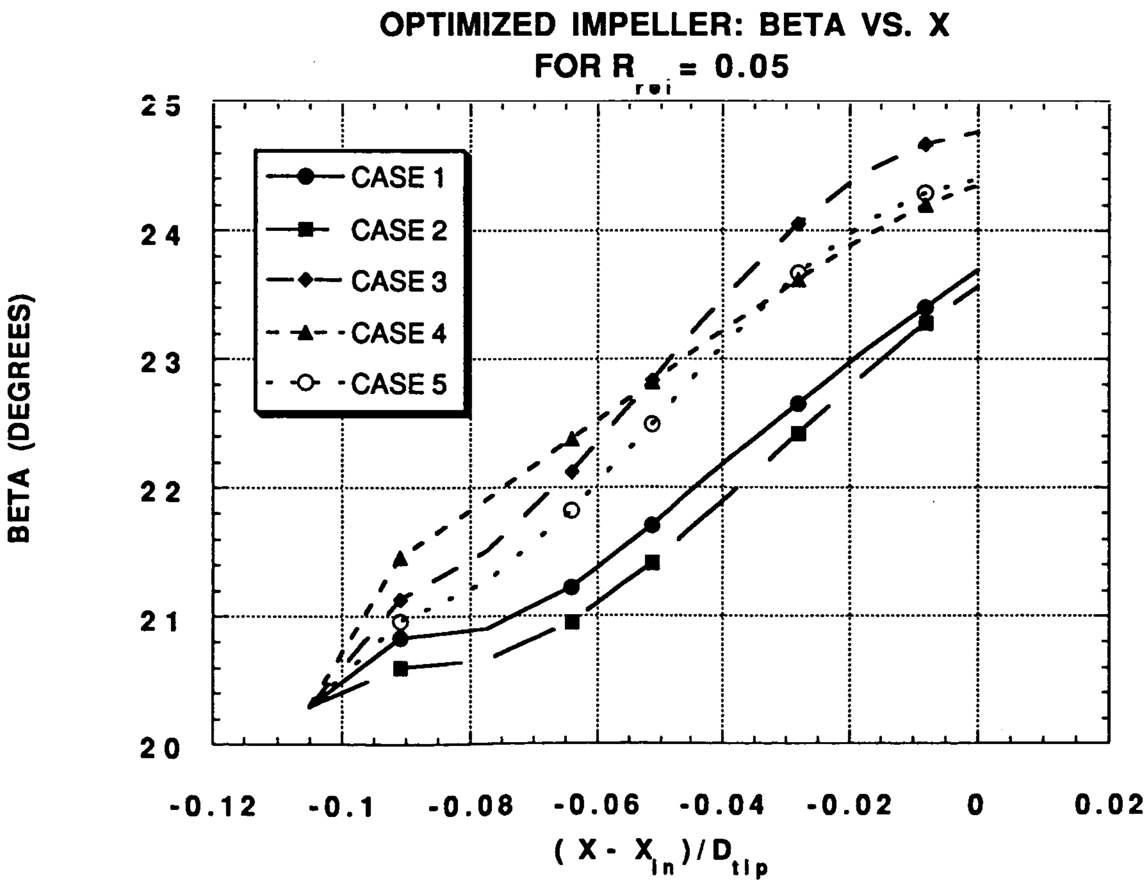
OPTIMIZED IMPELLER: BETA VS. X
FOR R_{rel} = 0.05
BETA (DEGREES)
25
24
23
22
21
20
CASE 1
CASE 2
CASE 3
CASE 4
CASE 5
-0.12
-0.1
-0.08
-0.06
-0.04
-0.02
0
0.02
$(X - X_{in})/D_{tip}$

AMES RESULTS: EXIT CM VS. X
FOR VARYING FLOW RATE

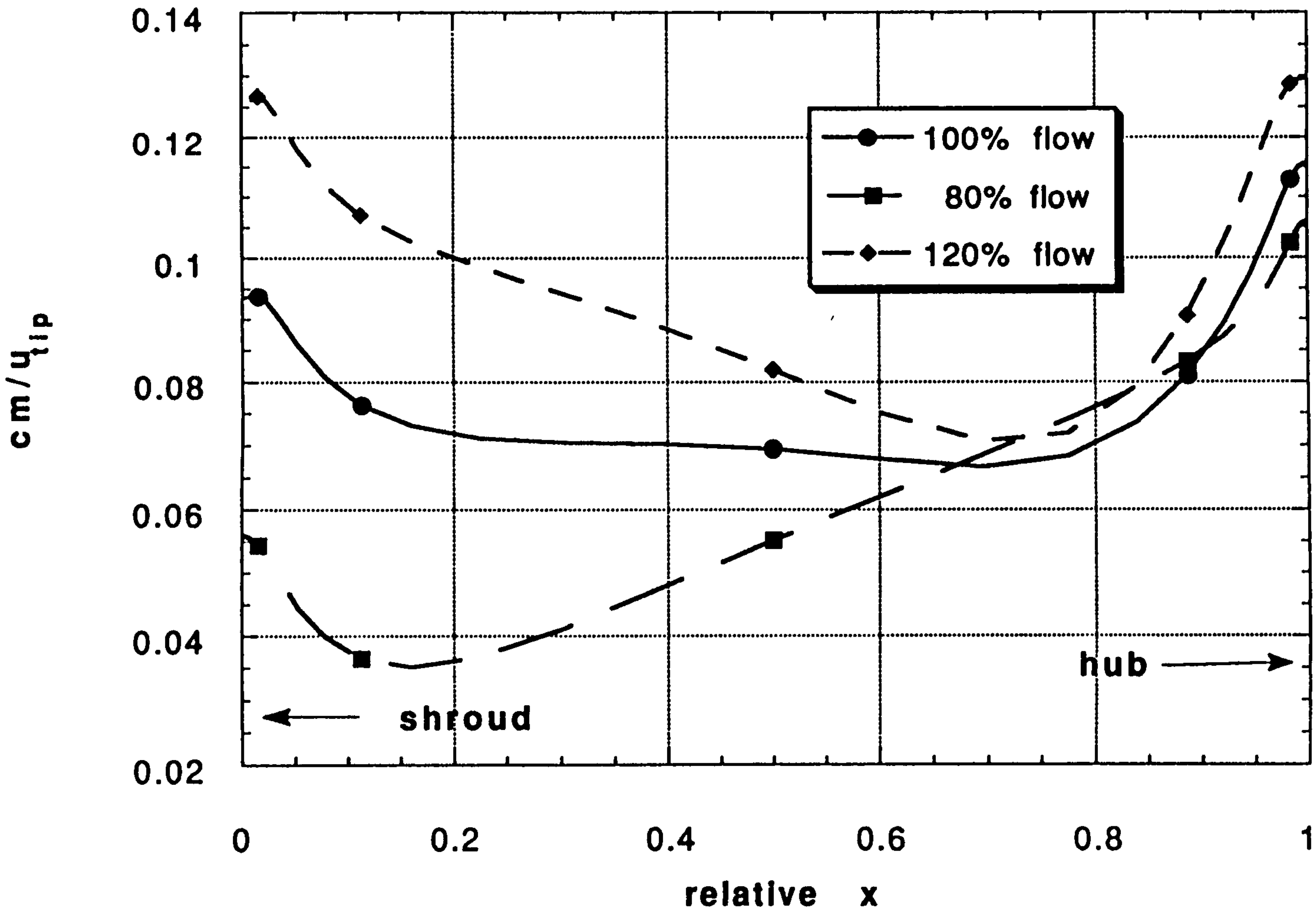

AMES RESULTS: HEAD COEFF. VS. X FOR VARYING FLOW RATE

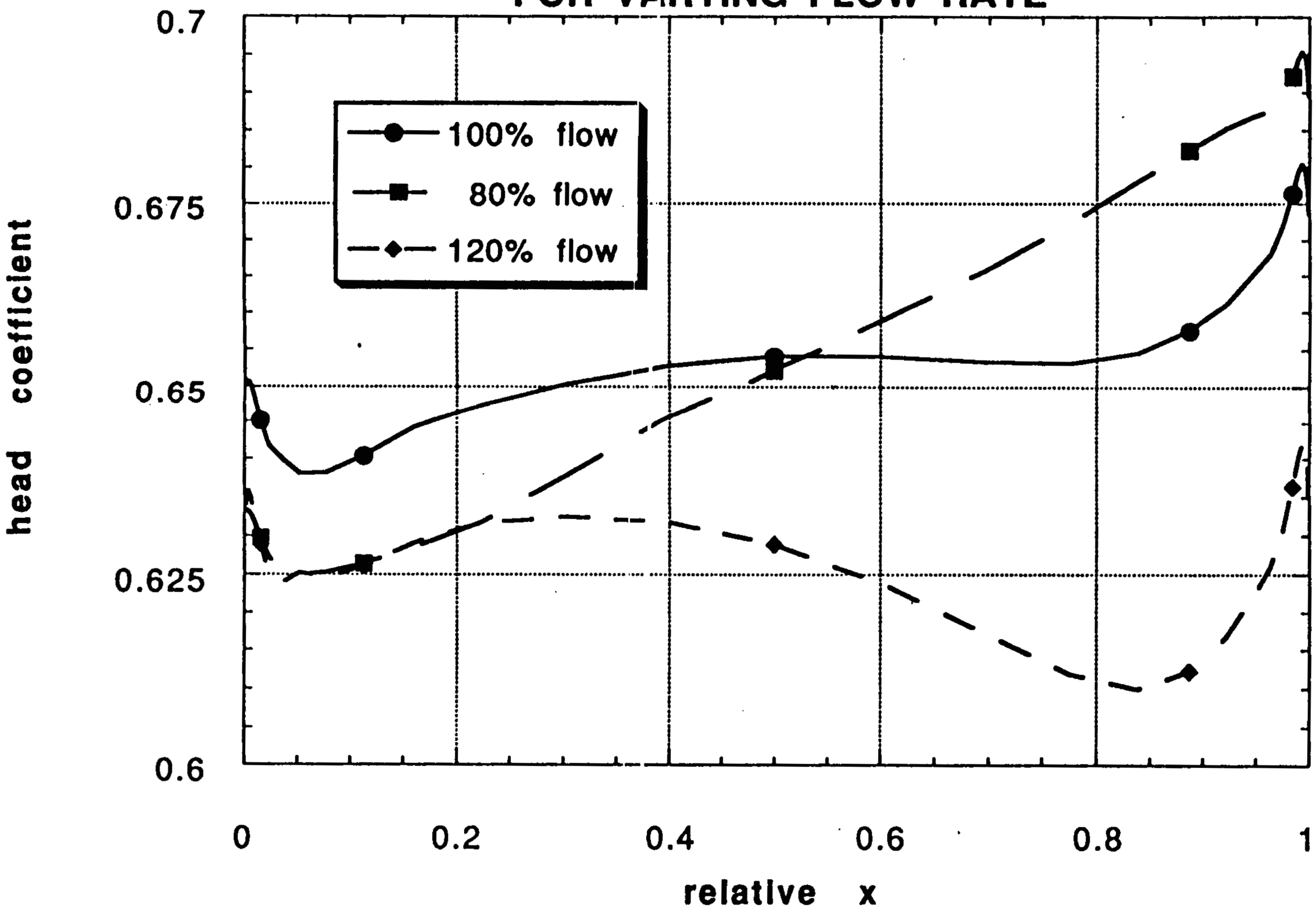

AMES RESULTS: CM UPSTREAM OF IMPELLER FOR 80% FLOW

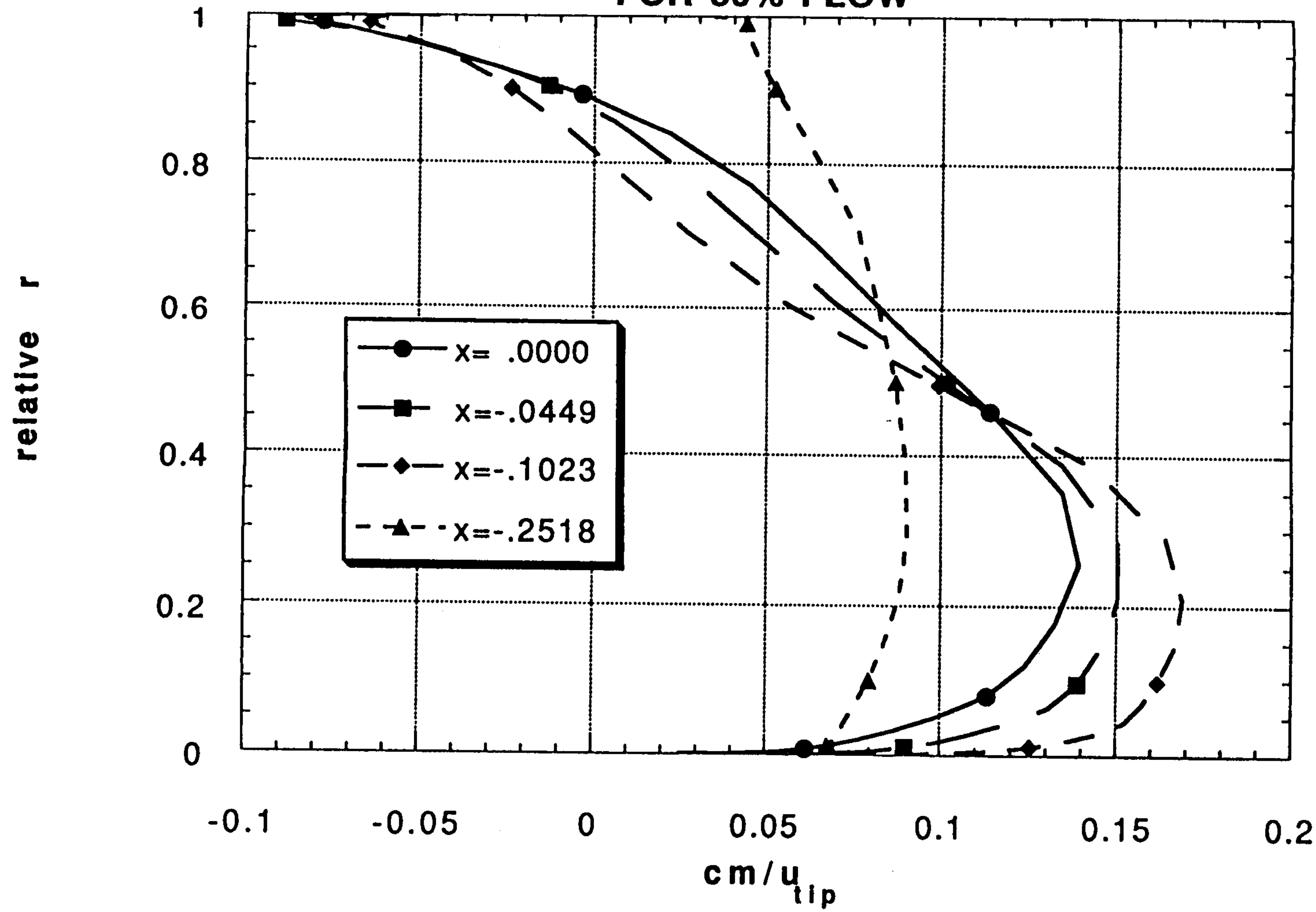

AMES RESULTS: CU UPSTREAM OF IMPELLER FOR 80% FLOW

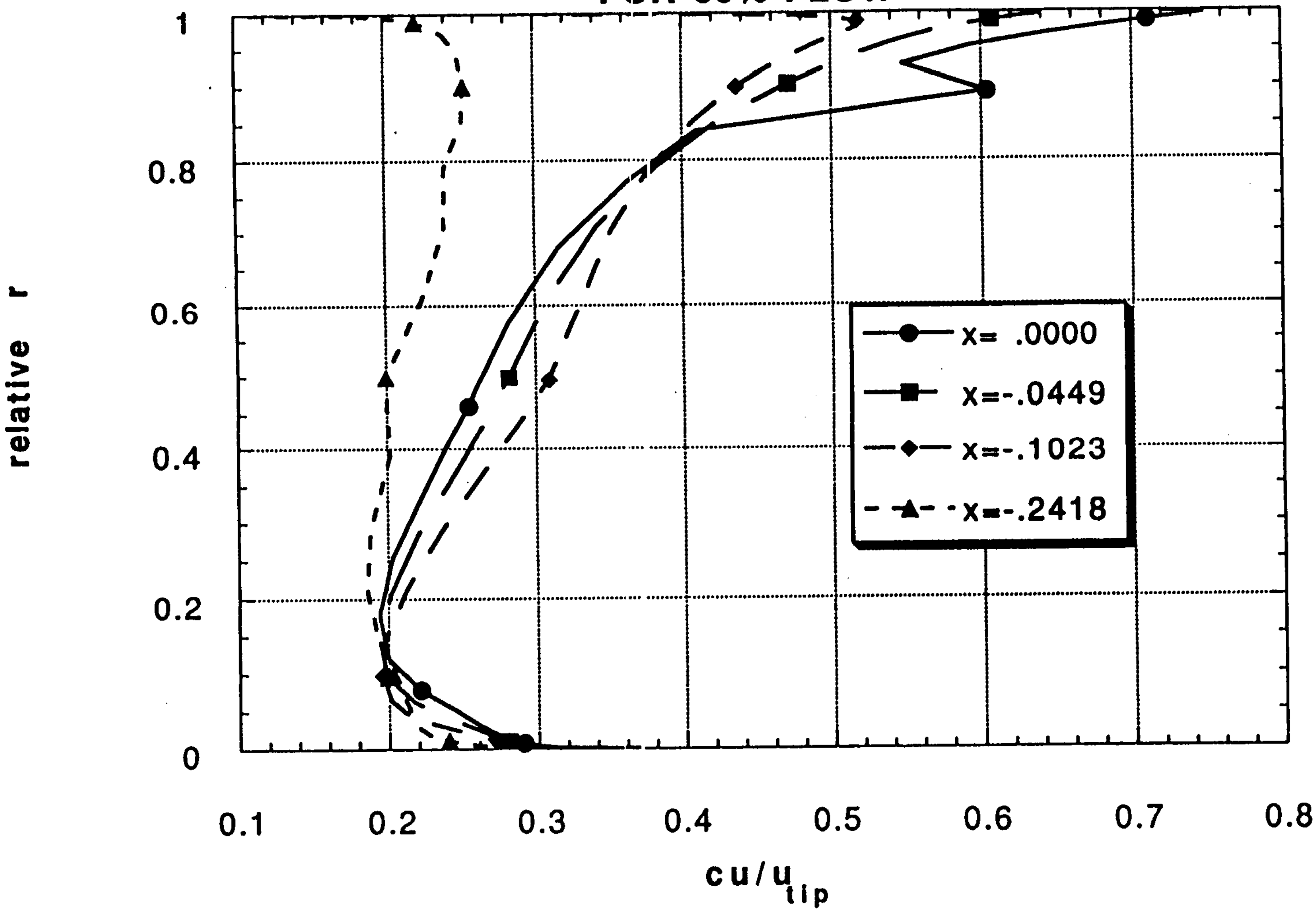

NASA
National Aeronautics and
Space Administration

A Summary of the Activities of the NASA/MSFC Pump Stage Technology Team

Summary/Conclusions

- Technology team in place and functioning efficiently
  - Participation by industry, universities, and government
- Detailed experimental data sets suitable for benchmarking have been or are being generated
- Preliminary evaluation of six different codes complete
- CFD codes being used to reduce the design development time and improve performance of advanced impellers
- Verification of advanced impeller predictions planned for the fall of 1992
- Future work to include impeller-diffuser interaction and inducer non-cavitating analysis

N92-32287

CFD ANALYSIS OF PUMP CONSORTIUM IMPELLER

Gary C. Cheng*, Y.S. Chen†, and R.W. Williams‡

Abstract

Current design of high performance turbopumps for rocket engines requires effective and robust analytical tools to provide design impact in a productive manner. The main goal of this study is to develop a robust and effective computational fluid dynamics (CFD) pump model for general turbopump design and analysis applications. A Navier-Stokes flow solver, FDNS, embedded with the extended k-ε turbulence model and with appropriate moving interface boundary conditions, is developed to analyze turbulent flows in the turbomachinery devices. The FDNS code has been benchmarked with its numerical predictions of the pump consortium inducer, and provides satisfactory results. In the present study, a CFD analysis of the pump consortium impeller will be conducted with the application of the FDNS code. The pump consortium impeller, with partial blades, is the new design concept of the advanced rocket engine. A 3-D flow calculation with 81 x 41 x 41 grid system was conducted for the team base-line impeller. The result shows a massive flow separation occurs between the full-blade pressure surface and the partial-blade suction surface. Similar result was predicted by the other consortium members. A pump consortium optimized impeller, a revision based on the base-line impeller, was then designed by Rocketdyne to remove the flow separation. A 3-D flow analysis, with 103 x 23 x 30 mesh system and with the inlet flow conditions provided by Rocketdyne, was performed for the optimized impeller. The numerical result indicates no flow separation occurs inside the flow passage, which is also consistent with the other consortium members' predictions. However, the flow field inside the optimized impeller as calculated by the team members showed great variations, especially near the exit shroud region. The discrepancy is suspected to be due to different exit boundary conditions used by the consortium members. Therefore, three different exit wall boundary conditions will be further examined by the FDNS code, those are fixed-wall, wall-slip (symmetry), and rotating wall boundary conditions. The computed results will be compared in order to address the effect of exit boundary conditions on the impeller flow field. Meanwhile, two off-design cases of the optimized impeller, 80% and 120% of the design flow, will also be analyzed with a particular exit boundary condition. All CFD analysis of the pump consortium base-line impeller, and the optimized impeller with various exit boundary conditions will be presented in the coming CFD workshop meeting.

* SECA, Inc., 3313 Bob Wallace Ave., Suite 202, Huntsville, AL

† Engineering Sciences, Inc., 4920 Corporate Dr., Suite K, Huntsville, AL

‡ ED 32, NASA/Marshall Space Flight Center, Huntsville, AL

CFD ANALYSIS OF PUMP CONSORTIUM IMPELLER

By

Gary C. Cheng, SECA, Inc.

Y.S. Chen, ESI

AND

R.W. Williams
NASA/Marshall Space Flight Center

NASA Contract No. NAS8-38868

TENTH ANNUAL CFD WORKSHOP MEETING, APRIL, 1992

- **INLET/EXIT WALL B.C. TESTED**

		Exit B.C.		
		Fixed-Wall	Rotating-Wall	Wall-Slip
Inlet B.C.	Fixed-Wall	Case 1	N/A	Case 2
	Rotating-Wall	Case 3	Case 4	Case 5

- **CALCULATED MASS FLOW RATE SPLIT**

	Case 1	Case 2	Case 3	Case 4	Case 5
S.F. - P.P. /S.P. - P.F.	50.4/49.6	49/51	43.2/56.8	42.4/57.6	40.6/59.4

DEFINITION OF PERFORMANCE PARAMETERS

- $C_u = c_u / U_{tip}$; $C_M = c_M / U_{tip}$ where c_u = Absolute Tangential Velocity, c_M = Meridional Velocity, U_{tip} = Wheel Tip Velocity
- β = Relative Flow Angle Relative to Tangential Direction
- Relative Radius = $(R_i - R_{hub}) / (R_{shroud} - R_{hub})$
- Relative X = $(X_i - X_{shroud}) / (X_{hub} - X_{shroud})$
- Relative Angle = $(Angle_i - Angle_{suction}) / (Angle_{pressure} - Angle_{suction})$
- Ψ (Head Coefficient) = $\Delta H_t g / U_{tip}^2$
- η (Efficiency) = Head Rise / Euler Head Rise

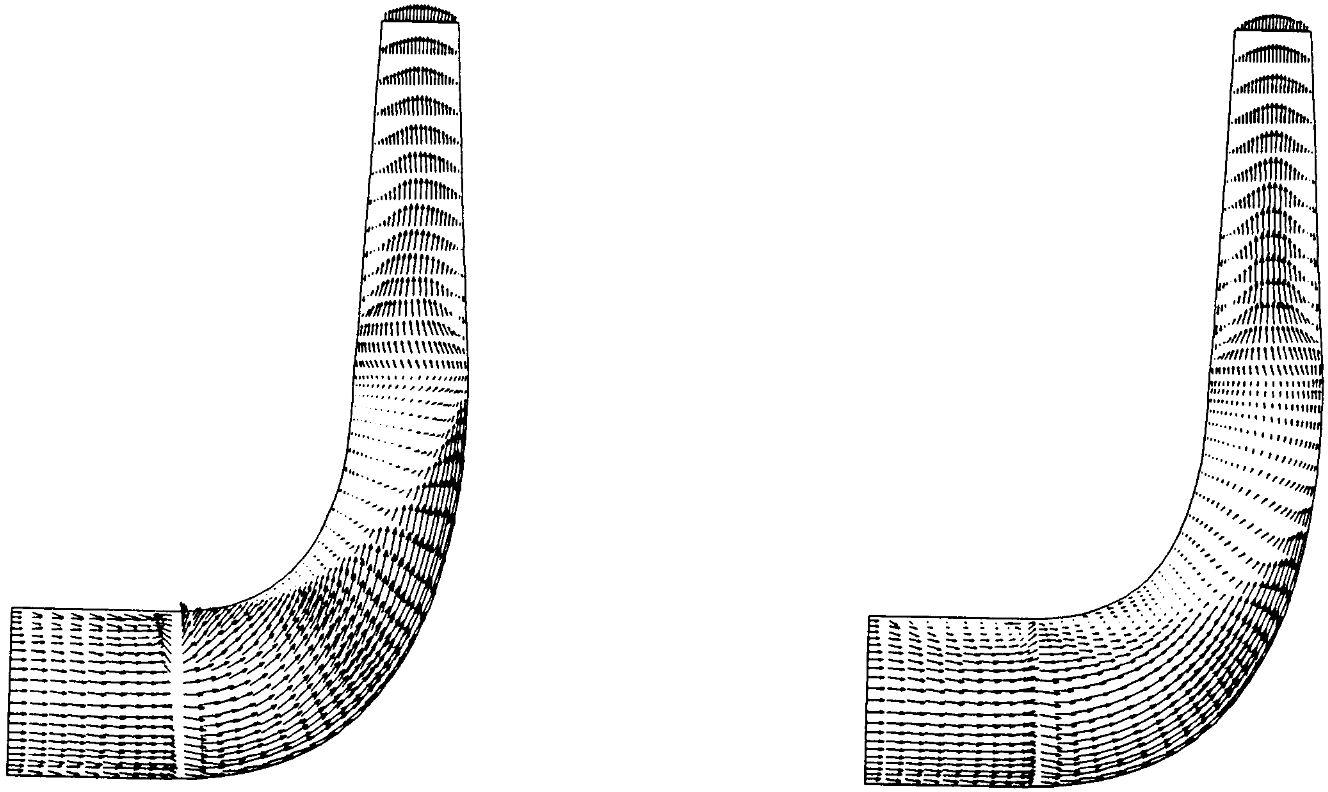

Case 1

Case 3

VELOCITY VECTORS NEAR SUCTION SIDE OF BLADE

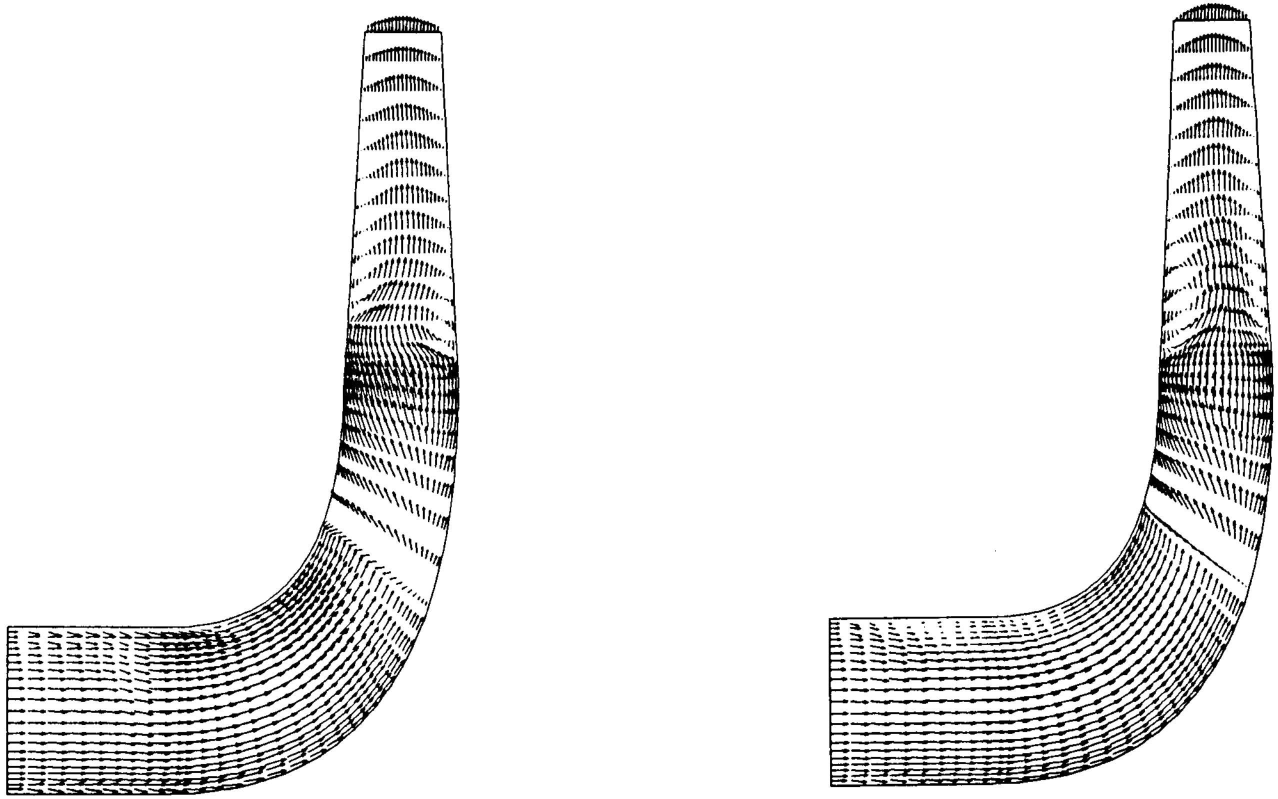

Case 1

Case 3

VELOCITY VECTORS NEAR PRESSURE SIDE OF SPLITTER

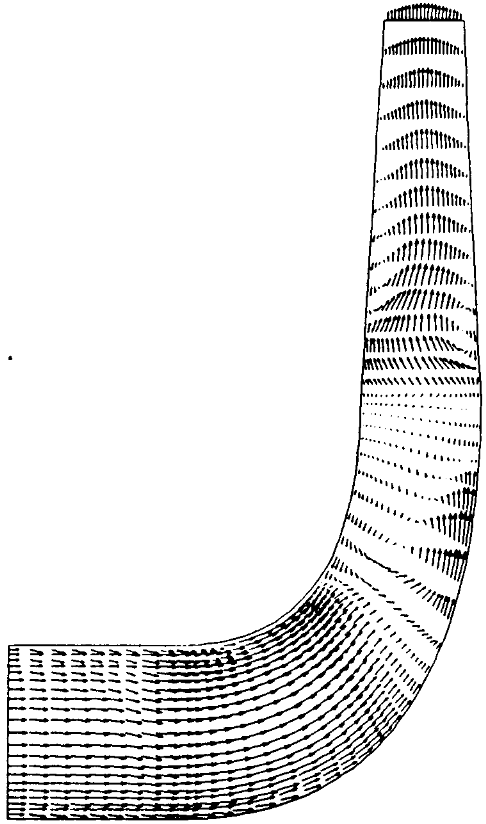

Case 1

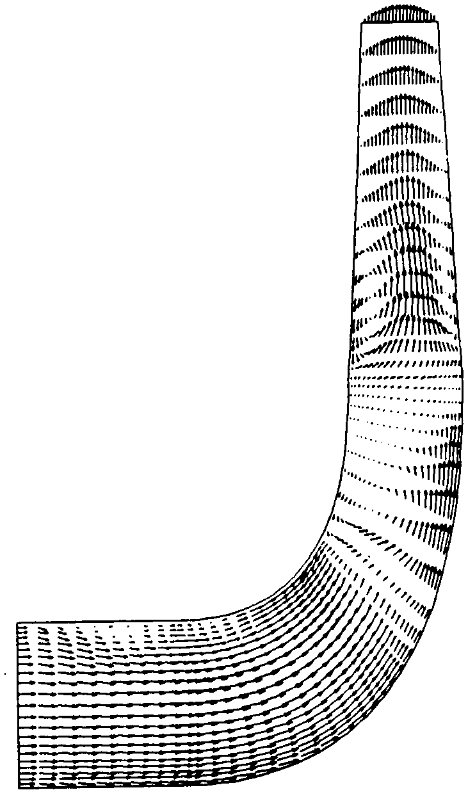

Case 3

VELOCITY VECTORS NEAR SUCTION SIDE OF SPLITTER

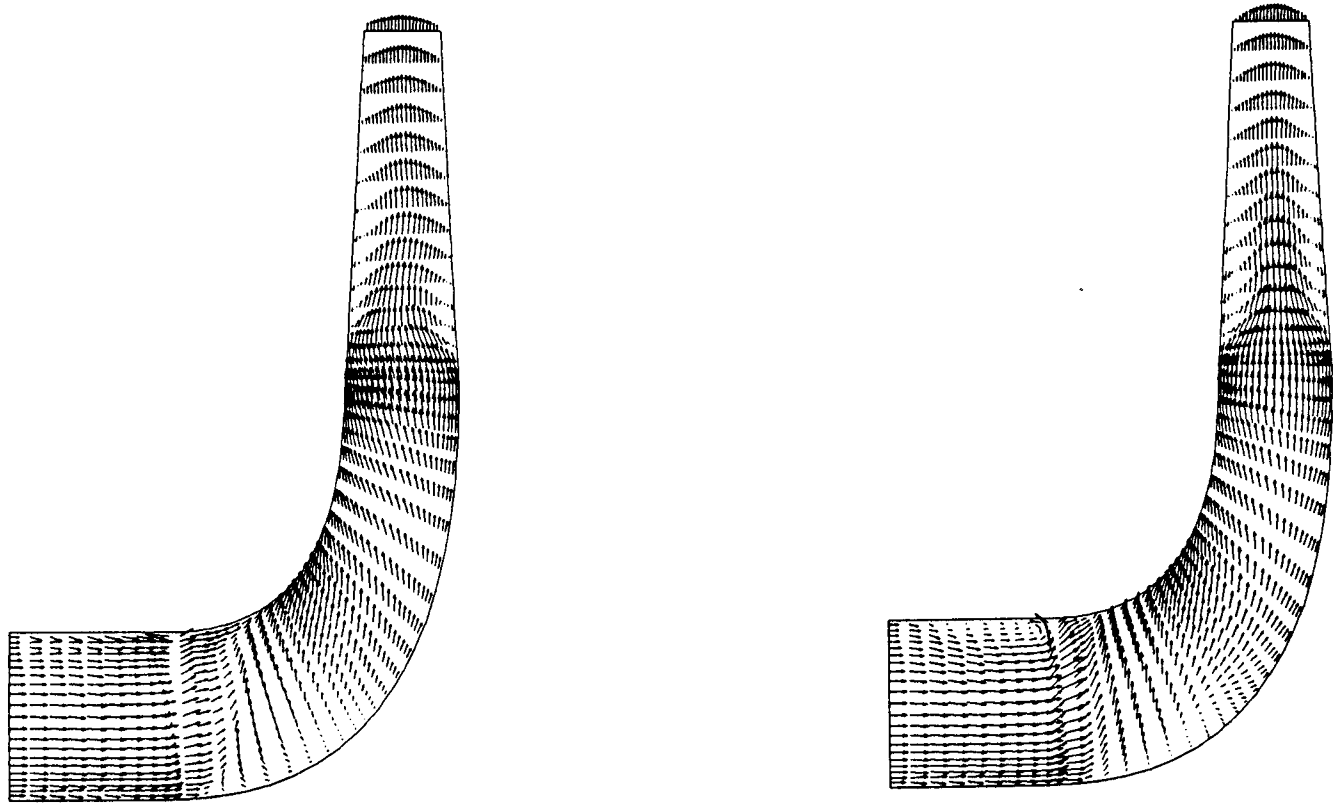

Case 1 Case 3

VELOCITY VECTORS NEAR PRESSURE SIDE OF BLADE

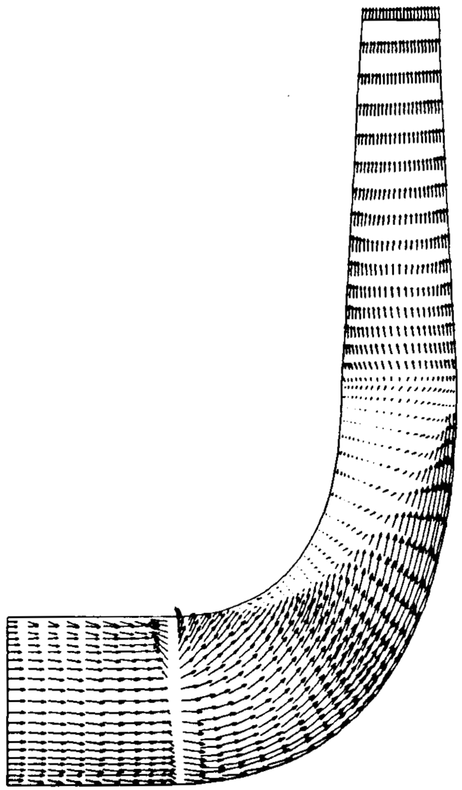

Case 2

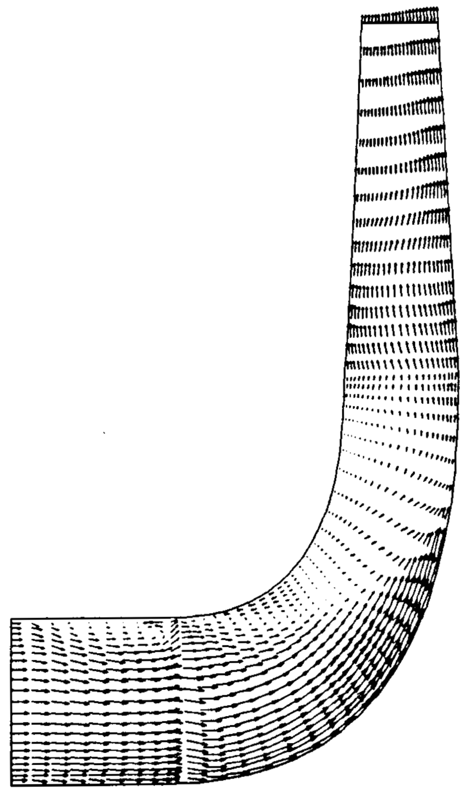

Case 5

VELOCITY VECTORS NEAR SUCTION SIDE OF BLADE

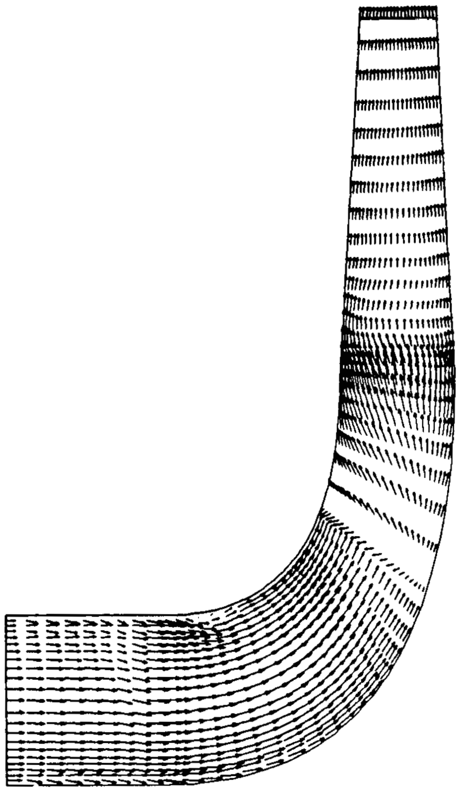

Case 2

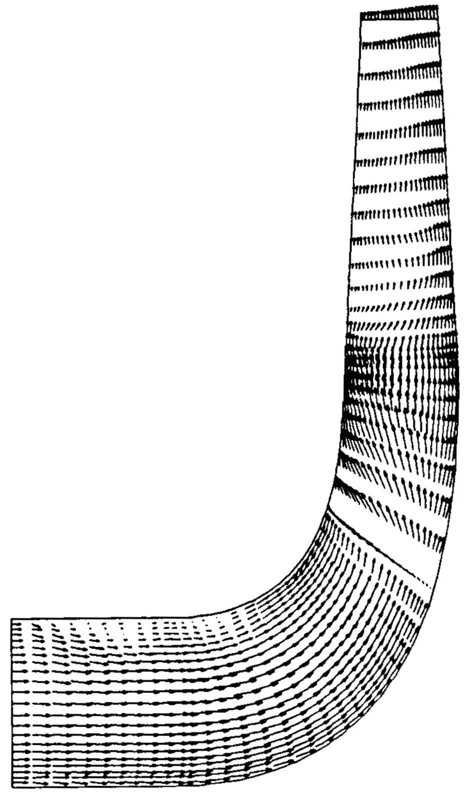

Case 5

VELOCITY VECTORS NEAR PRESSURE SIDE OF SPLITTER

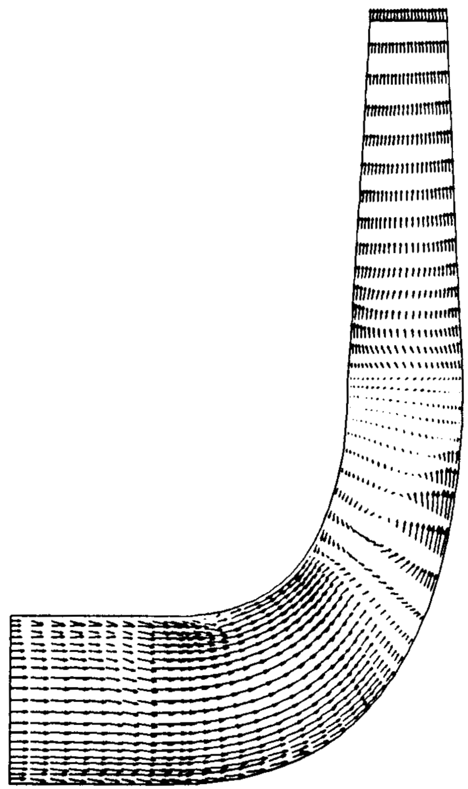

Case 2

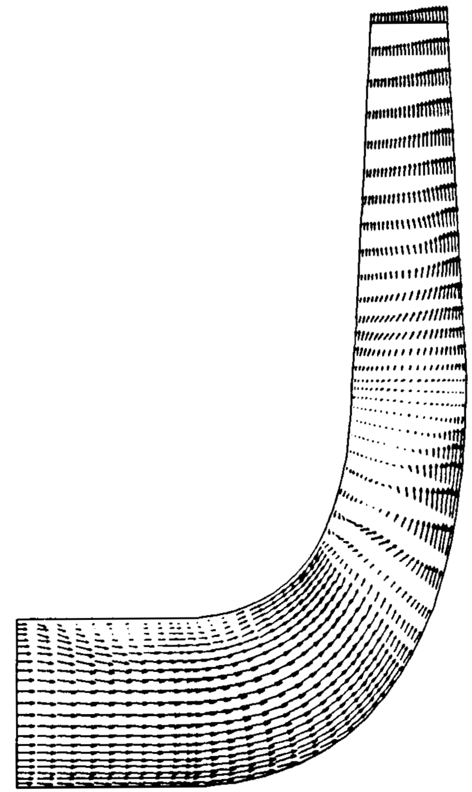

Case 5

VELOCITY VECTORS NEAR SUCTION SIDE OF SPLITTER

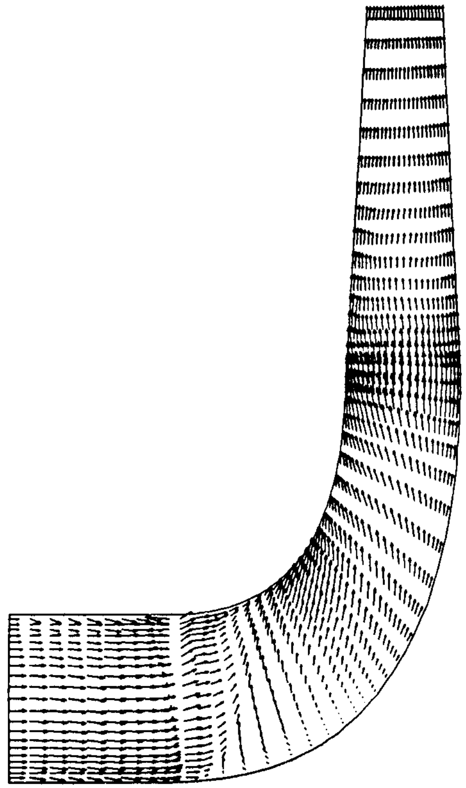

Case 2

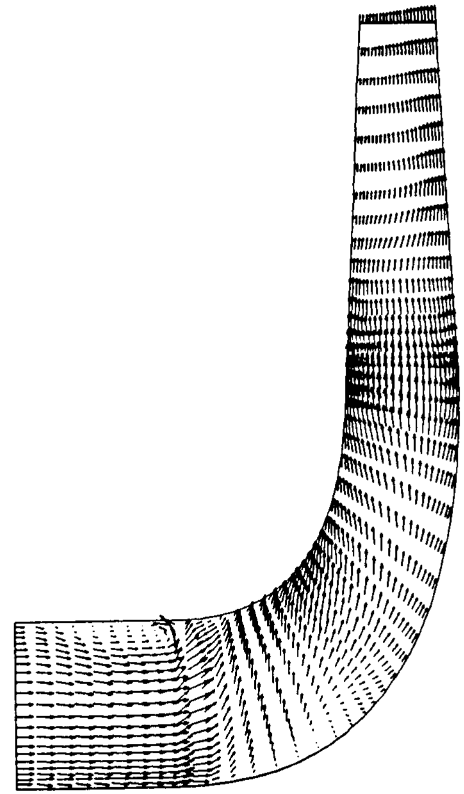

Case 5

VELOCITY VECTORS NEAR PRESSURE SIDE OF BLADE

OPTIMIZED IMPELLER: CM VS. X FOR R_{rel} = 0.05 (NEAR HUB)

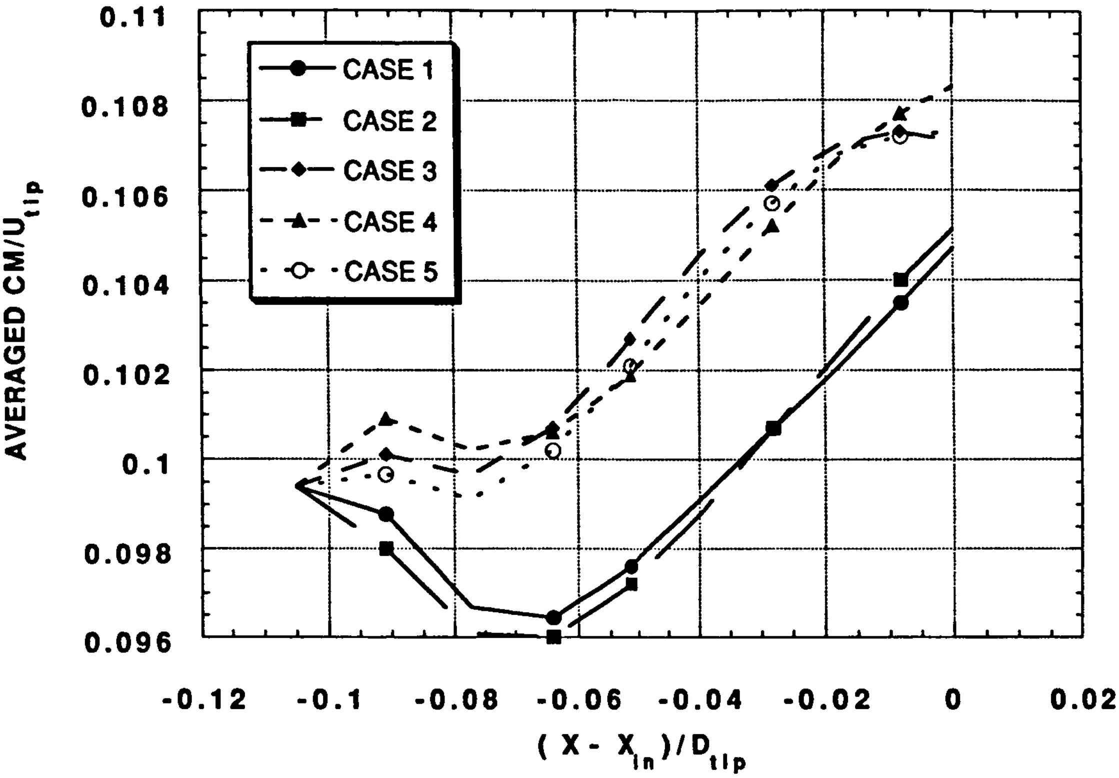

OPTIMIZED IMPELLER: BETA VS. X FOR R_{rel} = 0.05

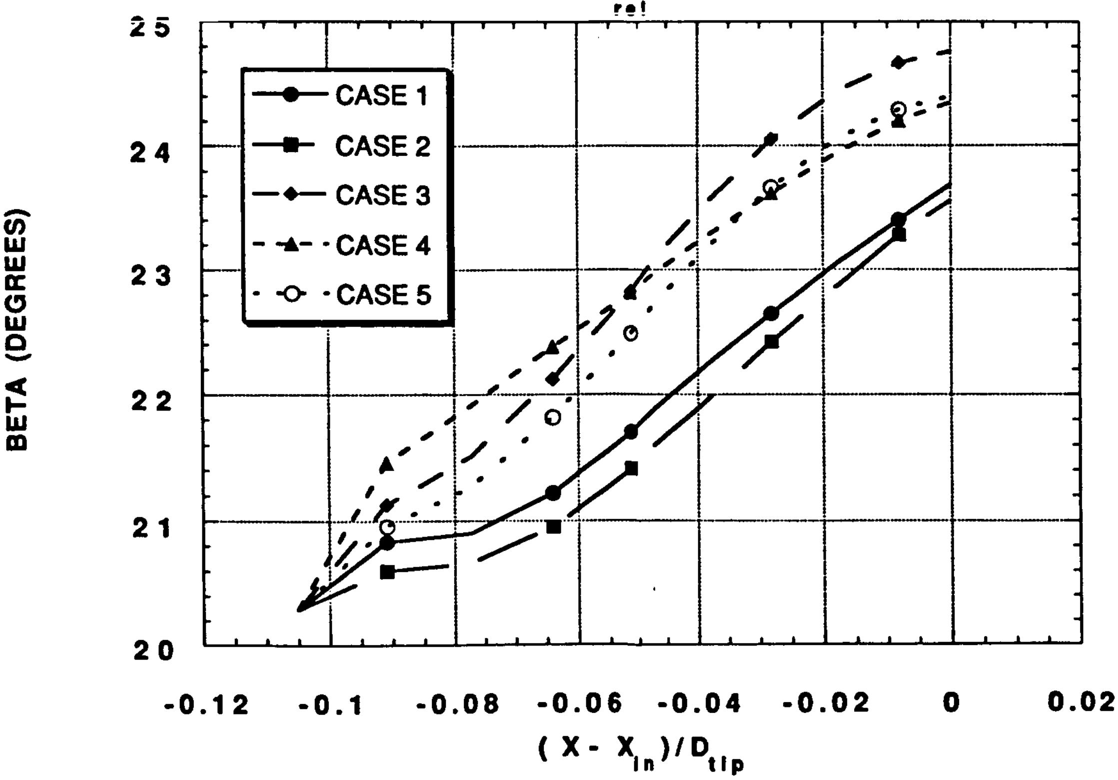

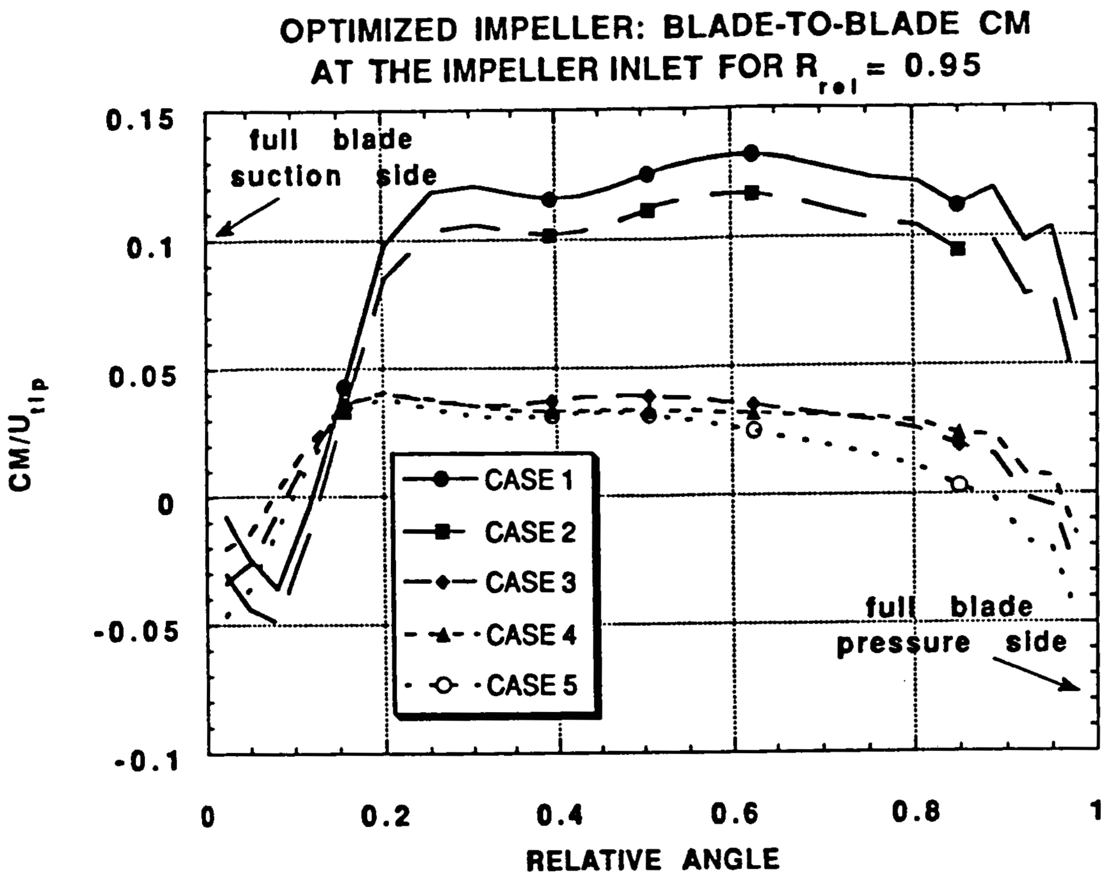
OPTIMIZED IMPELLER: BLADE-TO-BLADE CM
AT THE IMPELLER INLET FOR R_{rel} = 0.95
full blade
suction side
full blade
pressure side
CASE 1
CASE 2
CASE 3
CASE 4
CASE 5
CM/U_{tip}
RELATIVE ANGLE
0.15
0.1
0.05
0
-0.05
-0.1
0
0.2
0.4
0.6
0.8
1

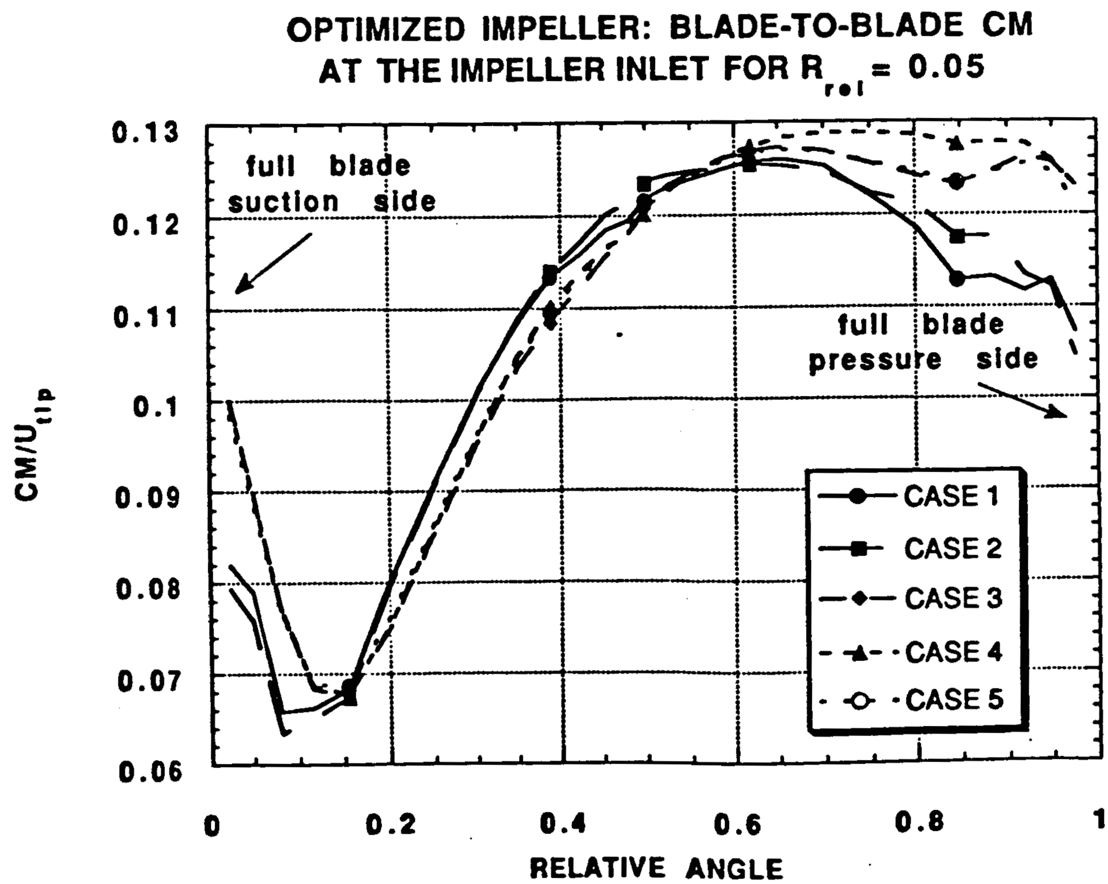
OPTIMIZED IMPELLER: BLADE-TO-BLADE CM
AT THE IMPELLER INLET FOR R_{rel} = 0.05
full blade
suction side
full blade
pressure side
CASE 1
CASE 2
CASE 3
CASE 4
CASE 5
CM/U_{tip}
RELATIVE ANGLE
0.13
0.12
0.11
0.1
0.09
0.08
0.07
0.06
0
0.2
0.4
0.6
0.8
1

OPTIMIZED IMPELLER: CM VS. X
FOR R_{rel} = 0.95 (NEAR SHROUD)

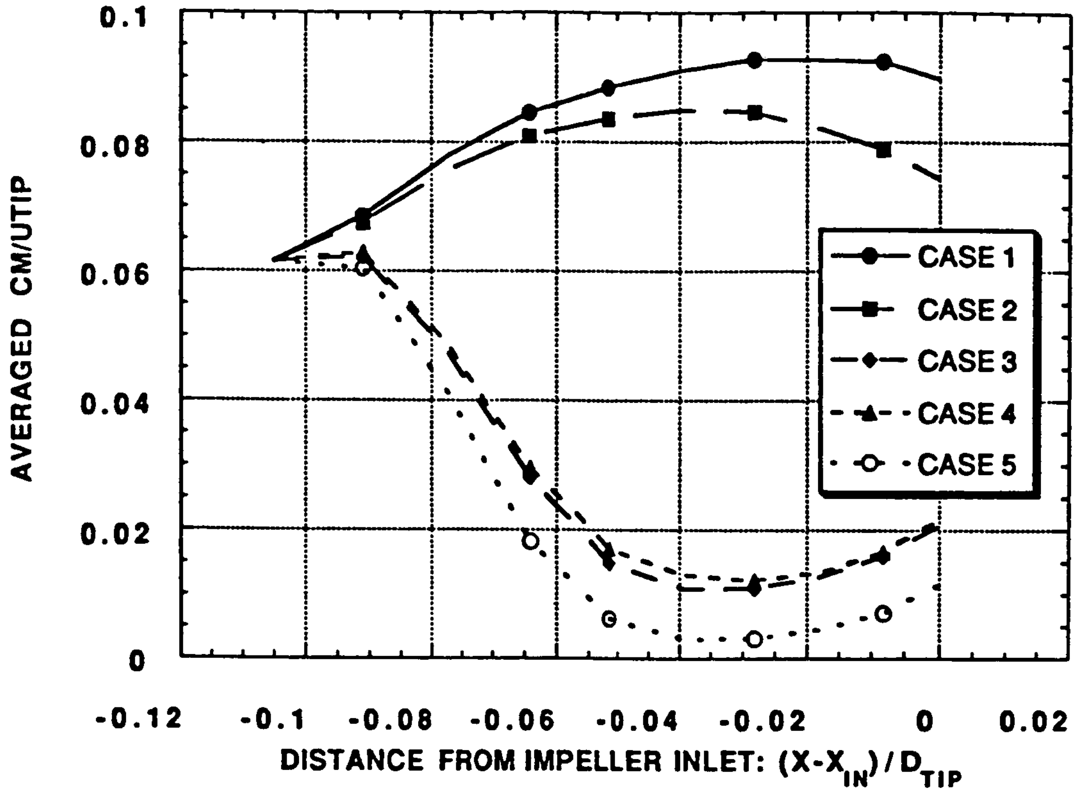

OPTIMIZED IMPELLER: BETA VS. X
FOR R_{rel} = 0.95

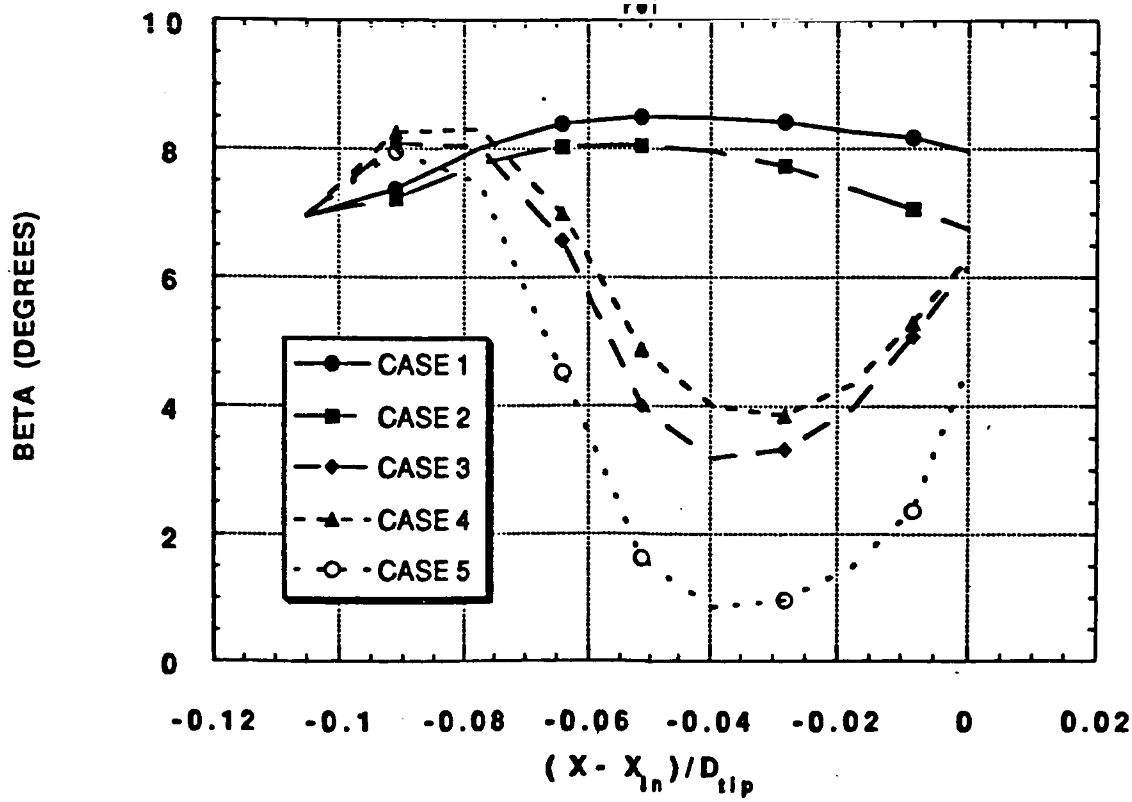

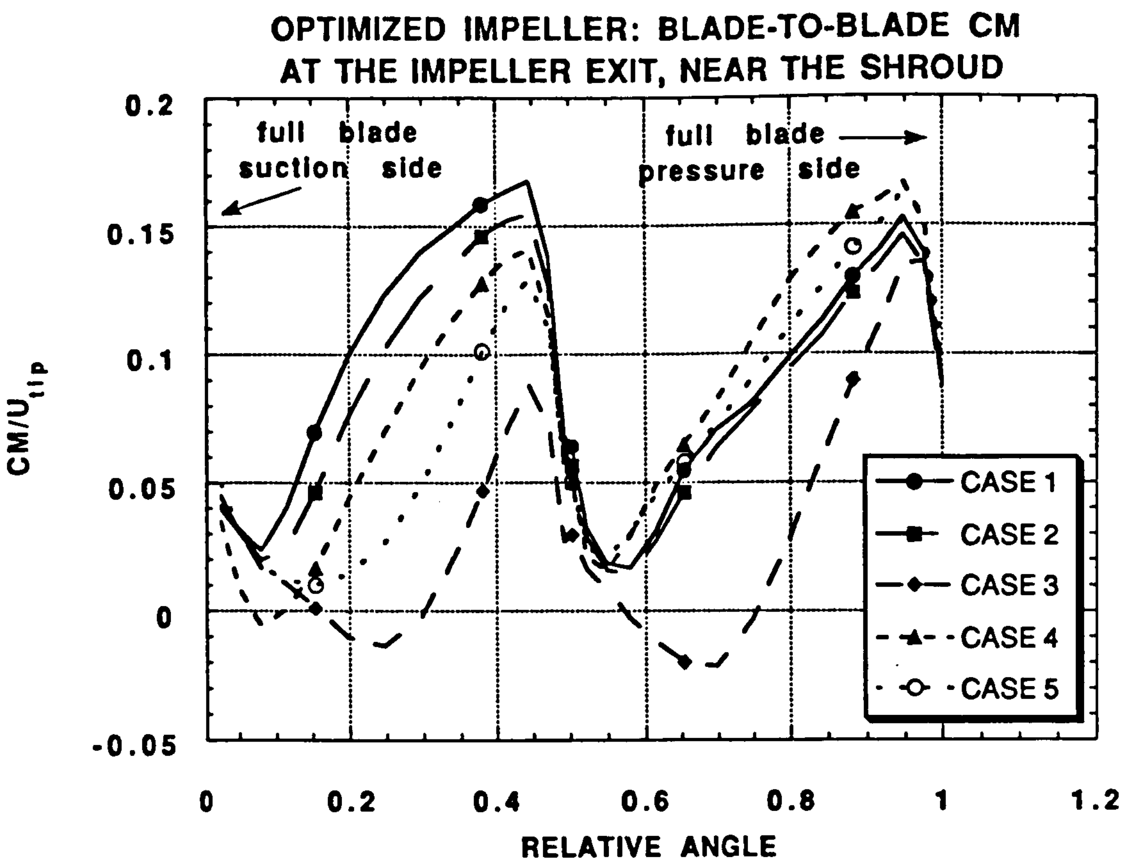
OPTIMIZED IMPELLER: BLADE-TO-BLADE CM
AT THE IMPELLER EXIT, NEAR THE SHROUD
full blade suction side
full blade pressure side
CASE 1
CASE 2
CASE 3
CASE 4
CASE 5
CM/U_tip
0.2
0.15
0.1
0.05
0
-0.05
0
0.2
0.4
0.6
0.8
1
1.2
RELATIVE ANGLE

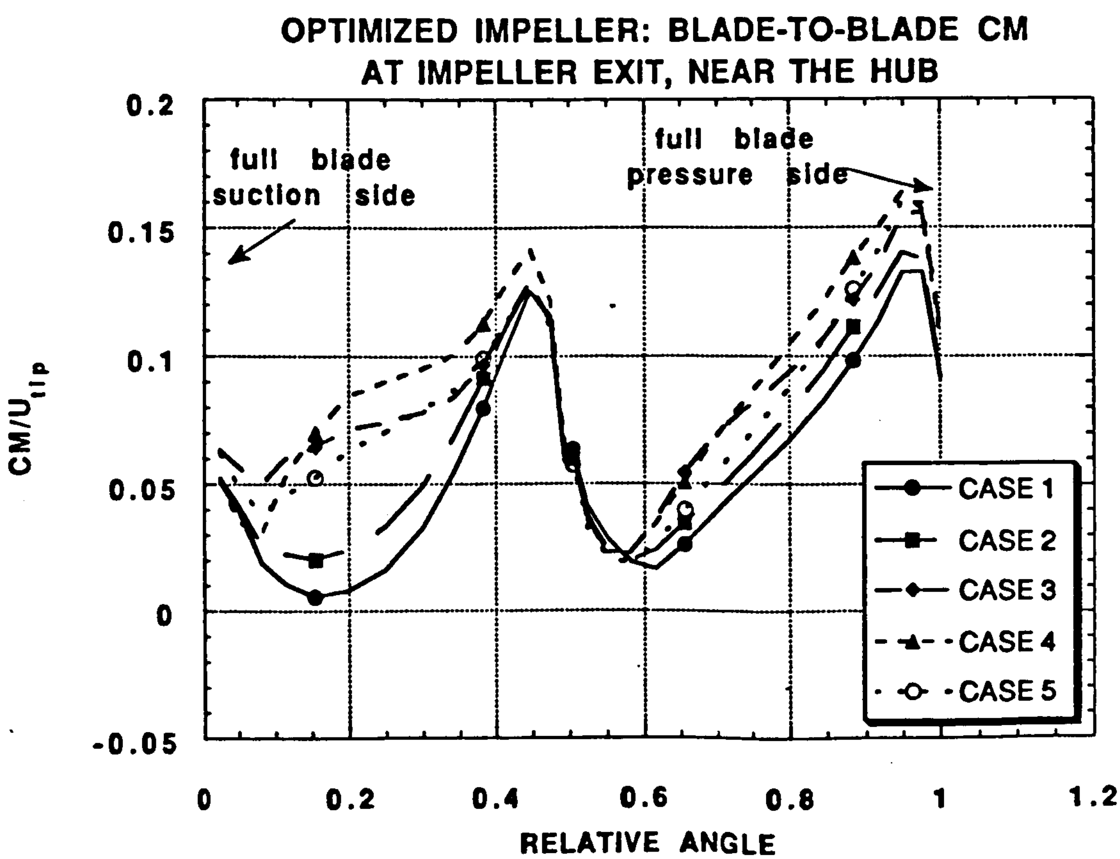
OPTIMIZED IMPELLER: BLADE-TO-BLADE CM
AT IMPELLER EXIT, NEAR THE HUB
full blade suction side
full blade pressure side
CASE 1
CASE 2
CASE 3
CASE 4
CASE 5
CM/U_tip
0.2
0.15
0.1
0.05
0
-0.05
0
0.2
0.4
0.6
0.8
1
1.2
RELATIVE ANGLE

OPTIMIZED IMPELLER: EFFICIENCY VS. X

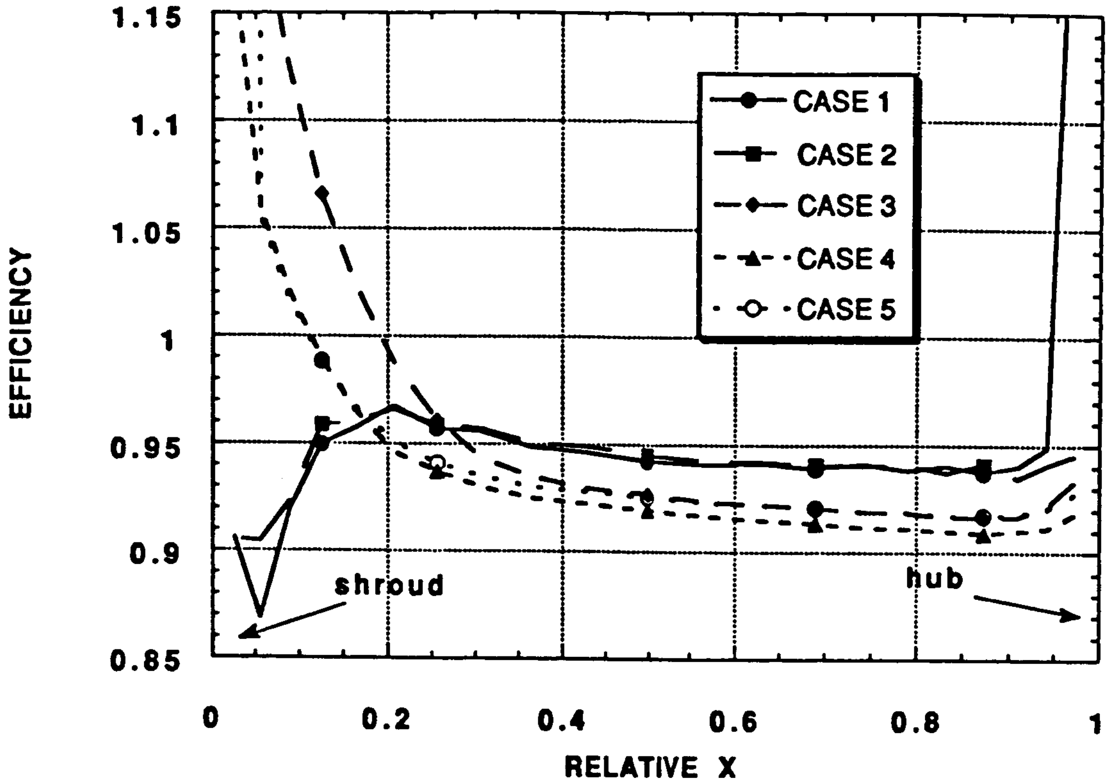

OPTIMIZED IMPELLER: HEAD COEFICIENT VS. X

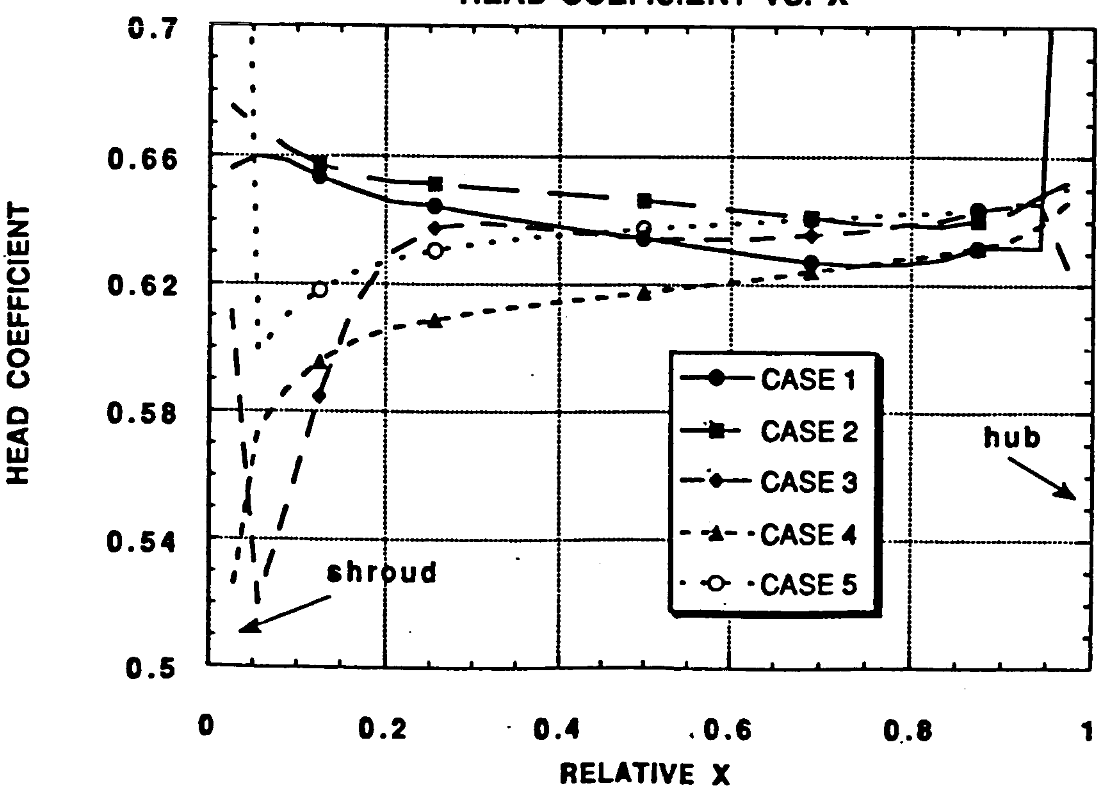

CONCLUSIONS

- THE PRESENT CFD RESULTS HAVE SHOWN SENSITIVITY OF INLET AND EXIT WALL BOUNDARY CONDITIONS ON THE FLOW STRUCTURE INSIDE THE OPTIMIZED CONSORTIUM IMPELLER DESIGN

- INLET SHROUD WALL BOUNDARY TREATMENTS HAVE SIGNIFICANT EFFECT ON THE FLOW SPLIT AROUND THE PARTIAL BLADE (MORE FLOW THROUGH THE PARTIAL/FULL-PRESSURE PASSAGE WHEN THE INLET SHROUD WALL IS ASSUMED ROTATING)

- ONLY MINOR IMPACT ON THE OVERALL IMPELLER PERFORMANCE DATA WAS REVEALED FOR DIFFERENT BOUNDARY CONDITIONS IMPOSED

N92-32288

Abstract of a proposed paper for the presentation at workshop for CFD Applications in Rocket Propulsion to be held at NASA Marshall Space Flight Center, AL, April 28-30, 1992

CFD APPLICATIONS IN PUMP FLOWS

Cetin Kiris, Liang Chang
MCAT Institute, Moffett Field, CA

and

Dochan Kwak
NASA-Ames Research Center, Moffett Field, CA

The objective of the proposed paper is to develop a computational procedure that solves incompressible Navier-Stokes equations for pump flows. The solution method is based on the pseudocompressibility approach and uses an implicit-upwind differencing scheme together with the Gauss-Seidel line relaxation method. The equations are solved in steadily rotating reference frames and the centrifugal force and the Coriolis force are added to the equation of motion. As a bench mark problem, the flow through the Rocketdyne inducer is numerically simulated. A coarse grid solution is obtained with a single zone by using an algebraic turbulence model. In multi-zone fine grid computation, one-equation Baldwin-Barth turbulence model is utilized. Numerical results are compared with experimental measurements and a good agreement is found between the two. The resulting computer code is then applied to the flow analysis inside two-stage fuel pump impeler operating at 80 %, 100 %, and 120 % of design flow.

CFD APPLICATIONS IN PUMP FLOWS

Cetin Kiris, Dochan Kwak, and Leon Chang
NASA-Ames Research Center

Workshop for CFD Applications in Rocket Propulsion
NASA-MSFC, April 28-30, 1992

Introduction

- Motivation
  - ≫ Increasing efficiency and reliability of the liquid rocket engine components is an important task.
  - ≫ Understand fluid dynamics of fuel and oxidizer flows from fuel tank to plume.
  - ≫ Role of CFD toward a better design.

- Goal
  - ≫ To implement CFD technology to simulate the flow through the pump components.

    First Step : Bench mark problems and component analysis.

    Second Step : Unsteady flows through the entire pump (future work).

Method of Solution

- Available algorithms for pump applications are : INS3D-UP and IND3D-LU.
- Currently INS3D-UP is used.
- Based on method of artificial compressibility.
- Both steady-state and time-accurate formulation.
- Steady-state formulation in steadily rotating reference frame.
- Multi-Zone and Operlapped grid scheme capability.
- Computing time: $\approx 1\text{x}10^{-4}$ sec/grid point/iteration
- Memory Usage: $\approx$ 45 times number of grid points in words

INS3D-UP Algorithm

- Central differencing for viscous fluxes
- Upwind differencing for convective fluxes
  - ≫ 3rd and 5th order flux-difference splitting is used for the right hand side terms
- Gauss-Seidel line relaxation relaxation
- Unlimited time step usage in steady-state formulation.
- Inflow and Outflow boundaries based on Method of Characteristics
  - ≫ Inflow Boundary : Three velocity components specified
  - ≫ Outflow Boundary : Static pressure specified
- Quasi-implicit boundary conditions at zonal interfaces.

Steady-State Formulation

- Introduce artificial compressibility term to the continuity equation

$$\frac{\partial p}{\partial \tau} = -\beta \left(\frac{\partial \hat{U}}{\partial \xi} + \frac{\partial \hat{V}}{\partial \eta} + \frac{\partial \hat{W}}{\partial \zeta} \right)$$

$$\frac{\partial \hat{q}}{\partial \tau} = -\frac{\partial}{\partial \xi}(\hat{e} - \hat{e}_v) - \frac{\partial}{\partial \eta}(\hat{f} - \hat{f}_v) - \frac{\partial}{\partial \zeta}(\hat{g} - \hat{g}_v) = -\hat{r} + S$$

  ≫ β is an artificial compressibility constant
  ≫ τ is a pseudo-time step
  ≫ S is a source term as centrifugal and coriolis forces.

- Euler Implicit time discretization

- Solve system of equations iteratively in pseudo-time until solution converges to a steady state

Time-accurate Formulation

- Discretize the time term in momentum equations using second-order three-point backward-difference formula

$$\left(\frac{\partial \hat{U}}{\partial \xi} + \frac{\partial \hat{V}}{\partial \eta} + \frac{\partial \hat{W}}{\partial \zeta}\right)^{n+1} = 0$$

$$\frac{3\hat{q}^{n+1} - 4\hat{q}^{n} + \hat{q}^{n-1}}{2\Delta t} = -\hat{r}^{n+1}$$

- Introduce a pseudo-time level and artificial compressibility

$$\frac{1}{\Delta \tau}(\hat{p}^{n+1,m+1} - \hat{p}^{n+1,m}) = -\beta \nabla \cdot q^{n+1,m+1}$$

$$\frac{1.5}{\Delta t}(\hat{q}^{n+1,m+1} - \hat{q}^{n+1,m}) = -\hat{r}^{n+1,m+1} - \frac{3\hat{q}^{n+1,m} - 4\hat{q}^{n} + \hat{q}^{n-1}}{2\Delta t}$$

- Iterate the equations in pseudo-time for each time step until incompressibility condition is satisfied.

Inducer Computations

- Grid size : 187 x 27 x 35
- Baldwin-Lomax algebraic turbulence model.
- Tip clearance region is included.
- Computer time : 5 - 6 Cray-YMP hours
- Multi-zone computation (**currently underway**)
- Grid 1 : 63 x 37 x 74 Upstream of inducer
- Grid 2 : 115 x 37 x 48 Inducer blades
- Grid 3 : 51 x 37 x 20 Bull-nose cavity
- Grid 4 : 51 x 37 x 49 Downstream of blades
- One-equation Baldwin-Barth turbulence model.

VALIDATION OF INS3D-UP

Pump Design Code Development for STME

Rocketdyne inducer geometry

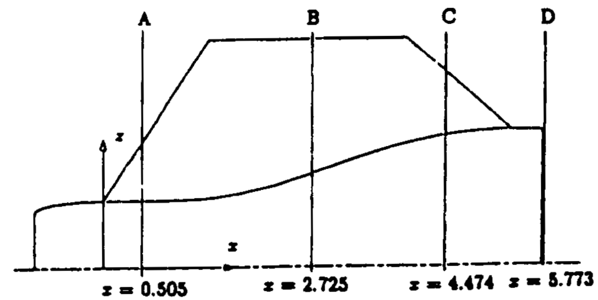

Schematic of the experimental measurement planes

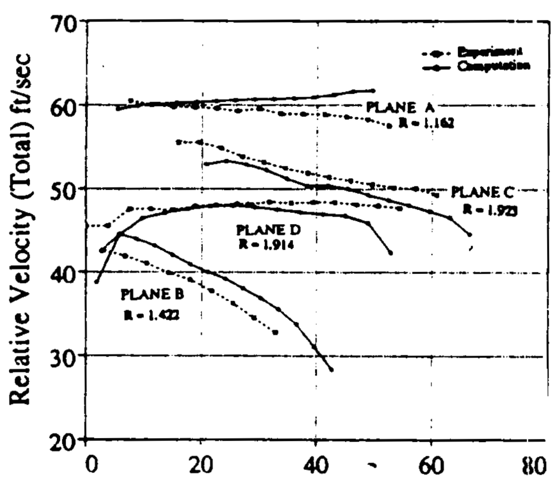

Comparison of relative total velocities

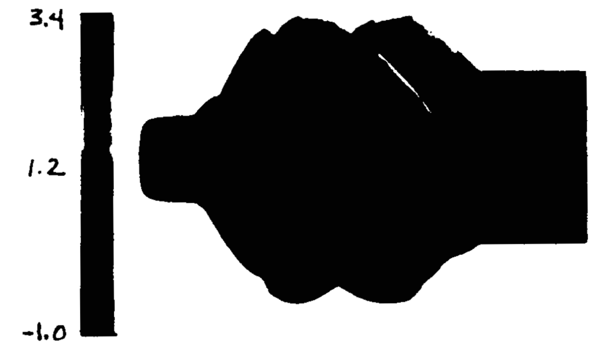

Computed surface pressure for Rocketdyne inducer

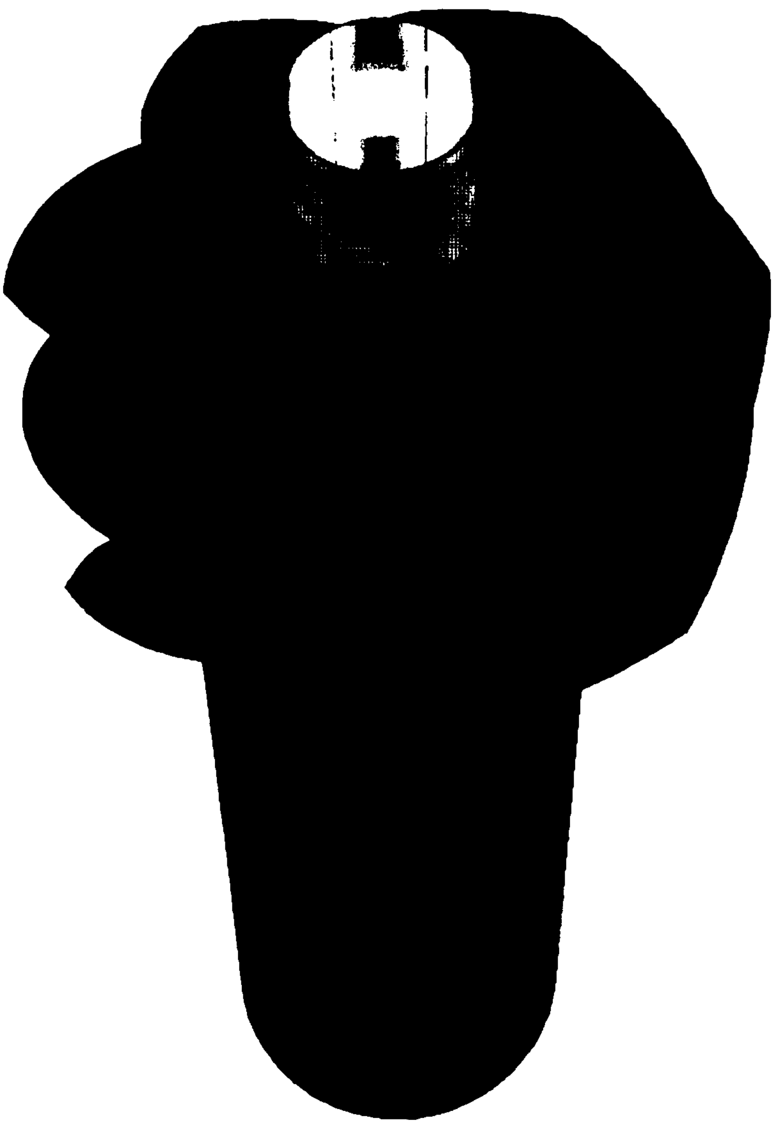

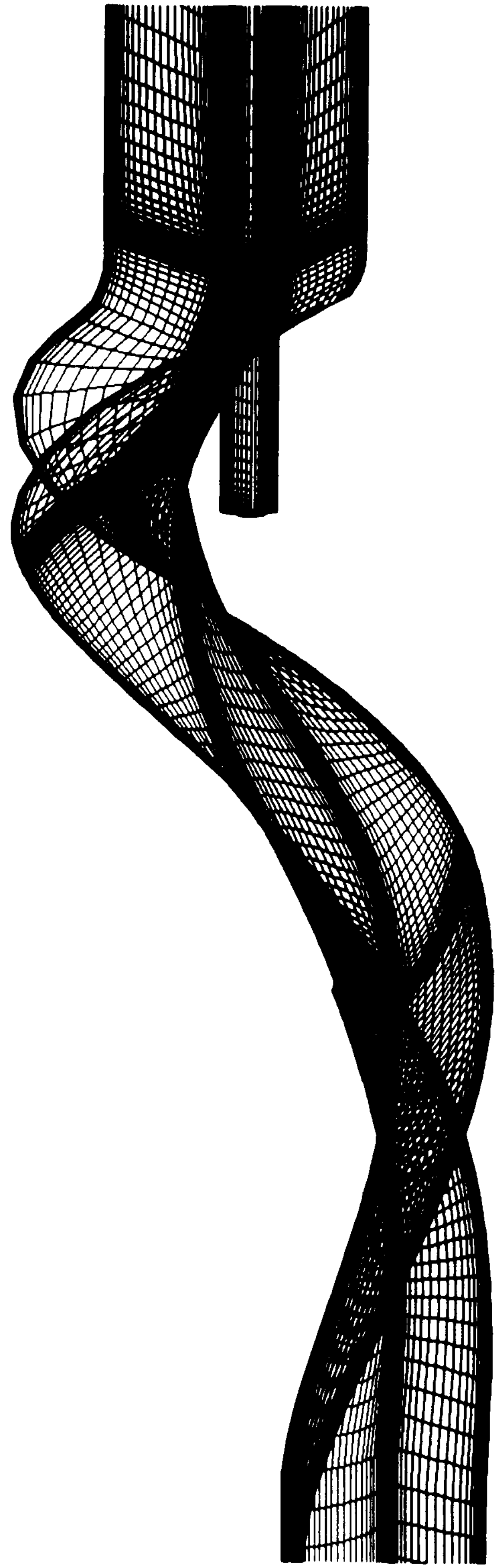

Impeller Water Test Conditions

• Number of Blades	6 full, 6 partial
• Design Speed, RPM	6632
• Design Flow, GPM	1205
• Reynolds Number, per inch	1.81e+5
• Inlet Tip Diameter, inch	6.0
• Inlet Hub Diameter, inch	3.9
• Outflow Diameter, inch	9.045
• Discharge Tip Speed, fps	249.5

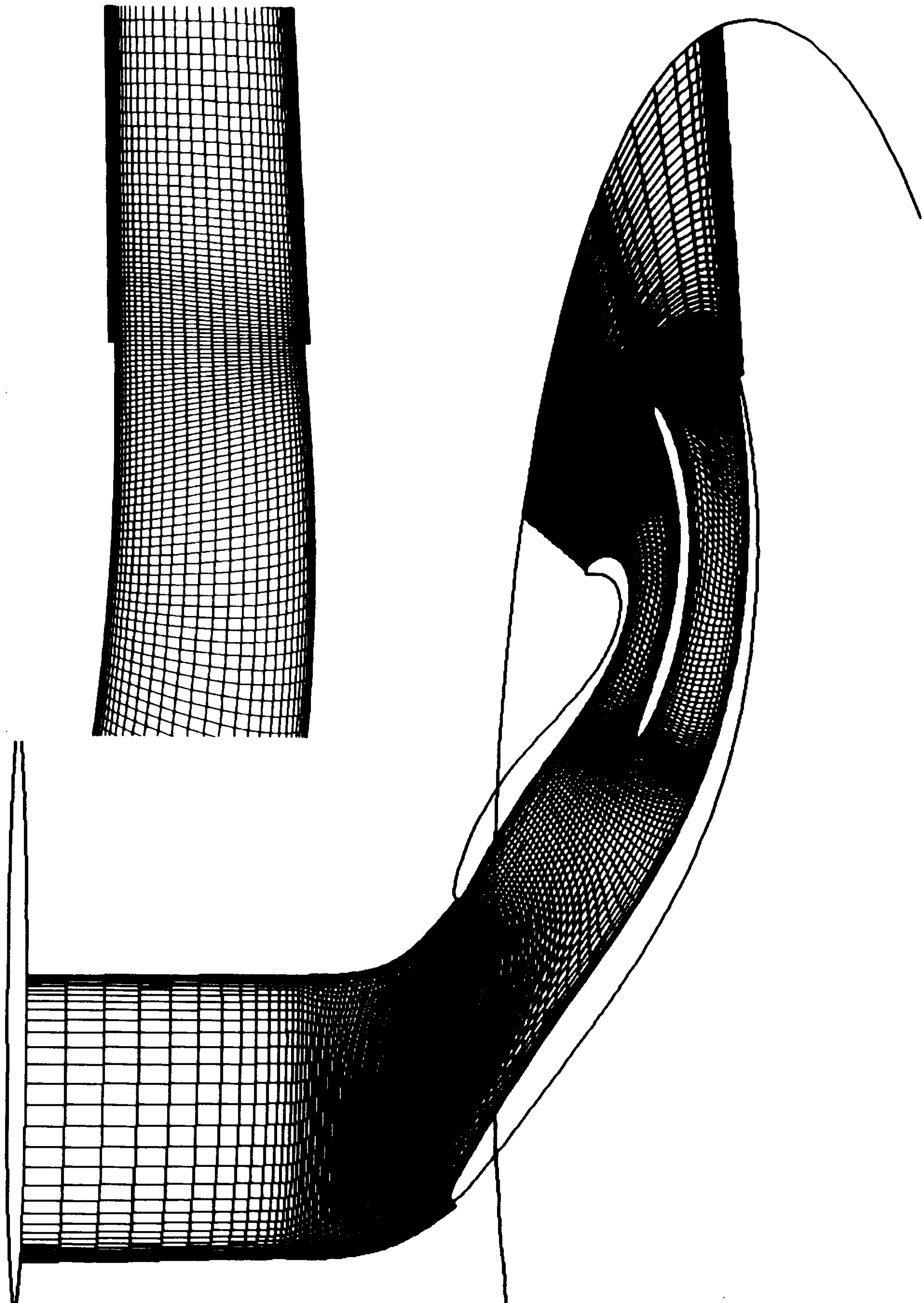

NLS Pump Impeller

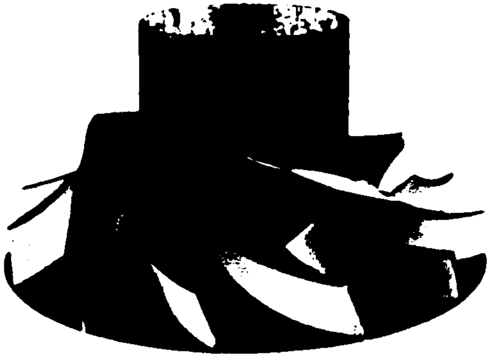

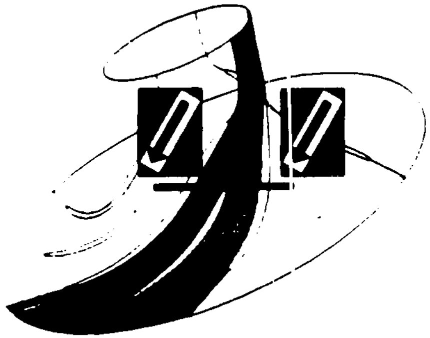

Surface Pressure

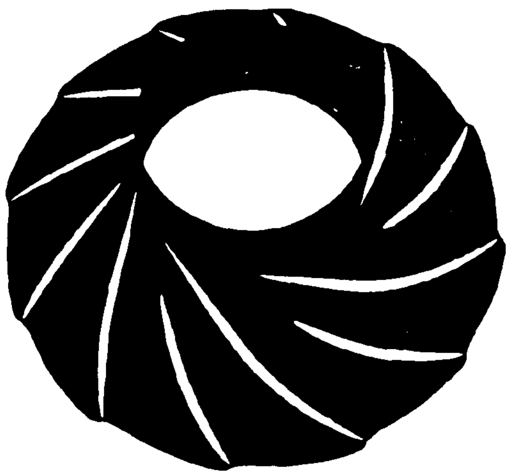

Pressure

-180.000
-178.000
-176.000
-174.000
-172.000
-170.000
-168.000
-166.000
-164.000
-162.000
-160.000
-158.000
-156.000
-154.000
-152.000
-150.000
-148.000
-146.000
-144.000
-142.000
-140.000
-138.000
-136.000
-134.000
-132.000
-130.000
-128.000
-126.000
-124.000
-122.000
-120.000

Relative Velocity Vectors Colored by Pressure

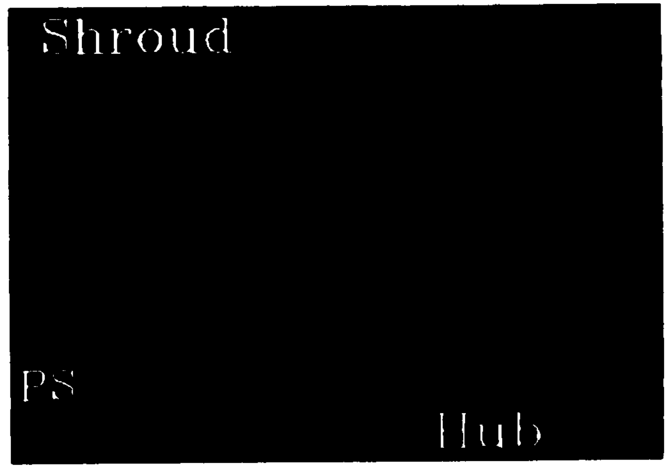

Old Design

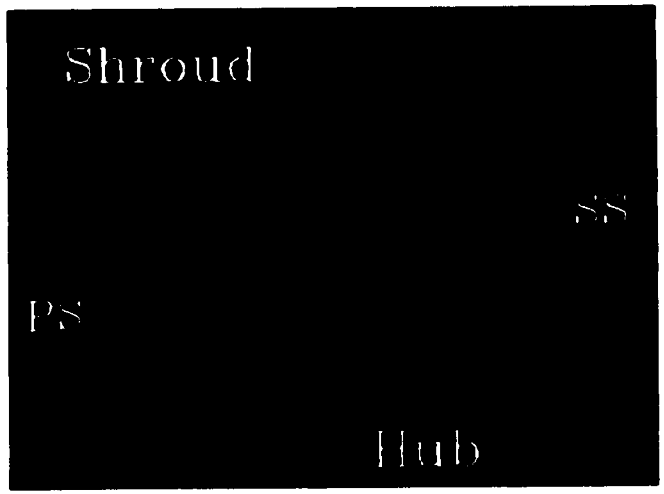

New Design

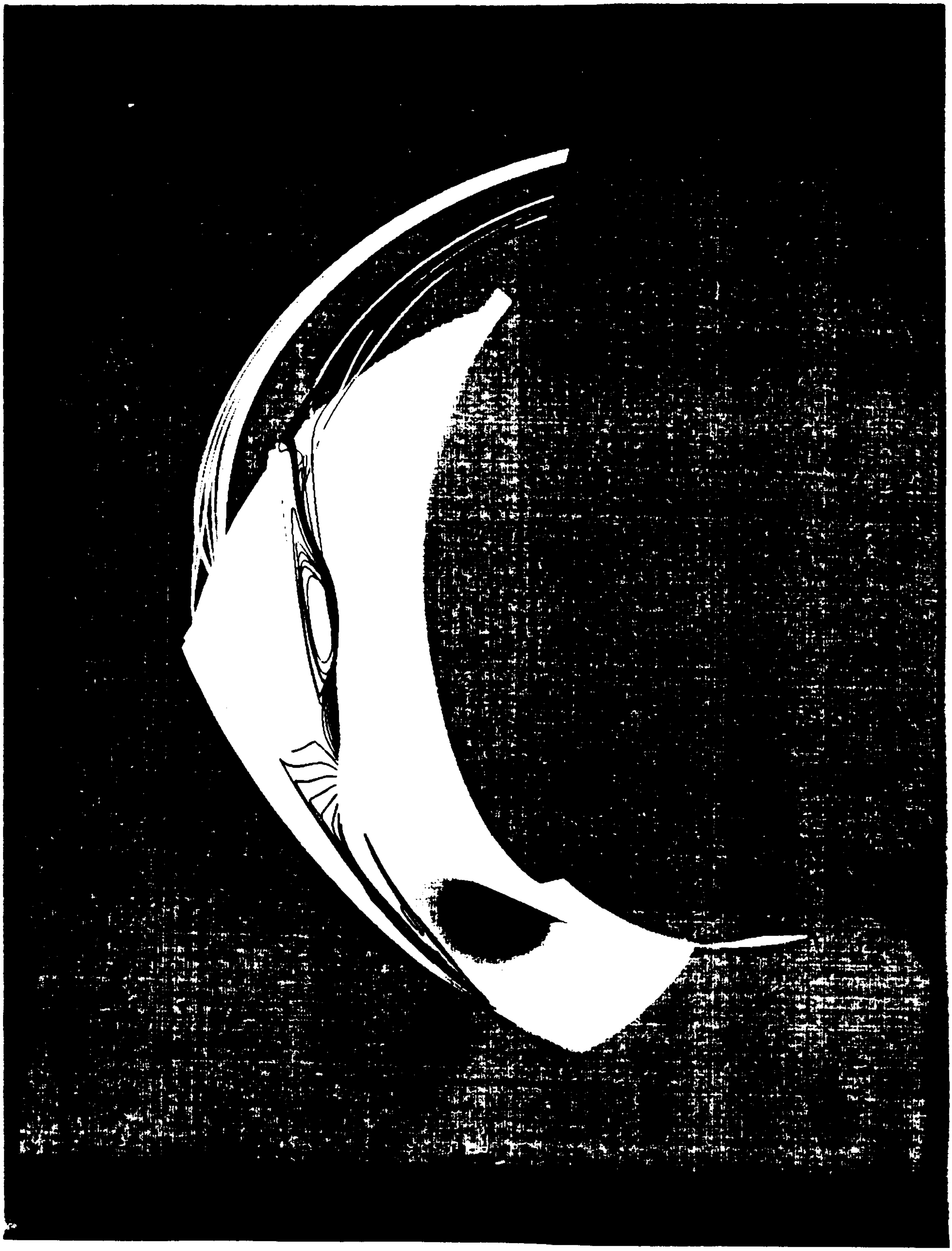

NLS Pump Impeller

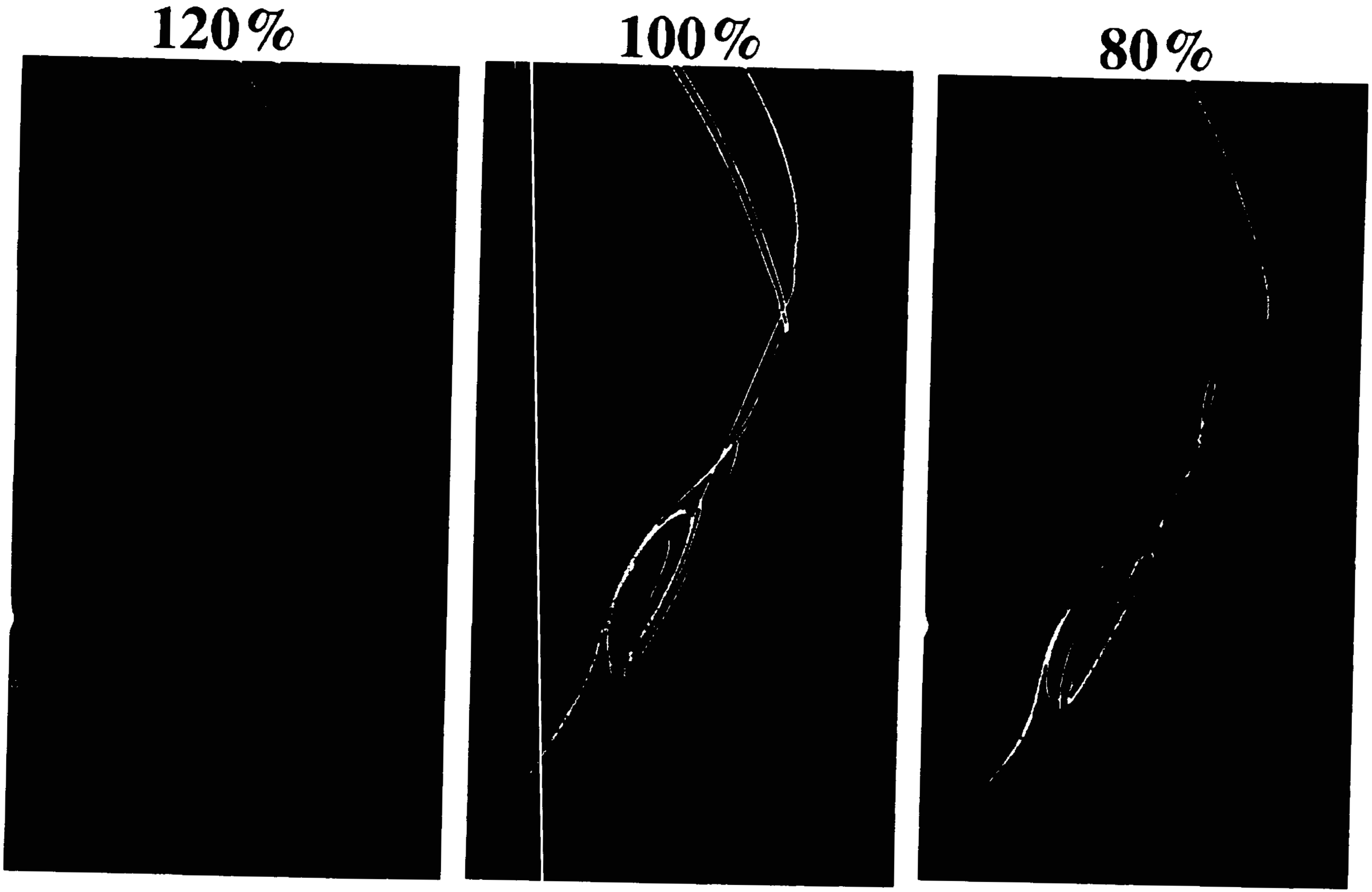

Particles are relased near shroud

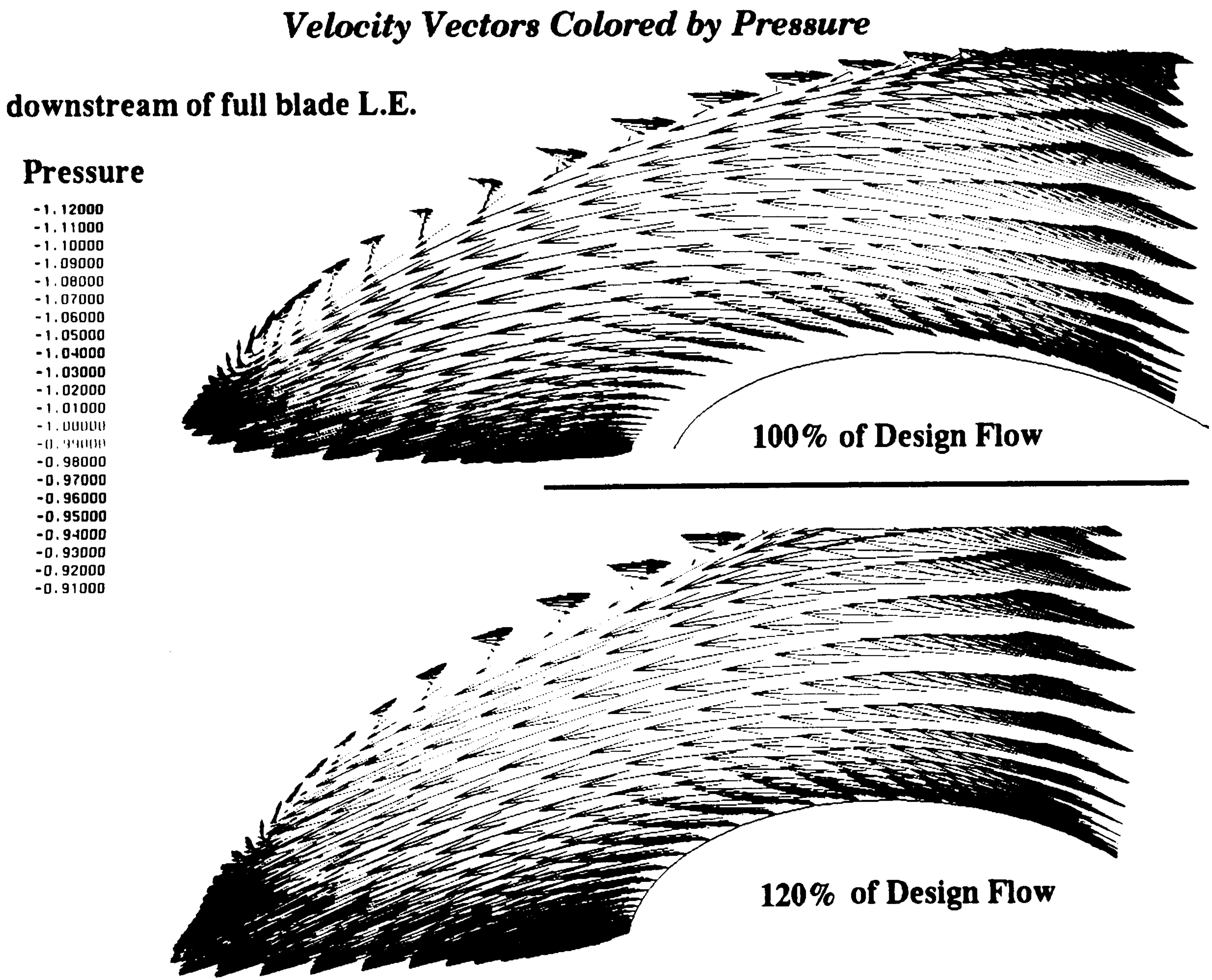
Velocity Vectors Colored by Pressure
downstream of full blade L.E.
Pressure
-1.12000
-1.11000
-1.10000
-1.09000
-1.08000
-1.07000
-1.06000
-1.05000
-1.04000
-1.03000
-1.02000
-1.01000
-1.00000
-0.99000
-0.98000
-0.97000
-0.96000
-0.95000
-0.94000
-0.93000
-0.92000
-0.91000
100% of Design Flow
120% of Design Flow

Velocity Vectors Colored by Pressure

downstream of full blade L.E.

Pressure

-1.12000
-1.11000
-1.10000
-1.09000
-1.08000
-1.07000
-1.06000
-1.05000
-1.04000
-1.03000
-1.02000
-1.01000
-1.00000
-0.99000
-0.98000
-0.97000
-0.96000
-0.95000
-0.94000
-0.93000
-0.92000
-0.91000

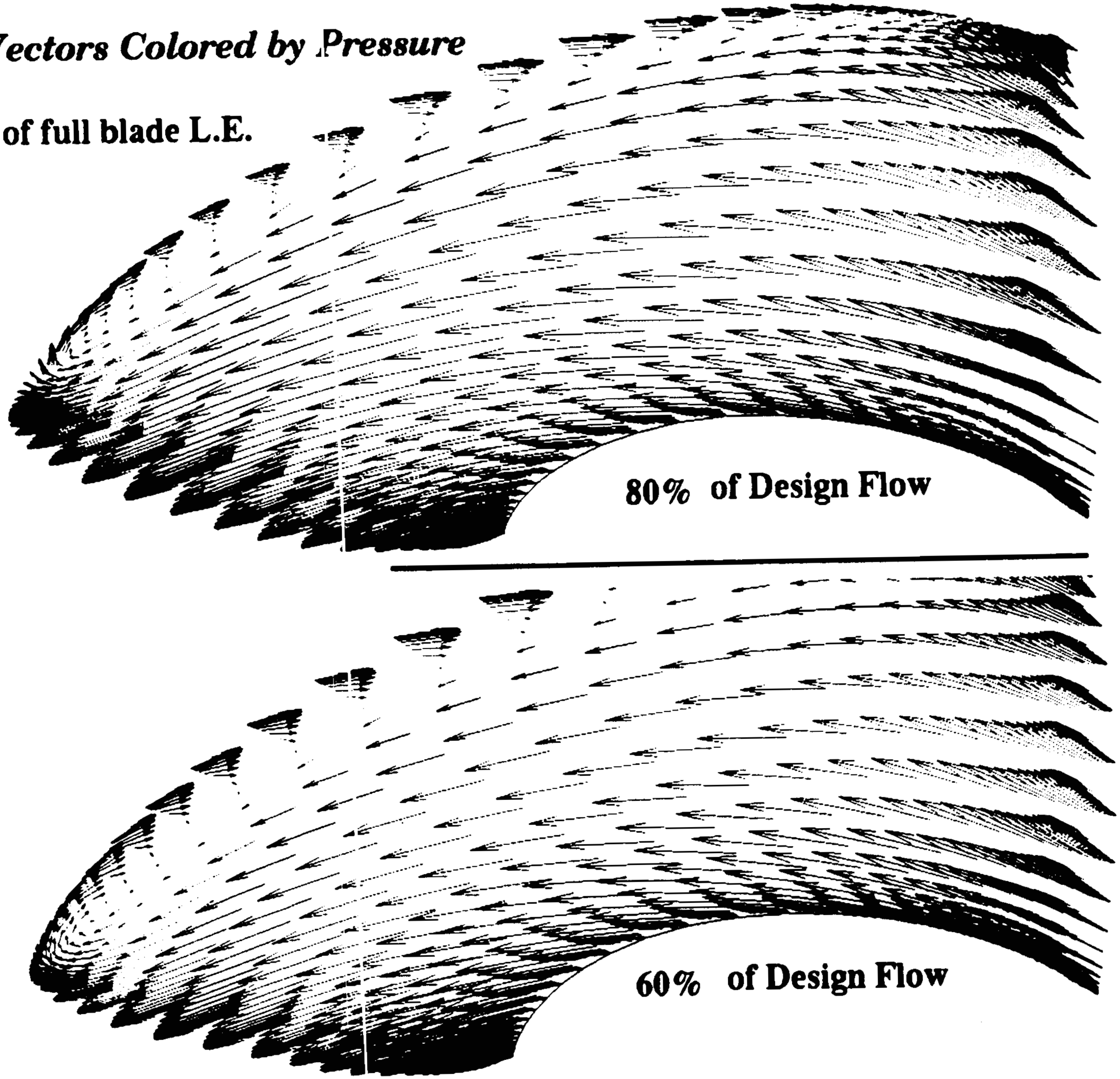

ORIGINAL PAGE IS
OF POOR QUALITY

Velocity Vectors Colored by Pressure upstream of discharge plane

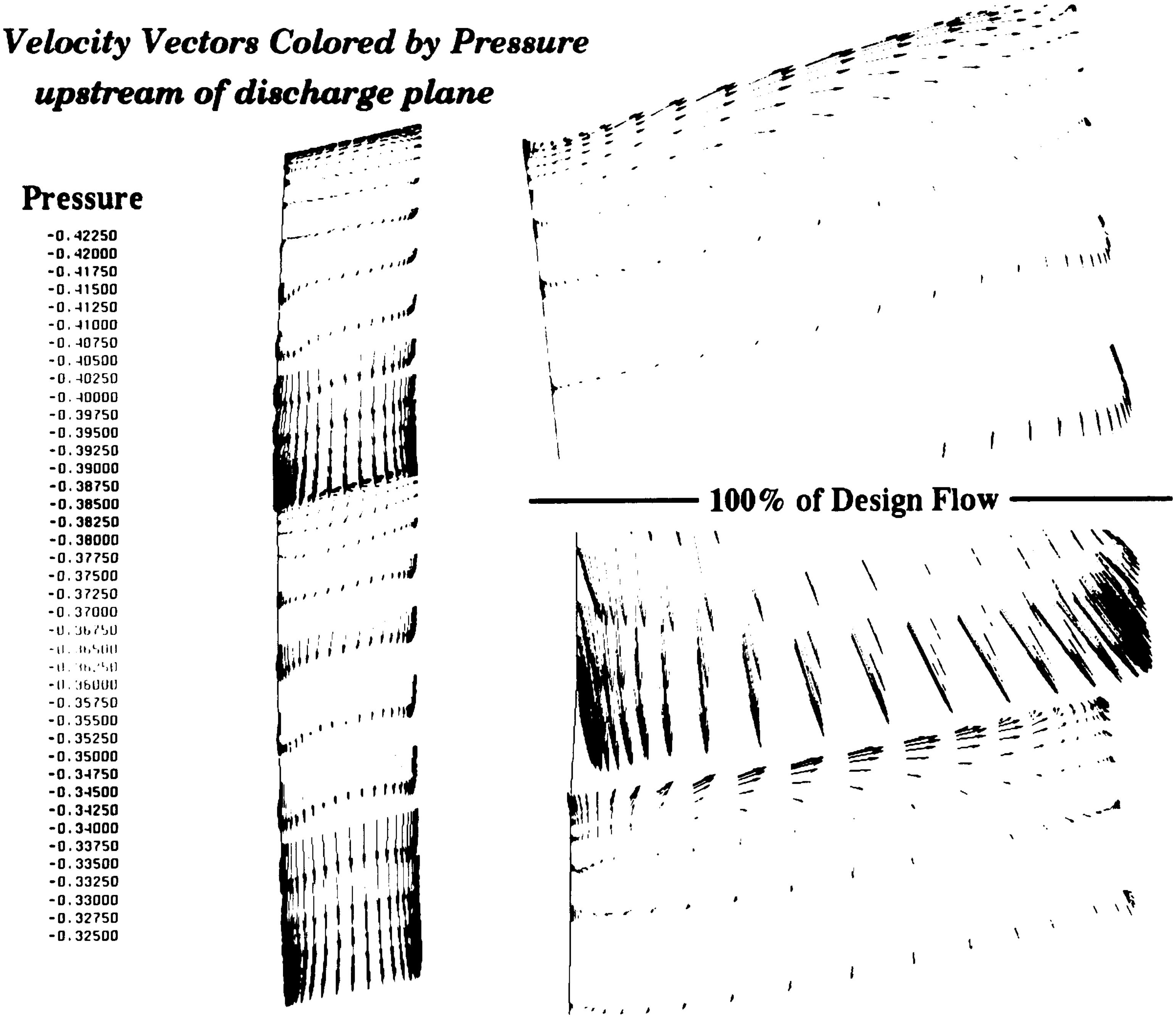

ORIGINAL PAGE IS
OF POOR QUALITY

Velocity Vectors Colored by Pressure upstream of discharge plane

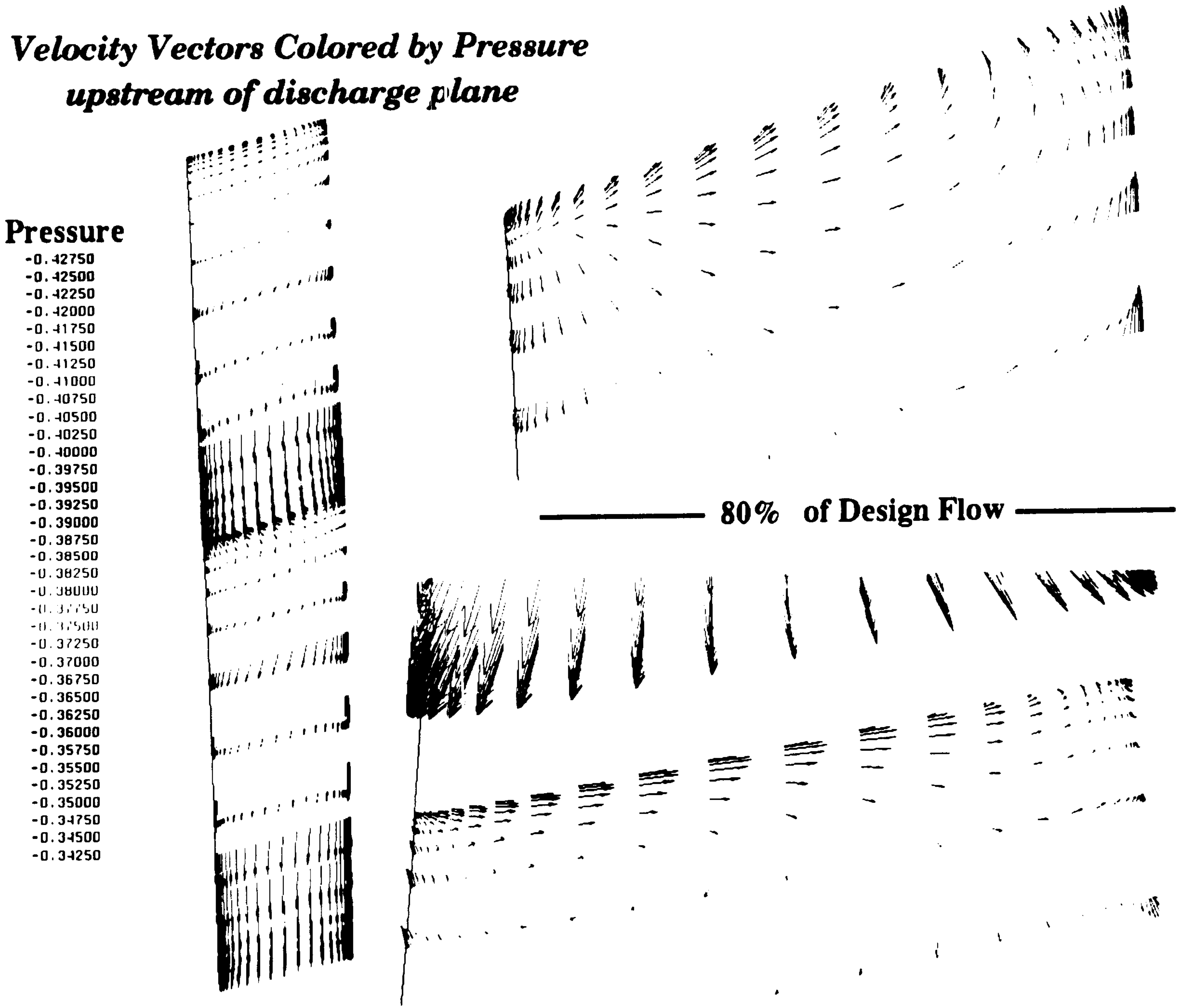

ORIGINAL PAGE IS OF POOR QUALITY

Velocity Vectors Colored by Pressure
upstream of discharge plane

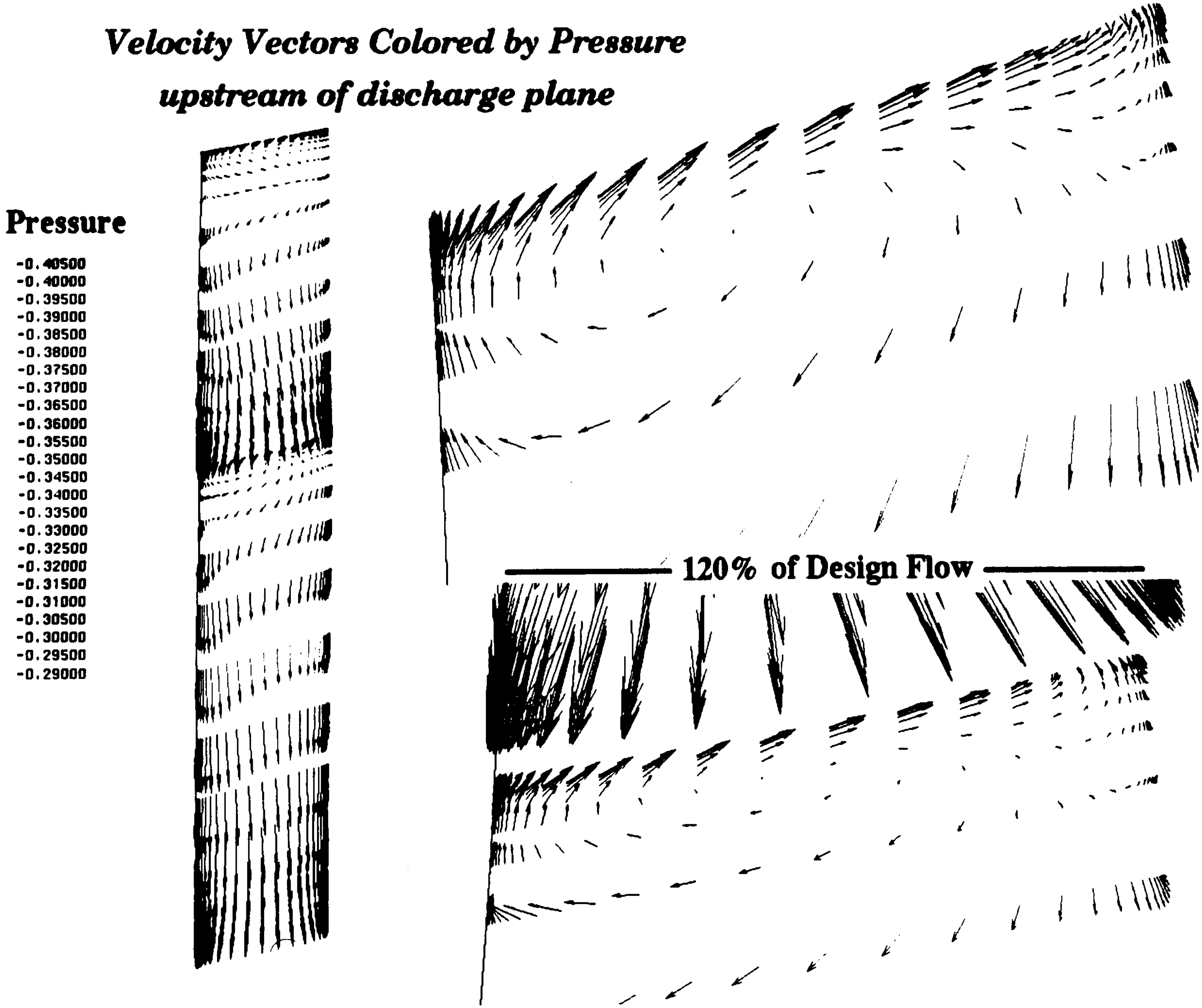

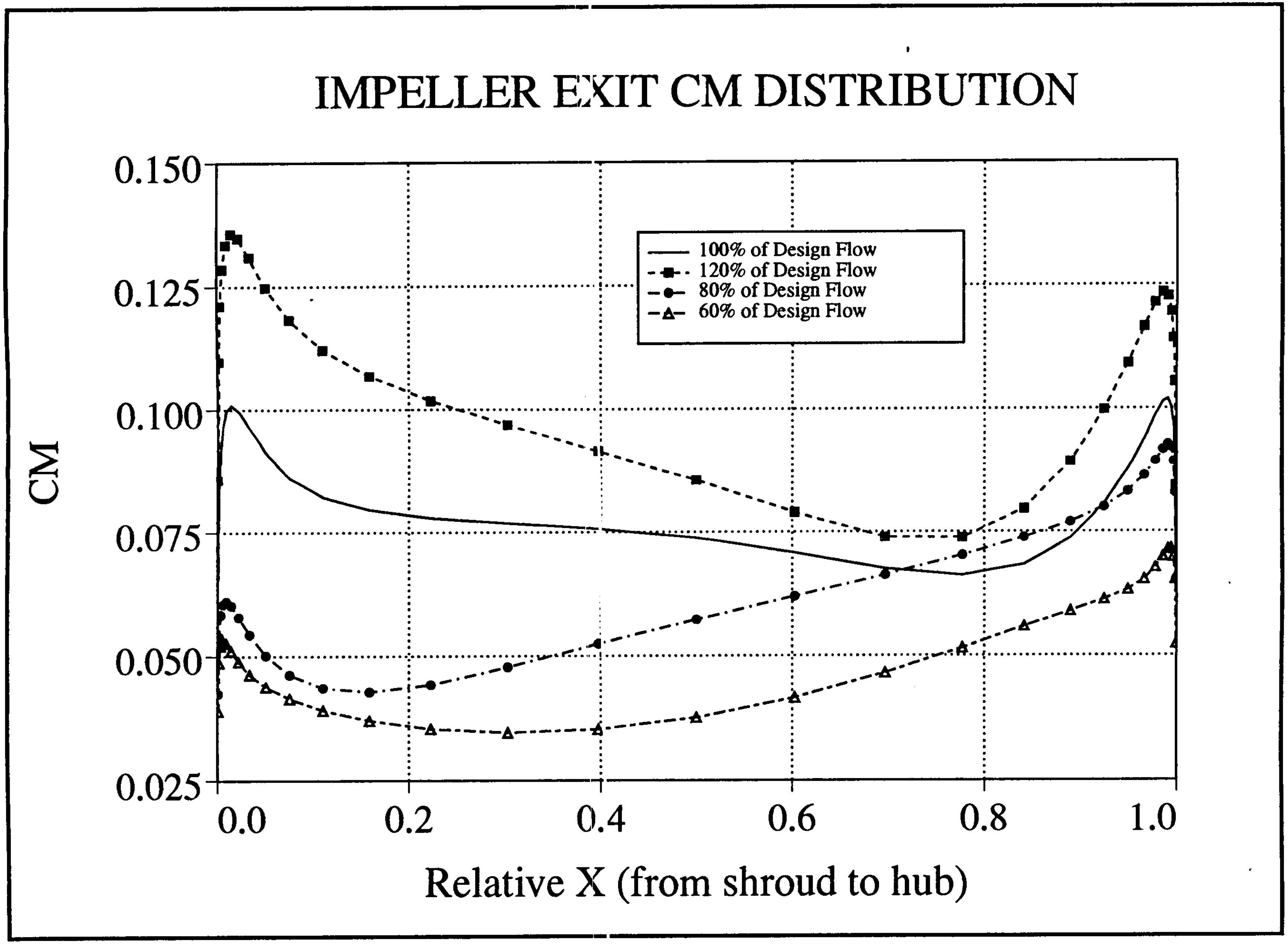
IMPELLER EXIT CM DISTRIBUTION
100% of Design Flow
120% of Design Flow
80% of Design Flow
60% of Design Flow
0.150
0.125
0.100
0.075
0.050
0.025
CM
0.0
0.2
0.4
0.6
0.8
1.0
Relative X (from shroud to hub)

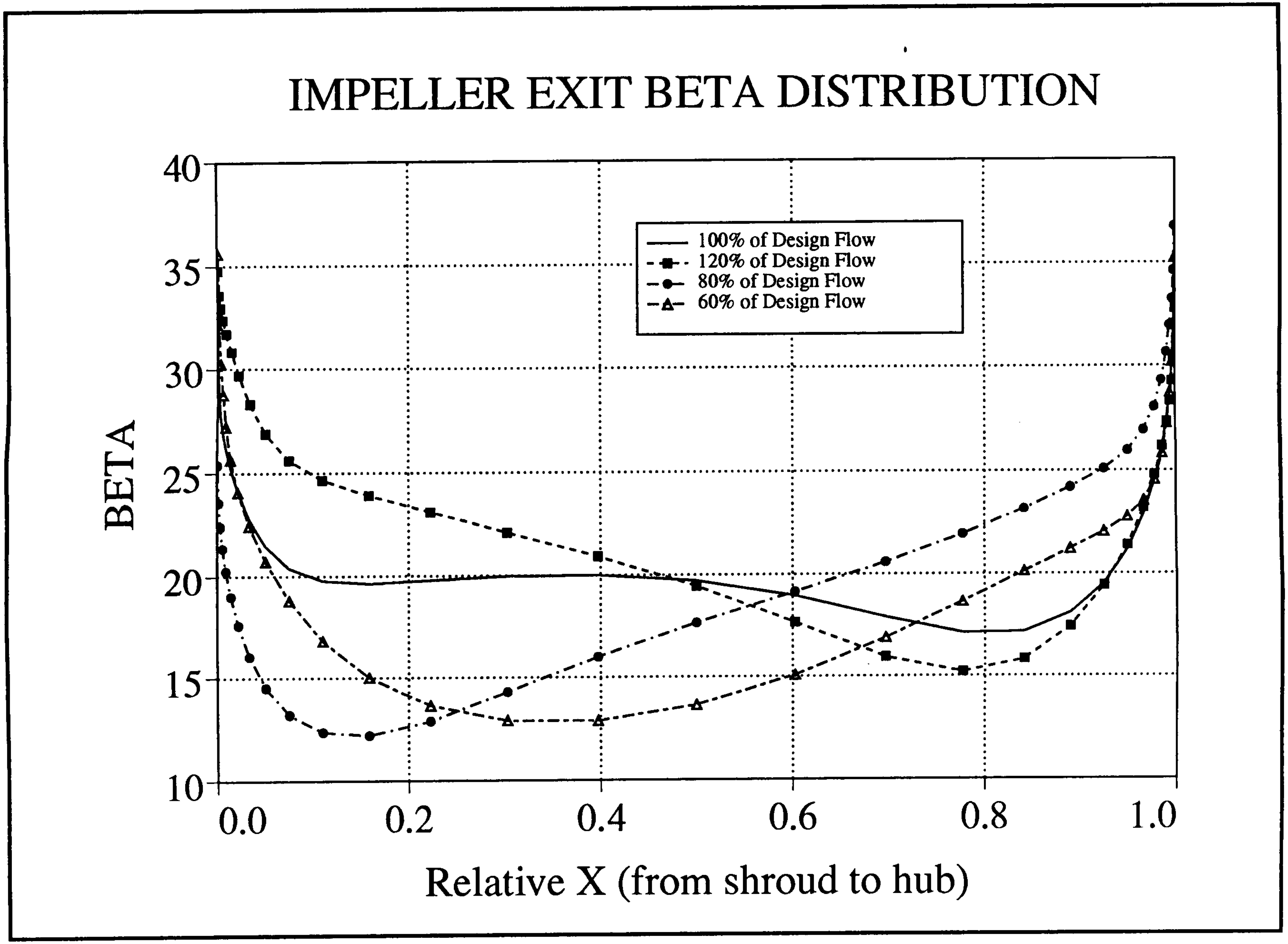

IMPELLER EXIT BETA DISTRIBUTION
100% of Design Flow
120% of Design Flow
80% of Design Flow
60% of Design Flow
BETA
Relative X (from shroud to hub)
40
35
30
25
20
15
10
0.0
0.2
0.4
0.6
0.8
1.0

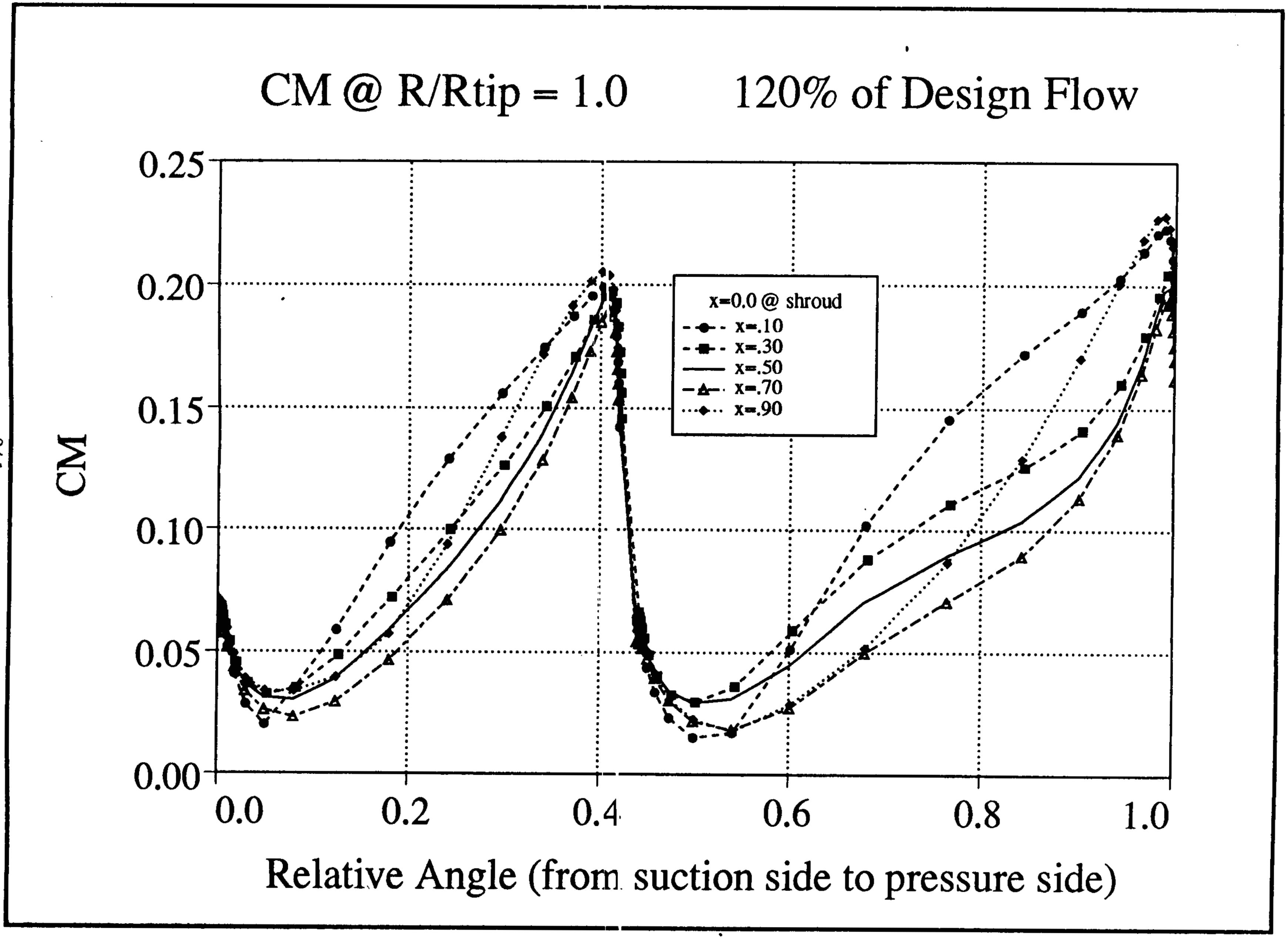
CM @ R/Rtip = 1.0 120% of Design Flow
0.25
0.20
0.15
0.10
0.05
0.00
CM
0.0
0.2
0.4
0.6
0.8
1.0
Relative Angle (from suction side to pressure side)
x=0.0 @ shroud
x=.10
x=.30
x=.50
x=.70
x=.90

IMPELLER OVERALL PARAMETERS

Design	Baseline	Optimized	Optimized	Optimized	Optimized	Opt.
Downstream Boundary	no-slip wall	no-slip wall	slip b.c.	slip b.c.	slip b.c.	slip b.c.
Design Flow	100 %	100 %	100 %	120 %	80 %	60 %
Efficiency	.946	.983	.943	.931	.955	.963
Head Coefficient	.663	.636	.659	.631	.667	.691
Relative Flow Angle, Deg	25.5	18.3	19.8	21.1	19.2	17.6
Absolute Flow Angle, Deg	7.01	6.44	6.63	7.31	4.33	3.10
Meridional Velocity	24.5	21.1	19.4	24.04	15.52	11.52
Flow Split	.45/.55	.47/.53	.43/.57	.435/.565	.415/585	.37/.63

Summary

- The present capability to compute a 3-D flow through a complex internal geometry is demonstrated. Advanced impeller analysis showed that overall parameters do not have a significant change between 80%, 100%, and 120% of design flow.

- Solution algorithm was tested and validated in model problems. Inducer computations indicate less than 10 % error in velocities. Tip and wake regions show biggest discrepancies. Future work will be focused on turbulence modeling.

- Solution procedure obtained here can be used in the design process of pump components.

N92-32289

COMPUTATION OF THE FLOW FIELD IN A CENTRIFUGAL IMPELLER WITH SPLITTER BLADES†

Frederik J. de Jong, Sang-Keun Choi, T.R. Govindan and Jayant S. Sabnis*
Scientific Research Associates, Inc.
Glastonbury, CT

ABSTRACT

To support the design effort of the STME Fuel Pump Stage, viscous flow calculations have been performed in a centrifugal impeller with splitter blades. These calculations were carried out with SRA's Navier-Stokes solver (MINT), which employs a linearized block-implicit ADI procedure to iteratively solve a finite difference form of the system of conservation equations of mass, momentum, and energy in body-fitted coordinates. A computational grid was generated algebraically for the "channel" between two main blades of the impeller and extended both upstream of the impeller inlet and downstream of the impeller exit so that the appropriate boundary conditions could be applied (viz. specified velocity profiles at the inflow boundary, and specified pressure at the outflow boundary).

The results of the calculations show that although the overall level of flow distortion near the impeller exit is not very large, there is a noticeable difference between the flow patterns in the two "passages" (one passage between the pressure side of the full blade and the suction side of the splitter blade, and the other one between the pressure side of the splitter blade and the suction side of the next full blade). For example, the pressure distribution shows that the splitter blade is loaded less heavily than the main blade. At the same time, the flow distortion near the suction side of the main blade is larger than that near the suction side of the splitter blade. A better understanding of these results can be obtained by studying "particle traces" (streamlines in a frame of reference fixed to the rotating impeller). These traces show that a significant amount of low momentum fluid (originating from the hub and shroud boundary layers) moves from the pressure side to the suction side in the impeller "channel" ahead of the splitter blade, and ends up in the passage between the pressure side of the splitter blade and the suction side of the full blade. This explains why the region of flow distortion in this passage is larger than that in the other passage, and why the mass flow through this channel is less. The understanding of the physics of impeller flow fields that results from analyzing viscous flow calculations such as the one described above is very valuable in pump stage design.

† This work was supported by NASA Marshall Space Flight Center under Contract NAS8-38866.

* Currently at United Technologies Research Center, East Hartford, CT

PRECEDING PAGE BLANK NOT FILMED

OBJECTIVES

- DEVELOPMENT OF A PREDICTIVE TOOL FOR THE VISCOUS FLOW IN CENTRIFUGAL IMPELLERS
- SUPPORT OF DESIGN EFFORT OF STME FUEL PUMP STAGE
- ENHANCEMENT OF UNDERSTANDING OF PHYSICAL FLOW PHENOMENA

Scientific Research Associates

APPROACH

- EQUATIONS SOLVED:

  REYNOLDS-AVERAGED NAVIER-STOKES EQUATIONS IN ROTATING BODY-FITTED COORDINATES

- METHOD OF SOLUTION:

  LINEARIZED BLOCK IMPLICIT (ADI) SCHEME

- TURBULENCE MODEL:

  MIXING LENGTH OR TWO-EQUATION (K-ε)

Scientific Research Associates

GEOMETRY

- SHROUDED IMPELLER
- SIX FULL ("MAIN") BLADES, SIX PARTIAL ("SPLITTER") BLADES
- ROTATING VANELESS DIFFUSER SECTION DOWNSTREAM
- ROTATING HUB AND NON-ROTATING END WALL UPSTREAM
- COMPUTATIONAL DOMAIN = "DUCT" BETWEEN TWO MAIN BLADES, WITH UPSTREAM AND DOWNSTREAM EXTENSIONS

Scientific
Research
Associates

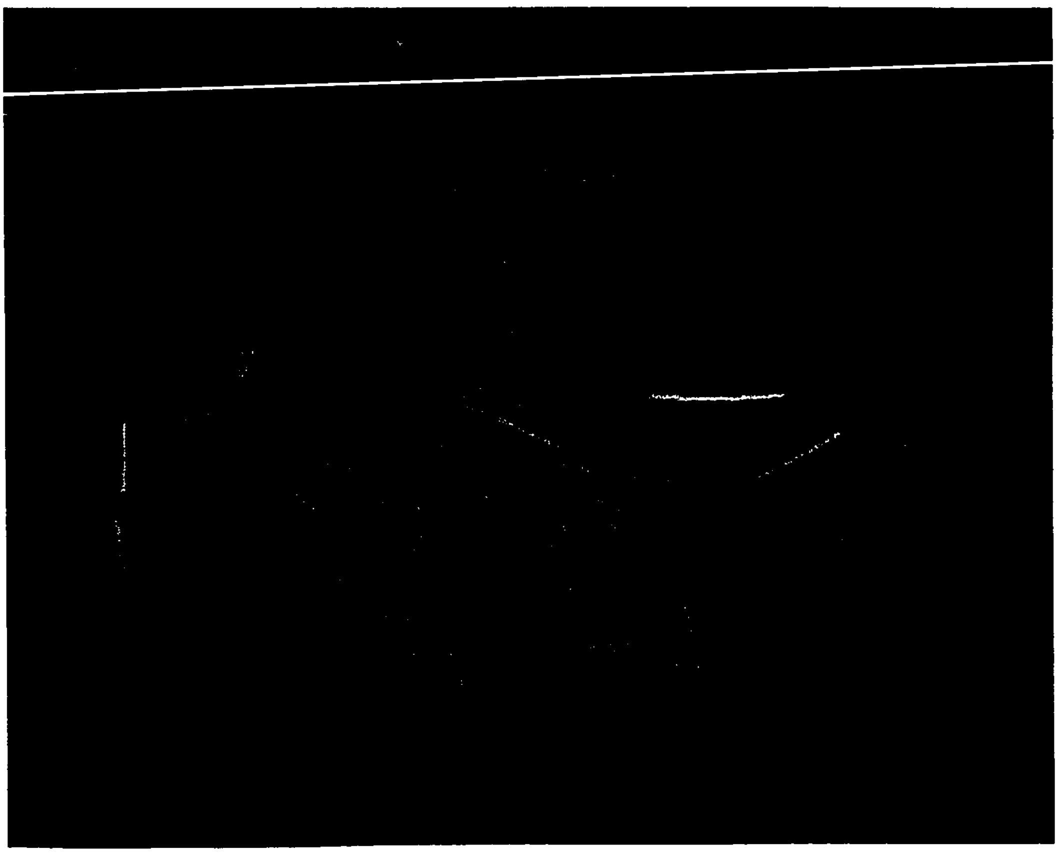

BOUNDARY CONDITIONS

- INFLOW:
  VELOCITY PROFILES, STAGNATION TEMPERATURE
- OUTFLOW:
  CONSTANT PRESSURE
- WALLS:
  NO-SLIP, ADIABATIC
- UPSTREAM AND DOWNSTREAM MAIN BLADE EXTENSIONS:
  PERIODICITY

Scientific Research Associates

WATER TEST CONDITIONS

- DIMENSIONS

INLET TIP DIAMETER		6.0	INCH	(=	0.1524	M)
INLET HUB DIAMETER		3.9	INCH	(=	0.0991	M)
EXIT TIP DIAMETER	D	9.045	INCH	(=	0.2297	M)

- FLOW CONDITIONS

DESIGN SPEED	ω	6322	RPM	(=	662	RAD/S)
TIP SPEED	u	249.5	FT/S	(=	76.05	M/S)
DESIGN FLOW	Q	1205	GPM	(=	0.0760	M^3/S)
AVERAGE INFLOW VELOCITY		23.7	FT/S	(=	7.22	M/S)
FLOW COEFFICIENT	ϕ	0.095				
REYNOLDS NUMBER	$Q/\upsilon D$	$5.5\ 10^4$				
	uD/υ	$2.9\ 10^6$				

Scientific Research Associates

COMPUTATIONAL GRID

- ALGEBRAICALLY GENERATED GRID
- NUMBER OF GRID POINTS = 160,446
  - 121 POINTS IN "STREAMWISE" DIRECTION (WITH 61 POINTS ON THE MAIN BLADE AND 41 POINTS ON THE PARTIAL BLADE)
  - 26 POINTS FROM HUB TO SHROUD
  - 51 POINTS IN CIRCUMFERENTIAL DIRECTION (FROM BLADE TO BLADE)
- GRID SPACING (BASED ON TIP DIAMETER)
  - 10^{-5} NEAR HUB AND SHROUD
  - $5\ 10^{-5} - 10^{-4}$ NEAR BLADE SURFACES

Scientific Research Associates

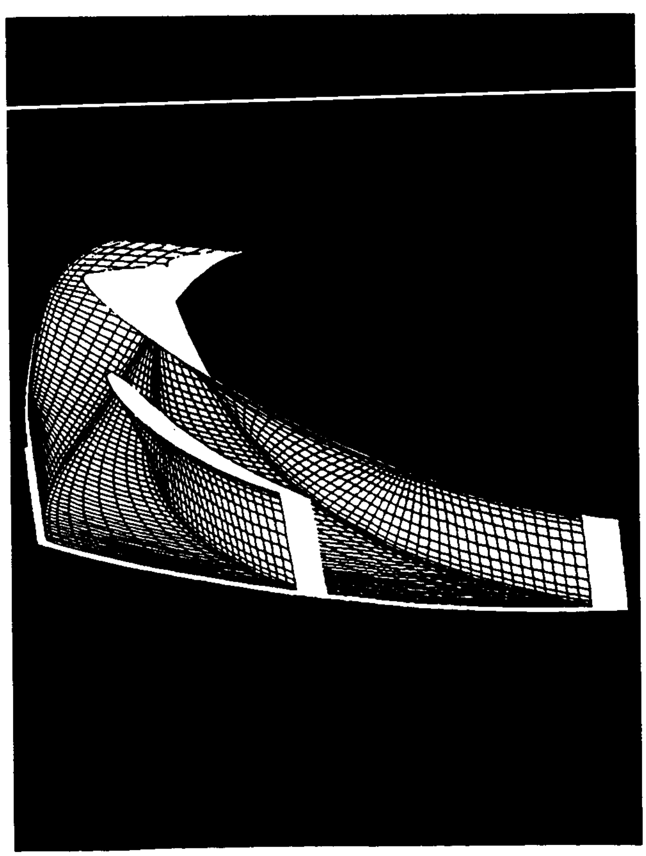

IMPELLER GEOMETRY
MERIDIONAL SURFACE

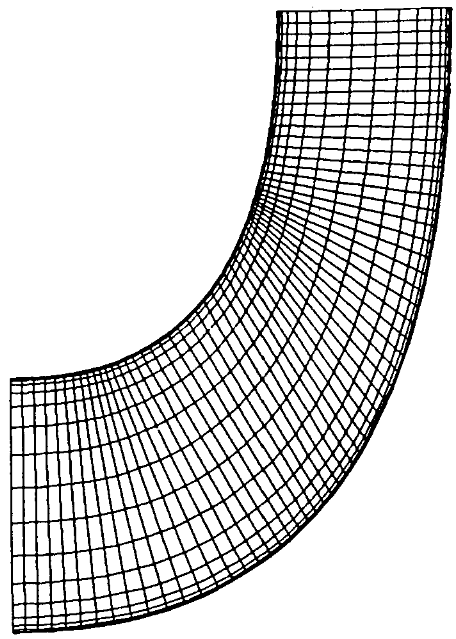

Scientific Research Associates

PRESSURE IN MERIDIONAL SURFACE
BETWEEN SPLITTER PRESSURE SIDE AND BLADE SUCTION SIDE

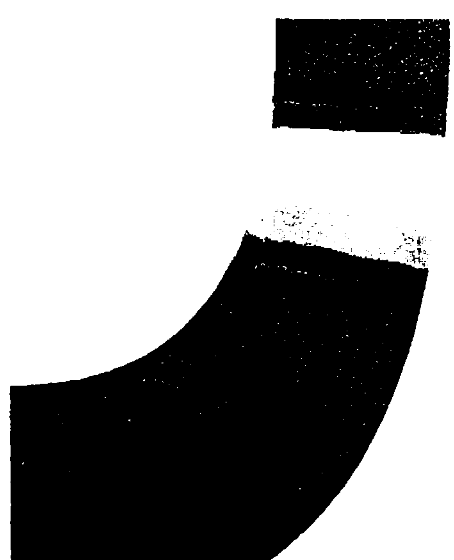

VELOCITY MAGNITUDE IN MERIDIONAL SURFACE

BETWEEN BLADE PRESSURE SIDE AND SPLITTER SUCTION SIDE

VELOCITY MAGNITUDE IN MERIDIONAL SURFACE

BETWEEN SPLITTER PRESSURE SIDE AND BLADE SUCTION SIDE

STREAMWISE VELOCITY IN MERIDIONAL SURFACE
BETWEEN BLADE PRESSURE SIDE AND SPLITTER SUCTION SIDE

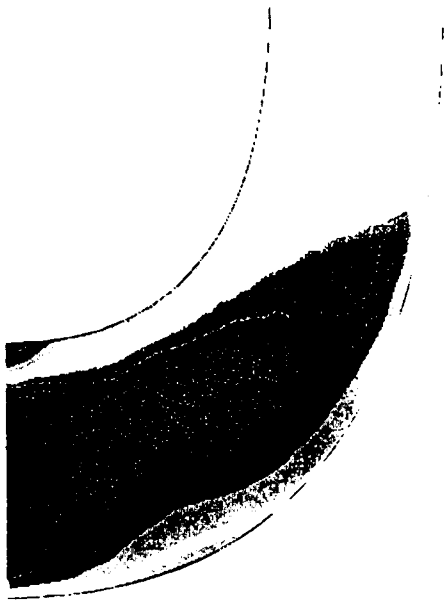

Scientific
Research
Associates

STREAMWISE VELOCITY IN MERIDIONAL SURFACE
BETWEEN SPLITTER PRESSURE SIDE AND BLADE SUCTION SIDE

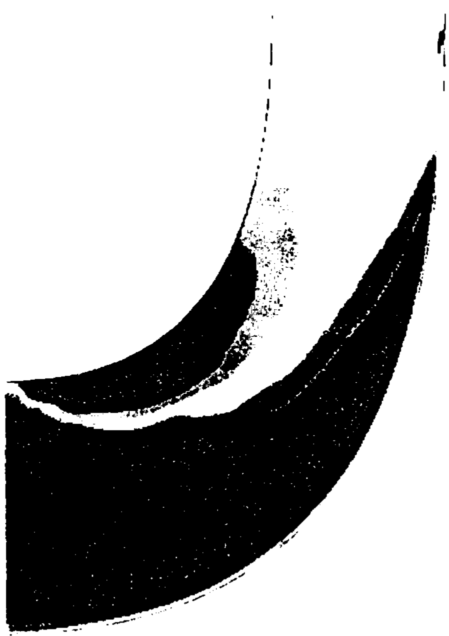

IMPELLER GEOMETRY
MID-SPAN BLADE-TO-BLADE SURFACE

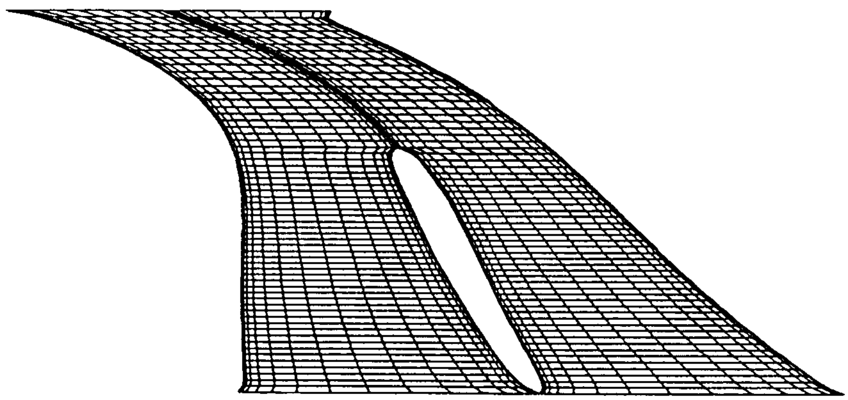

Scientific Research Associates

PRESSURE

VELOCITY MAGNITUDE

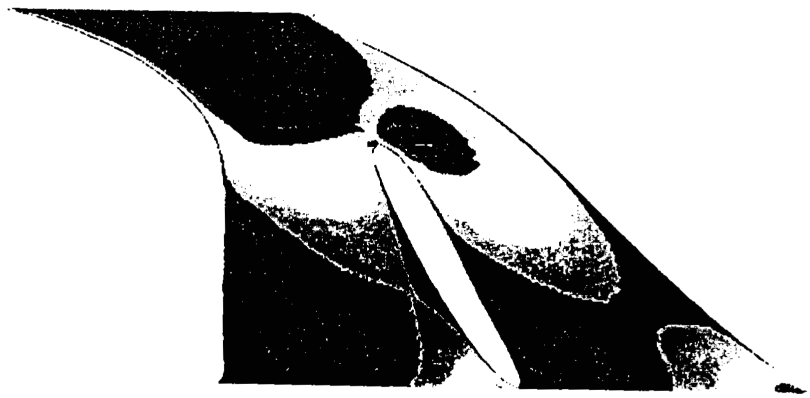

Scientific
Research
Associates

STREAMWISE VELOCITY

IMPELLER GEOMETRY

CROSS-SECTION NEAR TRAILING EDGE

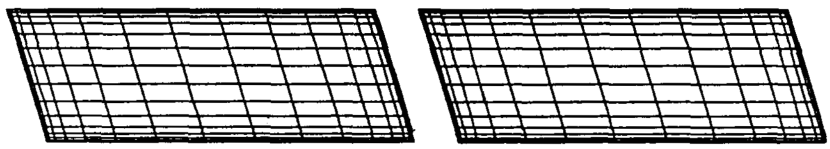

Scientific
Research
Associates

PRESSURE

VELOCITY MAGNITUDE

Scientific
Research
Associates

STREAMWISE VELOCITY

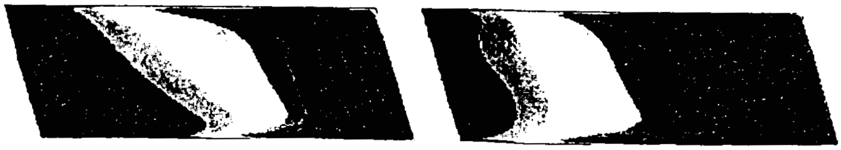

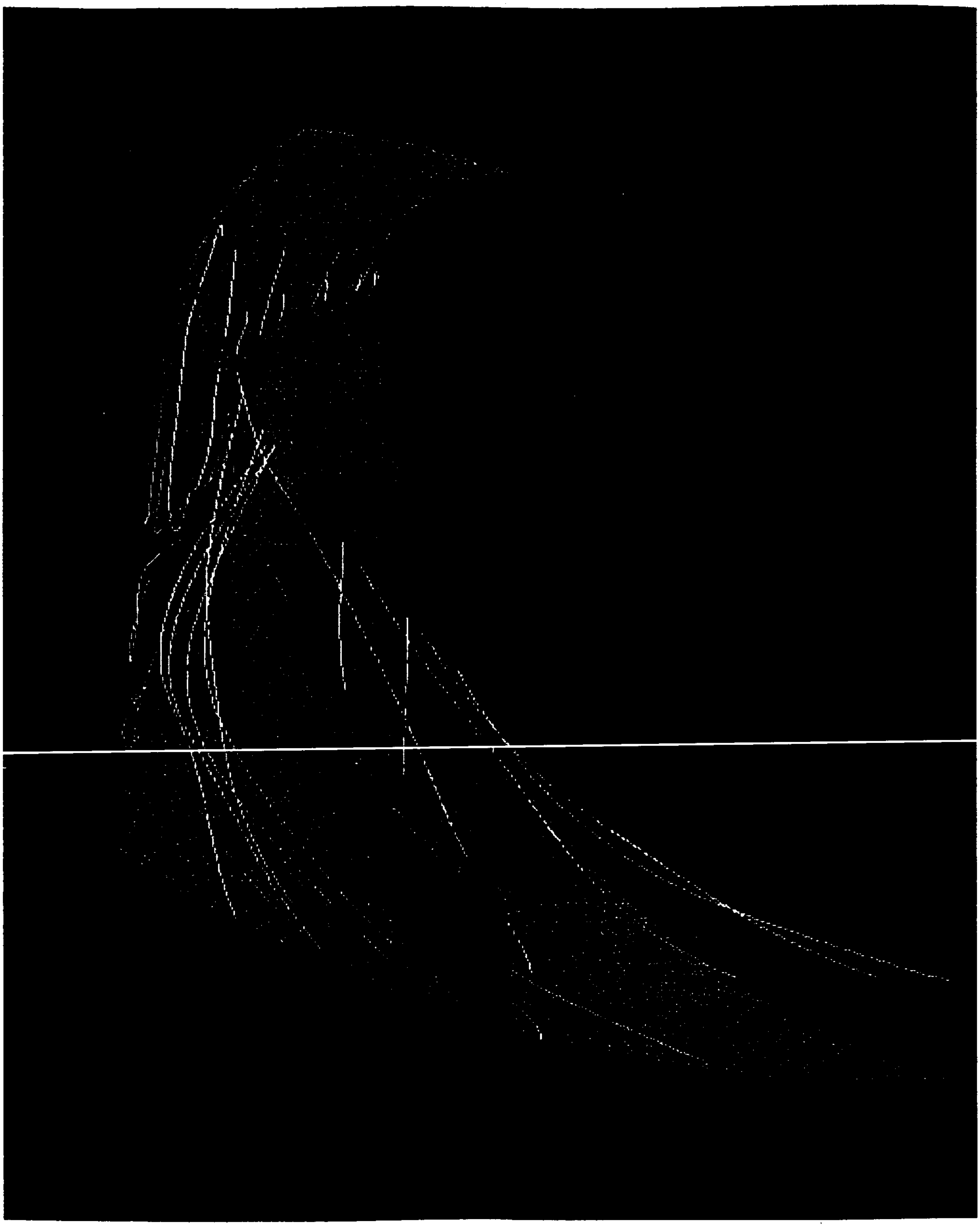

PARTICLE TRACES

SUMMARY

- NAVIER-STOKES PROCEDURE HAS BEEN USED TO SIMULATE THE FLOW FIELD IN A CENTRIFUGAL IMPELLER WITH SPLITTER BLADES
- ANALYSIS OF THE RESULTS PROVIDES UNDERSTANDING OF THE PHYSICAL FLOW PHENOMENA
    - VALUABLE IN PUMP STAGE DESIGN
    - USEFUL TO GUIDE CFD CODE DEVELOPMENT

Scientific
Research
Associates

N92-32290

IMPELLER TANDEM BLADE STUDY WITH GRID EMBEDDING FOR LOCAL GRID REFINEMENT

George Bache'

Aerojet Propulsion Division
Bldg. 2019; Dept. 5236
P.O. Box 13222
Sacramento CA 95813-6000

ABSTRACT

Flow non-uniformity at the discharge of high power density impellers can result in significant unsteady interactions between impeller blades and downstream diffuser vanes. These interactions result in degradation of both performance and pump reliability. The MSFC Pump Technology Team has regognized the importance of resolving this problem and has thus initiated the development and testing of a high head coefficient impeller. One of the primary goals of this program is to improve impeller performance and discharge flow uniformity. The objective of the present work is complimentary. Flow uniformity and performance gains were sought through the application of a tandem blade arrangement. The approach adopted was to numerically establish flow characteristics at the impeller discharge for the baseline MSFC impeller and then parametrically evaluate tandem blade configurations. A tandem design was sought that improves both impeller performance and discharge uniformity. The Navier-Stokes solver AEROVISC was used to conduct the study. Grid embedding is used to resolve local gradients while attempting to minimize model size. Initial results indicate that significant gains in flow uniformity can be achieved through the tandem blade concept and that blade clocking rather than slot location is the primary driver for flow uniformity.

ORIGINAL PAGE IS
OF POOR QUALITY

GENCORP
AEROJET

Propulsion Division

IMPELLER TANDEM BLADE STUDY WITH GRID EMBEDDING FOR LOCAL GRID REFINEMENT

GEORGE BACHE'

AEROJET PROPULSION DIVISION

10th WORKSHOP FOR COMPUTATIONAL FLUID DYNAMIC
APPLICATION IN ROCKET PROPULSION

APRIL 28-30, 1992

GENCORP
AEROJET

Propulsion Division

IMPELLER TANDEM BLADE STUDY WITH GRID EMBEDDING FOR LOCAL GRID REFINEMENT

George Bache'

Aerojet Propulsion Division
Bldg. 2019; Dept. 5236
P.O. Box 13222
Sacramento CA 95813-6000

ABSTRACT

Flow non-uniformity at the discharge of high power density impellers can result in significant unsteady interactions between impeller blades and downstream diffuser vanes. These interactions result in degradation of both performance and pump reliability. The MSFC Pump Technology Team has regognized the importance of resolving this problem and has thus initiated the development and testing of a high head coefficient impeller. One of the primary goals of this program is to improve impeller performance and discharge flow uniformity. The objective of the present work is complimentary. Flow uniformity and performance gains were sought through the application of a tandem blade arrangement. The approach adopted was to numerically establish flow characteristics at the impeller discharge for the baseline MSFC impeller and then parametrically evaluate tandem blade configurations. A tandem design was sought that improves both impeller performance and discharge uniformity. The Navier-Stokes solver AEROVISC was used to conduct the study. Grid embedding is used to resolve local gradients while attempting to minimize model size. Initial results indicate that significant gains in flow uniformity can be achieved through the tandem blade concept and that blade clocking rather than slot location is the primary driver for flow uniformity.

GENCORP
AEROJET

MOTIVATION FOR WORK

- HIGH POWER DENSITY IMPELLERS USED IN ROCKET PROPUSLION TURBOPUMPS PRODUCE SIGNIFICANT UNSTEADY INTERACTIONS BETWEEN IMPELLER BLADES AND DOWNSTREAM DIFFUSER VANES.

- PERFORMANCE DEGRADATION

- REDUCED COMPONENT LIFE (RELIABITY)

- GOAL: USE TANDEM BLADE CONCEPT TO IMPROVE IMPELLER PERFORMANCE AND/OR DISCHARGE FLOW UNIFORMITY

APPROACH

- PREDICT FLOW IN MSFC PUMP TECHNOLOGY TEAM BASELINE IMPELLER

- NUMERICALLY STUDY SEVERAL TANDEM BLADE CONFIGURATIONS

- PARAMETRICALLY VARY SLOT LOCATION AND CLOCKING

- PERFORM NUMERICAL PARAMETRICS WITH AEROVISC

- JUDGE IMPROVEMENTS BASED ON PERFORMANCE AND DISCHARGE FLOW UNIFORMITY

Aerovisc Numerics

- Formulation
  - Reynolds Stress Averaged Navier-Stokes Equations
  - Cartesian Primitive Variable Approach
  - Strongly Conservative, Colocated Form
  - k-e and ARS Turbulence Models With Wall Functions
  - 2 Layer Turbulence Model
- Discretization
  - Flux Element Based Finite Volume Method
  - General Non-Orthogonal Boundary-Fitted Structured Grid
  - Advection Schemes Have Two Components
    - Upwind Skew Scheme (UDS, MWS, LPS) ==> Transverse Gradients
    - Physically Based Correction Term (PAC) ==> Streamwise Gradients
  - Rhie Type 4th Order Pressure Redistribution
    - Pressure /Velocity Coupling For I.C. Flows
- Solver
  - Vectorized Gauss-Siedel or Incomplete Cholesky Base Solver
  - Multigrid (Large Grids) and Block Correction (High Aspect Ratio Grids)

GENCORP AEROJET

Demonstrated Code Capabilities

Propulsion Division

- Applicable Flow Ranges
  - Incompressible
  - Subsonic, Transonic and Supersonic
  - Laminar, Turbulent or Inviscid
  - Multi-Component
  - 2-Phase (Solid Particle / Gas)
- Coriolis and Centrifugal Terms For Turbomachinery Applications
- Conjugate Heat Transfer or Specified Wall Temperature / Flux
- Flexible Geometric Modeling Features
  - Arbitrary Periodicity
  - Multiple Blocked Regions
  - Grid Embedding or Attaching
- Fixed, Moving or Rotating Walls
- Variable Fluid and / or Solid Properties

GENCORP
AEROJET

Solid Model of Eckardt Compressor

Propulsion Division

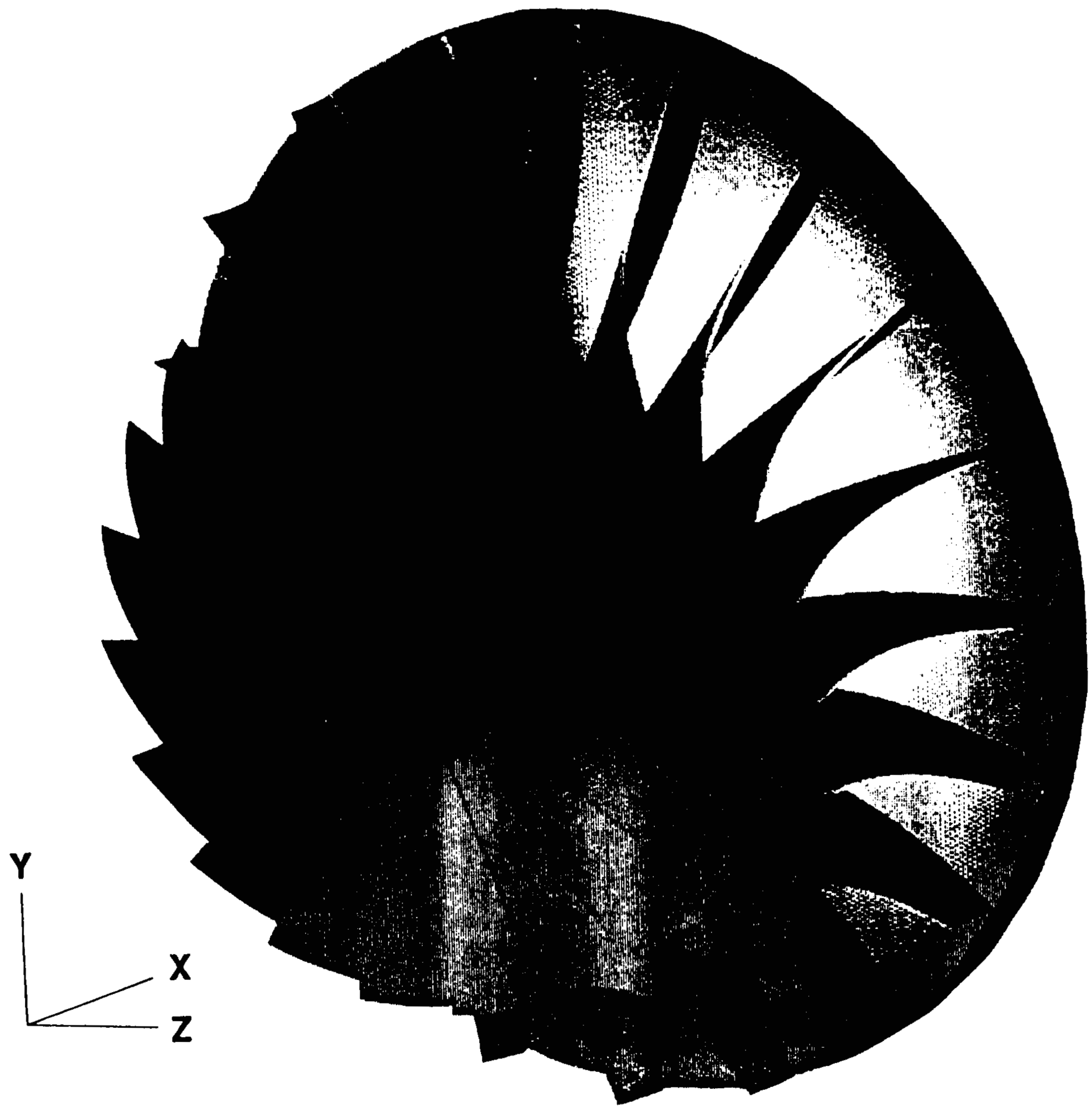

The Krain Impeller – Introduction

- 24 Blades, 22,363 rpm, 4.7 Design Pressure Ratio, 4.0 kg/s Total Mass Flow
- Computational Domain Includes Inlet, Tip Region, and Diffuser
- Absolute Frame Total Pressure and Total Temperature at Inlet, Mass Flow Specified at Outlet, Log-Law Used at Walls
- 80,000 Nodes, Second-Order-Accurate Skew Upwind Scheme, Coupled Multigrid
- Note: Inlet Geometry Was Estimated

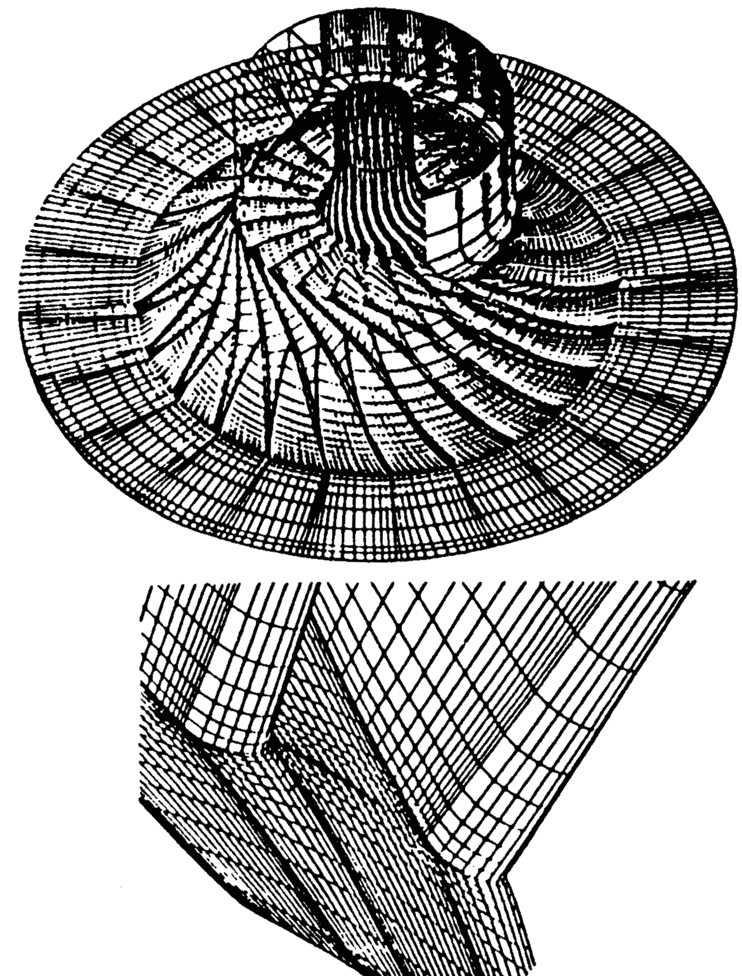

IR&D-7

The Krain Impeller – Comparisons to Data

- Total Run Time About 150 Hours on a Personal Iris 4D/25
- Measured Total Pressure Ratio Was About 4.1, the Code Predicted 4.26

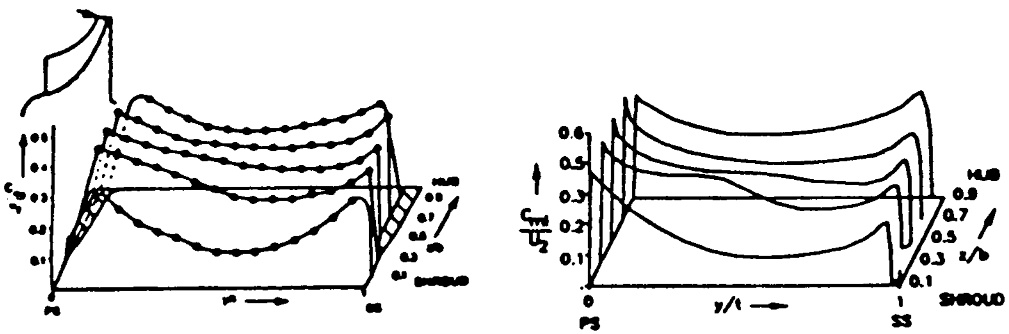

Meridional Velocity Components at Outlet Data (Left) Calculation (Right)

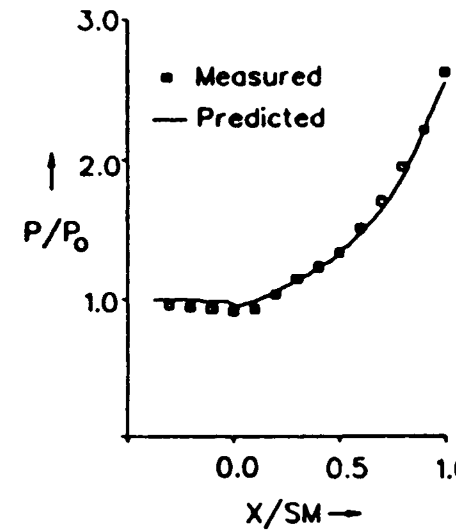

Circumferentially Averaged Shroud Static Pressure

IR&D-7


VALIDATION INDUCER
X
Y
Z

INDUCER CODE VALIDATION

PLANE B, X=2.725 IN., ANGLE=-133.755 DEG.

POSITION 5, RADIUS= 2.365 IN.

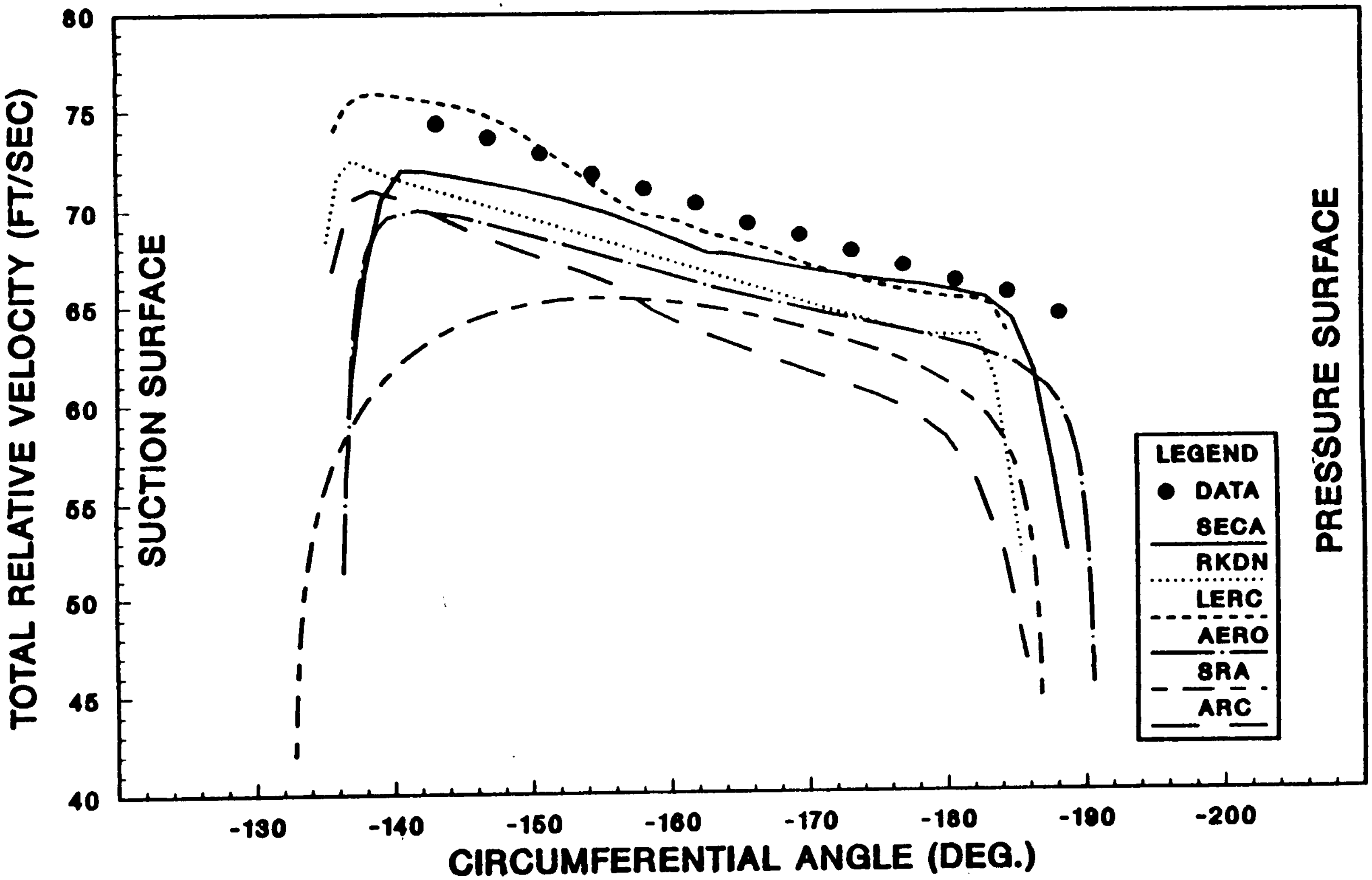

INDUCER CODE VALIDATION

PLANE B, X=2.725 IN., ANGLE=-133.755 DEG.

POSITION 5, RADIUS= 2.365 IN.

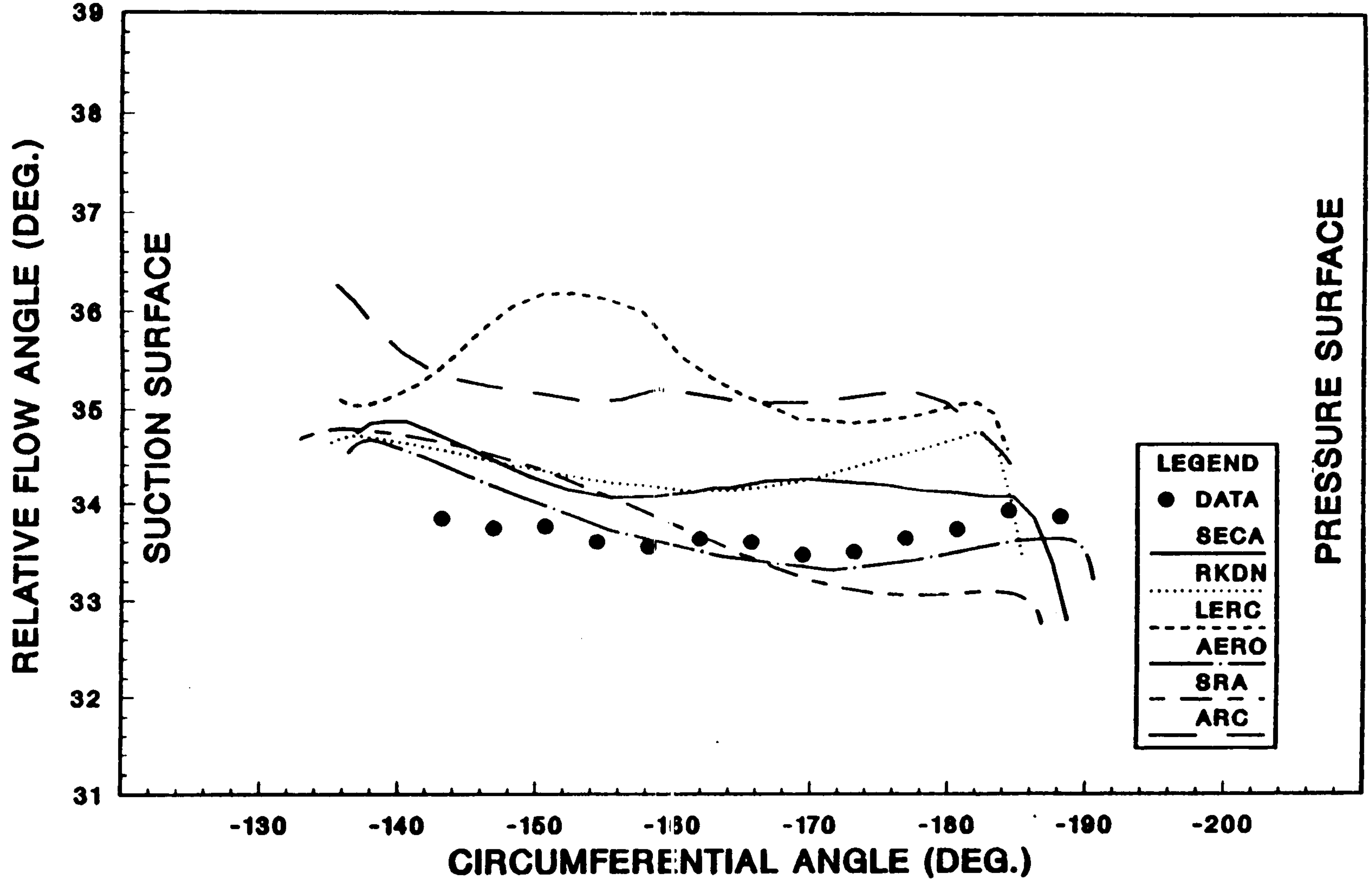

GENCORP
AEROJET
Propulsion Division

- FLUID - HYDROGEN
- 6 FULL + 6 PARTIAL
- N = 30108 RPM
- TIP DIAM. = 14.14 in.
- TIP SPEED = 1857 fps
- OUTLET BLADE ANGLE = 49.5 deg.
- SPECIFIC SPEED = 1141
- HEAD COEFF. = 0.572

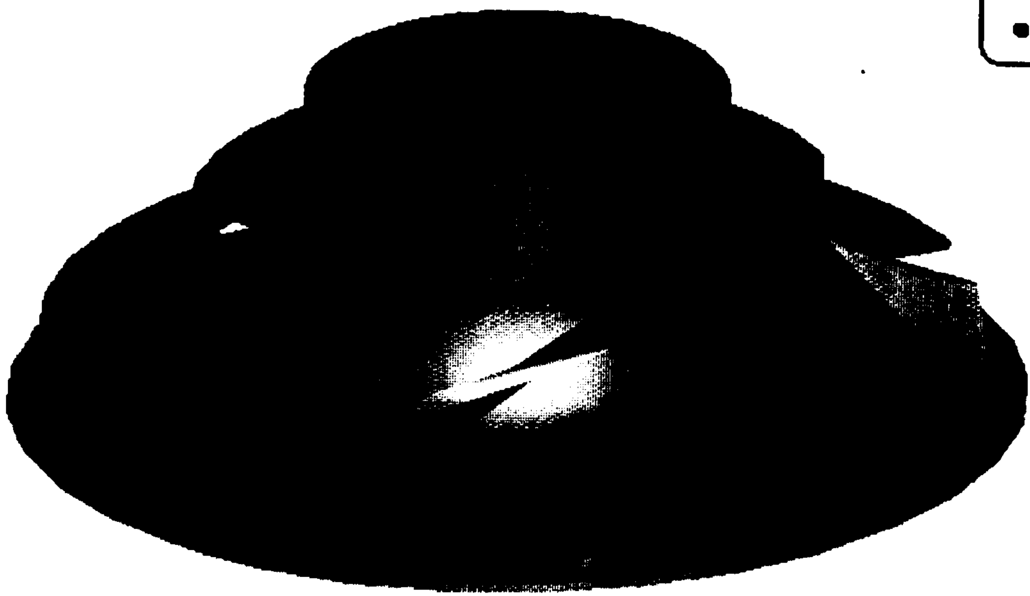

MSFC PUMP CFD CONSORTIUM IMPELLER

GenCorp
Aerojet
Propulsion Division

MSFC PUMP CFD CONSORTIUM IMPELLER

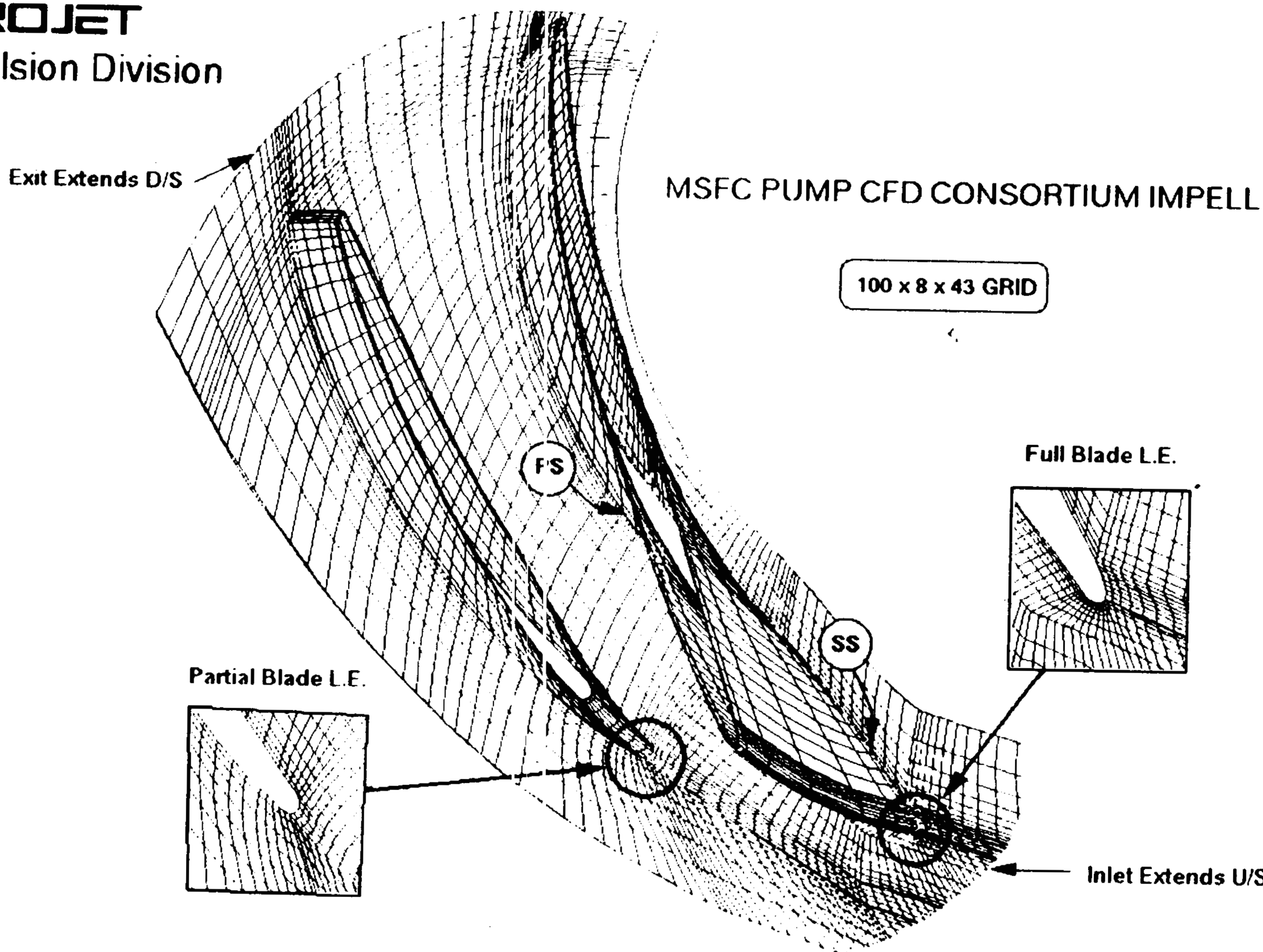

GENCORP AEROJET

Propulsion Division

BASELINE IMPELLER, VISCOUS SOLUTION

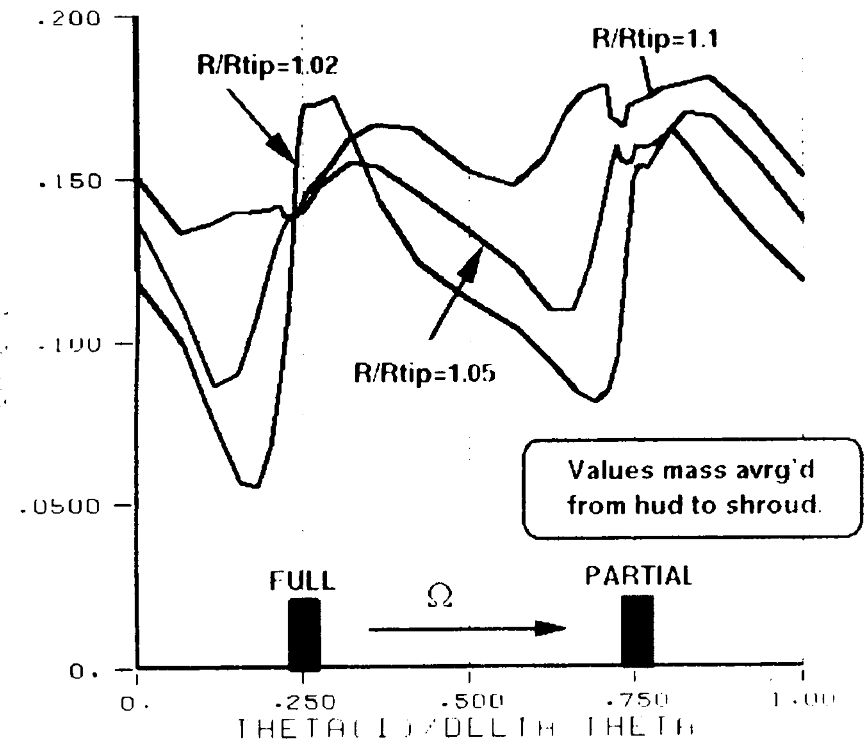

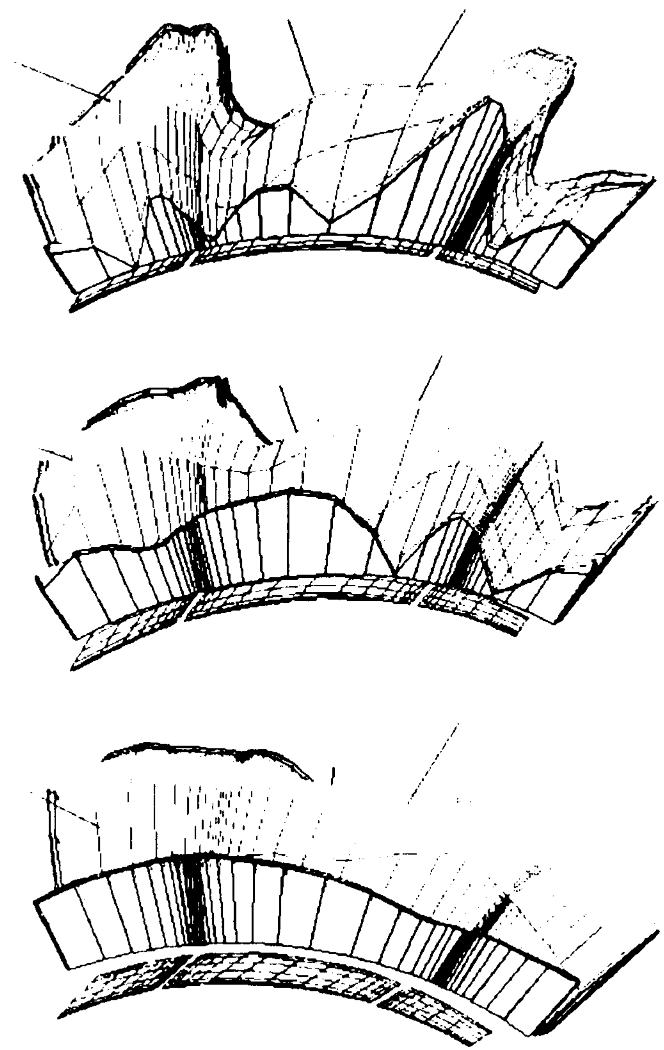

Utip=1858 fps , A0=60 Deg , mass flow split 45% - 55%

GENCORP
AEROJET
Propulsion Division

IMPELLER DOWNSTREAM PROFILE

BASELINE CONFIGURATION 34K NODES

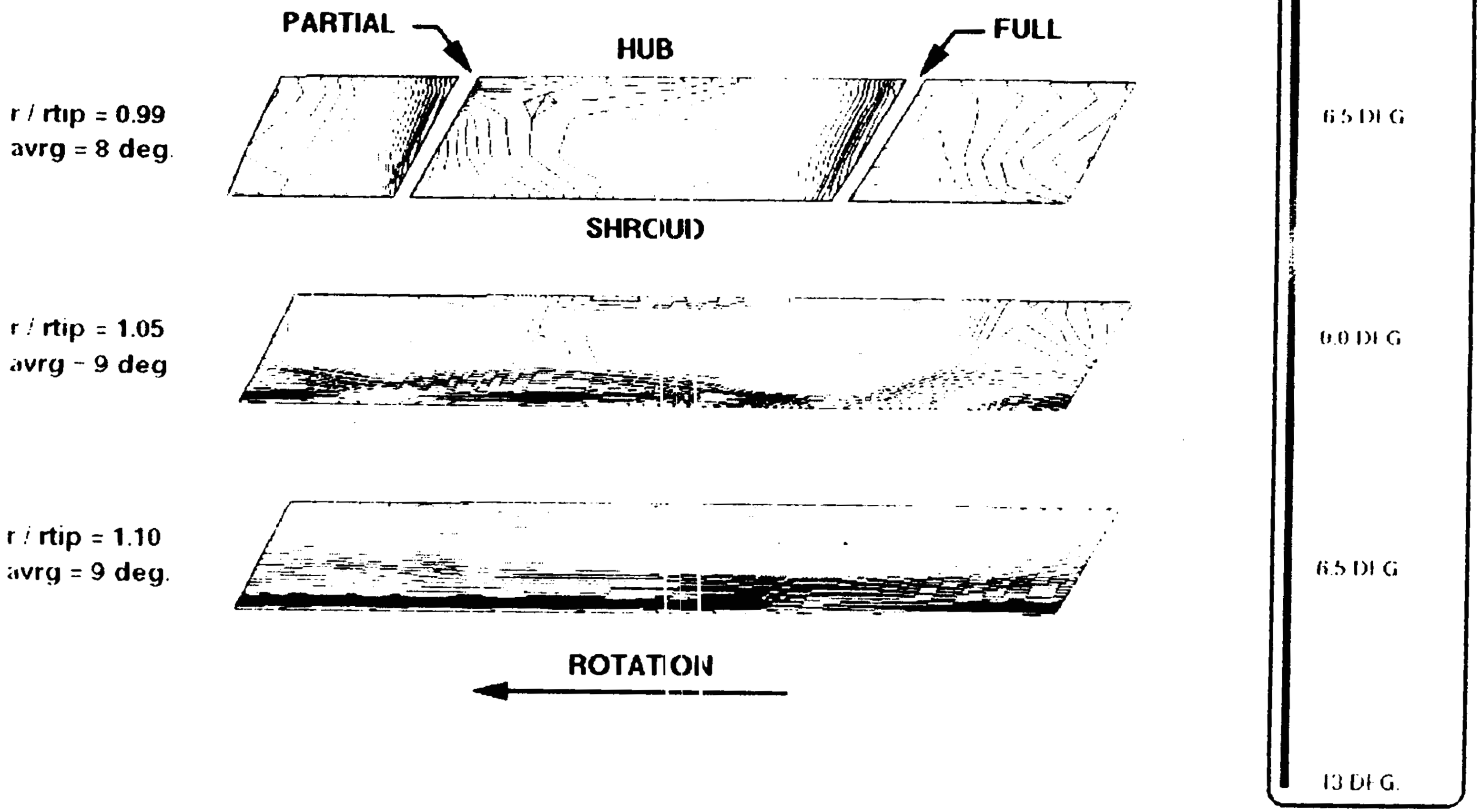

GENCORP
AEROJET
Propulsion Division

IMPELLER DOWNSTREAM PROFILE

BASELINE CONFIGURATION 34K NODES

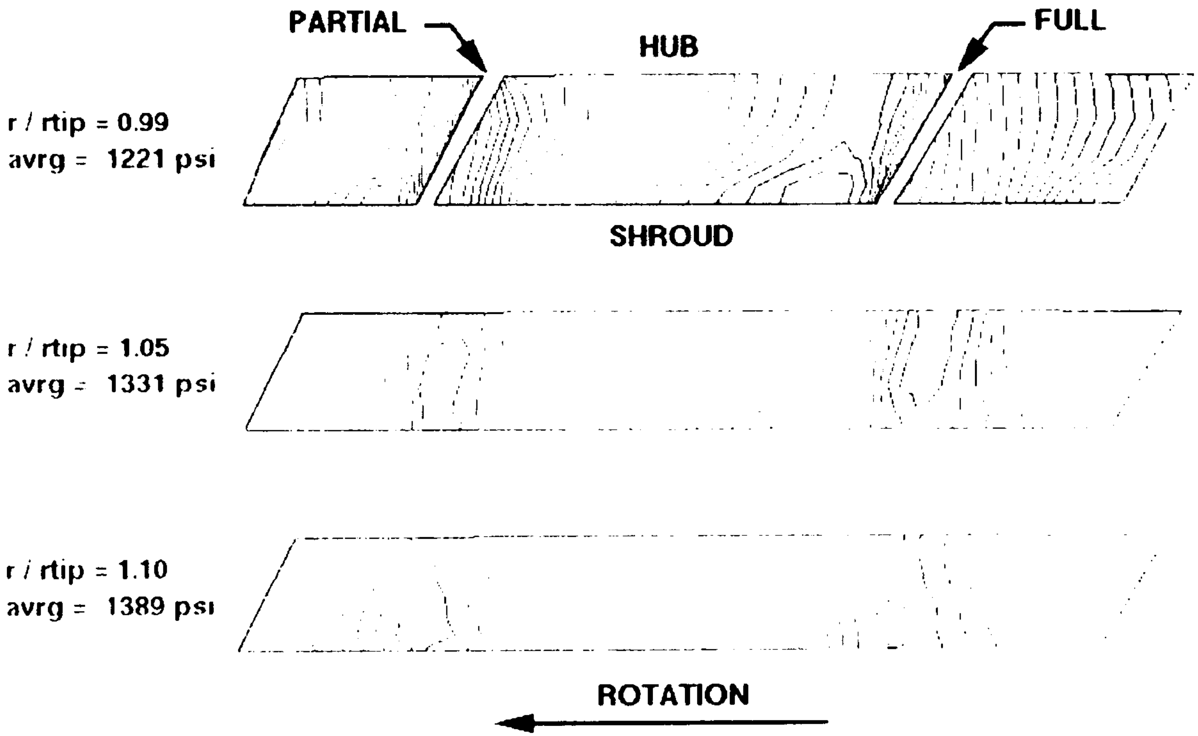

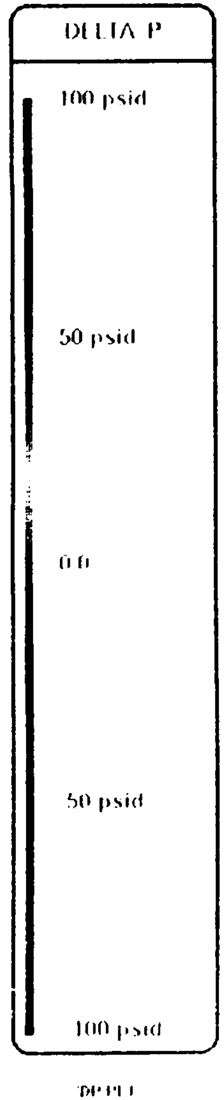

GenCorp
Aerojet

Propulsion Division

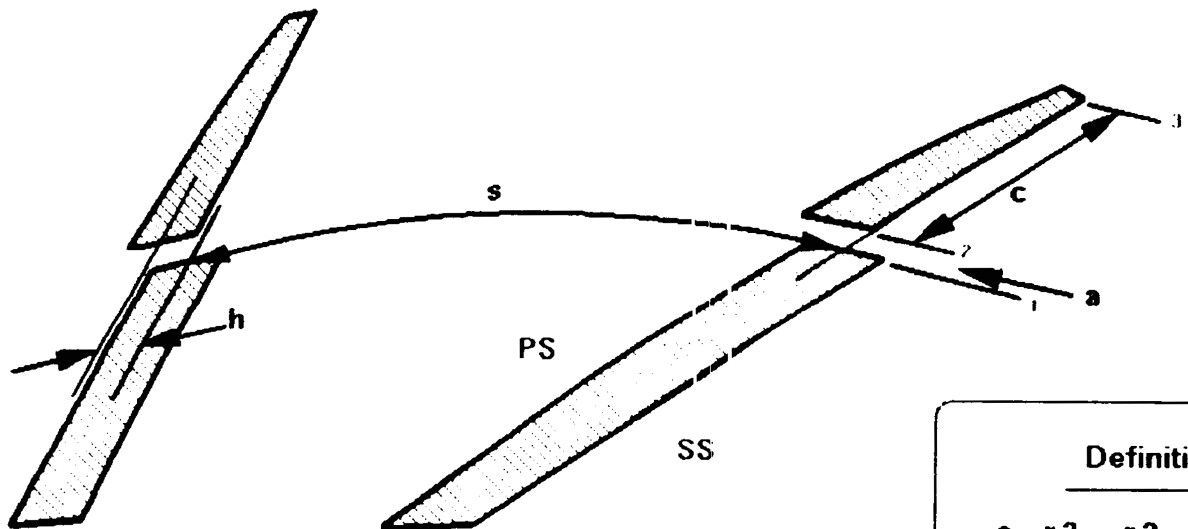

Definitions

c = r 3 - r 2
a = r 2 - r 1
s = r 1 × (delta theta) full - partial
h = r 1 × (delta theta) shift

GenCorp
Aerojet
Propulsion Division

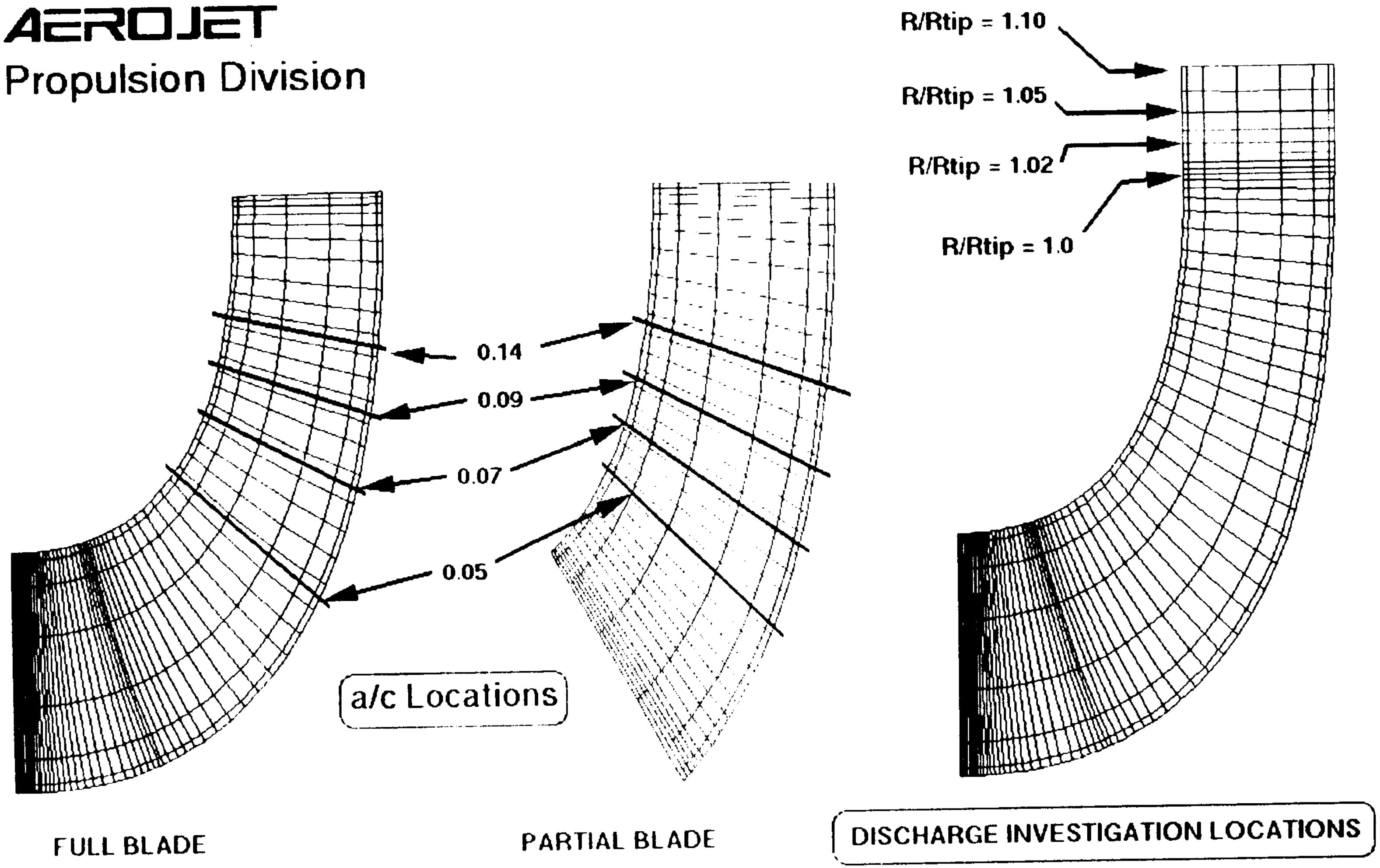

GENCORP AEROJET

CONFIGURATIONS AND STATUS

Propulsion Division

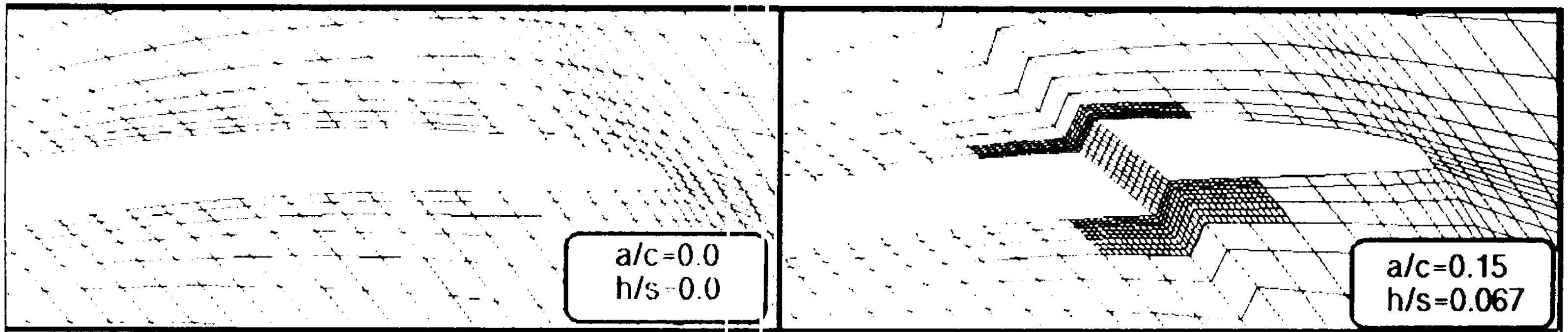

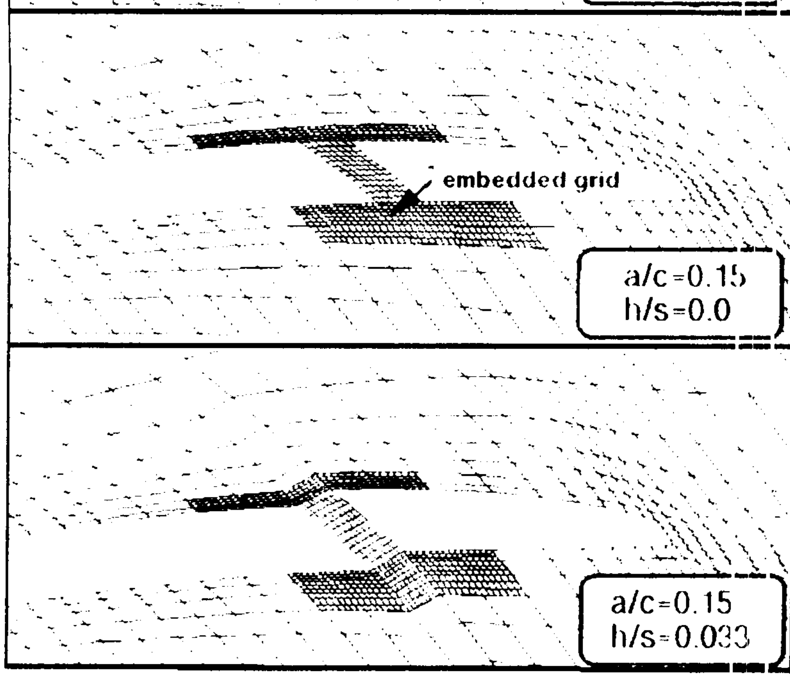

BASELINE INVISCID	→	Complete
BASELINE VISCOUS	→	Complete
a/c=0.14 ; h/s=0.0	→	Complete
h/s=0.033		Complete
h/s=0.067		Complete
a/c=0.09 ; h/s=0.0	→	Complete
a/c=0.07 ; h/s=0.0	→	Complete
a/c=0.05 ; h/s=0.0	→	Complete

100x8x43 Main Grid ; 36x8x28 and 36x8x40 Embedded Grids

GENCORP
AEROJET
Propulsion Division

IMPELLER DISCHARGE CIRC. Cm DISTRIBUTION
Mass Averaged Hub to Tip

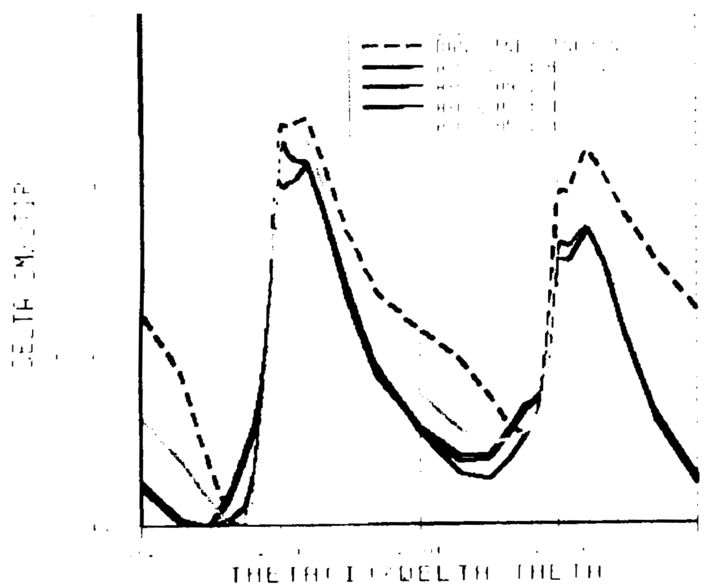

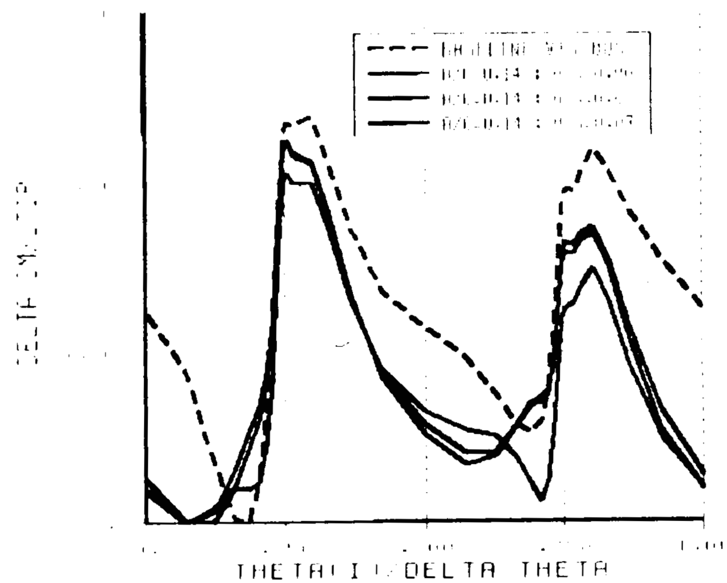

R/Rtip = 1.02

ORIGINAL PAGE IS
OF POOR QUALITY

GenCorp Aerojet

Propulsion Division

ORIGINAL PAGE IS OF POOR QUALITY

IMPELLER DISCHARGE CIRC. Cm DISTRIBUTION
Mass Averaged Hub to Tip

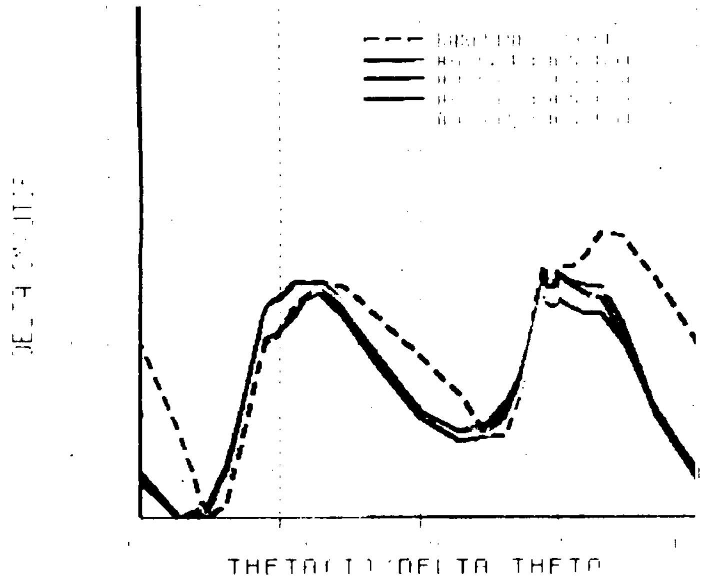

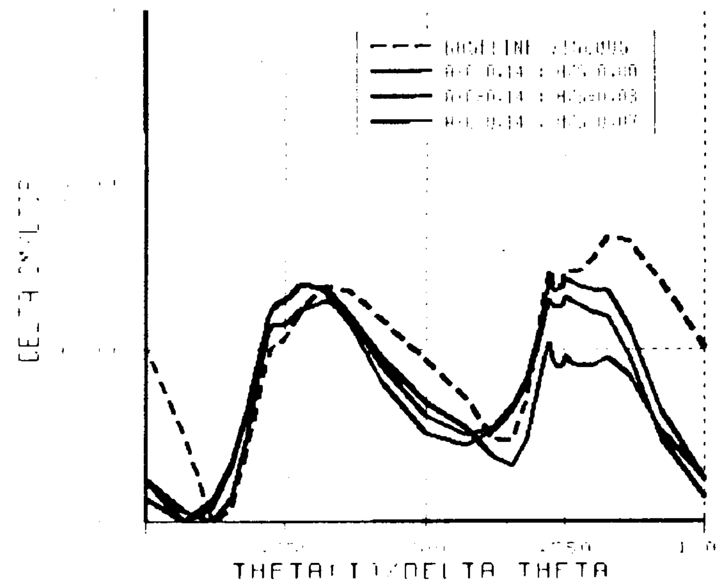

R/Rtip = 1.05

GENCORP AEROJET

Propulsion Division

IMPELLER DISCHARGE CIRC. Cm DISTRIBUTION
Mass Averaged Hub to Tip

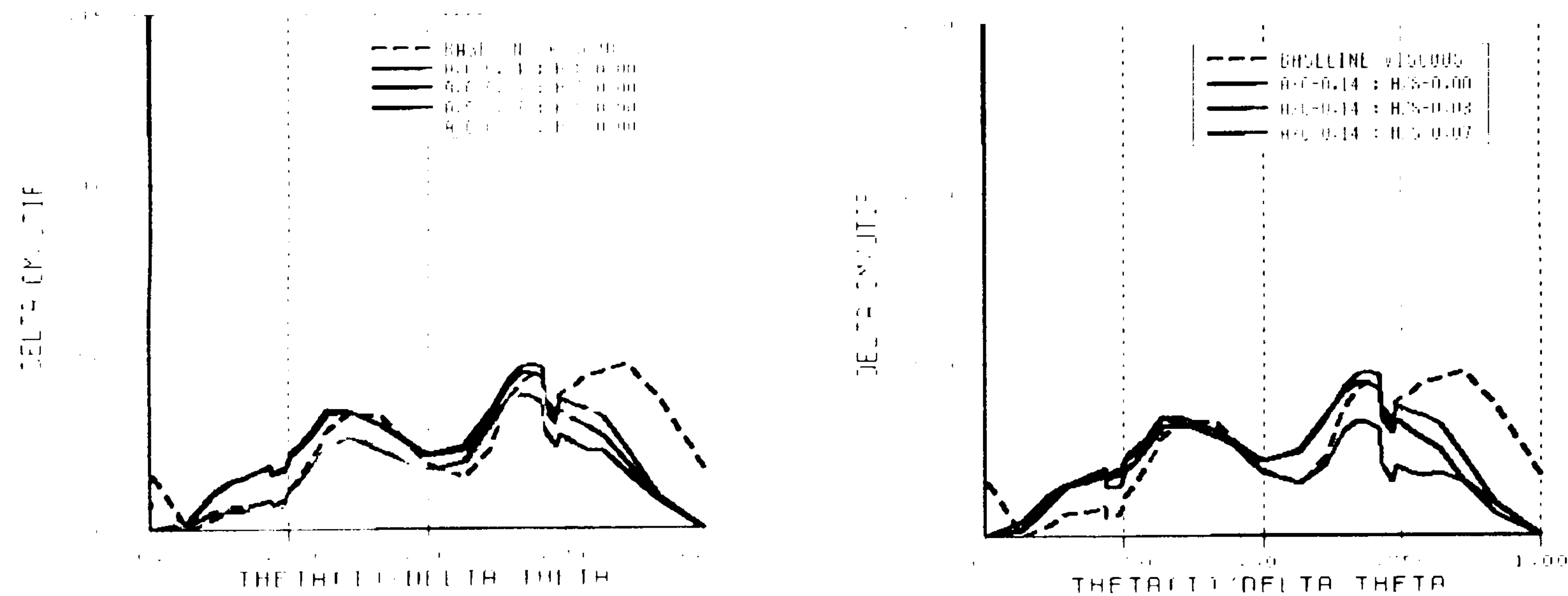

R/Rtip = 1.10

ORIGINAL PAGE IS OF POOR QUALITY

ORIGINAL PAGE IS
OF POOR QUALITY

BASELINE IMPELLER, VISCOUS SOLUTION

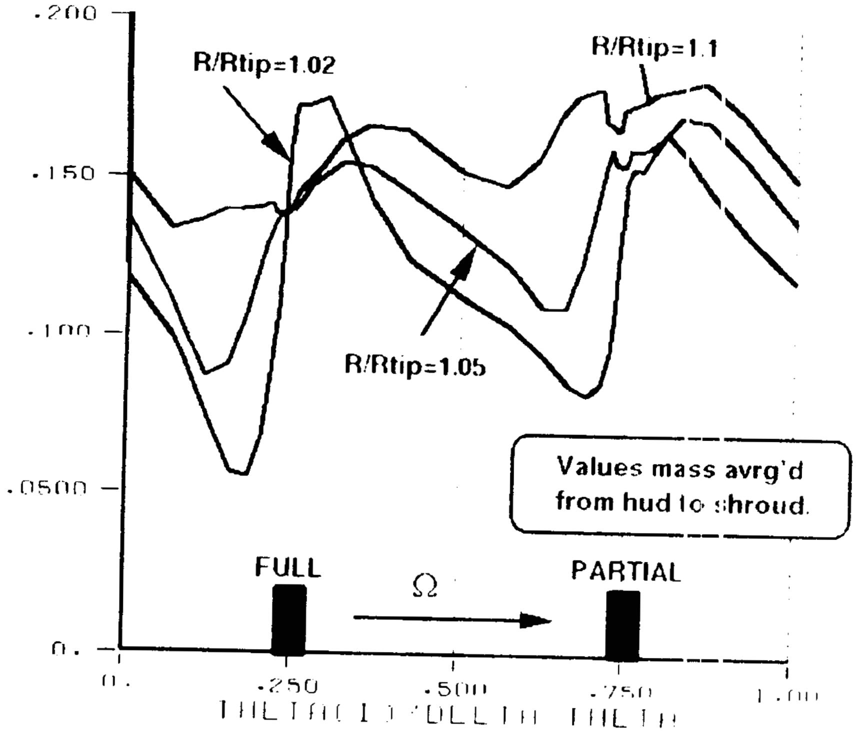

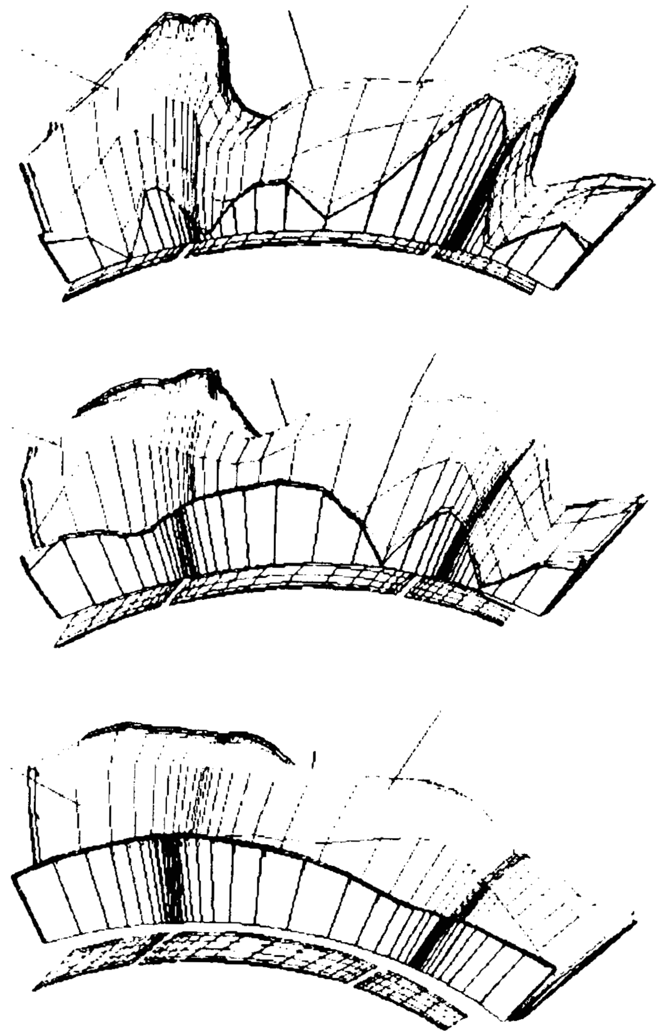

Utip=1858 fps, [illegible] Deg, mass flow split 45% - 55%

GenCorp
Aerojet
Propulsion Division

a/c=0.14 h/s=0.067, VISCOUS SOLUTION

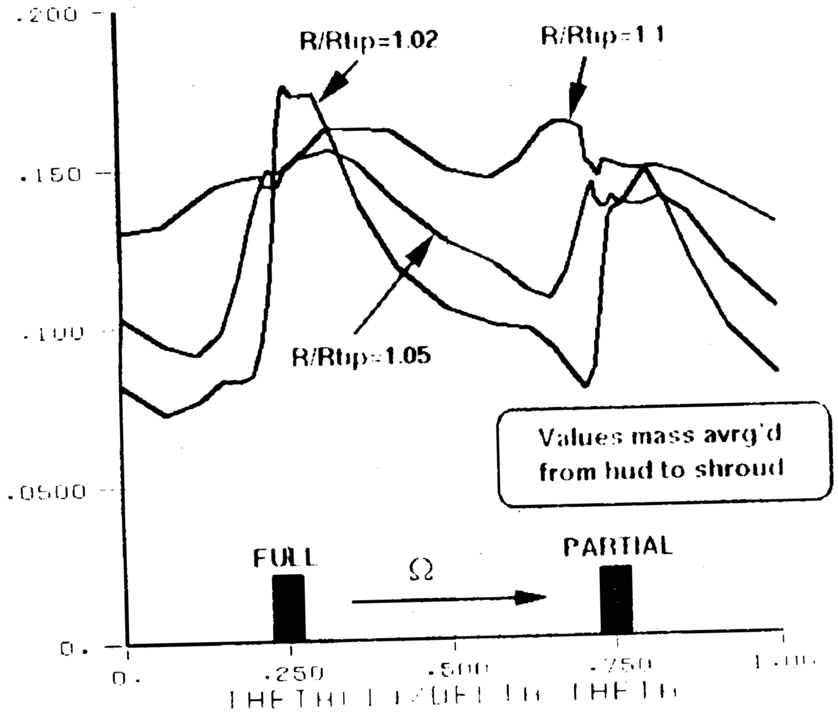

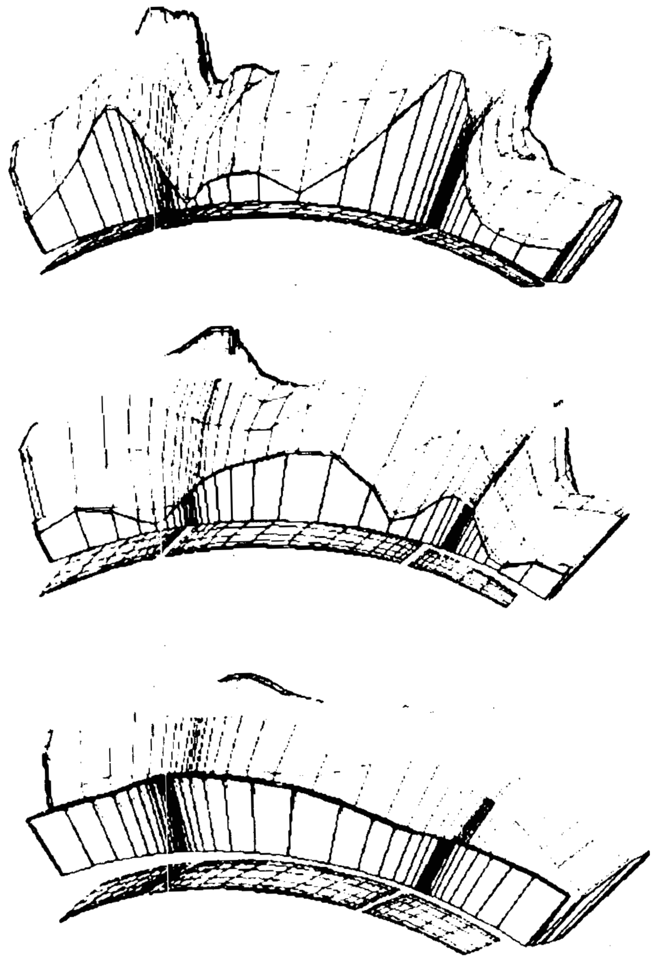

Utip=1858 fps ,

ORIGINAL PAGE IS OF POOR QUALITY

ORIGINAL PAGE IS OF POOR QUALITY

GENCORP AEROJET
Propulsion Division

BASELINE vs. a/c=0.14 ; 1 Deg. CLOCKED

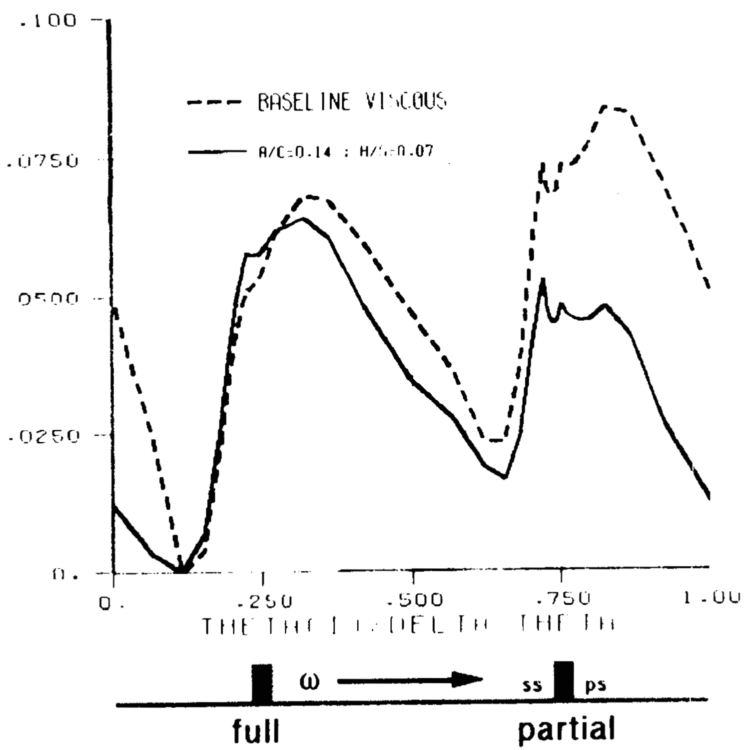

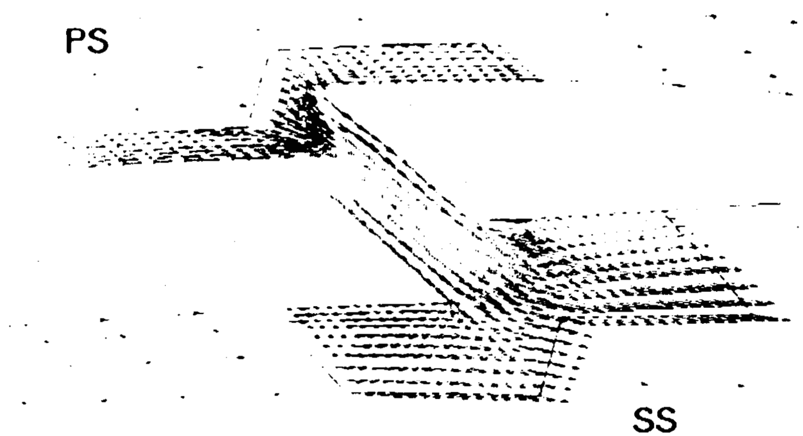

GENCORP AEROJET
Propulsion Division

Cm DISTRIBUTION JUST DOWNSTREAM OF SLOT LOCATION
R/RTIP = 0.94

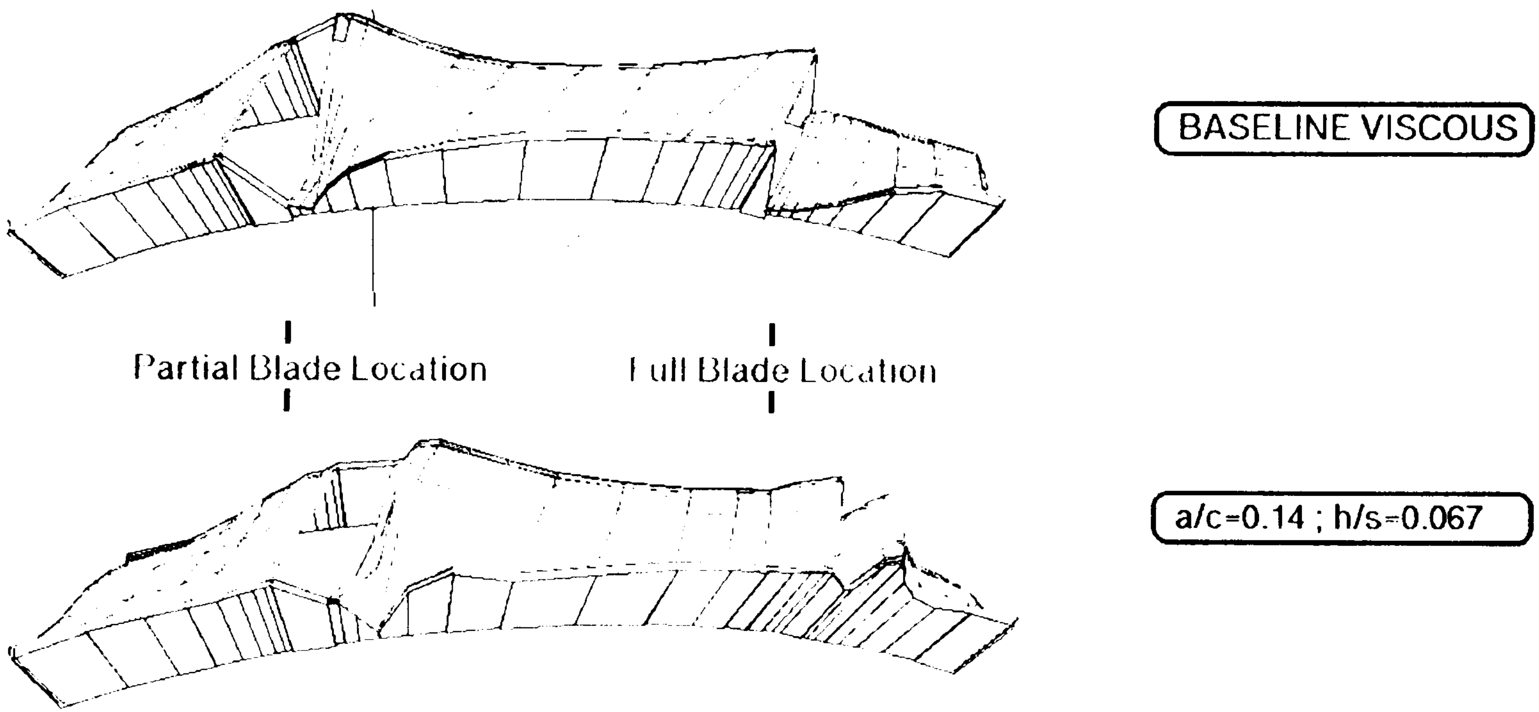

% BASELINE HEAD COEFF. vs SLOT LOCATION

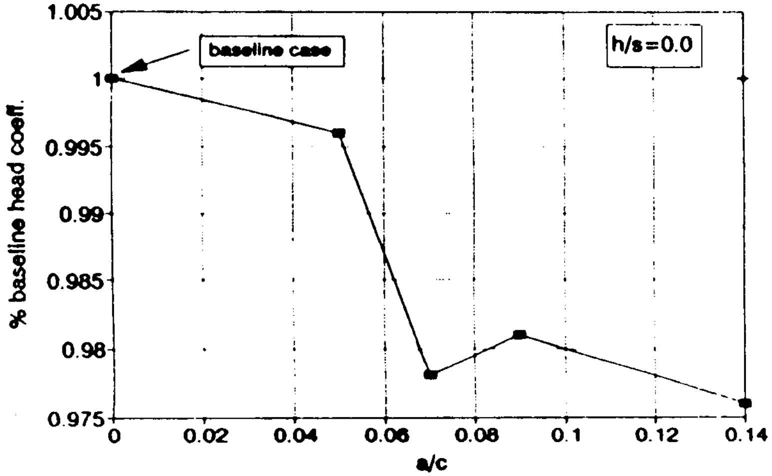

% BASELINE HEAD COEFF. vs CLOCKING

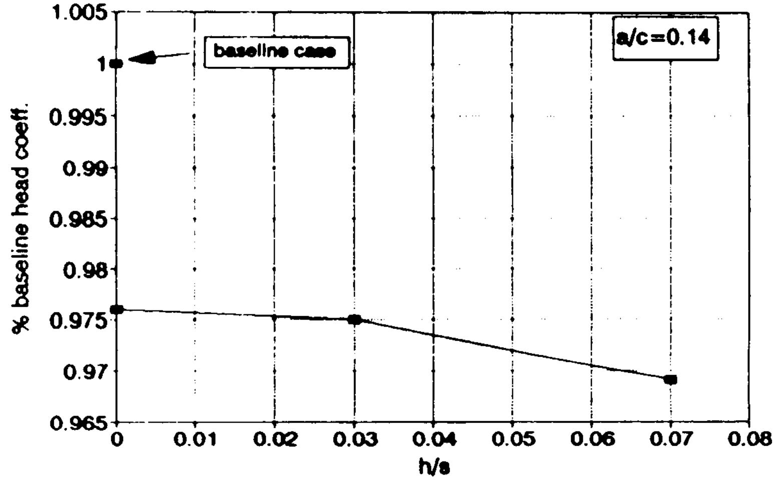

MASS FLOW SPLIT vs. SLOT LOCATION

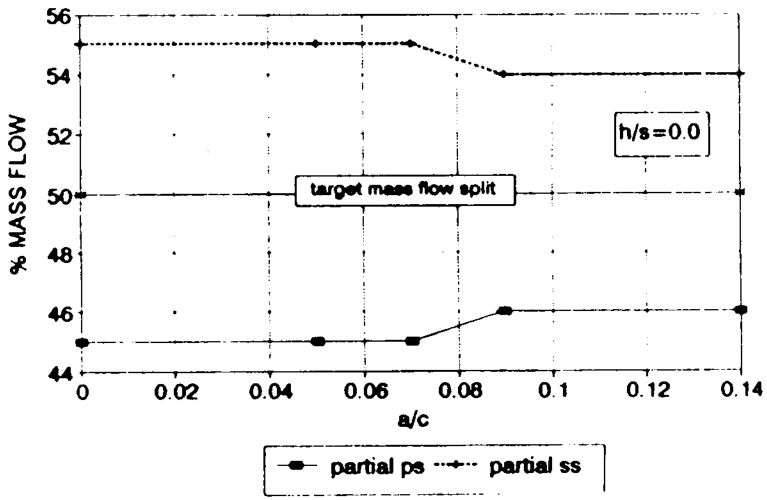

MASS FLOW SPLIT vs. CLOCKING

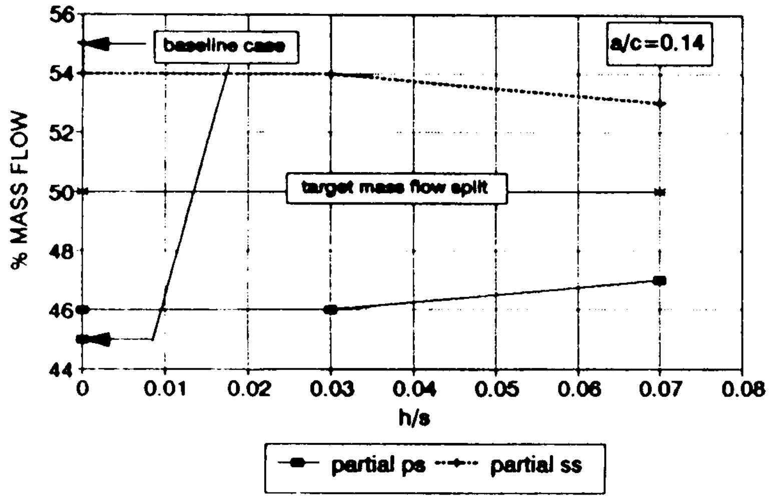

CONCLUSIONS

- FLOW NON-UNIFORMITY FOR THE BASELINE CASE WAS FOUND TO BE SIGNIFICANT
- SIGNIFICANT GAINS IN UNIFORMITY CAN POTENTIALLY BE ACHIEVED WITH TANDEM BLADE CONCEPT
- CLOCKING WAS SHOWN TO BE THE PRIMARY DRIVER FOR IMPELLER DISCHARGE FLOW UNIFORMITY
- CARE MUST BE TAKEN IN THE DESIGN PROCESS TO ACHIEVE POSITIVE PERFORMANCE GAINS RATHER THAN LOSSES
- GRID EMBEDDING CAN SIGNIFICANTLY REDUCE MODEL SIZE WHILE NOT SACRIFICING FLOW GRADIENT RESOLUTION

FURTHER OPTIMIZATION REQUIRED FOLLOWED BY GRID REFINEMENT

N92-32291

THREE-DIMENSIONAL FLOW FIELDS INSIDE A SHROUDED INDUCER AT DESIGN AND OFF-DESIGN CONDITIONS (CFD STUDY)

C. HAH, O. KWON, AND D. A. GREENWALD

NASA LEWIS RESEARCH CENTER

R. GARCIA

NASA MARSHALL SPACE FLIGHT CENTER

Three-dimensional flow phenomena in a shrouded inducer have been studied with a three-dimensional Navier-Stokes method.

The details of the three-dimensional flow structure inside the inducer at design and off-design conditions are analyzed and the results are compared with some flow visualization results obtained at the California Institute of Technology.

THREE-DIMENSIONAL FLOW FIELDS INSIDE A SHROUDED INDUCER AT DESIGN AND OFF-DESIGN CONDITIONS (CFD STUDY)

290

C. HAH, O. KWON, AND D. A. GREENWALD

NASA LEWIS RESEARCH CENTER

R. GARCIA

NASA MARSHALL SPACE FLIGHT CENTER

OBJECTIVES

3-D FLOW STRUCTURE AT LOW FLOW COEFFICIENT

FORMATION OF BACKFLOWS

LATERAL FORCES IN AXIAL FLOW INDUCERS

OVERALL APPROACHES

EXPERIMENTAL INVESTIGATION

CALIFORNIA INSTITUTE OF TECHNOLOGY

PH.D THESIS BY BHATTACHARYYA (PROF. ACOSTA)

ASME PAPER BY BHATTACHARYYA, ACOSTA, BRENNEN AND CAUGHEY ON " BACKFLOW IN INDUCER "

CFD INVESTIGATION

CURRENT SUBJECT

INDUCER 10

SHROUDED INDUCER (3 BLADES)

BLADE ANGLE = 12 DEGREES

TIP RADIUS = 1.9115 INCHES

TESTED FLOW COEFFICIENTS (0.074 & 0.041)

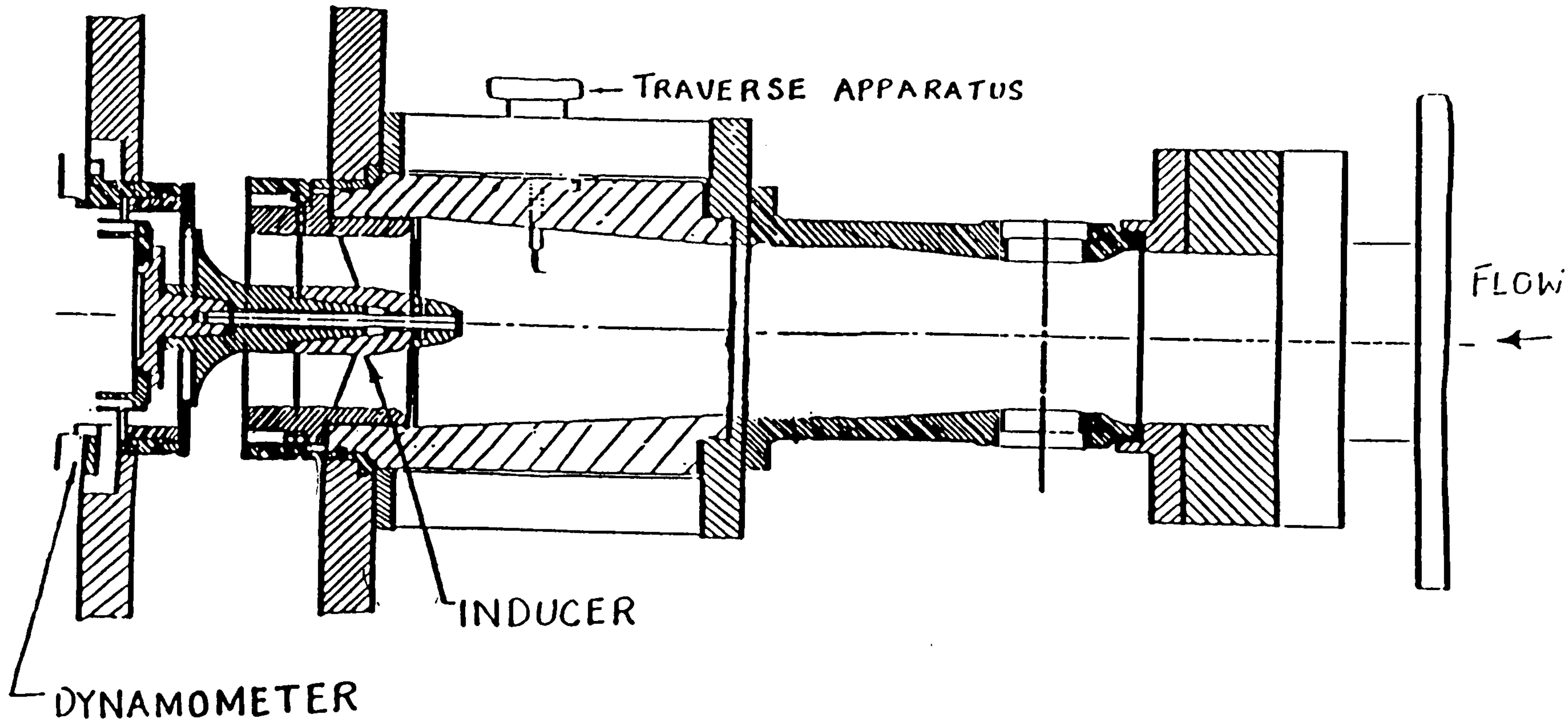

CALTECH INDUCER FACILITY

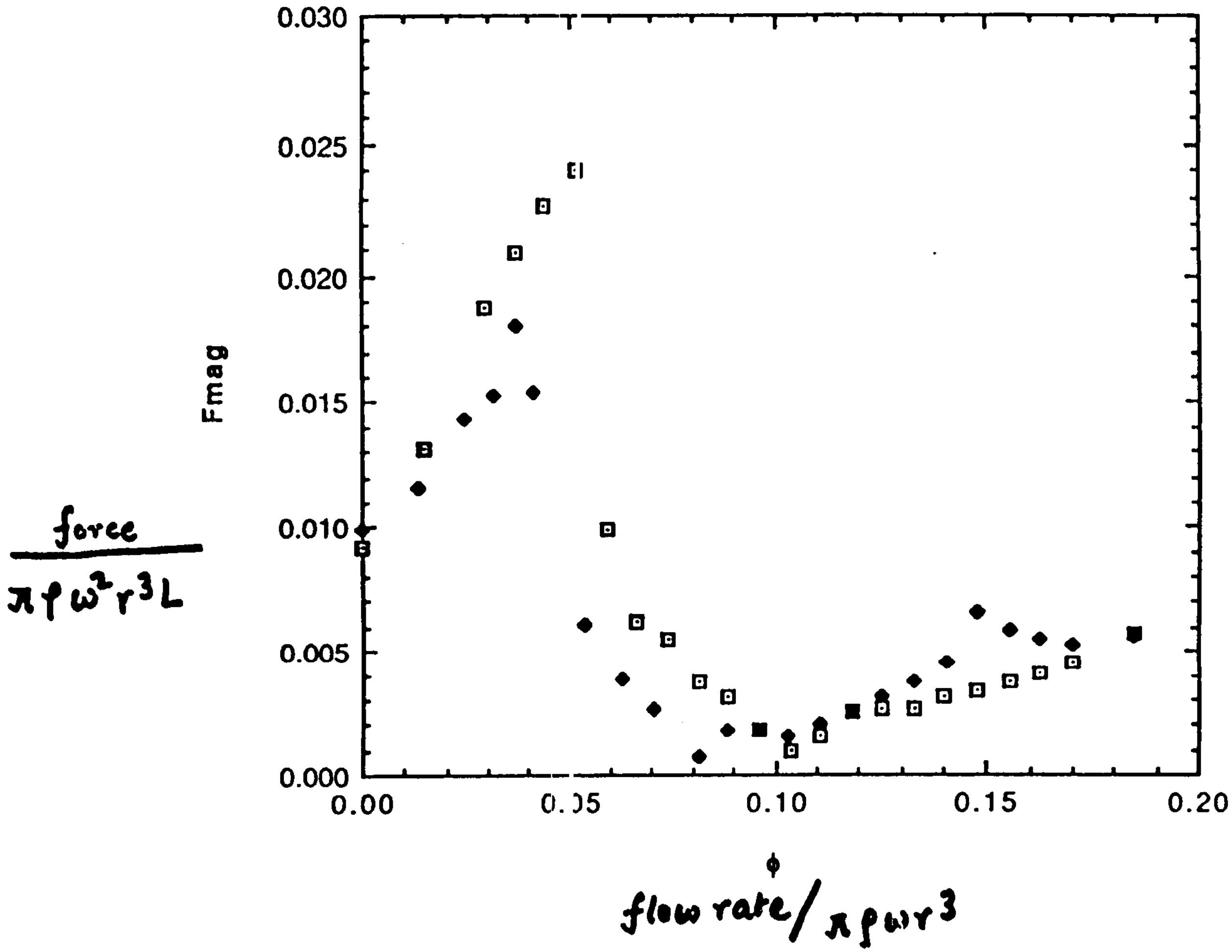

LATERAL FORCE AT VARIOUS FLOW COEFFICIENTS

(FROM CALTECH STUDY)

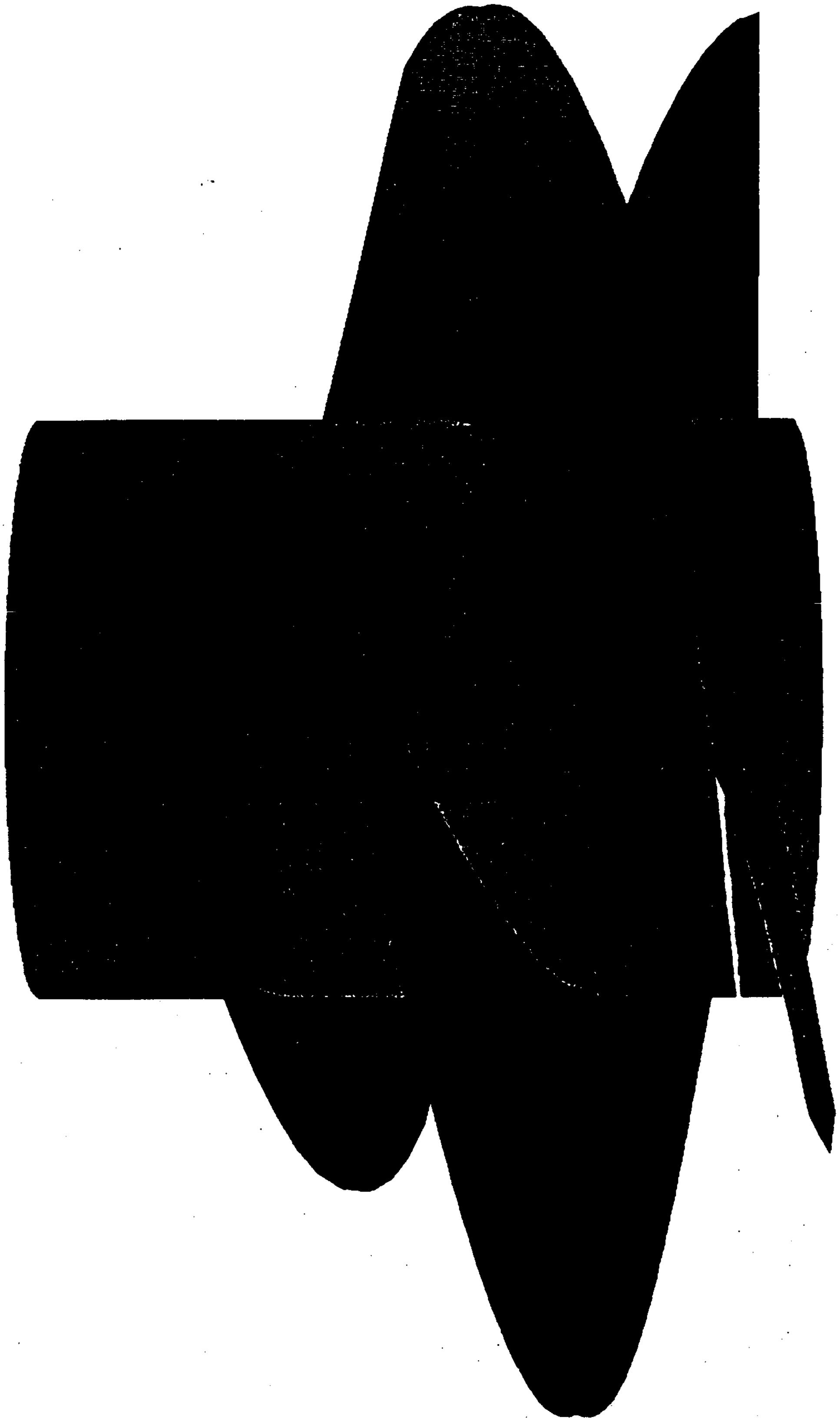

CALTECH SHROUDED INDUCER

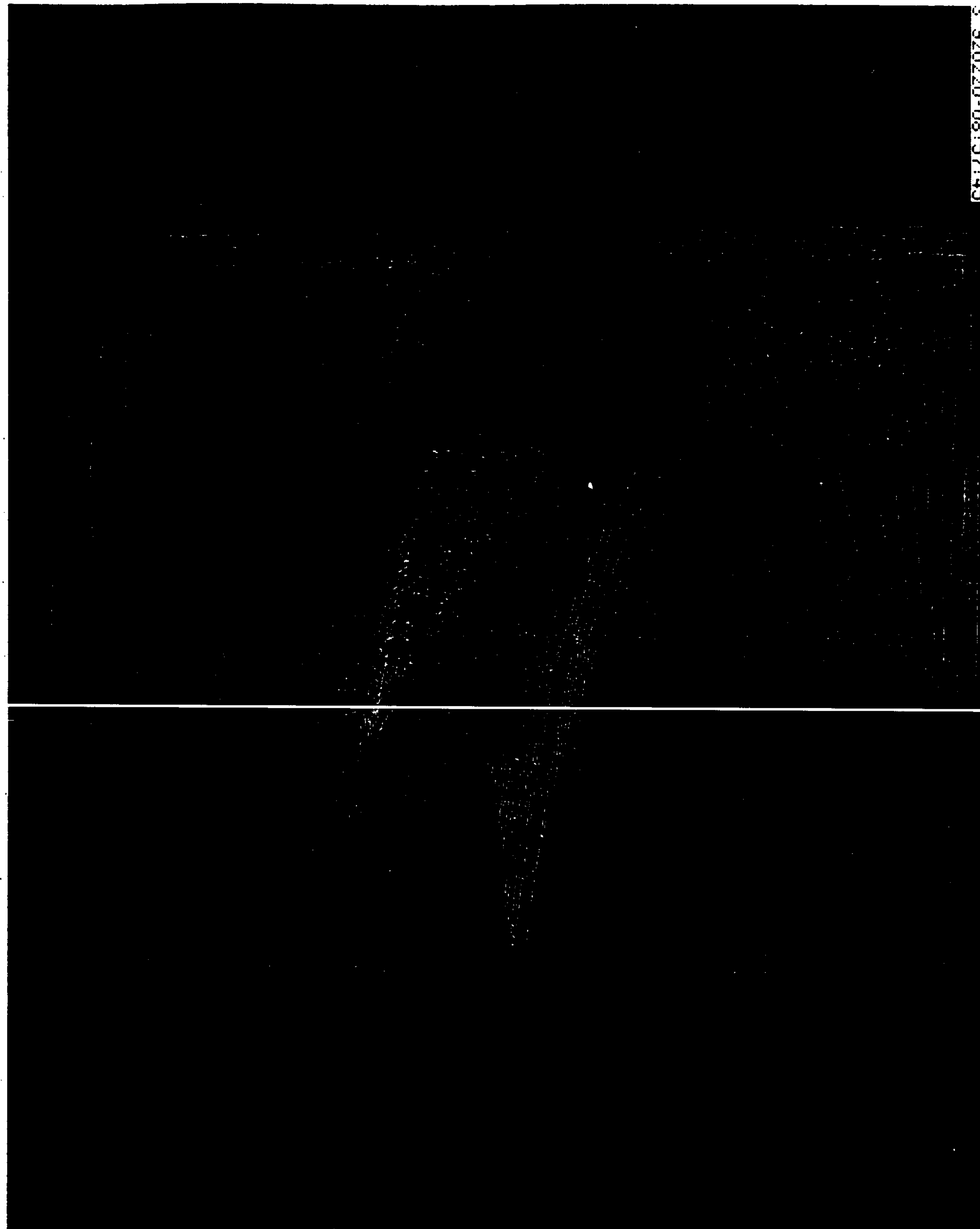

COMPUTATIONAL GRID (40*31*122)

FLOW COEFF. = 0.074

↓ FLOW

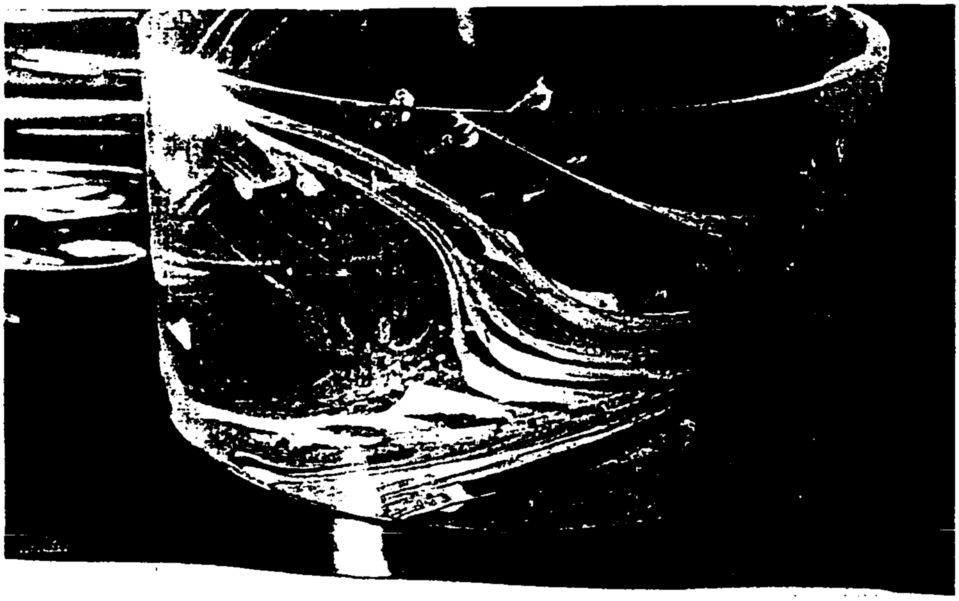

↓ FLOW

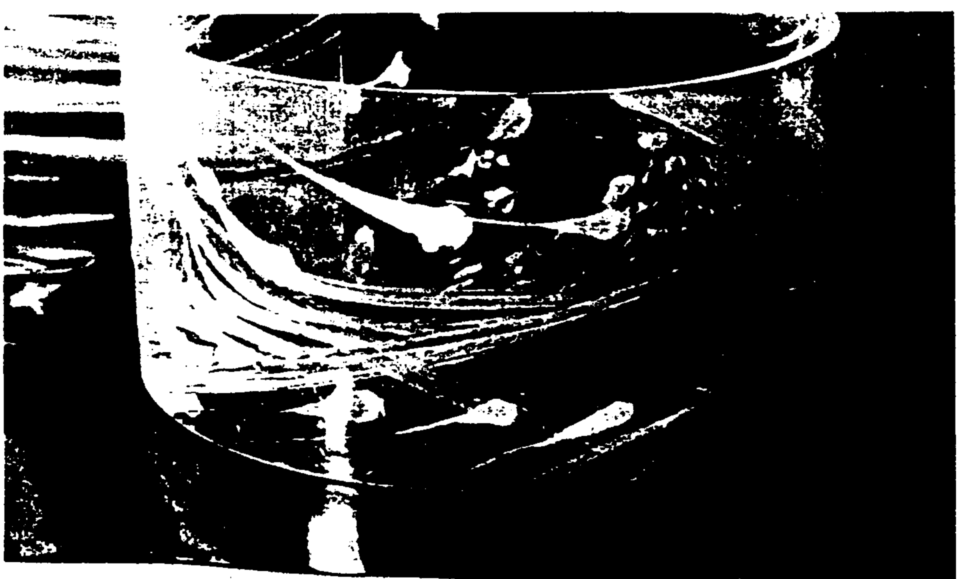

FLOW ON SHROUD (FROM CALTECH STUDY)

FLOW COEFF. = 0.074

Flow

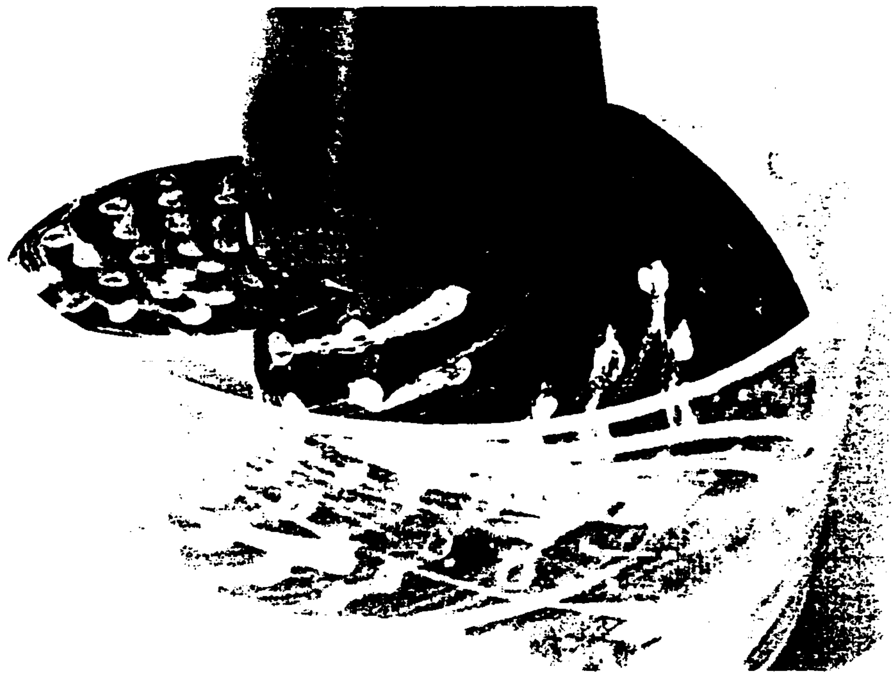

Flow

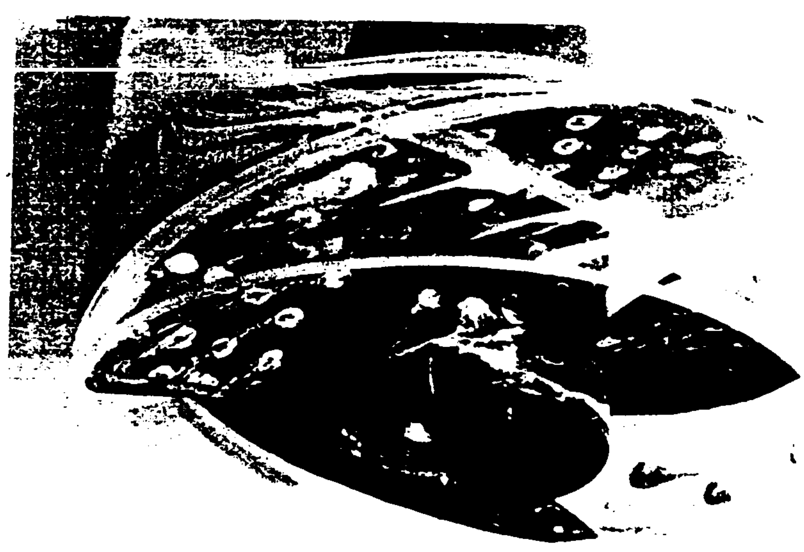

FLOW ON HUB (FROM CALTECH STUDY)

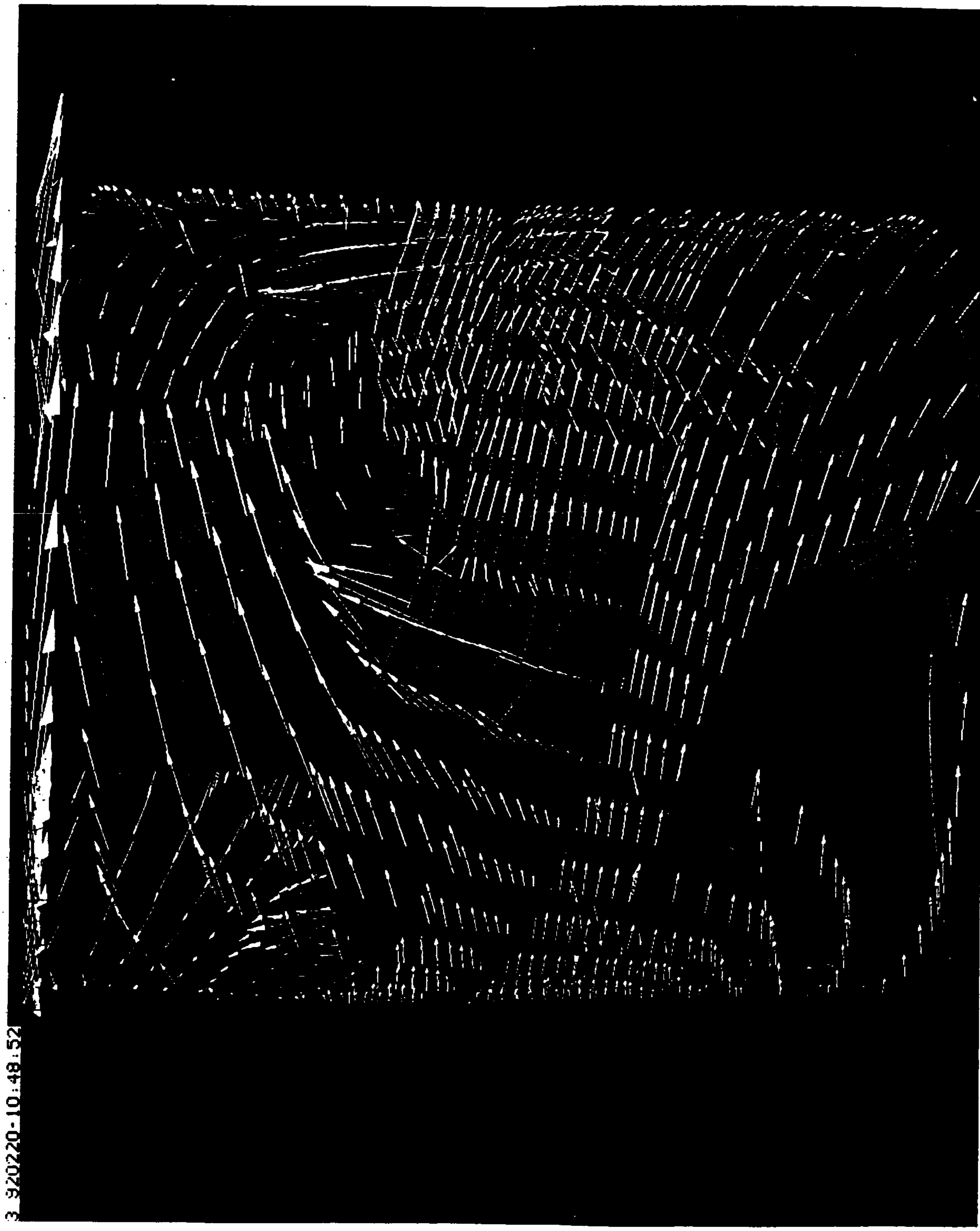

VELOCITY VECTORS NEAR SHROUD (FLOW COEFF.=0.074)

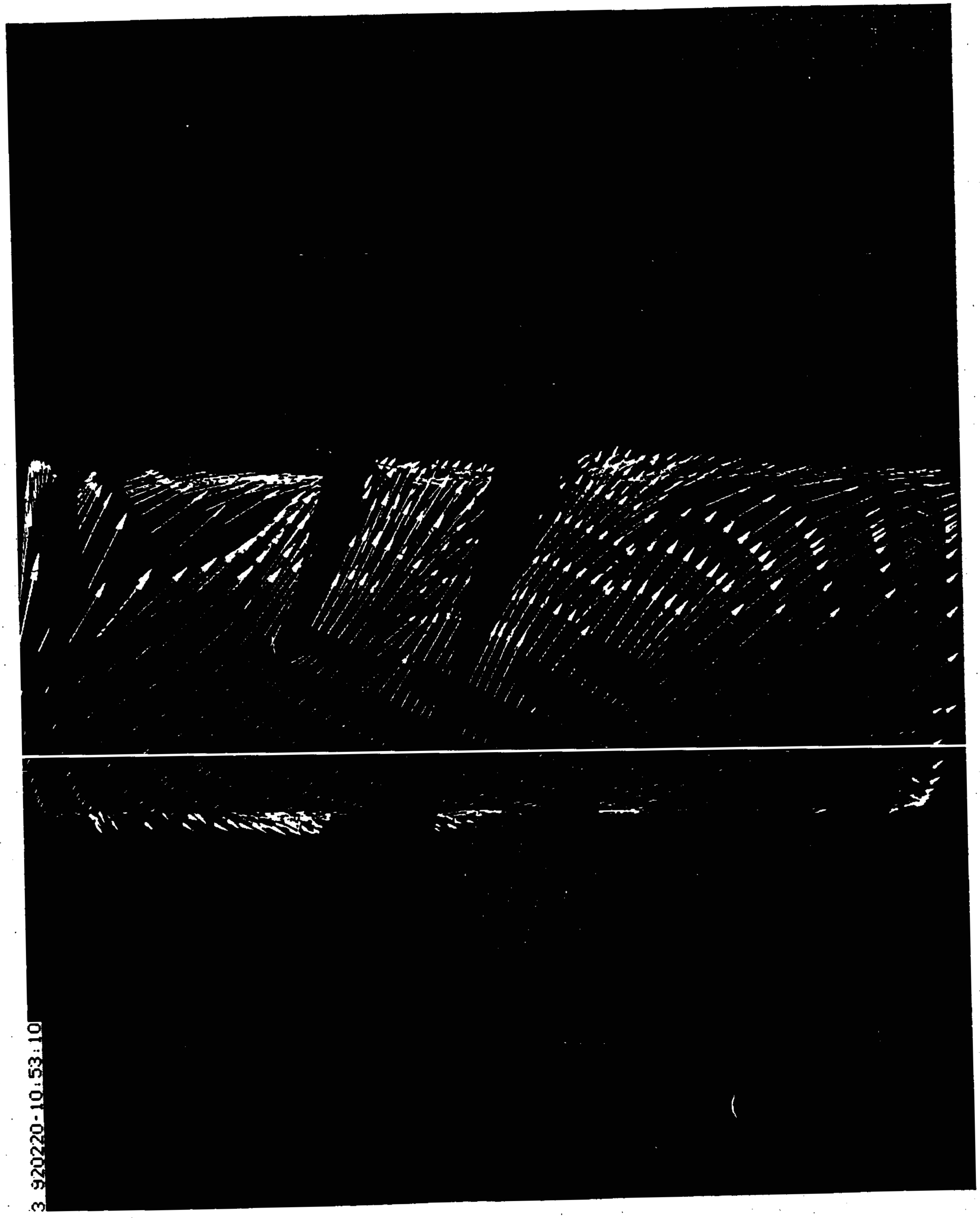

VELOCITY VECTORS NEAR HUB (FLOW COEFF.=0.074)

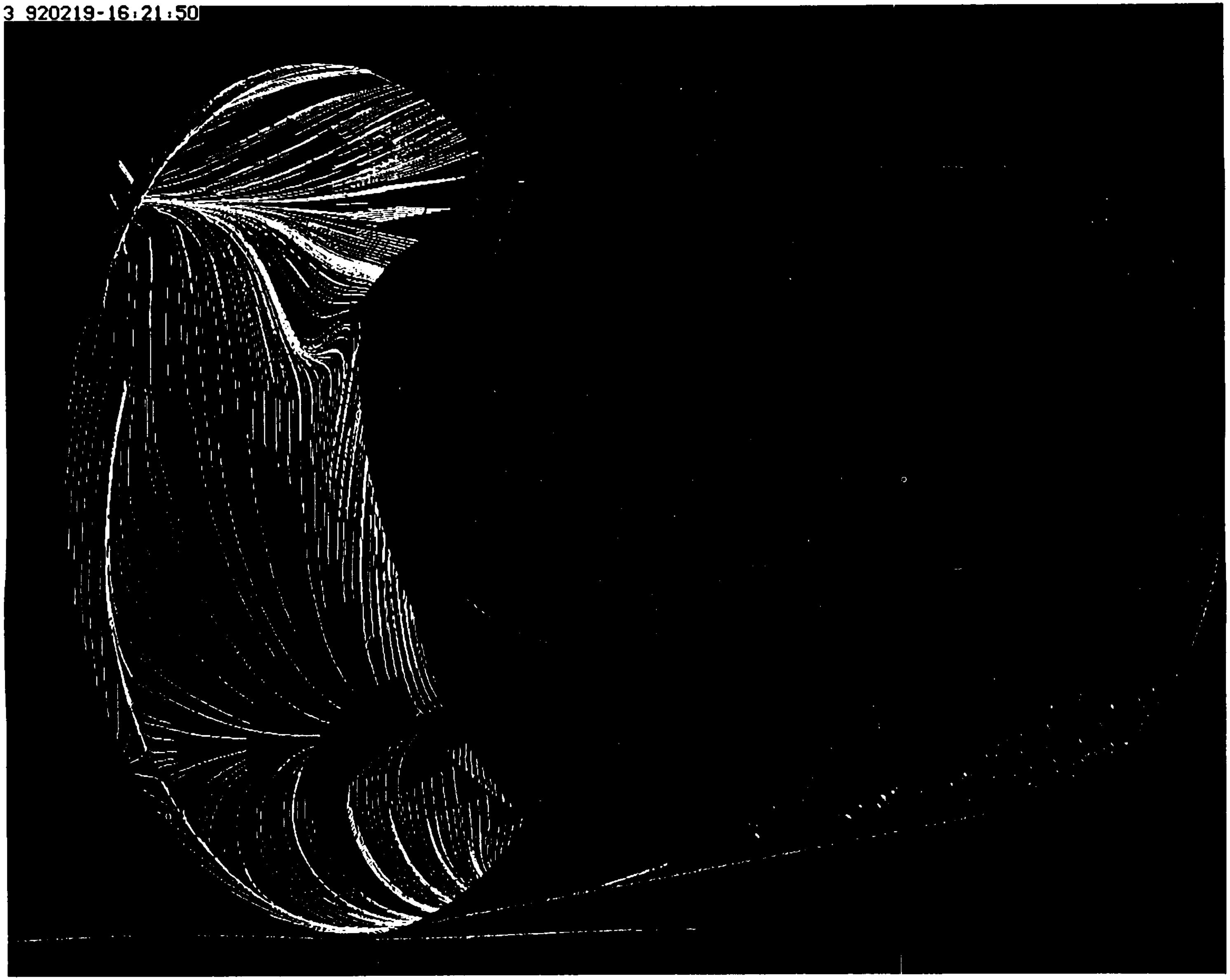

OIL FLOW ON SHROUD (FLOW COEFF.=0.074)

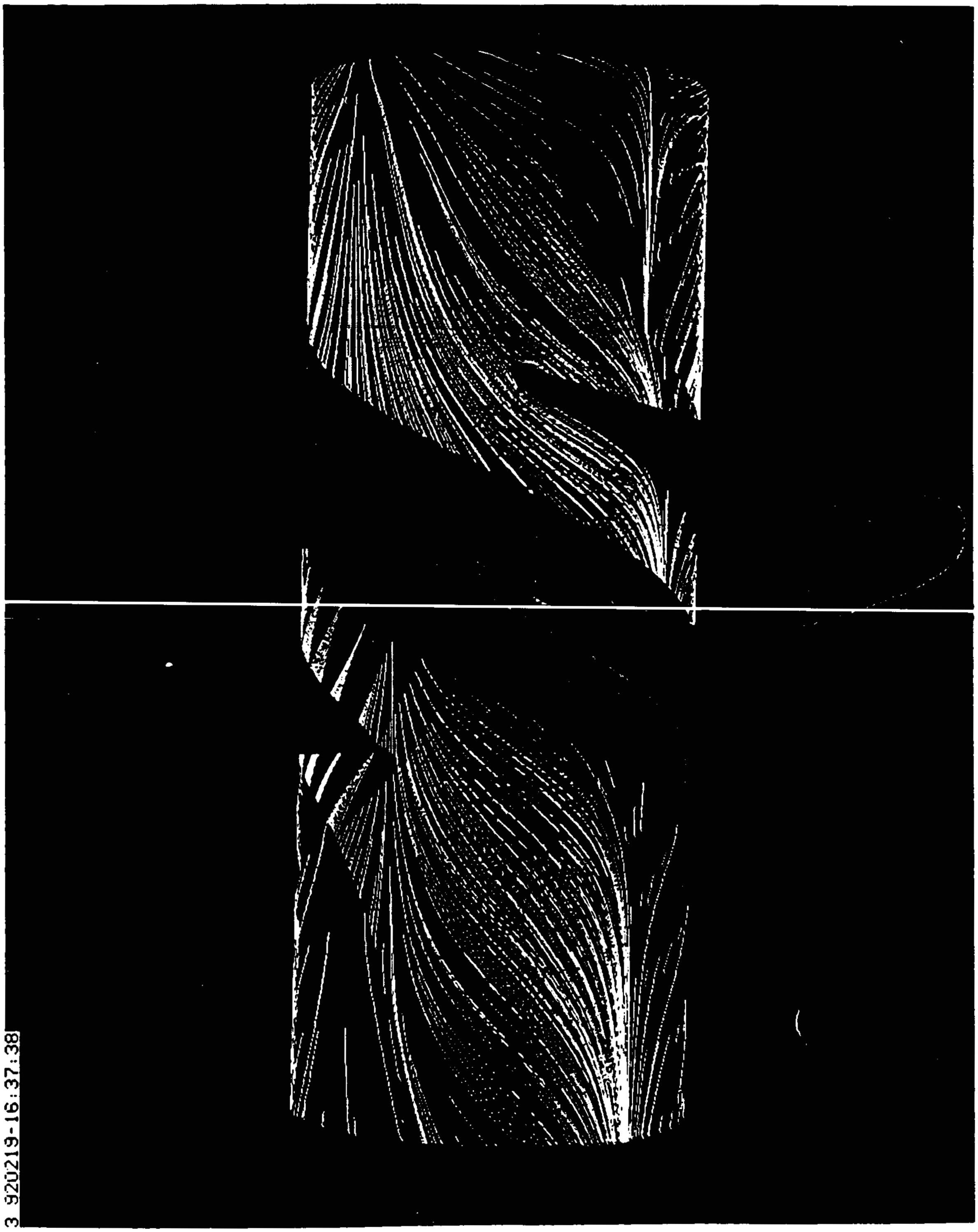

OIL FLOW ON HUB (FLOW COEFF.=0.074)

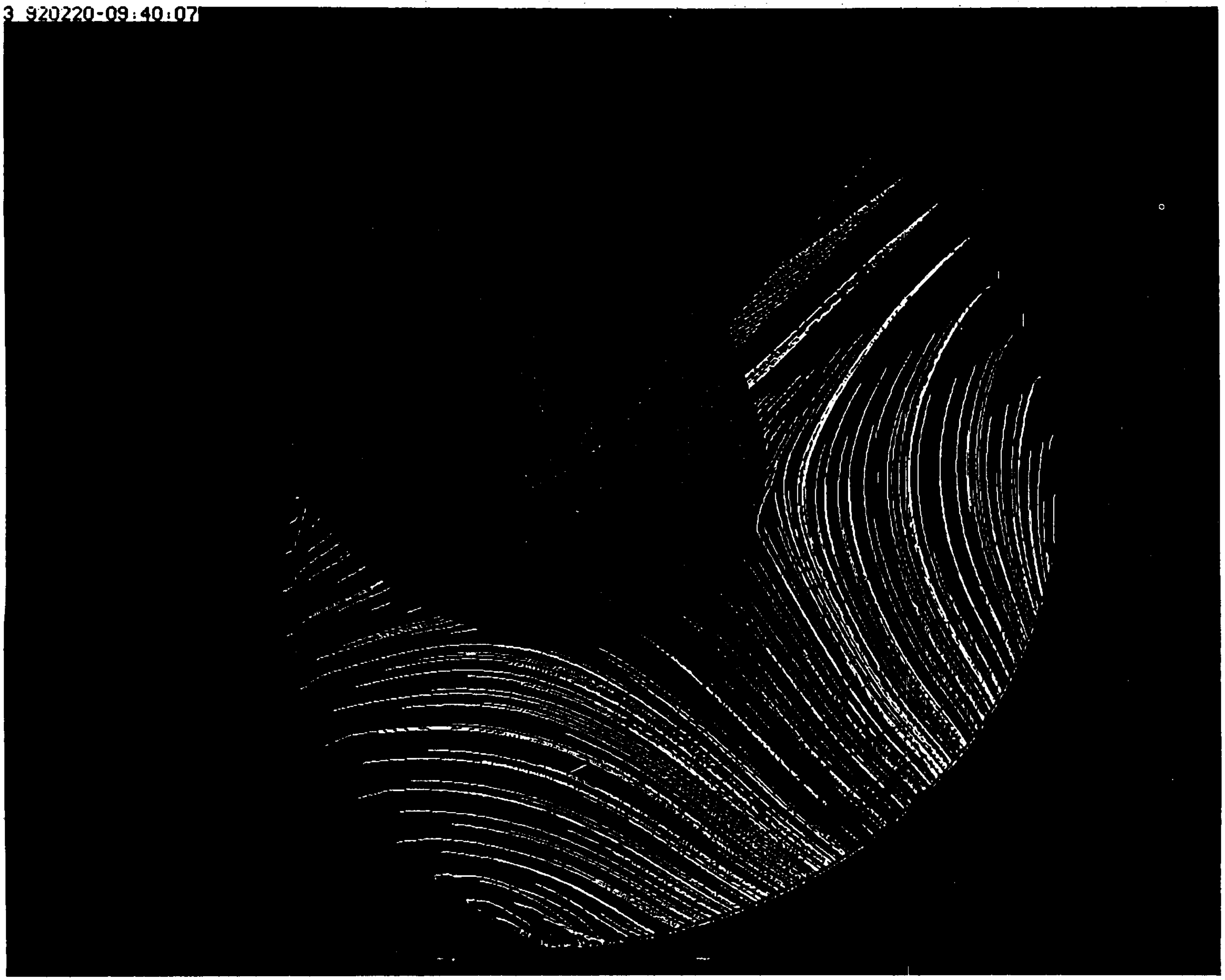

OIL FLOW ON SUCTION SIDE (FLOW COEFF.=0.074)

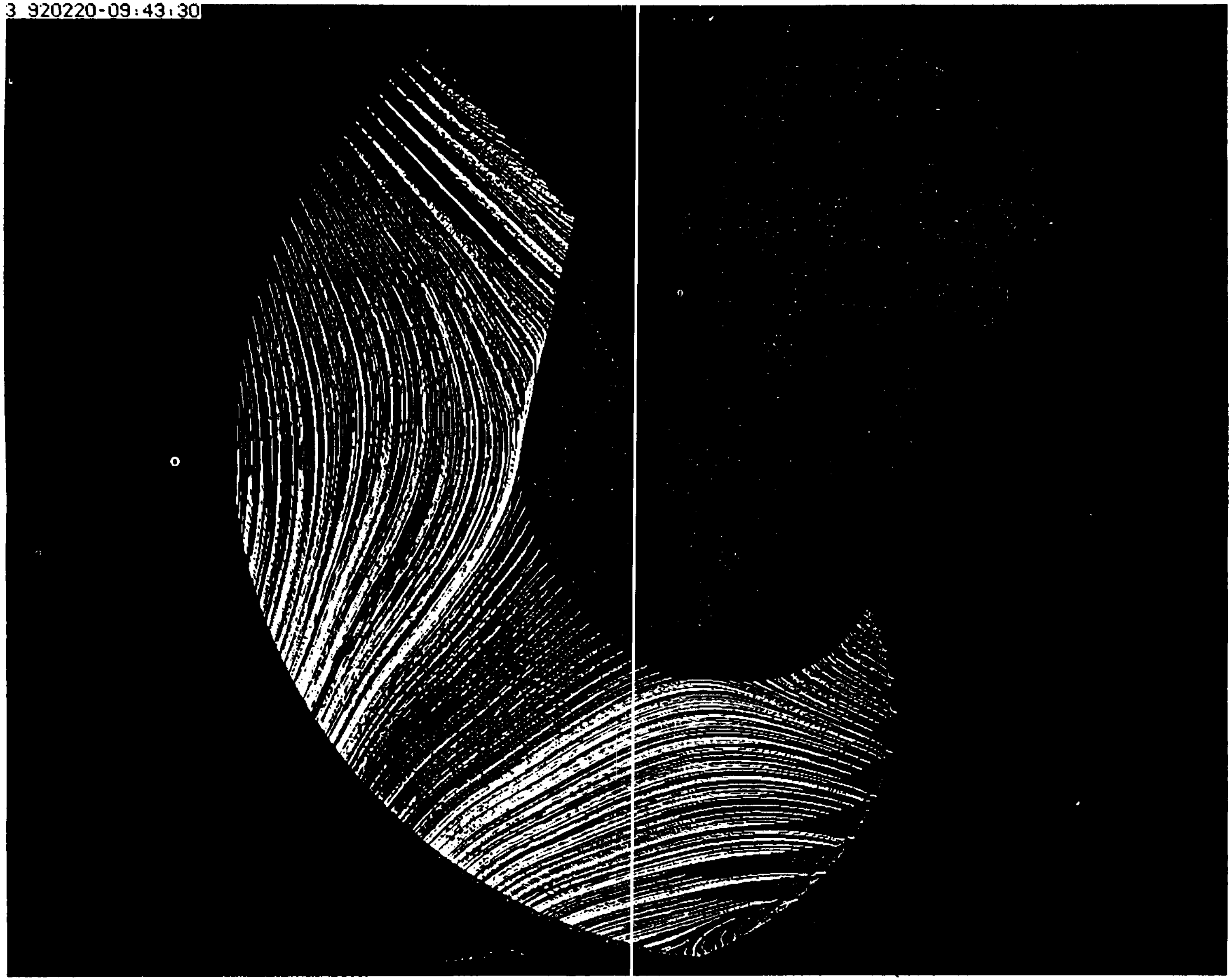

OIL FLOW ON PRESSURE SIDE (FLOW COEFF.=0.074)

FLOW COEFF. = 0.041

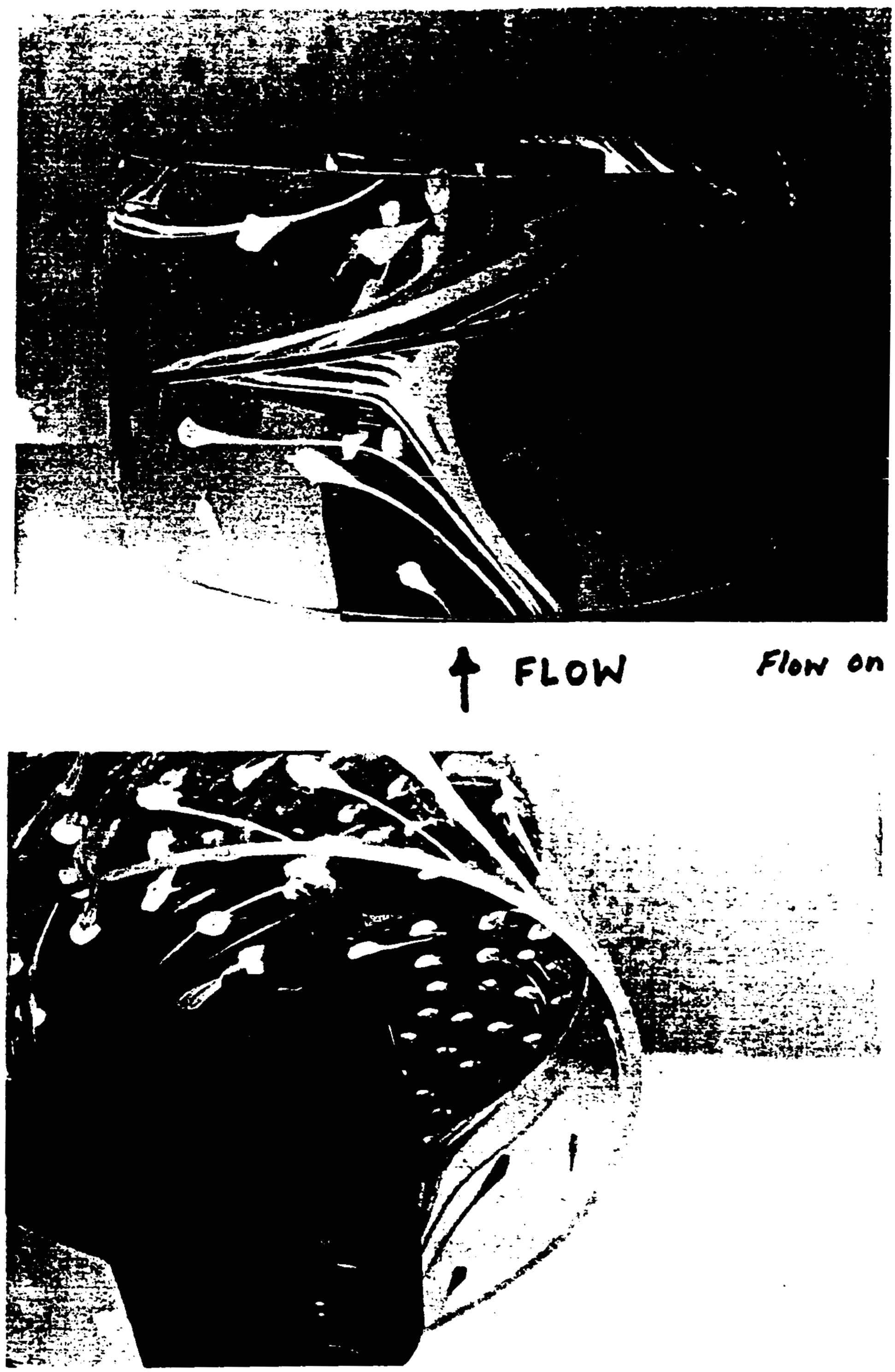

FLOW ON SHROUD (FROM CALTECH STUDY)

FLOW COEFF. = 0.041

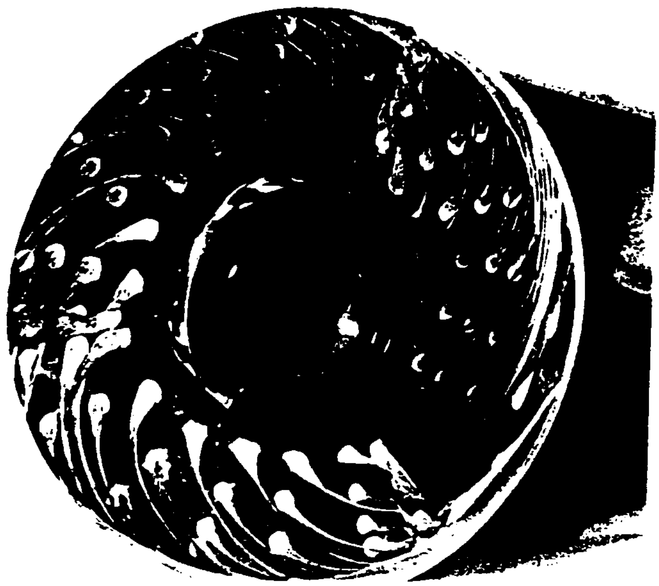

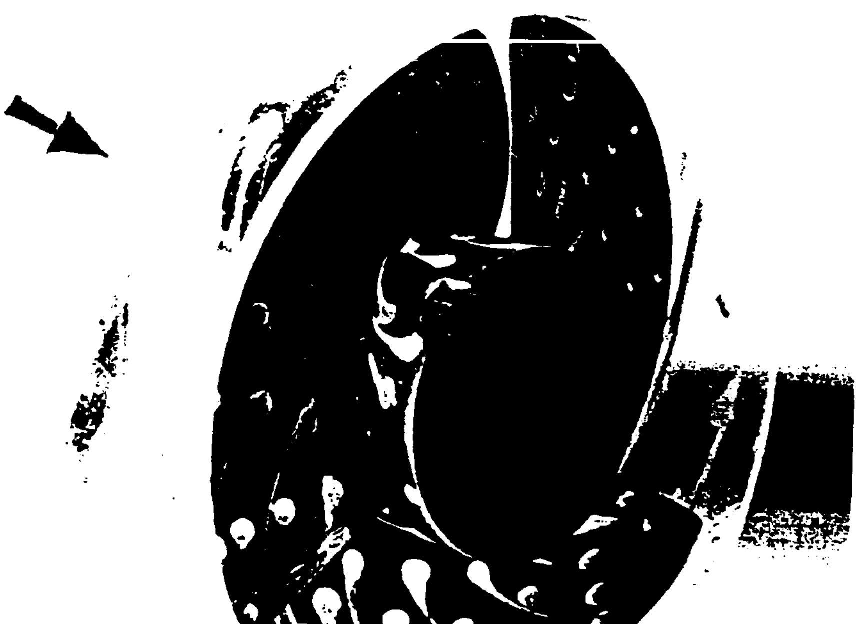

FLOW ON HUB (FROM CALTECH STUDY)

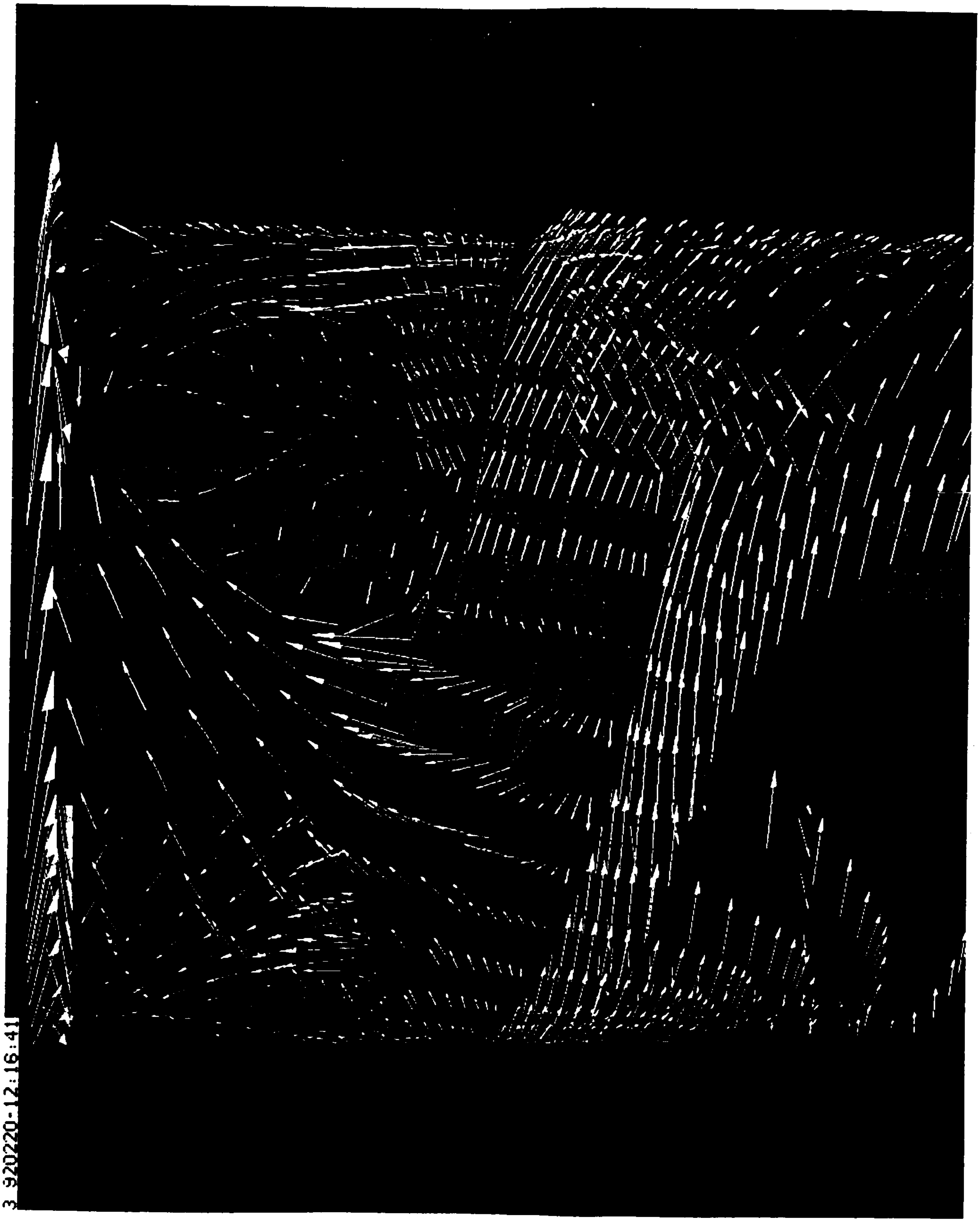

'ELOCITY VECTORS NEAR SHROUD (FLOW COEFF.=0.041)

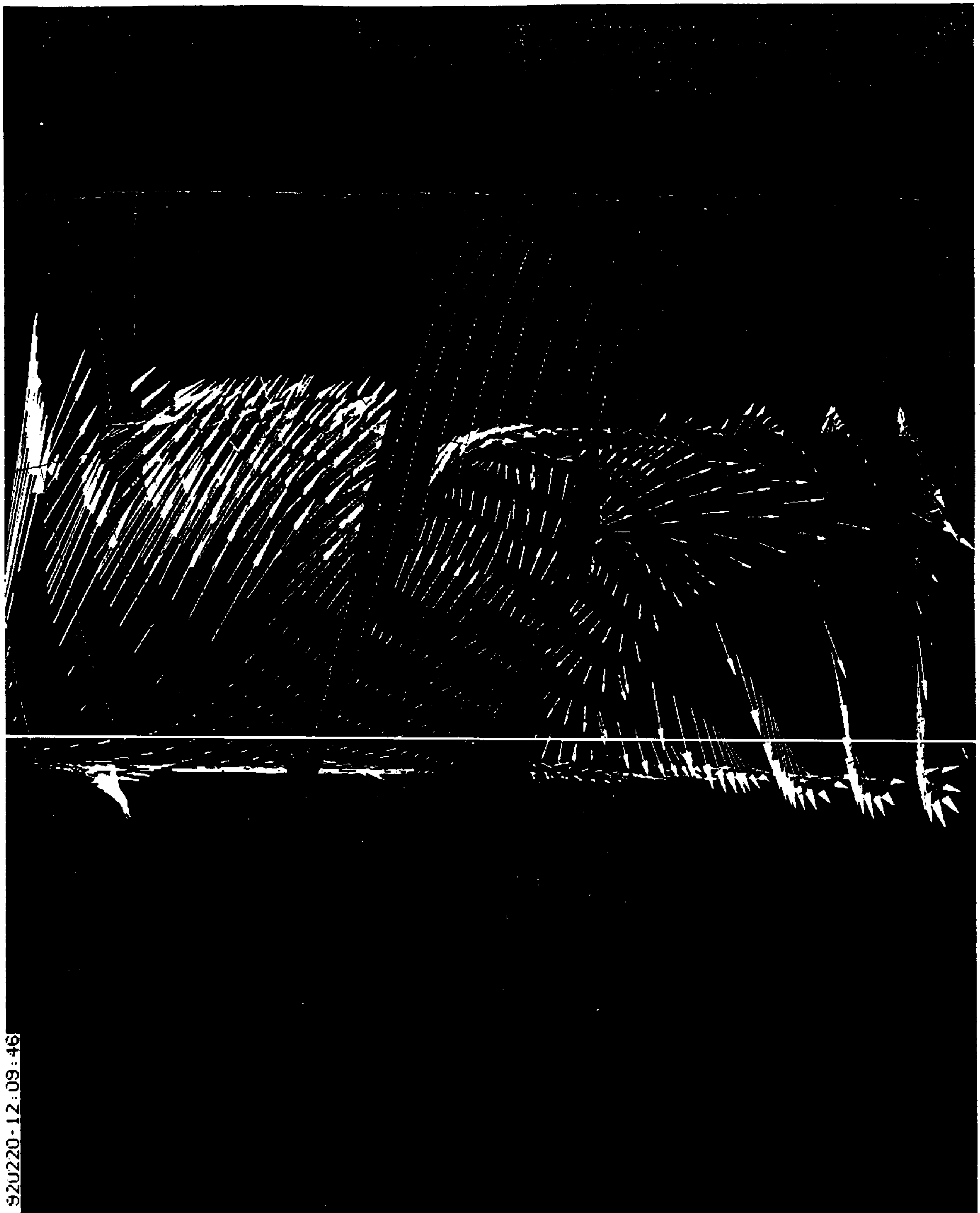

VELOCITY VECTORS NEAR HUB (FLOW COEFF.=0.041)

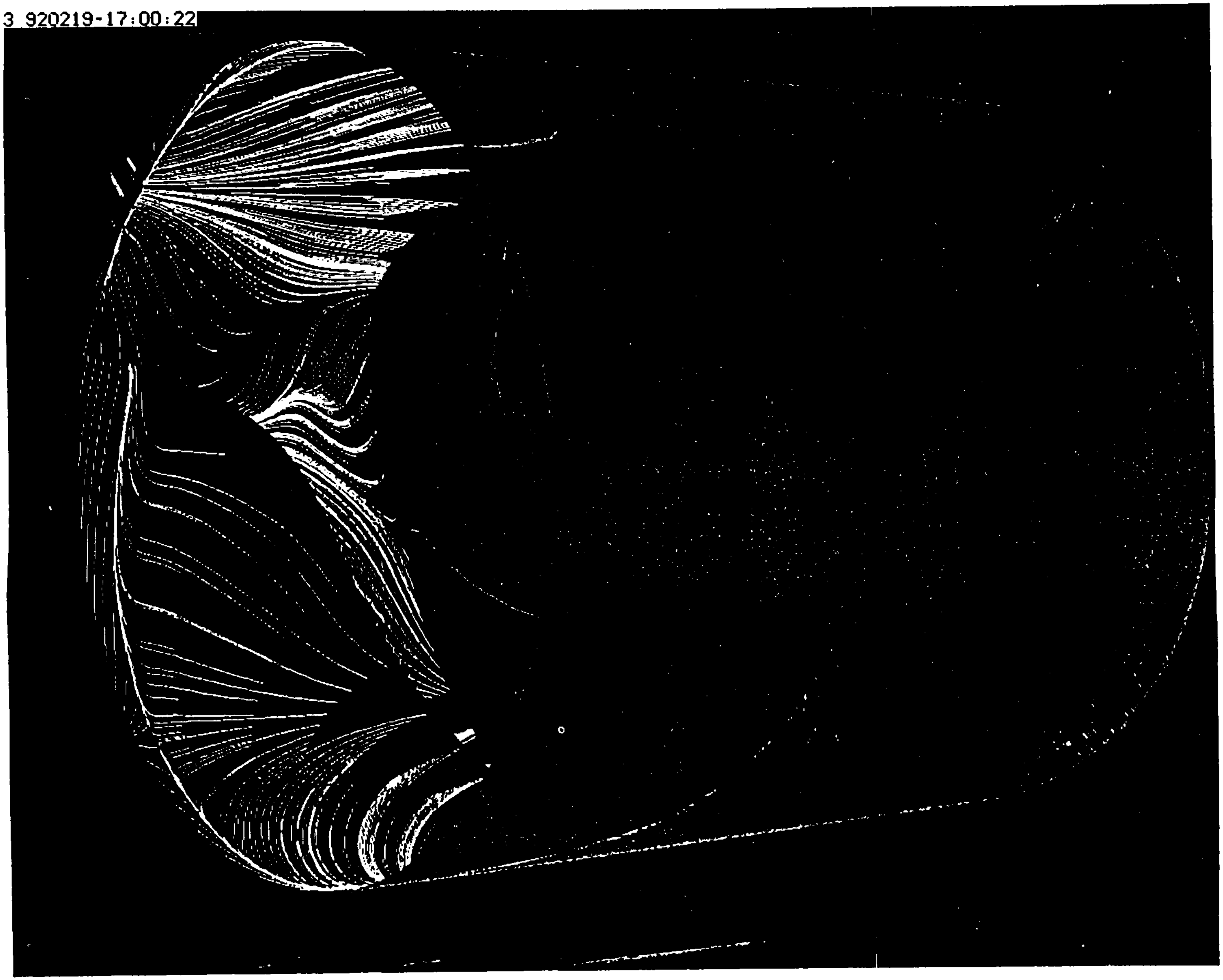

OIL FLOW ON SHROUD (FLOW COEFF.=0.041)

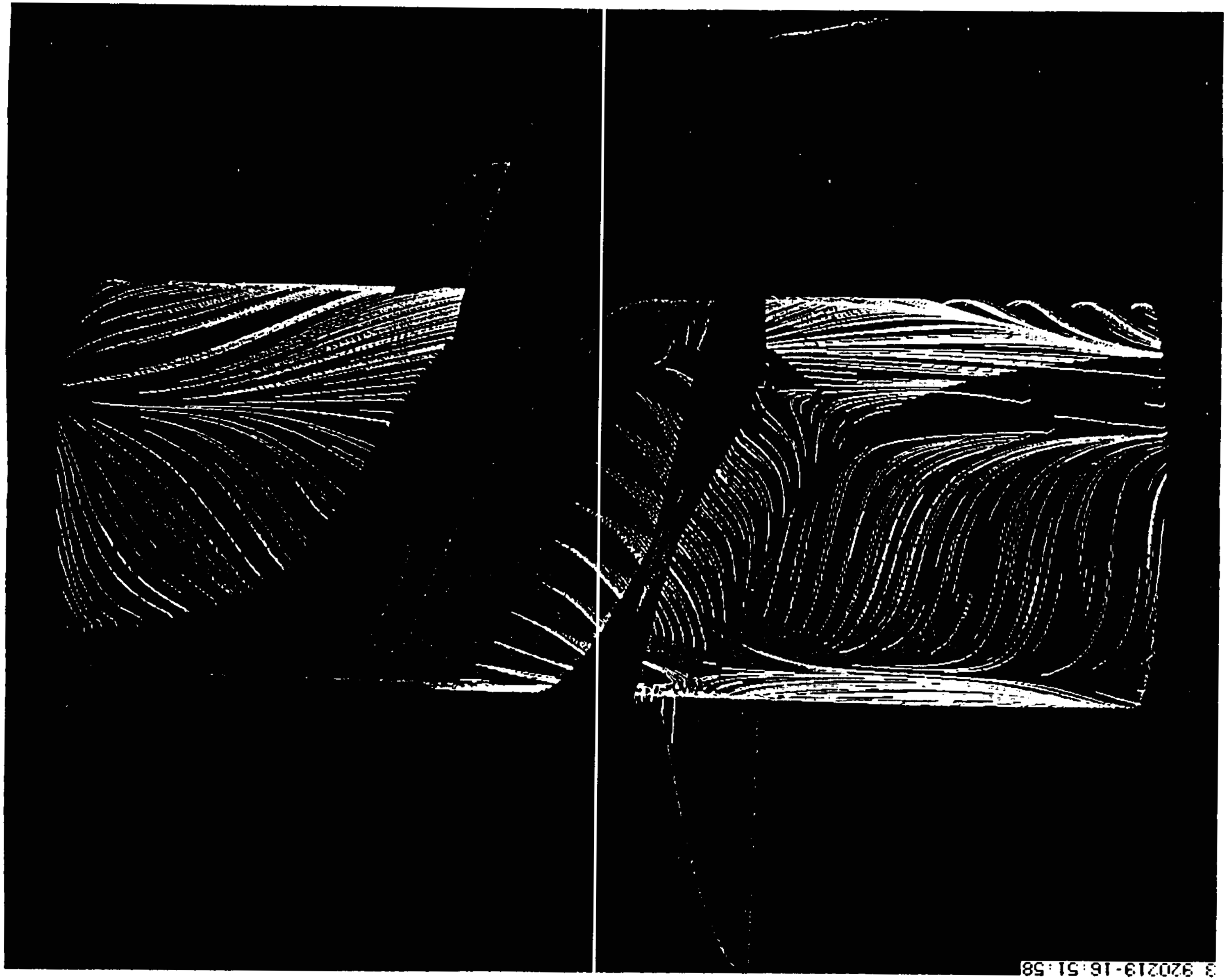

OIL FLOW ON HUB (FLOW COEFF.=0.041)

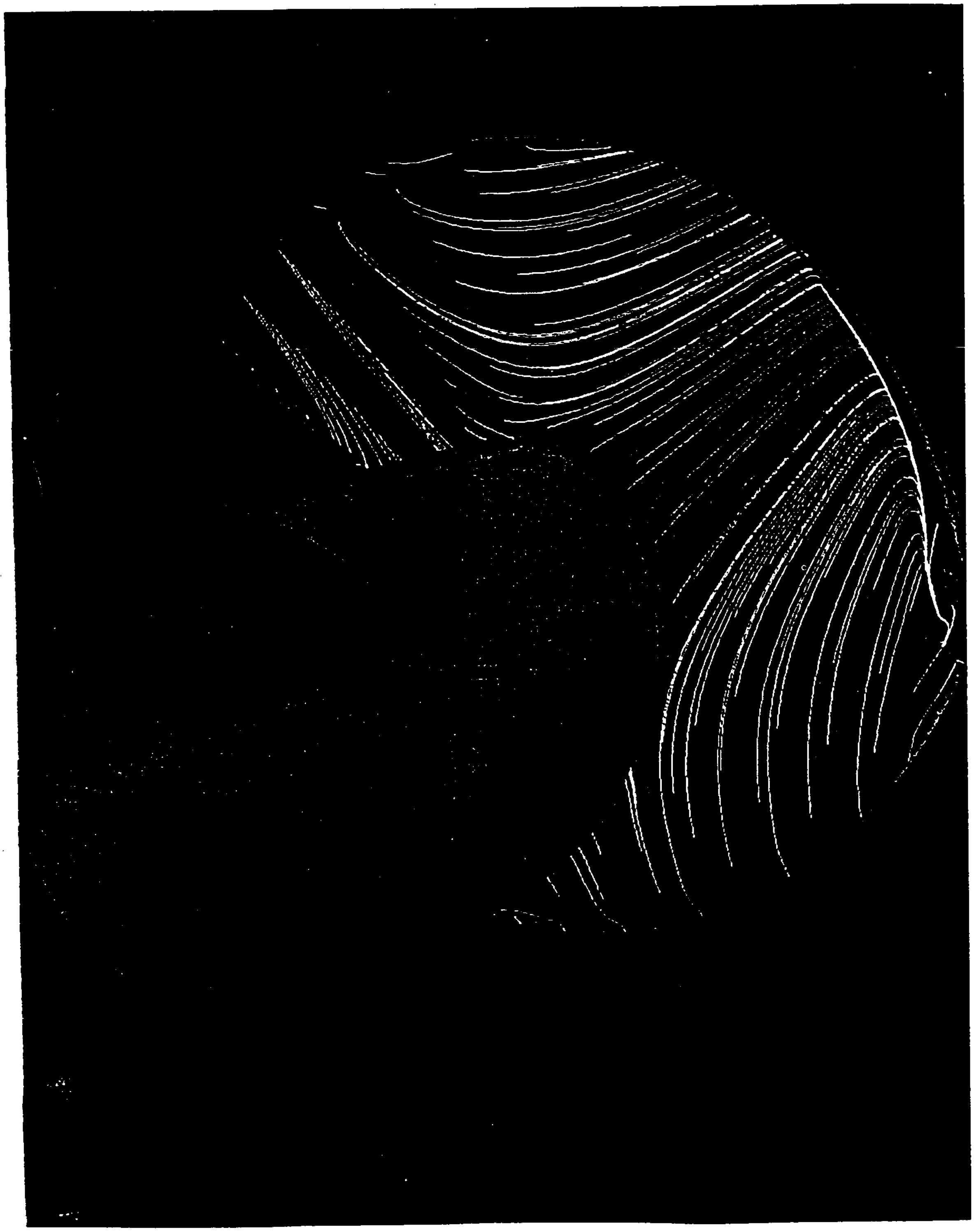

OIL FLOW ON SUCTION SIDE (FLOW COEFF.=0.041)

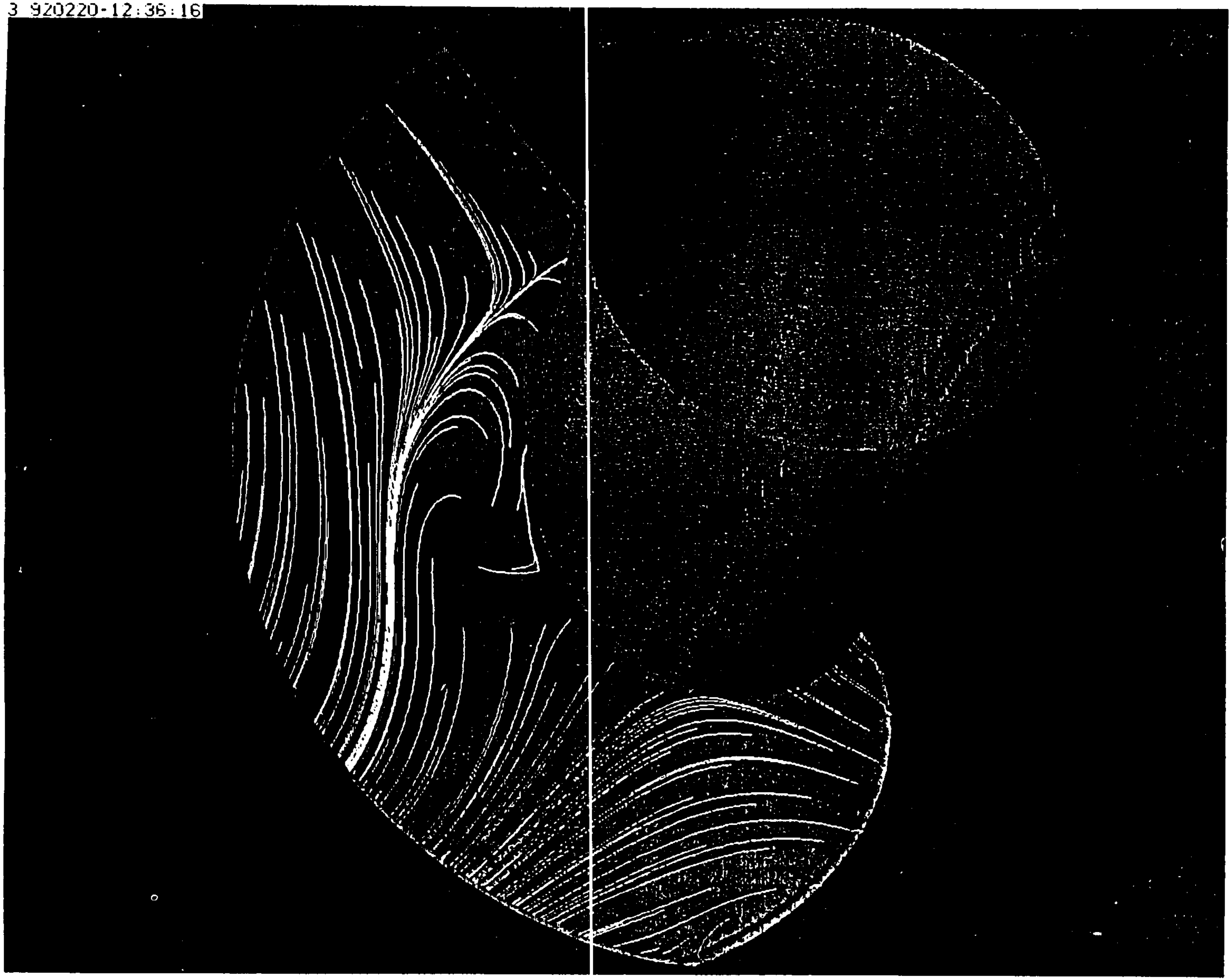

OIL FLOW ON PRESSURE SIDE (FLOW COEFF.=0.041)

OBSERVATIONS FROM CURRENT EXERCISE

MAJOR PHENOMENA WELL CALCULATED

FURTHER QUANTITATIVE COMPARISON NEEDED

CAVITATION MODELING NECESSARY

N92-32292

EFFECTS OF CURVATURE AND ROTATION ON TURBULENCE IN THE NASA LOW-SPEED CENTRIFUGAL COMPRESSOR IMPELLER

Joan G. Moore and John Moore

Mechanical Engineering Department
Virginia Polytechnic Institute and State University
Blacksburg, Virginia

The flow in the NASA Low-Speed Impeller is affected by both curvature and rotation. The flow curves due to

a) geometric curvature, e.g. the curvature of the hub and shroud profiles in the meridional plane and the curvature of the backswept impeller blades, and

b) secondary flow vortices, e.g. the tip leakage vortex.

Is the turbulence and effective turbulent viscosity in the impeller significantly affected by the curvature and rotation ?
Do these changes significantly affect the overall three-dimensional flow development ?
And do they also impact on the overall performance of the impeller ?

An answer to these questions is obtained by comparing two predictions of the flow in the impeller - one with, and one without modification to the turbulent viscosity due to rotation and curvature.

Some experimental and theoretical background for the modified mixing length model of turbulent viscosity will also be presented.

Prediction of Flow in the Impeller

using a Mixing Length Model for Turbulent Viscosity

$$\mu_t = \rho L^2 \text{"}\frac{du}{dy}\text{"}$$

L = smaller of 0.41"y"

0.08 δ

Van Driest correction used in 0.41y region

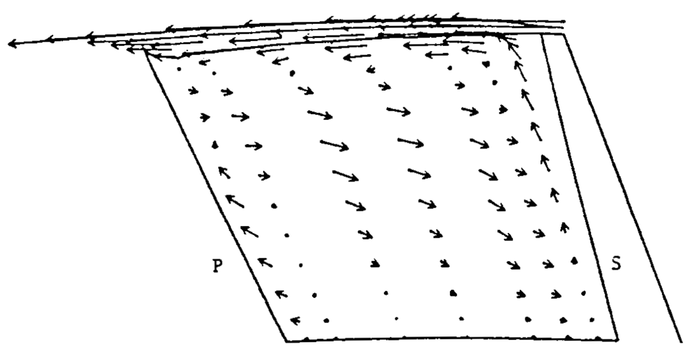

Calculated secondary flow velocity vectors on cross-sectional plane three quarters of the way through the impeller. Note contour of zero primary velocity near the shroud wall.

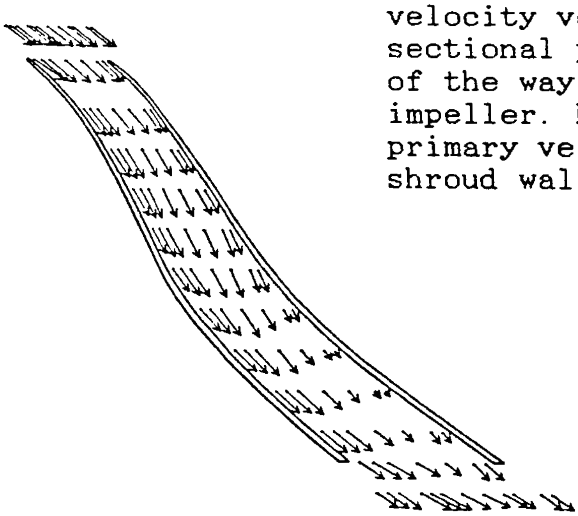

Throughflow velocity vectors projected onto the unrolled blade-to-blade plane at 80% of blade height.

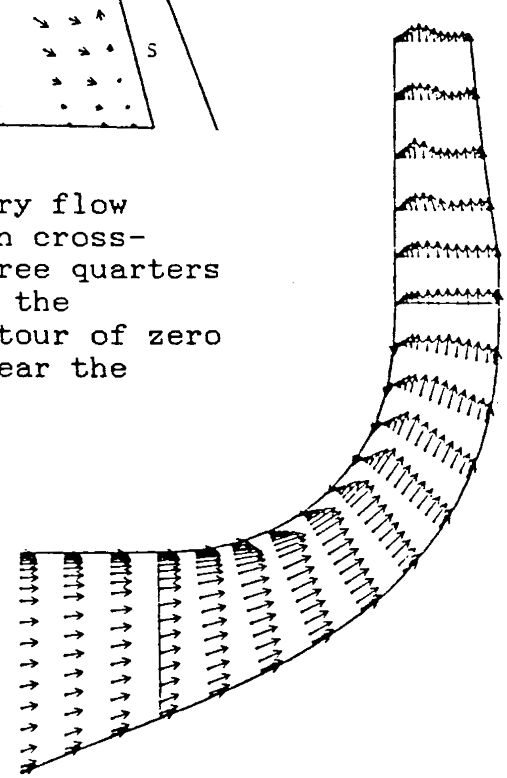

Meridional view of the velocity vectors at mid-passage.

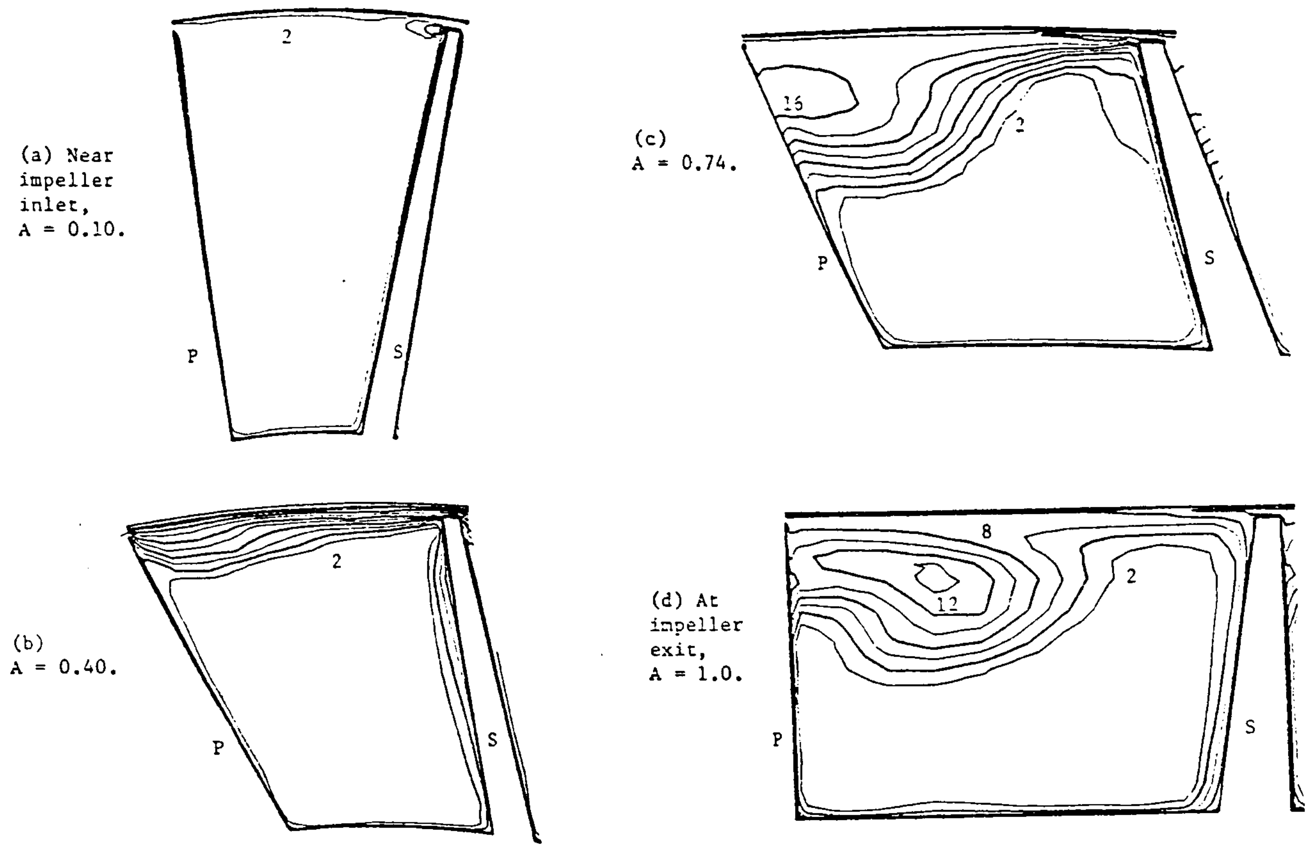

Distributions of entropy on cross-sectional planes through the impeller. Contour interval = 2.0 J/kg K. P, pressure side; S, suction side.

The effects of tip leakage dominate the calculated flow. The calculation was made with a tip gap which varied from 2.6% of blade height at the impeller inlet to 4% at the impeller exit. The secondary flow velocity vectors in the cross-sectional plane are dominated by the flow over the blade tip and the resulting vortex in the passage. The velocity vectors in the meridional view at mid passage show the extent of the backflow region near the shroud due to the tip leakage. The vectors in the blade-to-blade view show the penetration of the high loss/low velocity tip leakage fluid at 80% of the blade height.

The entropy on four cross-sectional planes show the build up of the losses to be dominated by the tip leakage flow with the high loss fluid covering the pressure-side/shroud quarter of the passage at the impeller exit.

Background of the Modification of the Mixing Length due to Curvature and Rotation

MIXING LENGTH MODEL

$$\mu_t = \rho L^2 \text{"}\frac{du}{dy}\text{"}$$

= Equilibrium form of one equation k-L model

Turbulence Kinetic Energy Equation

$$\rho \underline{u} \cdot \nabla k \quad - \quad \nabla \cdot \mu_{eff} \nabla k \quad = \quad P_k \quad - \quad D_k$$

Convection Diffusion Production Dissipation

Equilibrium

$$P_k = D_k$$

$$\Longrightarrow \quad \mu_t = \rho L^2 \left[\left(\frac{\partial u_i}{\partial x_j} + \frac{\partial u_j}{\partial x_i} \right) \frac{\partial u_i}{\partial x_j} \right]^{1/2}$$

$$\mu_t = \rho L^2 \text{"}\frac{du}{dy}\text{"}$$

The mixing length turbulence model may be viewed as the equilibrium form of a one-equation turbulence model. It can be derived by setting the production of turbulence kinetic energy equal to its dissipation.

The modification to the turbulent viscosity due to curvature and rotation may be derived by considering the Reynolds stress equations. So (1978), derived the reduction by considering the situation when rotation and curvature act in a plane. He used the equilibrium form (production = dissipation) of the three normal stress equations and one shear stress equation.

MIXING LENGTH MODEL WITH CURVATURE AND ROTATION

$$\mu_t = \rho (L_o F)^2 \text{"}\frac{du}{dy}\text{"}$$

= Equilibrium form of 6 equation $\overline{u_i' u_j'}$ - L model

Reynolds Stress Equations

$$\rho \underline{u} \cdot \nabla (\overline{u_i' u_j'}) - \nabla \cdot (\mu/\sigma)_{eff} \nabla (\overline{u_i' u_j'}) = P_{ij} - D_{ij}$$

Convection Diffusion Production Dissipation

Equilibrium

$$P_{ij} = D_{ij}$$

===> $$\mu_t = \rho \, (L_o F)^2 \text{"}\frac{du}{dy}\text{"}$$

F = F(Gradient Richardson Number)

MODIFICATION FACTOR FROM 2-D FLOW LITERATURE

$$F = 1 - \beta \, Ri \qquad \text{for } Ri < 0$$

$$F = 1/(1 + \beta \, Ri) \qquad \text{for } Ri > 0$$

Curvature and Rotation Acting in a Plane (So)

$$Ri = \frac{(2u/R - 2\Omega)\,(\partial u/\partial y + u/R - 2\Omega)}{(\partial u/\partial y - u/R)^2}$$

(R = radius of curvature)

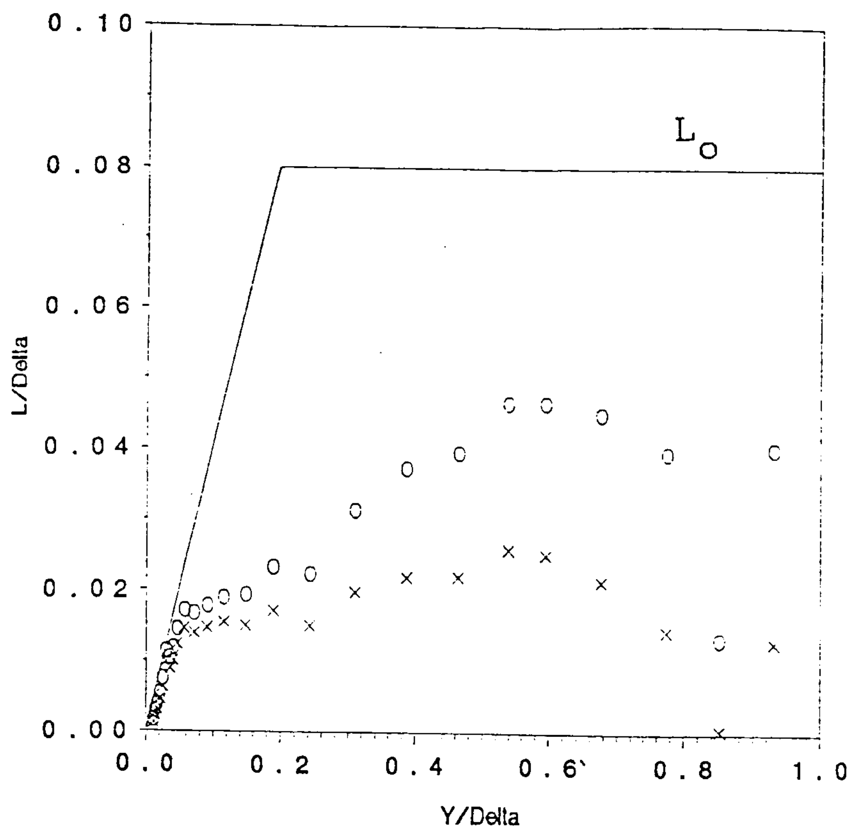

Modified Mixing Length from Experimental Data

2-D Flow in a Curved Channel (Gillis et al.)

$$-\rho u'v' = \mu_t \text{"}du/dy\text{"},$$

$$o - \quad \mu_t = \rho L^2 \text{"}du/dy\text{"}$$

$$\times - \quad \mu_t = C_\mu \rho L k^{1/2}$$

Gillis et al. measured the six Reynolds stresses and the velocity profile on the suction side of a curved channel. The local turbulent viscosity and the local mixing length for either a zero equation (Prandtl mixing length) or one-equation (k-L) turbulence model may then be determined from their measurements.

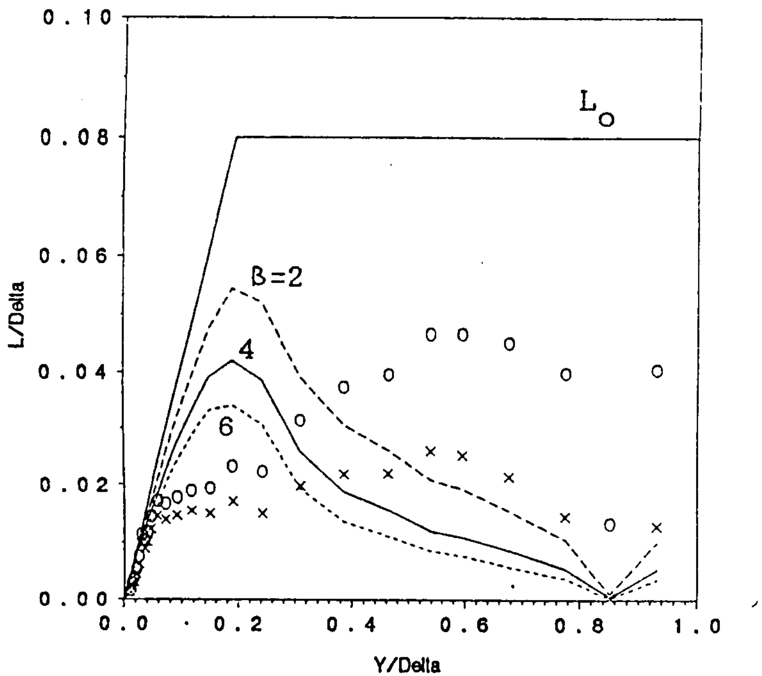

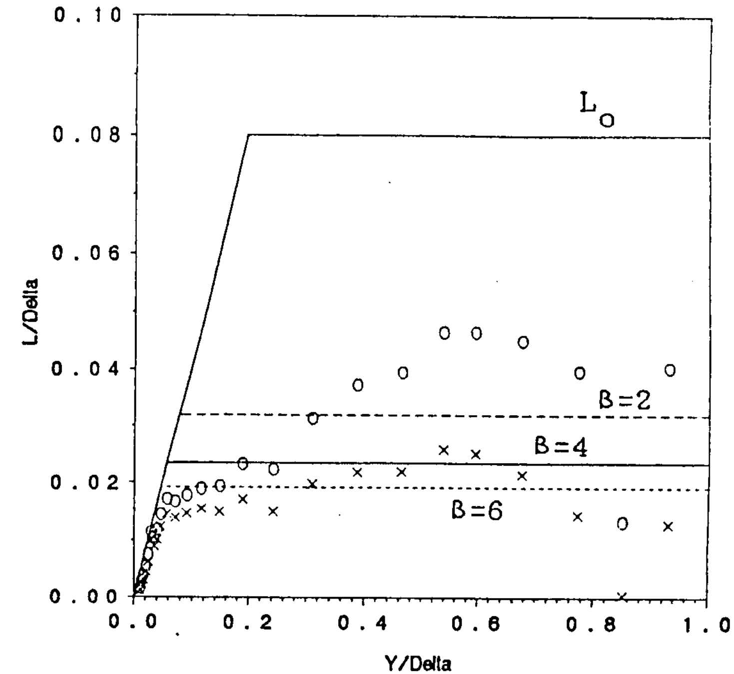

Modified L Model using local Factor:

$$L = L_o F$$

$$F = 1/(1 + \beta Ri)$$

Modified L Model using mean Factor:

L = smaller of 0.41"y"

$$0.08\delta \bar{F} = 0.08 \int_0^\delta F \, dy$$

When L, determined from the measurements, is compared to L from the model, to obtain ß, it is found that using a local modification factor results in the wrong shape for the L versus y profile through the boundary layer. A mean factor applied to L in the outer part of the boundary layer gives better results.

PREDICTED FLOW IN THE IMPELLER

using a CURVATURE/ROTATION

MODIFIED MIXING LENGTH MODEL FOR 3-D FLOW

$$\mu_t = \rho L^2 \text{"}\frac{du}{dy}\text{"}$$

$$L = \text{smaller of} \quad \begin{matrix} 0.41\text{"}y\text{"} \\ 0.08\delta\ \bar{F} \end{matrix}$$

Van Driest correction used in 0.41y region

$$F = 1 - \beta\ Ri \qquad \text{for } Ri < 0$$

$$F = 1/(1 + \beta\ Ri) \qquad \text{for } Ri > 0$$

$$\beta = 4$$

$$Ri = [2\varepsilon_{nkj}u_k u_i \partial u_j/\partial x_i - 2\varepsilon_{nlk}\varepsilon_{kji}u_l u_i \Omega_j]$$
$$\cdot\ [\varepsilon_{nla}\varepsilon_{akn}u_l u_m(\varepsilon_{kji}\partial u_j/x_i - 2\Omega_k)\ ]$$
$$/\ [\varepsilon_{nkj}u_k u_i(\partial u_i/\partial x_j + \partial u_j/\partial x_i)\ ]^2$$

The mixing length model, with L modified by a mean factor for curvature and rotation, was then used to obtain another prediction of the flow in the NASA low speed centrifugal impeller. β=4 was used with a generalized 3-d form of the Richardson number which reduces to the correct 2-d form in 2-d situations.

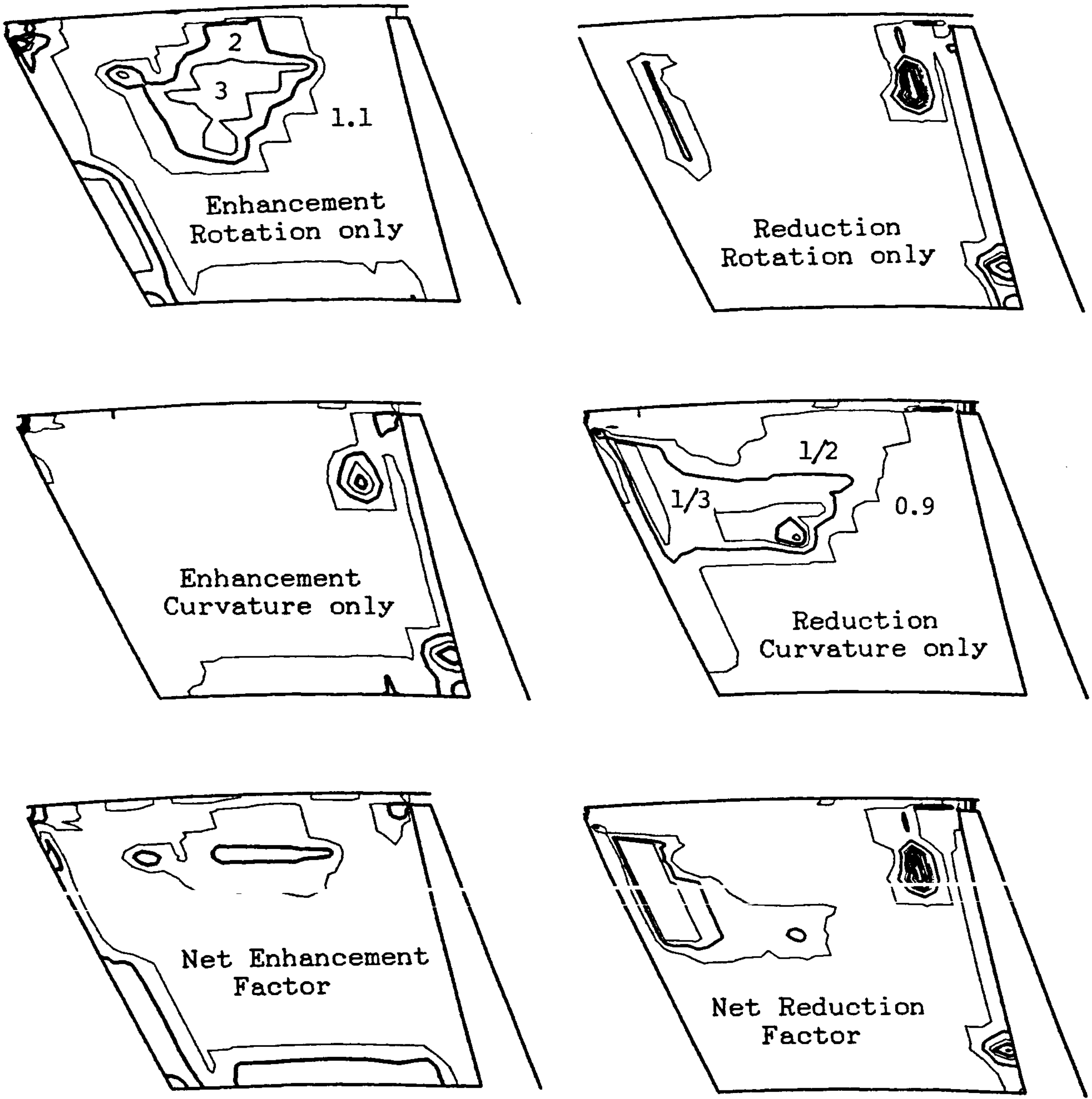

Modification factor for the turbulent viscosity, $\bar{F}^2$, 3/4ths of the way through the impeller.

The classical 2-d boundary layer modifications can be seen with enhancement due to rotation in the pressure side boundary layer, reduction due to rotation in the suction side boundary layer, and enhancement due to curvature on the concave hub wall. In the tip leakage vortex there is an enhancement due to rotation near mid-passage where the entropy gradient is in the same sense as in a pressure side boundary layer. The tip vortex also sees a reduction due to curvature near mid-height where the entropy gradient is in the same sense as for a shroud wall (convex wall) boundary layer.

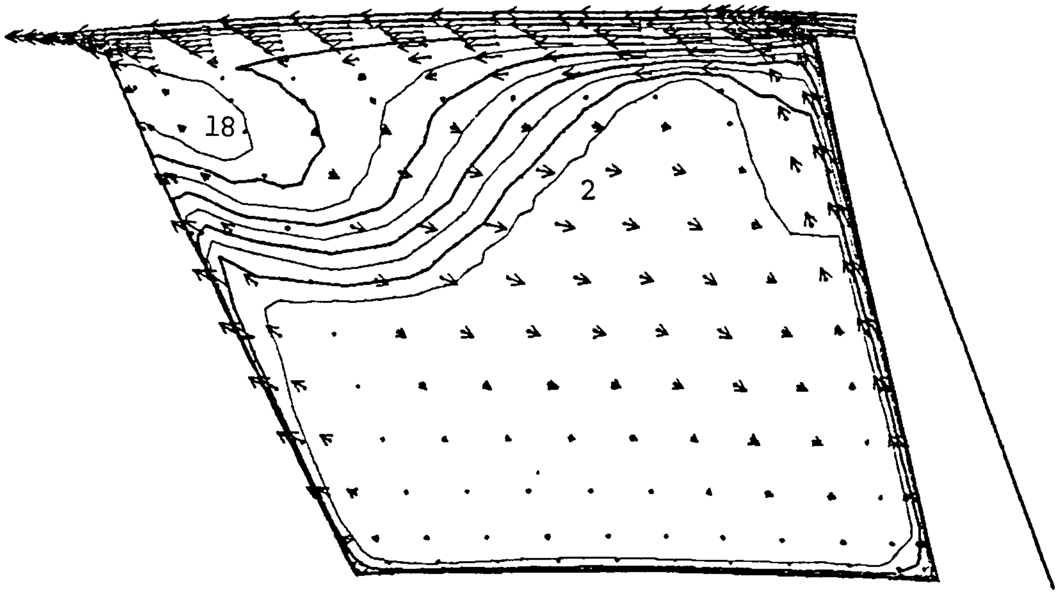

A = 0.74

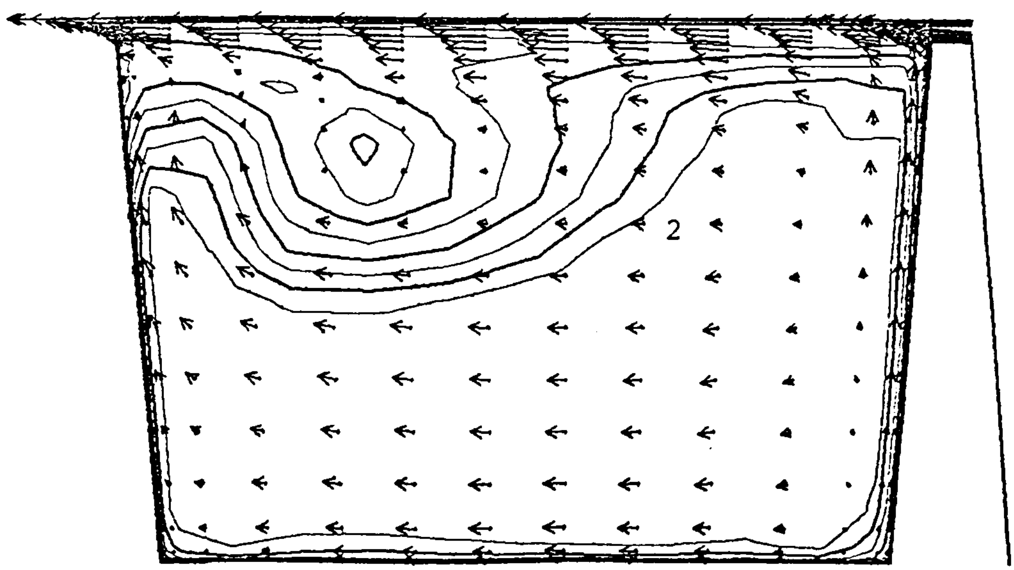

A = 0.97

Secondary flow velocity vectors and entropy contours on cross-sectional planes 3/4ths through, and near the exit of the impeller. Contour interval δs = 2 J/kgK.

The character of the flow in the impeller and the mean (mass-averaged) levels of entropy were essentially the same as for the first prediction. The shape and location of the tip leakage vortex were slightly modified by the increased turbulence at mid-shroud and the reduced turbulence in the tip vortex near the pressure side near mid-height.

Comparison of Rotor Performance Predictions at 1920 RPM and 30 kg/s (66 lbm/s) with Preliminary Measurements

	NASA Design (Streamline Curvature)	Prediction Mixing Length Turb. Model	Prediction Curv/Rot Modified L	NASA Preliminary Measurements
P_{t2}/P_o	1.173	1.128	1.127	1.13
η_{t-ti2}	0.934	0.922	0.922	0.93
$\Delta H/U^2$	0.607	0.469	0.467	0.50
$M_{reli,tip}$	0.31	0.31	0.31	
M_{rel2}	0.20	0.272		
M_{abs2}	0.287	0.244		
Reaction	0.763	0.843	0.846	

Plane i is at the impeller inlet; Plane 2 is at the impeller exit.

TOTAL PRESSURE RISE IN THE IMPELLER

o - NASA Preliminary Measurements

Predictions

——— MEFP, Mixing Length Turbulence Model

- - - MEFP, Rot/Curv Modified L Model

- - NASA Design (Streamline Curvature)

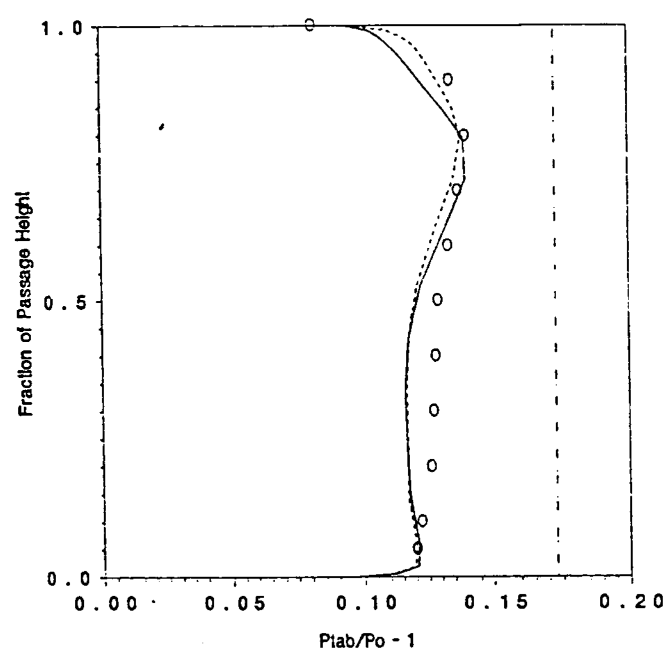

Both MEFP predictions compare well with the preliminary measurements made by NASA. Comparisons with preliminary measurements are included here because NASA has decided to reduce the tip clearance before making detailed measurements of flow in the impeller.

CONCLUSIONS

- A local modification factor due to curvature and rotation is inappropriate in a mixing length model.

  Data suggests that an average factor for the layer is appropriate.

- Typical modification factors for the turbulent viscosity in the NASA Low Speed Centrifugal Impeller were 2-4.

- Changes to the predicted flow were small:
  - Slight increase in secondary flow velocities on the pressure side.
  - Slight change in shape and relocation of the tip leakage vortex.

- No change in overall performance.

- The NASA Low Speed Centrifugal Impeller is a good test case for verification of 3-d N-S solvers which include mixing length, one-equation, or two-equation turbulence models.

- The Upwind Control Volume* discretization used in MEFP makes this code a good vehicle for the evaluation of turbulence models in 3-d flow. Calculated vortex structure is sensitive to small changes in the turbulence model.

* The Upwind Control Volume approach introduces no numerical mixing either directly through second or fourth order smoothing or indirectly through inconsistencies in the discretization of the convection term such as upwind differencing.

EFFECTS OF CURVATURE AND ROTATION ON TURBULENCE IN THE NASA LOW-SPEED CENTRIFUGAL COMPRESSOR IMPELLER

Joan G. Moore and John Moore

Mechanical Engineering Department
Virginia Polytechnic Institute and State University
Blacksburg, Virginia

The flow in the NASA Low-Speed Impeller is affected by both curvature and rotation. The flow curves due to

a) geometric curvature, e.g. the curvature of the hub and shroud profiles in the meridional plane and the curvature of the backswept impeller blades, and

b) secondary flow vortices, e.g. the tip leakage vortex.

Is the turbulence and effective turbulent viscosity in the impeller significantly affected by the curvature and rotation ?
Do these changes significantly affect the overall three-dimensional flow development ?
And do they also impact on the overall performance of the impeller ?

An answer to these questions is obtained by comparing two predictions of the flow in the impeller - one with, and one without modification to the turbulent viscosity due to rotation and curvature.

Some experimental and theoretical background for the modified mixing length model of turbulent viscosity will also be presented.

Prediction of Flow in the Impeller

using a Mixing Length Model for Turbulent Viscosity

$$\mu_t = \rho L^2 \text{"}\frac{du}{dy}\text{"}$$

L = smaller of 0.41"y"

0.08 δ

Van Driest correction used in 0.41y region

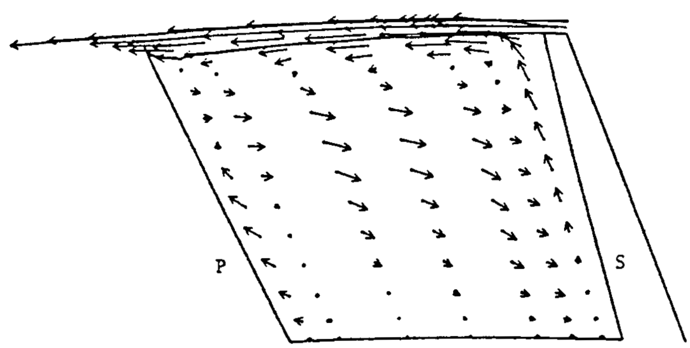

Calculated secondary flow velocity vectors on cross-sectional plane three quarters of the way through the impeller. Note contour of zero primary velocity near the shroud wall.

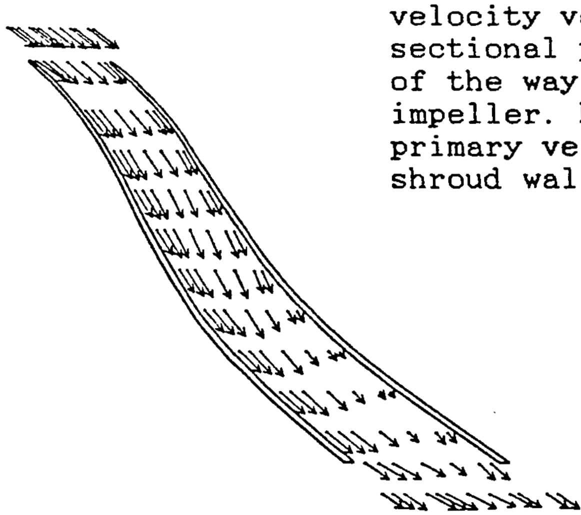

Throughflow velocity vectors projected onto the unrolled blade-to-blade plane at 80% of blade height.

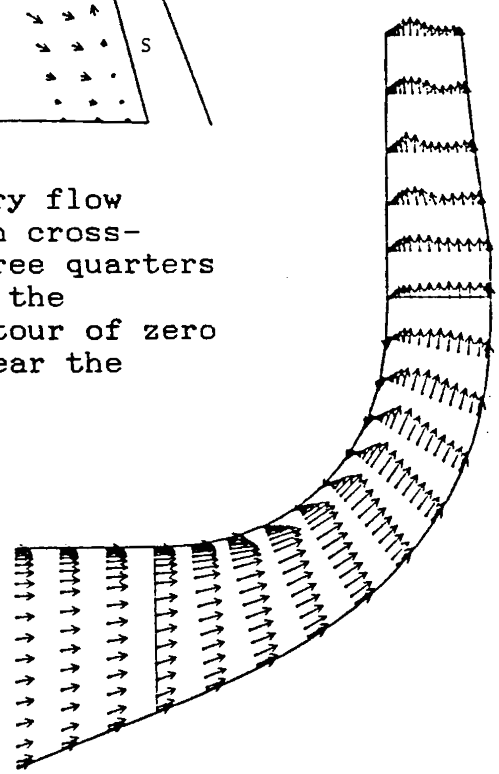

Meridional view of the velocity vectors at mid-passage.

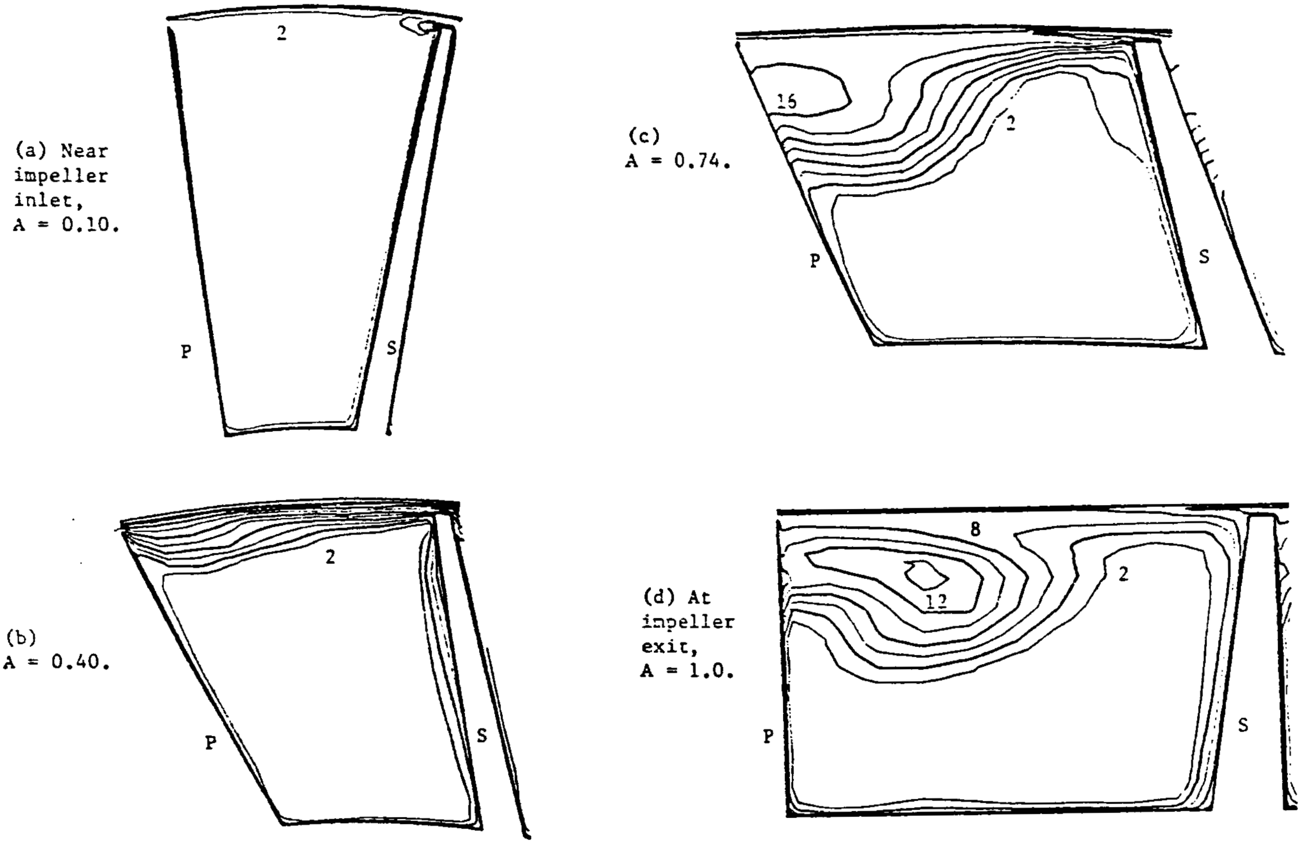

Distributions of entropy on cross-sectional planes through the impeller. Contour interval = 2.0 J/kg K. P, pressure side; S, suction side.

The effects of tip leakage dominate the calculated flow. The calculation was made with a tip gap which varied from 2.6% of blade height at the impeller inlet to 4% at the impeller exit. The secondary flow velocity vectors in the cross-sectional plane are dominated by the flow over the blade tip and the resulting vortex in the passage. The velocity vectors in the meridional view at mid passage show the extent of the backflow region near the shroud due to the tip leakage. The vectors in the blade-to-blade view show the penetration of the high loss/low velocity tip leakage fluid at 80% of the blade height.

The entropy on four cross-sectional planes show the build up of the losses to be dominated by the tip leakage flow with the high loss fluid covering the pressure-side/shroud quarter of the passage at the impeller exit.

Background of the Modification of the Mixing Length due to Curvature and Rotation

MIXING LENGTH MODEL

$$\mu_t = \rho L^2 \text{"}\frac{du}{dy}\text{"}$$

= <u>Equilibrium form of one equation k-L model</u>

Turbulence Kinetic Energy Equation

$\rho \underline{u} \cdot \nabla k$	$-$	$\nabla \cdot \mu_{eff} \nabla k$	$=$	P_k	$-$	D_k
Convection		Diffusion		Production		Dissipation

<u>Equilibrium</u>

$$P_k = D_k$$

$$\Longrightarrow \quad \mu_t = \rho L^2 \left[\left(\frac{\partial u_i}{\partial x_j} + \frac{\partial u_j}{\partial x_i} \right) \frac{\partial u_i}{\partial x_j} \right]^{1/2}$$

$$\mu_t = \rho L^2 \text{"}\frac{du}{dy}\text{"}$$

The mixing length turbulence model may be viewed as the equilibrium form of a one-equation turbulence model. It can be derived by setting the production of turbulence kinetic energy equal to its dissipation.

The modification to the turbulent viscosity due to curvature and rotation may be derived by considering the Reynolds stress equations. So (1978), derived the reduction by considering the situation when rotation and curvature act in a plane. He used the equilibrium form (production = dissipation) of the three normal stress equations and one shear stress equation.

MIXING LENGTH MODEL WITH CURVATURE AND ROTATION

$$\mu_t = \rho(L_o F)^2 \, "\frac{du}{dy}"$$

= <u>Equilibrium form of 6 equation $\overline{u_i' u_j'}$ - L model</u>

Reynolds Stress Equations

$$\underset{\text{Convection}}{\rho \underline{u} \cdot \nabla(\overline{u_i' u_j'})} - \underset{\text{Diffusion}}{\nabla \cdot (\mu/\sigma)_{eff} \nabla(\overline{u_i' u_j'})} = \underset{\text{Production}}{P_{ij}} - \underset{\text{Dissipation}}{D_{ij}}$$

<u>Equilibrium</u>

$$P_{ij} \doteq D_{ij}$$

===> $$\mu_t = \rho \, (L_o F)^2 \, "\frac{du}{dy}"$$

F = F(<u>Gradient Richardson Number</u>)

MODIFICATION FACTOR FROM 2-D FLOW LITERATURE

$$F = 1 - \beta \, Ri \qquad \text{for } Ri < 0$$

$$F = 1/(1 + \beta \, Ri) \qquad \text{for } Ri > 0$$

Curvature and Rotation Acting in a Plane (So)

$$Ri = \frac{(2u/R - 2\Omega)\,(\partial u/\partial y + u/R - 2\Omega)}{(\ \partial u/\partial y - u/R\ )^2}$$

(R = radius of curvature)

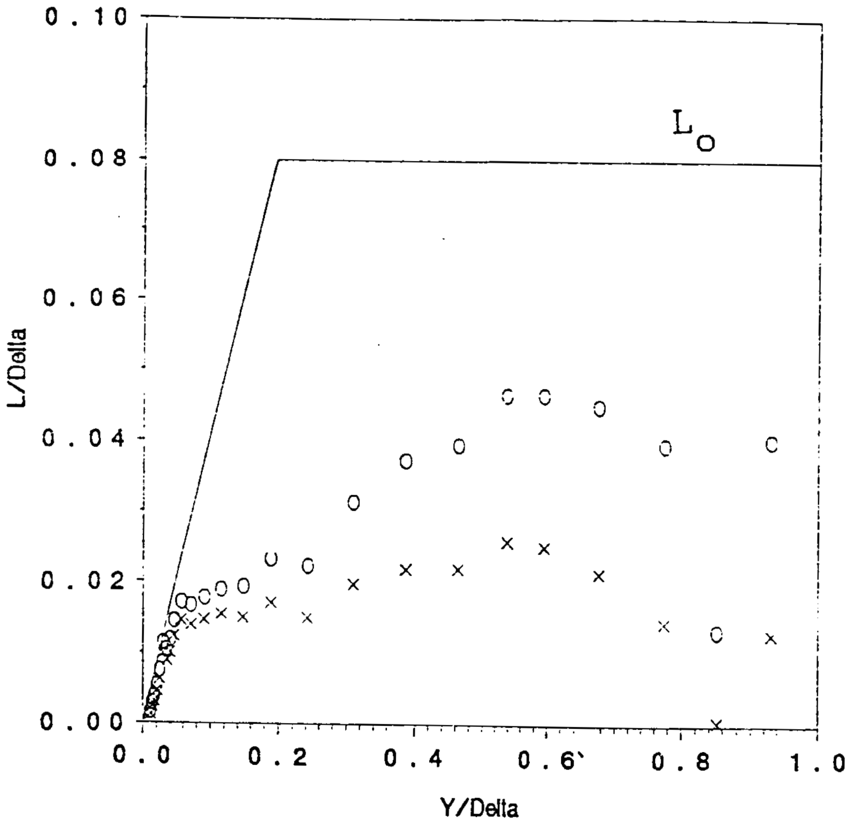

Modified Mixing Length from Experimental Data

2-D Flow in a Curved Channel (Gillis et al.)

$$-\rho u'v' = \mu_t \text{"}du/dy\text{"},$$

$$\text{o} - \quad \mu_t = \rho L^2 \text{"}du/dy\text{"}$$

$$\times - \quad \mu_t = C_\mu \rho L k^{1/2}$$

Gillis et al. measured the six Reynolds stresses and the velocity profile on the suction side of a curved channel. The local turbulent viscosity and the local mixing length for either a zero equation (Prandtl mixing length) or one-equation (k-L) turbulence model may then be determined from their measurements.

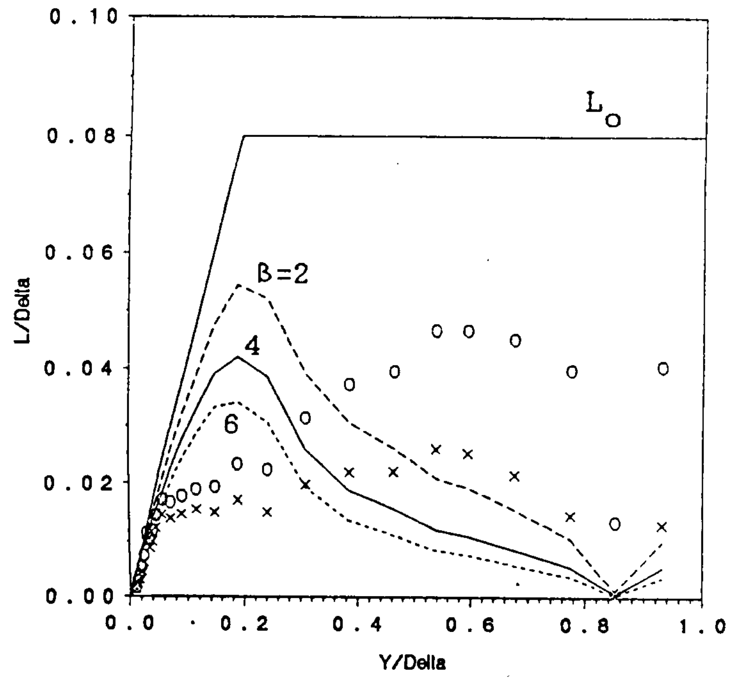

Modified L Model using local Factor:

$$L = L_o F$$

$$F = 1/(1 + \beta Ri)$$

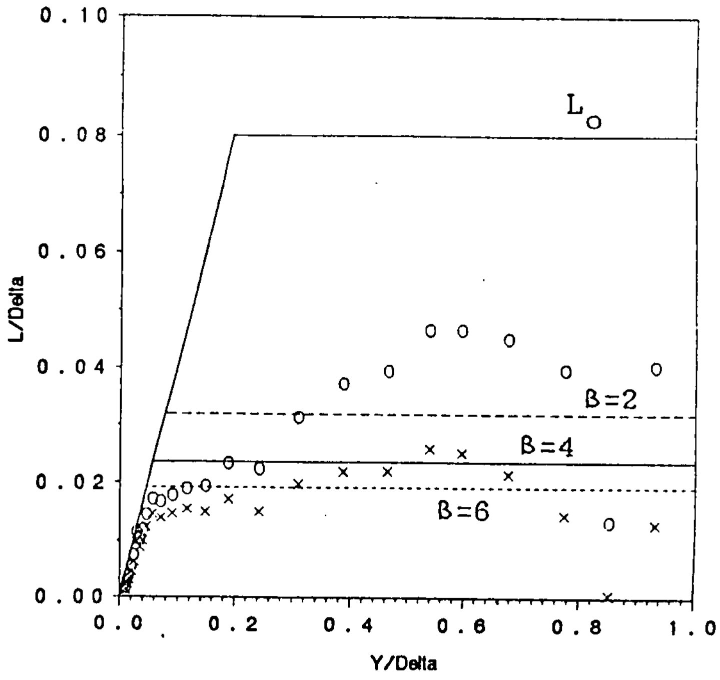

Modified L Model using mean Factor:

L = smaller of 0.41"y"

$$0.08\delta \bar{F} = 0.08 \int_0^\delta F \, dy$$

When L, determined from the measurements, is compared to L from the model, to obtain ß, it is found that using a local modification factor results in the wrong shape for the L versus y profile through the boundary layer. A mean factor applied to L in the outer part of the boundary layer gives better results.

PREDICTED FLOW IN THE IMPELLER

using a CURVATURE/ROTATION

MODIFIED MIXING LENGTH MODEL FOR 3-D FLOW

$$\mu_t = \rho L^2 \text{"}\frac{du}{dy}\text{"}$$

$$L = \text{smaller of } \begin{cases} 0.41\text{"}y\text{"} \\ 0.086\ \bar{F} \end{cases}$$

Van Driest correction used in 0.41y region

$$F = 1 - \beta\, Ri \qquad \text{for } Ri < 0$$

$$F = 1/(1 + \beta\, Ri) \qquad \text{for } Ri > 0$$

$$\beta = 4$$

$$Ri = [2\varepsilon_{nkj}u_k u_i \partial u_j/\partial x_i - 2\varepsilon_{nlk}\varepsilon_{kji}u_l u_i \Omega_j] \cdot [\varepsilon_{nla}\varepsilon_{akn}u_l u_m(\varepsilon_{kji}\partial u_j/x_i - 2\Omega_k)\ ] \,/\, [\varepsilon_{nkj}u_k u_i(\partial u_i/\partial x_j + \partial u_j/\partial x_i)\ ]^2$$

The mixing length model, with L modified by a mean factor for curvature and rotation, was then used to obtain another prediction of the flow in the NASA low speed centrifugal impeller. β=4 was used with a generalized 3-d form of the Richardson number which reduces to the correct 2-d form in 2-d situations.

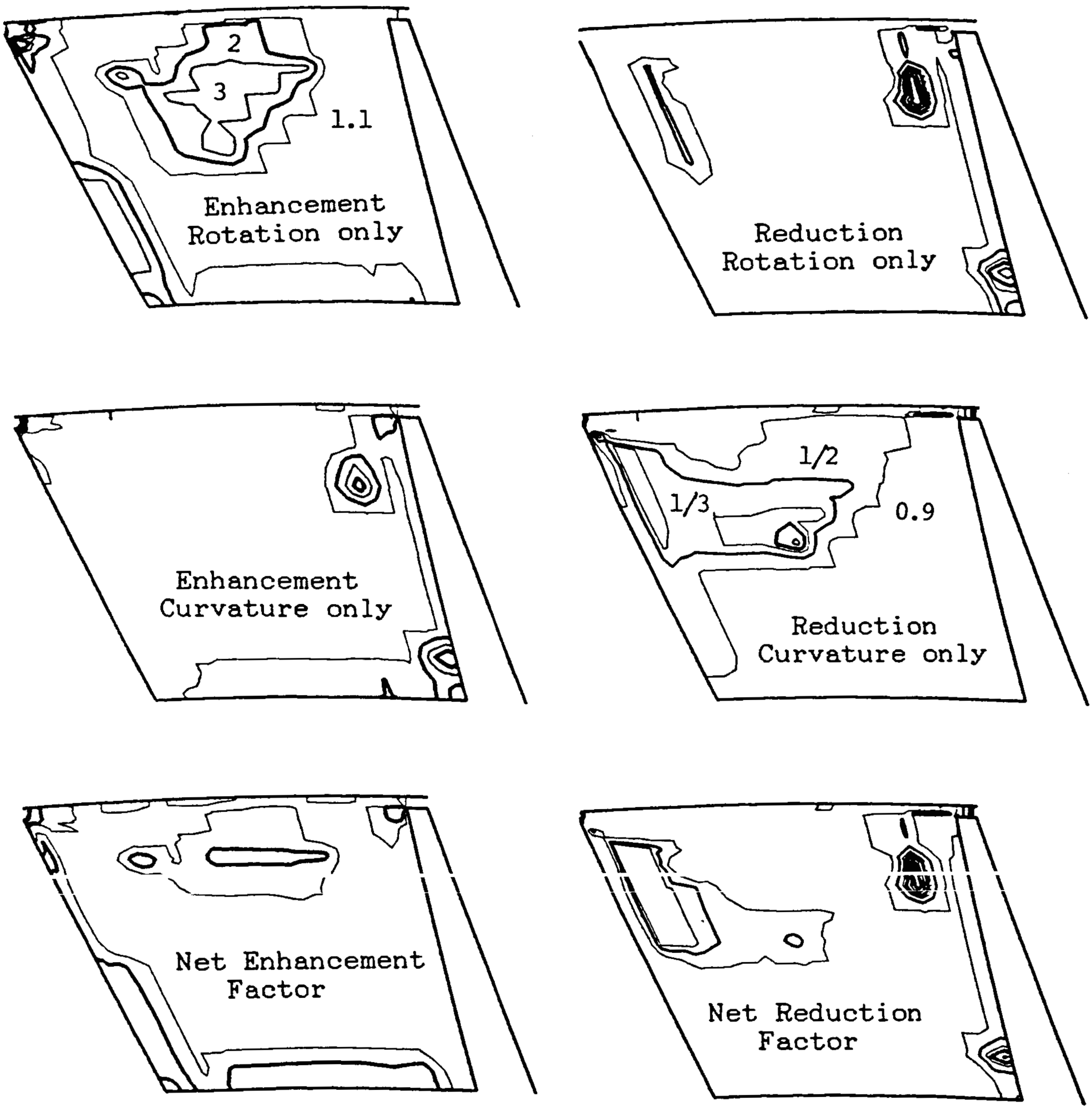

Modification factor for the turbulent viscosity, $\bar{F}^2$, 3/4ths of the way through the impeller.

The classical 2-d boundary layer modifications can be seen with enhancement due to rotation in the pressure side boundary layer, reduction due to rotation in the suction side boundary layer, and enhancement due to curvature on the concave hub wall. In the tip leakage vortex there is an enhancement due to rotation near mid-passage where the entropy gradient is in the same sense as in a pressure side boundary layer. The tip vortex also sees a reduction due to curvature near mid-height where the entropy gradient is in the same sense as for a shroud wall (convex wall) boundary layer.

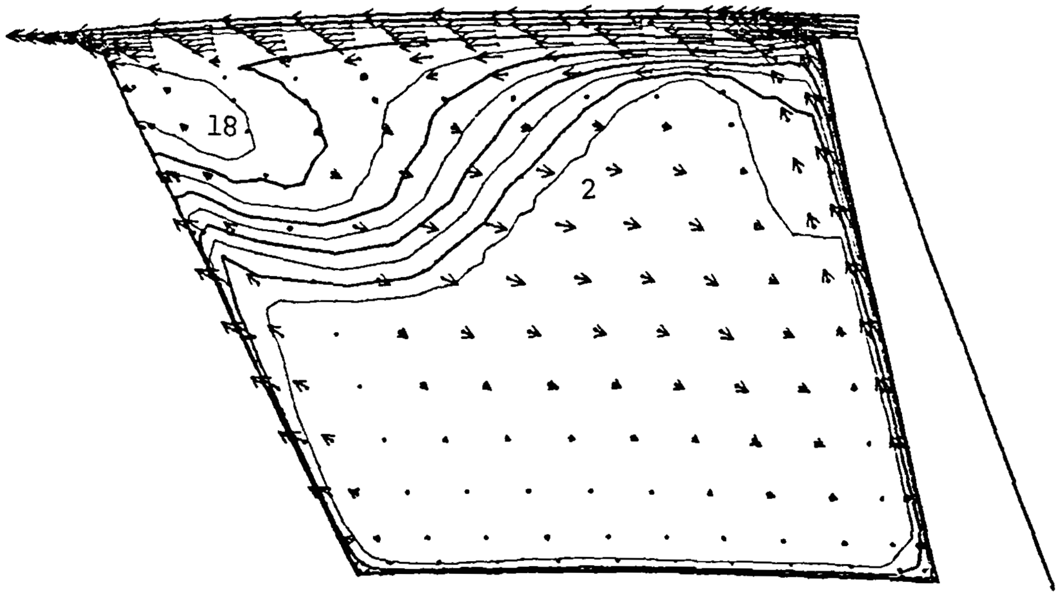

A = 0.74

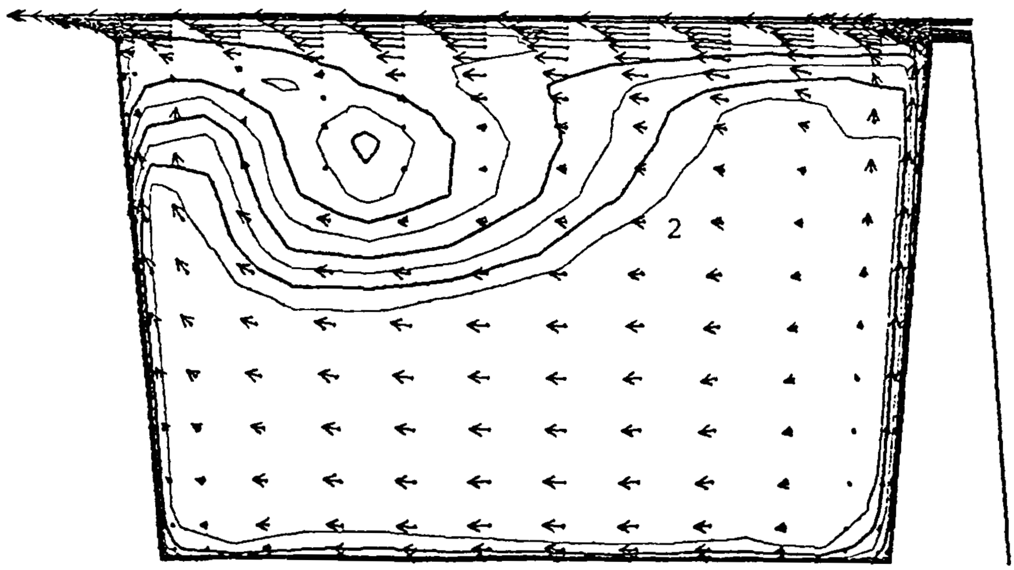

A = 0.97

Secondary flow velocity vectors and entropy contours on cross-sectional planes 3/4ths through, and near the exit of the impeller. Contour interval δs = 2 J/kgK.

The character of the flow in the impeller and the mean (mass-averaged) levels of entropy were essentially the same as for the first prediction. The shape and location of the tip leakage vortex were slightly modified by the increased turbulence at mid-shroud and the reduced turbulence in the tip vortex near the pressure side near mid-height.

Comparison of Rotor Performance Predictions at 1920 RPM and 30 kg/s (66 lbm/s) with Preliminary Measurements

	NASA Design (Streamline Curvature)	Prediction Mixing Length Turb. Model	Prediction Curv/Rot Modified L	NASA Preliminary Measurements
P_{t2}/P_o	1.173	1.128	1.127	1.13
η_{t-ti2}	0.934	0.922	0.922	0.93
$\Delta H/U^2$	0.607	0.469	0.467	0.50
$M_{reli,tip}$	0.31	0.31	0.31	
M_{rel2}	0.20	0.272		
M_{abs2}	0.287	0.244		
Reaction	0.763	0.843	0.846	

Plane i is at the impeller inlet; Plane 2 is at the impeller exit.

TOTAL PRESSURE RISE IN THE IMPELLER

o - NASA Preliminary Measurements

Predictions

——— MEFP, Mixing Length Turbulence Model

- - - MEFP, Rot/Curv Modified L Model

\- \- NASA Design (Streamline Curvature)

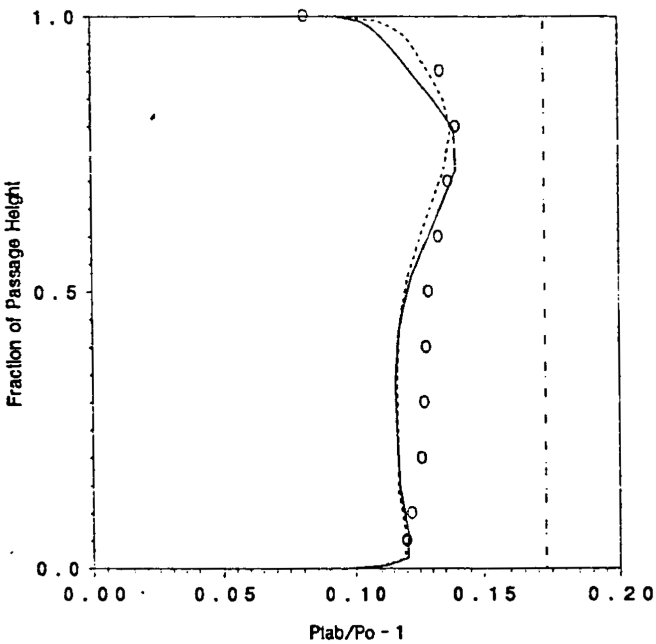

Both MEFP predictions compare well with the preliminary measurements made by NASA. Comparisons with preliminary measurements are included here because NASA has decided to reduce the tip clearance before making detailed measurements of flow in the impeller.

CONCLUSIONS

- A local modification factor due to curvature and rotation is inappropriate in a mixing length model.

  Data suggests that an average factor for the layer is appropriate.

- Typical modification factors for the turbulent viscosity in the NASA Low Speed Centrifugal Impeller were 2-4.

- Changes to the predicted flow were small:
  - Slight increase in secondary flow velocities on the pressure side.
  - Slight change in shape and relocation of the tip leakage vortex.

- No change in overall performance.

- The NASA Low Speed Centrifugal Impeller is a good test case for verification of 3-d N-S solvers which include mixing length, one-equation, or two-equation turbulence models.

- The Upwind Control Volume* discretization used in MEFP makes this code a good vehicle for the evaluation of turbulence models in 3-d flow. Calculated vortex structure is sensitive to small changes in the turbulence model.

* The Upwind Control Volume approach introduces no numerical mixing either directly through second or fourth order smoothing or indirectly through inconsistencies in the discretization of the convection term such as upwind differencing.

N92-32293

Computational Fluid Dynamic Design of Rocket Engine Pump Components

by
Wei-Chung Chen, George H. Prueger, Daniel C. Chan and Anthony H. Eastland
Rocketdyne Division, Rockwell International Corp.

Integration of CFD for design and analysis of turbomachinery components is needed as the requirements of pump performance and reliability become more stringent for the new generation of rocket engine. A fast grid generator, designed specially for centrifugal pump impeller, which allows a turbomachinery designer to use CFD to optimize the component design will be presented. The CFD grid is directly generated from the impeller blade G-H blade coordinates. The grid points are first generated on the meridional plane with the desired clustering near the end walls. This is followed by the marching of grid points from the pressure side of one blade to the suction side of a neighboring blade. This fast grid generator has been used to optimize the consortium pump impeller design. A grid dependency study has been conducted for the consortium pump impeller. Two different grid sizes, one with 10,000 grid points and one with 80,000 grid points were used for the grid dependency study. The effects of grid resolution on the turnaround time, including the grid generation and completion of the CFD analysis, is discussed. The impeller overall mass average performance is compared for different designs. Optimum design is achieved through systematic change of the design parameters. In conclusion, it is demonstrated that CFD can be effectively used not only for flow analysis but also for design and optimization of turbomachinery components.

CFD DESIGN OF ROCKET ENGINE COMPONENT

by

Wei-Chung Chen, George H. Prueger
Daniel C. Chan, Anthony H. Eastland

Rocketdyne Division
Rockwell International Corporation

340

Presented at NASA Marshall Space Flight Center
Tenth Workshop for Computational Fluid Dynamic Applications
in Rocket Propulsion
April 28-30, 1992

CFD DESIGN OF ROCKET ENGINE PUMP COMPONENT

TYPICAL TURBOPUMP LAYOUT

- KEY COMPONENTS
  - INDUCER, STATOR, IMPELLER, VOLUTE, TURBINE, BEARING
  - IMPELLER SERVES AS THE HEART OF PUMP

- ADVANCED IMPELLER DESIGNS REQUIRE HIGH HEAD COEFFICIENTS
  - RELIABILITY AND COST REQUIREMENTS LIMIT MAXIMUM ALLOWABLE TIP SPEED
  - LOW COST REQUIRES MINIMUM NUMBER OF STAGES

- HIGH PUMP HEAD COEFFICIENTS INCREASE FLOW TURNING AND DIFFUSION
  - INCREASE EXIT FLOW NON-UNIFORMITY

- CFD INCORPORATED FOR PUMP IMPELLER DESIGN
  - IDENTIFY FLOW PROBLEMS INSIDE IMPELLER PASSAGE AND DISCHARGE
  - OPTIMIZE IMPELLER CONFIGURATION DURING DESIGN PROCESS

CONSORTIUM 2-STAGE FUEL PUMP

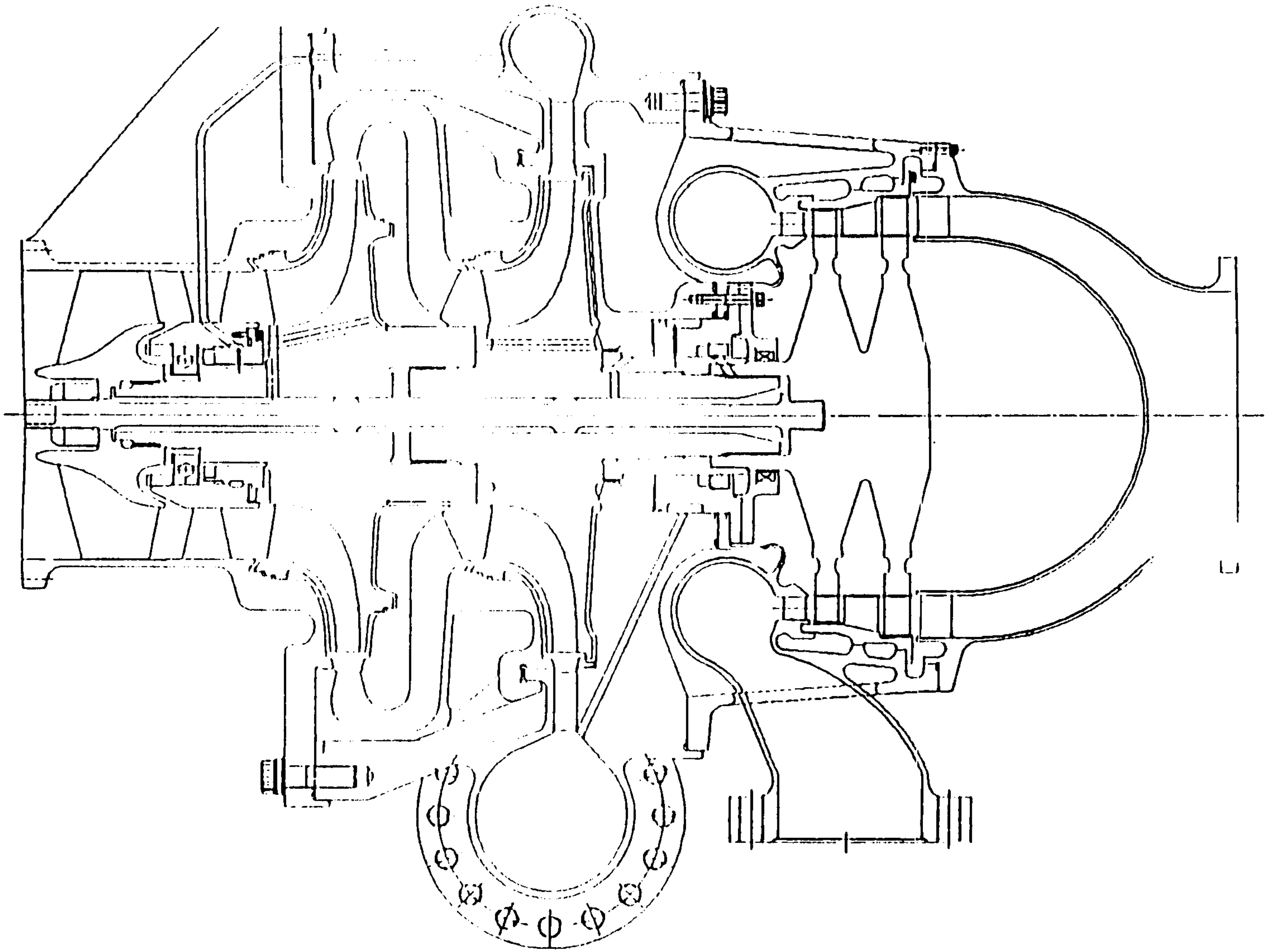

CFD DESIGN OF ROCKET ENGINE PUMP COMPONENT

CONSTRUCTION OF IMPELLER BLADE

- GENERATE BLADE MEANLINE G-H CURVE ALONG EACH STREAMLINE
  - REDUCE 3-D PROBLEM TO 2-D COORDINATE SYSTEM
  - EACH STREAMLINE INDEPENDENTLY GENERATED TO MATCH FLOW FIELD
  - CHANGE BLADE WRAP ANGLE TO CONTROL SOLIDITY
  - STACK BLADE TO ACHIEVE OPTIMUM IMPELLER PERFORMANCE

- CONSTRUCT BLADE SURFACE FROM MEANLINE COORDINATES
  - SURFACE COORDINATE GENERATED ACCORDING TO BLADE THICKNESS DISTRIBUTION
  - FLEXIBILITY OF USING MEANLINE, PRESSURE SIDE, SUCTION SIDE OR HYBRID FAIRING

- SURFACE INFORMATION DIRECTLY USED FOR
  - BLADE LAYOUT IN CATIA MODEL
  - CFD GRID GENERATION

Rockwell International
Rocketdyne Division

IMPELLER MEANLINE BLADE GENERATION

CONSORTIUM PUMP IMPELLER
STREAMLINE DEFINITION (ITERATION 22)

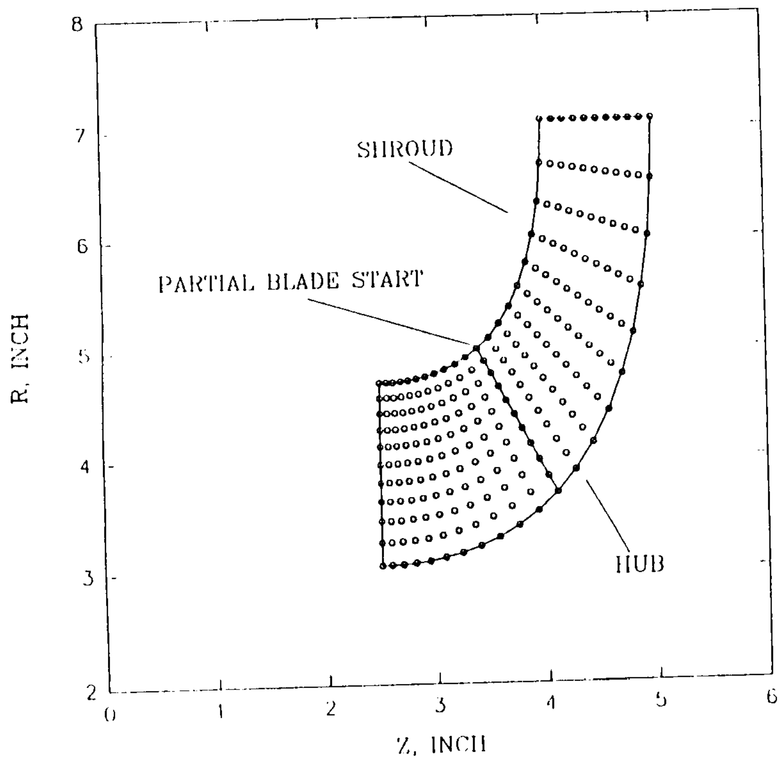

CONSORTIUM PUMP
IMPELLER BLADE G-H CURVE (ITERATION 22)

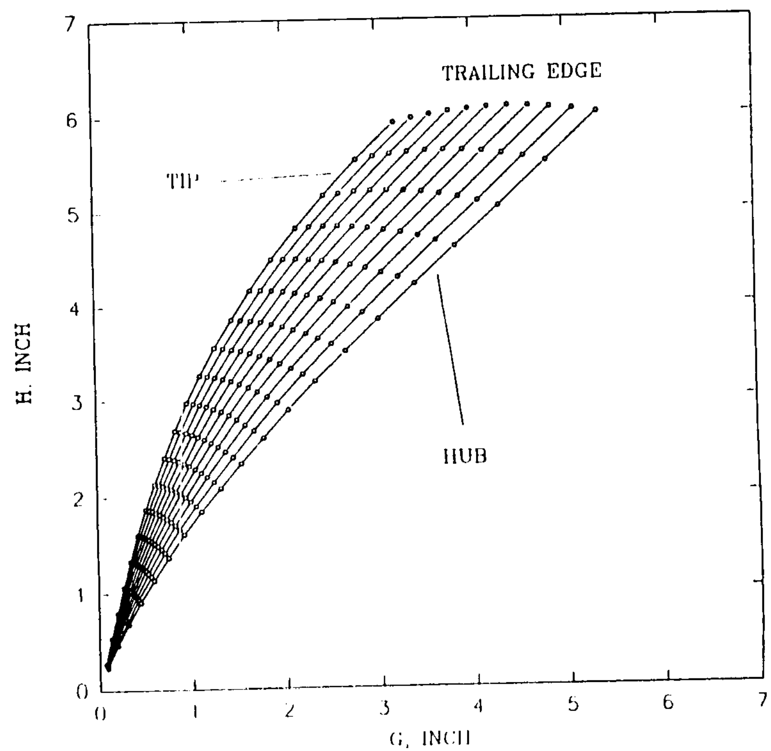

Rockwell International
Rocketdyne Division

CFD DESIGN OF ROCKET ENGINE PUMP COMPONENT

FAST GRID GENERATOR

- USE BLADE SURFACE PRESSURE AND SUCTION SURFACE G-H INFORMATION
  - BOTH FULL AND PARTIAL BLADES
- GENERATE GRID IN MERIDIONAL PLANE
  - DETERMINE L.E. TO T.E. STATION NUMBER
  - SELECT HUB TO TIP STREAMLINE NUMBER
- INTERPOLATE BLADE SURFACE COORDINATES TO GRID MESH POINTS
  - REQUIRE SURFACE INTERPOLATION
- CREATE 3-D GRID POINTS BETWEEN TWO BLADE SURFACES
- EXTEND GRID POINTS OUTWARDS
  - ACCORDING TO INLET AND OUTLET BLADE ANGLE DISTRIBUTION
- H-GRID ALGEBRAICALLY GENERATED
  - POISSON GRID SMOOTHER INCORPORATED

Rockwell International

Rocketdyne Division

DEVELOPMENT OF 10K IMPELLER GRID

COMPUTATIONAL GRID

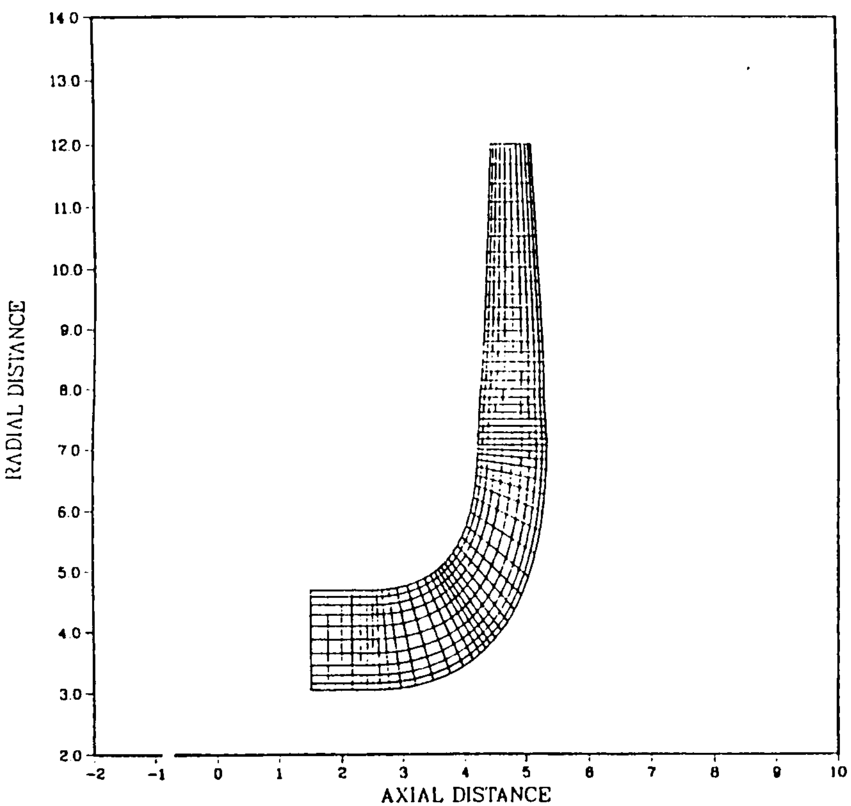

COMPUTATIONAL GRID

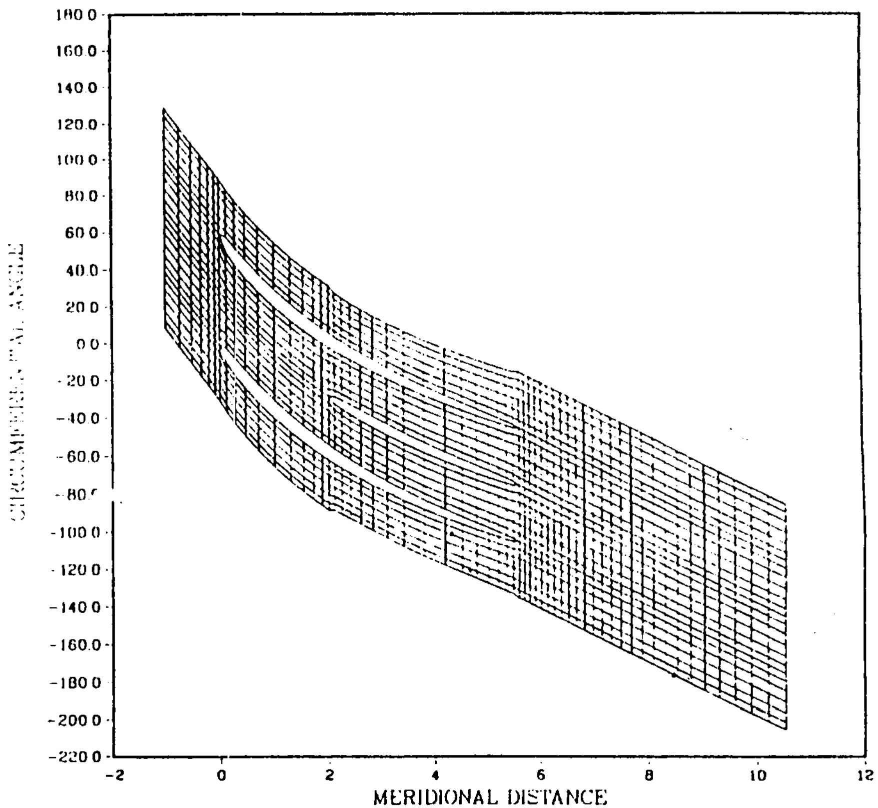

Rockwell International
Rocketdyne Division

DEVELOPMENT OF 80K IMPELLER GRID

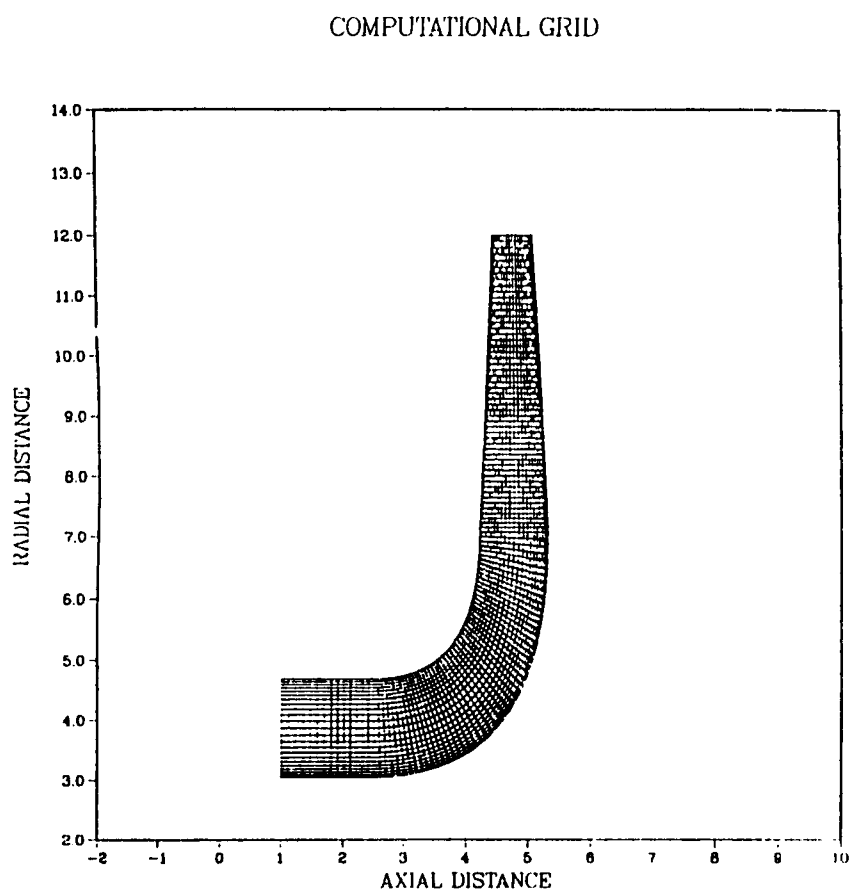

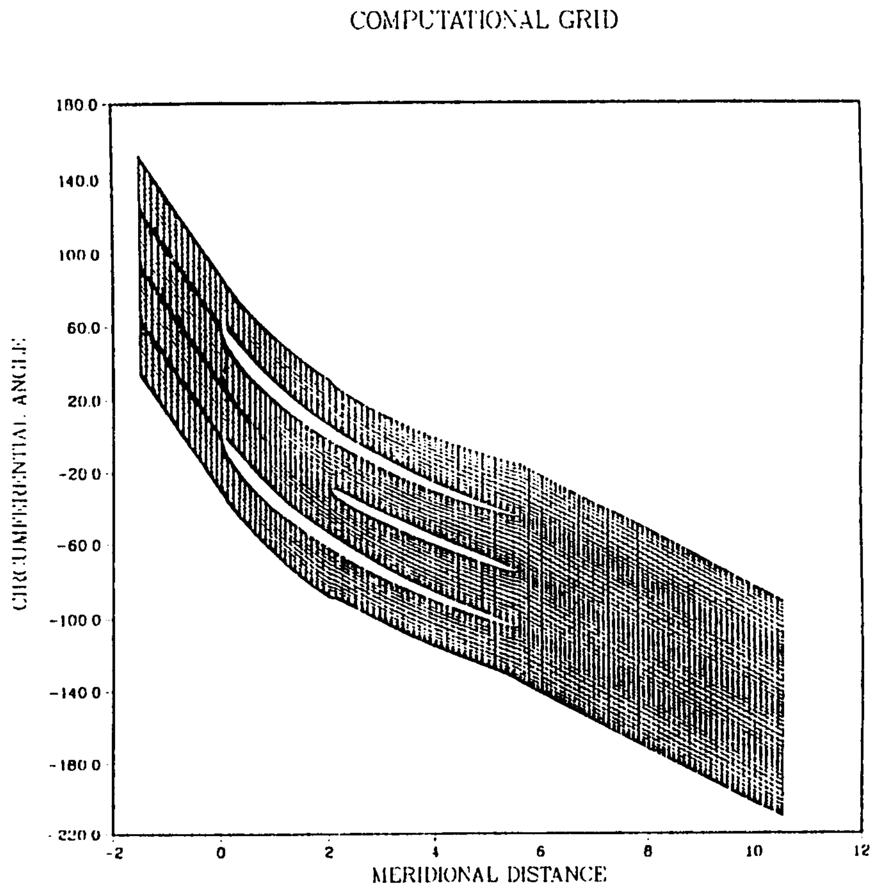

347

Rockwell International
Rocketdyne Division

CFD DESIGN OF ROCKET ENGINE PUMP COMPONENT

BOUNDARY AND INITIAL CONDITIONS

- BOUNDARY CONDITIONS AT INLET
  - MERIDIONAL AND TANGENTIAL VELOCITY PRESCRIBED FROM MEASUREMENT OR PREDICTION
- BOUNDARY CONDITION AT OUTLET
  - VELOCITY EXTRAPOLATED FROM INTERIOR POINTS
  - MASS AND ANGULAR MOMENTUM CONSERVED
- ALONG BLADE SURFACES AND END WALLS
  - NO-SLIP BOUNDARY CONDITION IMPOSED
  - SLIP END WALL EFFECTS STUDIED
- PERIODICITY APPLIED AT INLET AND OUTLET IN BLADE-TO-BLADE DIRECTION
- INITIAL CONDITIONS
  - UNIFORM VELOCITY ASSUMED AT EACH STREAMWISE STATION
  - VELOCITY BASED ON 1-D PREDICTION
  - FLOW DIRECTION IS ALIGNED WITH LOCAL GRID ORIENTATION

CFD DESIGN OF ROCKET ENGINE PUMP COMPONENT

ACCURACY OF CFD RESULTS

- FLOW SOLVER REACT3D
  - ROCKETDYNE ELLIPTIC ANALYSIS CODE FOR TURBOMACHINERY USED
  - VALIDATED FOR INDUCER AND TURBINE PERFORMANCE

- COMPARE TO ONE-DIMENTIONAL PROGRAM FOR IMPELLER PERFORMANCE
  - IMPELLER HYDRO EFFICIENCY AGREE WITH 1-D PROGRAM (94.5%)
  - EULER HEAD 8% HIGHER THAN THAT OF 1-D PREDICTION

- EULER HEAD DISCREPENCY ATTRIBUTED TO DIFFERENCES IN DEVIATION ANGLE AND BLOCKAGE
  - 1-D MODEL EXTRAPOLATED TO HIGH HEAD COEFFICIENT
  - UNCERTAINTY IN SOLIDITY CALCULATION WITH PARTIAL BLADE
  - SIMPLIFIED BLADE TRAILING EDGE MODELING IN REACT3D

- WATER TEST PLANNED TO RESOLVE THESE ISSUES

Rockwell International
Rocketdyne Division

CFD DESIGN OF ROCKET ENGINE PUMP COMPONENT

DISCUSSION OF GRID DEPENDENCY

- 2 GRID SIZE USED FOR IMPELLER ANALYSIS
  - 10K (59X14X11, STREAMWISE X BLADE-TO-BLADE X HUB-TO-TIP)
  - 80K (119X30X23, STREAMWISE X BLADE-TO-BLADE X HUB-TO-TIP)
- GRID GENERATED ON APOLLO WORKSTATION
  - 2 CPU MINUTES FOR 10K CASE
  - 10 CPU MINUTES FOR 80K CASE
- CFD ANALYSIS ALSO CARRIED OUT ON APOLLO WORKSTATION
  - 4 CPU HOURS FOR 10K CASE
  - 15 CPU HOURS FOR 80K CASE
- COMPARISON OF CFD RESULTS BETWEEN 10K AND 80K
  - CONSISTENT RESULTS FOR BOTH BASELINE AND OPTIMUM DESIGN
  - EFFICIENCY AND PUMP HEAD WITHIN 2%
  - TRENDS IN EVALUATION CRITERIA SIMILAR
  - USE 10K FOR IMPELLER DESIGN OPTIMIZATION
  - USE 80K FOR FINAL OPTIMUM DESIGN FLOW ANALYSIS

Rockwell International
Rocketdyne Division

COMPARISON OF CFD SOLUTIONS

CASE	HEAD (FT)	EFFICIENCY	FLOW SPLIT*	IMPELLER DISCHARGE		CROSSOVER INLET	
				EC 1	EC 2	EC 1	EC 2
10K BASELINE	1256.6	94.2%	+/- 6%	3.26 DEG	0.142	4.35 DEG	0.0809
80K BASELINE	1256.5	94.1%	+/- 6.6%	5.48 DEG	0.148	7.67 DEG	0.0657
10K OPTIMUM	1255.6	94.2%	+/- 2.5%	2.08 DEG	0.121	2.996 DEG	0.0603
80K OPTIMUM	1272.9	94.8%	+/- 5%	2.36 DEG	0.142	5.516 DEG	0.0536

* HIGH ON FULL BLADE PRESSURE SURFACE TO PARTIAL BLADE SUCTION SURFACE

CFD DESIGN OF ROCKET ENGINE PUMP COMPONENT

DISCUSSION OF END WALL EFFECTS

- 3 CASES USED FOR PARAMETRIC STUDY
  - CASE 1: ROTATING WALL WITH NO SLIP AT IMPELLER UPSTREAM AND DOWNSTREAM
  - CASE 2: SAME AS CASE 1 EXCEPT SLIP CONDITIONS AT DOWNSTREAM
  - CASE 3: SAME AS CASE 1 EXCEPT STATIONARY SHROUD AT UPSTREAM
- SMALL CHANGE FOR ALL PARAMETERS EVALUATED
  - DIFFERENCE OF HEAD AND EFFICIENCY WITHIN 1%
  - SMALL CHANGE OF IMPELLER DISCHARGE CM AND CU DISTRIBUTION
- FOURTH CASE WITH STATIONARY DOWNSTREAM WALL DID NOT FULLY CONVERGE
  - UNCONVERGED RESULTS (RESIDUALS 10^{-2}) SHOWED EXTENSIVE RECIRCULATION AT DISCHARGE HUB AND SHROUD

Rockwell International
Rocketdyne Division

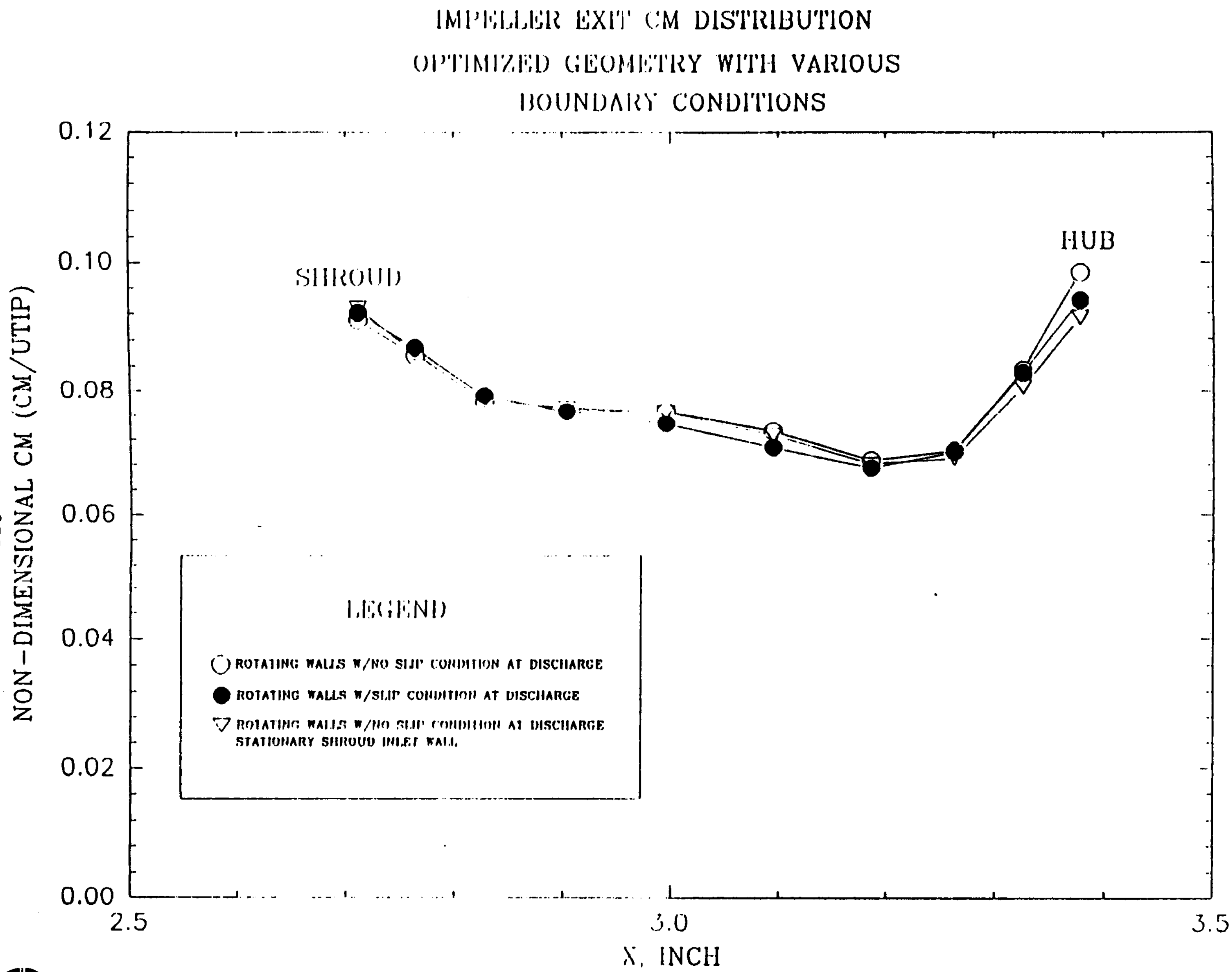

Rockwell International
Rocketdyne Division

IMPELLER EXIT CU DISTRIBUTION
OPTIMIZED GEOMETRY WITH VARIOUS
BOUNDARY CONDITIONS

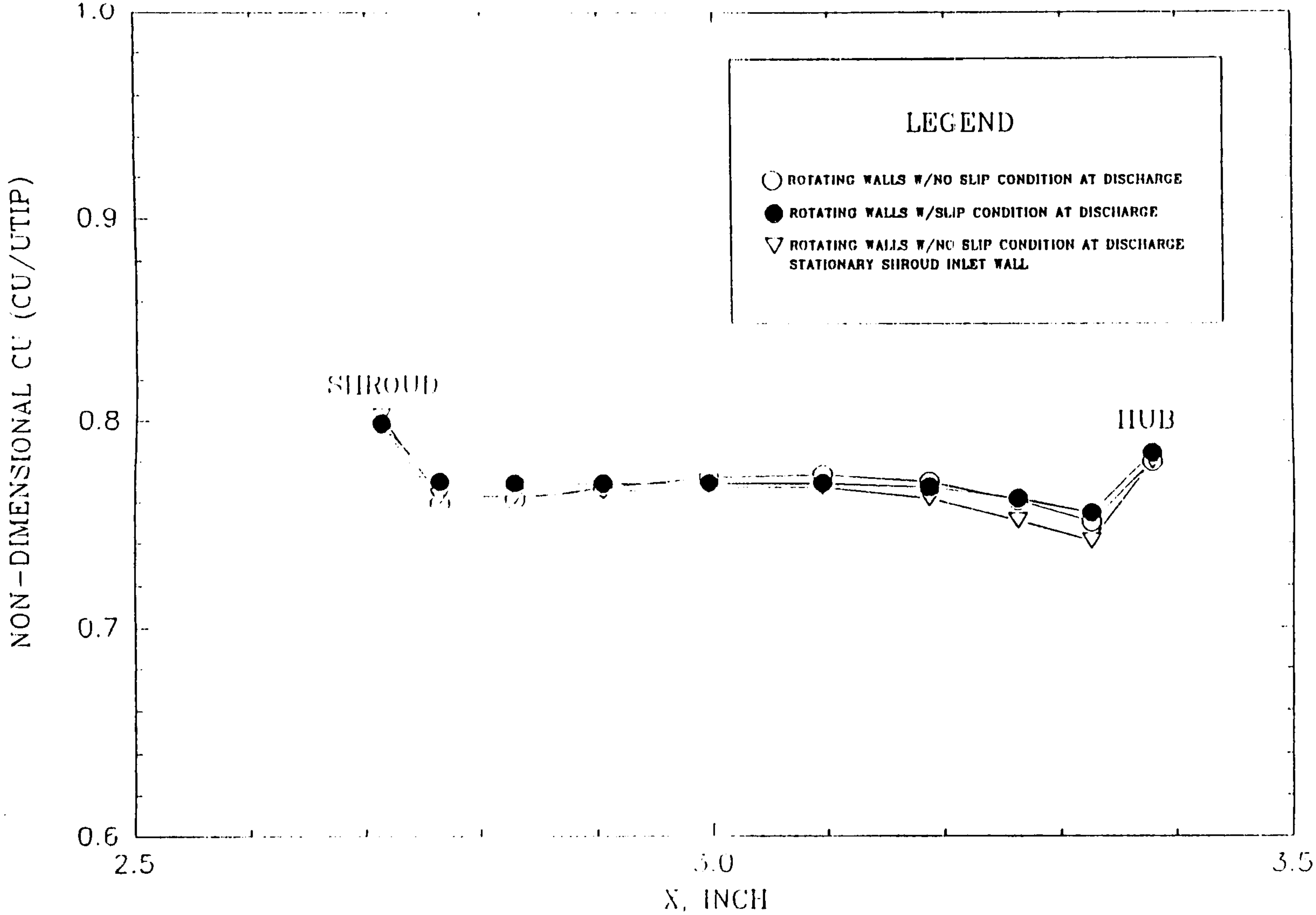

Rockwell International
Rocketdyne Division

CFD DESIGN OF ROCKET ENGINE PUMP COMPONENT

DESIGN PARAMETRIC CHANGES

- IMPELLER DISCHARGE HUB-TO-TIP WIDTH
  - RANGE FROM 0.88 TO 1.20 INCHES
- IMPELLER DISCHARGE BLADE ANGLE FROM TANGENTIAL
  - RANGE FROM 38 TO 54 DEGREES
- IMPELLER AXIAL LENGTH FROM 2.38 TO 3.0 INCHES
- BLADE TOTAL WRAP ANGLES
  - 65 TO 90 DEGREES FOR TIP
  - 65 TO 115 DEGREES FOR HUB
- WRAP DIFFERENCE BETWEEN HUB AND TIP
  - RANGE FROM 0 TO 5.0 DEGREES
- ALL CHANGES ACHIEVE REQUIRED HEAD WITH CONSTANT RPM AND DIAMETER

Rockwell International
Rocketdyne Division

CONSORTIUM IMPELLER CONFIGURATION STUDIED

KEY PARAMETER CASES	DISCHARGE B2 WIDTH	DISCHARGE BLADE ANGLE	AXIAL LENGTH	TOTAL WRAP TIP(HUB)	DISCHARGE WRAP DIFFERENCE	CFD GRID POINT
BASELINE	1.00	47.2	2.50	65 (85)	5	10000
BASELINE	1.00	47.2	2.50	65 (85)	5	**80000**
CASE 1	1.00	47.2	2.50	65 (85)	**0**	10000
CASE 2	**0.88**	54.0	2.38	55 (78)	3	10000
CASE 3	**1.12**	39.0	2.62	77 (100)	2.7	10000
CASE 4	**1.20**	34.4	2.70	90 (115)	5.0	10000
CASE 5	1.00	47.2	**3.00**	72 (92)	5.0	10000
OPTIMUM	**1.12**	38.0	**2.82**	83 (105)	**2.6**	10000
OPTIMUM	**1.12**	38.0	**2.82**	83 (105)	**2.6**	**80000**

Rockwell International
Rocketdyne Division

REACT USED TO OPTIMIZE HIGH PERFORMANCE IMPELLER

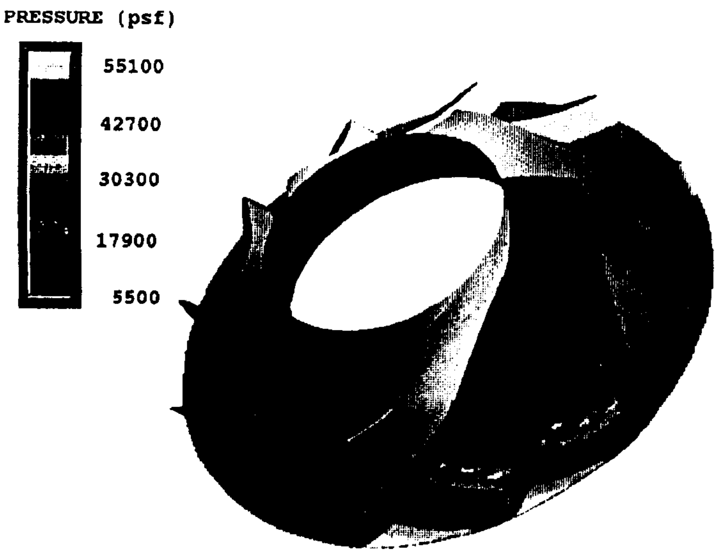

BASELINE GEOMETRY 80K GRID
IMPELLER DISCHARGE RADIAL VELOCITY (FPS)

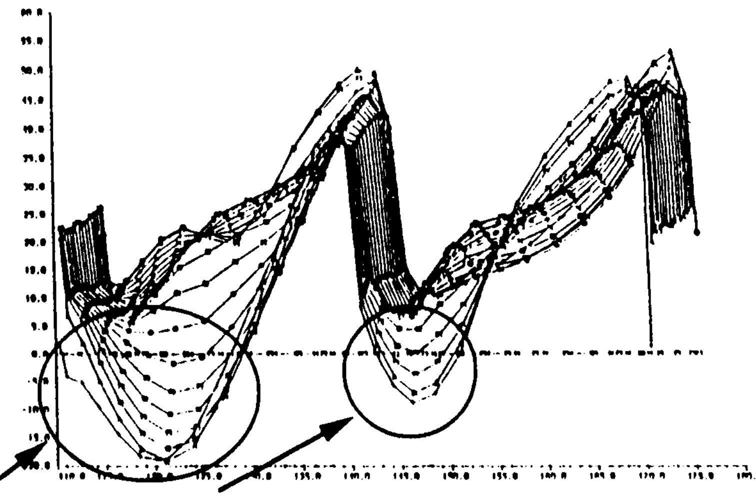

OPTIMUM GEOMETRY 80K GRID
IMPELLER DISCHARGE RADIAL VELOCITY (FPS)

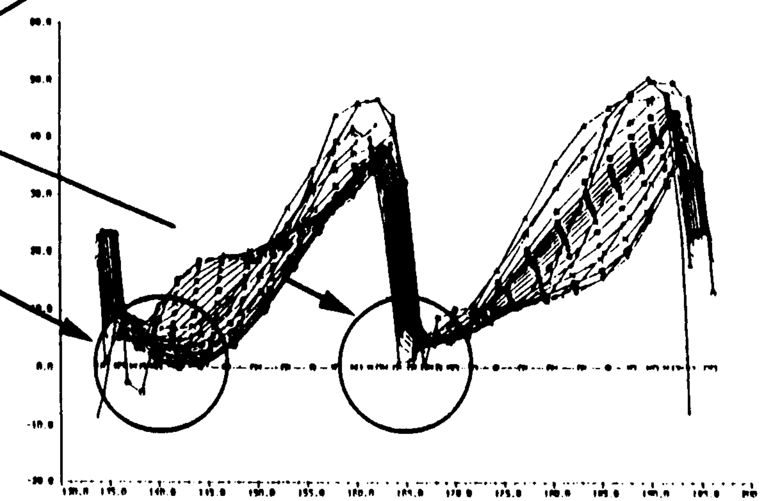

FLOW RECIRCULATION
ELIMINATED AT IMPELLER
DISCHARGE

Rockwell International
Rocketdyne Division

CFD DESIGN OF ROCKET ENGINE PUMP COMPONENT

CONCLUSIONS

- A FAST GRID GENERATOR HAS BEEN DEVELOPED
  - USED FOR DESIGN OPTIMIZATION OF CONSORTIUM IMPELLER
  - USED FOR SSME HPFTP IMPELLER FOR CFD CODE VALIDATION
  - SUCCESFULLY APPLIED FOR INDUCER
- CFD INCORPORATED INTO PUMP DESIGN PROCESS
  - IMPELLER PERFORMANCE EVALUATION CRITERIA DEVELOPED
  - OPTIMUM DESIGN ACHIEVED THROUGH CFD ANALYSIS
  - TURNAROUND TIME ACCEPTABLE FOR DESIGN PROCESS

Rockwell International
Rocketdyne Division

CFD DESIGN OF ROCKET ENGINE PUMP COMPONENT

CONCLUSIONS (continued)

- CFD GRID DEPENDENCY
  - SMALL GRID SIZE ACCEPTABLE FOR PARAMETRIC STUDIES
  - FINE GRID REQUIRED (300K) TO FINALIZE GRID DEPENDENCY STUDY
- END WALL BOUNDARY EFFECTS
  - CHANGE OF IMPELLER HEAD AND EFFICIENCY WITHIN 1%
  - SMALL CHANGE OF IMPELLER DISCHARGE CM AND CU DISTRIBUTION
- TEST DATA REQUIRED
  - CONFIRM HIGH HEAD COEFFICIENT IMPELLER PERFORMANCE
  - VALIDATE CFD RESULTS FOR CENTRIFUGAL PUMP APPLICATION

Rockwell International
Rocketdyne Division

N92-32294

SSME HPOTP IMPELLER BACKCAVITY CFD ANALYSIS

W.W. HSU and S.J. LIN

Rockwell International Corp., Rocketdyne Division
6633 Canoga Avenue, MS IA34
Canoga Park, California 91303

The ball bearings behind the SSME HPOTP preburner pump have a history of premature wear requiring their replacement. Extensive tests have been conducted in an attempt to identify the operating factors that contribute to the wear. It has been conjectured that the coolant inflow velocity swirl pattern can aid bearing operation by matching ball orbit speed and thus affect bearing life. However, control of the velocity distribution up to now could only be achieved by trial and error following hardware testing. Observation of hardware from recent flight and development operation led to the hypothesis that certain assemblies with more extensive grinding patterns on the backwall of the impeller for rotor balancing correlated with improved bearing wear.

To analytically evaluate the effect of cavity configuration on the flowfield, 3-D CFD analyses of various geometries was successfully executed using REACT3D. Height of the anti-vortex ribs on the stationary wall was varied, as was the configuration of the rotating wall, from smooth to simulations of various grindout patterns. The results obtained indicate the effects of the various geometries and provide valuable guidelines for cavity modification to optimize bearing cooling.

PRECEDING PAGE BLANK NOT FILMED

SSME HPOTP PREBURNER IMPELLER BACKCAVITY CFD ANALYSIS

W.W. HSU, S.J. LIN
ROCKWELL INERNATIONAL, ROCKETDYNE DIVISION
APRIL 1992

Rockwell International
Rocketdyne Division

BACKGROUND

SSME HPOTP BALL BEARINGS #1 AND #2 BEHIND PREBURNER IMPELLER HAVE HISTORY OR WEAR AND PREMATURE REPLACEMENT

EXTENSIVE ENGINE AND SUBCOMPONENT TESTS HAVE IDENTIFIED VARIOUS OPERATING FACTORS THAT AFFECT WEAR

LUBRICATION	CAGE COATINGS SUCH AS FEP, BRAYCOTE
AXIAL PRE-LOAD	CORRECT SPRING STIFFNESS TO MAINTAIN PRE-LOAD
MATERIALS	SILICON NITRIDE BALLS, PLATINGS
COOLANT FLOW	MAINTAIN ADEQUATE VAPOR MARGIN

RECENT TESTS CORRELATED MORE EXTENSIVE ROTOR BALANCING GRINDOUTS ON IMPELLER REAR FACE WITH REDUCED BEARING WEAR

Rockwell International
Rocketdyne Division

PHASE II
HIGH PRESSURE OXYGEN TURBOPUMP

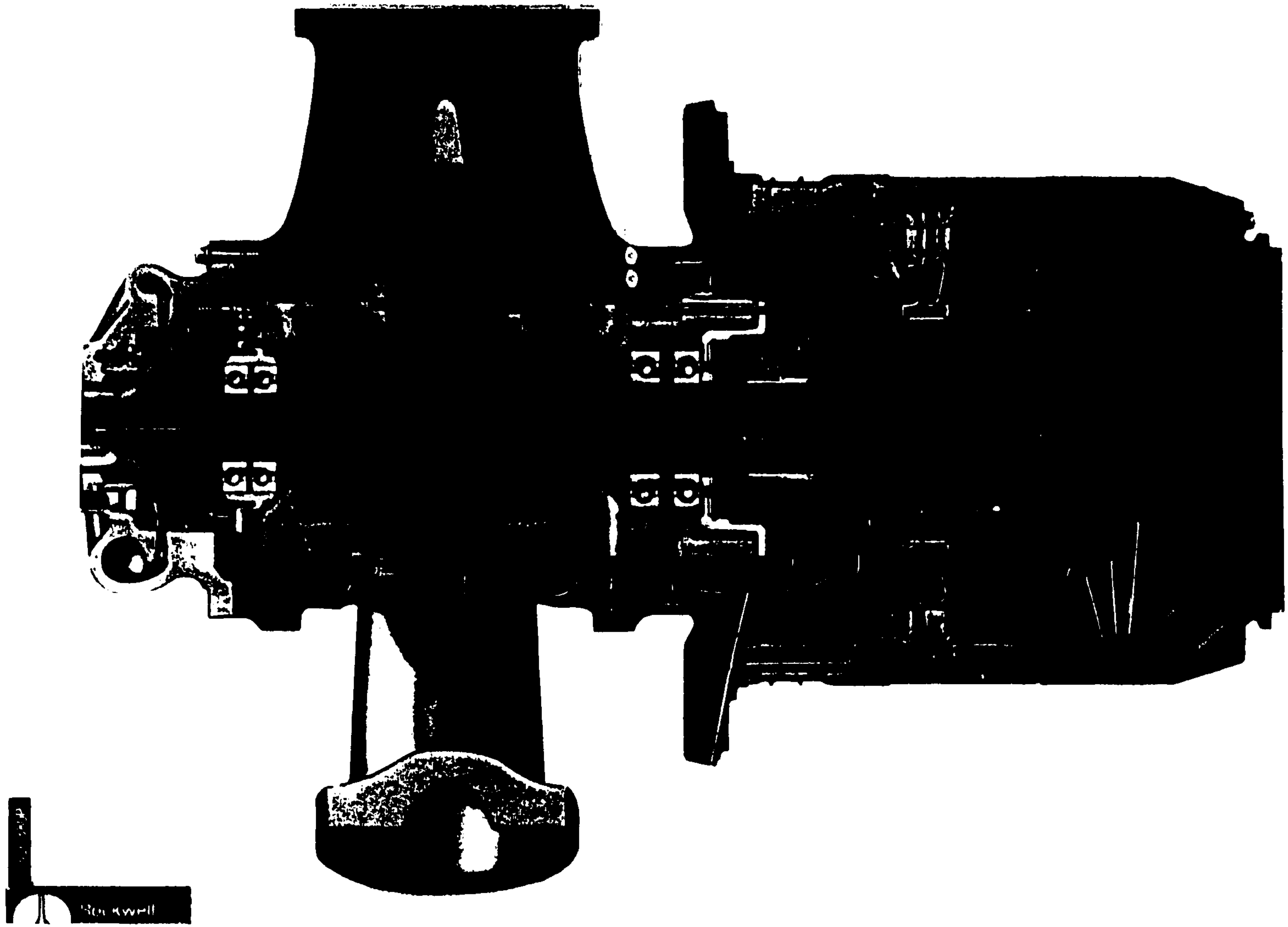

INCENTIVE FOR CFD ANALYSIS

COOLANT INFLOW SWIRL DISTRIBUTION CONJECTURED TO AFFECT BEARING WEAR

MATCHING BALL ORBIT SPEED REDUCES INFLOW RESISTANCE AND DRAG TORQUE ON BALLS AND CAGE

SUGGESTS DESIGN CHANGES TO UPSTREAM CAVITY COULD REDUCE BEARING WEAR

OPTIMIZE MAGNITUDE AND RADIAL DISTRIBUTION OF INLET SWIRL VELOCITY

ADJUST HEIGHT OF ANTI-VORTEX RIBS AND/OR SIZE OF IMPELLER GRINDOUTS TO ACHIEVE DESIRED DISTRIBUTION

CFD ANALYSIS OBJECTIVES

DEFINE VARIATION OF INLET SWIRL VELOCITY WITH GEOMETRY

EFFECT OF ANTI-VORTEX RIBS AND IMPELLER GRINDOUTS INDIVIDUALLY AND TOGETHER

UNDERSTAND FLOW WELL ENOUGH TO SUGGEST DESIGN CHANGES

NARROW CAVITY WITH HIGH WALL TANGENTIAL VELOCITY

RIBS ON STATIONARY WALL

HIGH VELOCITY JET AT INLET

CFD MODELING

REACT3D STEADY NAVIER-STOKES ANALYSIS, SINGLE ZONE

- GRINDOUTS ANALYZED IN ROTATING FRAME OF REFERENCE
- RIBS ANALYZED IN STATIONARY FRAME OF REFERENCE
- QUASI-STEADY APPROACH PROPOSED FOR GRINDOUT-RIB COMBINATIONS

FLOWFIELD SIMPLIFICATIONS

- SMALL LEAKAGE PATH PARALLEL TO BEARINGS IGNORED
- EFFECTS OF ROTATING CAGE AND ROLLING BALLS NOT SIMULATED

GRID EXTENDED DOWNSTREAM BEYOND BEARING INLET

- AIDS CONVERGENCE WITH POTENTIAL BACKFLOW

Rockwell International
Rocketdyne Division

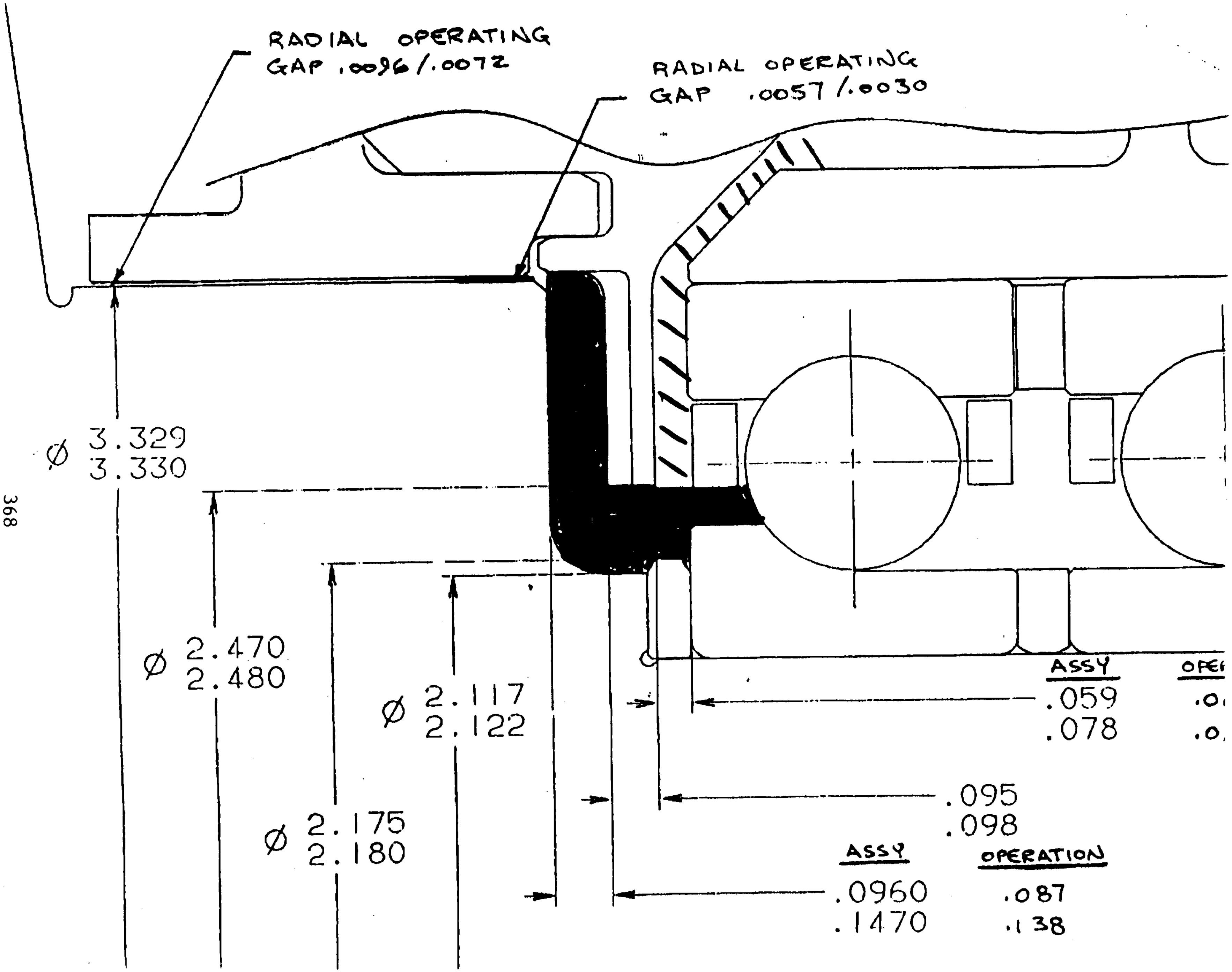
RADIAL OPERATING
GAP .0096/.0072
RADIAL OPERATING
GAP .0057/.0030
Ø 3.329
3.330
Ø 2.470
2.480
Ø 2.117
2.122
Ø 2.175
2.180
ASSY
.059
.078
.095
.098
ASSY
.0960
.1470
OPERATION
.087
.138

GEOMETRIES INVESTIGATED

FOUR BASIC GEOMETRIES TO BE INVESTIGATED (3 COMPLETE)

- RIBBED STATIONARY WALL / SMOOTH ROTATING WALL
- SMOOTH STATIONARY WALL / SMOOTH ROTATING WALL
- SMOOTH STATIONARY WALL / ROTATING WALL WITH GRINDOUTS
- RIBBED STATIONARY WALL / ROTATING WALL WITH GRINDOUTS

GRINDOUTS SIMULATED WITH SMOOTH INDENTATIONS ON ROTATING WALL

- RADIAL HEIGHT MATCHED TO AVERAGE OBSERVED
- TOTAL CIRCUMFERENTIAL EXTENT 180 DEG.

GEOMETRY VARIATIONS

- RIB HEIGHTS 100%, 50%, 25% OF CURRENT DESIGN
- GRINDOUTS WITH 4 LOBES 0.05" DEEP, 6 LOBES 0.1" DEEP

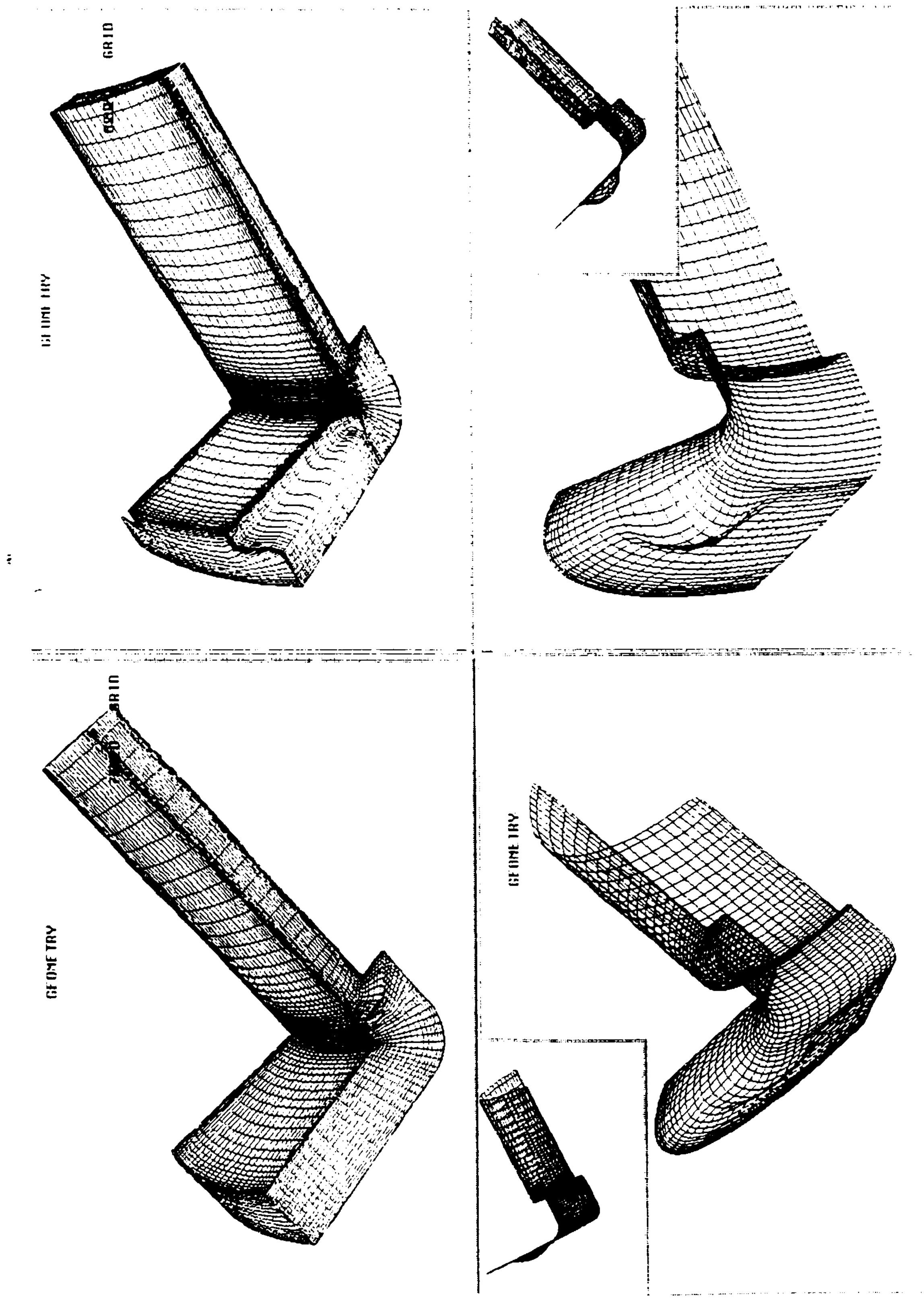
GEOMETRY
GRID
GEOMETRY
GRID
GEOMETRY

CFD ANALYSIS CONDITIONS

GRID SIZE	MERIDIONAL DIRECTION		I = 75 TO 85
	CIRCUMFERENTIAL DIRECTION		J =15 TO 30
	NORMAL DIRECTION		K = 15 TO 20
GEOMETRY	IMPELLER	ROTATION	29141 RPM
		HUB SEAL RADIUS	1.67 INCH
		SEAL GAP	0.005 INCH
		HUB INNER RADIUS	1.06 INCH
	CAVITY	AXIAL WIDTH	0.113 INCH
		RIB HEIGHT	0.05 INCH
FLUID	LOX, DENSITY 57.4 LB/CUB. FT.		
FLOW RATE	10.8 LB/SEC		
JET VELOCITY	AXIAL	245 FT/SEC (SEAL EXIT CHAMFERED)	
	TANGENTIAL	50% WHEEL SPEED (PHASE 1)	
		30% WHEEL SPEED (PHASE 2)	

C-5

Rockwell International
Rocketdyne Division

RESULTS

REACT3D RESULTS QUALITATIVELY AS EXPECTED

GRINDOUTS SIGNIFIICANTLY INCREASE INLET TANGENTIAL VELOCITY

RIBS SIGNIFICANTLY DECREASE INLET TANGENTIAL VELOCITY

STRONG VORTEX MOTIONS DRIVEN BY JET FROM DAMPING SEAL AND ROTATING WALLS

NO SIGNIFICANT IMPACT ON AXIAL VELOCITY

FLOW SEPARATIONS OFF INNER RACE MAY SIGNIFICANTLY REDUCE THROUGHFLOW

LESS SIGNIFICANT SEPARATION AT BOTTOM OF RIBS

RIB DEPTH CAN BE USED TO CONTROL INLET VELOCITY

JET INLET TANGENTIAL VELOCITY HAS LITTLE EFFECT ON BEARING INLET VELOCITY PROFILE

Smooth Rotating Wall with Rib

Tangential Velocity (ft/s)

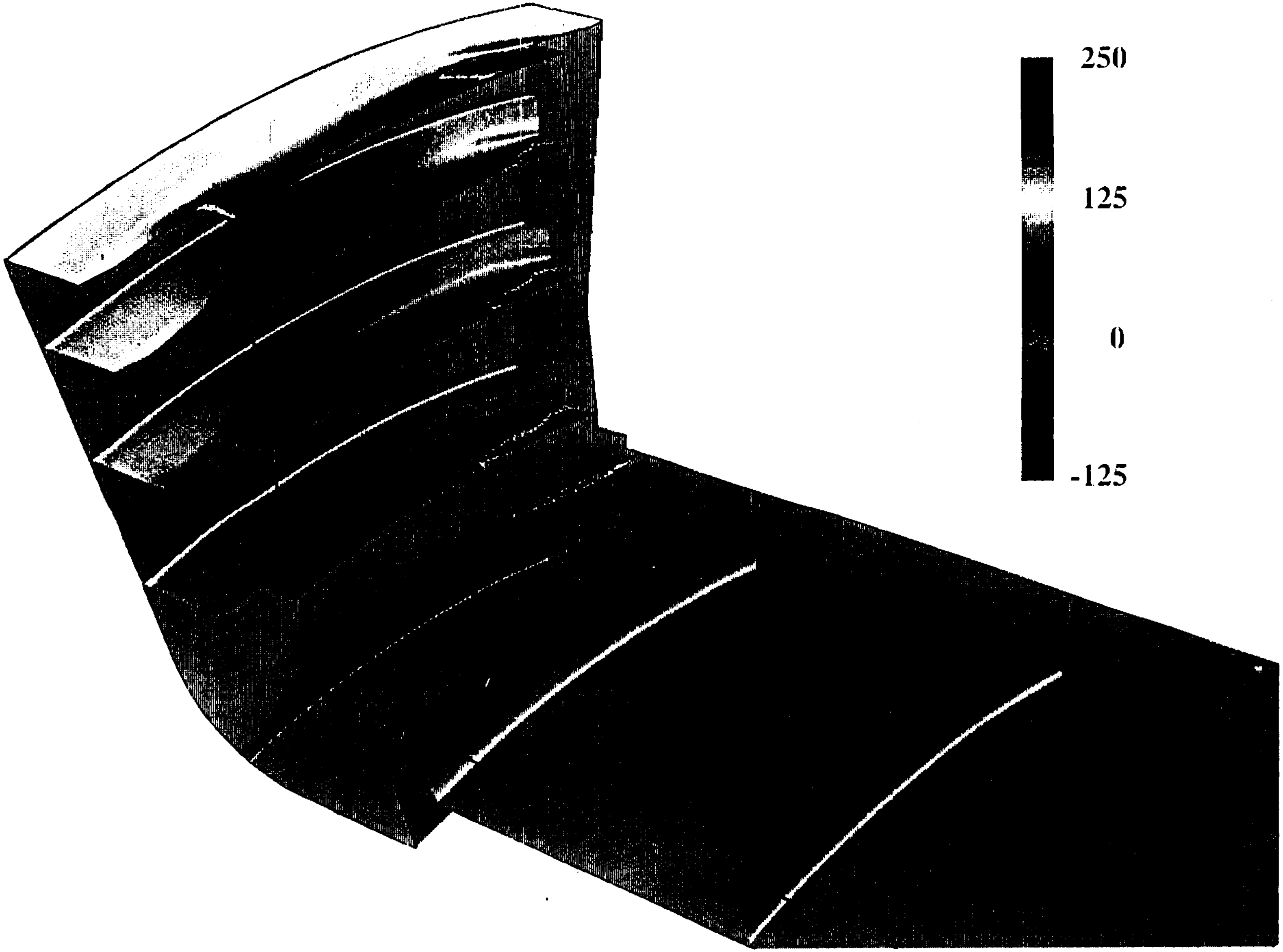

Smooth Rotating Wall without Rib

Tangential Velocity (ft/s)

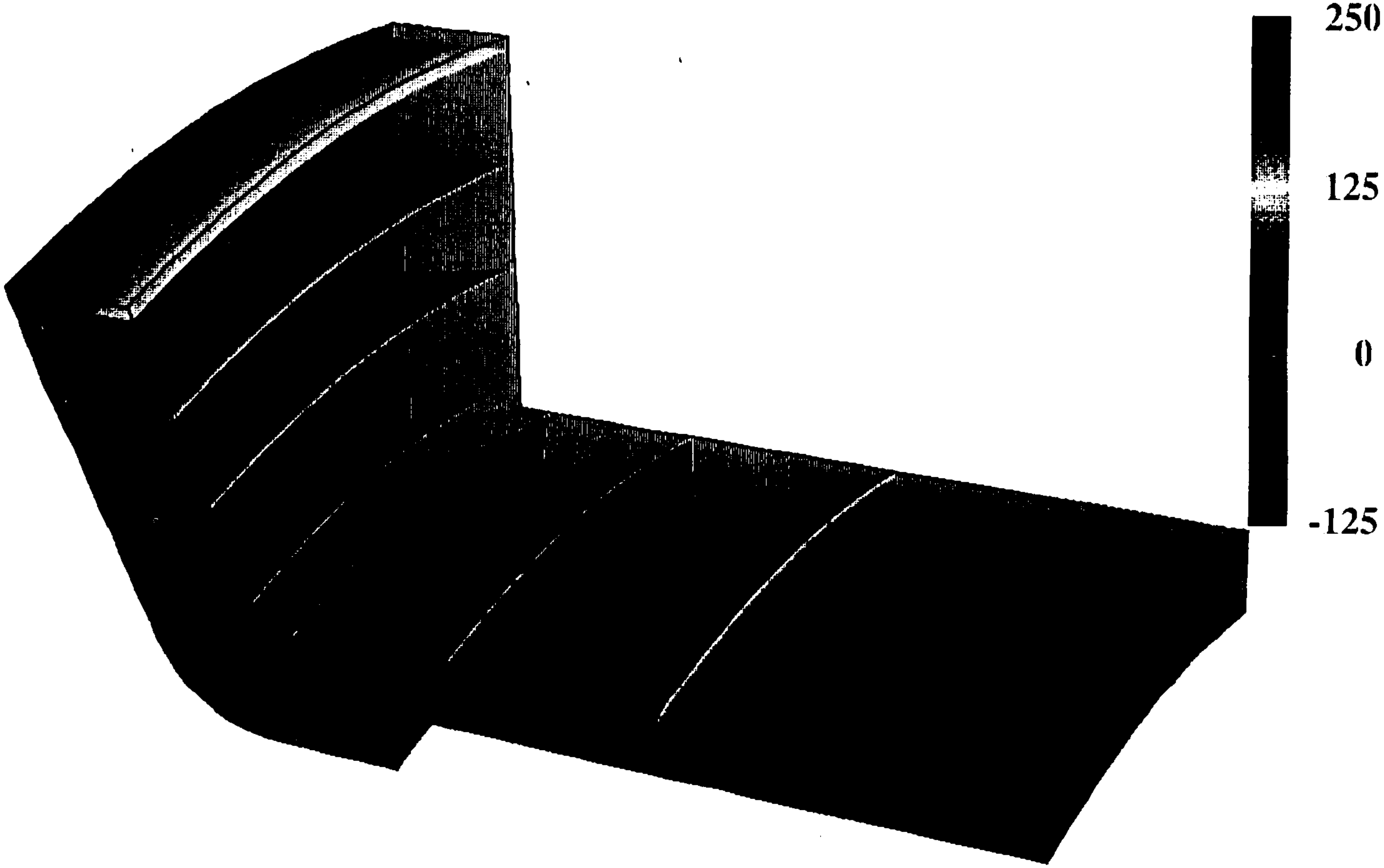

Ground Rotating Wall without Rib

Tangential Velocity (ft/s)

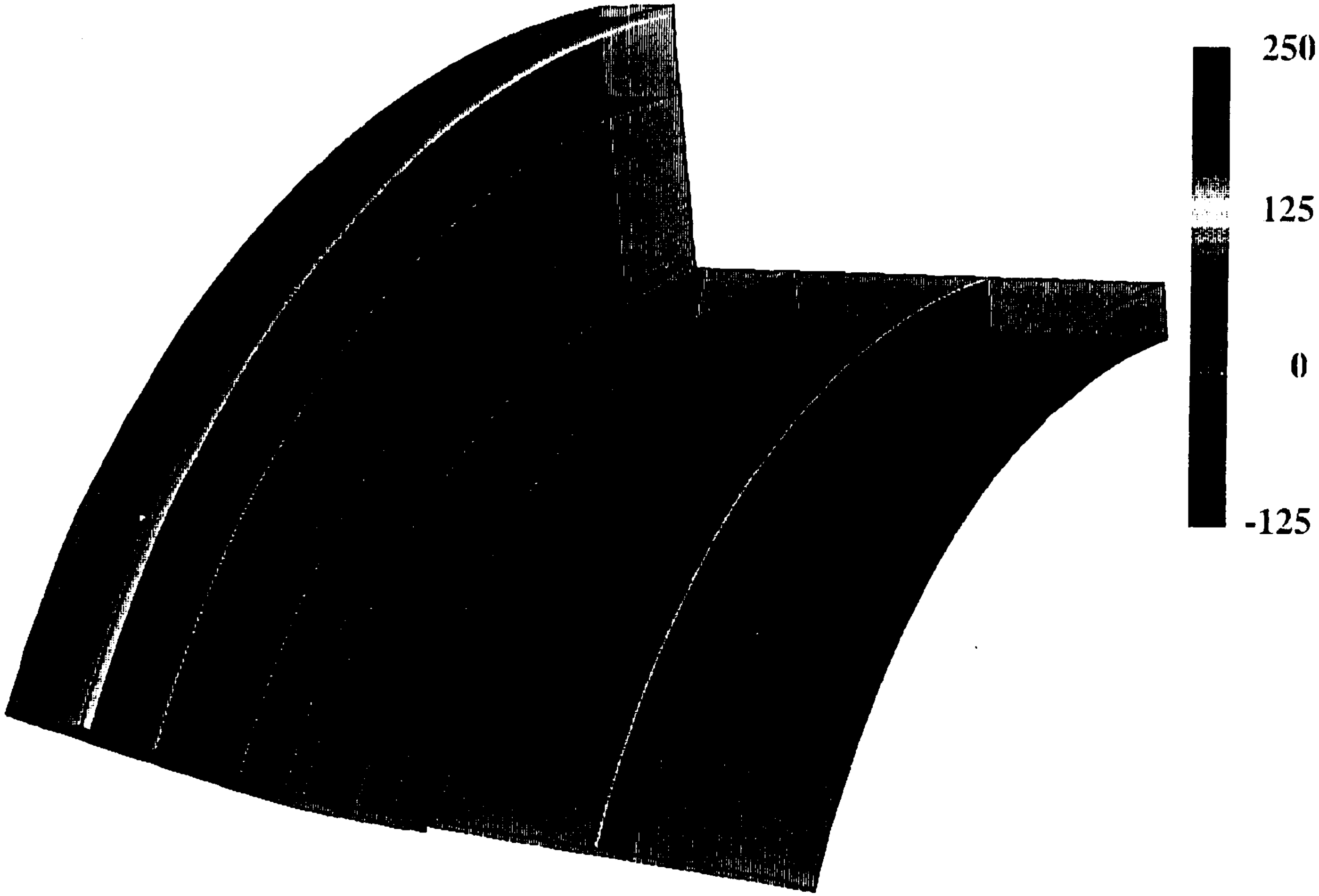

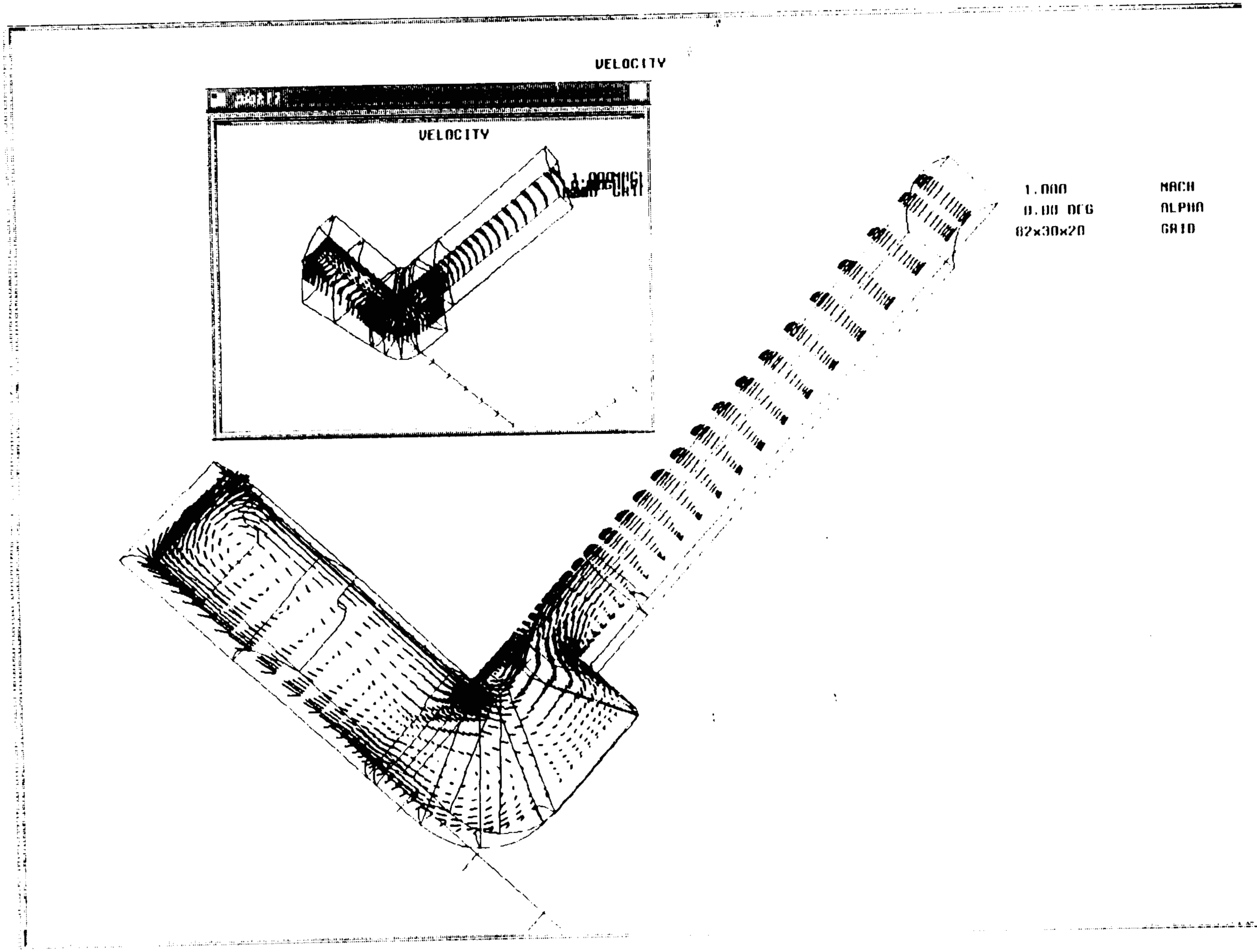
VELOCITY
VELOCITY
1.000 MACH
0.00 DEG ALPHA
82x30x20 GRID

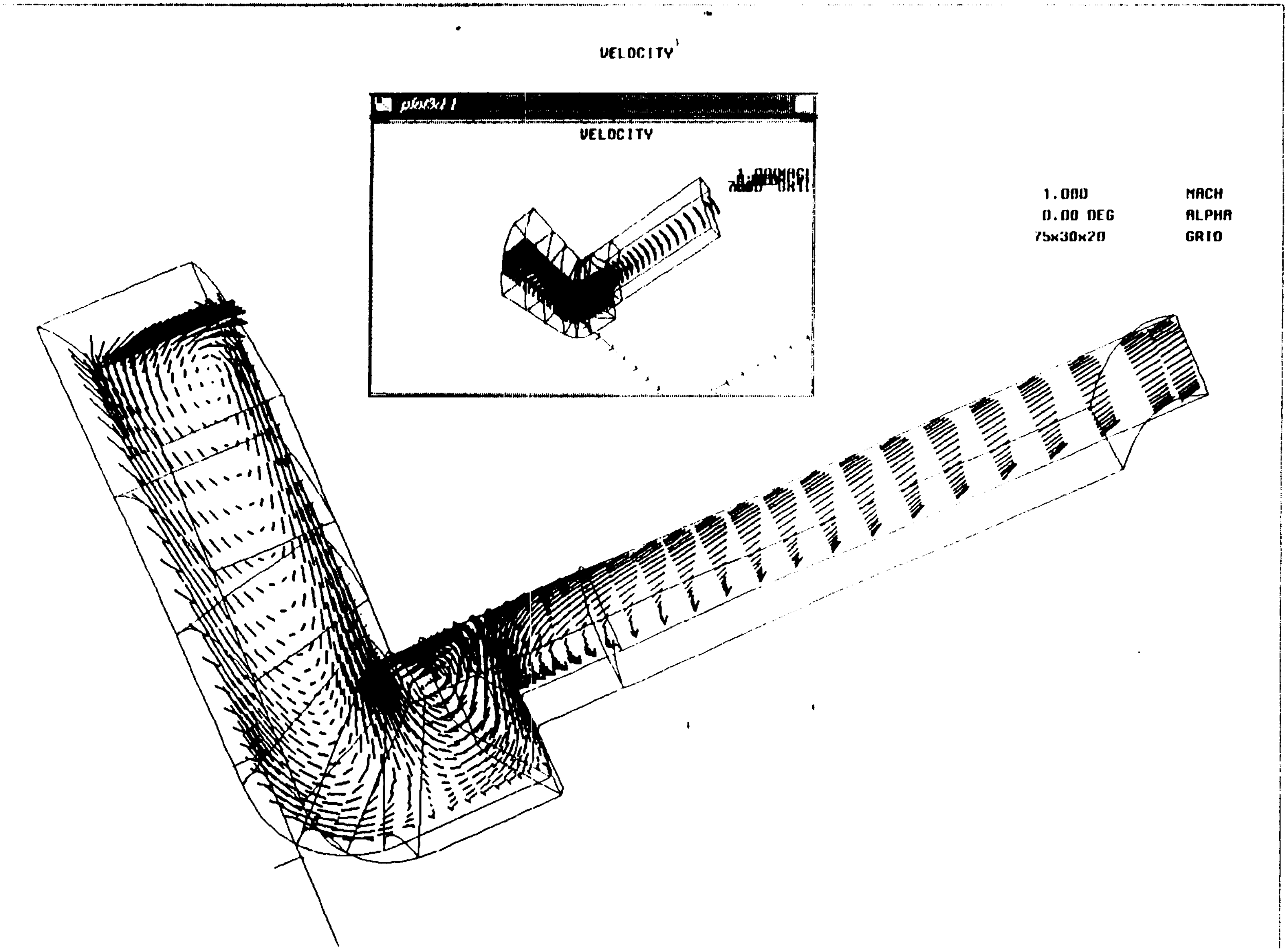
VELOCITY
VELOCITY
1.000 MACH
0.00 DEG ALPHA
75x30x20 GRID

Smooth Rotating Wall with Rib

Axial Velocity (ft/s)

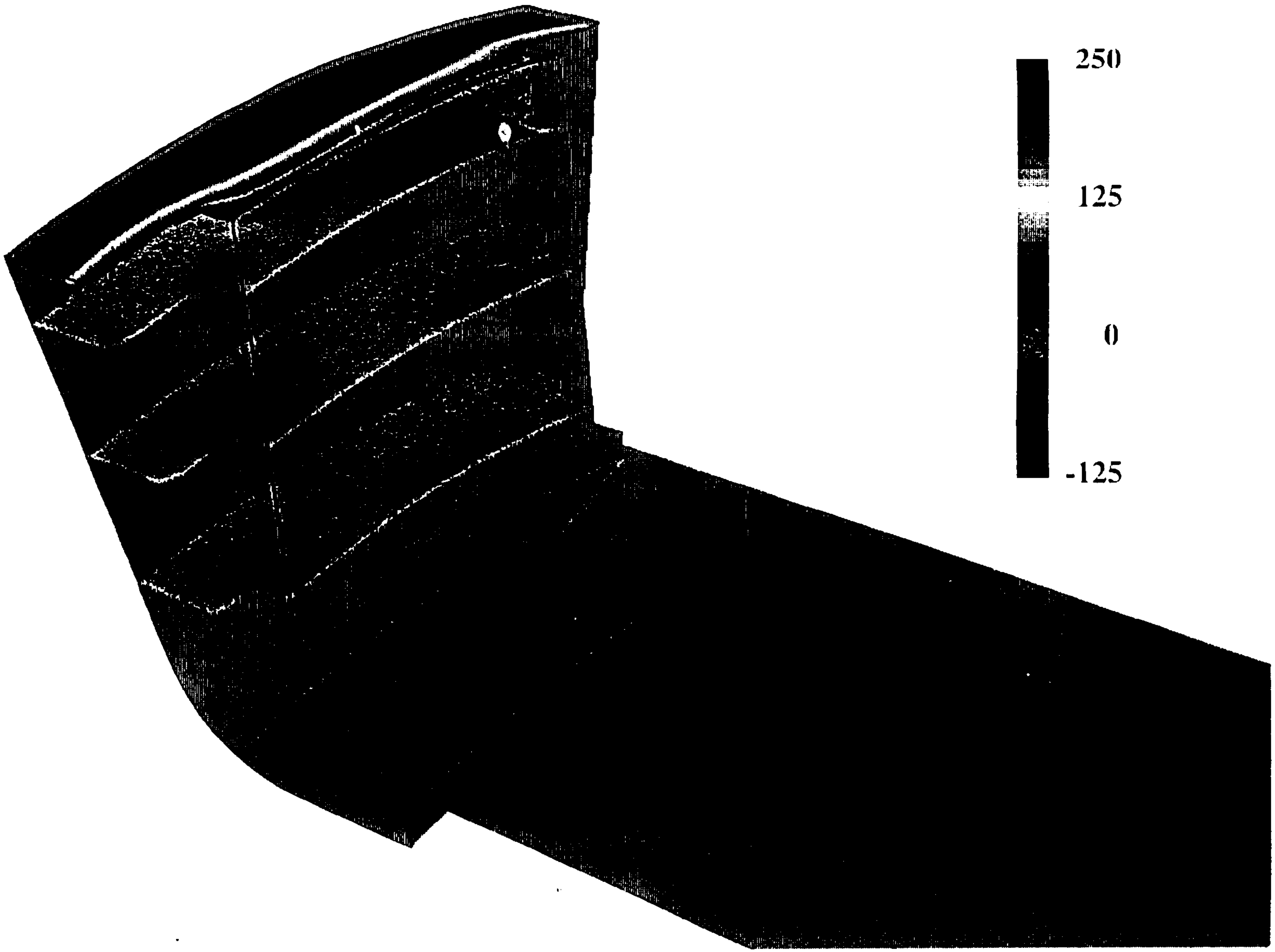

Smooth Rotating Wall without Rib

Axial Velocity (ft/s)

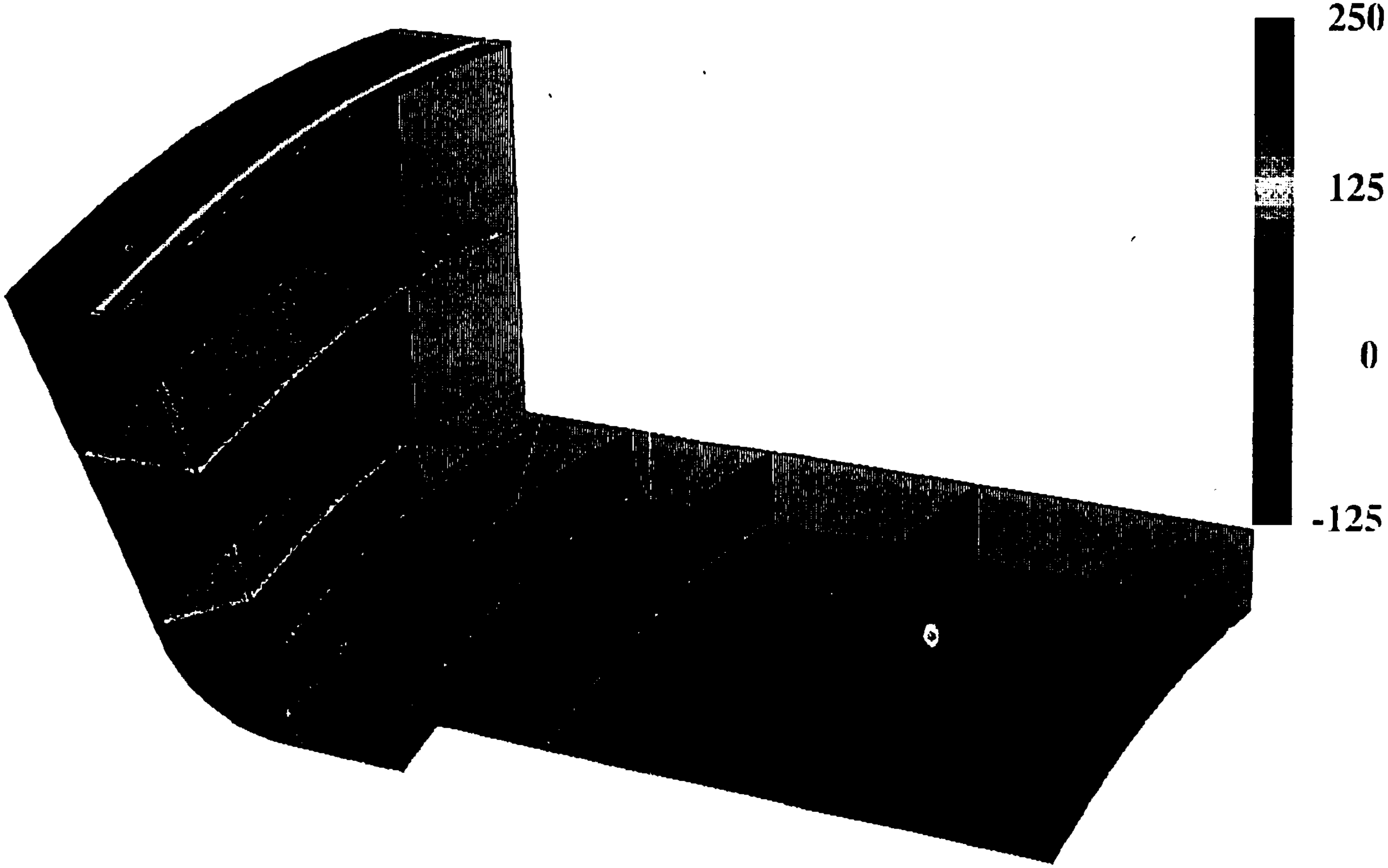

Ground Rotating Wall without Rib

Axial Velocity (ft/s)

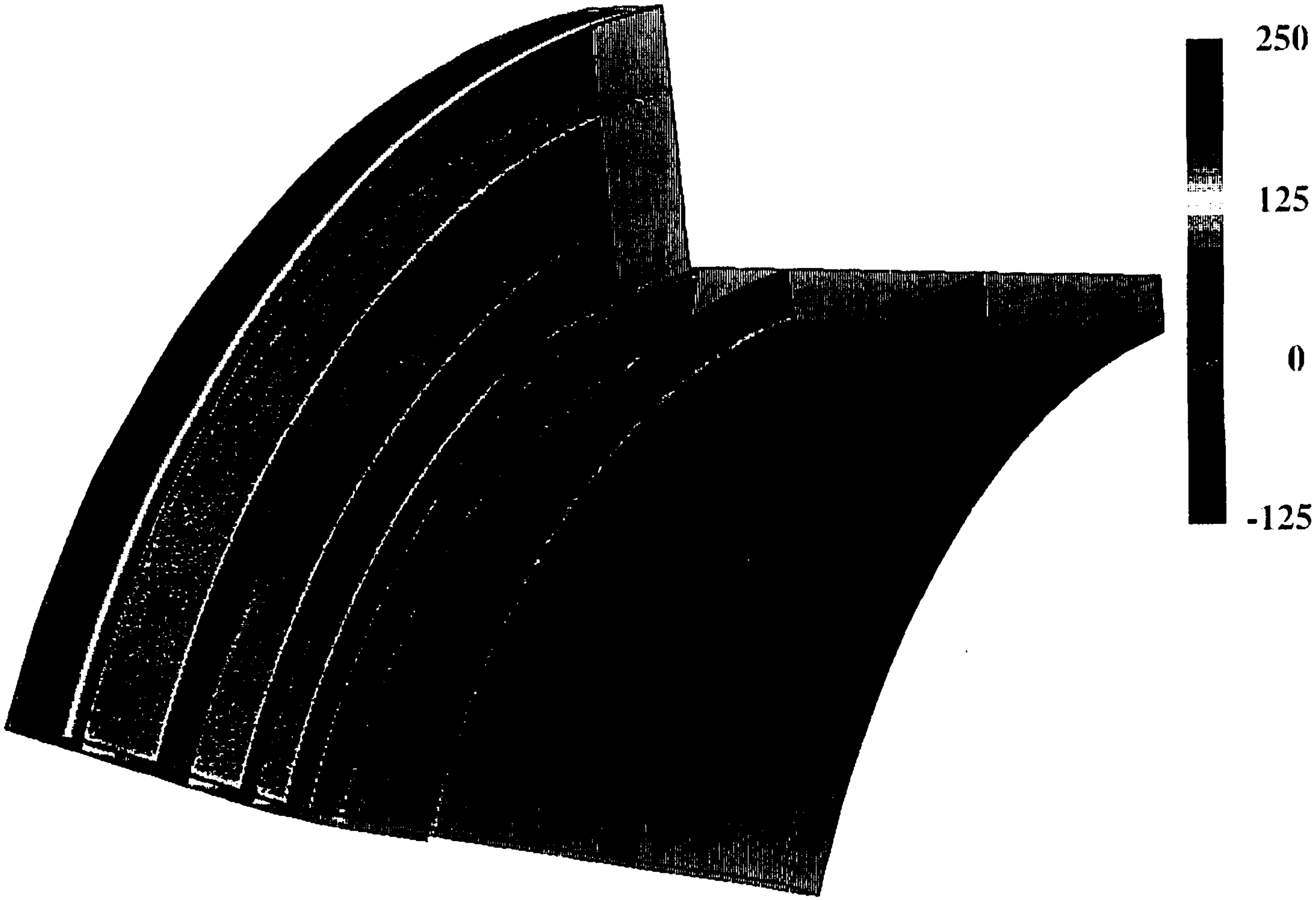

Smooth Rotating Wall with Rib

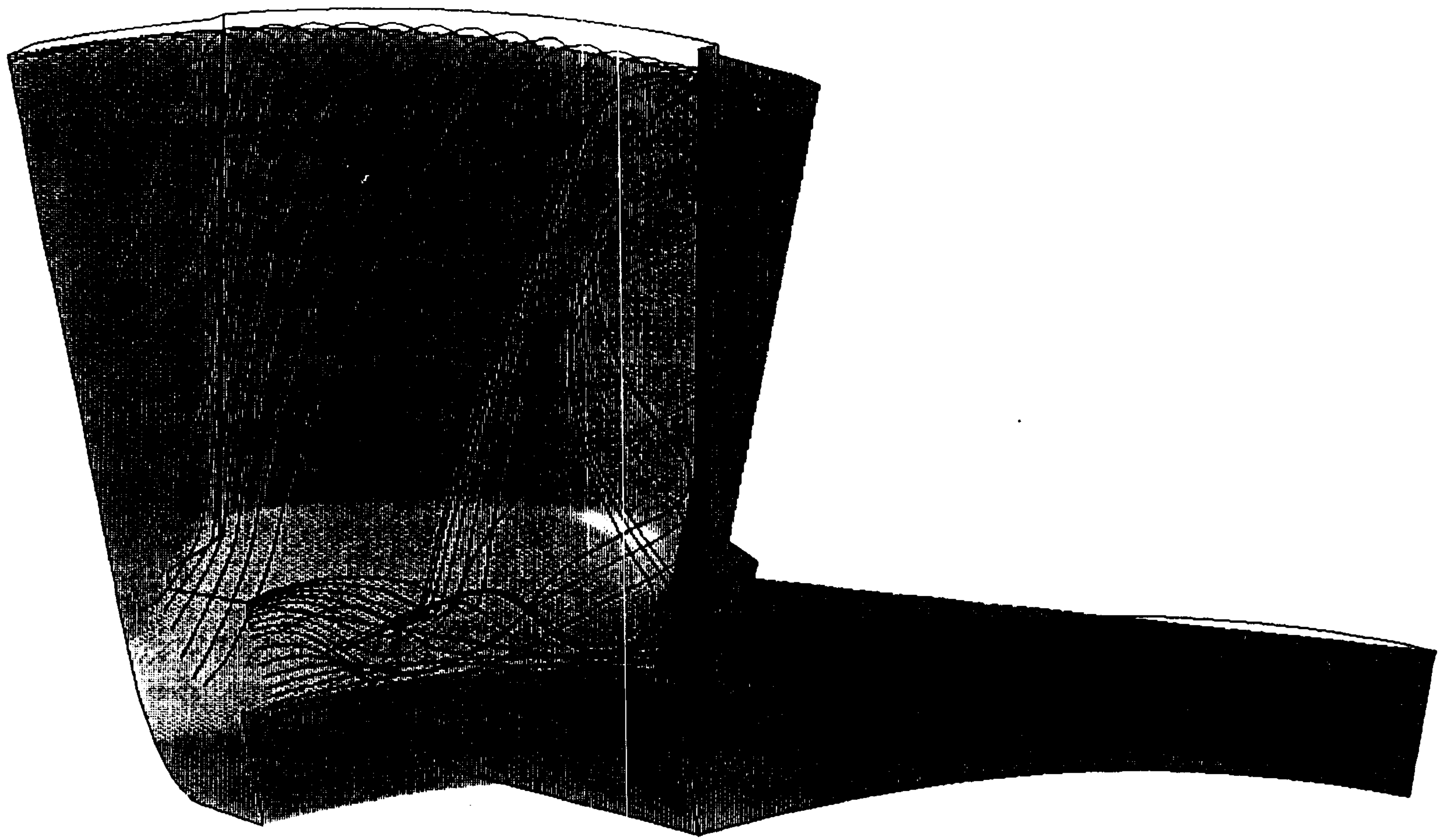

Smooth Rotating Wall with Rib

Smooth Rotating Wall without Rib

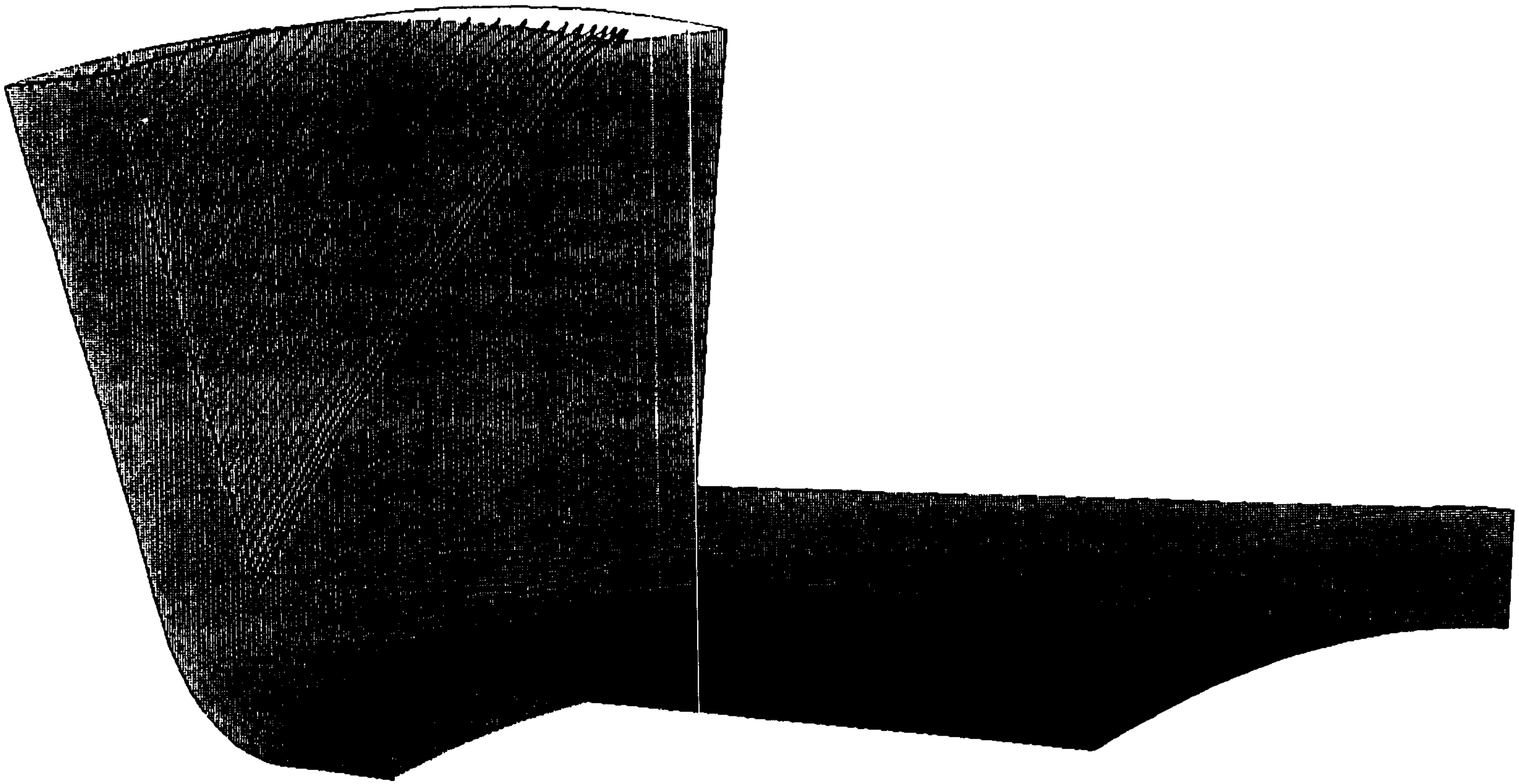

Smooth Rotating Wall without Rib

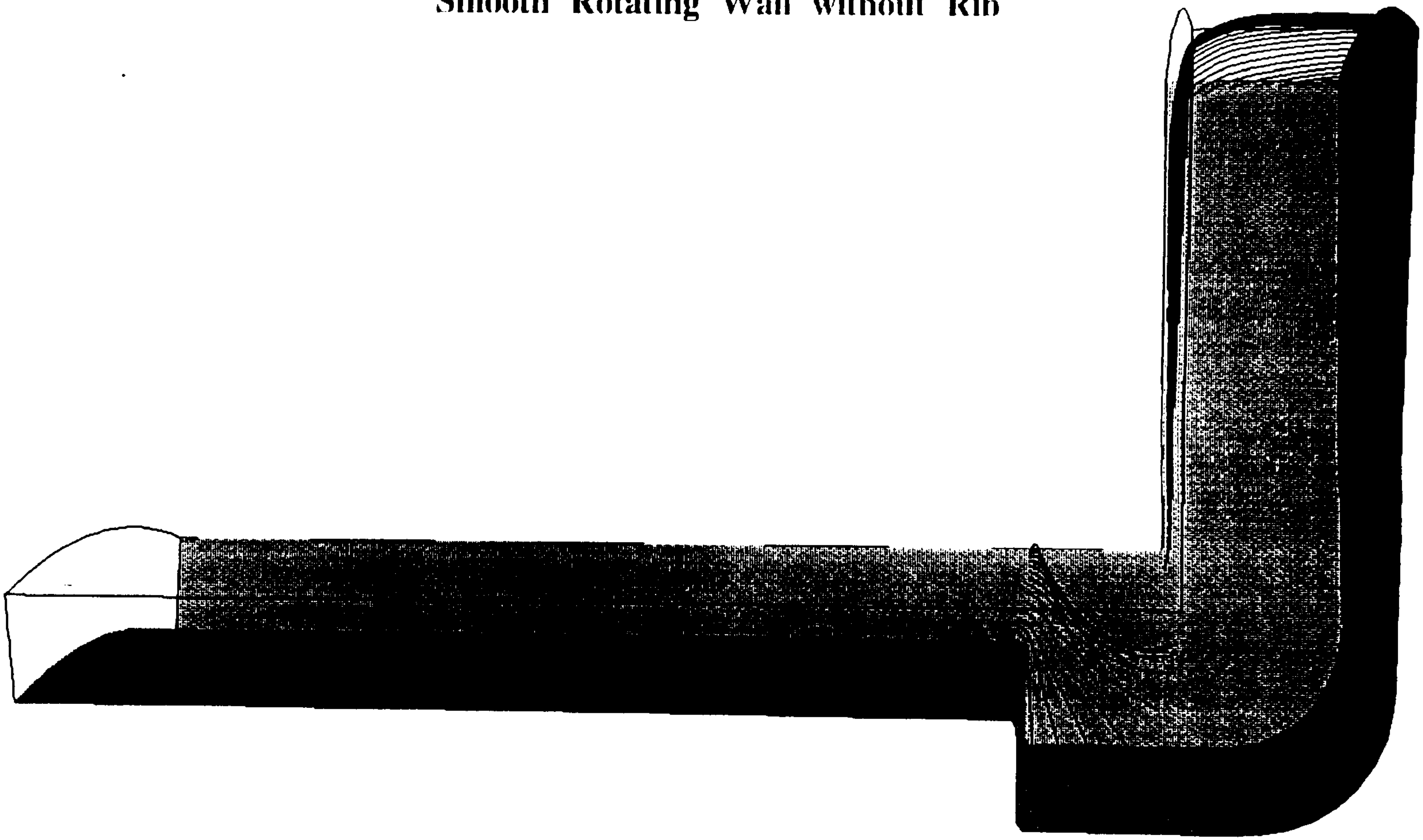

Ground Rotating Wall without Rib

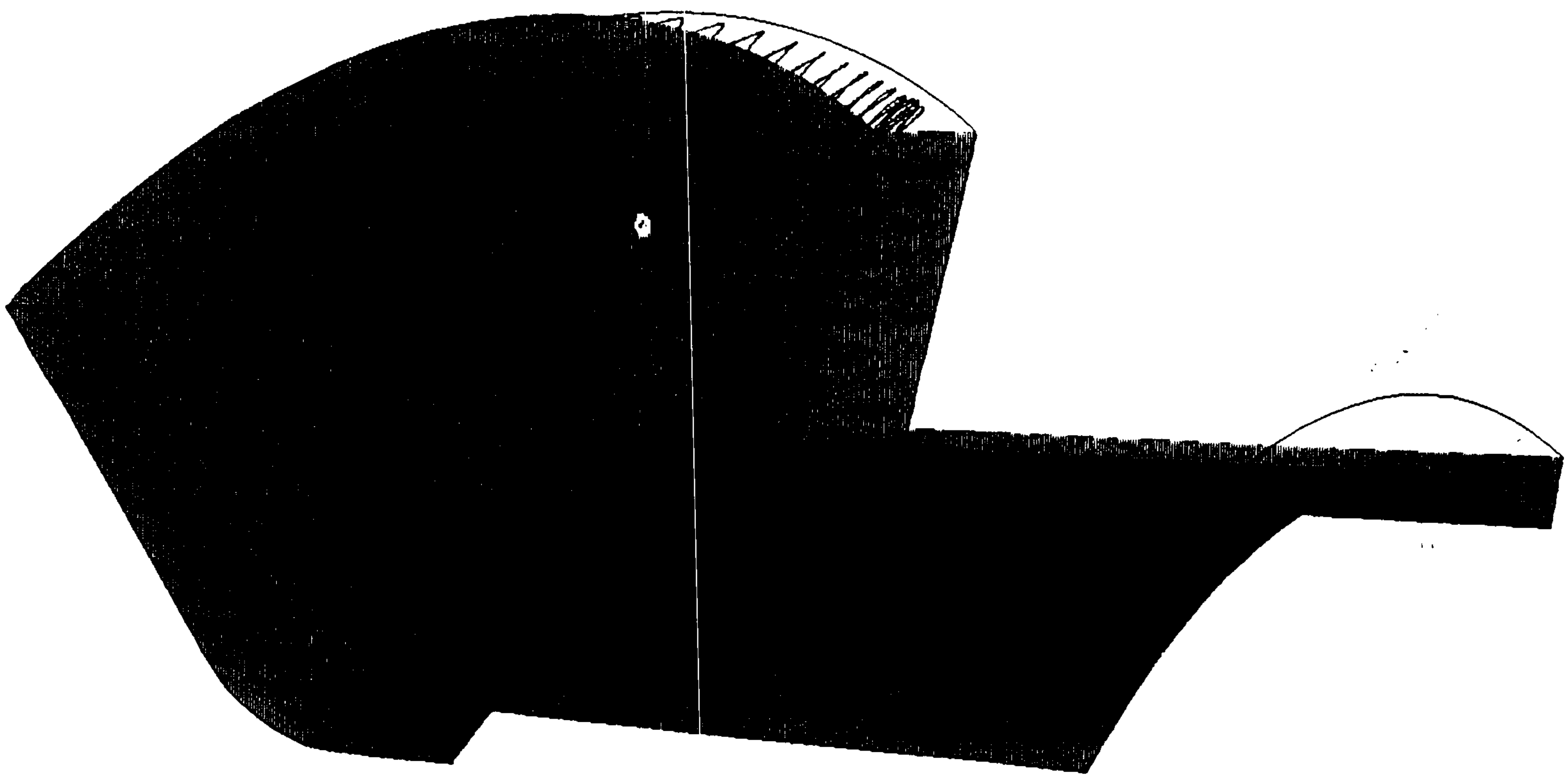

Ground Rotating Wall without Rib

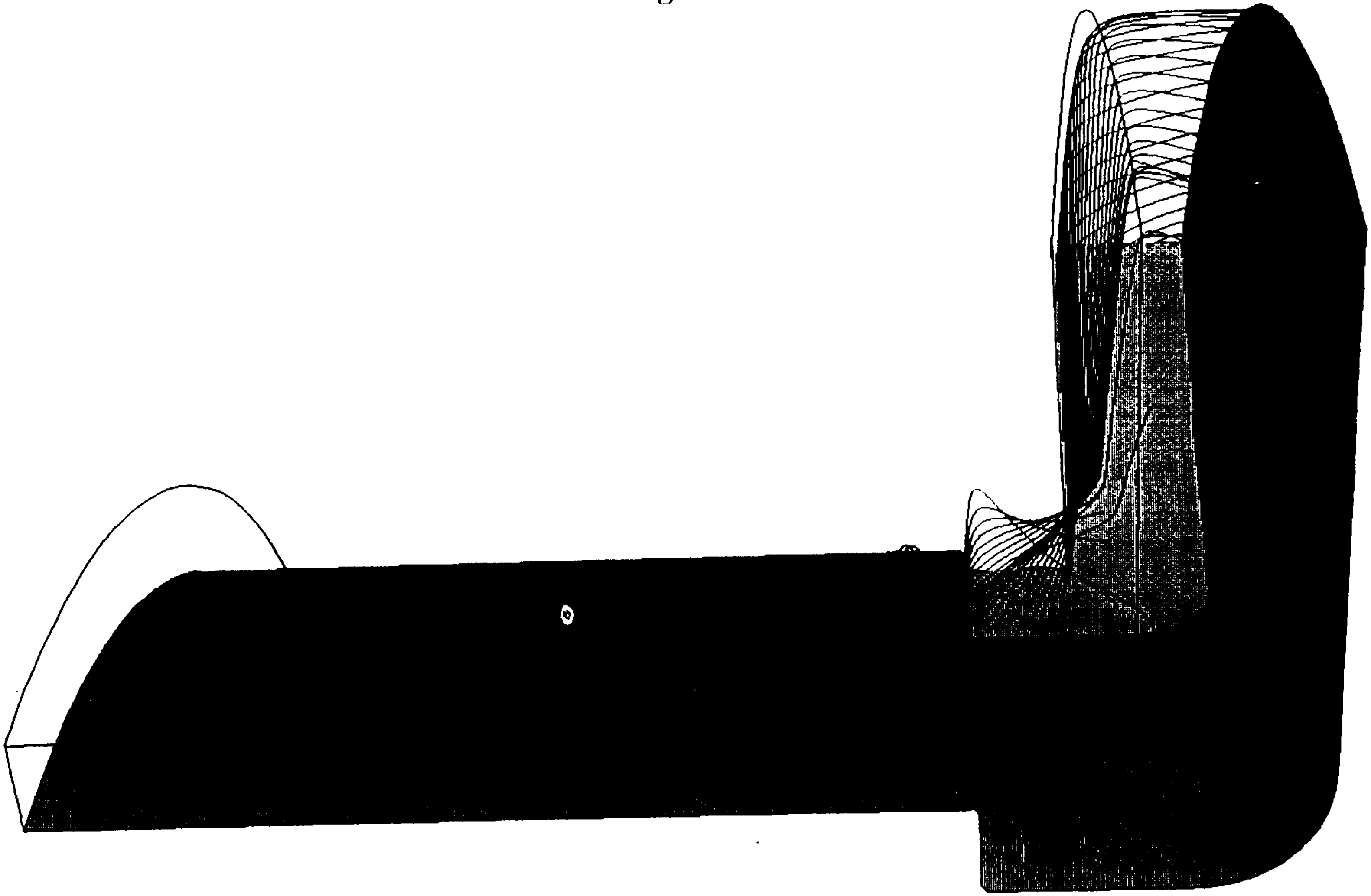

HPOTP PREBURNER BACKCAVITY (AT INNER–RACE INLET)

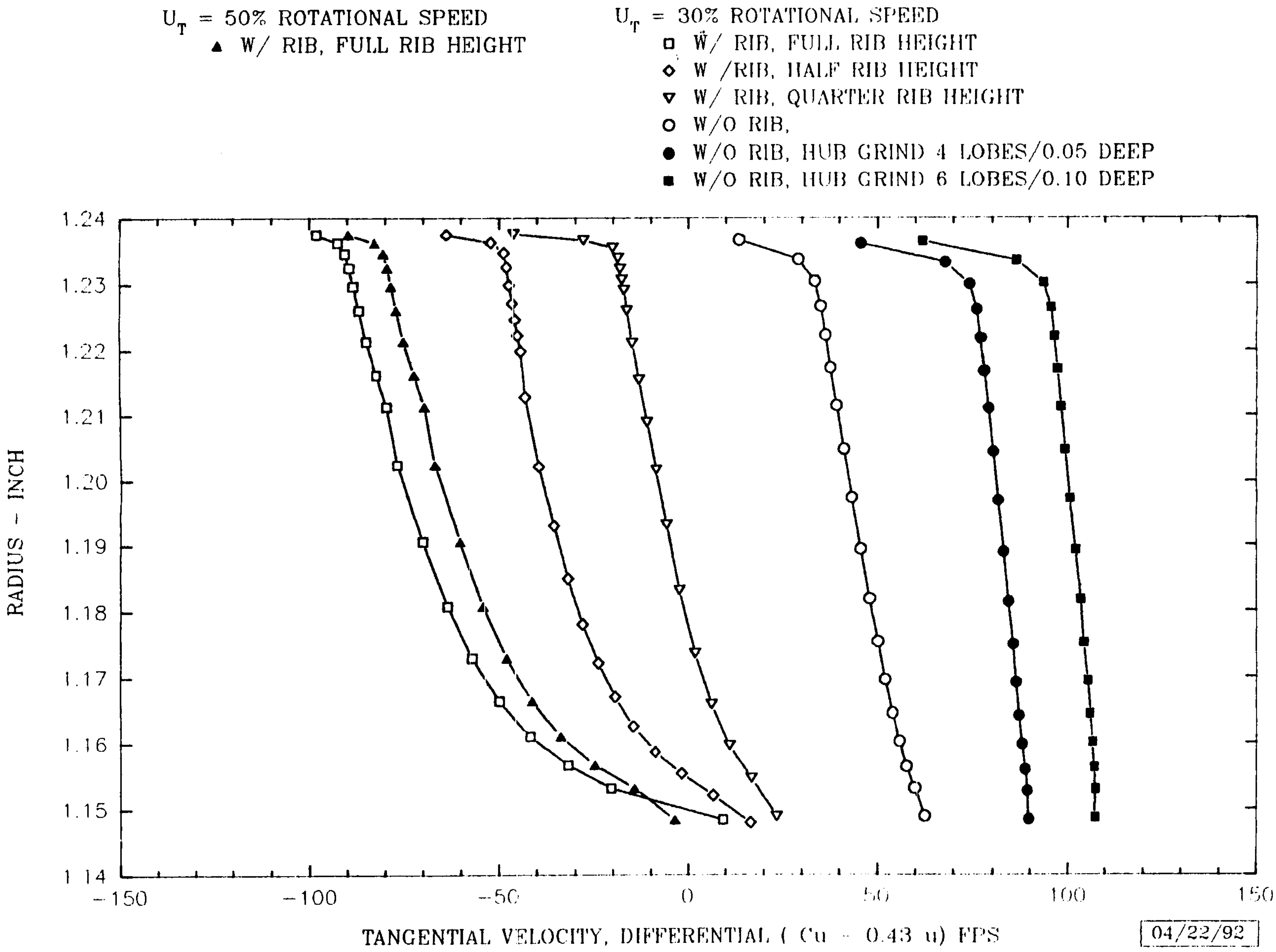

CONCLUSIONS / FUTURE WORK

REACT3D CFD RESULTS PROVIDE INSIGHT INTO COMPLEX FLOW PHYSICS

ADVANCED POST-PROCESSING ESSENTIAL TO UNDERSTANDING FLOW

RESULTS CAN BE USED TO DIRECT REDESIGN EFFORTS

CASE COMBINING RIBS AND GRINDOUTS IN WORK

N92-32295

NLS CLUTCHING BEARING CAVITY FLOW ANALYSIS

Ken Tran, Daniel C. Chan and Armen Darian
Rocketdyne Division - Rockwell International
6633 Canoga Ave., Canoga Park - CA 91303

In turbopumps with hydrostatic bearings, clutching bearings are one technique that can be used to control the transient axial thrust. At steady state operation, the clutching bearing inner race is decoupled from the rotating shaft and spins at a speed which is determined by the fluid driving forces in the bearing cavity and the ball bearing resistance. The life of the clutching bearing depends on the speed of rotation of the inner race; therefore, it is important to predict the latter with accuracy.

Cavity flow analysis is difficult due the complicated nature of the geometry, which often results in a totally skewed mesh. A quick study of a simple cavity flow was performed to gain insight into important parameters. It was concluded that the multi-domain (or multi-zone) approach, the double precision code, the initial condition and a good combination of relaxation factors are the 4 essential features in the search for a quick converged solution. The multi-domain approach enables the user to divide the model into small blocks which are gridded separately; therefore insuring the creation of a reasonable mesh. The double precision code solves the problem of various scales in different regions of the flow and the good initial guess in conjunction with a good selection of relaxation factors helps reduce the computational time.

A flow model of the NLS clutching bearing cavity was built for 2-D axisymmetric viscous analyses. From the CFD output, the tangential force exerted on the surfaces of the inner race was integrated to calculate the driving torque which, in conjunction with the resistance torque, was used to predict the operating speed of the inner race.

In order to further reduce the inner race rotation, the swirling flow at the cavity inlet was partially re-directed to generate an opposing torque. Thirty six slanted slots was incorporated into the anti-vortex rib to achieve this goal. A 3-D flow analysis performed on this configuration indicated a drastic reduction of the driving torque and inner race RPM.

NLS CLUTCHING BEARING FLOW ANALYSIS

By Ken Tran, Daniel C. Chan and Armen Darian

Rocketdyne Division, Rockwell International

Rockwell International
Rocketdyne Division

CONTENT

- Clutching bearing description
- Objective and Methodology
- Two-Dimensional analysis
- Three-Dimensional analysis
- Concluding remarks

CLUTCHING BEARING FUNCTION

- During transient operation:
  - Bearing element is used to control transient axial thrust
- At steady state operation:
  - Bearing is decoupled from the rotating shaft
  - Balance piston takes over the control of the axial thrust
  - Inner race is induced to rotate by fluid friction

ROCKETDYNE ADP FUEL TURBOPUMP

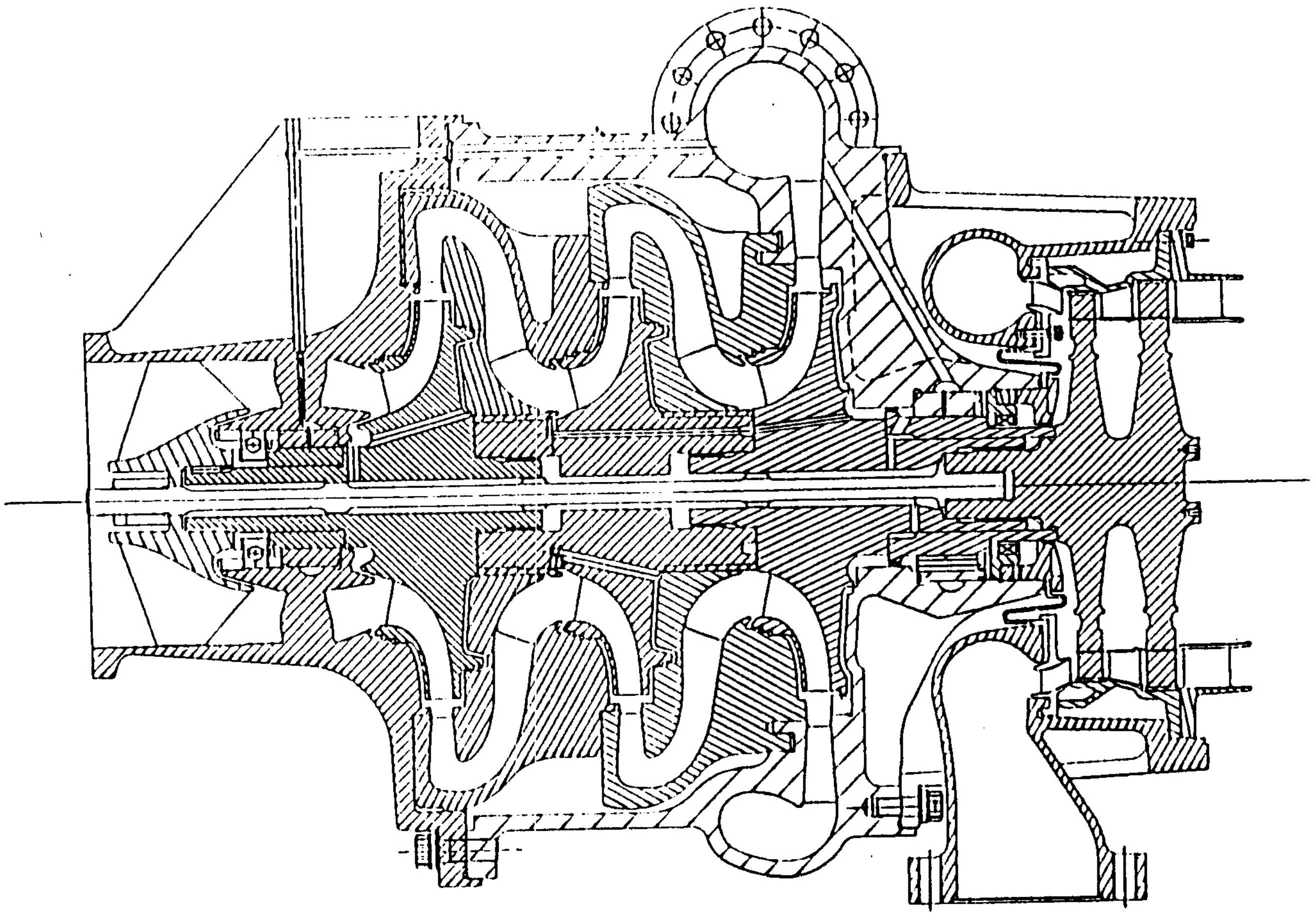

NLS CLUTCHING BEARING CONFIGURATION

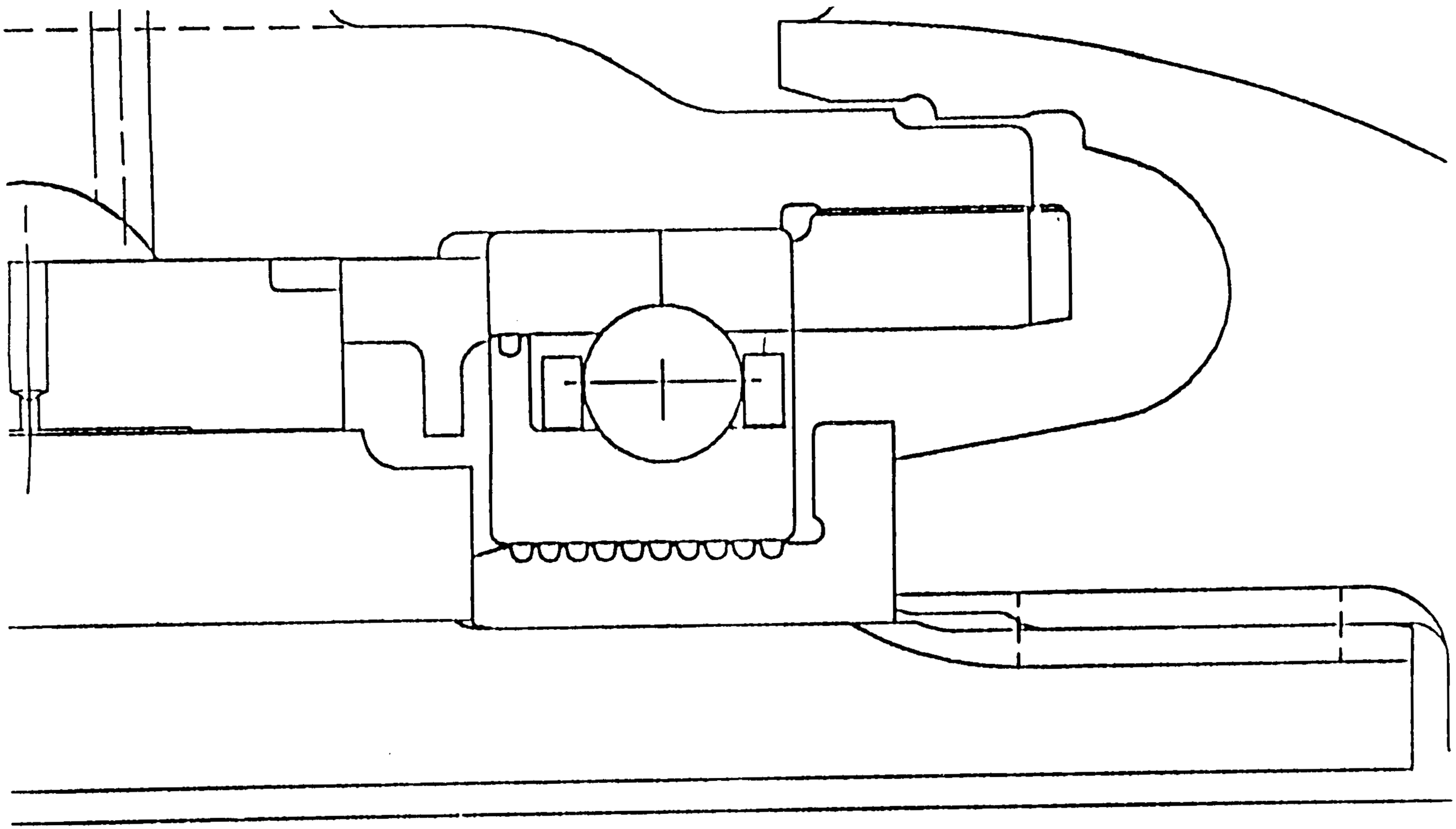

Rockwell International
Rocketdyne Division

OBJECTIVE

- Determine life of the clutching bearing
- Predict the inner race RPM
- Calculate the torque acting on the bearing inner race faces
- Investigate design features to minimize inner race speed

APPROACH

- Estimate resistance torque as a function of inner race RPM from bearing mechanical characteristics
- Determine driving torque in function of inner race RPM
- Intersection of 2 torque curves determines inner race speed
- Simplify the flow geometry
  - Labys are not modeled
  - Flow through the balls not included

CFD METHODOLOGY

- Reynolds averaged Navier-Stokes solver (REACT):
  - Control volume, pressure correction method
  - Two-equation k-ε turbulence model
- Validation:
  - Daily and Nece cavity

Rockwell International
Rocketdyne Division

COMPUTATIONAL MODEL

- Following elements are important to achieve converged solution:

  - Multi-domain grid: better mesh and control of Y+

  - Double precision code

  - Good initial condition

  - Relaxation factors: Taguchi parametrics for simple case performed on u,v,w (0.35 , 0.5, 0.8)and p (0.1, 0.15, 0.2) relaxation factor

Rockwell International
Rocketdyne Division

COMPUTATIONAL MODEL (cont.)

- Grid resolution:

  - Y+ ~ 50-500

  - 4205 grid points for 2-D model

  - 95366 grid points for 3-D model: meridional grid identical to 2-D mesh

- Boundary conditions:

  - Swirling jet imposed at one circumferencial node line

    The jet represents the exit condition of the hydrostatic bearing

Rockwell International
Rocketdyne Division

COMPUTATIONAL MESH

SINGLE ZONE

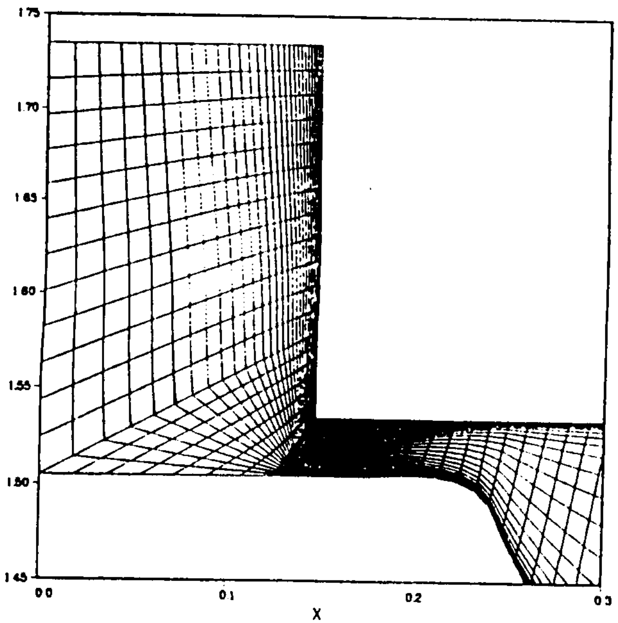

MULTI-ZONE

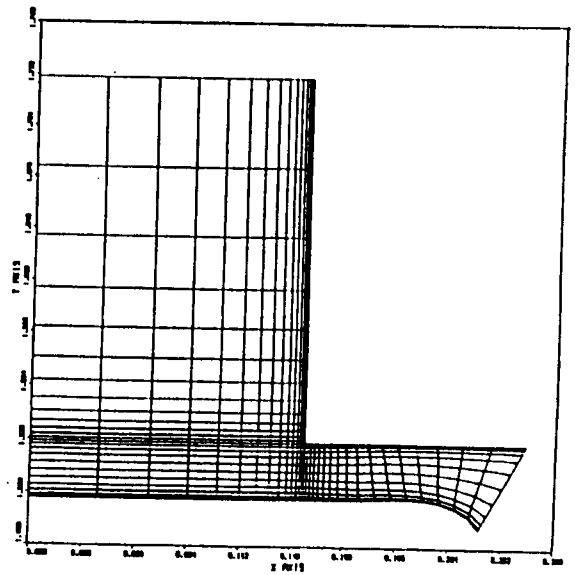

Rockwell International
Rocketdyne Division

TAGUCHI ANALYSIS OF RELAXATION FACTORS

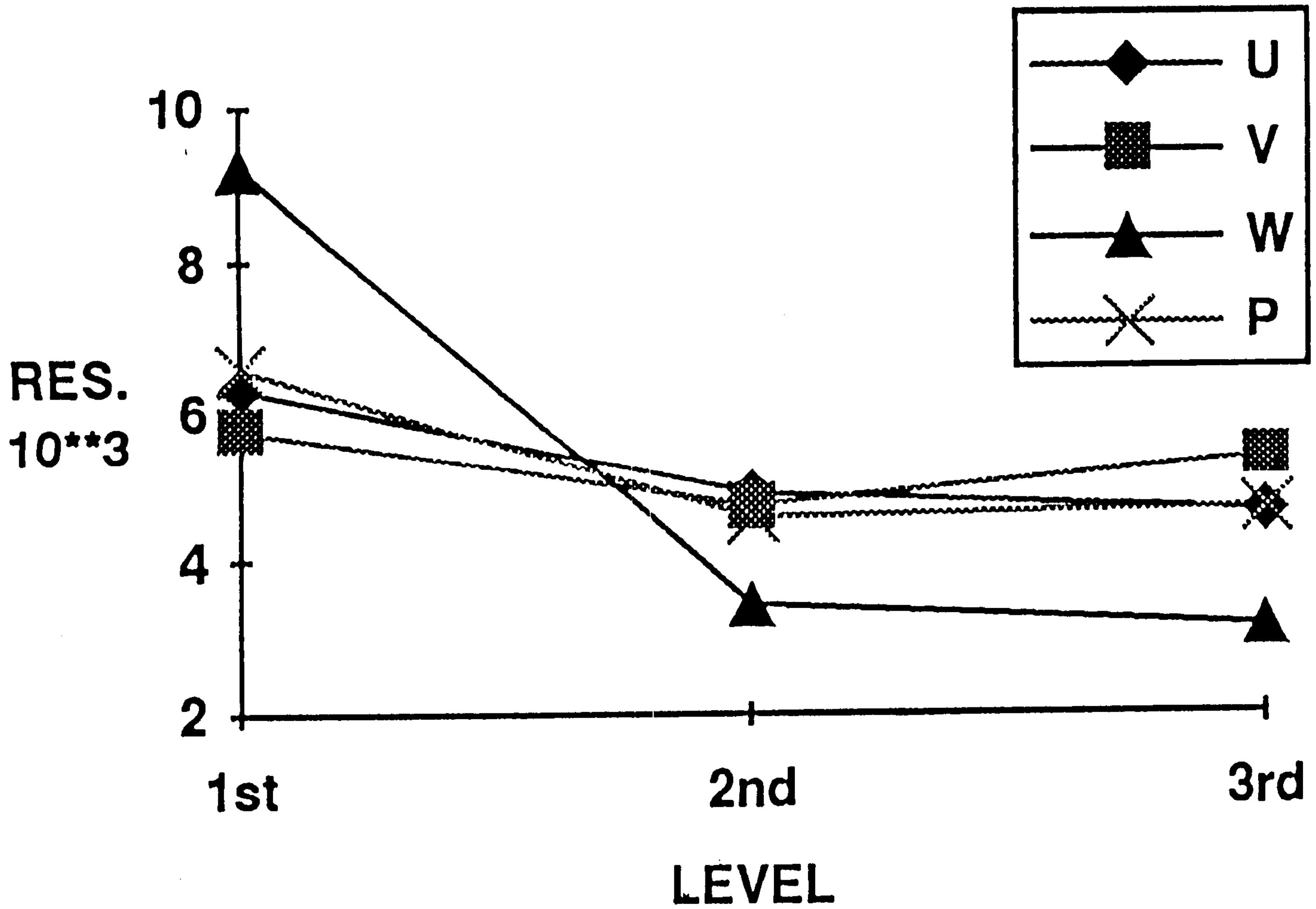

Rockwell International
Rocketdyne Division

COMPUTATIONAL GRID

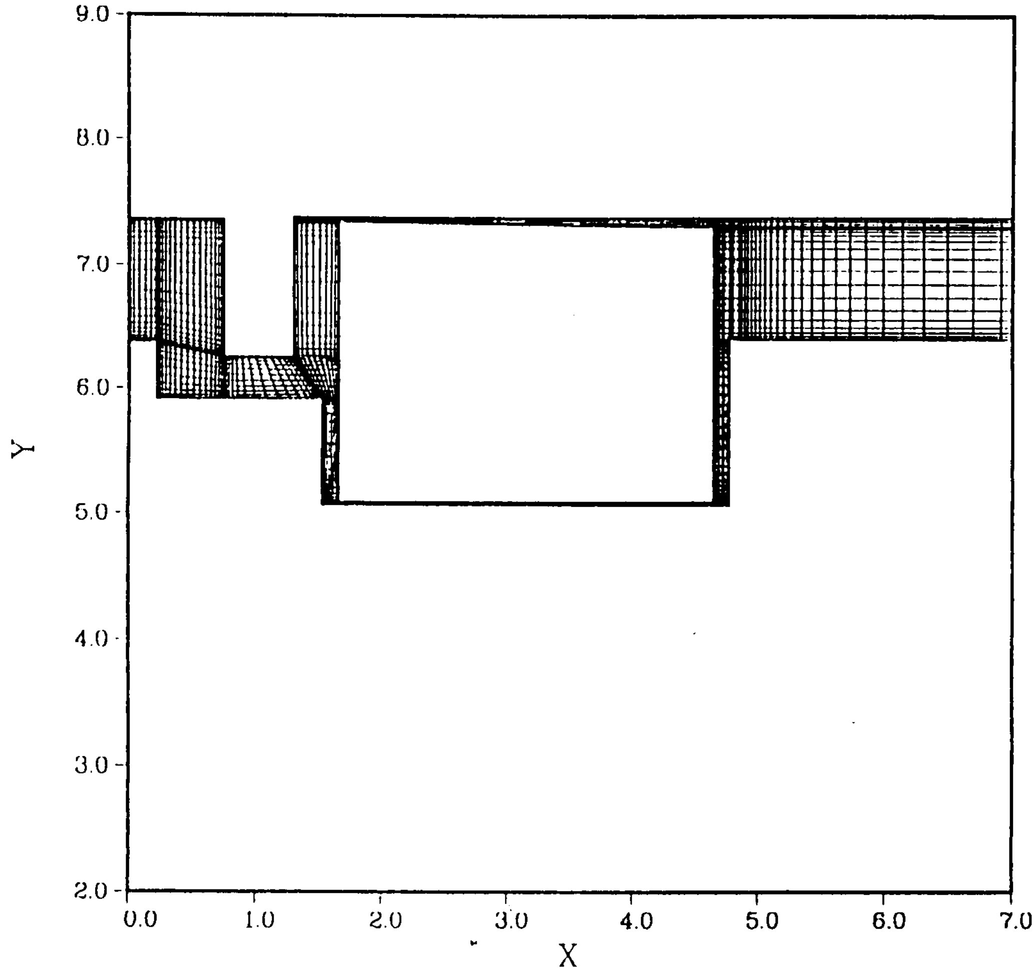

Rockwell International
Rocketdyne Division

2-D CFD RESULTS

- Streamlines show the jet diffusion is slow
- Swirl flow is still present near the inner race front face
- Radial pressure distribution on the inner race front face is relatively uniform except at stagnation point:
  - -1-D model can be used to estimate axial load
- Predicted axial load is independent of inner race speed

2-D CFD RESULTS (cont.)

- Integrated torque acting on the inner race indicates that:
  - At zero RPM, the inner race front face contributes over 50% to the total torque
  - At 10000. RPM, this contribution is only 25%
- Resistance and driving torque characteristics determine inner race RPM:
  - Predicted RPM is about 9000

MERIDIONAL STREAMLINES

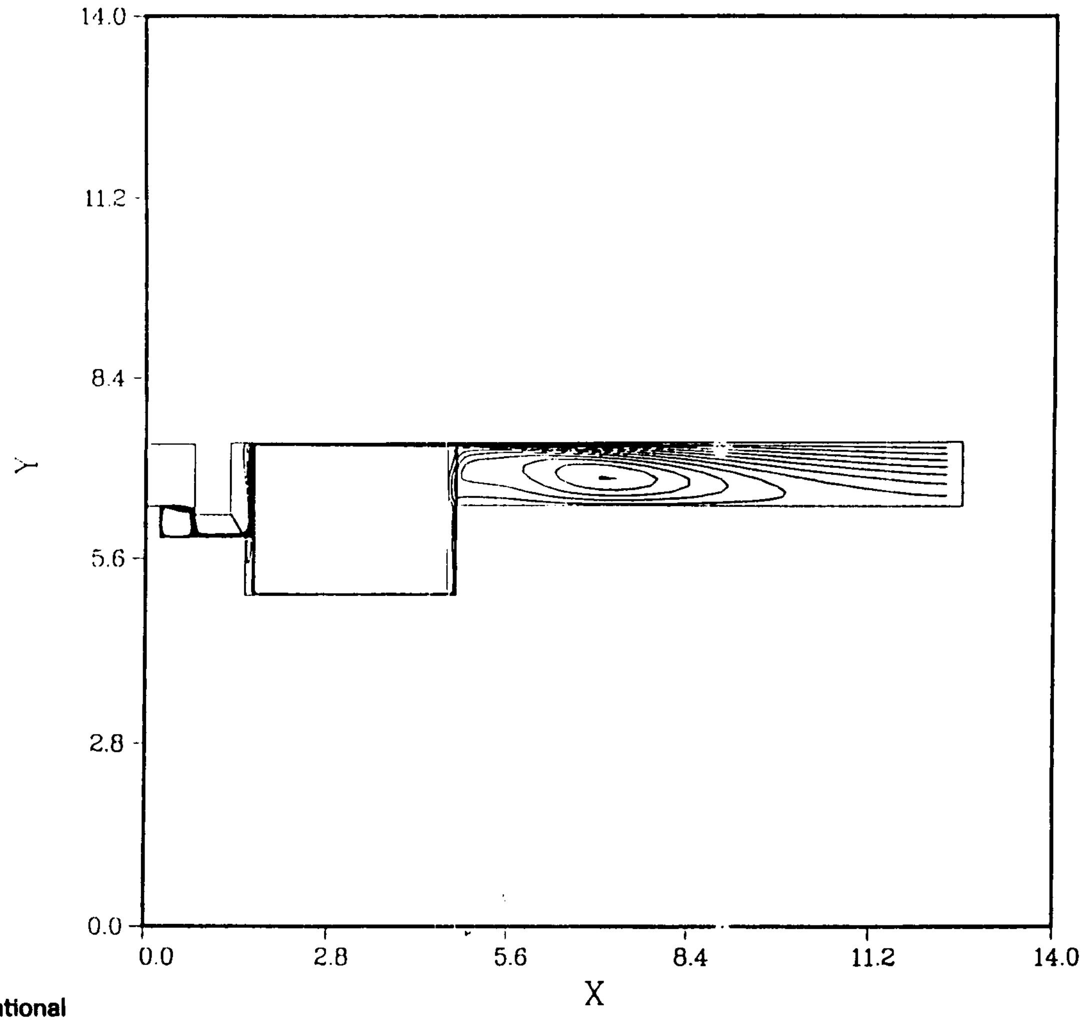

MERIDIONAL VELOCITY

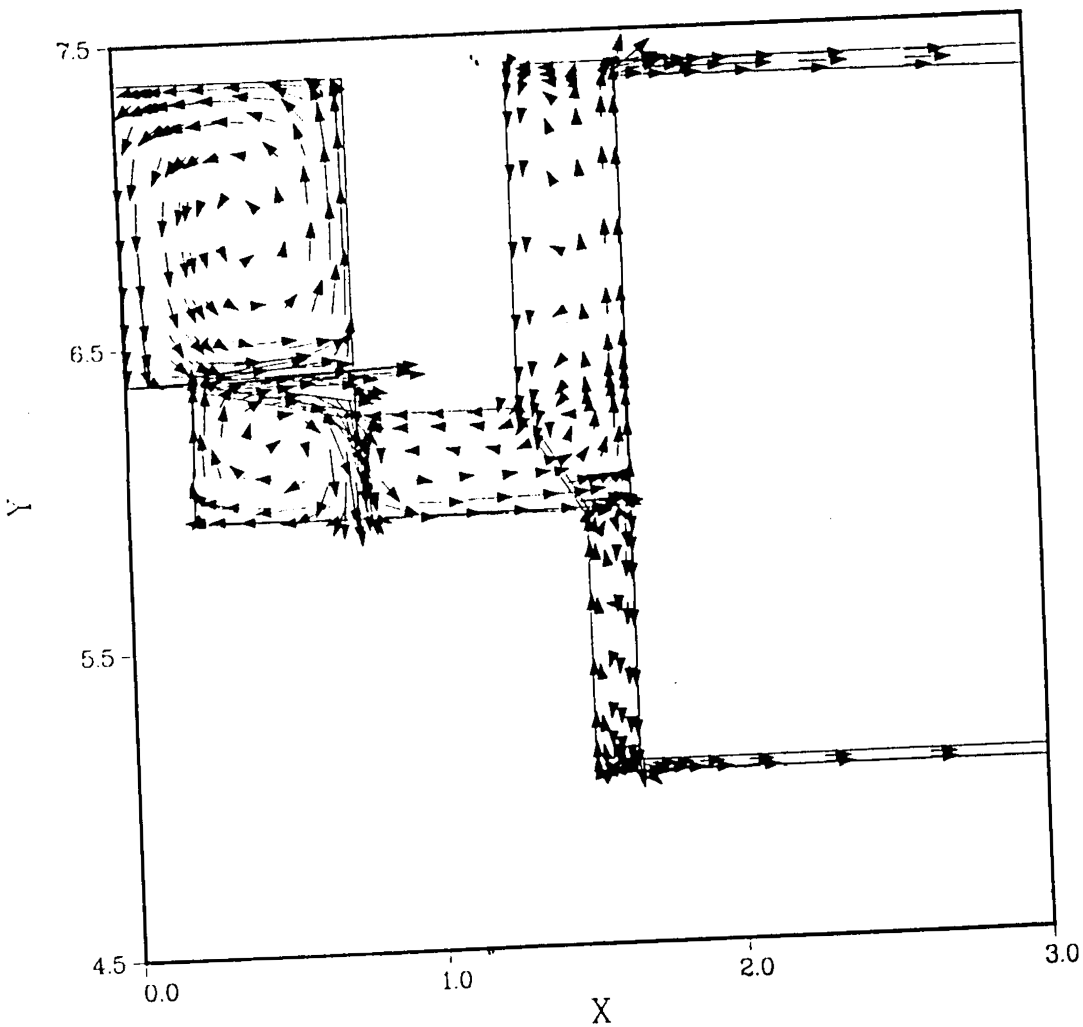

Rockwell International

Rocketdyne Division

TORQUE VERSUS INNER RACE RPM

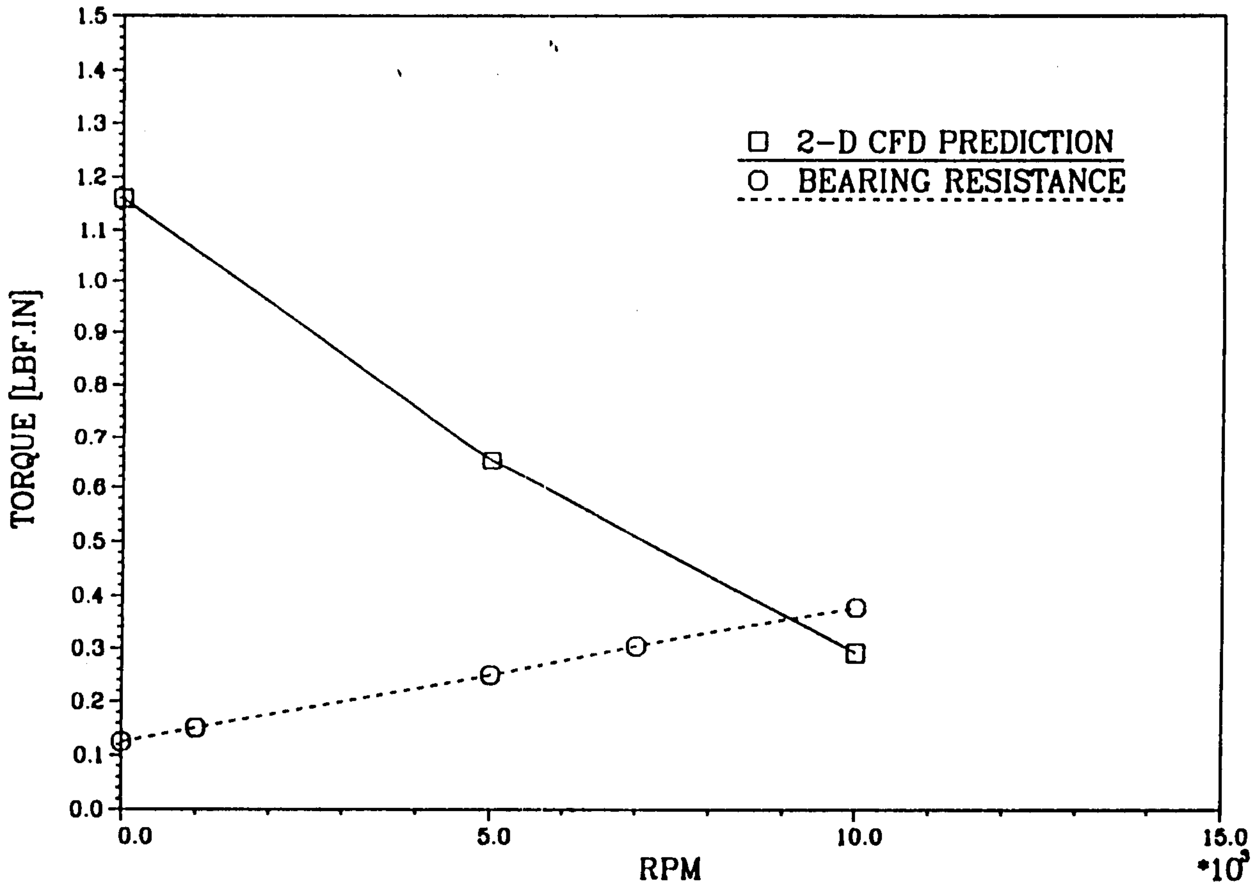

Rockwell International

Rocketdyne Division

PRESSURE DISTRIBUTION ON INNER RACE FRONT FACE

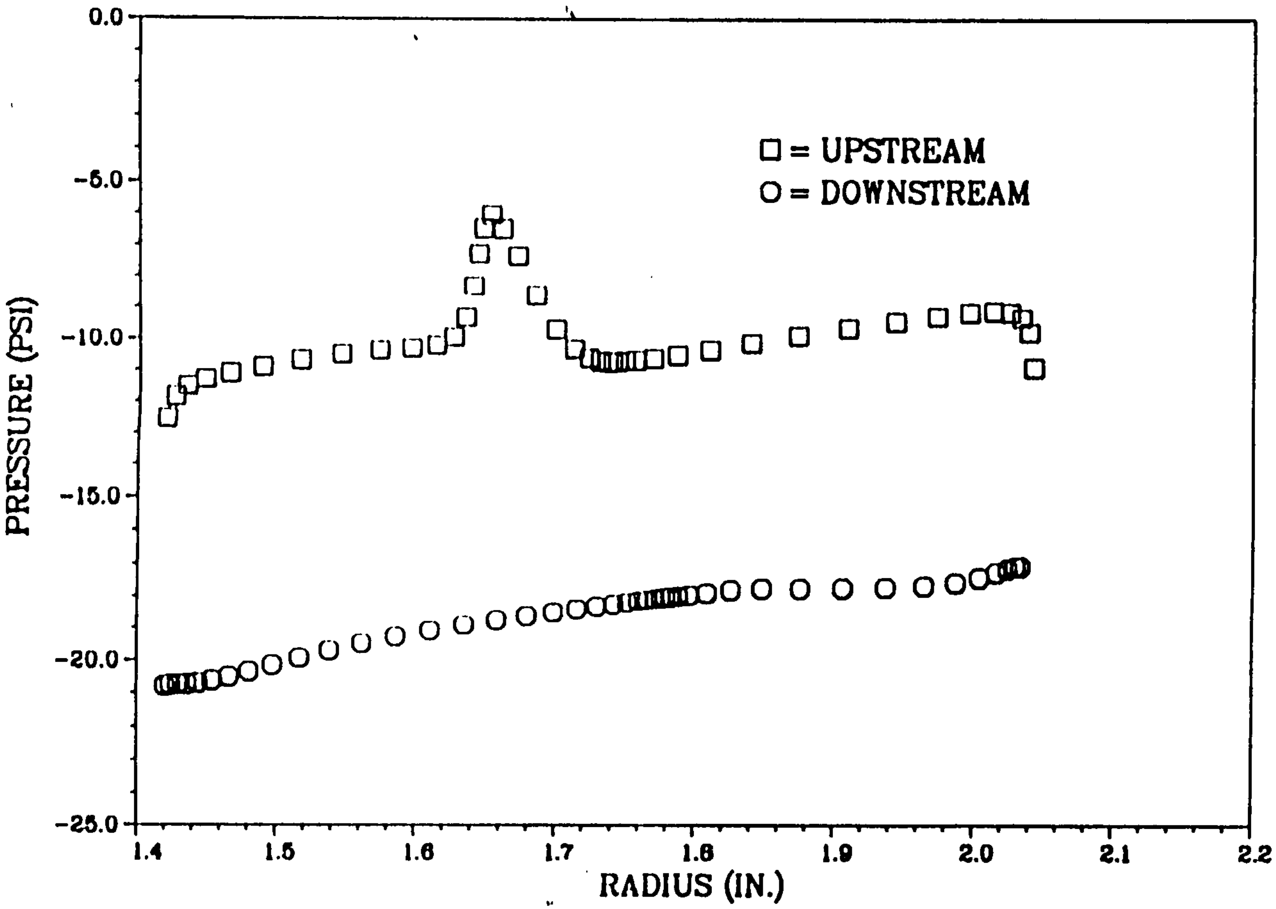

Rockwell International
Rocketdyne Division

METHODS TO REDUCE INNER RACE SPEED

- Increase axial load to raise resistance torque:

  -Tighter laby clearance: unacceptable due to high assembly cost

- Reduce the effect of the swirl:

  - Anti-vortex ribs: limited result because of small contribution of the front face torque

  - Redirecting the jet against direction of rotation to offset driving torque

Rockwell International
Rocketdyne Division

3-D CFD ANALYSIS

- Feature: 36 Slots on rib used to redirect jet (20 deg. from axial)
- Results:
  - Driving torque reduced significantly
  - Inner race speed lowered to 7000 RPM
  - 12 Hrs of YMP Cray CPU time per case
- Slots can be modified to increase effectiveness

TORQUE VERSUS INNER RACE SPEED

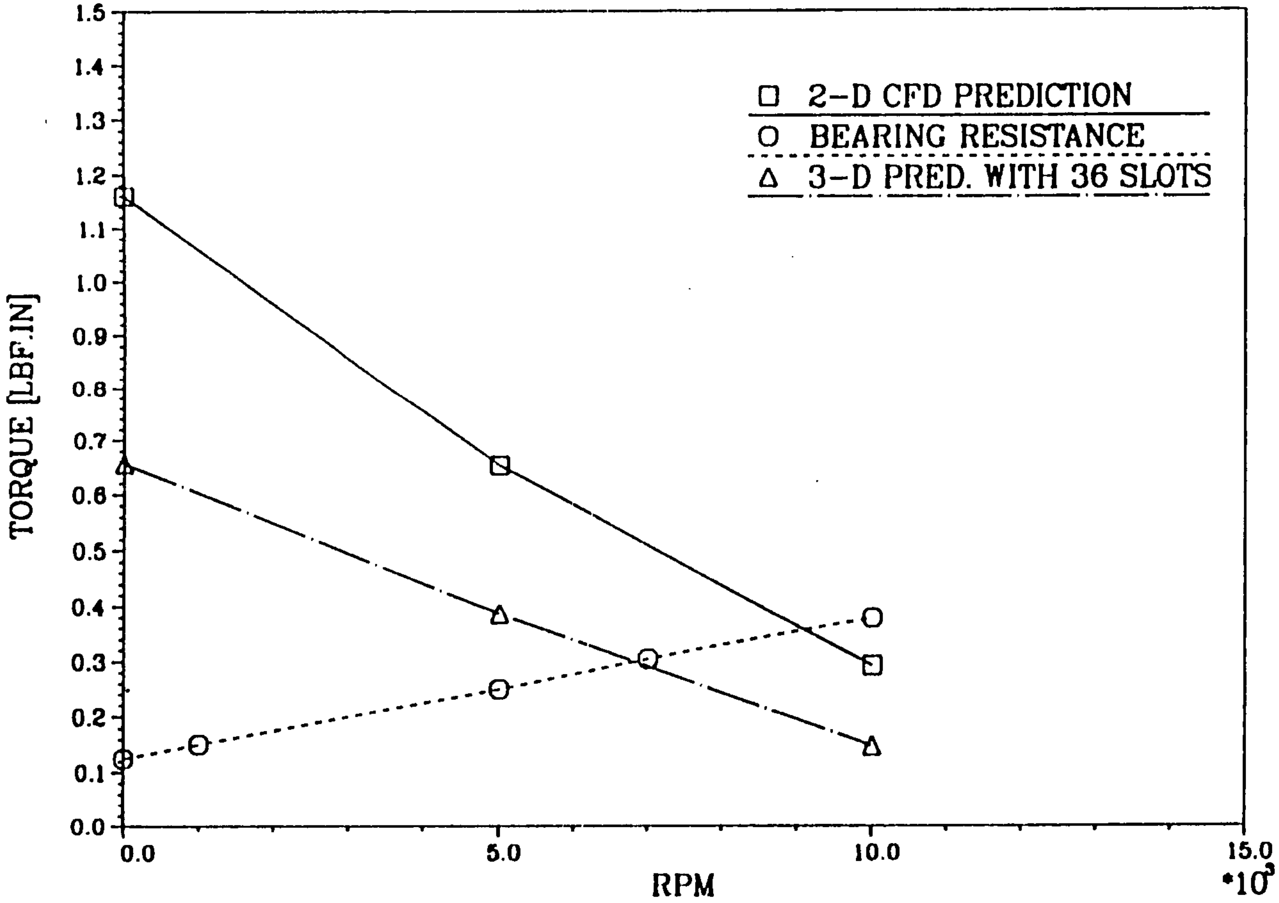

Rockwell International
Rocketdyne Division

NLS CLUTCHING BEARING

COMPUTATIONAL GRID

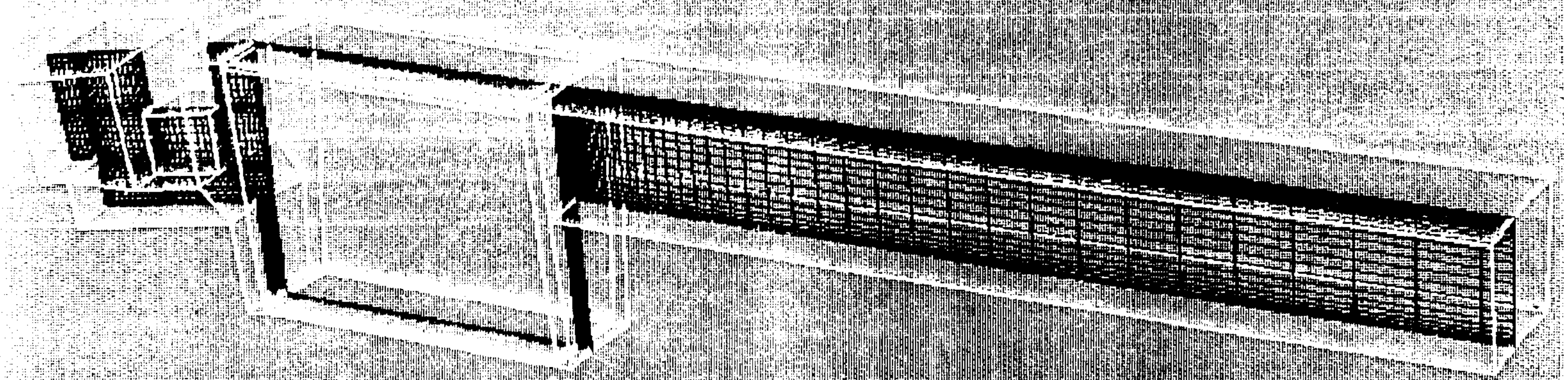

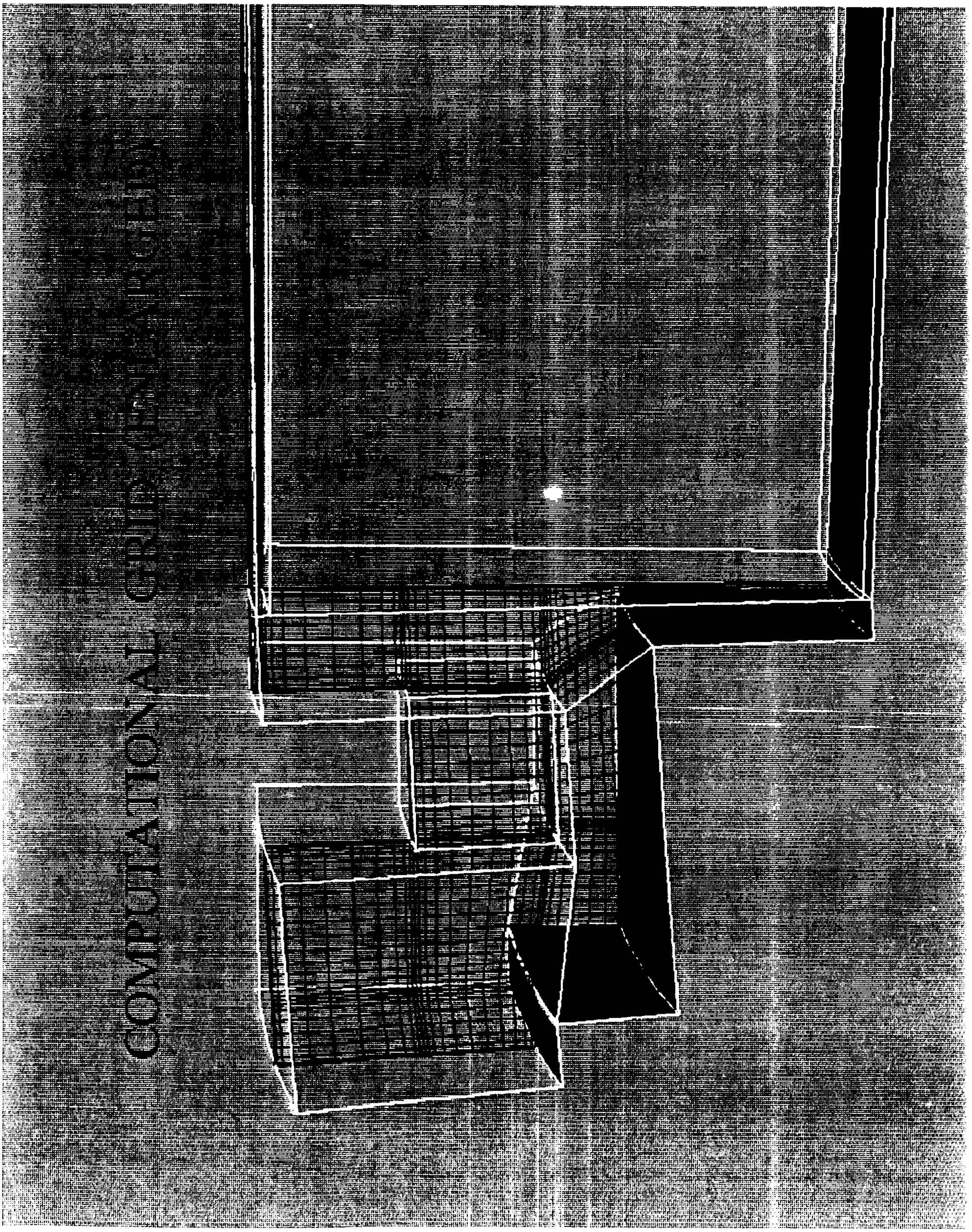

COMPUTATIONAL GRID

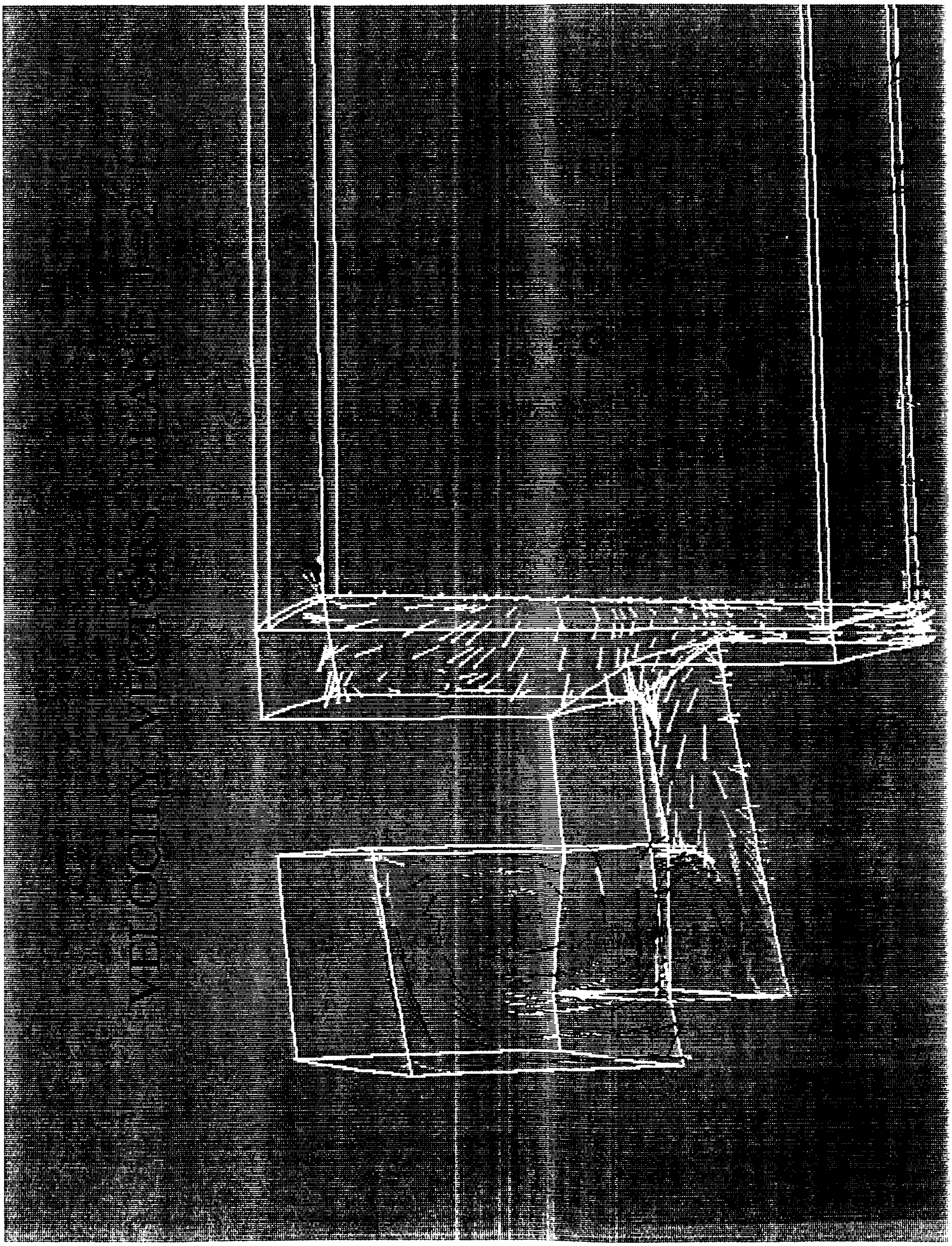
VELOCITY VECTORS

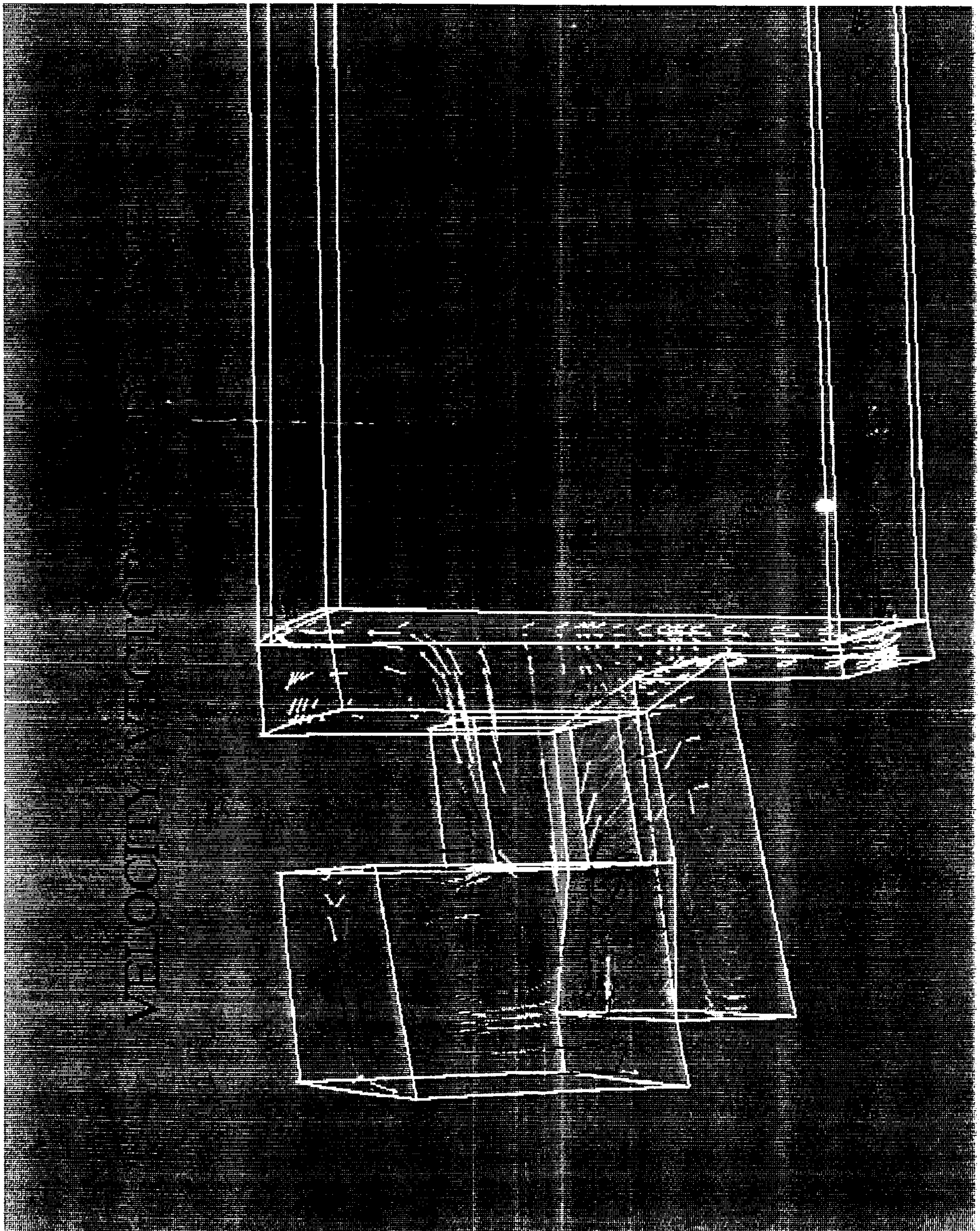
VELOCITY

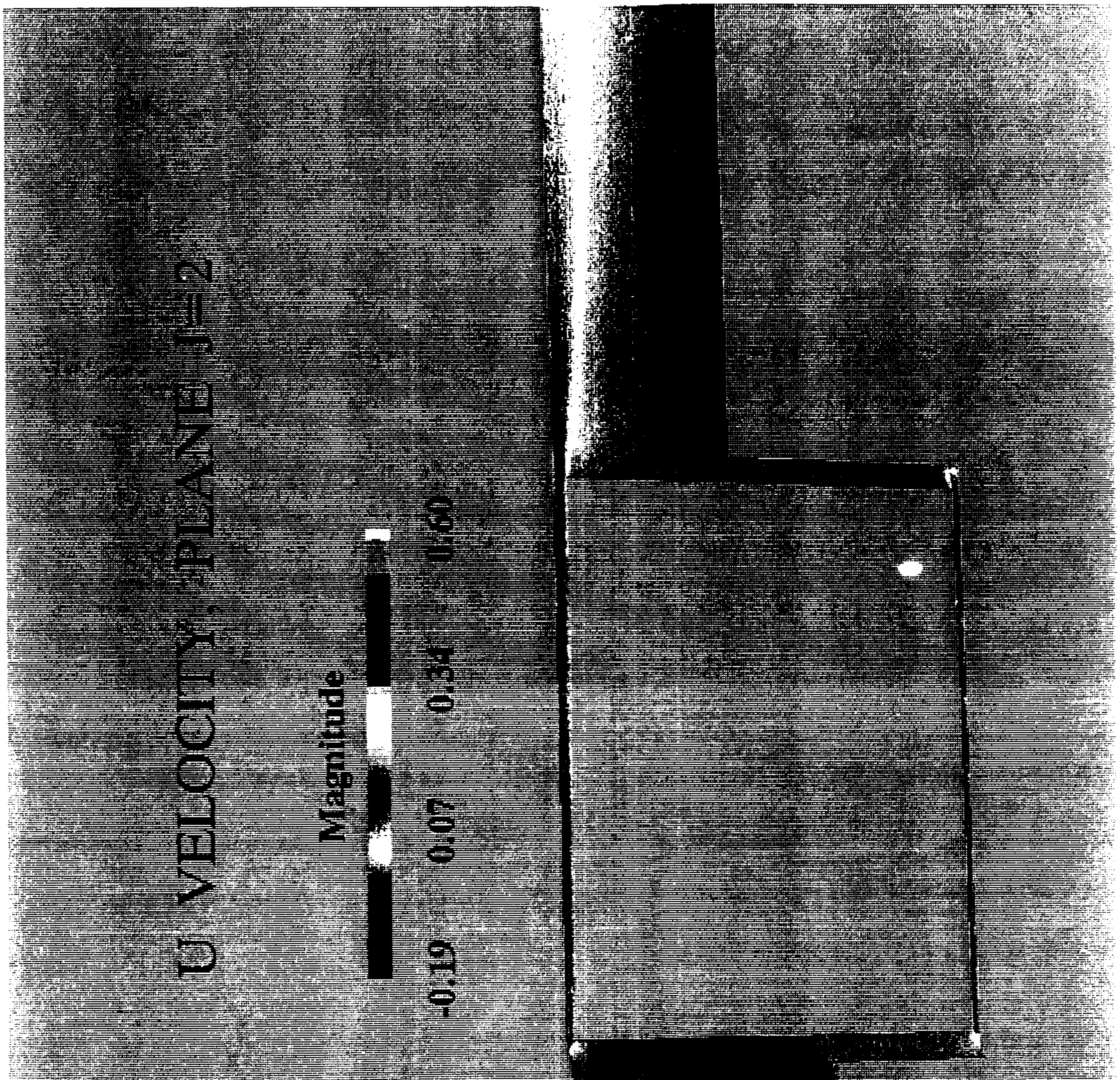
U VELOCITY, PLANE J=2
Magnitude
-0.19
0.07
0.34
0.60

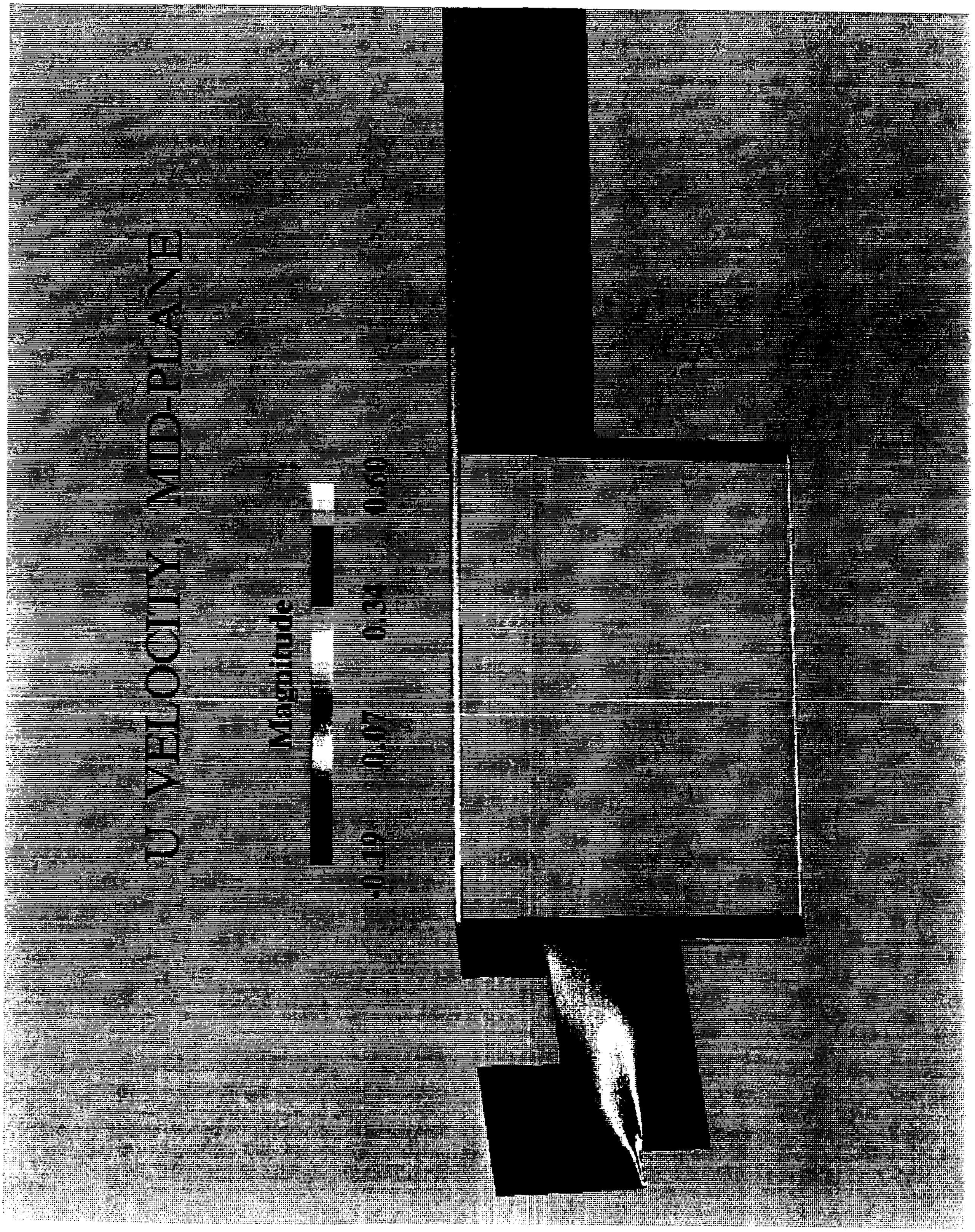
U VELOCITY, MID-PLANE
Magnitude
-0.19
0.07
0.34
0.60

CONCLUDING REMARKS

- Multi-domain methodology is needed for complicated geometry
- REACT is a mature code:
  - Enables the exploration of new design concepts
  - Helps determine optimum configurations
- Graphics post-processing is an important tool:
  - Assists users in the understanding of the flow field
  - Highlights flow features

Rockwell International
Rocketdyne Division

N92-32296

CFD Analysis to Optimize a Design Modification of BSMT

Mark Ratcliff and Ram Avva
CFD Research Corporation, Huntsville, Alabama
Robert Williams
NASA MSFC, Huntsville, Alabama

The Bearings, Seals and Material Tester (BSMT) is a test article being used at MSFC to evaluate the performance of conventional rolling contact bearings. Pressure differentials between the BSMT inlet and exit cavities are found to cause large parasitic axial loads on the bearing-carrier walls. These parasitic loads, besides being detrimental to the life of bearings, make the testing and evaluation of bearing performance very difficult, and need to be eliminated if at all possible.

CFDRC is currently under contract to MSFC to perform a detailed analysis of the flow fields inside the BSMT cavities and manifolds. The objectives of this study are to estimate the hydrodynamic loads on the bearings and to recommend feasible design modifications for BSMT to eliminate the parasitic loads.

Three-dimensional computational analyses of inlet and exit cavities in their baseline configuration were performed with REFLEQS which is an advanced finite-volume Navier-Stokes code. Computations were performed with and without a 1/4 inch diameter temperature probe included in each of the cavities. The results of the analyses indicate that the temperature probes substantially alter the flow field and reduce the pressure drop/rise in the cavities. The overall pressure drop across the tester compares quite well with the measurements.

One of the potential design modifications to reduce the parasitic loads on the bearings is to place baffles in the inlet cavities to isolate the coolant flow from the slinger wall. Three-dimensional analyses of the inlet cavities with the baffle were performed to assess the effect of baffles on the axial load. The baffle length was varied as a parameter. Results suggest that axial loading should be reduced considerably with the baffle extended inward to the radius of the outer race.

Thermal analyses of the inlet cavities were performed to determine the temperature rise due to viscous dissipation. The deflection of the baffle due to the hydrodynamic pressure load was also determined by performing structural analysis. The analyses suggest that the temperature rise and the baffle deflection are not of much concern. Therefore the considered design modification seems feasible and should be investigated further from structural, manufacturing, and test assembly considerations.

CFD Research Corporation **CFDRC**

3325-D Triana Blvd. ■ Huntsville, AL 35805 ■ (205) 536-6576 ■ FAX: (205) 536-6590

CFD ANALYSIS TO OPTIMIZE A DESIGN MODIFICATION OF BSMT

by

Mark Ratcliff and Ram Avva
CFD Research Corporation
Huntsville, Alabama 35805

and
Robert Williams
NASA Marshall Space Flight Center
Marshall Space Flight Center, Alabama

April 28, 1992

OUTLINE

CFDRC

- Overview

- Modeling of Inlet and Exit Cavities

- Results of 3D Analyses

- Summary and Concluding Remarks

Bearings, Seals & Material Tester

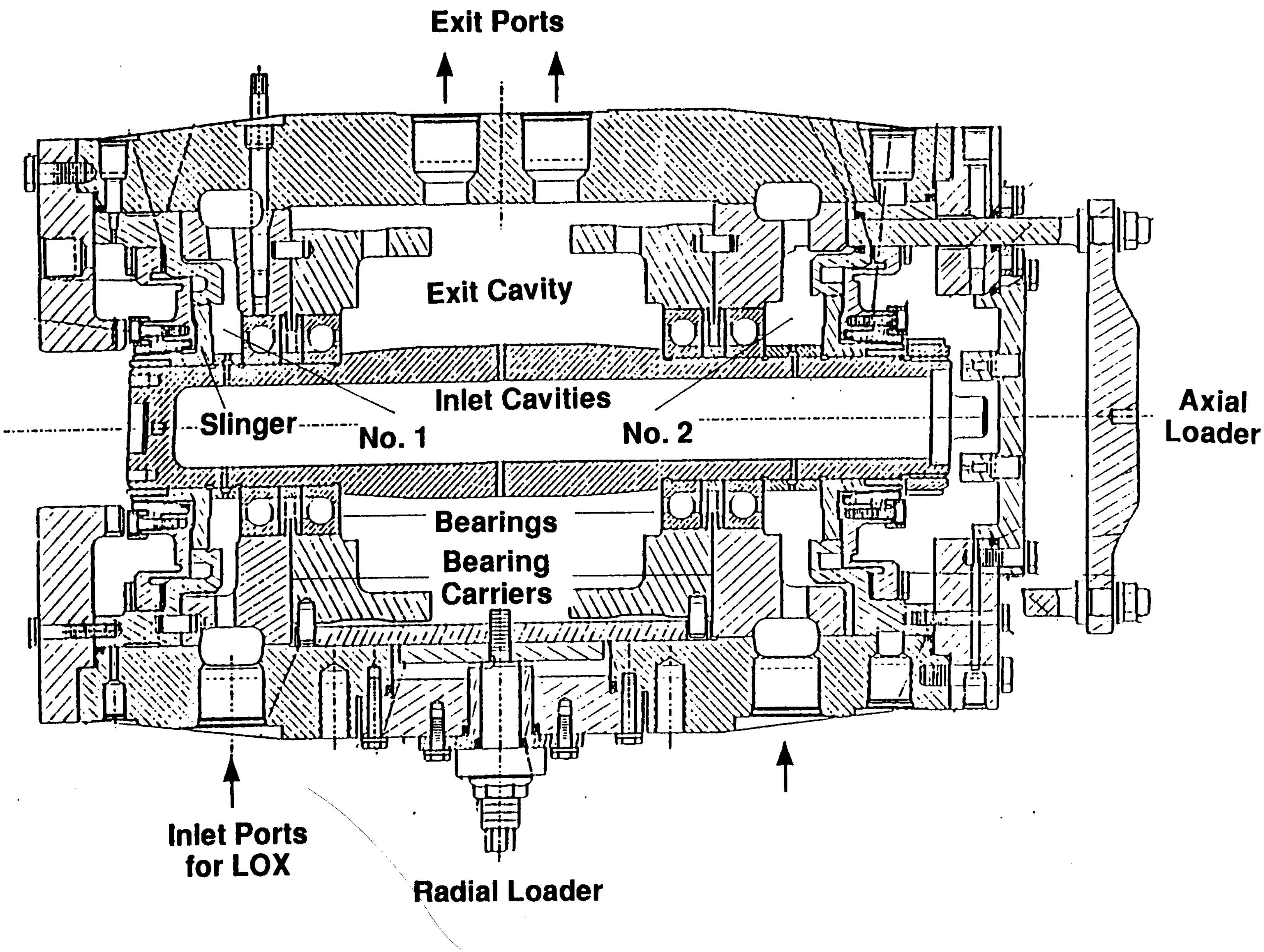

BSMT INSTRUMENTATION

CFDRC

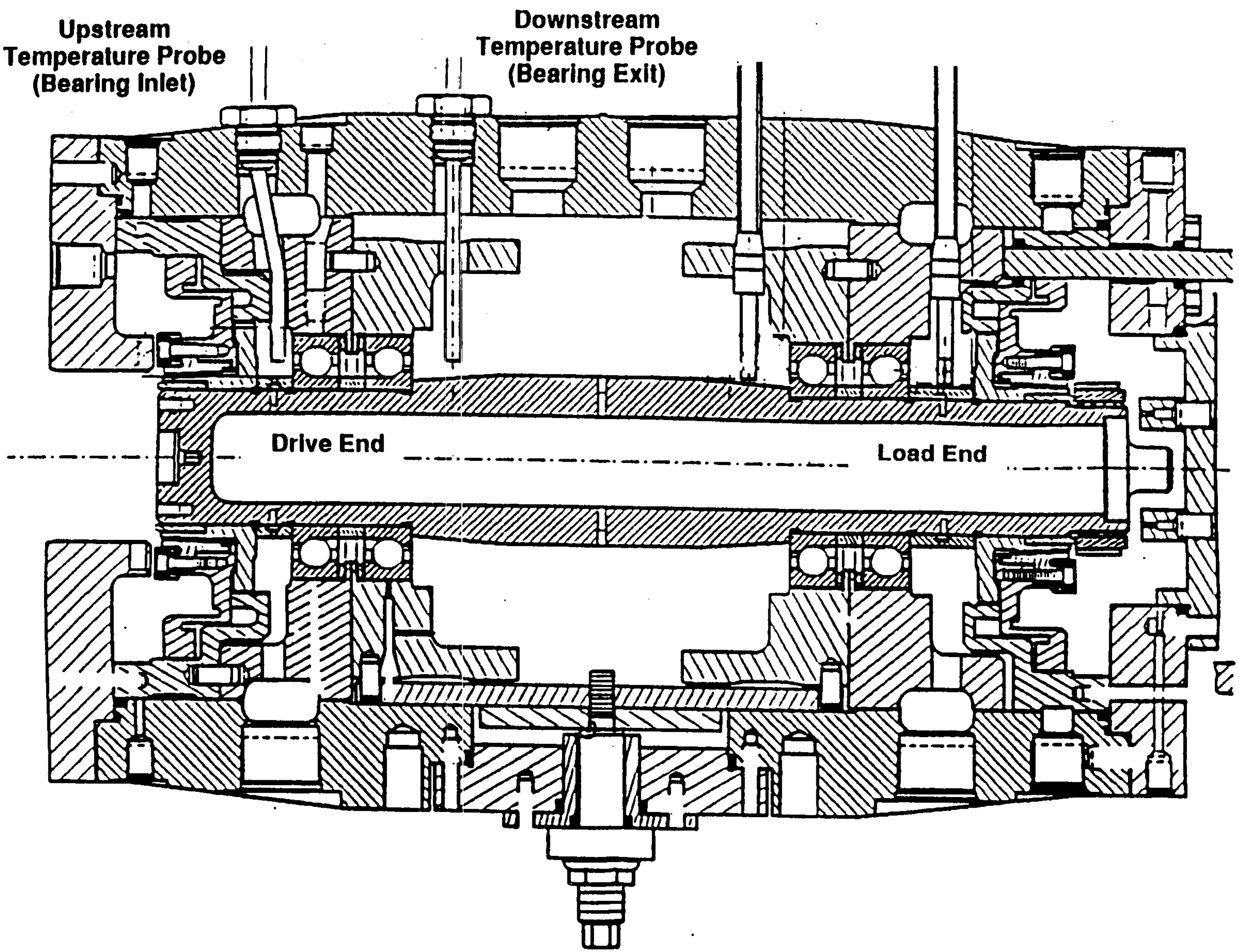

STATEMENT OF PROBLEM

CFDRC

- Problem
  - Tester Designed with Improper Cavity Pressure Distribution
  - Pressure Differentials Between BSMT Inlet and Exit Cavities Cause Large Parasitic Axial Loads

- Objective of Design Modification
  - Reduce Axial Loads in BSMT

NUMERICAL CODE

REactive FLow EQation Solver (REFLEQS)

- Density Averaged N-S Equations
- Finite Volume
- Pressure-Based Algorithm (SIMPLEC)
- Incompressible and Compressible Flows
- Cartesian, Axisymmetric and BFC Options
- Turbulence and Combustion Models

MODELING OF BSMT CAVITIES

CFDRC

LOX at -279°F (100°K) and 600 PSI (4×10^6 Pa)

Assumptions:

- Incompressible
- Isothermal
- Constant Properties
- Single Phase

MODELING OF INLET CAVITIES

CFDRC

Mass Flux Matched

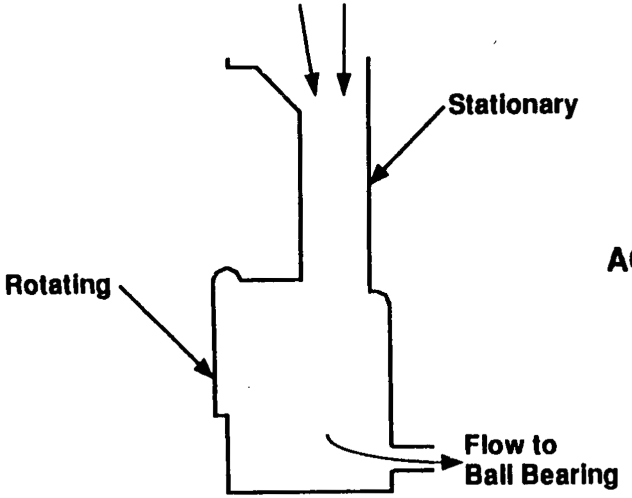

ACTUAL GEOMETRY

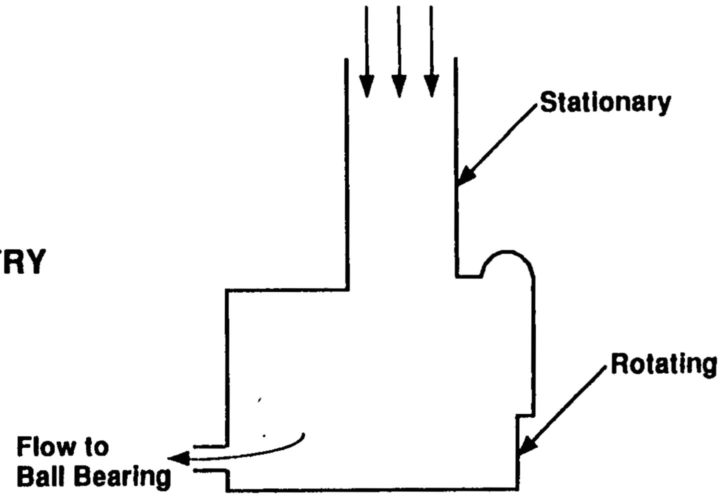

INLET CAVITY NO. 1

INLET CAVITY NO. 2

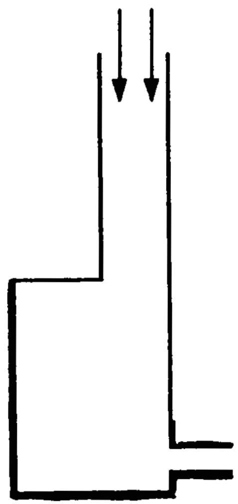

MODELED GEOMETRY

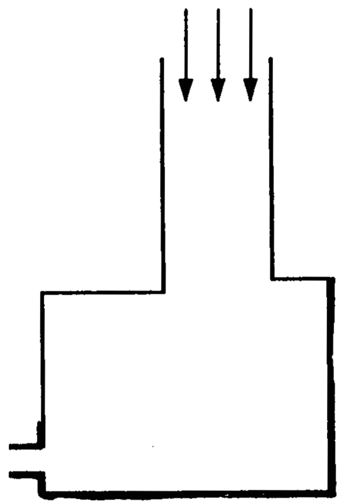

MODELING OF EXIT CAVITY

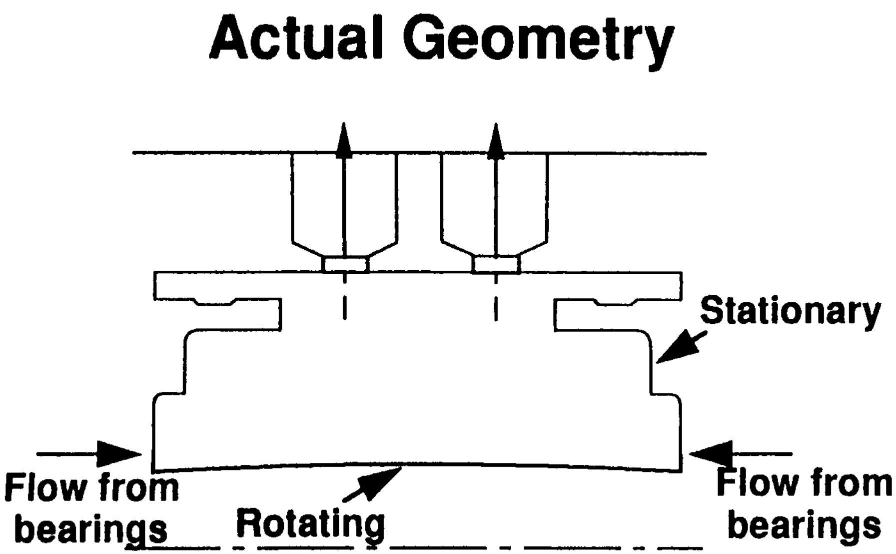

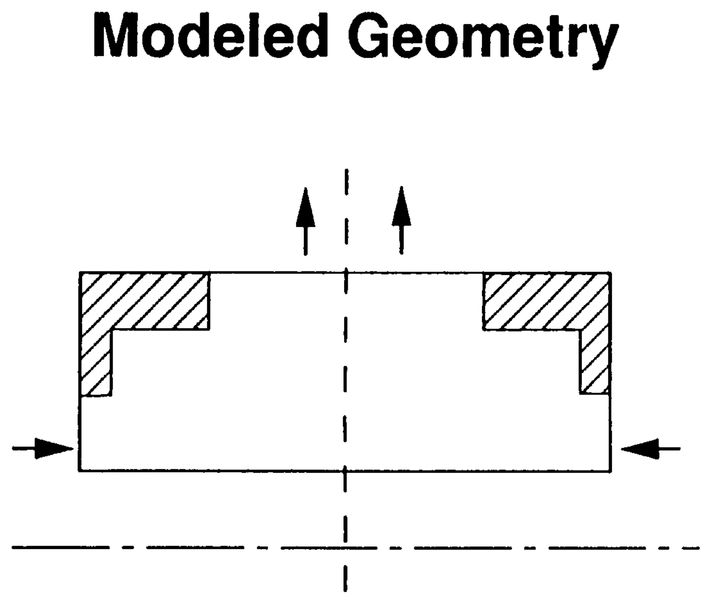

BOUNDARY CONDITIONS

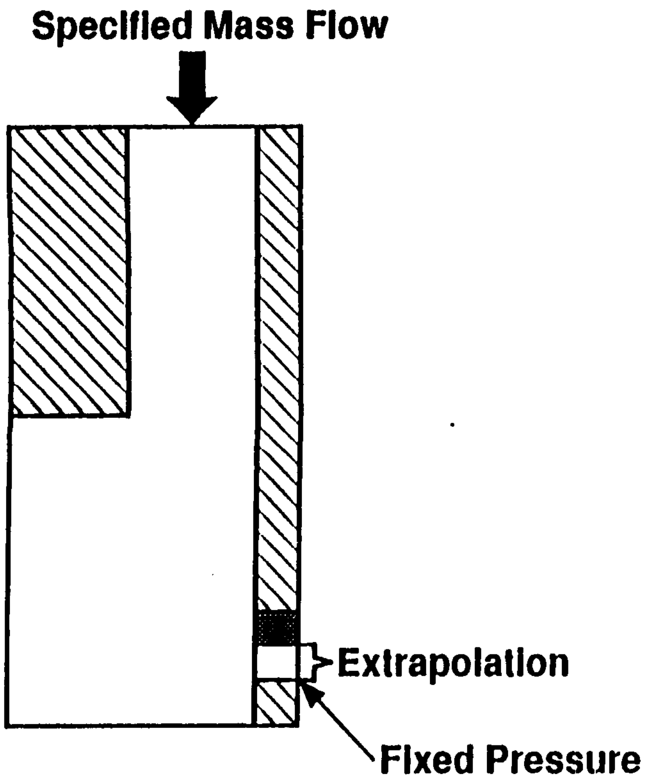

INLET CAVITY NO. 1

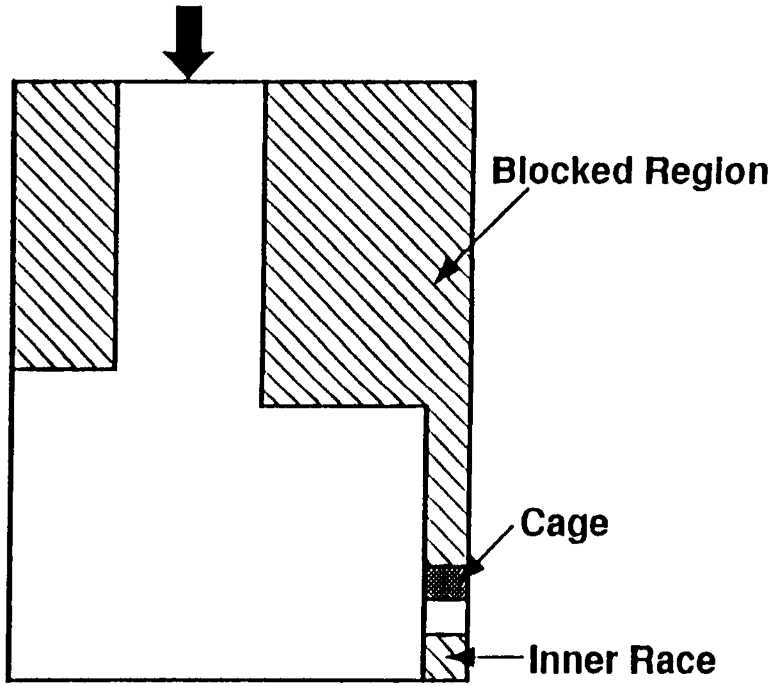

INLET CAVITY NO. 2

CAVITY NO. 1

COMPUTATIONAL GRID

30 x 30 x 34

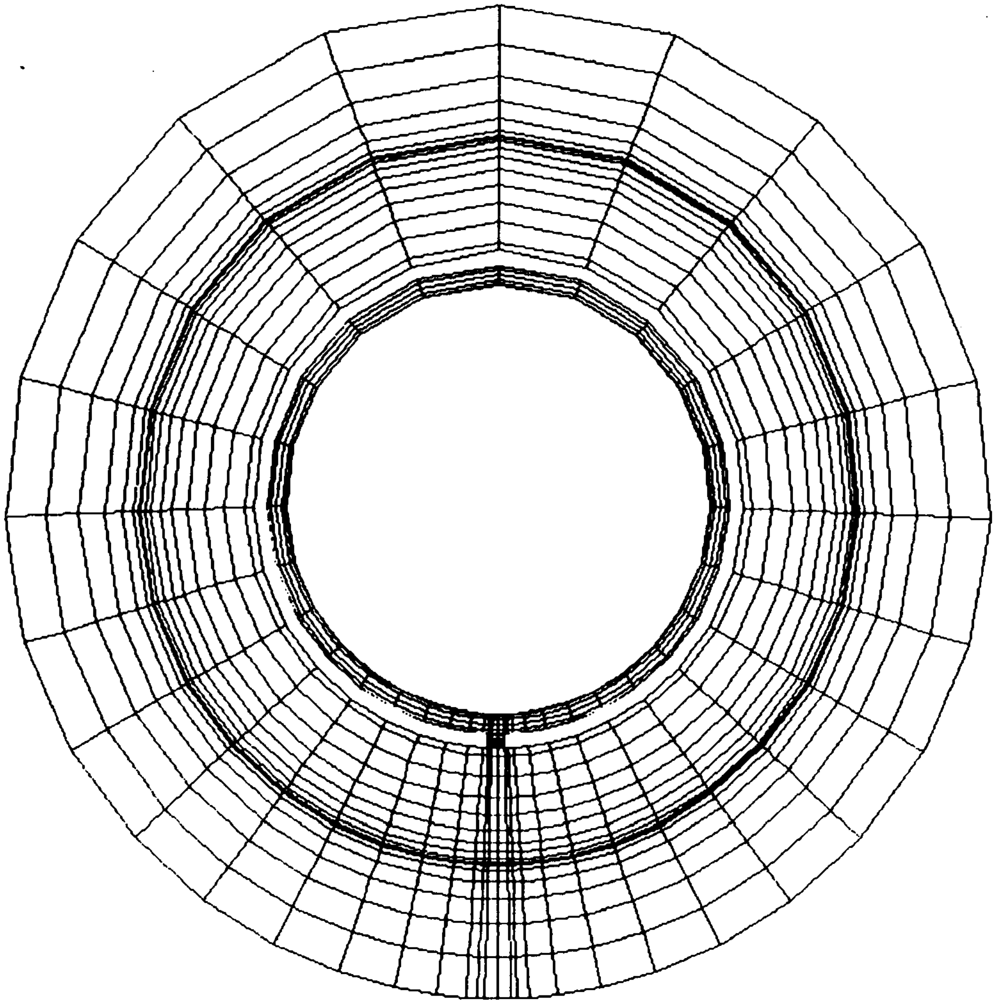

rθ - PLANE

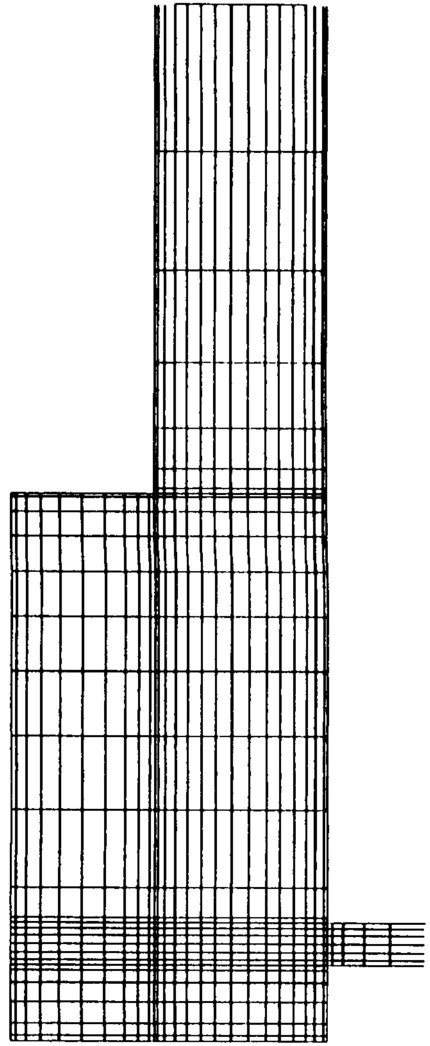

Xr - PLANE

CAVITY NO. 1 (BASELINE)

STATIC PRESSURE ON CARRIER WALL

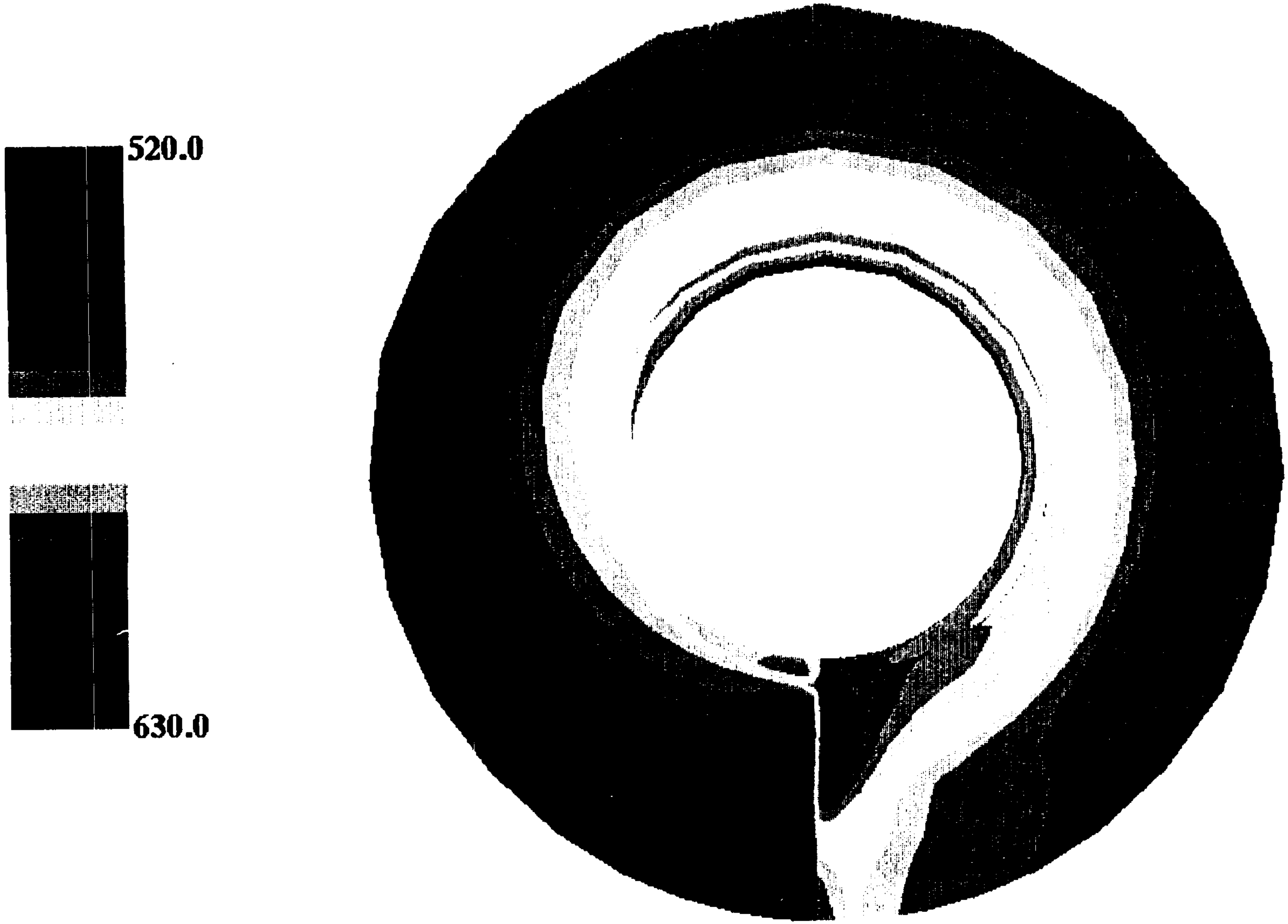

INLET & EXIT LOCATIONS

CFDRC

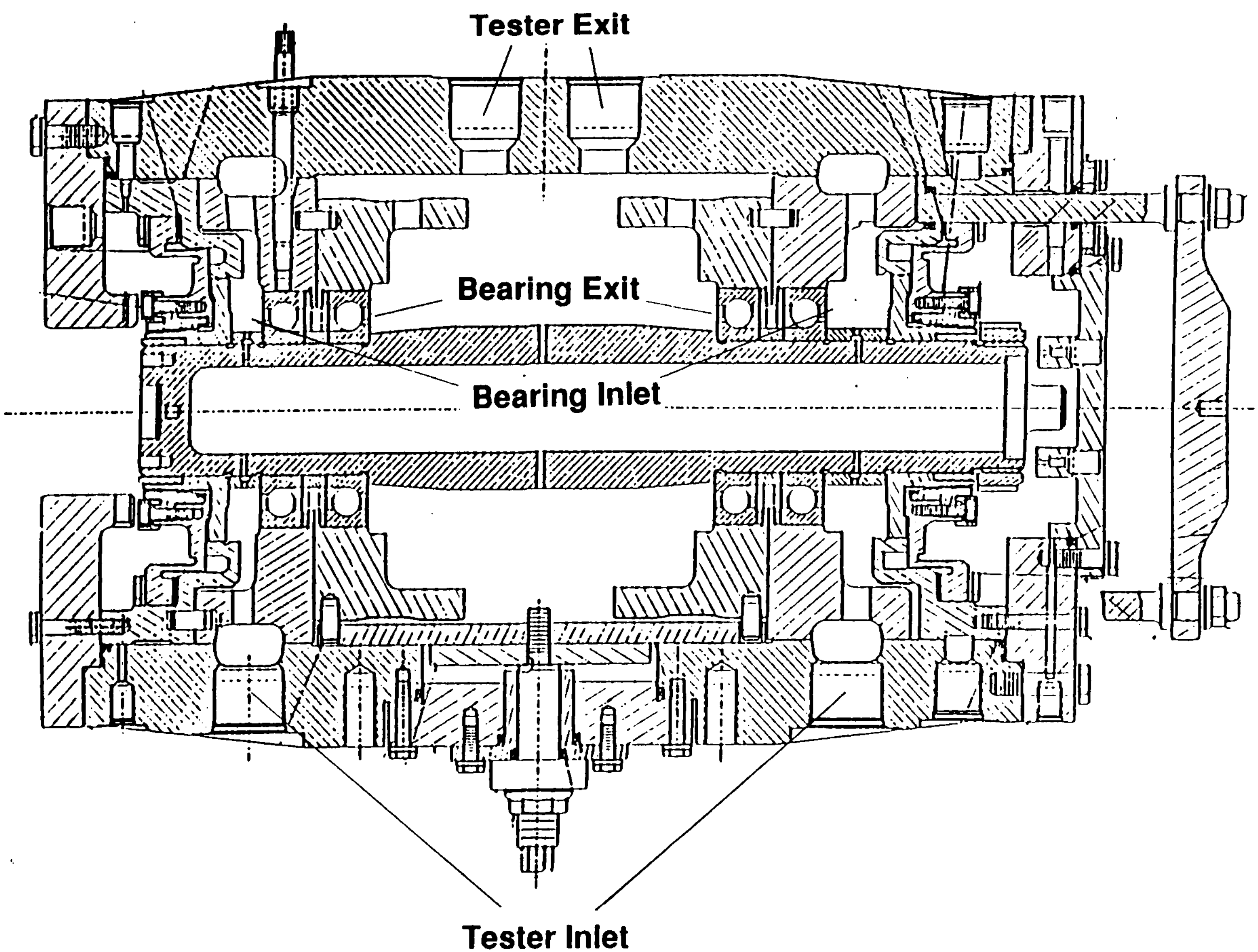

SUMMARY OF 3D ANALYSES

CFDRC

Baseline with Probes

Case	Static Pressure at (psi)				Net Δ P across Tester (psi)		Bearing Inlet Swirl % cage speed	Net Load lbf
	Tester Inlet	Bearing Inlet	Bearing Exit	Tester Exit	Computed	Measured		
Cavity No. 1 with probe	600	570	555	578	22	24	42	945
Cavity No. 2 with probe	600	556	541	564	36	38	60	1,495

POTENTIAL DESIGN MODIFICATION

CFDRC

Problem: Large axial (parasitic) loads

Cause: Strong vortex generated due to slinger rotation

Solution: Isolate fluid from slinger

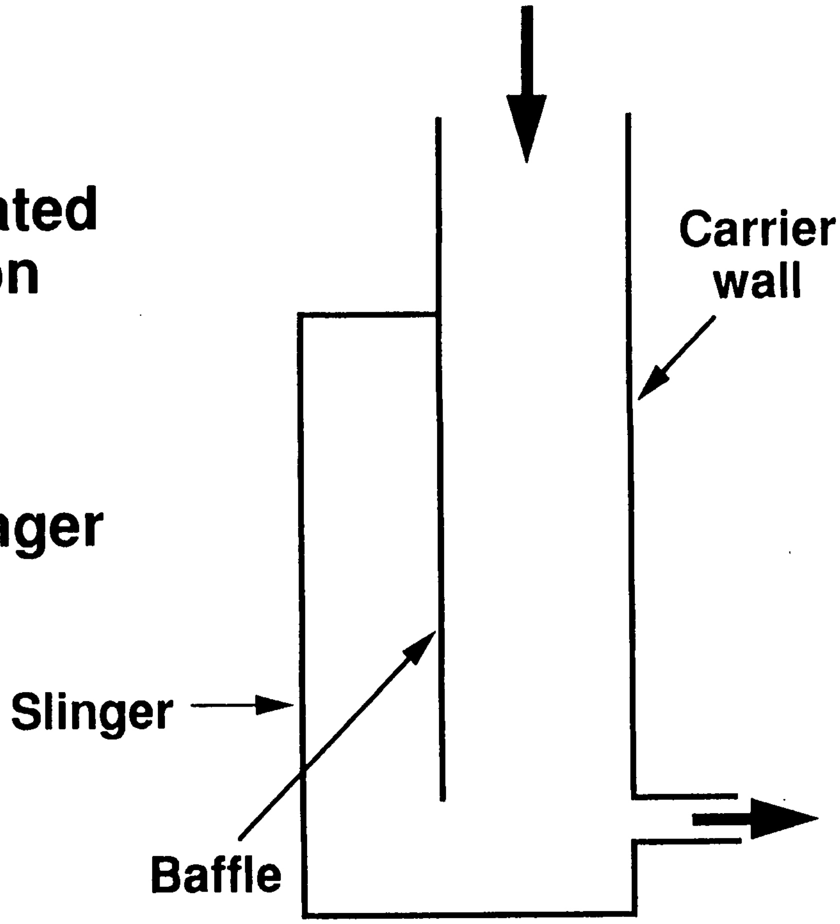

CAVITY NO. 1 (66% BAFFLE)

STATIC PRESSURE ON CARRIER WALL

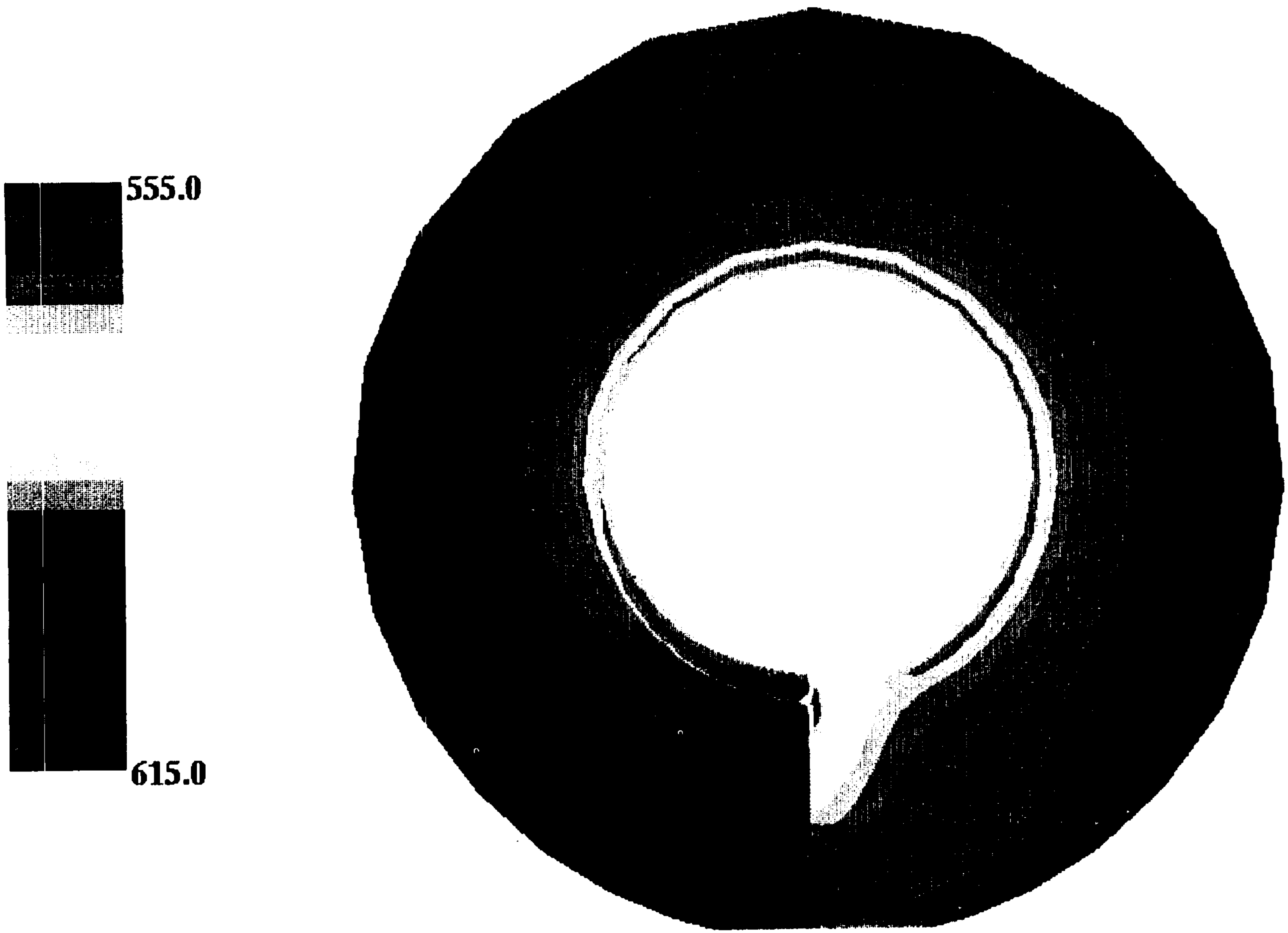

CAVITY NO. 1 (100% BAFFLE)

STATIC PRESSURE ON CARRIER WALL

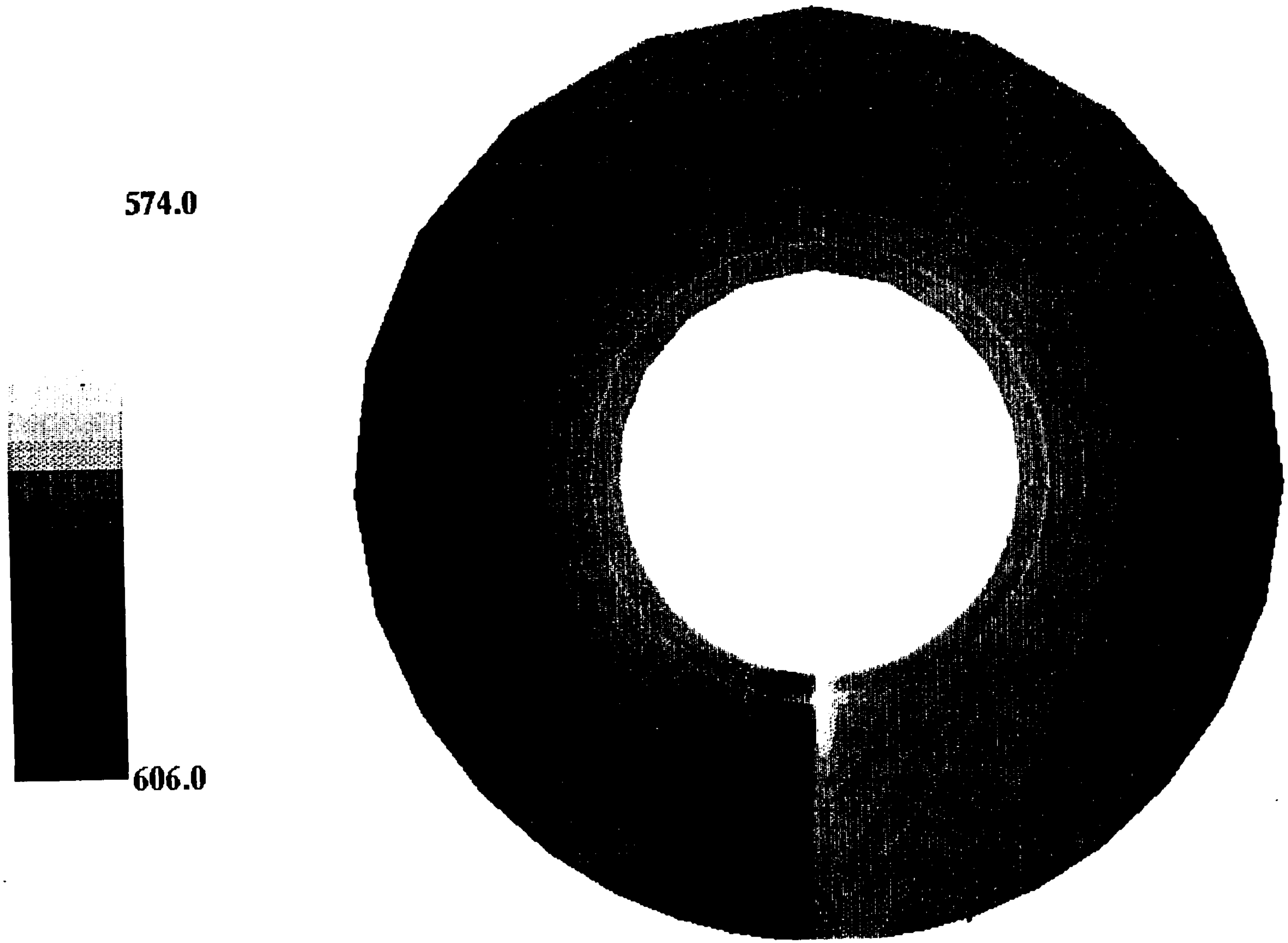

SUMMARY OF 3D ANALYSES

CFDRC

Case	Static Pressure at (psi)				Net ΔP across Tester (psi)		Bearing Inlet Swirl % cage speed	Net Axial Load on Bearings lbf
	Tester Inlet	Bearing Inlet	Bearing Exit	Tester Exit	Computed	Measured		
Drive-side								
Baseline	600	570	555	578	22	24	42	945
66% Baffle	600	585	570	593	7		27	345
100 % Baffle	600	591	576	599	1		21	105
Load-side								
Baseline	600	556	541	564	36	38	60	1,495
66% Baffle	600	586	571	594	6		41	265
100 % Baffle	600	591	576	599	1		38	75

BSMT THERMAL ANALYSIS

CFDRC

1st Law of Thermodynamics

Assuming adiabatic walls

$$\dot{W} = \dot{m}\left[(h + KE)_{out} - (h + KE)_{in}\right]$$

$$\text{Bulk } \Delta T = \frac{h_{out} - h_{in}}{c_p}$$

Solving Enthalpy Equation ➡ Peak ΔT

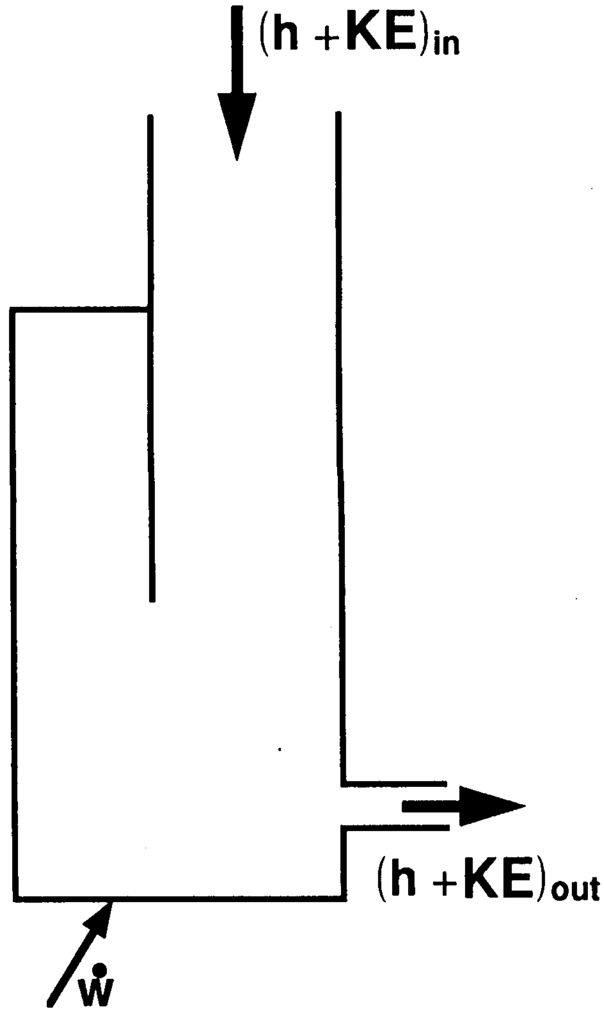

Inlet Cavity No. 1 (Drive-Side)

Case	Power HP	Bulk Temp Rise °F	Peak Temp Rise °F
Baseline	24.9	6.72	17.5
33% baffle	27.5	7.4	
66% baffle	25.5	7.0	24.3
100% baffle	22.9	6.5	

STRUCTURAL ANALYSIS

CFDRC

$$\nabla^4 \omega = \frac{q}{D}$$

where $D = \frac{Et^3}{12(1-\nu^2)}$

E = Elasticity Modulus

ν = Poisson's ratio

t = thickness

ω = deflection

66% Baffle

t (inches)	ω (mil)
1/16	0.4
1/32	3.3

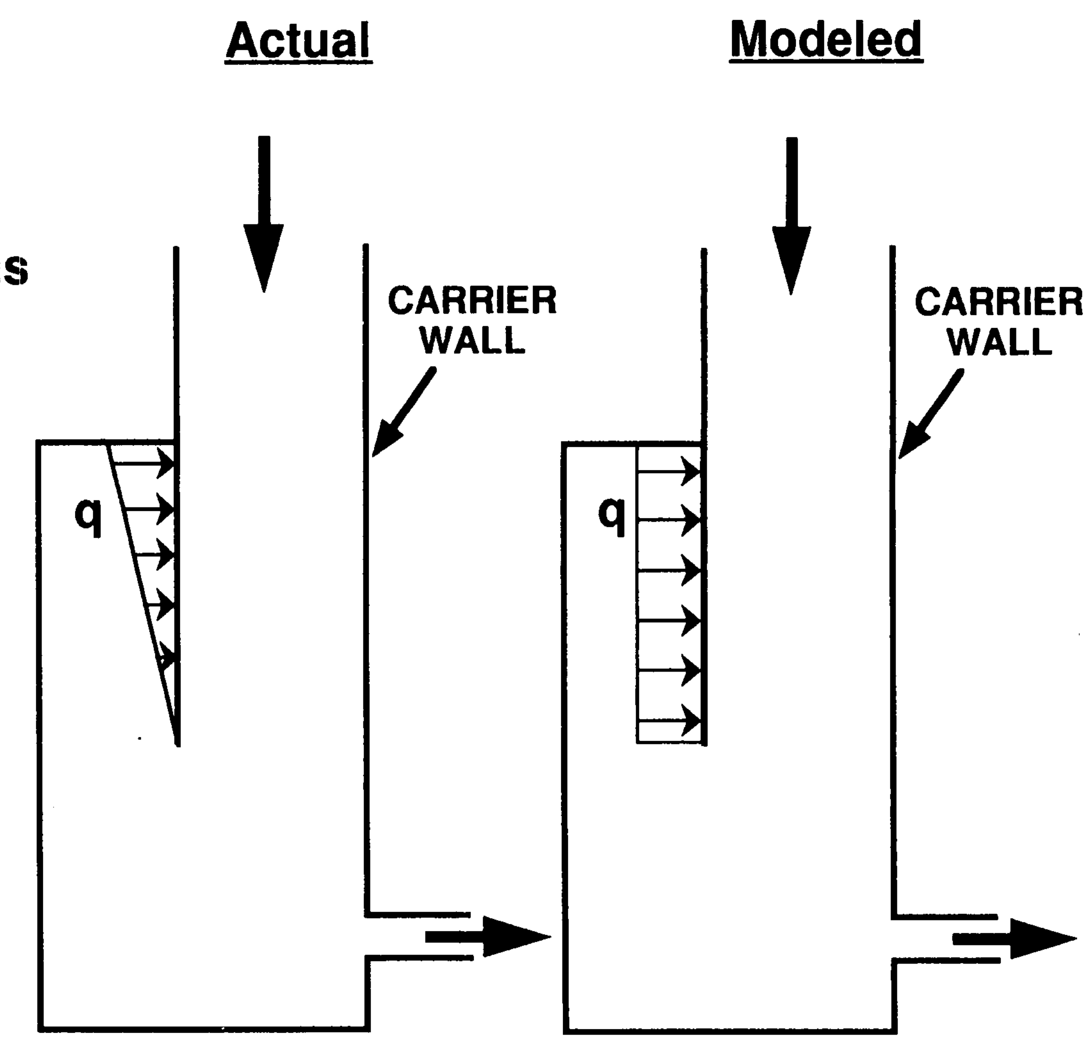

CONCLUDING REMARKS

CFDRC

- Predicted axial (Parasitic) loads are comparable to earlier estimates

- Axial loads can be reduced with baffles

- Baffle deflection and temperature rise are of little concern

N92-32297

Combustion Instability Analysis For Liquid Propellant Rocket Engines

Y.M. Kim, C.P. Chen, and J.P. Ziebarth

University of Alabama in Huntsville
Huntsville, Alabama 35899

Abstract

The multi-dimensional numerical model has been developed to analyze the nonlinear combustion instabilities in liquid-fueled engines. The present pressure-based approach can handle the implicit pressure-velocity coupling in a non-iterative way. The additional scalar conservation equations for the chemical species, the energy, and the turbulent transport quantities can be handled by the same predictor-corrector sequences. This method is time-accurate and it can be applicable to the all-speed, transient, multi-phase, and reacting flows.

Special emphasis is given to the acoustic/vaporization interaction which may act as the crucial rate-controlling mechanism in the liquid-fueled rocket engines. The subcritical vaporization is modeled to account for the effects of variable thermophysical properties, non-unitary Lewis number in the gas-film, the Stefan flow effect, and the effect of transient liquid heating. The test cases include the one- dimensional fast transient non-reacting and reacting flows, and the multi-dimensional combustion instabilities encountered in the liquid-fueled rocket thrust chamber. The present numerical model successfully demonstrated the capability to simulate the fast transient spray-combusting flows in terms of the limiting-cycle amplitude phenomena, correspondence between combustion and acoustics, and the steep-fronted wave & flame propagation. The investigated parameters include the spray initial conditions, air-fuel mixture ratios, and the engine geometry. Stable and unstable operating conditions are found for the liquid-fueled combustors. Under certain conditions, the limiting cycle behavior of the combusting flowfields is obtained. The numerical results indicate that the spray vaporization processes play an important role in releasing thermal energy and driving the combustion instability.

COMBUSTION INSTABILITY ANALYSIS FOR LIQUID PROPELLANT ROCKET ENGINES

Y.M. Kim, C.P. Chen, and J.P. Ziebarth
University of Alabama in Huntsville

10th Workshop for CFD Applications in Rocket Propulsion
April 28-30, 1992
NASA/Marshall Space Flight Center

MOTIVATION

- To predict the nonlinear instability phenomena in liquid-fueled rocket engines.
- To gain deeper understanding of the effects of the design parameters.
- To get the detailed information about driving mechanism of combustion instabilities influenced by the physical processes such as atomization, vaporization , and drop breakup & collision.
- To develop an efficient, accurate, and stable numerical model(pressure-based) for fast transient spray-combusting flows.

APPROACH

- Eulerian-Lagrangian Formulation
  - Pressure-based method
  - Applicable to all speed flows
  - Non-iterative for transient calculations
- Stochastic Particle Tracking Technique
  - Delta function stochastic separated flow(SSF) model
  - Stochastic dispersion width transport(SDWT) model
- Equilibrium, Non-equilibrium, PDF Combustion Models.
- Infinitive & Effective Conductivity Vaporization Model
- Second-Order Upwind Scheme

ISSUES

- Physical processes involved in the driving mechanism of combustion instability.
- Correlation between the vaporization response characteristics and the oscillating flowfield.
- Prediction capabilities for the limiting cycle and the triggered instability.
- Effects of operating conditions, combustor geometry, and stabilization devices.
- Validation of numerical model for nonlinear chamber wave phenomea.

SHOCK TUBE PROBLEM

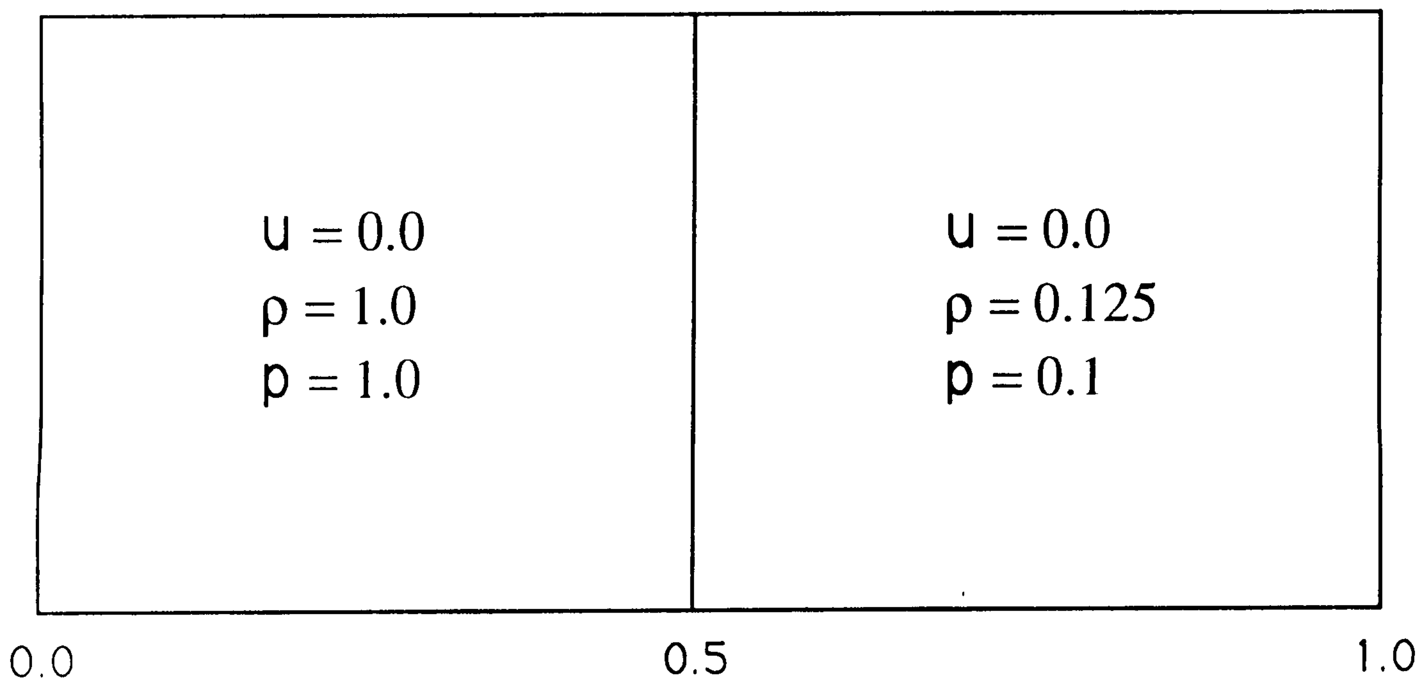

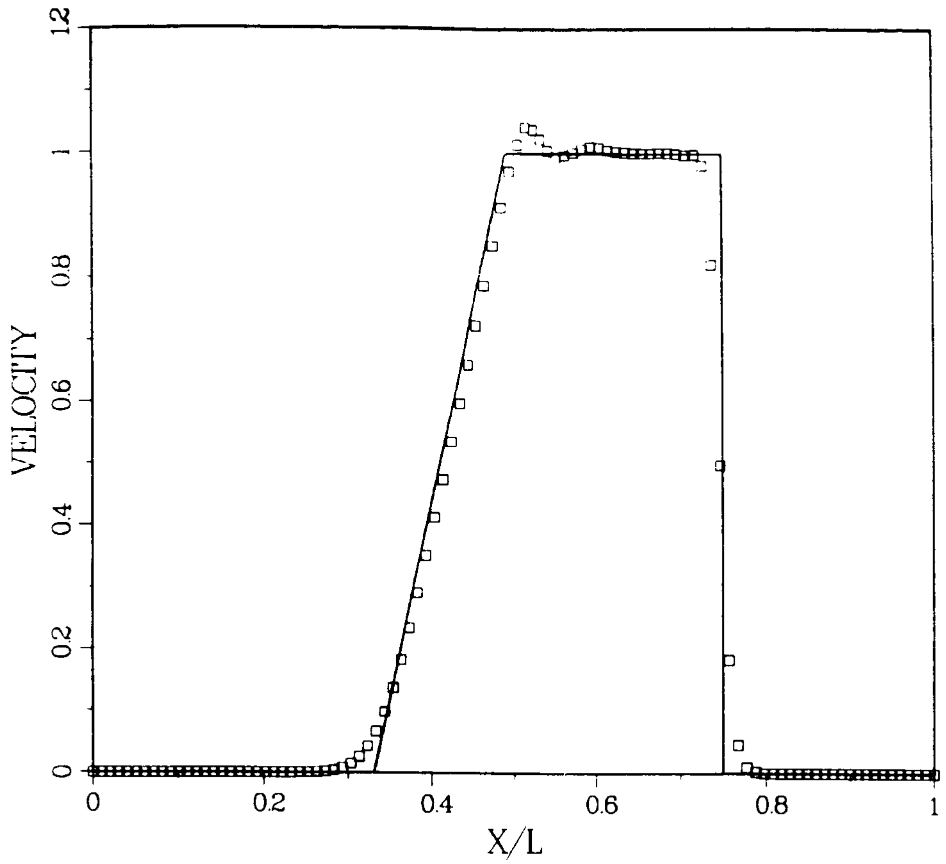

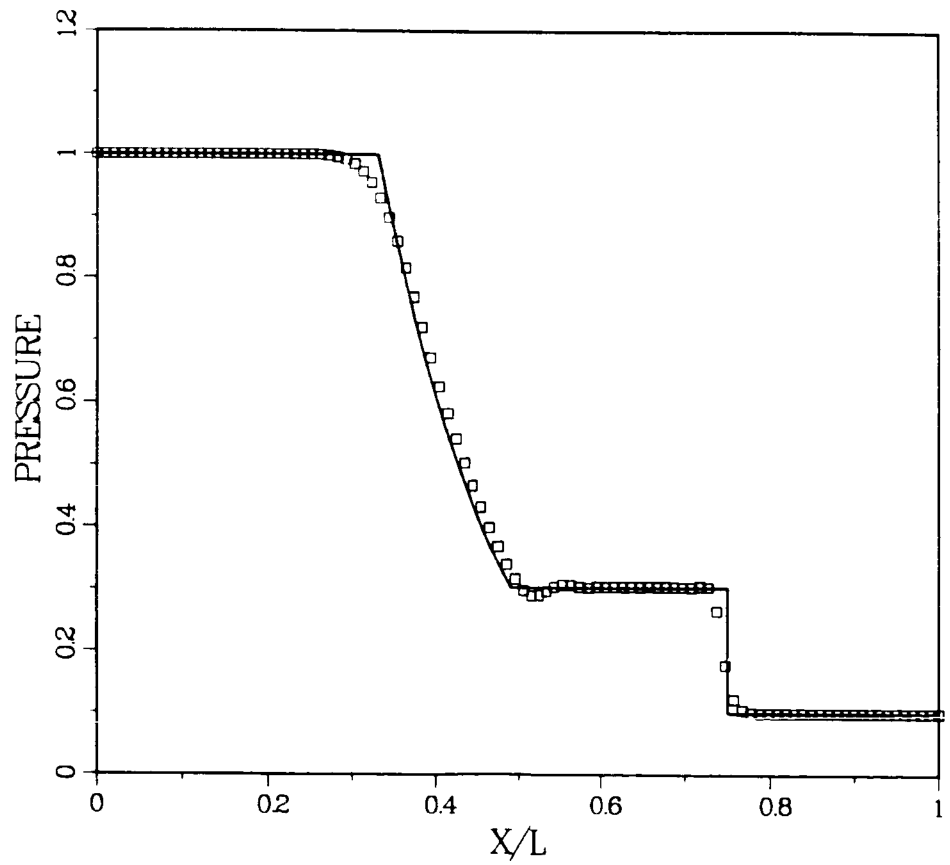

Shock tube problem($CFL = 0.5, N = 100, t = 0.143s$)

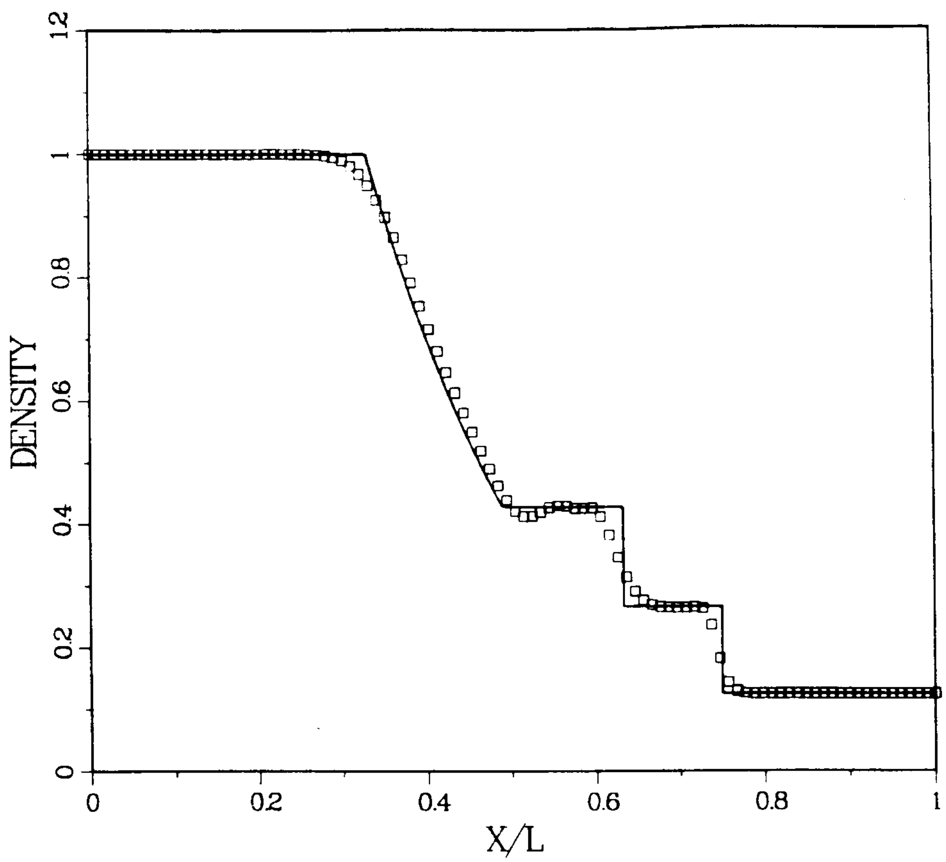

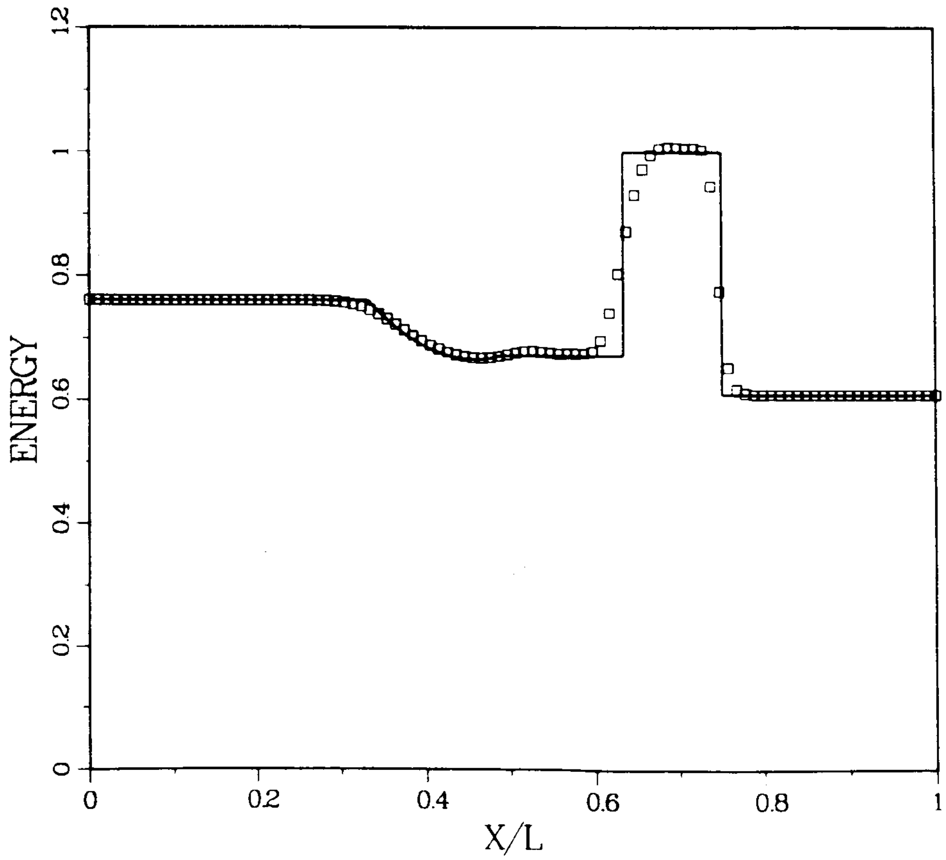

Shock tube problem($CFL = 0.5, N = 100, t = 0.143s$)

FLAME PROPAGATION IN A CLOSED TUBE

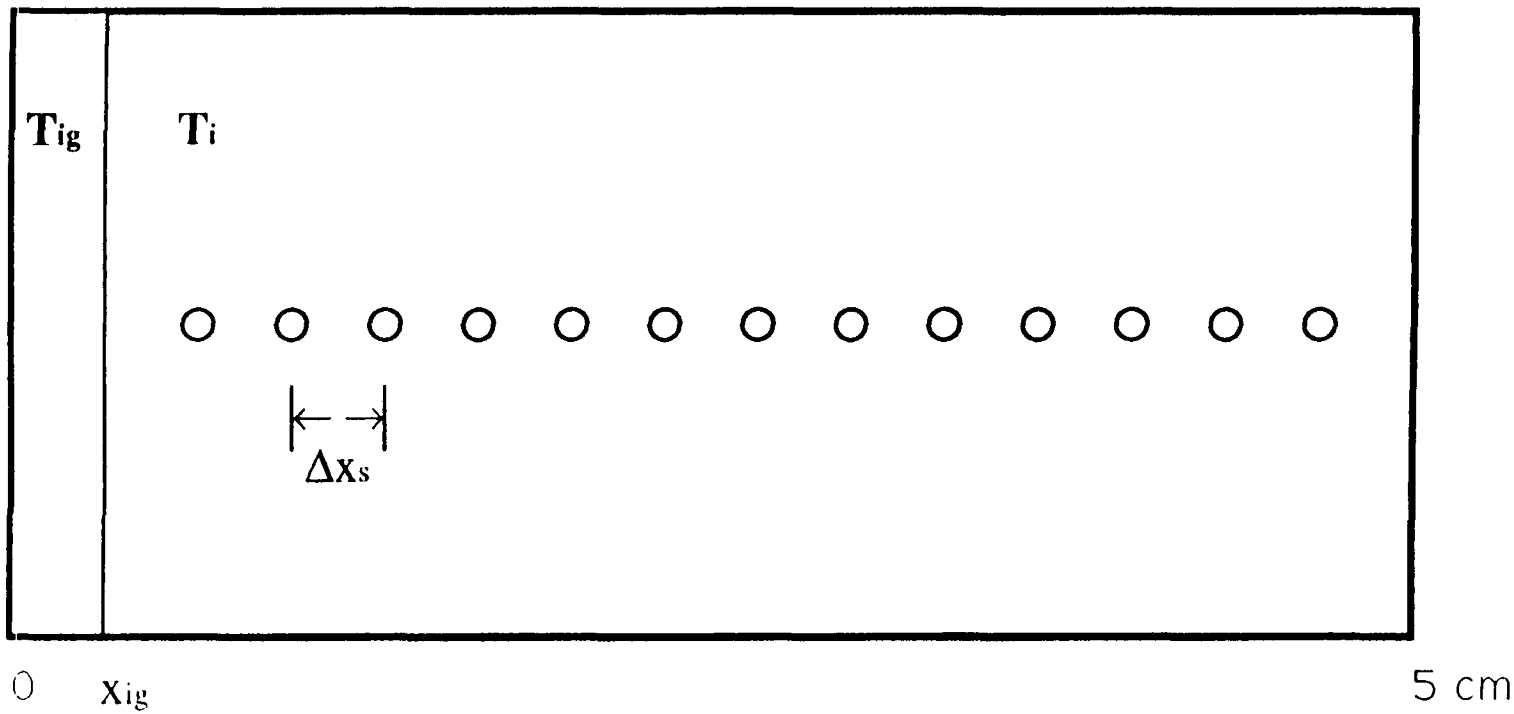

T_{ig} : 1500 K

x_{ig} : 0.25 cm

Δx_s : 0.19 cm

Δx : 0.05 cm

ϕ : 1.0

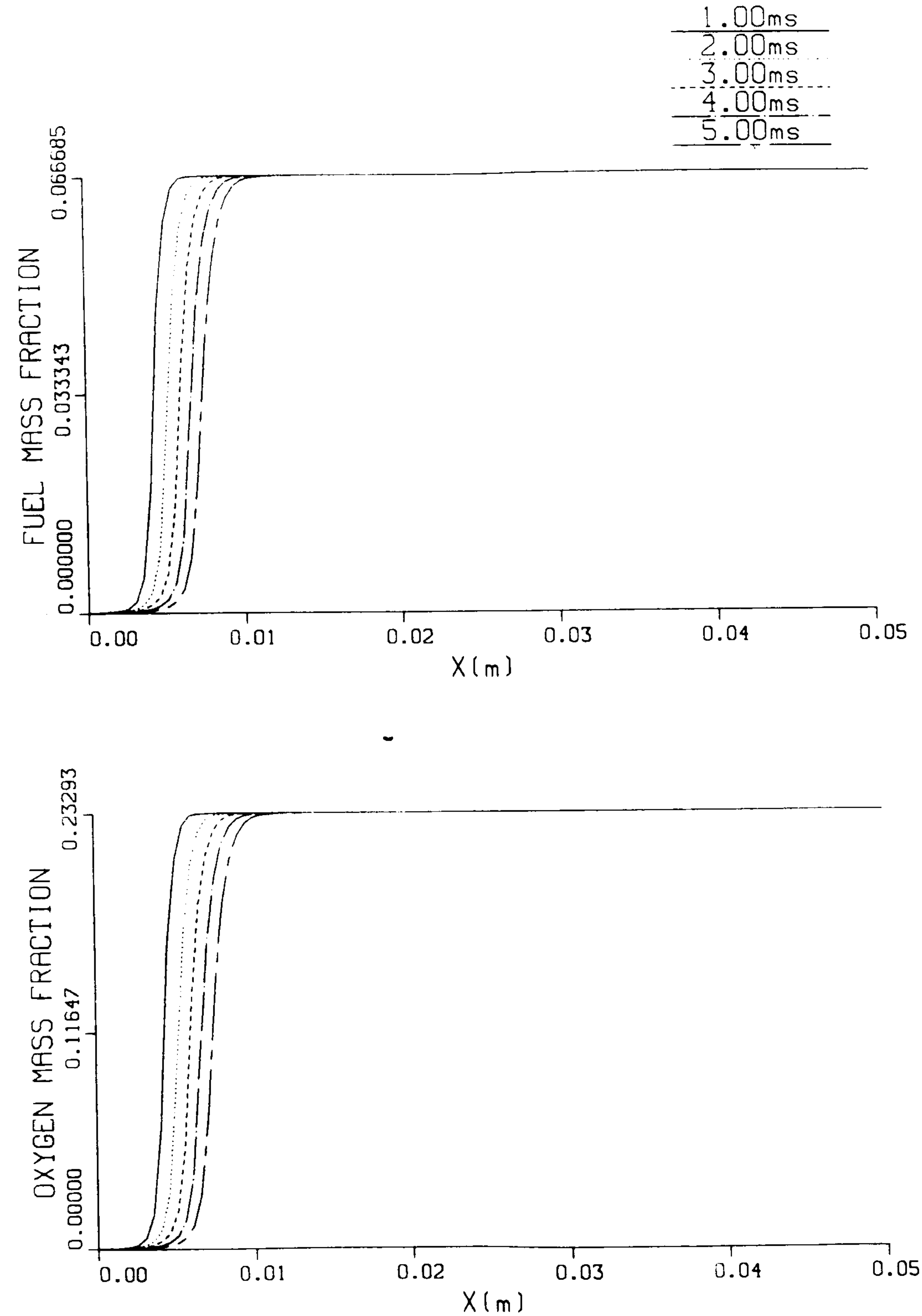

Premixed flame propagation($T_i = 600K, D = 1.8\text{x}10^{-4} m^2/s$)

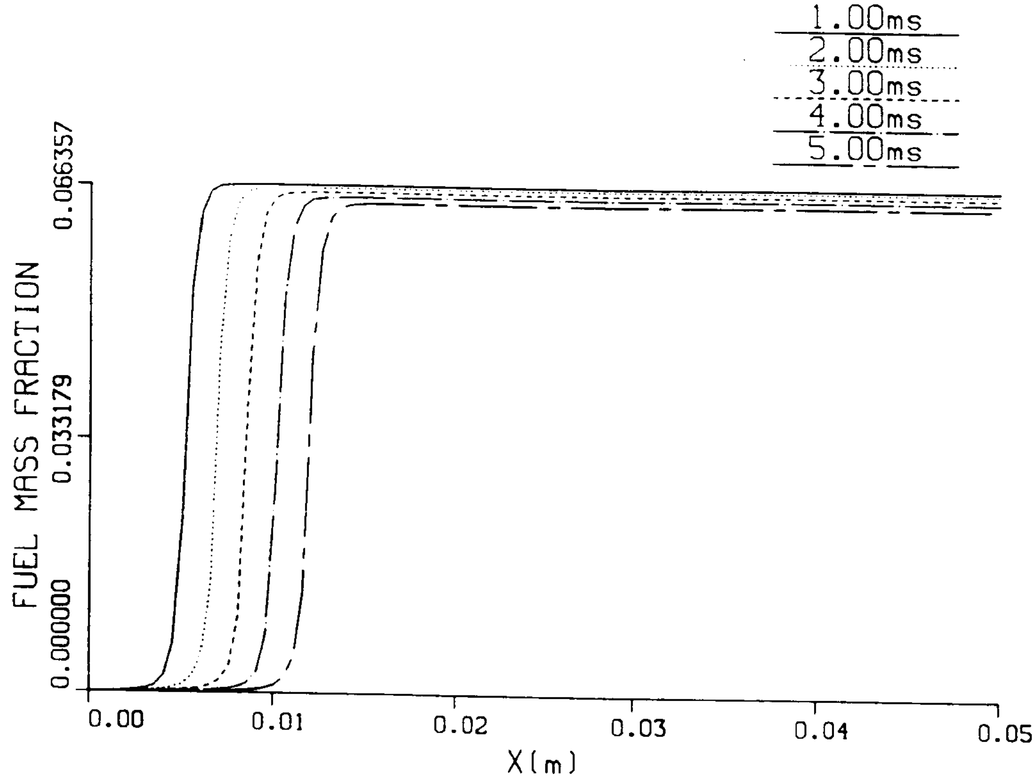

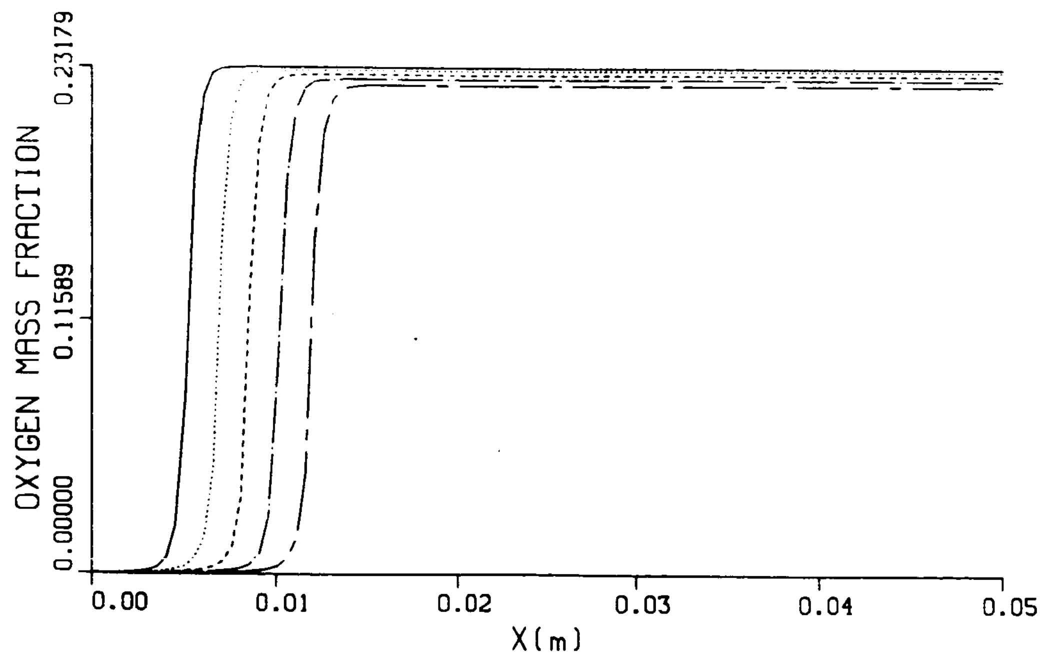

Premixed flame propagation($T_i = 800K, D = 1.8\text{x}10^{-4}m^2/s$)

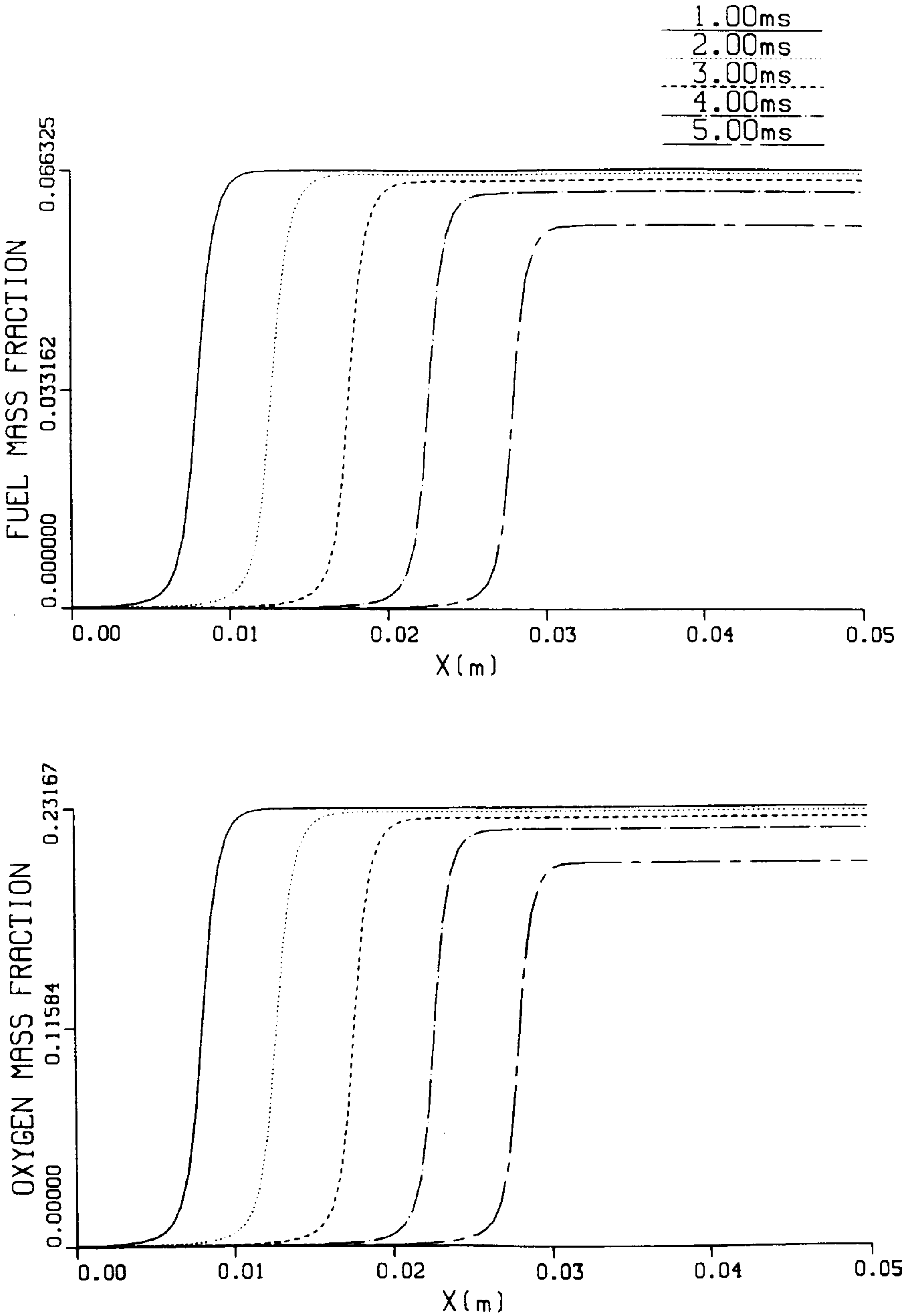

Premixed flame propagation($T_i = 800K, D = 9.0\text{x}10^{-4} m^2/s$)

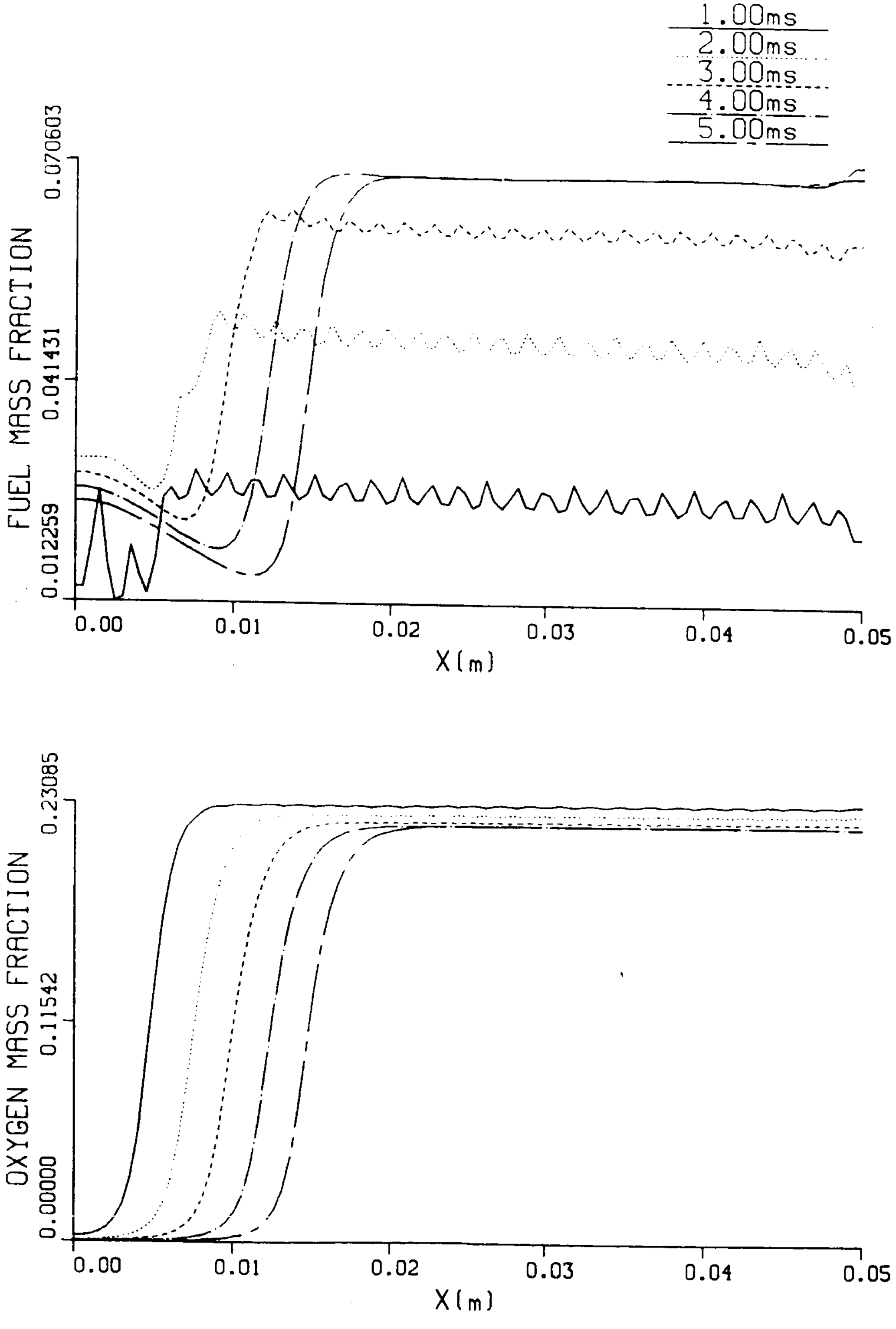

Spray flame propagation($T_i = 800K, D = 9.0\text{x}10^{-4}m^2/s, r_{k,o} = 15\mu m$)

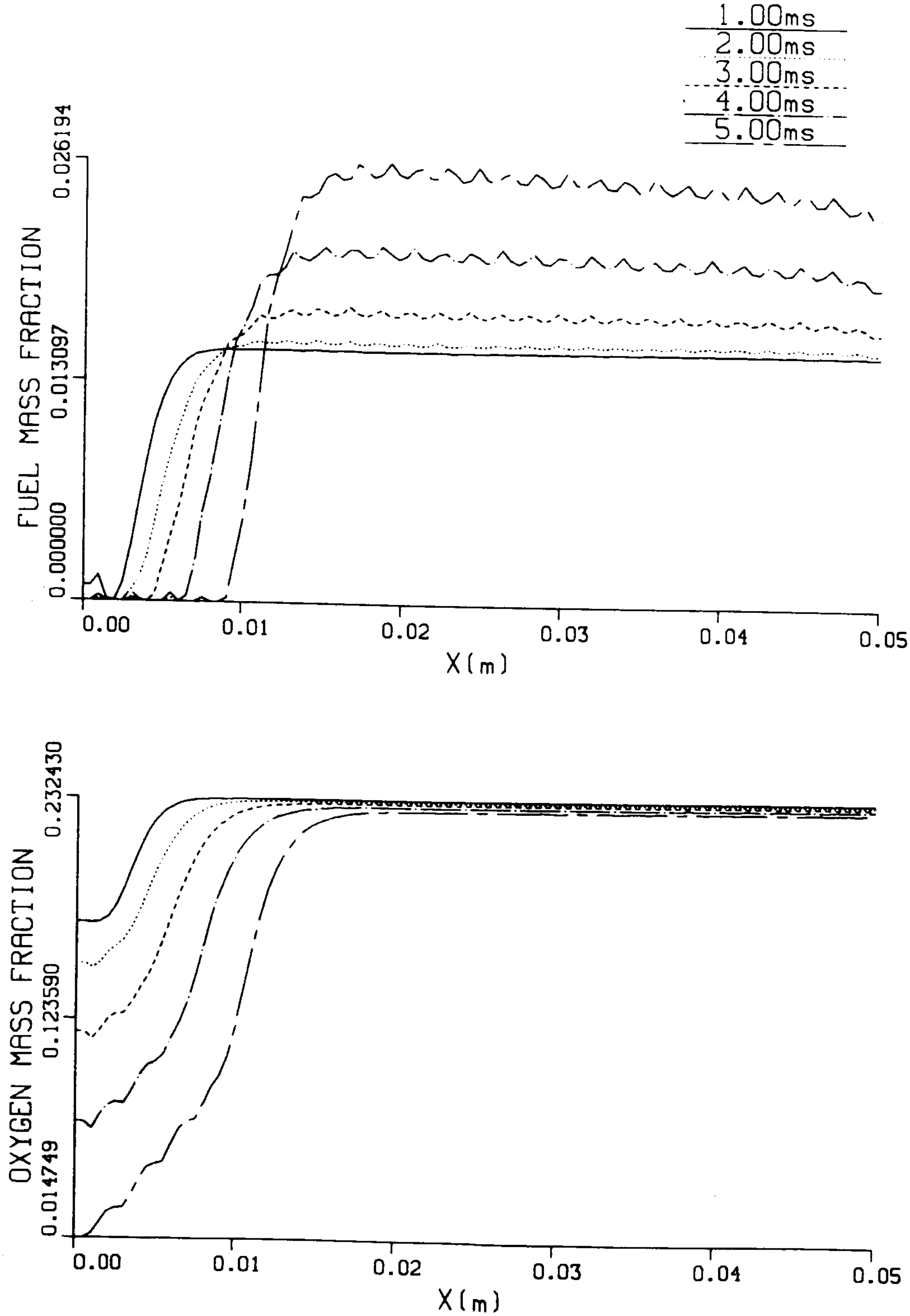

Spray flame propagation($T_i = 800K, D = 9.0\text{x}10^{-4}m^2/s, r_{k,o} = 30\mu m$)

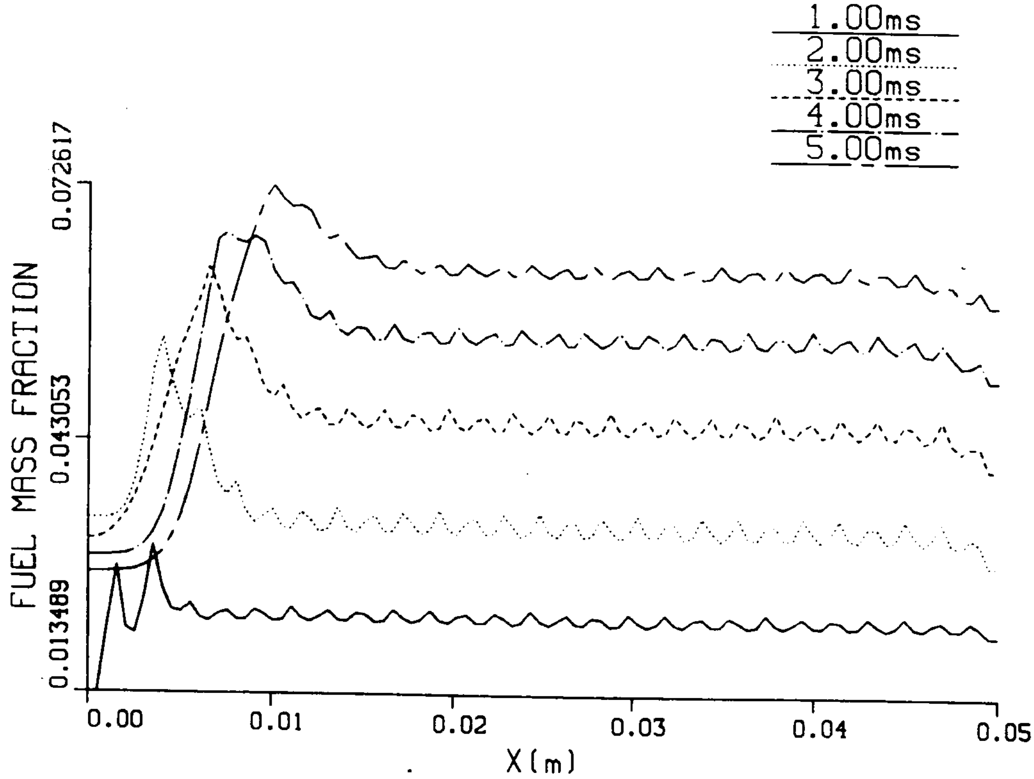

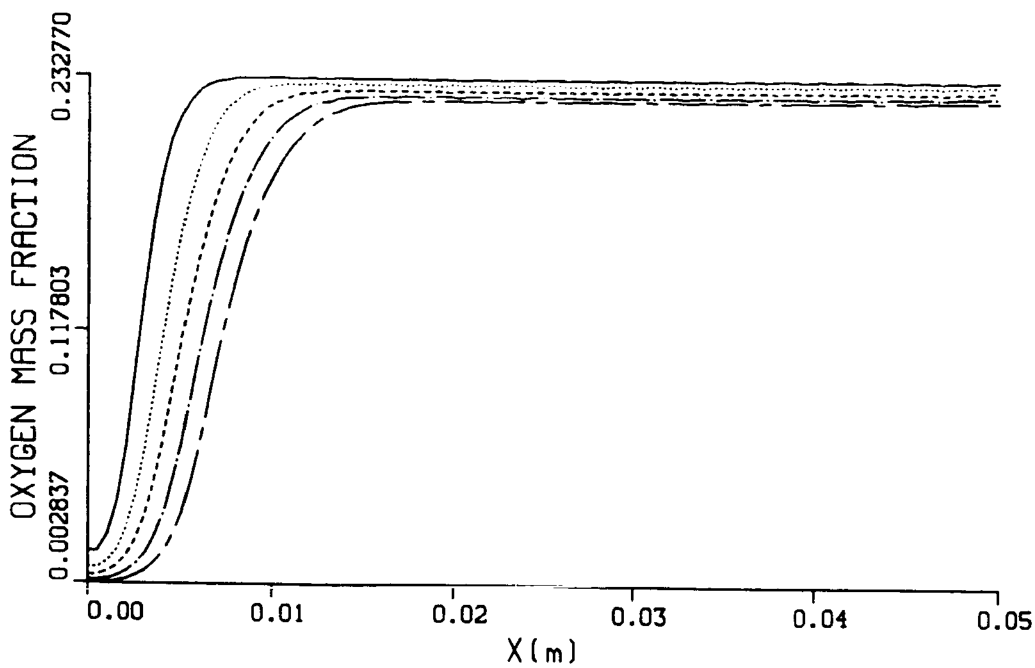

Spray flame propagation($T_i = 600K, D = 9.0\mathrm{x}10^{-4} m^2/s, r_{k,o} = 15\mu m$)

Table 1. Dimensions of Three Liquid-Fuel Rocket Engines.

Engine	L_1(m)	L_2(m)	R(m)	R_t(m)	Θ(deg)
E_1	0.3534	0.2094	0.2266	0.1309	65.44
E_2	0.1767	0.2094	0.2266	0.1309	65.44
E_3	0.1767	0.1047	0.2266	0.1309	47.57

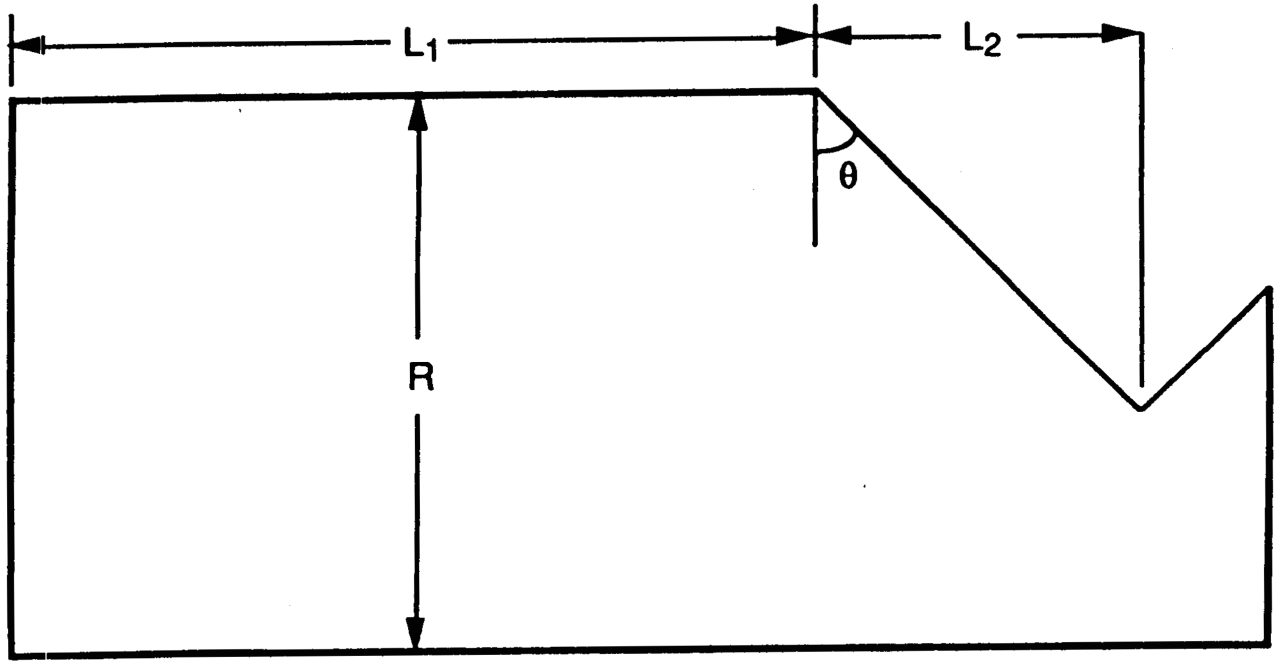

(Atomization + Vaporization + Turbulent Mixing + Chemical Reaction + etc)

$\downarrow$

τ_c (Overall Combustion Time Scale)

IF $\tau_c \approx \tau_a$ (characteristic acoustic time scale) $\longrightarrow$ Combustion Instability

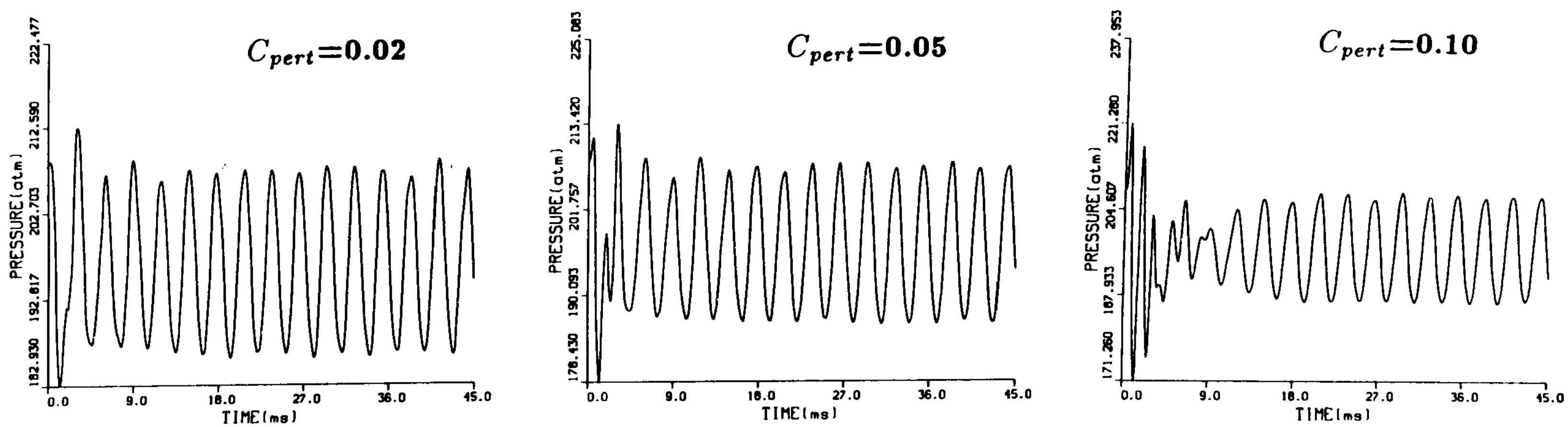

Figure 2 Pressure oscillations for three perturbation levels; ($r_{k,o}$=100μm, ϕ=1.3, X/L_1=1.0, Y/R=0.5, E_1)

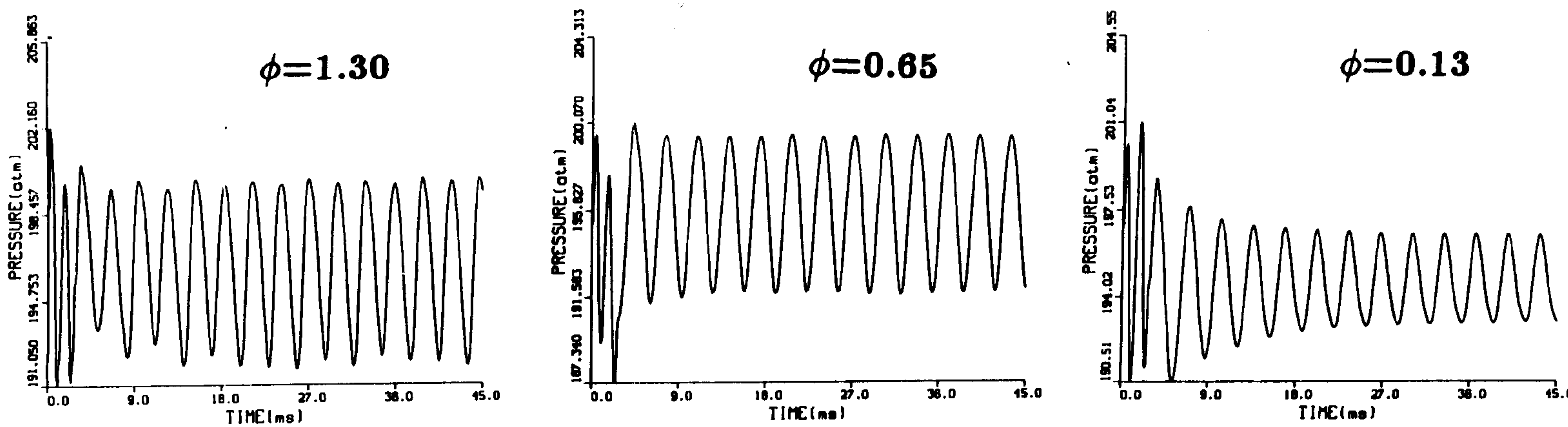

Figure 3 **Pressure oscillations for three overall equivalence ratios; ($r_{k,o}$=100μm, C_{pert}=0.02, X/L_1=0.0, Y/R=0.5, E_1)**

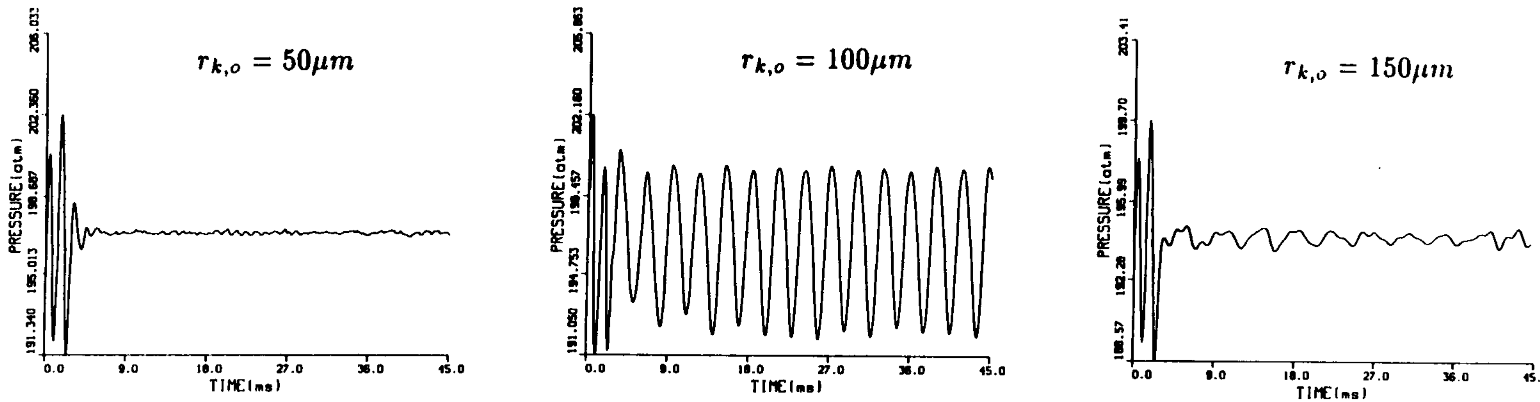

Figure 4 **Pressure oscillations for three initial spray conditions; (ϕ=1.3, C_{pert}=0.02, X/L_1=0.0, Y/R=0.5, E_1)**

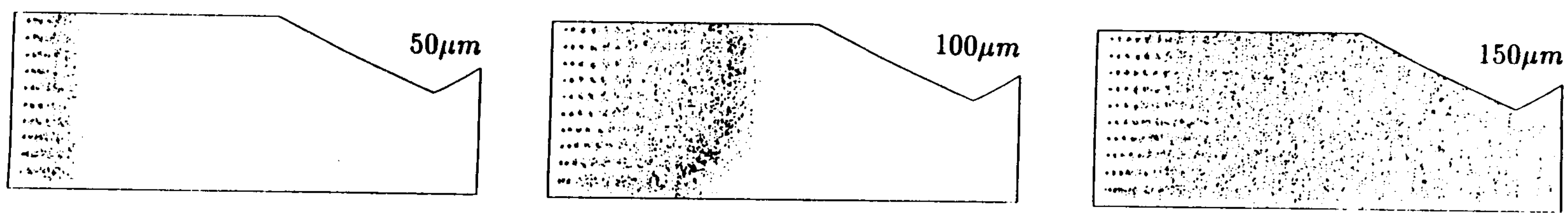

Figure 5 **Spray parcel distribution for three initial spray conditions; (ϕ=1.3, C_{pert}=0.02, E_1)**

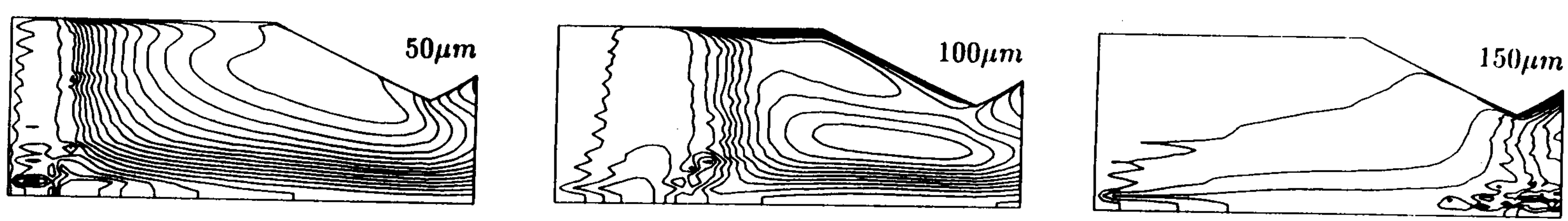

Figure 6 **Contours of temperature for three initial spray conditions; (ϕ=1.3, C_{pert}=0.02, X/L_1=0.0, E_1)**

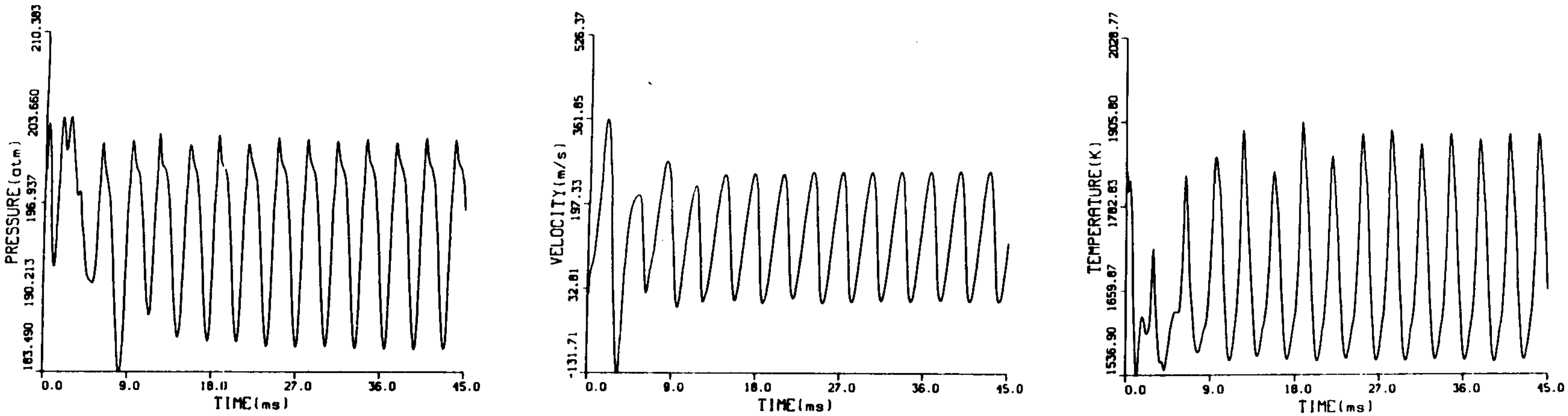

Figure 7 Flow oscillations of pressure, velocity, and temperature; ($r_{k,o}$=120μm, ϕ=1.3, C_{pert}=0.02, X/L_1=0.0, Y/R=0.5, E_1)

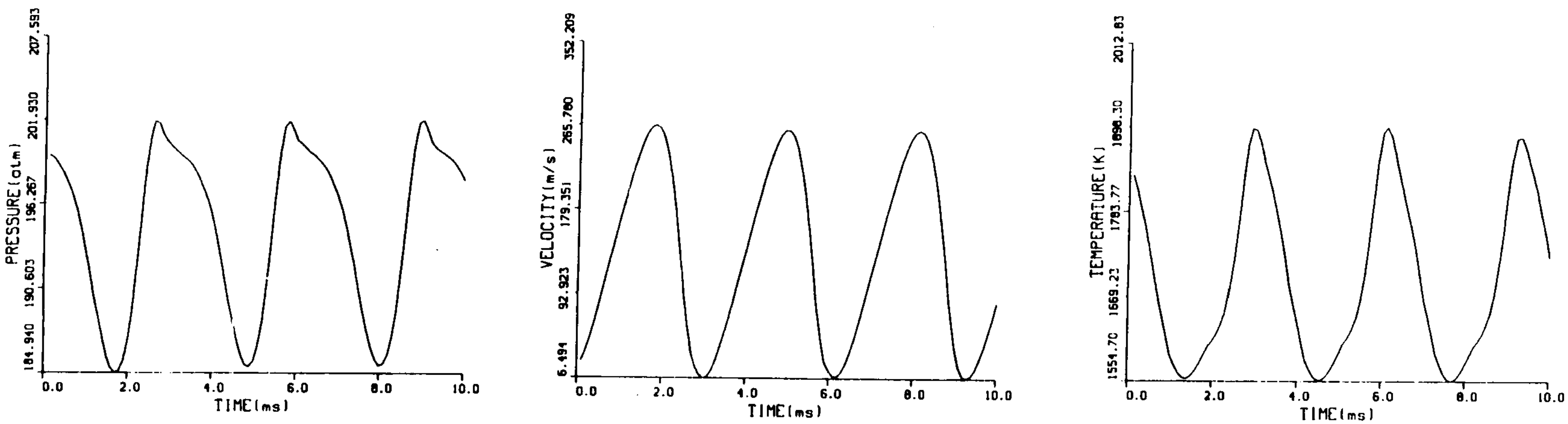

Figure 8 Limit-cycle flow oscillations of pressure, velocity, and temperature; ($r_{k,o}$=120μm, ϕ=1.3, X/L_1=0.0, Y/R=0.5, E_1)

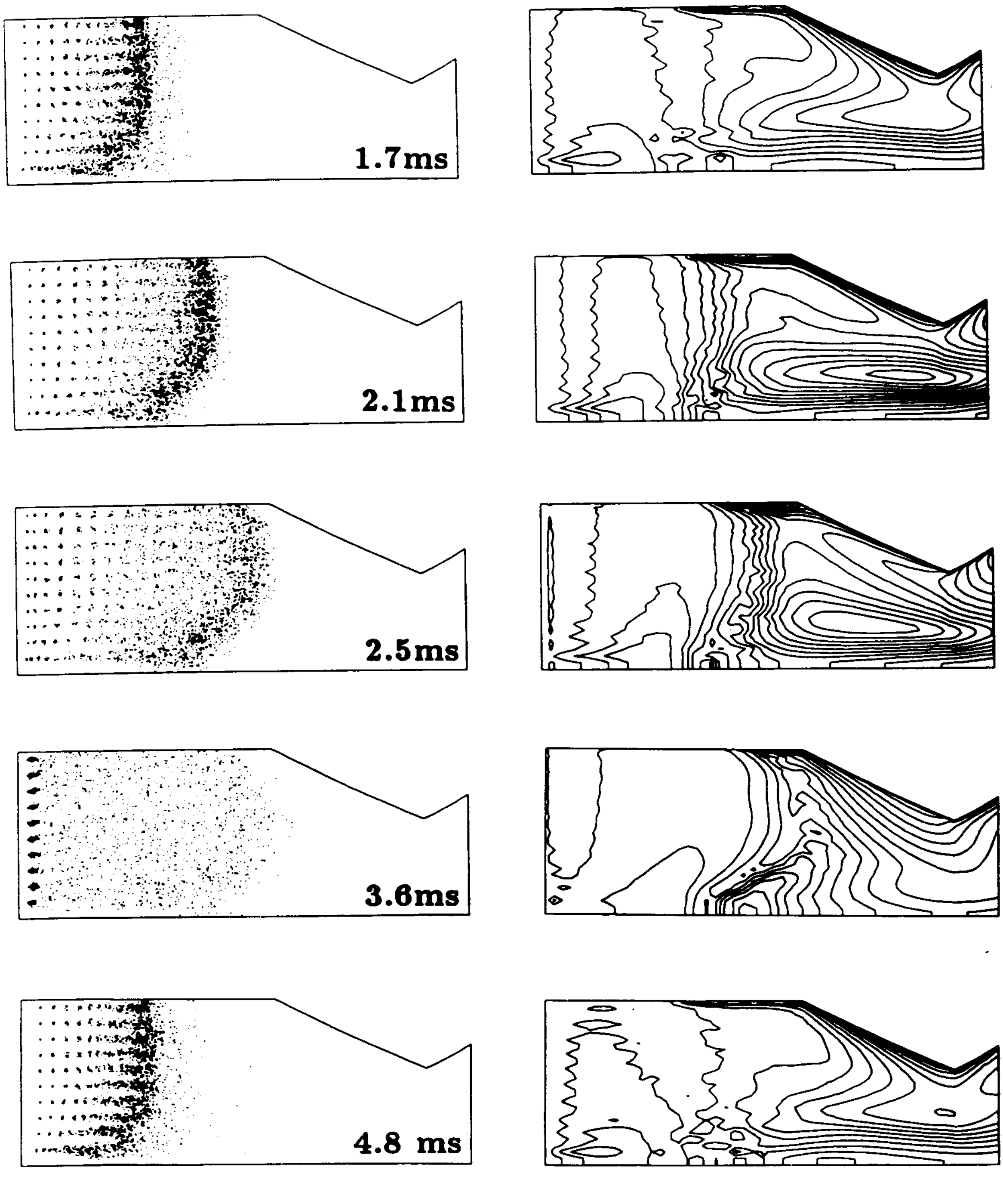

Figure 9 Spray parcel distribution and temperature contours; ($r_{k,o}$=120μm, ϕ=1.3, C_{pert}=0.02, E_1)

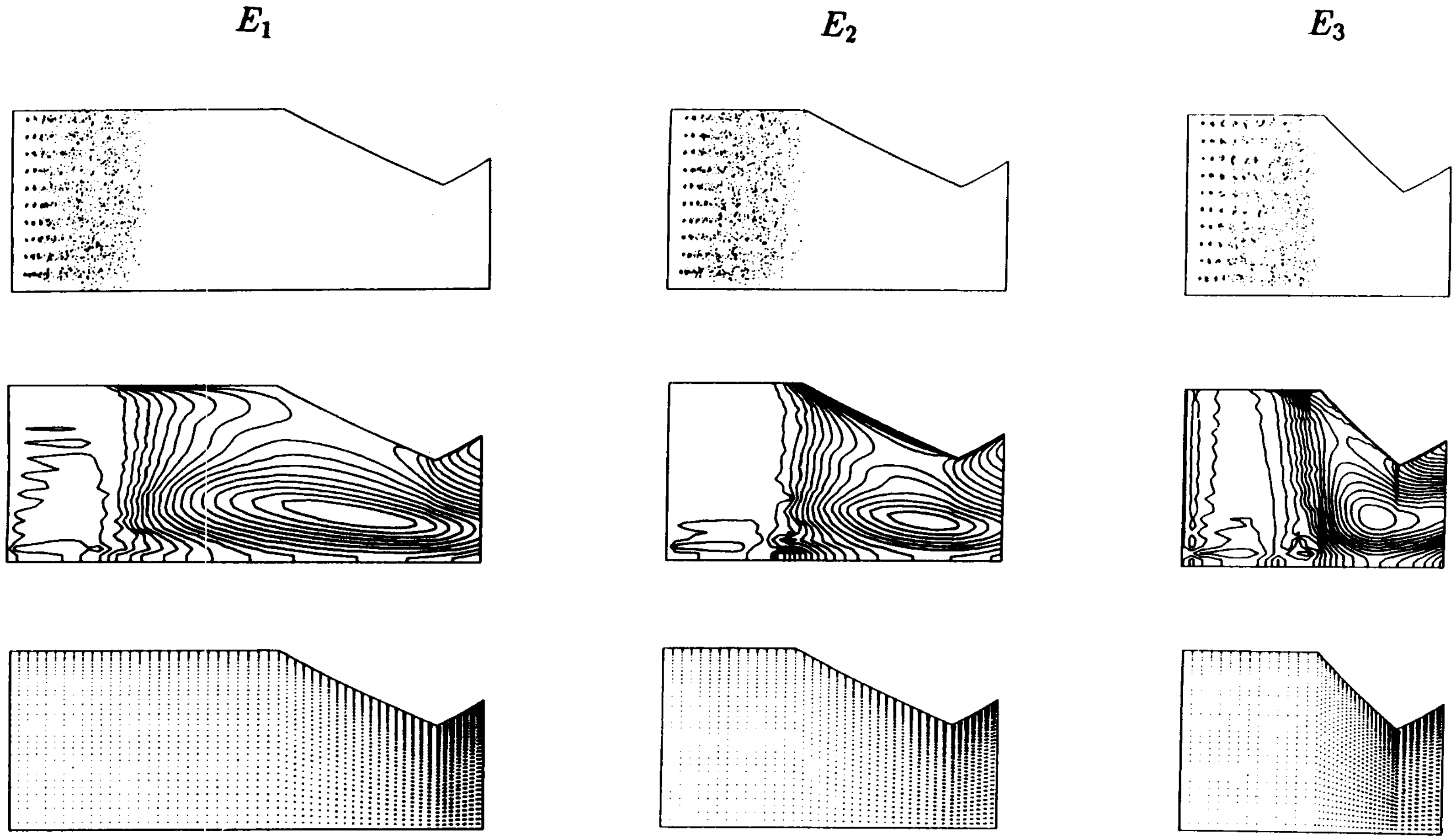

Figure 10 **Spray parcel distribution, temperature contours, and velocity vectors for three engines; ($r_{k,o}$= 70μm, ϕ=0.65, C_{pert}=0.02, Y/R=0.5)**

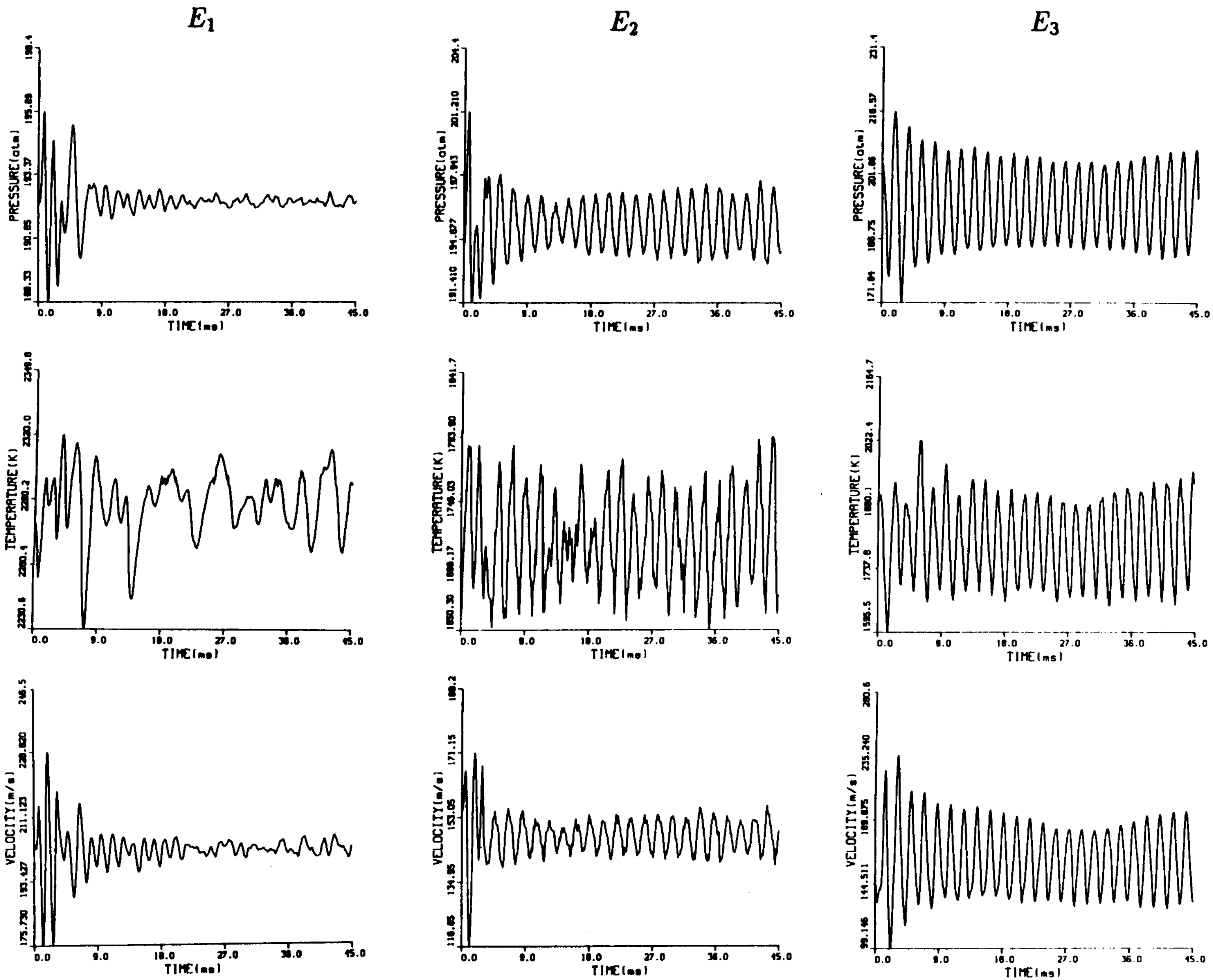

Figure 11 **Stability characteristics for three engines;**

SUMMARIES

- Successful predictions for the unsteady non-reacting, flame-propagating, and spray-combusting flows.
- Variations in the droplet size, the combustor length, and the nozzle length of converging section have a significant effect on the combustion instability.
- Extension to transverse mode instability analysis and incorporation of physical submodels dominantly involved in the driving mechanism of combustion instability.
- Validation of numerical model for linear and nonlinear chamber wave phenomena.

D-6

N92-32298

Inverse Design of a Proper Number, Shapes, Sizes, and Locations of Coolant Flow Passages

George S. Dulikravich
Department of Aerospace Engineering, 233 Hammond Building
The Pennsylvania State University, University Park, PA 16802, USA

During the past several years we have developed an inverse method that allows a thermal cooling system designer to determine proper sizes, shapes, and locations of coolant passages (holes) in, say, an internally cooled turbine blade, a scram jet strut, a rocket chamber wall, etc. Using this method the designer can enforce a desired heat flux distribution on the hot outer surface of the object, while simultaneously enforcing desired temperature distributions on the same hot outer surface as well as on the cooled interior surfaces of each of the coolant passages. This constitutes an over-specified problem which is solved by allowing the number, sizes, locations and shapes of the holes to adjust iteratively until the final internally cooled configuration satisfies the over-specified surface thermal conditions and the governing equation for the steady temperature field.

The problem is solved by minimizing an error function expressing the difference between the specified and the computed hot surface heat fluxes. The computed outer surface heat flux q_{out}^{comp} will not be the same as the specified outer surface heat flux, q_{out}^{spec}. A properly scaled L-2 norm of the difference between the specified outer surface heat flux, q_{out}^{spec}, and the computed outer surface heat flux, q_{out}^{comp}, is then minimized by iteratively changing the sizes, shapes, and locations of coolant passages. Starting with a large number of guessed holes, all unnecessary coolant passages are efficiently eliminated when their sizes reduce below a prespecified minimal allowable value. The minimization has been performed automatically using a standard optimization algorithm of Davidon-Fletcher-Powell. Local minimas in the optimization process were successfully avoided by changing the formulation for the objective function whenever the local minimas were detected. The temperature field analysis was performed using our highly accurate boundary integral element code with linearly varying temperature along straight surface panels. Examples of the inverse design applied to internally cooled turbine blades and scram jet struts (coated and non-coated) having circular and non-circular coolant flow passages will be shown.

PRECEDING PAGE BLANK NOT FILMED

1. Mathematical model

Steady heat conduction in internally cooled objects is modeled as a boundary value problem for Laplace's equation over a multiply-connected domain.

Assumptions are:
- temperature field is steady
- solid material of the blade is thermally isotropic.
- thermal expansion is neglected

Governing equation is Laplace's equation:

$$\boxed{\nabla^2 T = 0} \qquad (1)$$

2. Objectives

Determine:
- the exact number of the holes,
- radii of the holes,
- locations of the holes,

such that relative error between specified and computed heat fluxes at the outer boundary is minimized.

3. Boundary Conditions - Ill Posed Boundary Value Problem

Both, Dirichlet and Neumann boundary conditions are specified on the outer boundary. Such an overspecified problem can be solved by inverse (design) approach. The problem is solvable since the domain is multi-connected: positions, shapes and dimensions of the holes will provide additional degrees of freedom.

4. Constraints

Besides minimizing the heat flux error, optimized shape has to satisfy these constraints:
- minimum distance between holes,
- minimum distance between holes and the outer boundary

5. Objective Functions

Two different definitions of objective function were used. The difference between the specified and the heat flux and heat flux obtained by the current design can be computed as a global error:

$$F_1(x) = \frac{\sum_{j=1}^{N} \left(q_j^c - q_j^r\right)^2}{\sum_{j=1}^{N} \left(q_j^r\right)^2} \tag{2}$$

or as a local error in heat flux at each node:

$$F_2(x) = \sum_{j=1}^{N} \frac{\left(q_j^c - q_j^r\right)^2}{\left(q_j^r\right)^2} \tag{3}$$

Two constraints were incorporated into the objective function using a barrier function

$$B(g(x), w_b) = \frac{1}{w_b} \sum_{i=1}^{M} \left[\sum_{j=1}^{N_2} \frac{d^s}{\left(D_j^s - d^s - r_i\right)} + \sum_{k=1}^{M} \frac{d^h}{\left(D_k^h - d^h - r_i - r_k\right)} \right] \tag{4}$$

The composite objective function can have two forms:

$$F_i(g(x), w_b) = F_i(x) + B(g(x), w_b), \quad i = 1, 2 \tag{5}$$

depending whether global or local objective function is used for its evaluation.

2. The Optimization Procedure

The optimization procedure consists of the following steps:

(1) Specify shape of the outer surface and coating of the turbine blade.

(2) Specify desired temperature T_j^r values on the outer and inner surfaces.

(3) Specify desired heat flux q_j^r values on the outer surface.

(4) Specify manufacturing constraints:

(i) minimum distance d^s between holes and the outer surface,

(ii) minimum distance d^h between any two neighboring holes.

(5) Specify initial guess for the number of holes, M, their dimensions, r_i, and locations of the centers of the holes, x_i and y_i. Thus, there will be 3×M design variables if we limit ourselves to circular holes only.

(6) Using the Boundary Element Method, the Laplace's equation for a given domain and temperature boundary conditions is solved and heat fluxes at the outer boundary are computed. The Laplace's equation is solved 3×M times, ones for each perturbed design variable to compute the gradient.

(7) Determine relative error between specified and computed heat fluxes and evaluate the objective function. At the same time the barierr function has to be evaluated to determine the composite objective function F_i.

(8) Davidon-Powel-Fletcher technique is used to find the new values of design variables repeating the optimization procedure from the step (6) until the corresponding composite objective function F is less than a prespecified value If the dimension of a hole becomes less than a prespecified value, the hole is eliminated from further optimization. If the optimization procedure stalls in a local minimum the objective function formulation is changed from Eq. 2 to Eq. 3 while continuing with optimization from the step (6).

References

Kennon, S.R. and Dulikravich, G.S., (1985), "The Inverse Design of Internally Cooled Turbine Blades," *ASME Journal of Eng. Gas Turbines and Power*, January 1985, pp. 123-126.

Kennon, S.R. and Dulikravich, G.S., (1986a), "Inverse Design of Multiholed Internally Cooled Cooled Turbine Blades," *Int. Jour. of Num. Meth. in Eng.*, Vol. 22, pp. 363-375.

Kennon, S. R. and Dulikravich, G. S. (1986b), "Inverse Design of Coolant Flow Passages Shapes With Partially Fixed Internal Geometries," *International Journal ofTurbo & Jet Eng.*, Vol. 3, (1), pp. 13-20.

Chiang, T.L. and Dulikravich, G.S., (1986), "Inverse Design of Composite Turbine Blade Circular Coolant Flow Passages," *ASME Journal of Turbomachinery*, Vol. 108, pp. 275-282.

Dulikravich, G.S., (1988), "Inverse Design and Active Control Concepts in Strong Unsteady Heat Conduction," *Applied Mechanics Reviews*, Vol. 41, No. 6, June 1988, pp. 270-277.

Dulikravich, G.S. and Kosovic, B., (1991), "Minimization of the Number of Cooling Holes in Internally Cooled Turbine Blades", ASME paper 91-GT-103, ASME Gas Turbine Conference, Orlando, FL, June 2-6, 1991; also to appear in *Internat. Jour. of Turbo & Jet Engines*, 1992.

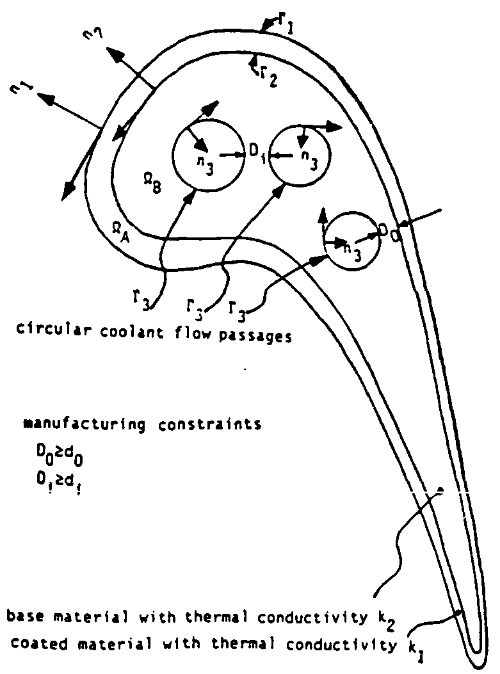

Fig. 1 Geometry and manufacturing constraints

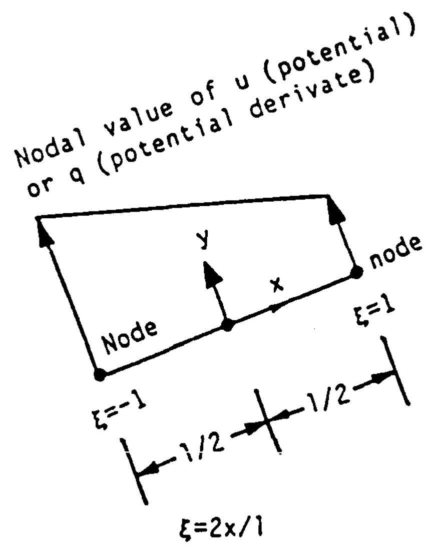

Fig. 2b Linear element

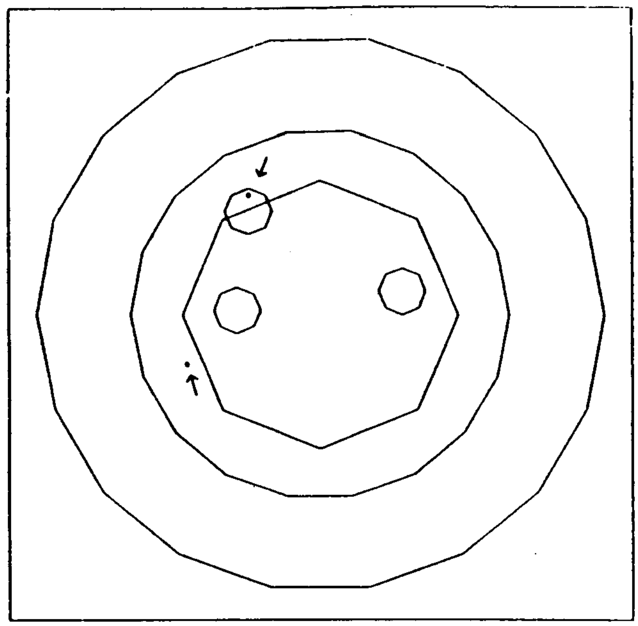

Fig. 1.1 Initial configuration (three holes) and final configuration (one large centrally located hole and two dots marked with arrows) corresponding to a solution with 0.1% integrated flux error.

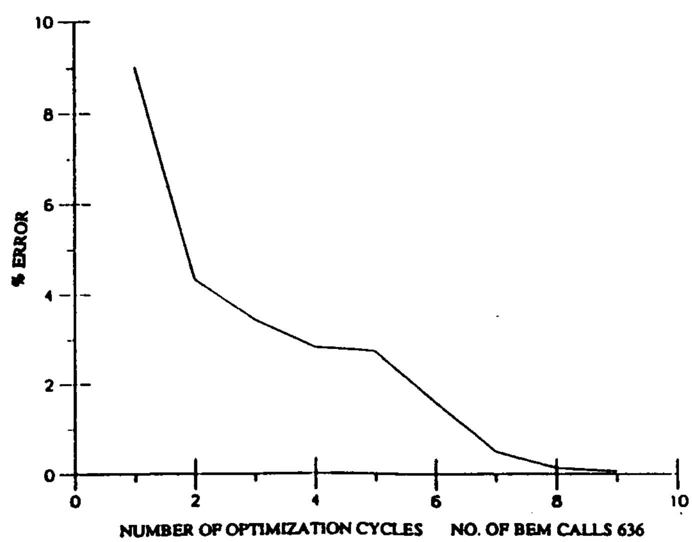

Fig. 1.2 Integrated heat flux error (L_2 norm) convergence history during the optimization.

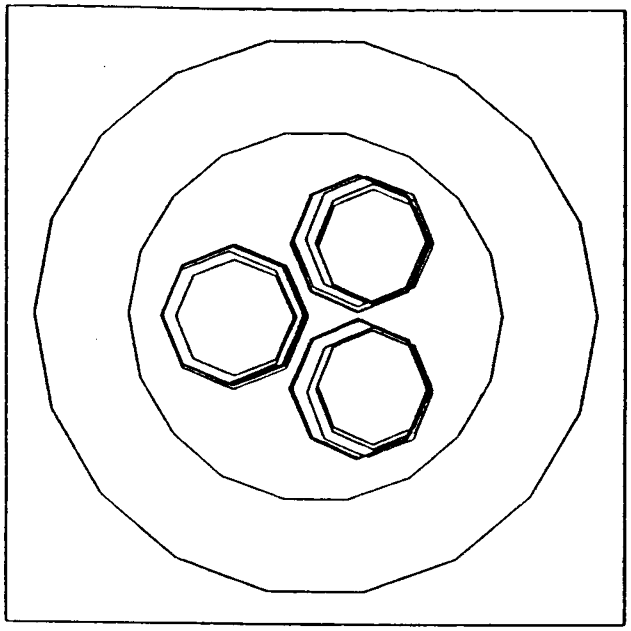

Fig. 1.3 Initially symmetrically located holes of identical size maintain a symmetric configuration throughout the iterative process.

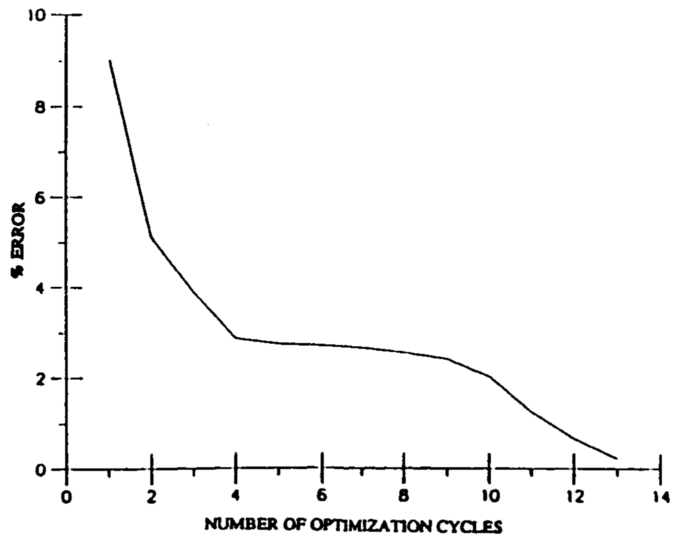

Fig. 1.4 Convergence history of the three-hole symmetrical configuration.

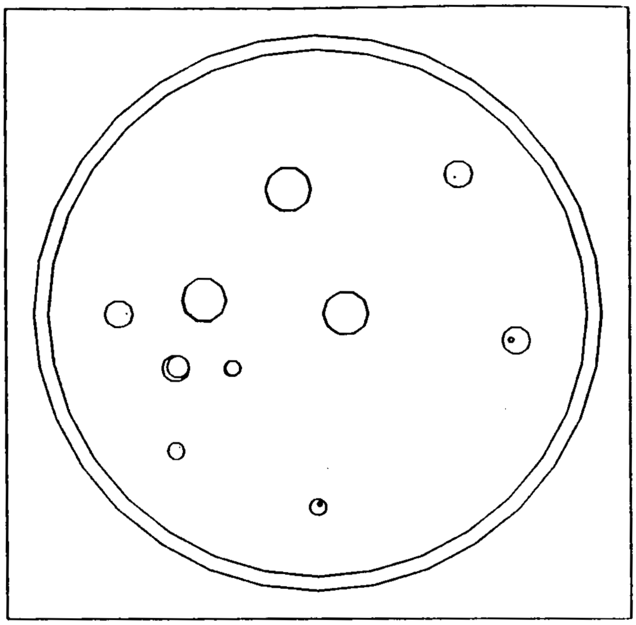

Fig. 1.5 Coated disk problem with initially ten holes. Convergence history shows five holes are reduced to zero. Hole elimination method was not used.

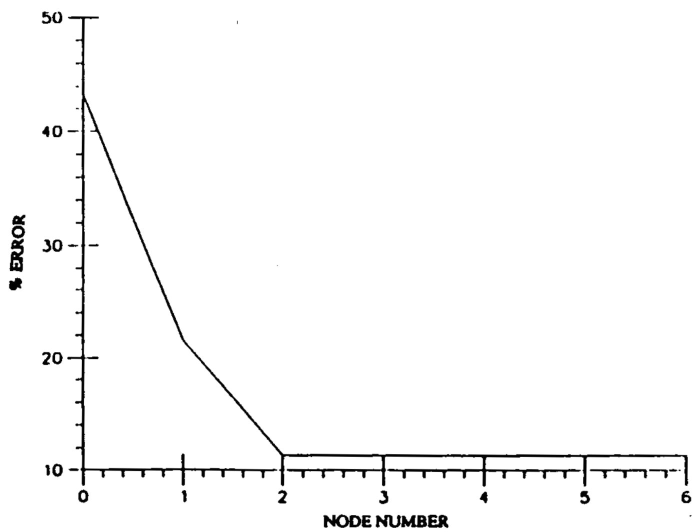

Fig. 1.6 Convergence history for a circular domain with initially ten holes. Hole elimination method was not used. Minimization process terminates in a local minimum.

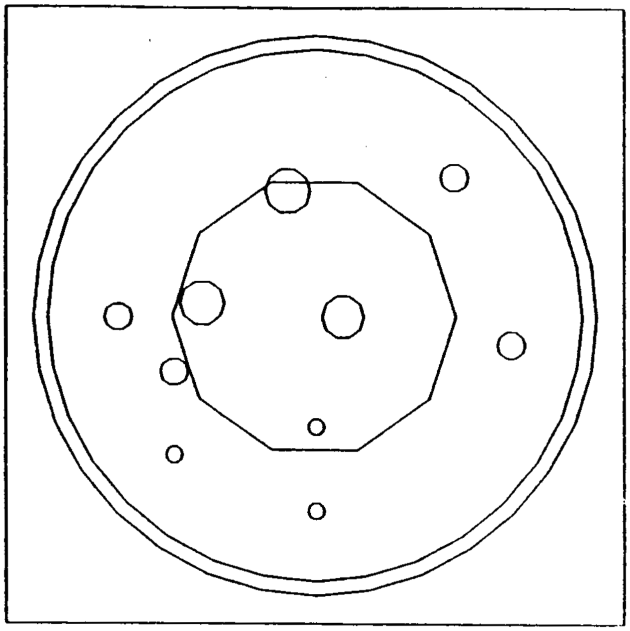

Fig. 1.7 Coated disk problem with initially ten holes. Hole elimination method was used together with objective function switching.

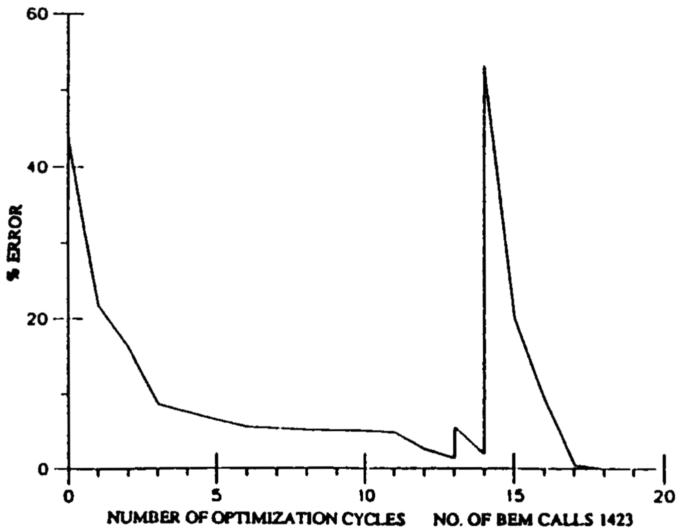

Fig. 1.8 Convergence history for a circular domain with initially ten holes when hole elimination method is applied together with objective function switching. Discontinuities represent changing of the objective function.

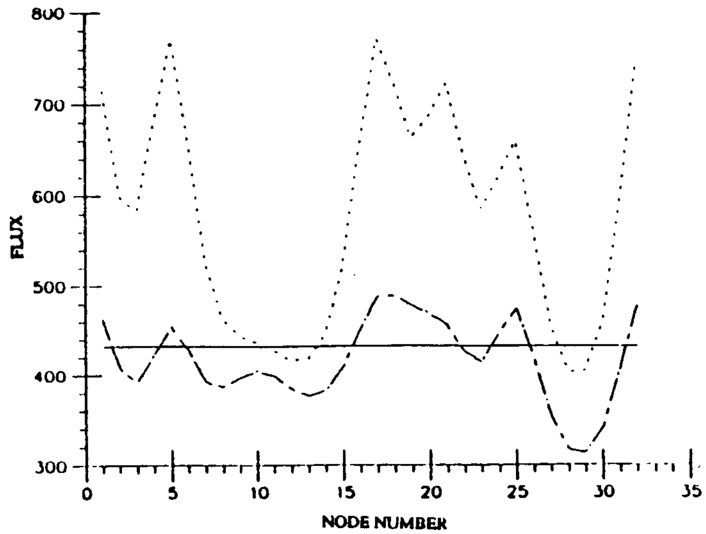

Fig. 1.9 Initial (·········), intermediate (– · – · –) and final (———) heat flux distribution through the outer boundary for a cylinder with ten holes initially. Hole elimination method was not used.

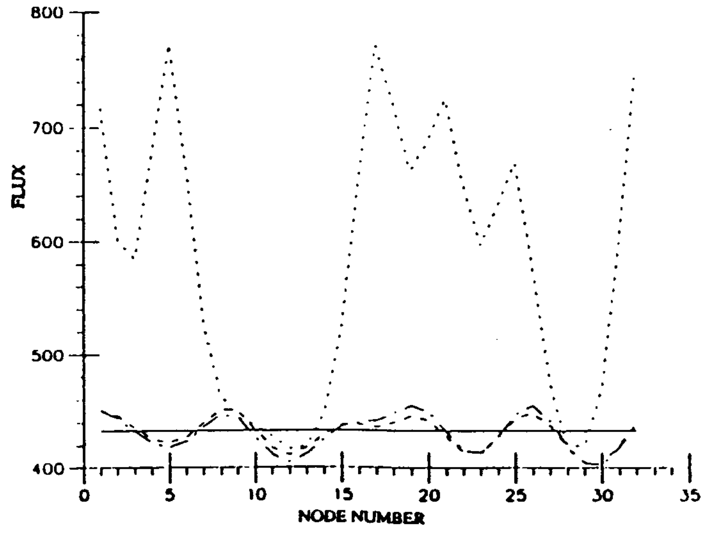

Fig. 1.10 Initial (·········), after 5 cycles (– · – · –) , after 10 cycles (– – – –) and final (———) heat flux distribution through the outer boundary for a cylinder with ten holes initially. Hole elimination method and objective function switching was used.

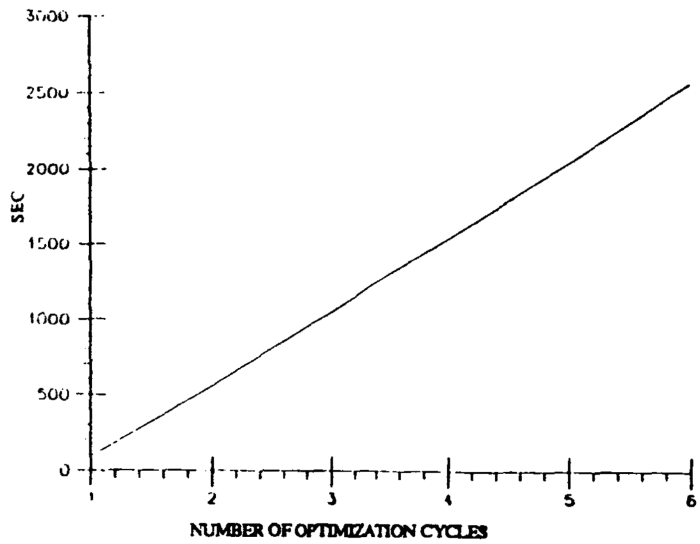

Fig. 1.11 Total CPU time (IBM 3090) vs. number of iterations for a circular cylinder with ten holes initially. Hole elimination method was not applied. Total number of analysis code calls (BEM code) was 1428.

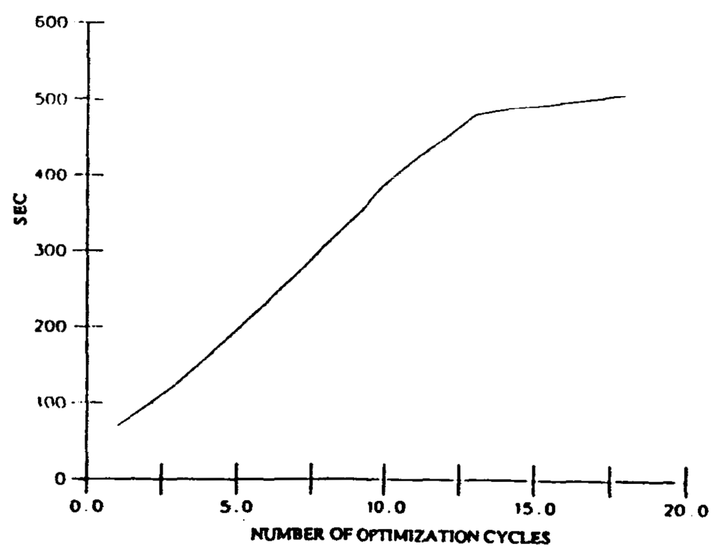

Fig. 1.12 Total CPU time (IBM 3090) vs. number of iterations for a circular cylinder with ten holes initially when hole elimination method was applied together with objective function switching.

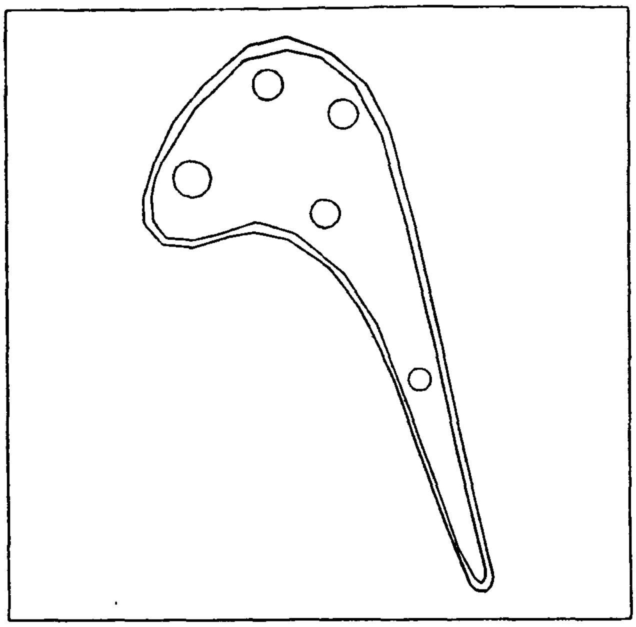

Fig. 1.13 A five-hole coated turbine blade from which thermal boundary conditions were used represents an actual solution for the case of the turbine blade with ten holes initially

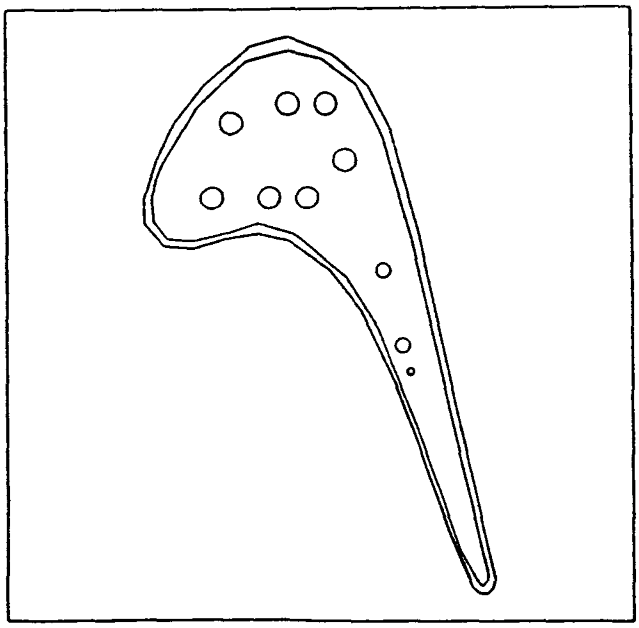

Fig. 1.14 Initial guess for a coated turbine blade configuration with ten holes using thermal boundary conditions from the five-hole configuration

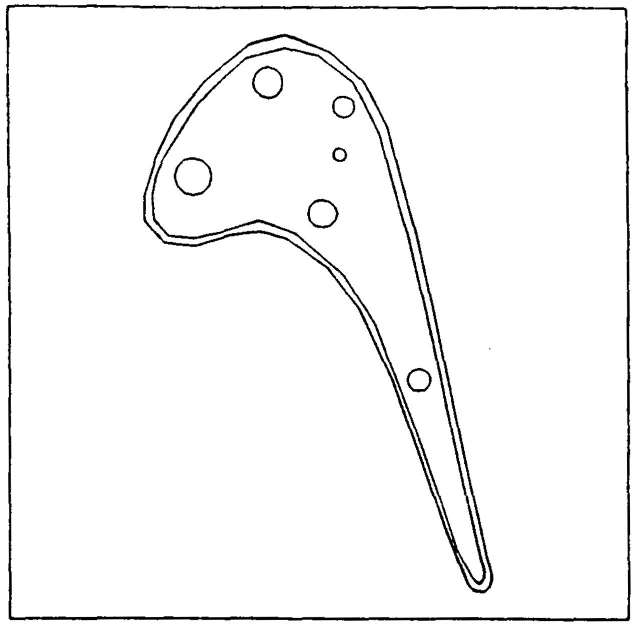

Fig. 1.15 Optimized solution for initial configuration with ten holes. Number of holes is minimized to six, where the sixth hole continues to shrink. Hole elimination method was used together with objective function switching.

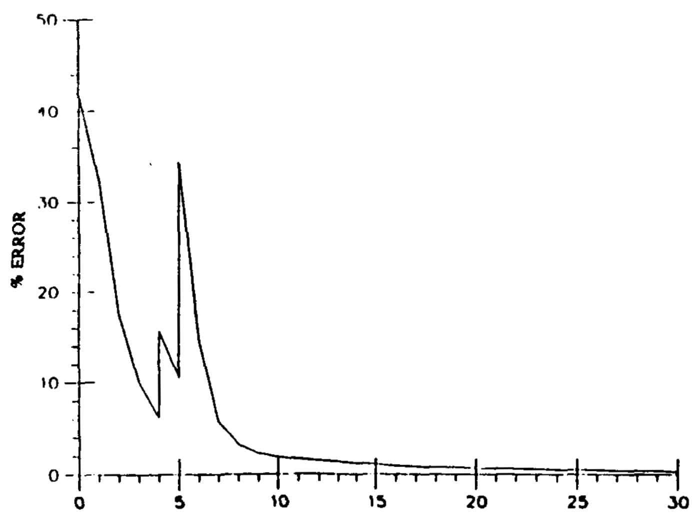

Fig. 1.16 Convergence history for a coated turbine blade with ten holes initially when hole elimination method was applied together with objective function switching. Discontinuities represent changing of the objective function.

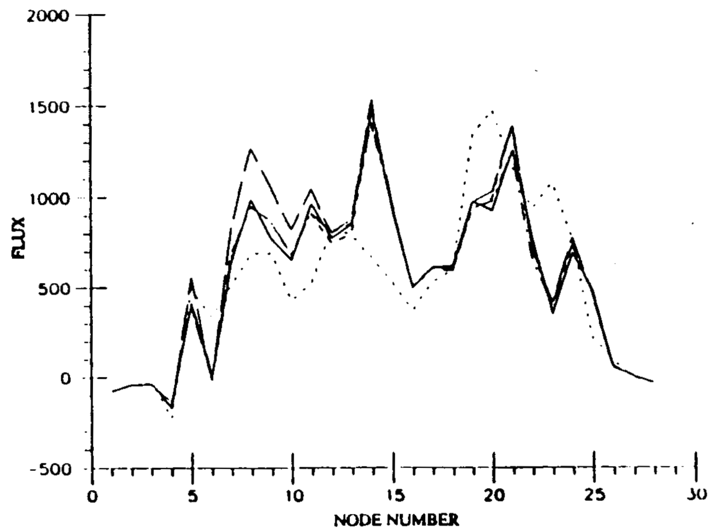

Fig. 1.17 Initial (·········), after 5 cycles (– – – –) , after 10 cycles (– · – · –) and final (———) heat flux distribution through the outer boundary for a turbine blade with initially ten holes. Hole elimination method was used together with objective function switching.

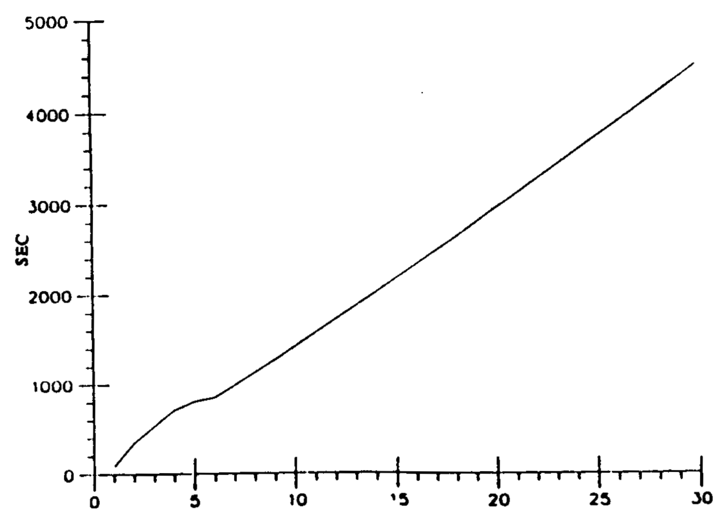

Fig. 1.18 Total CPU time (IBM 3090) vs. number of iterations for a turbine blade with ten holes initially. Hole elimination method was applied together with objective function switching.

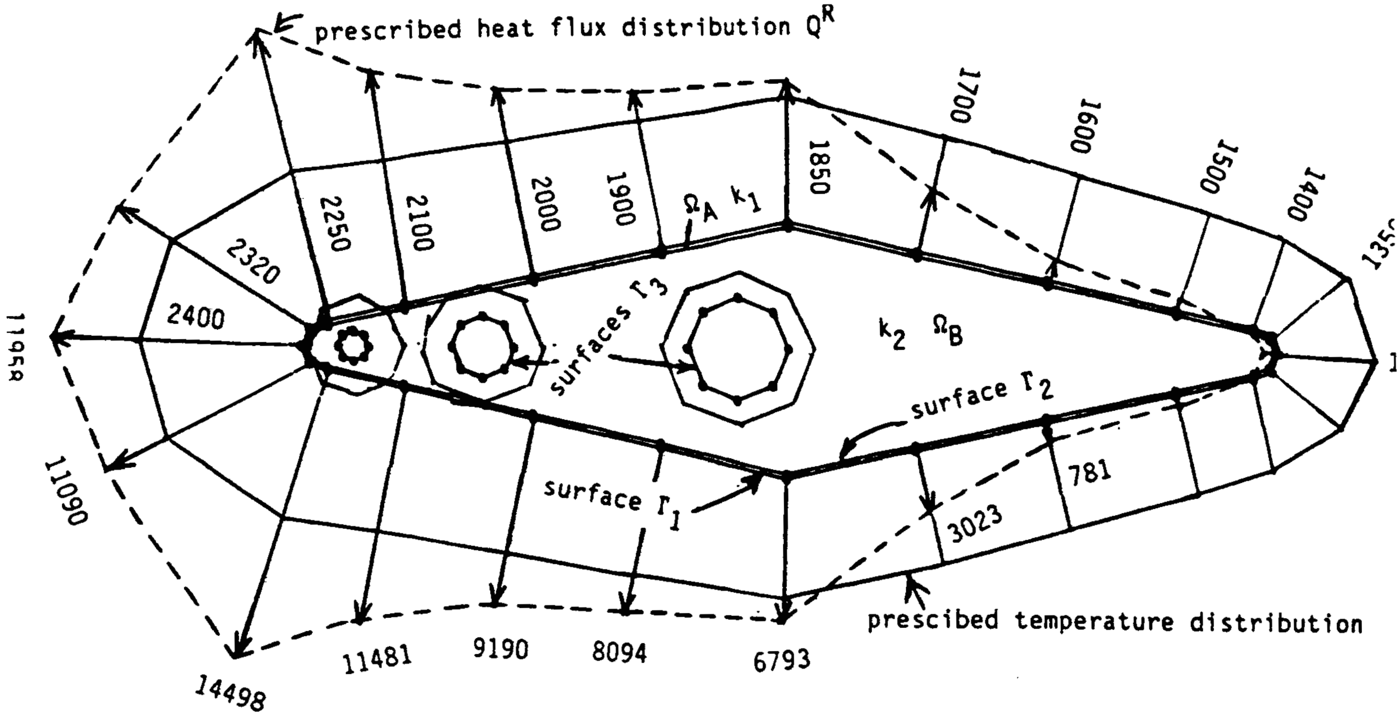

Fig. 1 Discretized Ceramically Coated Scram Jet Combustor strut
With prescribed Temperatures and Outer Surface Heat Flux
chord length of the strut : 19.
maximum thickness of the strut : 5.

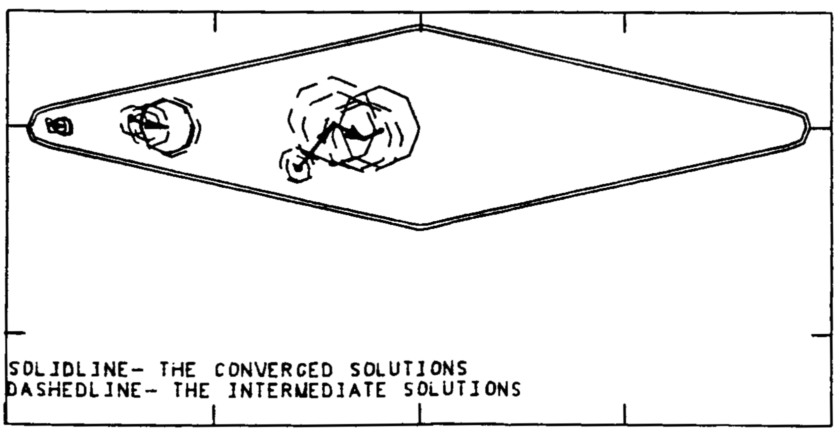

Fig. 2 Iteration sequence of case 1 (norm error = 0.554 %)

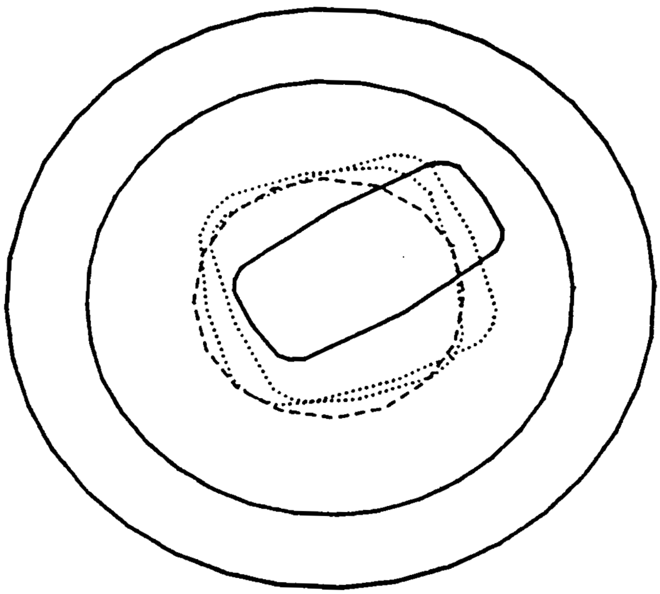

Fig. 2.1 Initial configuration (an off-center inclined almost rectangular hole) and optimized configuration (one large centrally located hole) for one-hole coated disk with intermediate hole shapes.

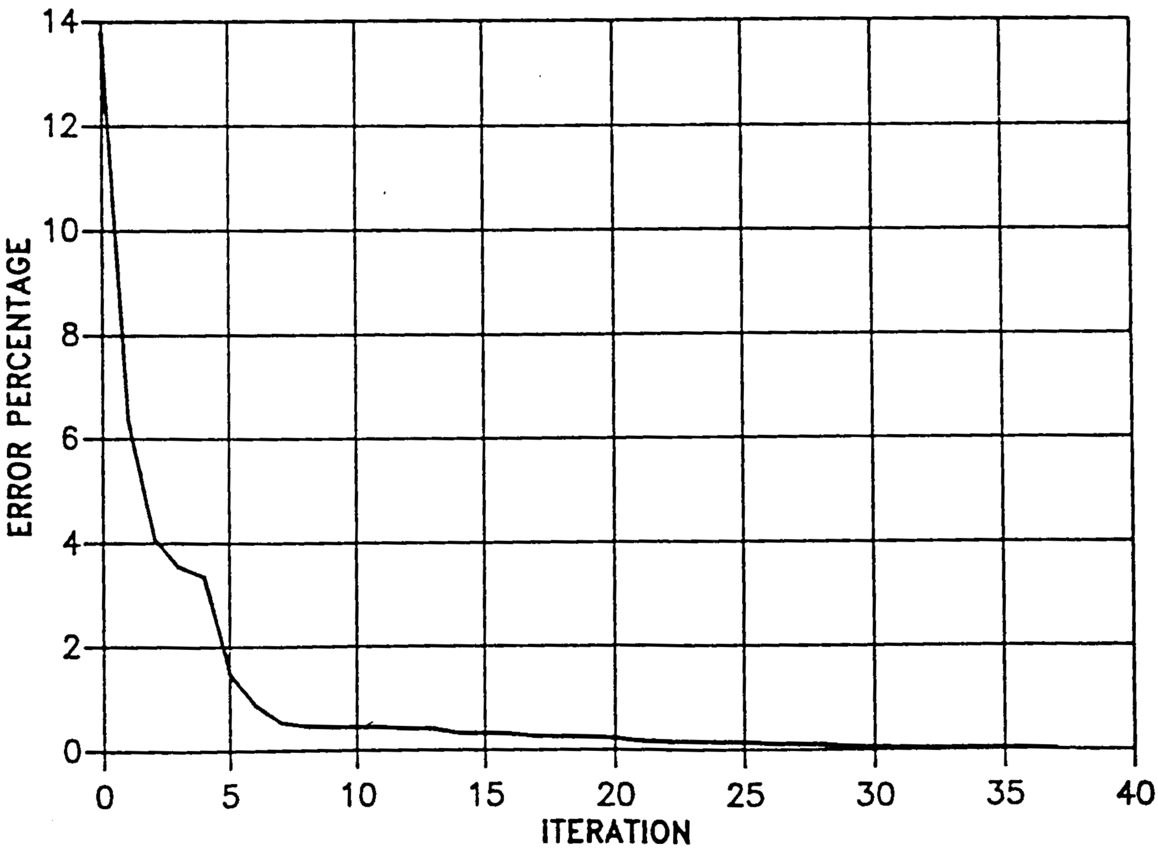

Fig. 2.2 Convergence history of the coated disk with one-hole configuration.

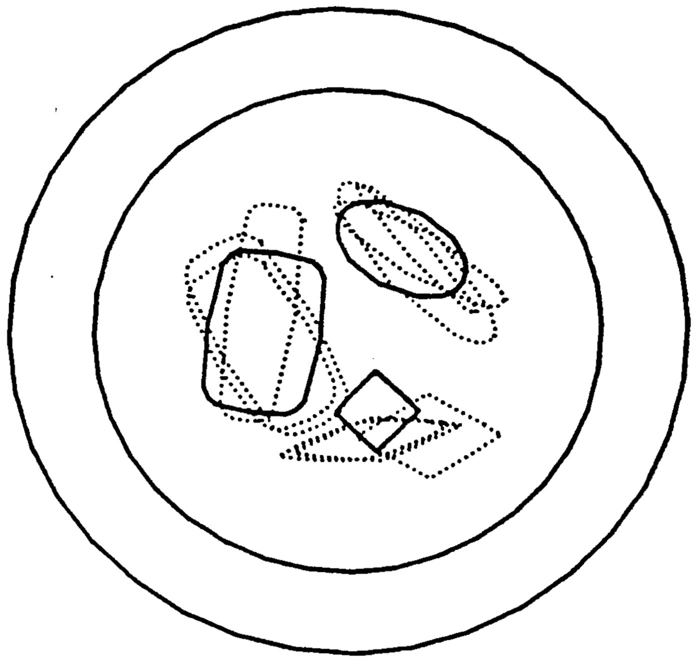

Fig. 2.3 Initial configuration consisting of three different holes (solid line) and their inermediate shapes during the first 64 optimization cycles for a coated disk.

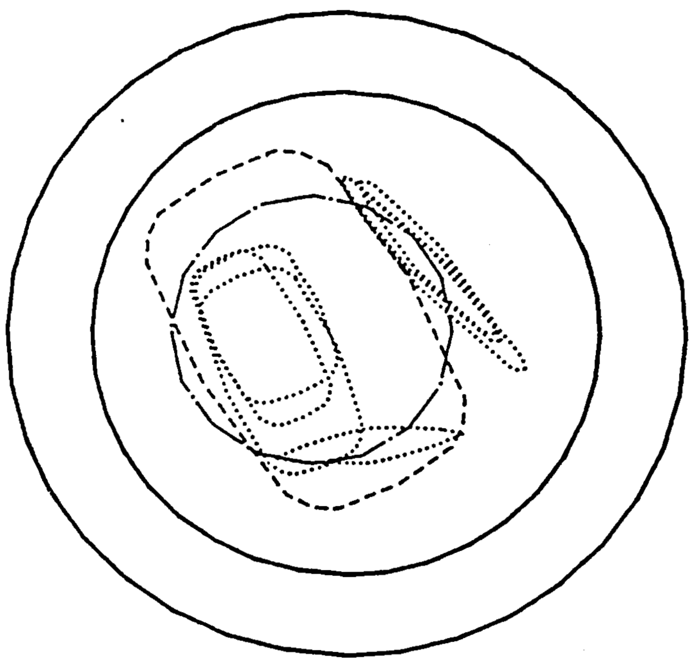

Fig. 2.4 Inermediate shapes of the three different holes during the optimization cycles 65-121 for a coated disk.

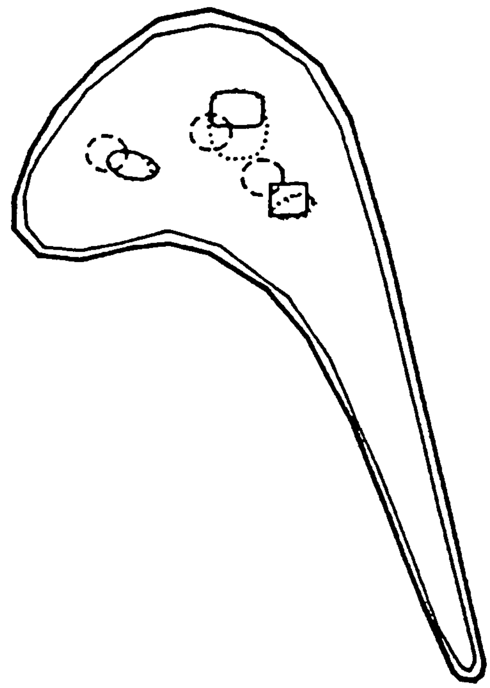

Fig. 2.5 Initial configuration (three circular holes) and optimized configuration (ellipse, rectangle, and a square) for a coated turbine blade with intermediate hole shapes (dotted).

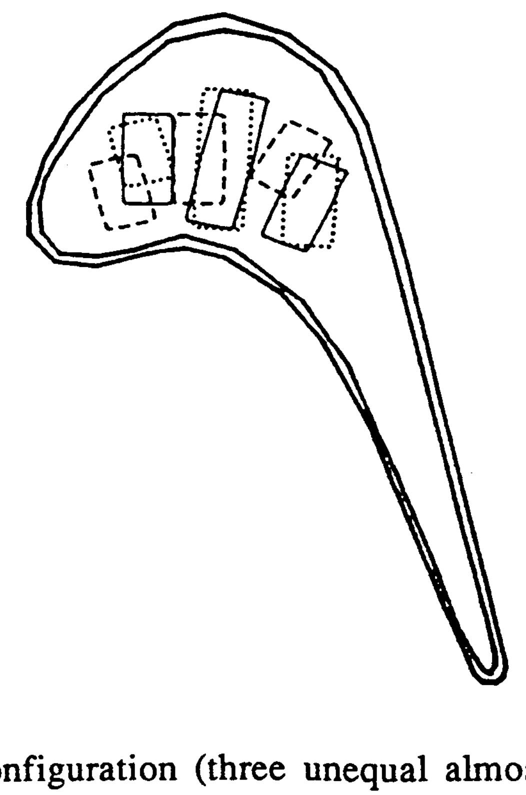

Fig. 2.6 Initial configuration (three unequal almost rectangular holes) and optimized configuration (three diffeently sized, positioned almost rectangular partially constrained holes) for the coated turbine blade airfoil with intermediate hole shapes.

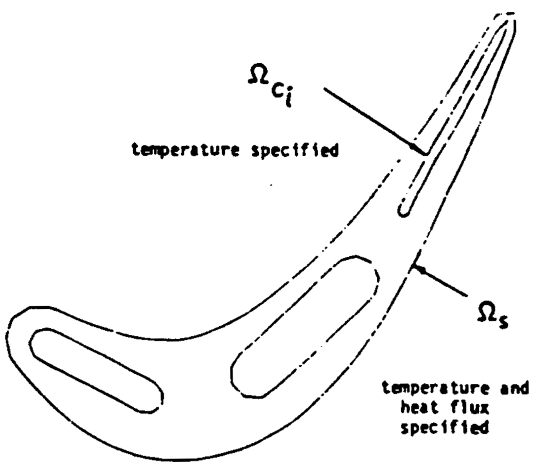

Fig. 1. Geometry and boundary conditions /9/.

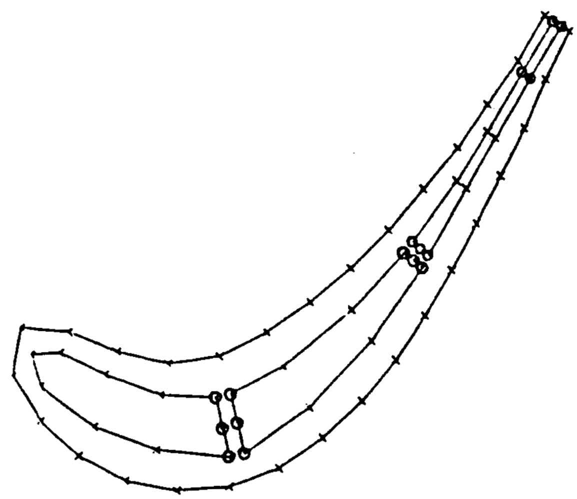

Fig. 2. Inner and outer contours discretized with panels (O denotes fixed end points).

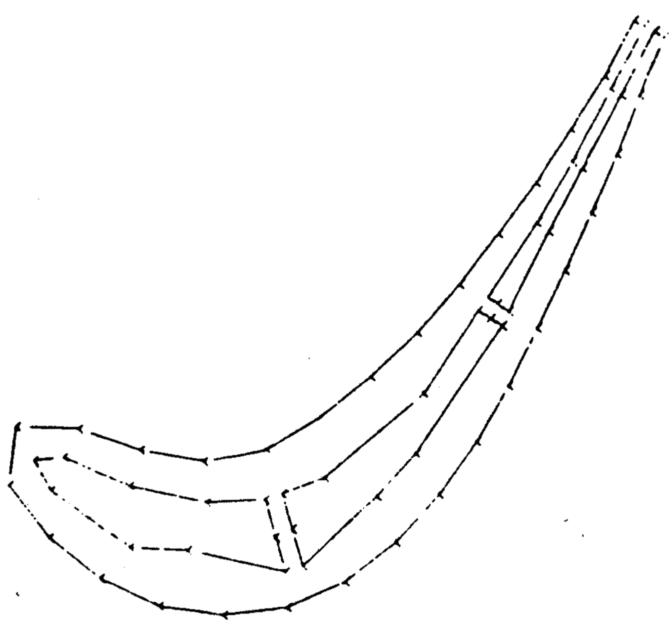

Fig. 4. Turbine design for case 1.

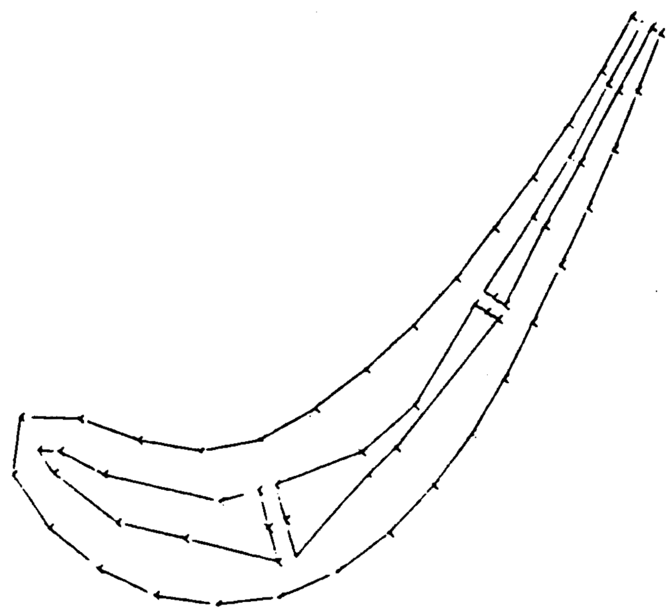

Fig. 5. Turbine design for case 2.

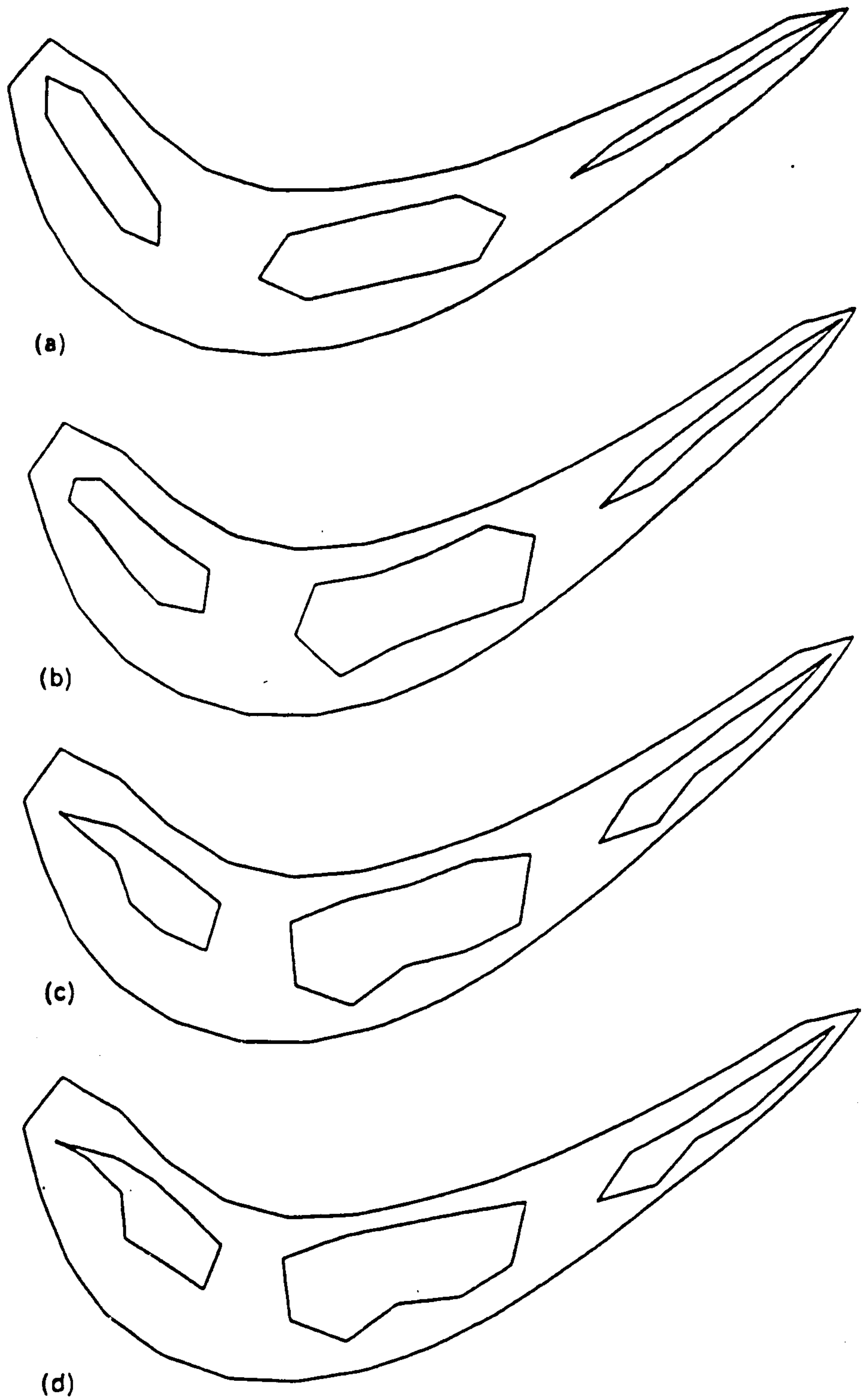

Iteration sequence for turbine design case 1: (a) initial configuration; (b) solution after 6 iterations; (c) solution after 14 iterations; (d) solution after 18 iterations

N92-32299

NUMERICAL ANALYSIS OF THE HOT-GAS-SIDE AND COOLANT-SIDE HEAT TRANSFER IN LIQUID ROCKET ENGINE COMBUSTORS

T.S. WANG
Computational Fluid Dynamics Branch
NASA - Marshall Space Flight Center
Marshall Space Flight Center, AL 35812

V. LUONG
Thermal Analysis Branch
NASA - Marshall Space Flight Center
Marshall Space Flight Center, AL 35812

Abstract

The objectives of this paper are to develop computational methods to predict the hot-gas-side and coolant-side heat transfer, and to use these methods in parametric studies to recommend optimized design of the coolant channels for regeneratively cooled liquid rocket engine combustors. An integrated numerical model which incorporates computational fluid dynamics (CFD) for the hot-gas thermal environment, and thermal analysis for the coolant channels, was developed. The model was validated by comparing predicted heat fluxes with those of hot-firing test and industrial design methods. Parametric studies were performed to find a strategy for optimized combustion chamber coolant channel design.

NUMERICAL ANALYSIS OF THE HOT-GAS-SIDE AND COOLANT-SIDE HEAT TRANSFER IN LIQUID ROCKET ENGINE COMBUSTORS

BY

TEN-SEE WANG
ED32,CFD BRANCH
NASA/MSFC

AND

VAN LUONG
ED64, THERMAL ANALYSIS BRANCH
NASA/MSFC

FOR
WORKSHOP FOR CFD ALLPICATIONS IN ROCKET PROPULSION
APRIL 28-30
HUNTSVILLE, ALABAMA

OBJECTIVES

- ★ TO DEVELOP COMPUTATIONAL METHODS FOR THE PREDICTION OF THE COUPLED HOT-GAS-SIDE AND COOLANT-SIDE HEAT TRANSFER IN A LIQUID ROCKET ENGINE COMBUSTOR

- ★ TO PERFORM PARAMETRIC STUDIES TO RECOMMEND OPTIMIZED DESIGN OF THE COOLANT CHANNELS FOR REGENERATIVELY COOLED LIQUID ROCKET ENGINE COMBUSTORS

THE AERO-THERMAL MODEL

- ☆ CFD MODEL FOR HOT-GAS-SIDE ENVIRONMENT
  - AXISYMMETRIC MCC FLOWFIELD
  - FULLY VISCOUS FLOW
  - SHOCK CAPTURING
  - SEVEN SPECIES EQUILIBRIUM CHEMISTRY
- ☆ SINDA THERMAL MODEL FOR LINER, RIB, AND JACKET
  - THREE-DIMENSIONAL
  - VARIABLE WALL THICKNESS, CHANNEL DIMENSIONS AND NUMBER OF CHANNELS
  - RADIATION CORRECTED
  - WALL TEMPERATURE AND THERMAL GRADIENT
- ☆ SINDA HYDRAULIC MODEL FOR COOLANT FLOW
  - COOLANT TEMPERATURE AND PRESSURE DROP

AERO-THERMAL MODEL

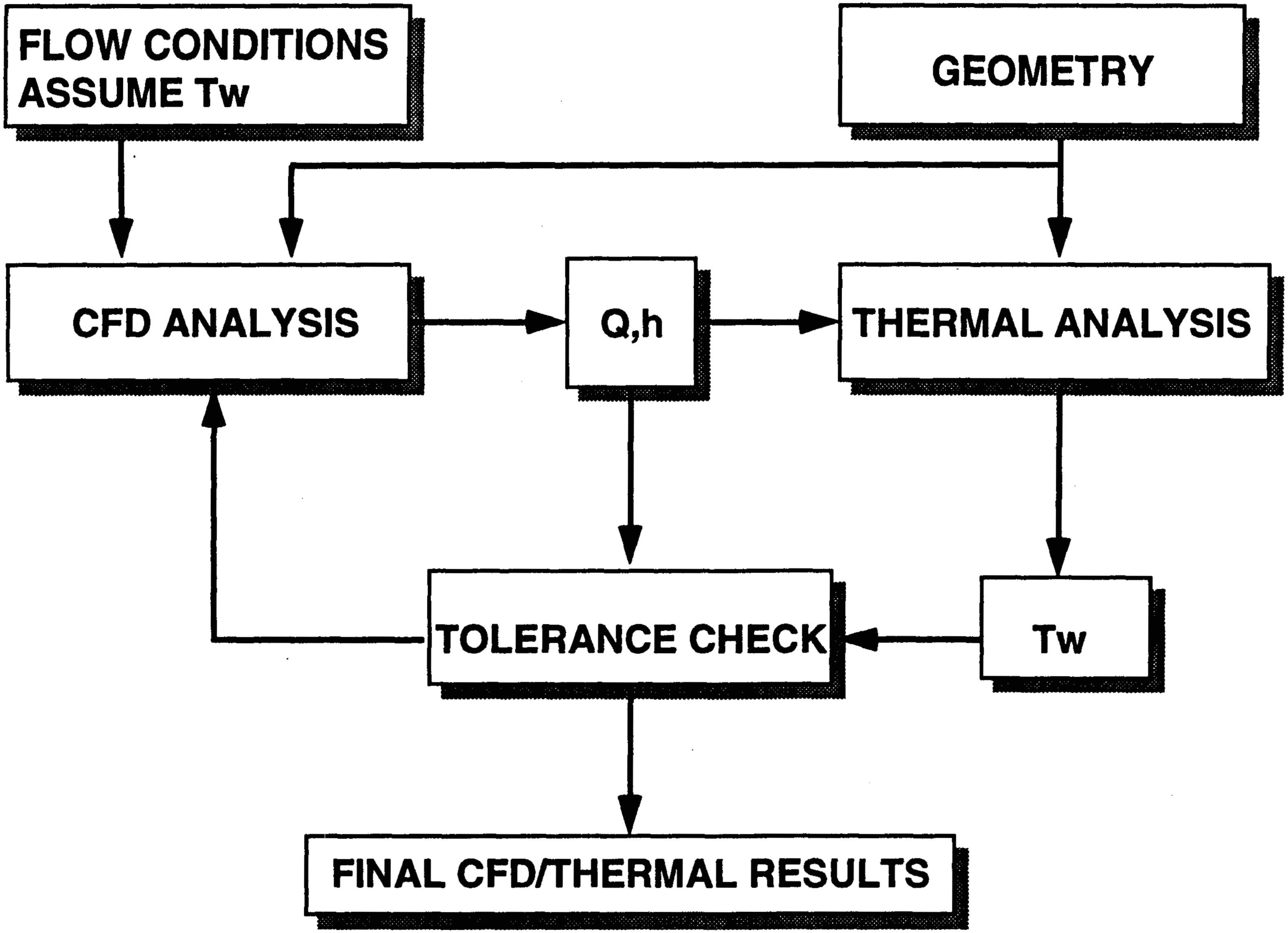

TEST CASES

- ★ 40K CALORIMETER THRUST CHAMBER TEST VALIDATION
- ★ BASELINE STANDARD THROAT SSME MCC COMPARISON
- ★ LARGE THROAT AMCC DESIGN PARAMETRIC STUDIES

SCHEMATIC OF 40K TEST CONFIGURATION

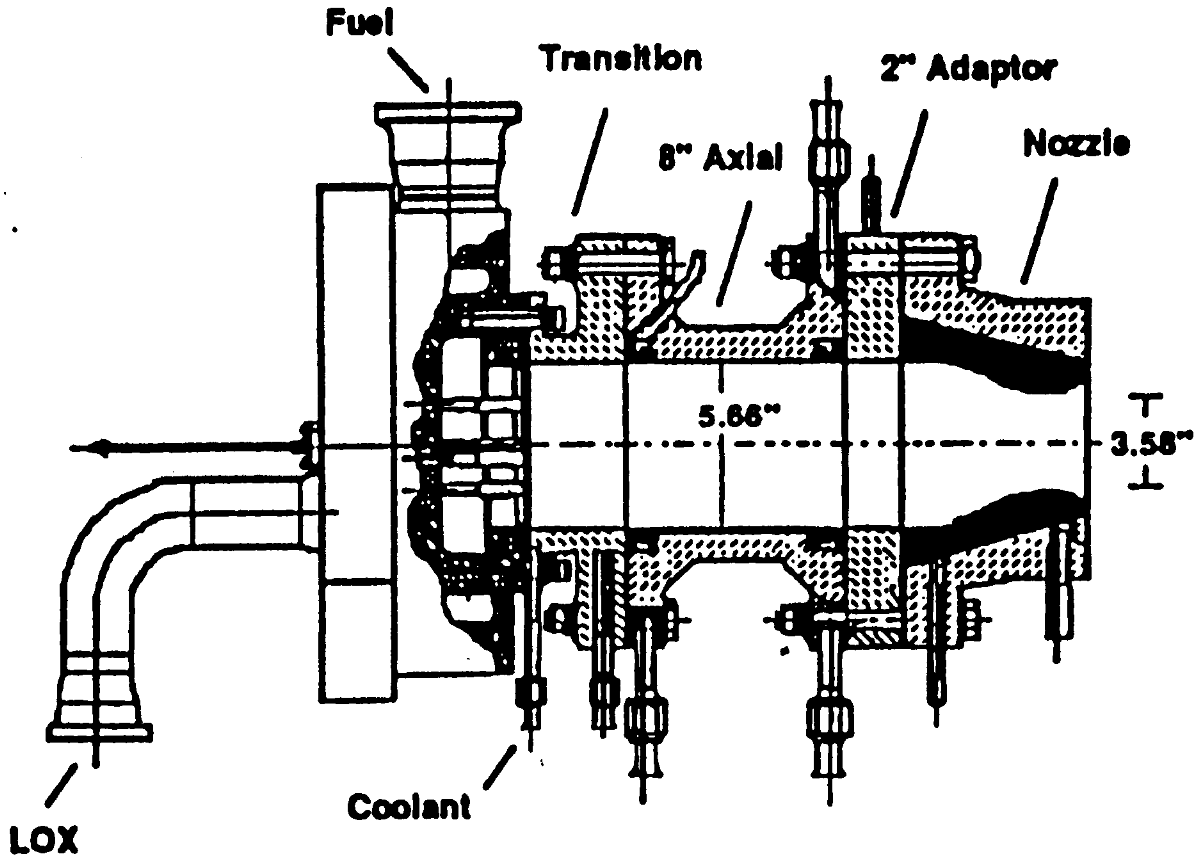

40K Coolant Discharge Temperature

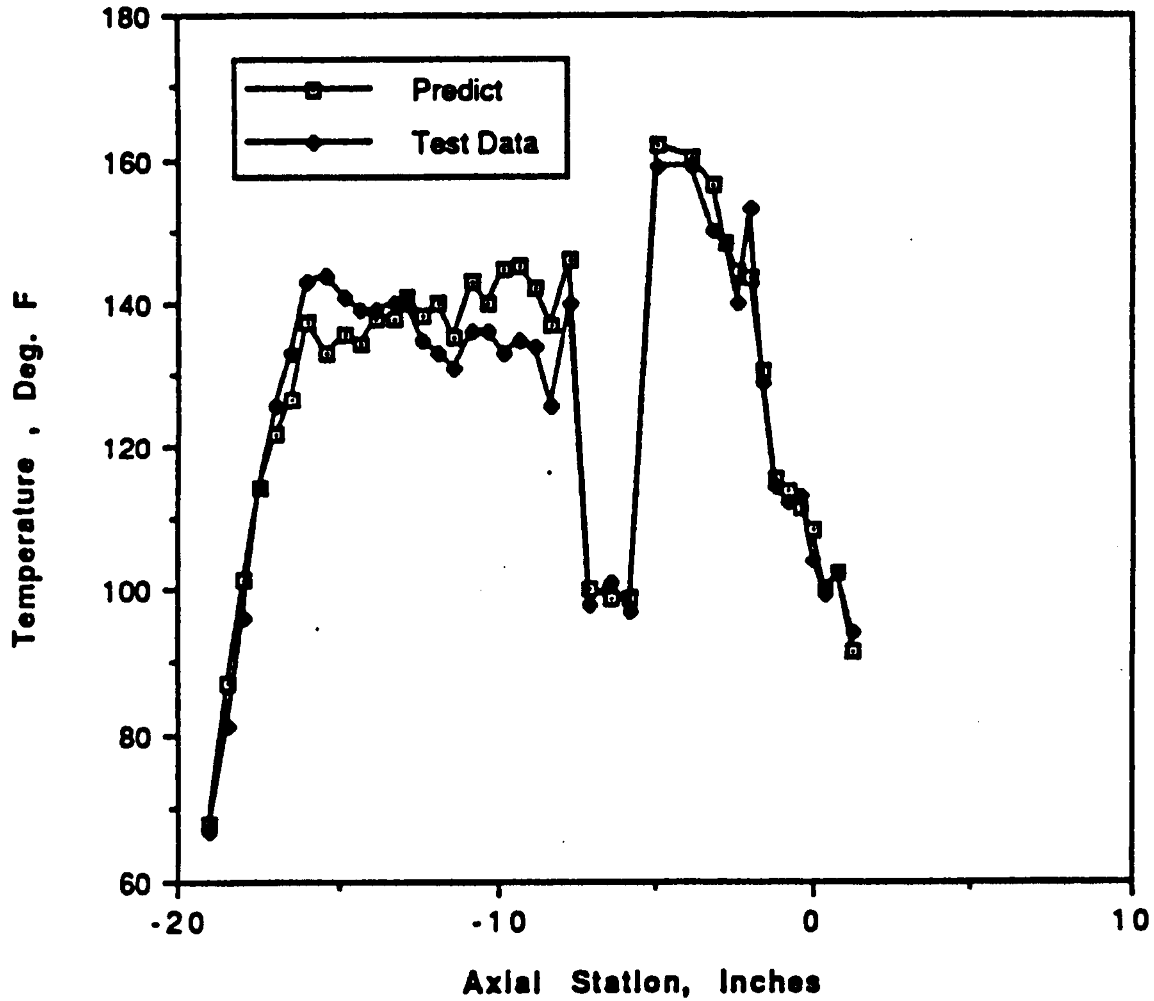

40K Wall Heat Flux

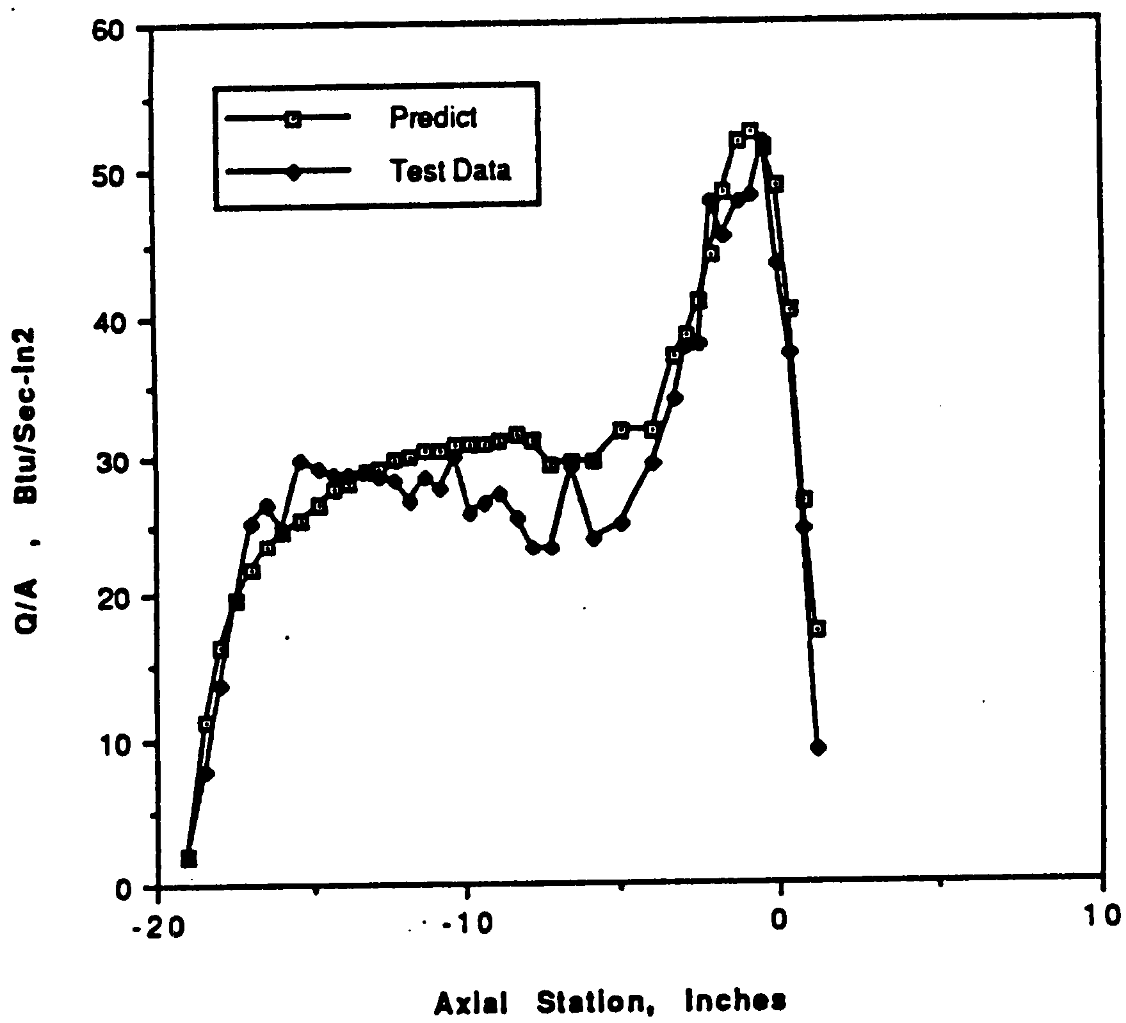

SSME MCC WALL HEAT FLUX

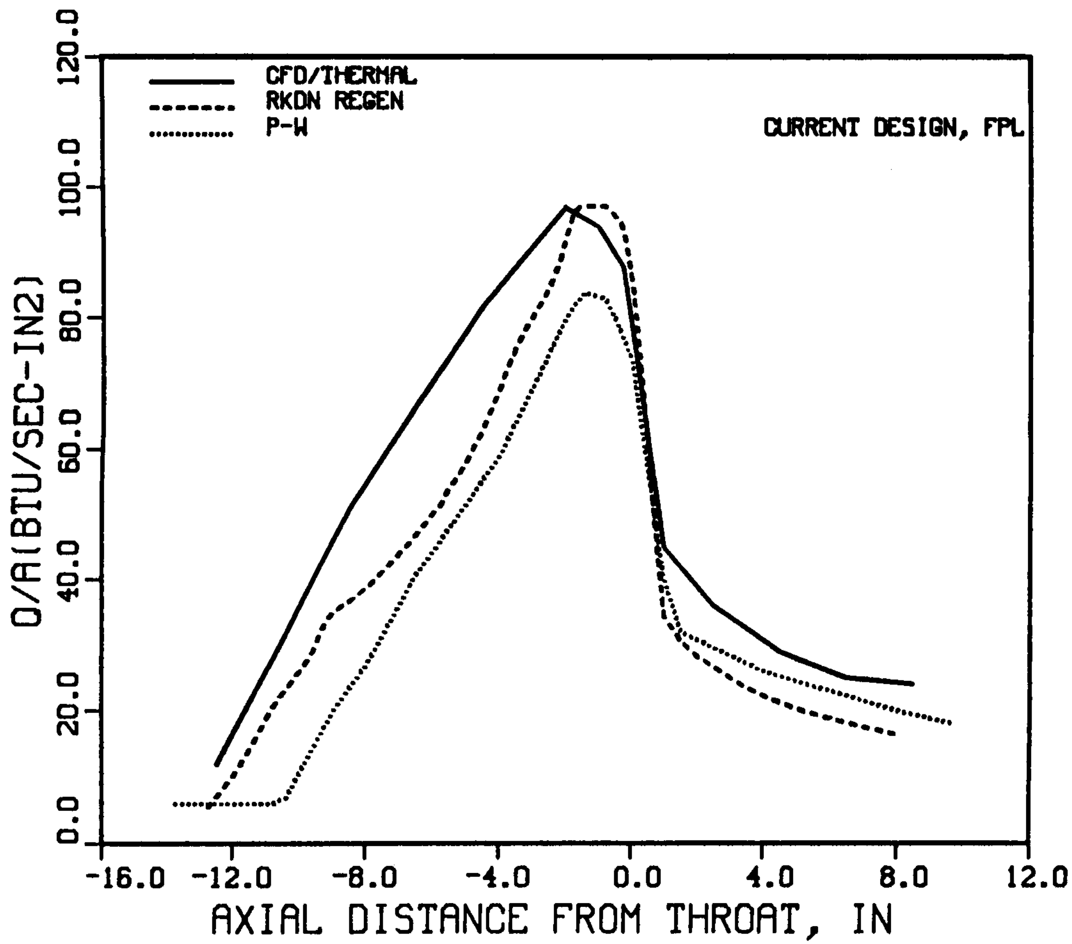

SSME MAIN COMBUSTION CHAMBER
HOT AND COLD WALL TEMPERATURE PROFILE

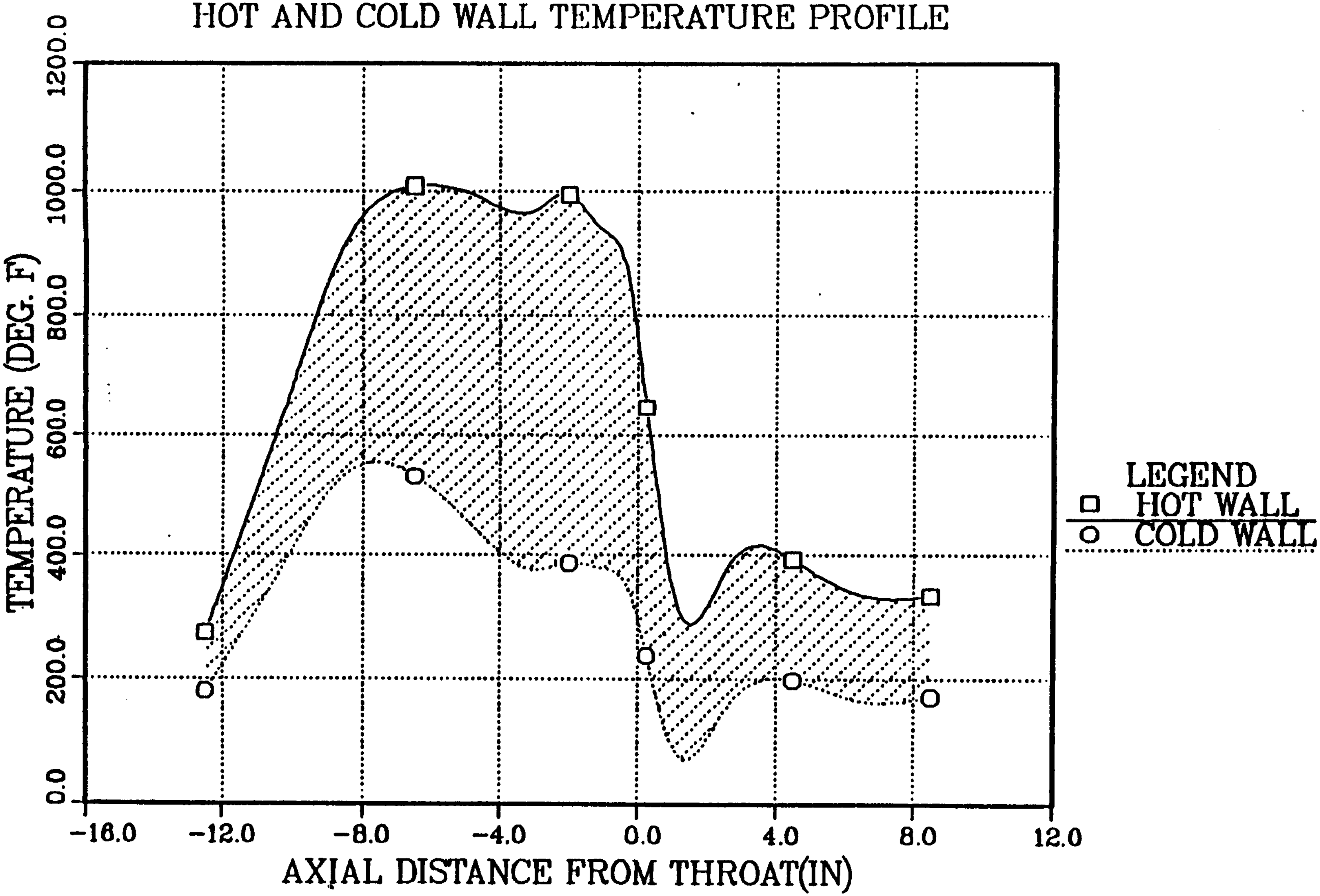

SSME MAIN COMBUSTION CHAMBER

HOT AND COLD GAS PRESSURE DISTRIBUTION

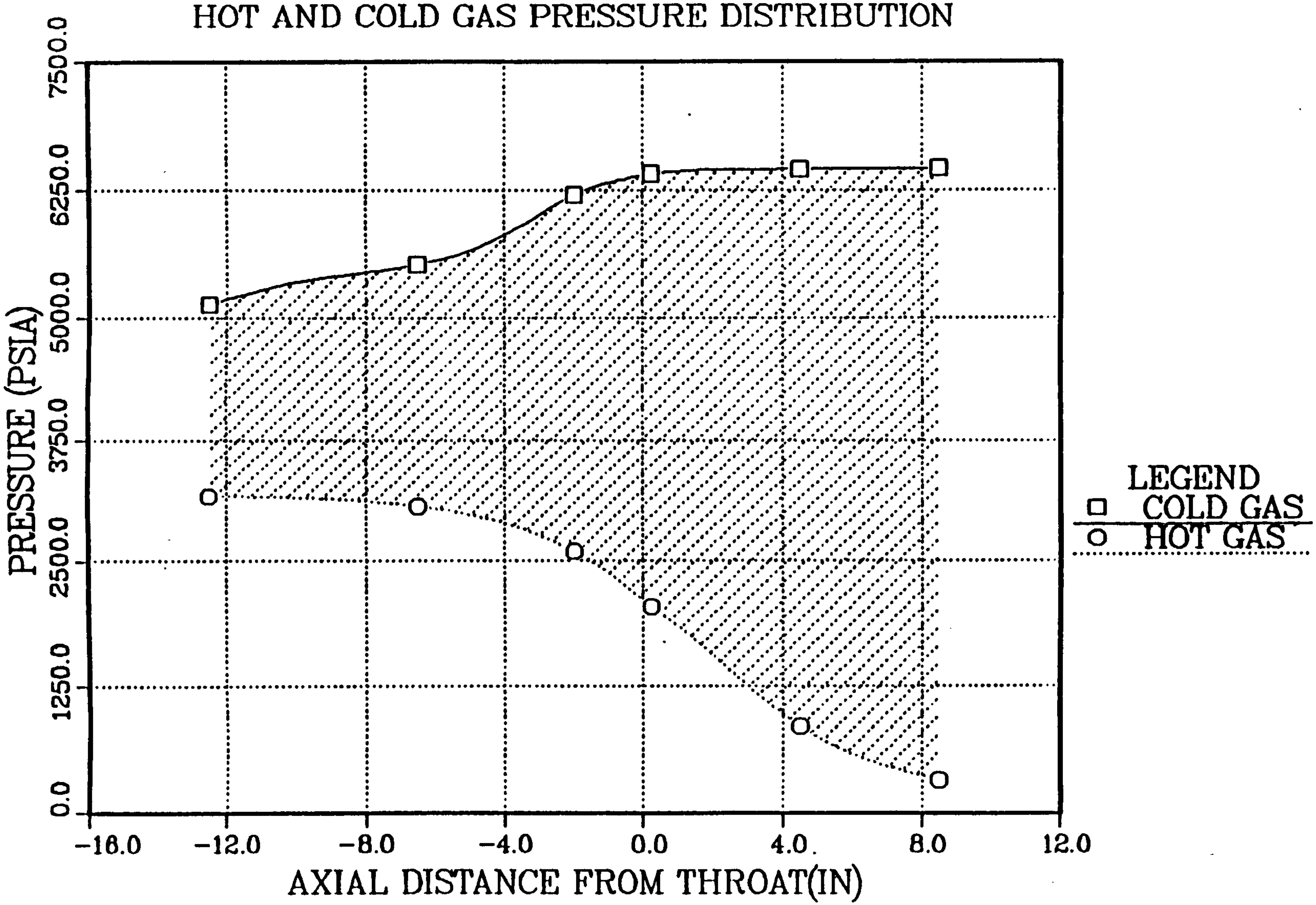

SSME COMBUSTION CHAMBER COOLANT LINER
COOLANT BULK TEMPERATURE PROFILE

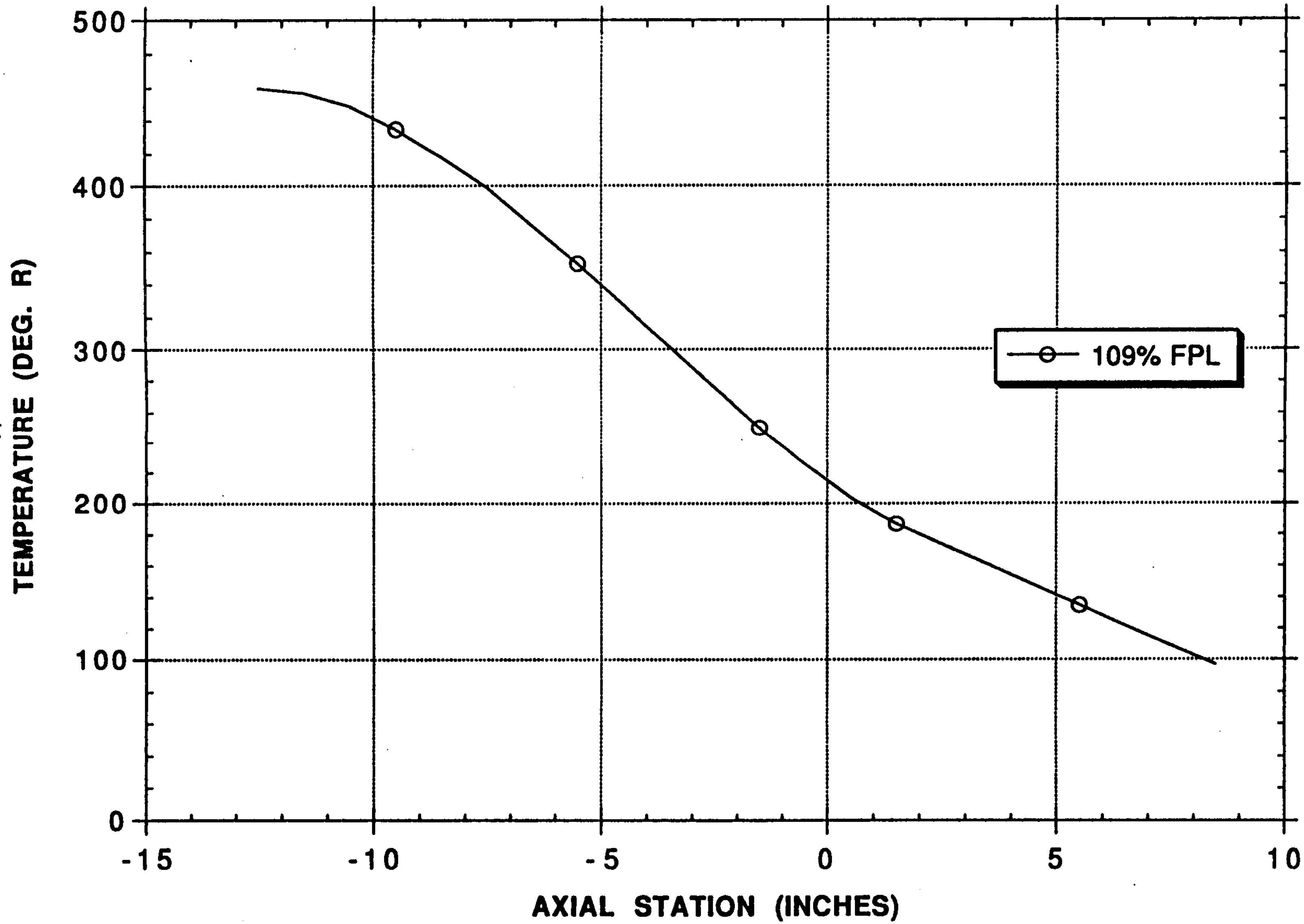

SSME VPS MAIN COMBUSTION CHAMBER
430 CHANNEL TO 550 CHANNEL COMPARISON
HOT GAS WALL SURFACE TEMPERATURE

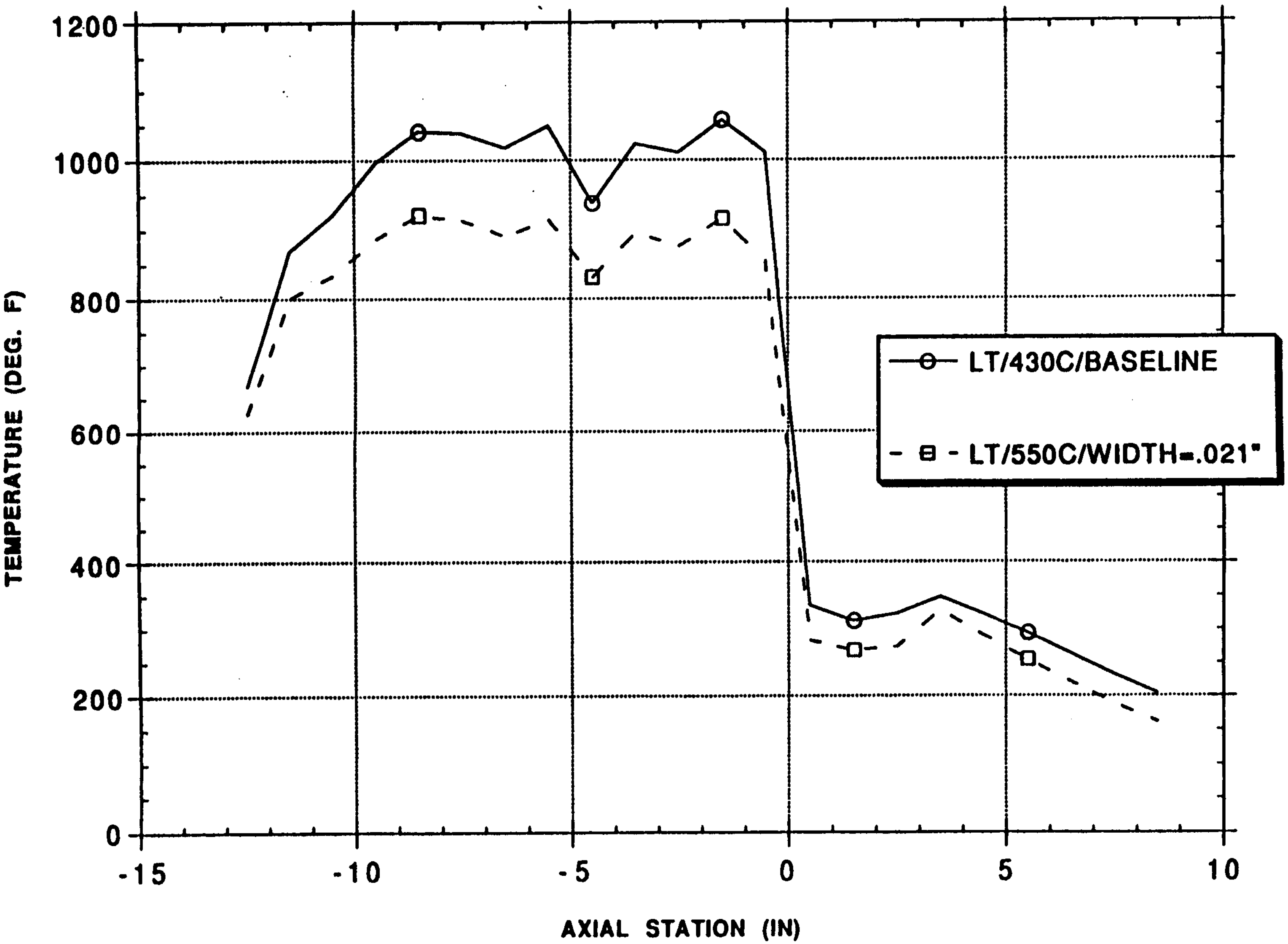

SSME VPS MAIN COMBUSTION CHAMBER
EFFECT OF HOT GAS WALL THICKNESS
HOT GAS WALL SURFACE TEMPERATURE

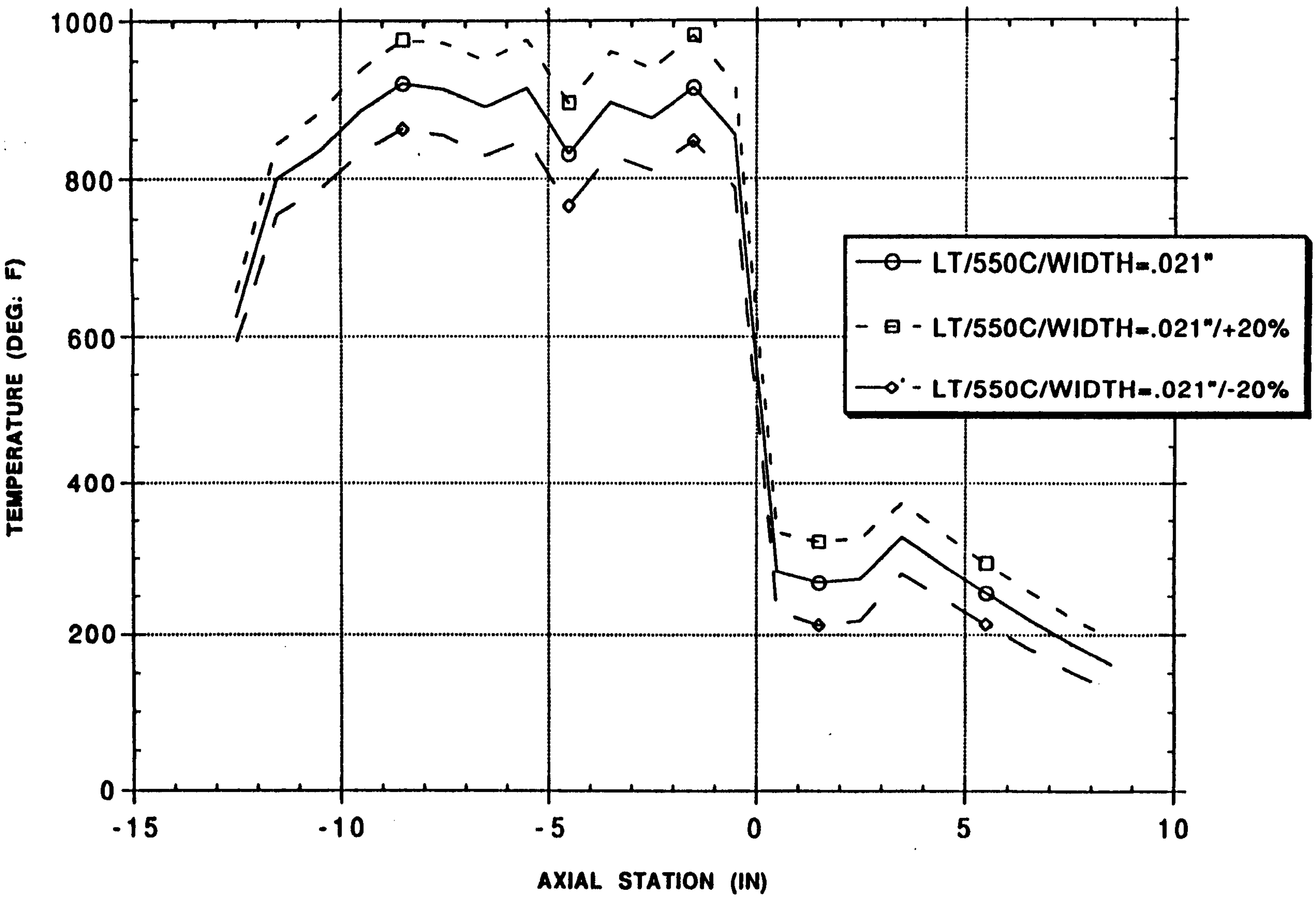

SUMMARY

- ★ AN INTEGRATED CFD/THERMAL MODEL HAS BEEN DEVELOPED TO PREDICT THE HOT-GAS-SIDE AND COOLANT SIDE HEAT TRANSFER FOR LIQUID ROCKET COMBUSTION CHAMBER
- ★ MODEL VALIDATED FOR 40K CALORIMETER THRUST CHAMBER TEST
- ★ MODEL COMPARED FOR BASELINE STANDARD THROAT SSME MCC HEAT TRANSFER
- ★ PERFORMED LARGE THROAT AMCC DESIGN PARAMETRIC STUDIES
  - INCREASED ASPECT RATIO AND NUMBER OF CHANNELS REDUCE THE WALL TEMPERATURE AND THERMAL GRADIENT
  - REDUCED WALL THICKNESS REDUCES THE SURFACE WALL TEMPERATURE

An Efficient and Robust Grid Optimization Algorithm

By

Bharat K. Soni
Associate Professor
NSF Engineering Research Center
for Computational Field Simulation

and

Shaochen Yang
Assistant Professor
Mississippi University for Women

N92-32300

ABSTRACT

The development of an efficient and robust grid optimization algorithm is presented. This algorithm is developed by combining the best characteristics of algebraic, elliptic and hyperbolic grid generation techniques (Ref. 1-3). This development is based on the following observations and evaluations:

Algebraic systems are fast and economical.

Precise spacing control (well distributed grid) is always achieved with algebraic systems.

Grid generation by elliptic system is always smooth.

Algebraic system may cause grids to everlap, however, elliptic system resist grid line overlapping.

Weighted transfinite interpolation method blended with Bezier, B–spline curves/surfaces can produce well-distributed, orthogonal(at Boundaries) and smooth grids (not in all cases, but most all).

The control functions can be formulated to achieve boundary orthogonality and spacing control (near solid boundary surface) by elliptic generation system.

The control functions can be formulated to accomplish field orthogonality in a given computational direction (h, x, or z) and spacing control by elliptic generation system by iteratively updating various terms in the generation system. This is very time consuming especially in three dimensional problems.

Algebraic systems require a high degree of understanding and visual user interaction. However, elliptic systems can be readily adaptable for generalization. This is extremely useful in grid adaptation.

The hyperbolic system preserves the orthogonality at the solid boundary and the point distribution in the field. However, its applicability is restricted to external flows where the accurate geometrical shape of the outer boundaries/surfaces are not important as long as their location is a certain distance away from the body. Also in three dimensional applications of hyperbolic system the grid quality is directly influenced by the characteristics of the surfaces associated with the computational domain.

Computational examples representing practical internal flow configurations are presented to demonstrate the success of this algorithm.

References:

1. B. K. Soni, "Grid Generation for Internal Flow Configurations", to appear, *Journal of Computers & Mathematics with Applications.*

2. B. K. Soni, "Elliptic Grid Generation System: Control Functions Revisited", accepted for publication, *Journal of Computers & Mathematics with Applications*, February 1991.

3. B. K. Soni, "Grid Optimization: A Mixed Approach", *Proceedings of the 3rd International Conference of Numerical Grid Generation in Computational Fluid Dynamics*, Barcelona, Spain, June 1991, edited by A. S. Arcilla, J. Hauser, P. R. Eiseman and J. F. Thompson, North–Holland, P. 617–628.

Grid Methods

Direct (Algebraic)

- Fast and Economical
- Precise Spacing Control
- Propogation of Slope Discontinuities
- Interactive User Interface
- Possible Overlapping
  - can be avoided !
- High Degree of Understanding and Visual User Interaction
- Orthogonality and Smoothness
- Transfinite : Lagrange, Hermite, Bezier, B-Splines, NURBS

Indirect (PDES)

- Time Consuming
- Distribution Loss !
- Inherent Smoothness
- Iterative Background Crunching
- Resistant to Grid Line Overlapping
- Readily Adaptable for Generalization
- Competitive Enhancement of Smoothness, Orthogonality, and Concentration
- Elliptic Hyperbolic

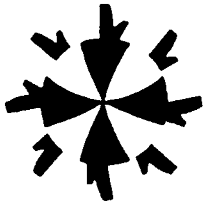

APPROACH

Objective: Accomplish othogonality – smoothness without any distribution loss.

- **Work hard with Algebraic**
  - Precise Spacing Control (Grid Spacings, Areas, Volume)
  - Inexpensive and Fast
  - Interior Bezier Curve/Surface Specification for Sub-blocks
  - Weighted Transfinite Lagrange and Hermite Interpolation
  - Precise Spacing Control (Grid Spacings, Areas, Volume)
- **Use elliptic for a quick fix**
  - Smart Forcing Functions
  - 3-5 Iterations (maximum)

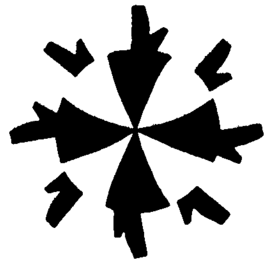

Conflicting Features

- **Smoothness**

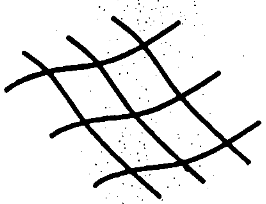

- **Resolution**

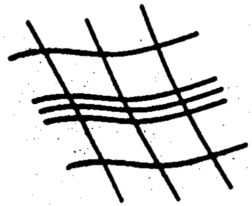

- **Orthogonality**

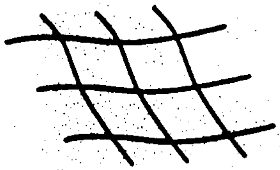

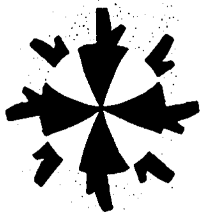

Transfinite Interpolation

$$P_\zeta = \sum_k \sum_n \phi(\zeta) r^{(k)}(\xi_n, \eta)$$

$$P_\eta = \sum_l \sum_m \Psi(\eta) r^{(l)}(\zeta, \eta_m)$$

$$P_\zeta P_\eta = \sum_k \sum_n \sum_m \phi(\zeta)\Psi(\eta) r^{(kl)}(\zeta_n, \eta_m)$$

$$P_\zeta \oplus P_\eta = P_\zeta + P_\eta - P_\zeta P_\eta$$

HERMITE TRANSFINITE INTERPOLATION

Slope Evaluation:

Going in ξ direction $\longrightarrow$

$$\begin{aligned} \mathbf{r}_\xi \cdot \mathbf{r}_\eta &= 0 \\ \left\| \mathbf{r}_\xi \times \mathbf{r}_\eta \right\| &= A \end{aligned} \quad \text{OR} \quad \begin{aligned} \mathbf{r}_\xi \cdot \mathbf{r}_\eta &= 0 \\ \mathbf{r}_\eta \cdot \mathbf{r}_\eta &= g_{22} \end{aligned}$$

Going in η direction $\longrightarrow$

$$\begin{aligned} \mathbf{r}_\xi \cdot \mathbf{r}_\eta &= 0 \quad , \quad & \mathbf{r}_\xi \cdot \mathbf{r}_\eta &= 0 \\ \left\| \mathbf{r}_\xi \times \mathbf{r}_\eta \right\| &= A \quad , \quad & \mathbf{r}_\xi \cdot \mathbf{r}_\xi &= g_{11} \end{aligned}$$

A Two Dimensional Elliptic Grid System

$$g_{22}(\underline{r}_{\xi\xi}-\phi\underline{r}_{\xi})+g_{11}(\underline{r}_{\eta\eta}-\Psi\underline{r}_{\eta})-2g_{12}\underline{r}_{\xi\eta}=0$$

$\underline{r}=(x,y)$ physical space

(ξ,η) computational space

$g_{11}=\underline{r}_{\xi}\cdot\underline{r}_{\xi}=x_{\xi}^{2}+y_{\xi}^{2}$

$g_{11}=\underline{r}_{\xi}:\underline{r}_{\eta}=x_{\xi}x_{\eta}+y_{\xi}y_{\eta}$

$g_{22}=\underline{r}_{\eta}\cdot\underline{r}_{\eta}=x_{\eta}^{2}+y_{\eta}^{2}$

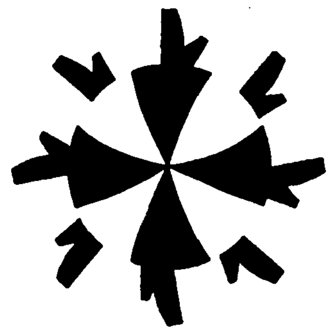

ϕ,Ψ control functions

Control Functions

$$\phi = \frac{\underline{\mathbf{r}}_{\xi\xi} \cdot \underline{\mathbf{r}}_{\xi}}{\underline{\mathbf{r}}_{\xi} \cdot \underline{\mathbf{r}}_{\xi}} + \frac{\underline{\mathbf{r}}_{\eta\eta} \cdot \underline{\mathbf{r}}_{\xi}}{\underline{\mathbf{r}}_{\eta} \cdot \underline{\mathbf{r}}_{\eta}}$$

$$\Psi = \frac{\underline{\mathbf{r}}_{\eta\eta} \cdot \underline{\mathbf{r}}_{\eta}}{\underline{\mathbf{r}}_{\eta} \cdot \underline{\mathbf{r}}_{\eta}} + \frac{\underline{\mathbf{r}}_{\xi\xi} \cdot \underline{\mathbf{r}}_{\eta}}{\underline{\mathbf{r}}_{\xi} \cdot \underline{\mathbf{r}}_{\xi}}$$

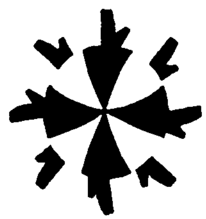

Cell Area Approach (I)

- Evaluation of $\underline{r}_\eta$

$$\underline{r}_\xi \cdot \underline{r}_\eta = x_\xi x_\eta + y_\xi y_\eta = 0$$

$$\left|\underline{r}_\xi \times \underline{r}_\eta\right| = x_\xi y_\eta - x_\eta y_\xi = v$$

$$\begin{bmatrix} x_\xi & y_\xi \\ -y_\xi & x_\xi \end{bmatrix} \begin{bmatrix} x_\eta \\ y_\eta \end{bmatrix} = \begin{bmatrix} 0 \\ v \end{bmatrix}$$

$$\begin{bmatrix} x_\xi & y_\xi \\ -y_\xi & x_\xi \end{bmatrix}$$

$$g_{11} = x_\xi^2 + y_\xi^2 \neq 0$$

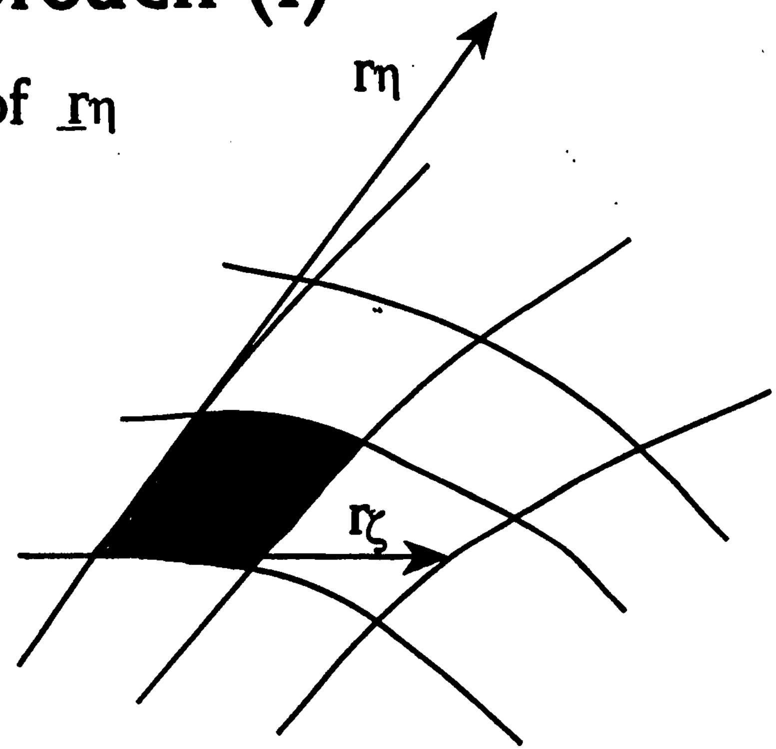

Cell Area Approach (II)

- Evaluation of $\underline{r}_{\zeta\eta}$

$$(\underline{r}_\xi \cdot \underline{r}_\eta)_\xi = (x_\xi x_\eta + y_\xi y_\eta)_\xi = 0$$

$$\left\| r_\xi \times r_\eta \right\|_\xi = (x_\xi y_\eta - x_\xi y_\xi)_\xi = v_\xi$$

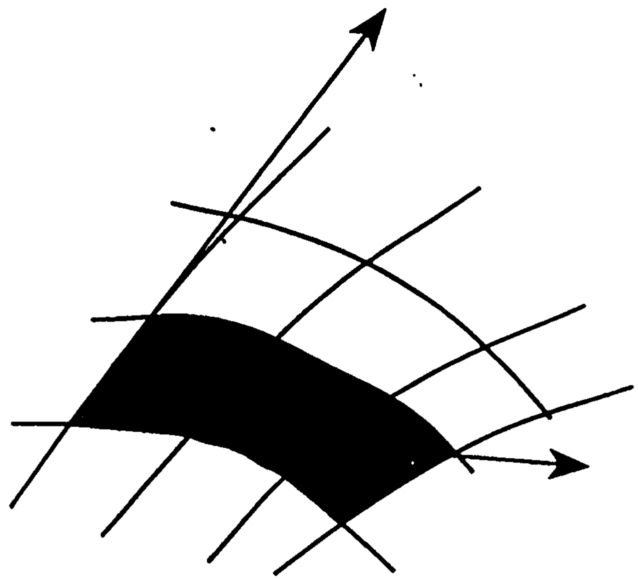

$$\begin{bmatrix} x_\xi & y_\xi \\ -y_\xi & x_\xi \end{bmatrix} \begin{bmatrix} x_{\xi\eta} \\ y_{\xi\eta} \end{bmatrix} = \begin{bmatrix} -x_{\xi\xi} x_\eta - y_{\xi\xi} y_\eta \\ v_\xi - x_{\xi\xi} y_\eta + x_\eta y_{\xi\xi} \end{bmatrix}$$

Cell Area Approach (III)

- Evaluation of $\underline{r}_{\eta\eta}$

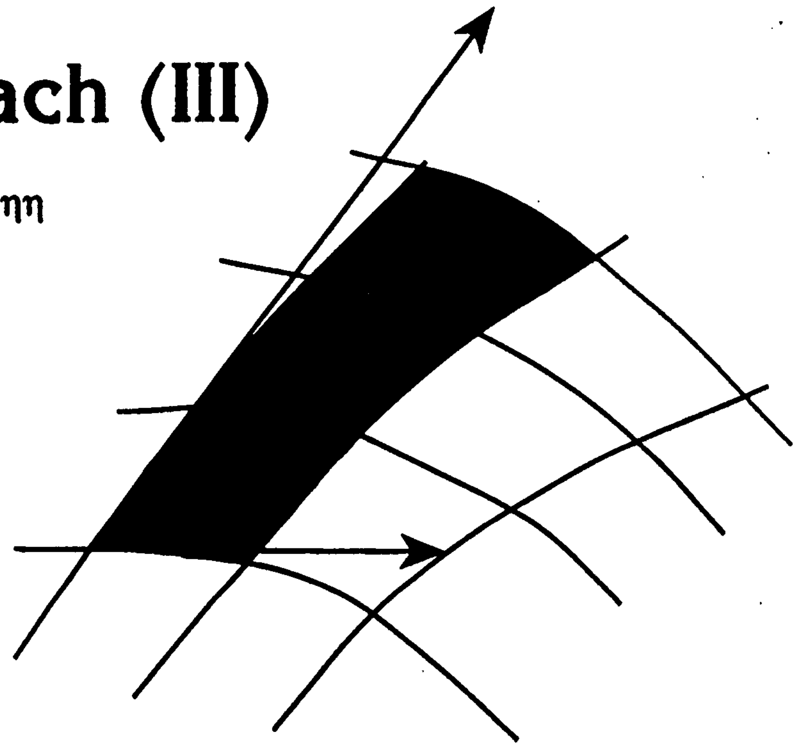

$$(r_\xi \cdot r_\eta)_\eta = (x_\xi x_\eta + y_\xi y_\eta)_\eta = 0$$

$$\left\| r_\xi \times r_\eta \right\|_\eta = (x_\xi y_\eta - x_\eta y_\xi)_\eta = v_\eta$$

$$\begin{bmatrix} x_\xi & y_\xi \\ -y_\xi & x_\xi \end{bmatrix} \begin{bmatrix} x_{\eta\eta} \\ y_{\eta\eta} \end{bmatrix} = \begin{bmatrix} -x_{\xi\eta} x_\eta - y_{\xi\eta} y_\eta \\ v_\eta - x_{\xi\eta} y_\eta + x_\eta y_{\xi\eta} \end{bmatrix}$$

Grid Spacing Approach

- Evaluation of $\underline{r}_\eta$

$$(\underline{r}_\xi \cdot \underline{r}_\eta)_\eta = (x_\xi x_\eta + y_\xi y_\eta)_\eta = 0$$

$$x_\eta^2 + y_\eta^2 = \bar{g}_{22}$$

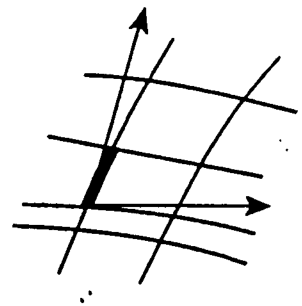

- Evaluation of $\underline{r}_{\xi\eta}$

$$(\underline{r}_\xi \cdot \underline{r}_\eta)_\xi = (x_\xi x_\eta + y_\xi y_\eta)_\xi = 0$$

$$(\underline{r}_\eta \cdot \underline{r}_\eta)_\xi = (x_\eta^2 + y_\eta^2)_\xi = (\bar{g}_{22})_\xi$$

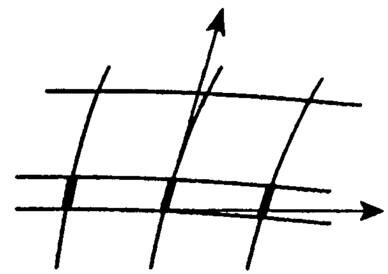

- Evaluation of $\underline{r}_{\eta\eta}$

$$(\underline{r}_\xi \cdot \underline{r}_\eta)_\eta = (x_\xi x_\eta + y_\xi y_\eta)_\eta = 0$$

$$(\underline{r}_\eta \cdot \underline{r}_\eta)_\eta = (x_\eta^2 + y_\eta^2)_\eta = (\bar{g}_{22})_\eta$$

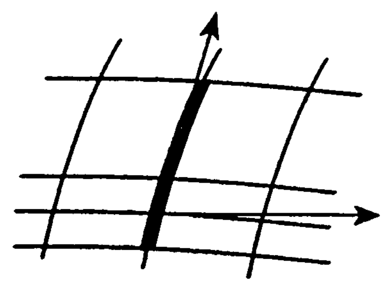

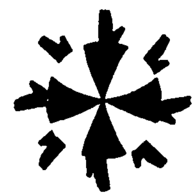

Control Functions Using Metric Terms

$$\mathbf{r} = \left(x, y\right)$$

$$g_{11} = x_\xi^2 + y_\xi^2 \qquad \left(g_{11}\right)_\xi = 2\mathbf{r}_\xi \cdot \mathbf{r}_{\xi\xi}\ ,\ \left(g_{11}\right)_\eta = 2\mathbf{r}_\xi \cdot \mathbf{r}_{\xi\eta}$$

$$g_{22} = x_\eta^2 + y_\eta^2 \qquad \left(g_{22}\right)_\eta = 2\mathbf{r}_\eta \cdot \mathbf{r}_{\eta\eta}\ ,\ \left(g_{22}\right)_\xi = 2\mathbf{r}_\eta \cdot \mathbf{r}_{\xi\eta}$$

$$g_{12} = x_\xi x_\eta + y_\xi y_\eta \qquad \left(g_{12}\right)_\xi = \mathbf{r}_\xi \cdot \mathbf{r}_{\xi\eta} + \mathbf{r}_\eta \cdot \mathbf{r}_{\xi\xi}\ ,\ \left(g_{12}\right)_\eta = \mathbf{r}_\eta \cdot \mathbf{r}_{\xi\eta} + \mathbf{r}_\xi \cdot \mathbf{r}_{\eta\eta}$$

Similarly in 3D

Working on ξ = Constant Surface

$$\begin{aligned} r_\xi \cdot r_\eta &= 0 \\ r_\xi \cdot r_\delta &= 0 \\ r_\xi \cdot (r_\eta \times r_\delta) &= v \end{aligned} \qquad \text{OR} \qquad \begin{aligned} r_\xi \cdot r_\eta &= 0 \\ r_\xi \cdot r_\delta &= 0 \\ r_\xi \cdot r_\xi &= g_{11} \end{aligned}$$

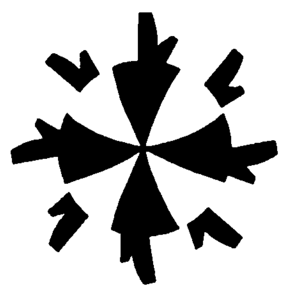

Control Functions Using Metric Term cont'd

Assuming $g_{12} = (g_{12})_\xi = (g_{12})_\eta = 0$

$$\phi = \frac{(g_{11})_\xi}{g_{11}} - \frac{(g_{22})_\xi}{g_{22}}$$

$$\psi = \frac{(g_{22})_\eta}{g_{22}} - \frac{(g_{11})_\eta}{g_{11}}$$

Assuming $g_{12} = (g_{12})_\xi = (g_{12})_\eta = 0$

$$\phi = \frac{1}{2}\left[\frac{(g_{11})_\xi}{g_{11}} - \frac{(g_{22})_\xi}{g_{22}}\right] = \frac{1}{2}\,\frac{d}{d_\xi}\left[\ln\left(\frac{g_{11}}{g_{22}}\right)\right]$$

$$\chi = \frac{1}{2}\left[\frac{(g_{22})_\eta}{g_{22}} - \frac{(g_{11})_\eta}{g_{11}}\right] = \frac{1}{2}\,\frac{d}{d_\eta}\left[\ln\left(\frac{g_{22}}{g_{11}}\right)\right]$$

Similarly In 3D

$$\phi = \frac{1}{2} \frac{d}{d_\xi} \left(\ln \left(\frac{g_{11}}{g_{22}\, g_{33}} \right) \right)$$

$$\chi = \frac{1}{2} \frac{d}{d_\eta} \left(\ln \left(\frac{g_{22}}{g_{11}\, g_{33}} \right) \right)$$

$$\theta = \frac{1}{2} \frac{d}{d_\delta} \left(\ln \left(\frac{g_{33}}{g_{11}\, g_{22}} \right) \right)$$

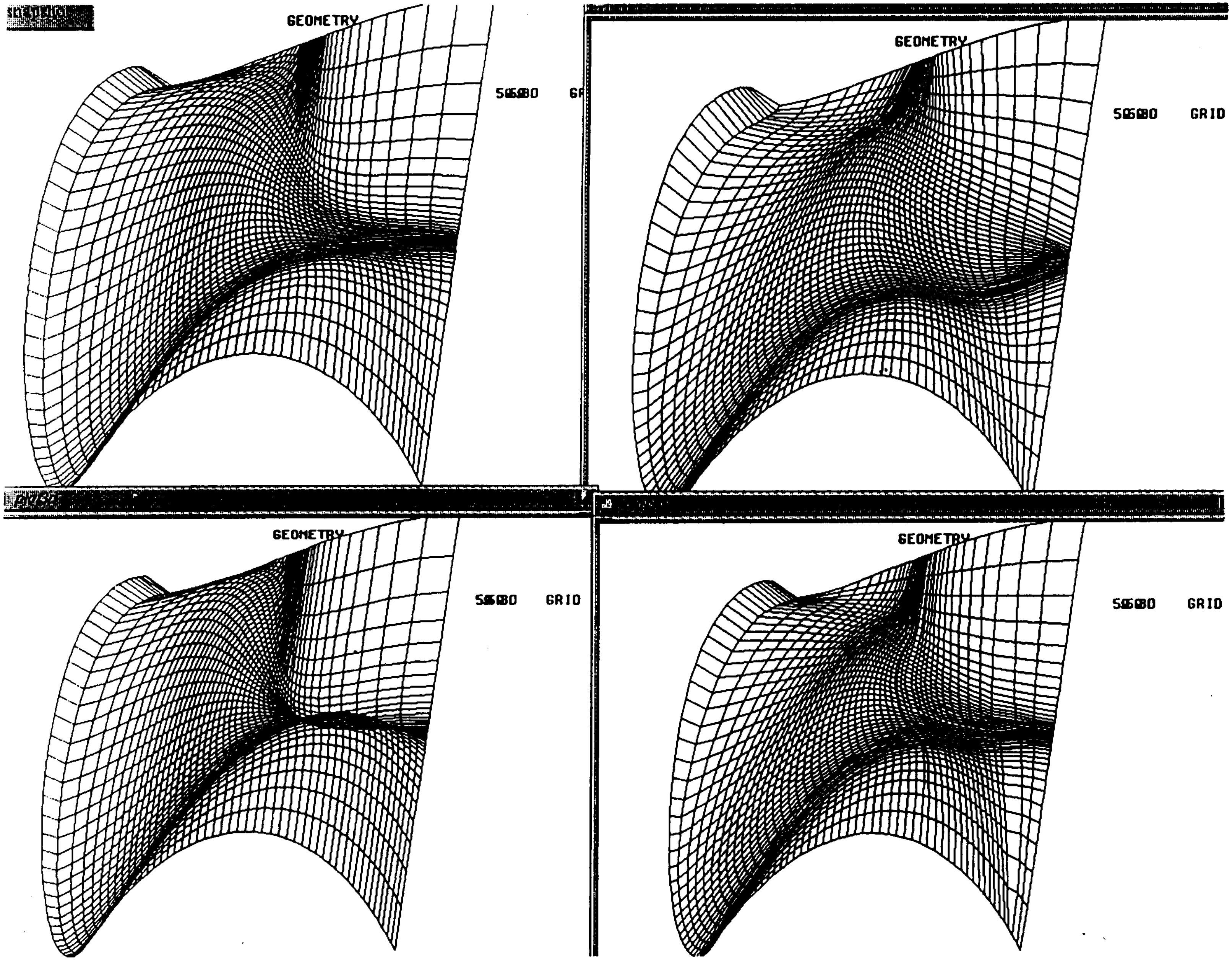
GEOMETRY
GRID
GEOMETRY
GRID
GEOMETRY
GRID
GEOMETRY
GRID

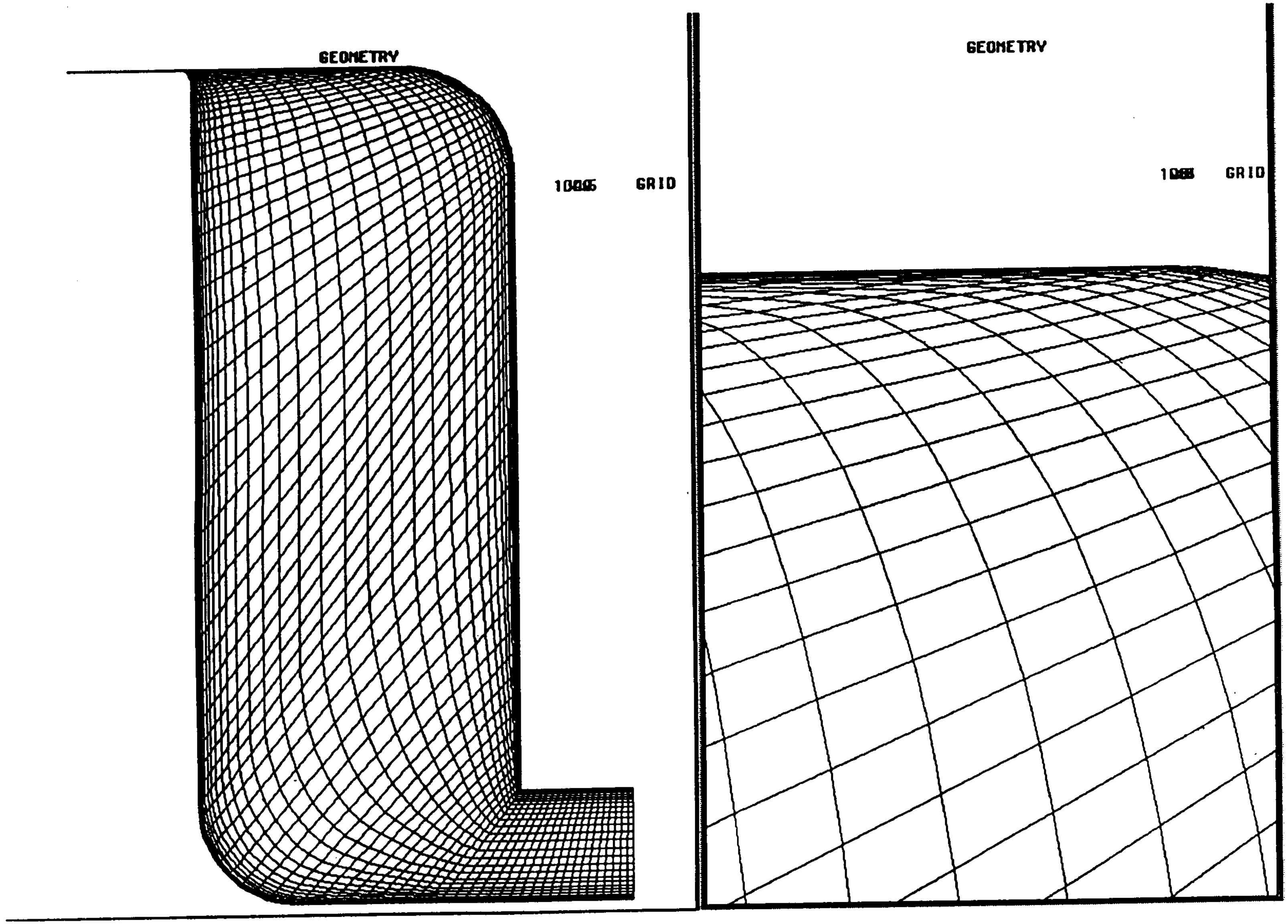
GEOMETRY
GRID
GEOMETRY
GRID

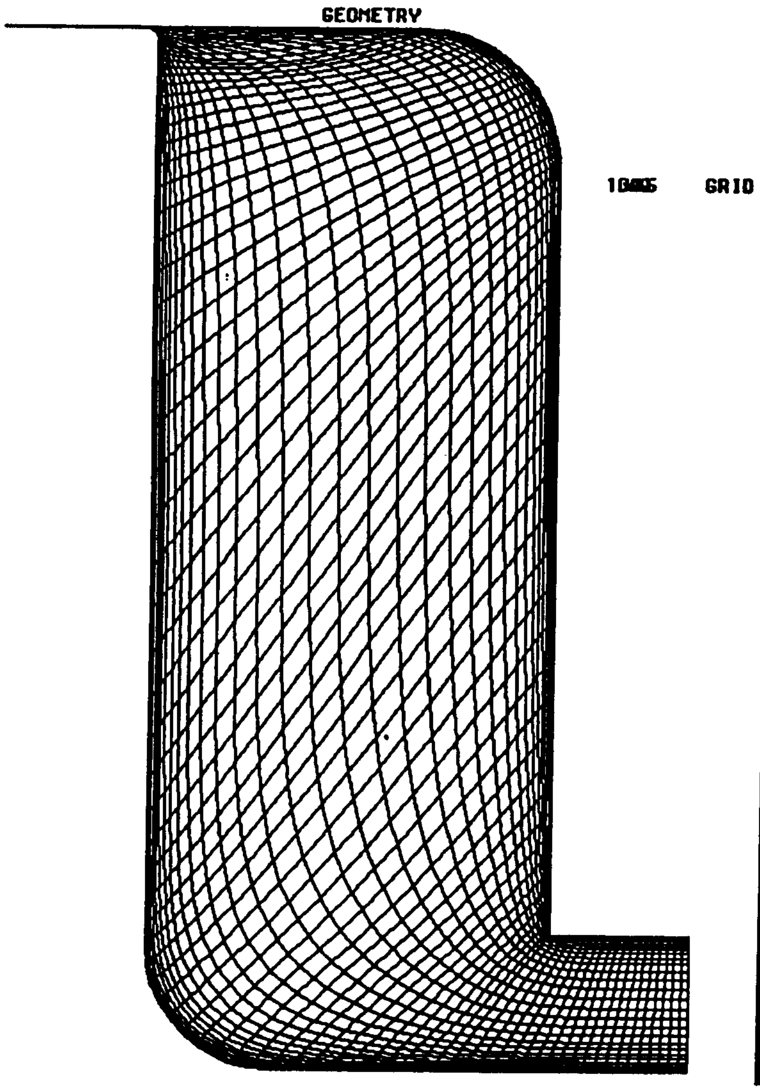
GEOMETRY
GRID

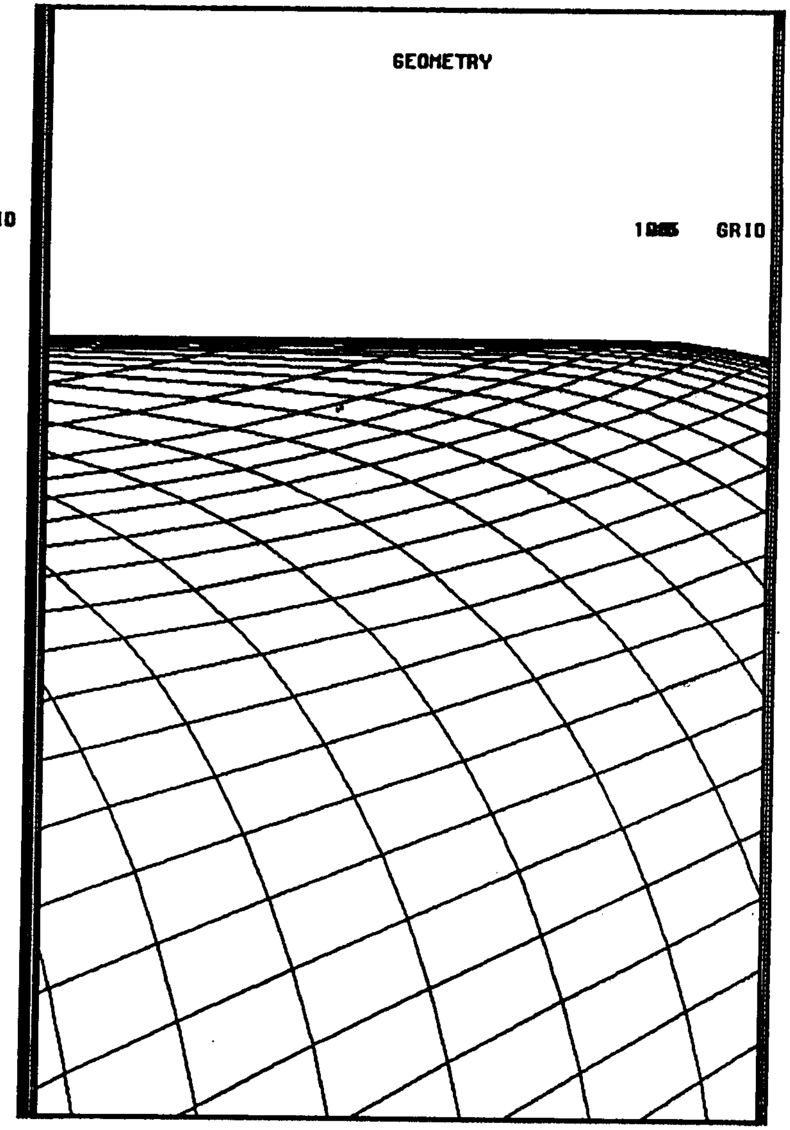
GEOMETRY
GRID

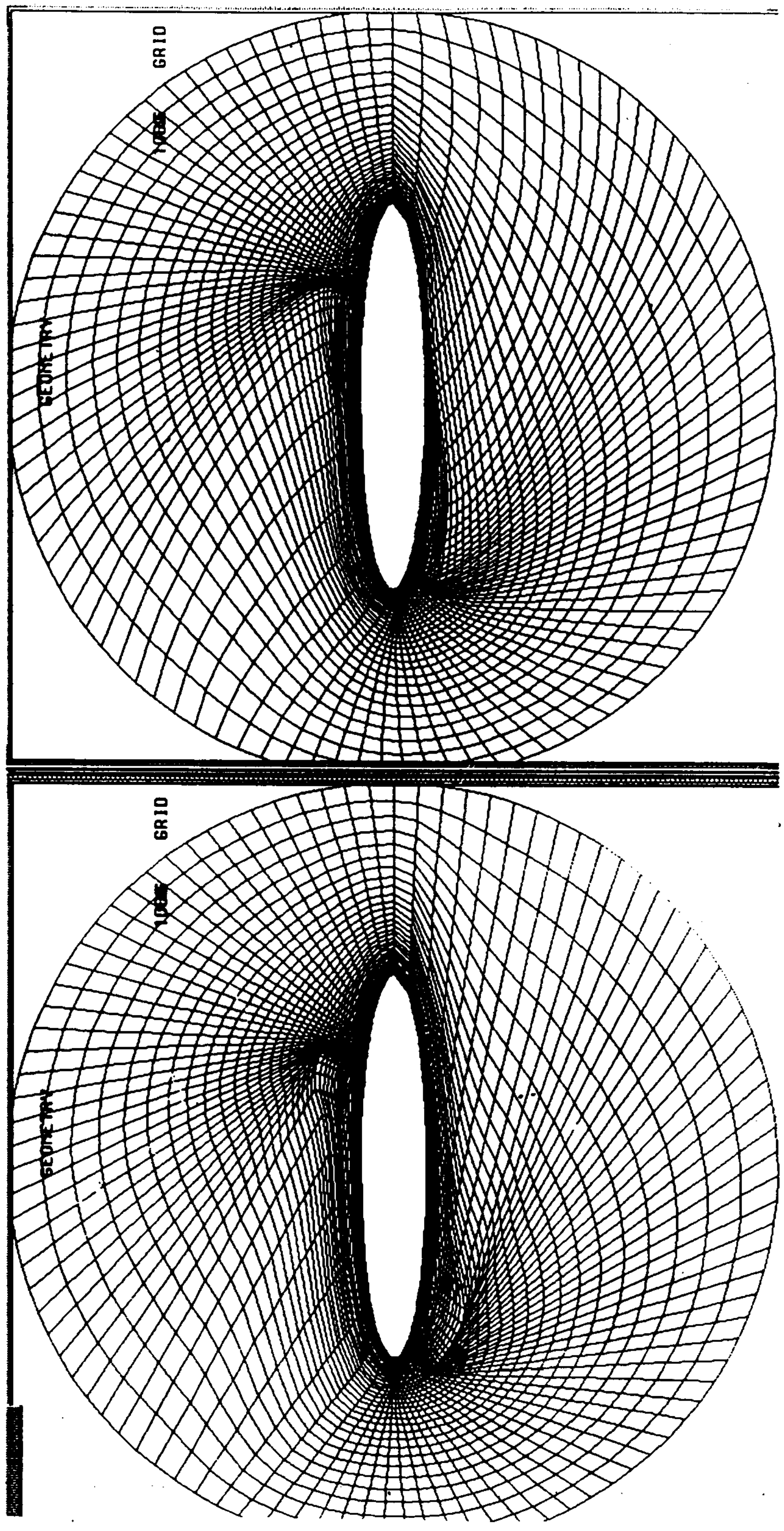
GEOMETRY
GRID
GEOMETRY
GRID

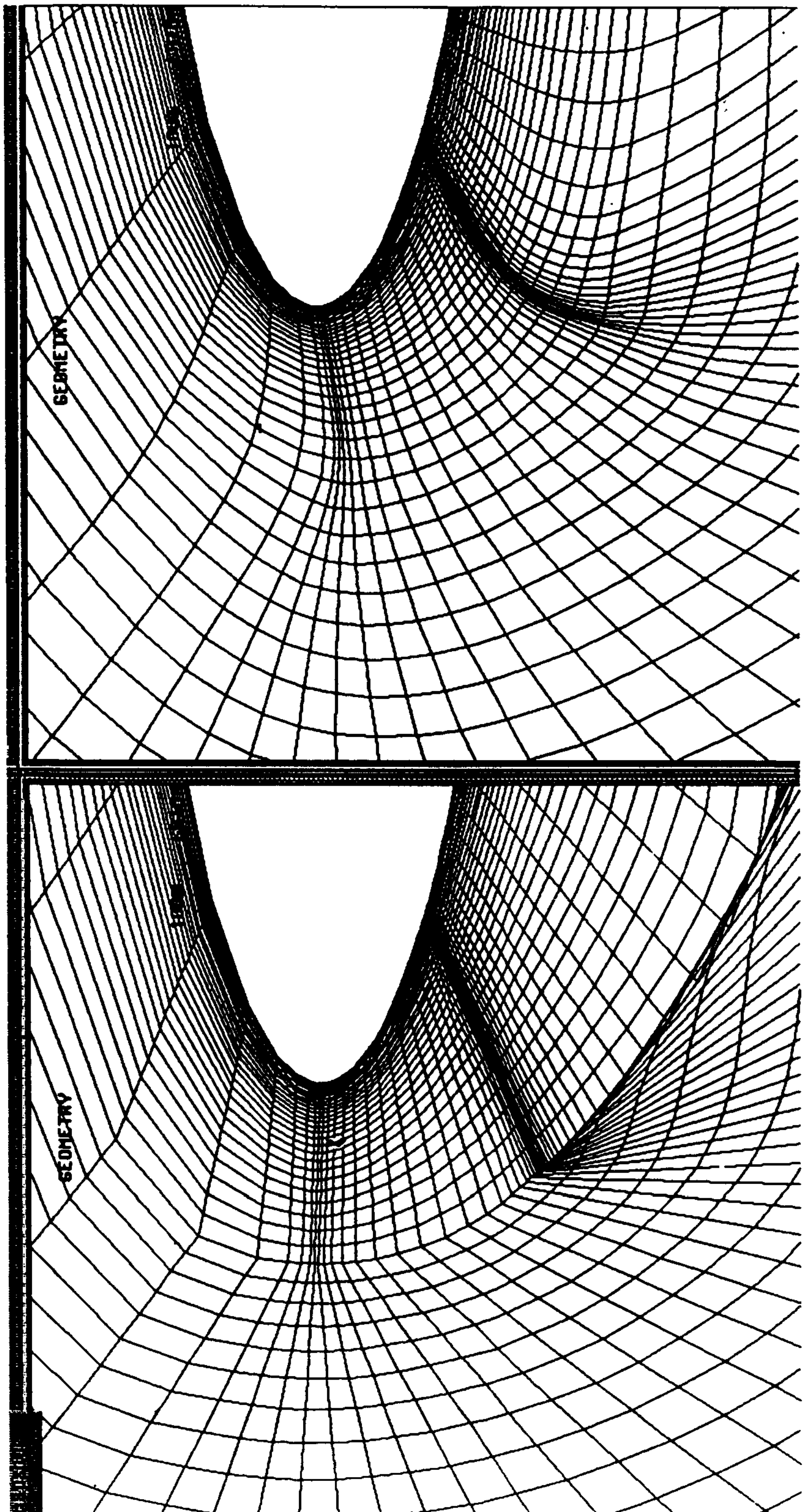
GEOMETRY
GEOMETRY

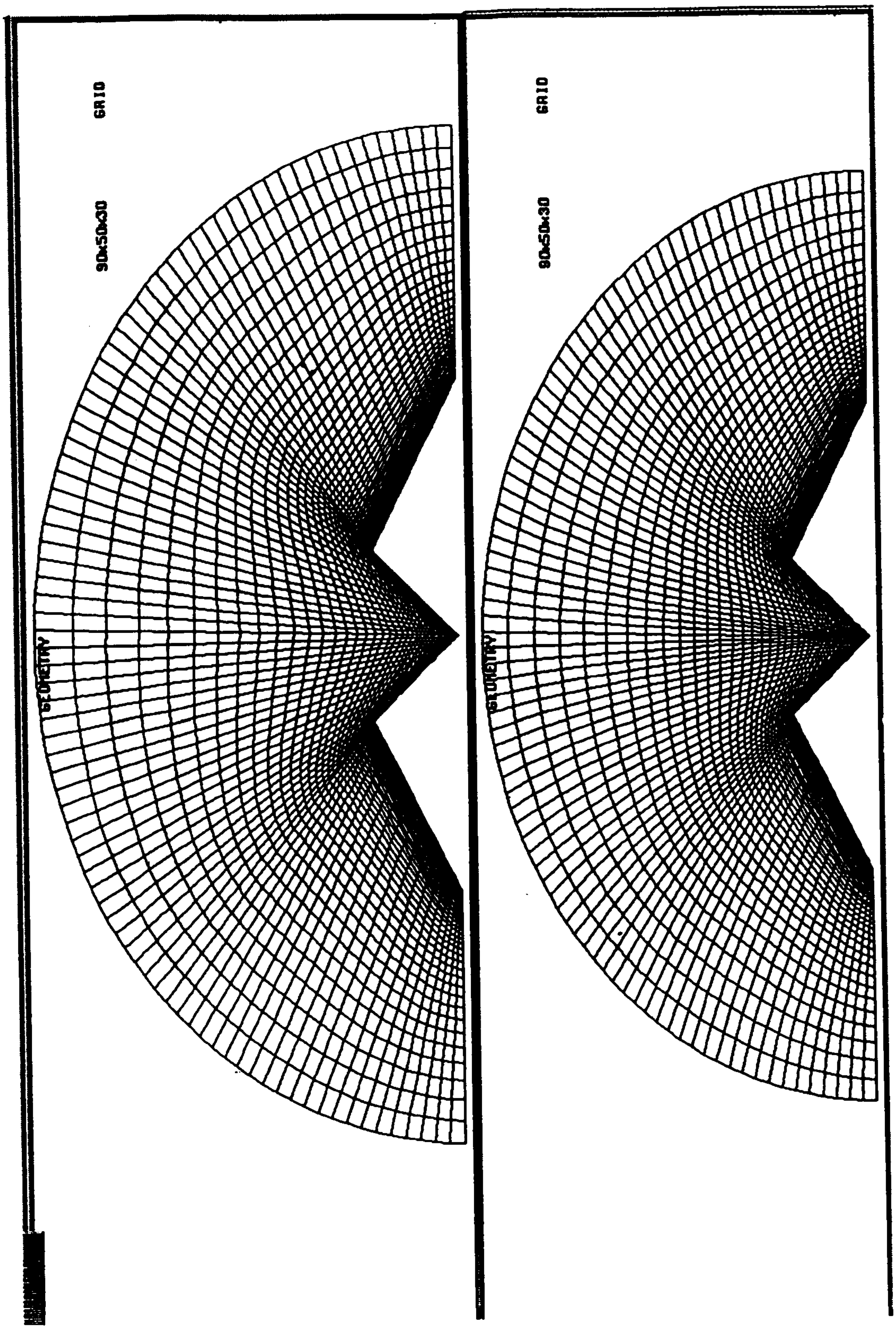
GEOMETRY
90x50x30
GRID
GEOMETRY
90x50x30
GRID

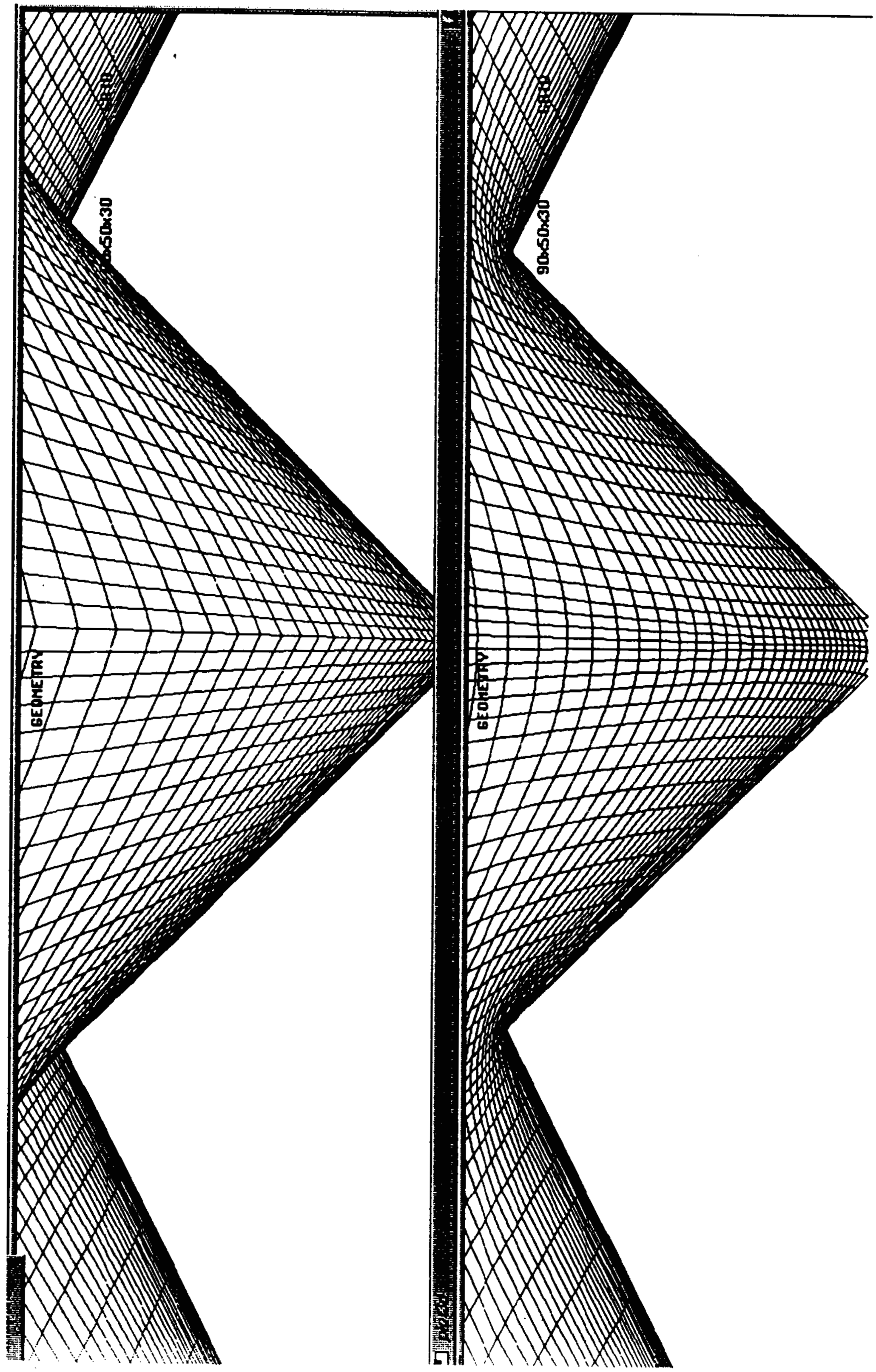
GEOMETRY
90x50x30
GEOMETRY
90x50x30

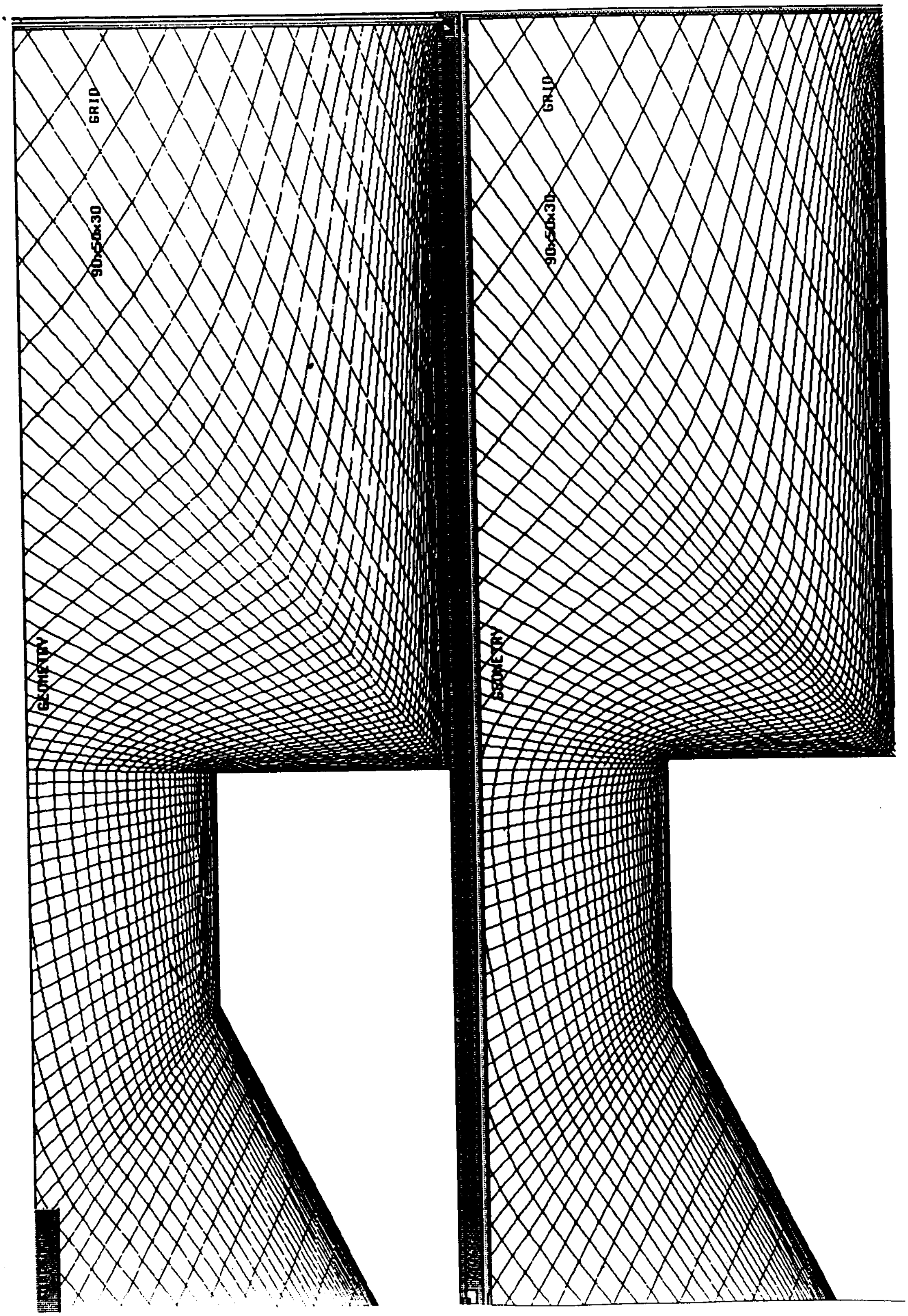
GRID
90x50x30
GEOMETRY
GRID
90x50x30
GEOMETRY

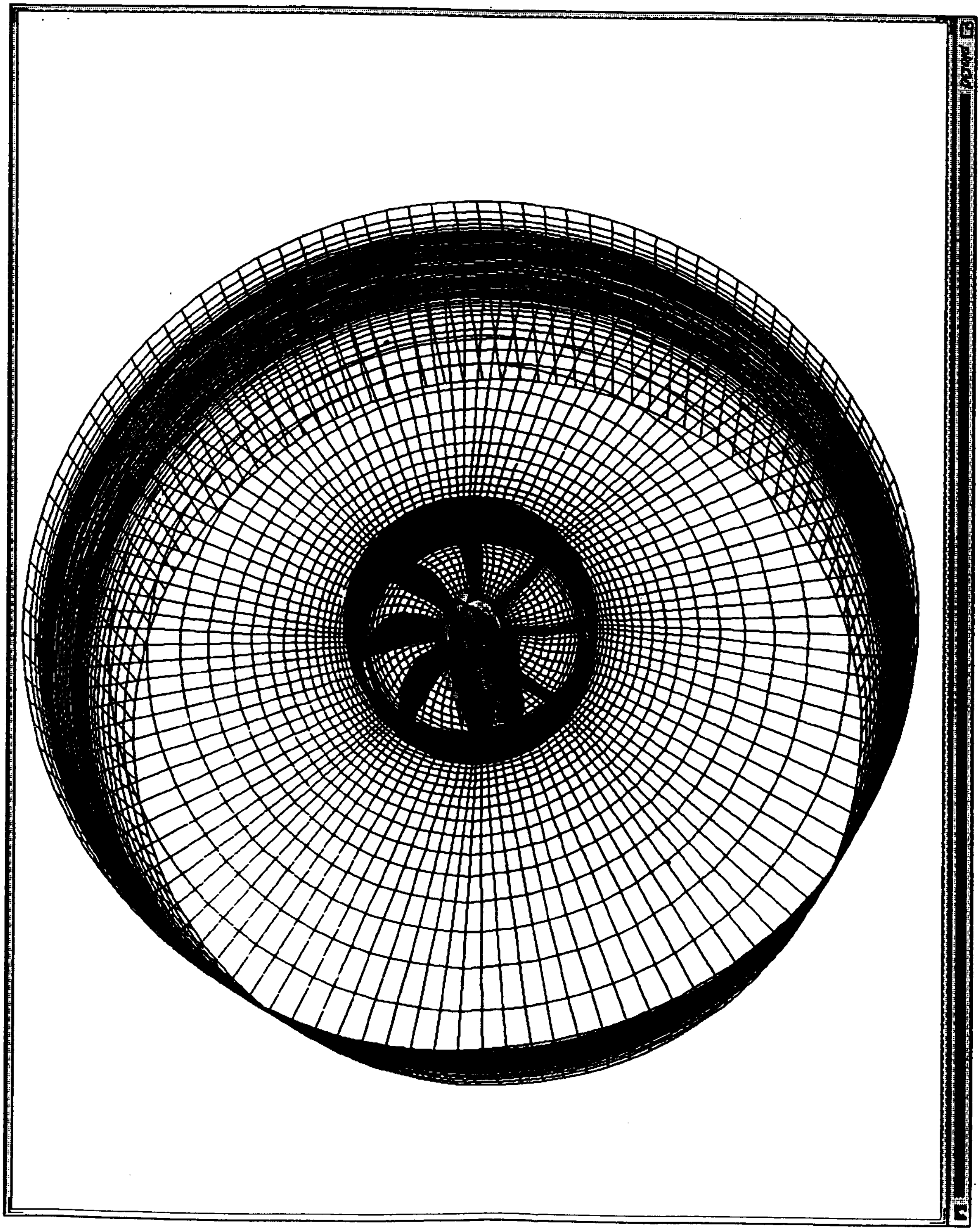

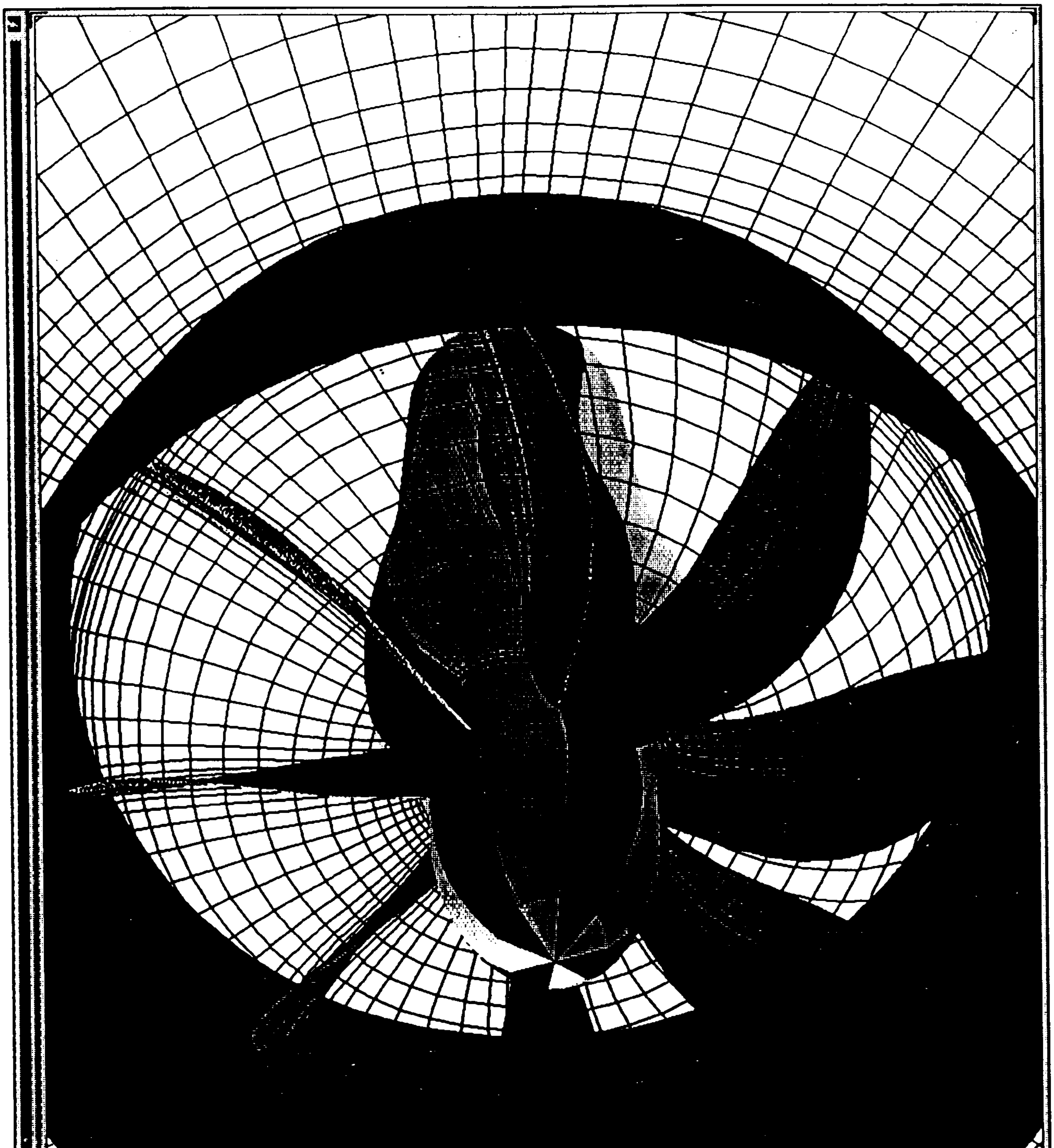
plot3d

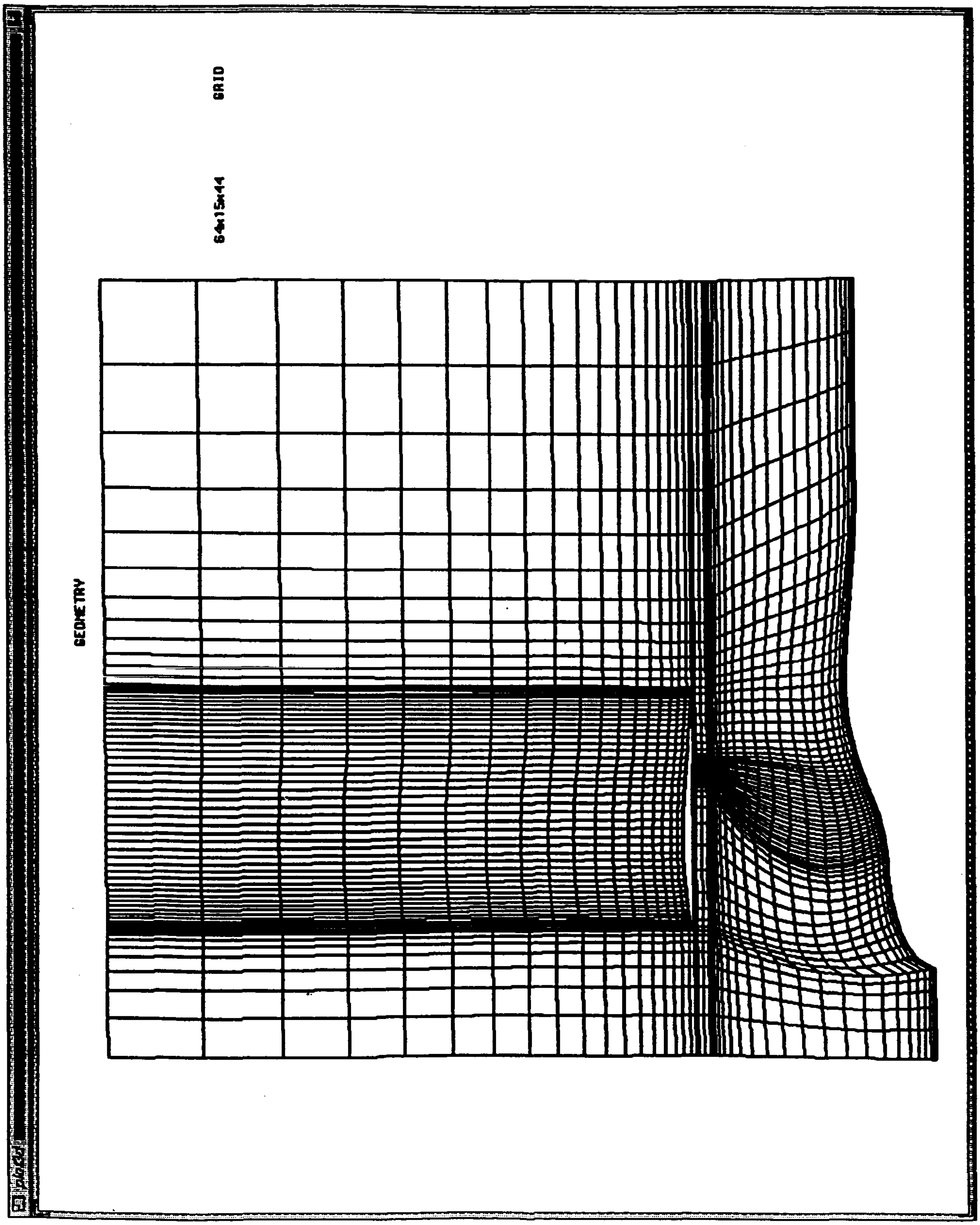
GEOMETRY
64x15x44
GRID

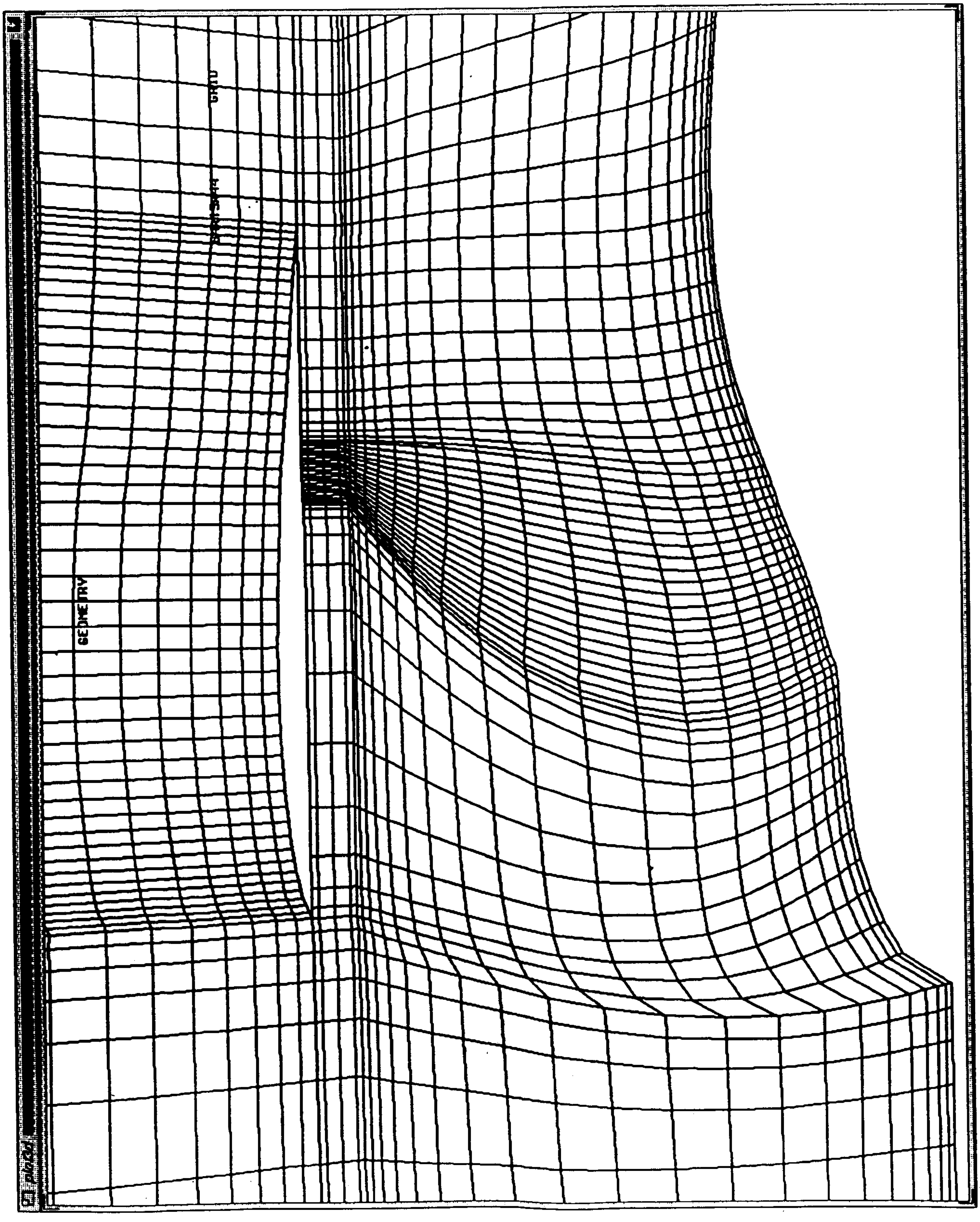
GRID
GEOMETRY

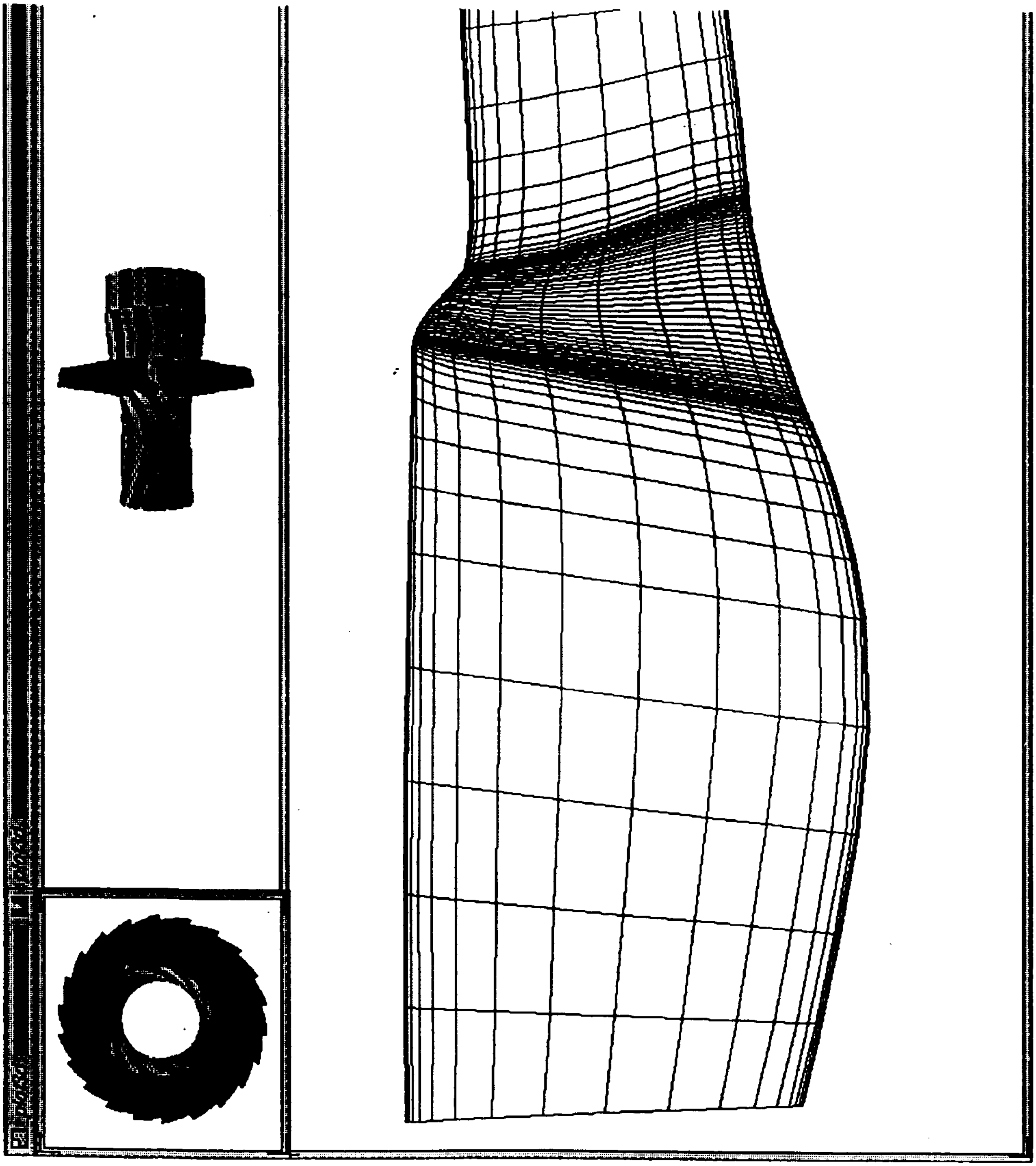

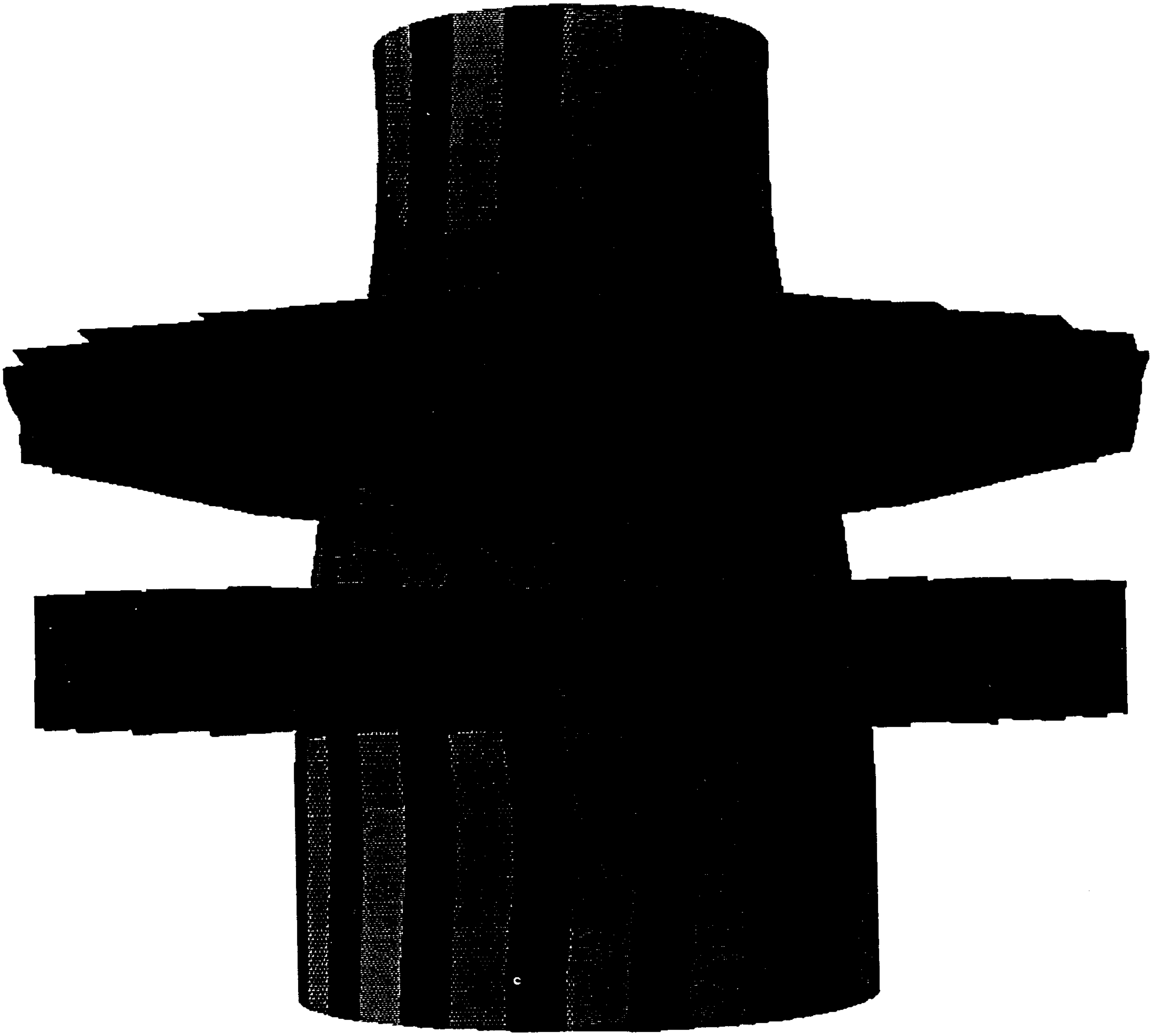

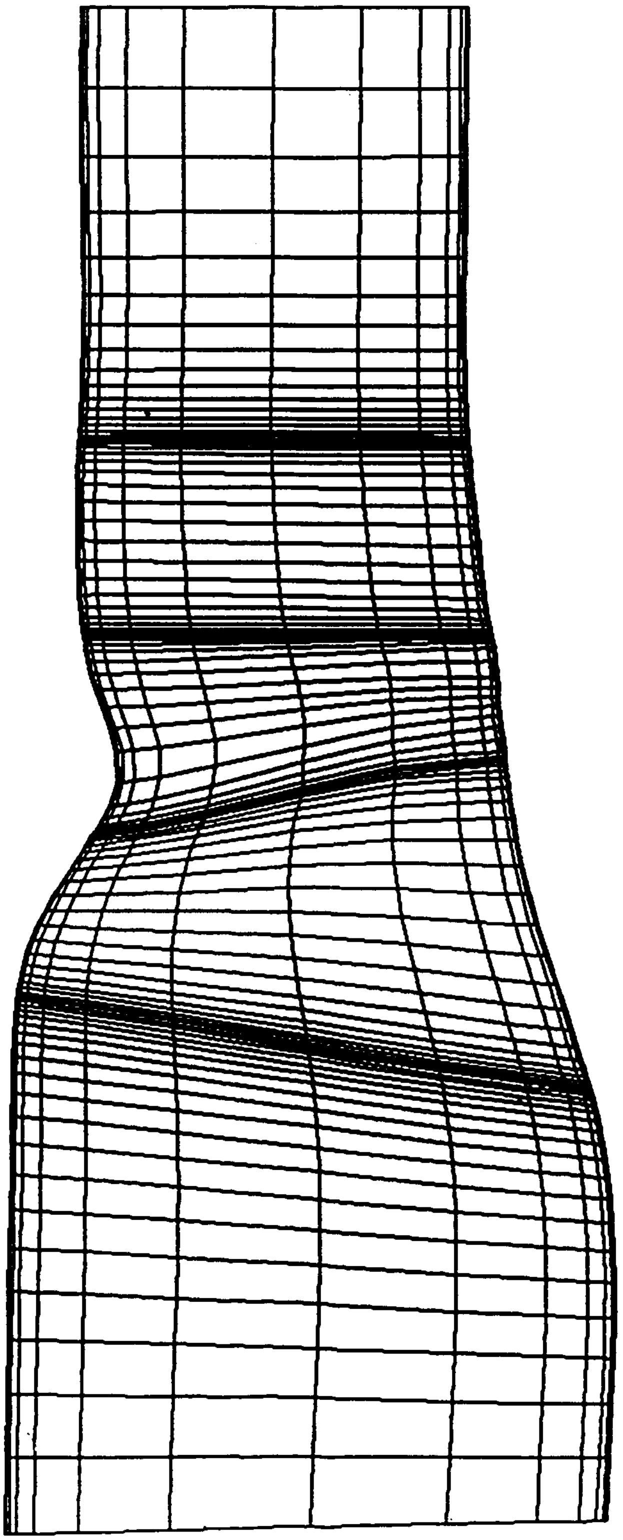

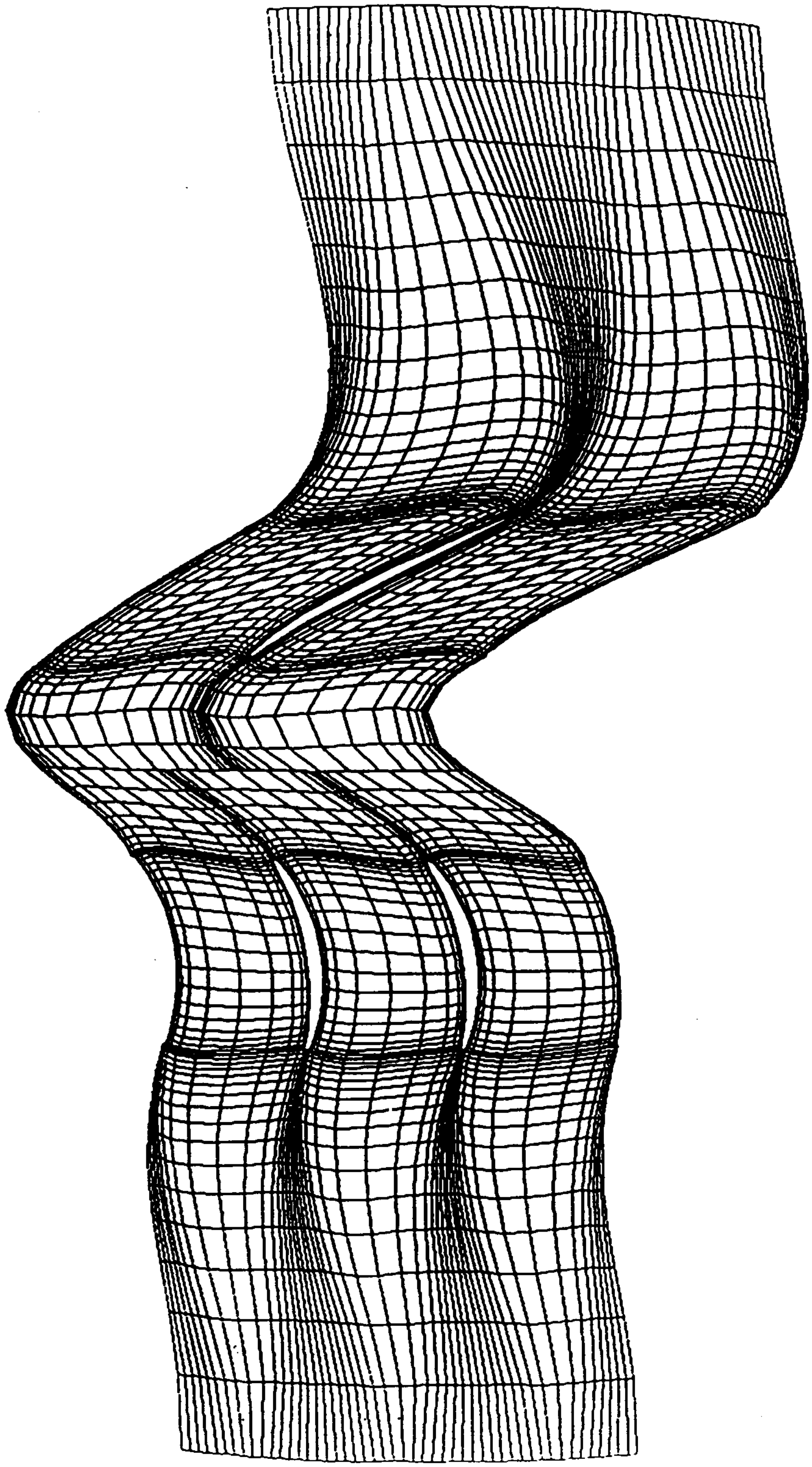

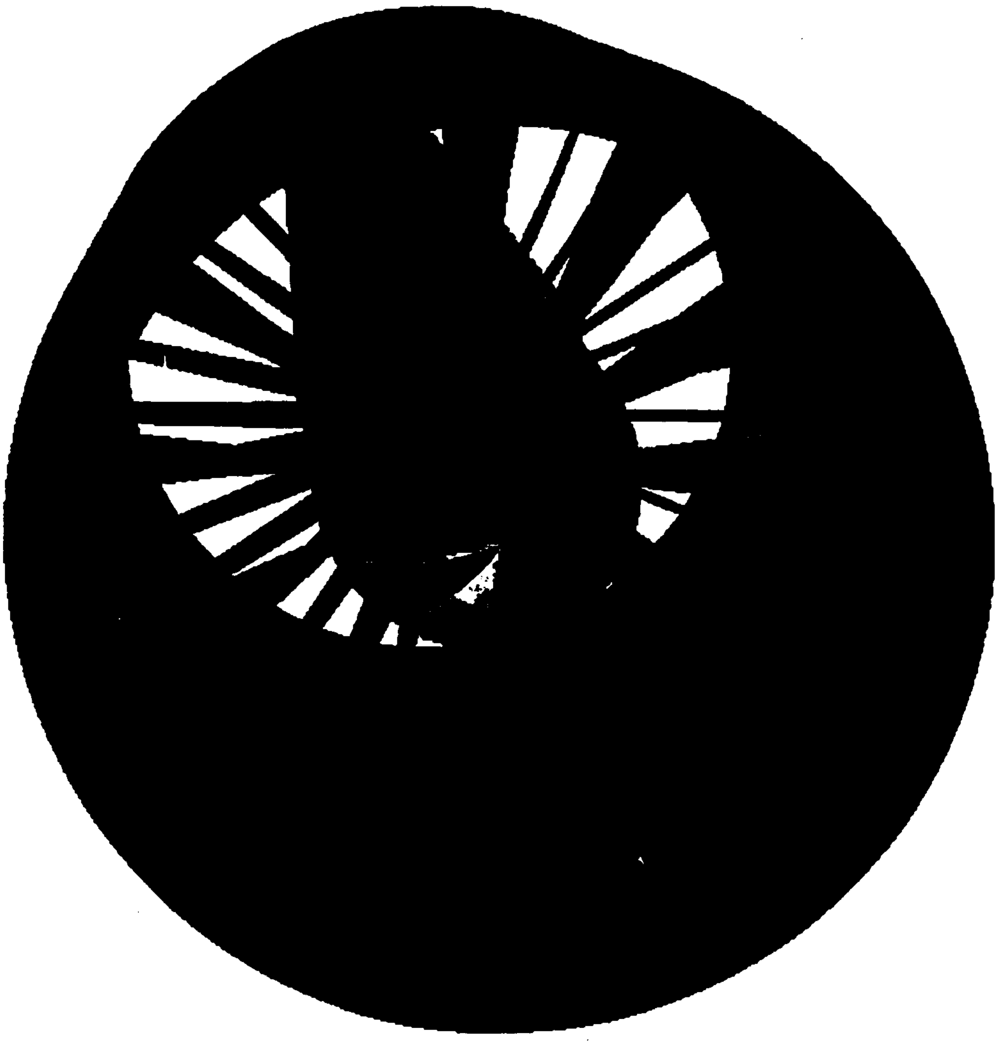

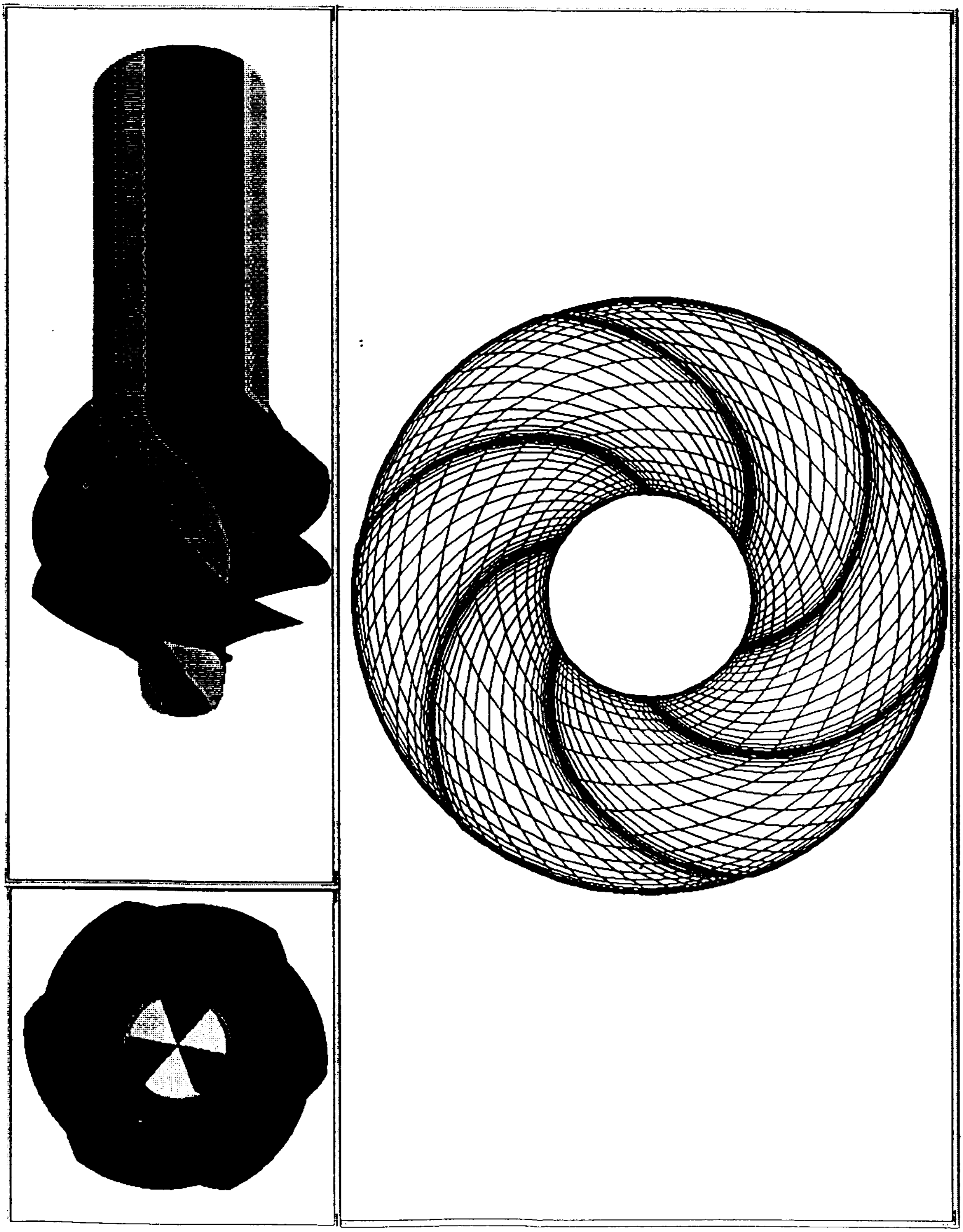

FUTURE

$$r_\xi \cdot r_\eta = 0$$
$$r_\xi \cdot r_\delta = 0$$
$$r_\xi \cdot (r_\eta \times r_\delta) = v$$

$$(r_\xi \cdot r_\eta)\eta = 0$$
$$(r_\xi \cdot r_\delta)\eta = 0$$
$$(r_\xi \cdot (r_\eta \times r_\delta))\eta = v_\eta$$

$$(r_\xi \cdot r_\eta)\delta = 0$$
$$(r_\xi \cdot r_\delta)\delta = 0$$
$$(r_\xi \cdot (r_\eta \times r_\delta))\delta = v_\delta$$

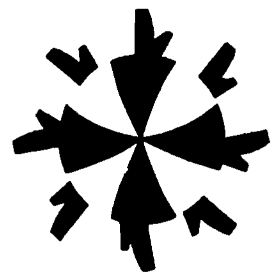

FUTURE

- Surface Grid Optimization Using NURBS Evaluation and Elliptic System Applications to the Parametric Space
- Full 3D Applications in a Multiblock Environment

N92-32301

Enhancements to the GRIDGEN Structured Grid Generation System for Internal and External Flow Applications

John P. Steinbrenner and John R. Chawner
MDA Engineering, Inc.
Arlington, Texas

GRIDGEN is a government domain software package for interactive generation of multiple block grids around general configurations. Though it has freely available since 1989, it has not been widely embraced by the internal flow community due to a misconception that it was designed for external flow use only. In reality GRIDGEN has always worked for internal flow applications, and GRIDGEN ongoing enhancements are increasing the quality of and efficiency with which grids for external *and* internal flow problems may be constructed.

The software consists of four codes used to perform the four steps of the grid generation process. GRIDBLOCK is first used to decompose the flow domain into a collection of component blocks and then to establish interblock connections and flow solver boundary conditions. GRIDGEN2D is then used to generate surface grids on the outer shell of each component block. GRIDGEN3D generates grid points on the interior of each block, and finally GRIDVUE3D is used to inspect the resulting multiple block grid. Three of these codes (GRIDBLOCK, GRIDGEN2D, and GRIDVUE3D) are highly interactive and graphical in nature, and currently run on Silicon Graphics, Inc. and IBM RS/6000 workstations. The lone batch code (GRIDGEN3D) may be run on any of several Unix based platforms.

The ease of flow domain decomposition using GRIDBLOCK has been improved through incorporation of edge point distribution commands and a new intermediate construction entity know as a *domain*. Grid point dimensions and distributions are now assigned to block boundary curves (connectors) *before* block construction. From here, block subsurfaces are defined by domains, which are simply a loop of connectors that represent the perimeter of the surface. The bounding connectors of the domain and the grid point distributions on the connectors provide sufficient data for the automatic initialization of surface grid points, which may be later refined as necessary in the GRIDGEN2D code. Blocks are then constructed by grouping domains into faces, and then by grouping 6 faces into a block. Grouping takes place in a point-and-click environment, and the reorientations of domains and faces needed to fit these components into the developing block is maintained automatically within the code, so that block construction may proceed in an intuitive manner. Further, block to block interfaces are determined automatically on the domain level, and domains without interblock connections may be assigned flow solver boundary conditions in a graphical interface.

Surface grid generation in GRIDGEN2D is being improved with the addition of higher order surface definitions (NURBS and parametric surfaces input in IGES format and bicubic surfaces input in PATRAN Neutral File format) and double precision mathematics. In addition, two types of automation have been added to GRIDGEN2D that reduce the learning curve slope for new users and eliminate work for experienced users.

Volume grid generation using GRIDGEN3D has been improved via the addition of an advanced hybrid control function formulation that provides both orthogonality and clustering control at the block faces and clustering control on the block interior.

PRECEDING PAGE BLANK NOT FILMED

Enhancements to the GRIDGEN Structured Grid Generation System for Internal and External Flow Applications

NASA Workshop for Computational Fluid Dynamic
Applications in Rocket Propulsion
28-30 April 1992

by

John P. Steinbrenner (presenter)
John R. Chawner

MDA Engineering, Inc.

OUTLINE

- Overview of the GRIDGEN System
- Review of current GRIDGEN capabilities (Version 6)
- Summary of GRIDGEN enhancements (Version 8)
- Continuing GRIDGEN improvement
- Conclusions

MDA Engineering, Inc.
Arlington, TX

Overview of the GRIDGEN System

- GRIDGEN is a series of four codes for the generation of 3D, multiple block, structured grids.
- GRIDBLOCK (interactive): domain decomposition.
- GRIDGEN2D (interactive): 3D surface grid generation.
- GRIDGEN3D (batch): volume grid generation.
- GRIDVUE3D (interactive): volume grid visualization.

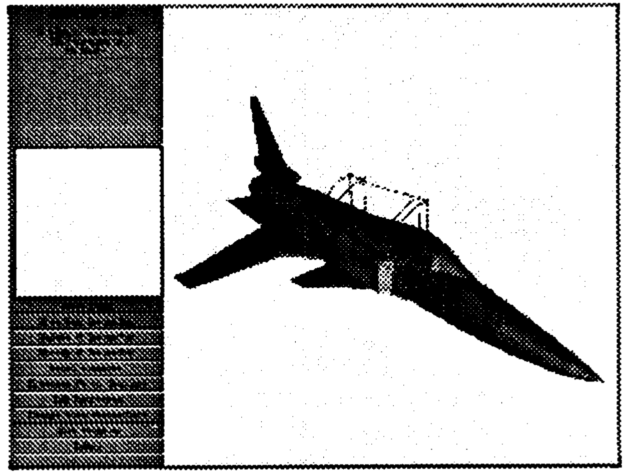

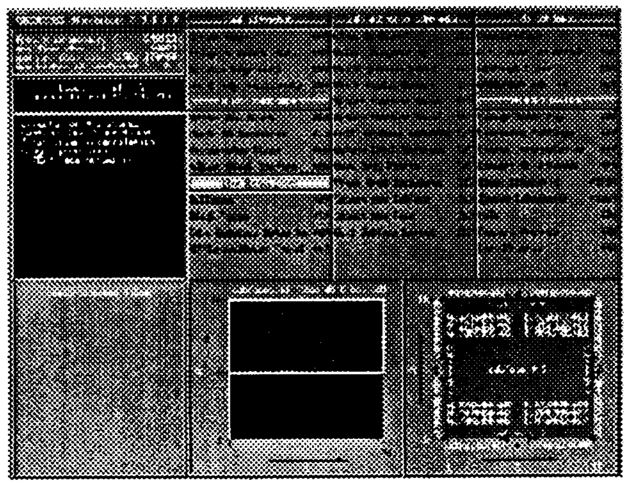

ORIGINAL PAGE IS
OF POOR QUALITY

MDA Engineering, Inc.
Arlington, TX

Overview of the GRIDGEN System

- The interactive codes have been written using IRIS GL and currently run only on Silicon Graphics 4D and IBM RS/6000 workstations.
- The interactive codes also require 24-bit planes and Z-buffer.
- GRIDGEN documentation consists of an official Air Force manual and several AIAA and AGARD papers.
  - "The GRIDGEN 3D Multiple Block Grid Generation System", Vols. I and II, WRDC-TR-90-3022, Flight Dynamics Lab., Wright-Patterson AFB, July 1990.
  - "Enhancements to the GRIDGEN System for Increased User Efficiency and Grid Quality", AIAA paper no. 92-0662, AIAA 30th Aerospace Sciences Meeting, January 1992.
  - "A Structured Approach to Interactive Multiple Block Grid Generation", from AGARD-CP-644 "Applications of Mesh Generation to Complex 3-D Configurations", 1989.

Overview of the GRIDGEN System

- Version 6, USAF
  - Developed for USAF at Wright-Patterson AFB, 1987-1990.
  - Technical Supervision: Dr. Donald W. Kinsey.
  - Software Distribution: Lt. John Seo (513) 255-2481, to U.S. government agencies and U.S. industry.
- Version 8, NASA Langley
  - Currently being developed for NASA Langley Research Center, 1991-1992.
  - Technical Supervision: Dr. Robert E. Smith.
  - Software Distribution: Dr. Jamshid Abolhassani (804) 864-5776 (Sept. 1992).
- Version 9, ? (currently being negotiated)

OUTLINE

- Overview of the GRIDGEN System
- Review of current GRIDGEN capabilities (Version 6)
- Summary of GRIDGEN enhancements (Version 8)
- Continuing GRIDGEN improvement
- Conclusions

Databases (Version 6)

- The user provides GRIDGEN with a geometric description (a database) of the configuration.
- A database consists of a collection of patches called networks.
- Each network is a 2D array of coordinate data on the configuration.
- The networks are *not* the same as the surface grid.
- The database may be obtained from a CAD system, an external user program, or GRIDGEN2D.

GRIDBLOCK (Version 6)

- GRIDBLOCK is used to decompose the domain surrounding the database into blocks.
- The user interactively draws 3D curves (connectors) that define the edges of each block.
  - Straight Line
  - Circular/Elliptical Arc
  - Piecewise Cubic
  - Line on Database
- Connectors may be drawn in any order and in any direction.

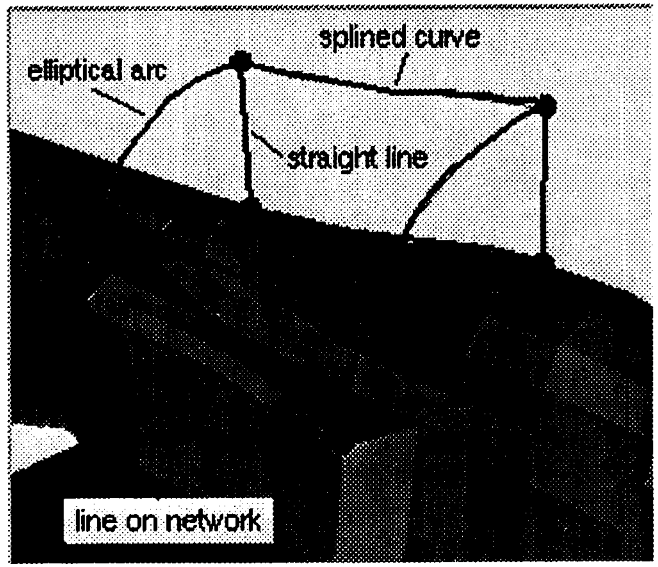

MDA Engineering, Inc.
Arlington, TX

GRIDBLOCK (Version 6)

- The user groups connectors into blocks.
- Blocks may contain up to 12 edges; singularities are allowed.
- The user interactively specifies computational (ξ, η, ζ) coordinate axes and number of points in each block.

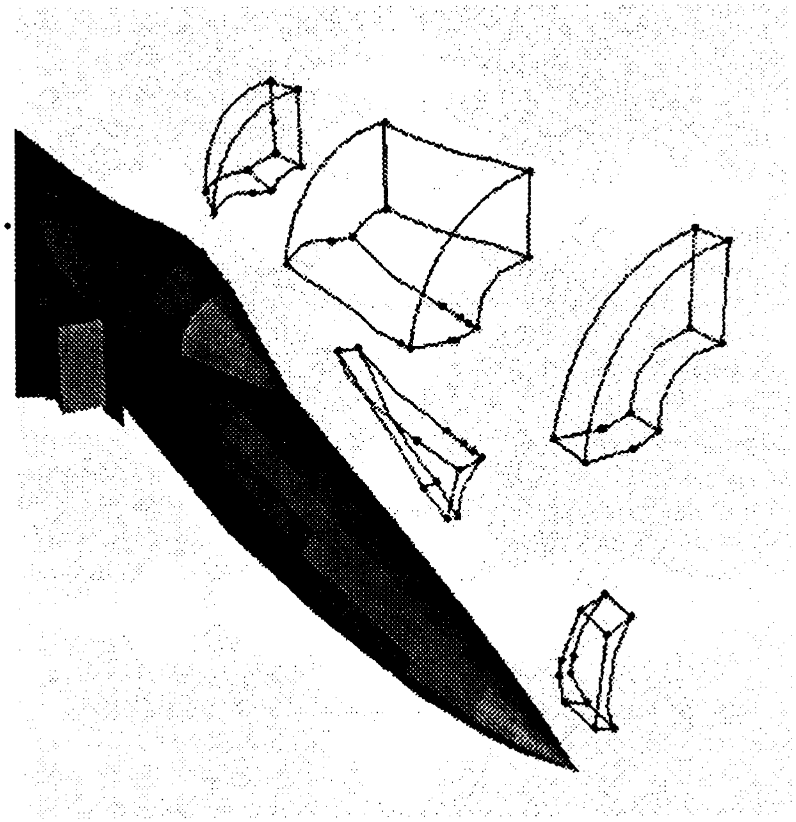

GRIDBLOCK (Version 6)

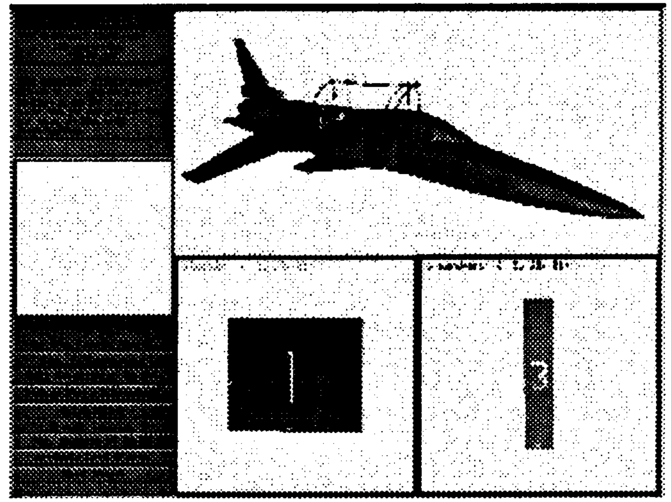

- The user specifies interblock connections and flow solver BCs.
- Interblock connections must be set.
  - GRIDGEN2D can then ensure consistency between blocks.
  - GRIDGEN3D can then provide slope continuity across interfaces.
- The user may set TEAM (USAF Euler solver) flow BC's.
  - TEAM restrictions on connections are checked to be sure grid is compatible.
  - GRIDGEN3D writes the connection and BC data in TEAM format.

MDA Engineering, Inc.
Arlington, TX

GRIDGEN2D (Version 6)

- GRIDGEN2D is used to generate the surface grids on the six faces of each block in the system.
- It may also be used to generate single block or single surface grids without running GRIDBLOCK first.
- For each face of each block...
  - Distribute points on each of the four edges.
  - Initialize surface points using algebraic methods.
  - Refine surface points using elliptic PDE methods.

GRIDGEN2D (Version 6)

- GRIDGEN2D edge point distribution.
  - GRIDBLOCK connectors are used to define edge shape or a new edge shape may be drawn interactively.
  - The edge may be divided into subedges for more control of point distribution.
  - Grid points are distributed using...
    * Two-sided tanh (Vinokur) stretching.
    * One-sided sinh and tanh stretching.
    * One-sided geometric progression.
    * Equal spacing.
    * Copy spacing from elsewhere in grid.
    * Cluster to edge curvature.

MDA Engineering, Inc.
Arlington, TX

GRIDGEN2D (Version 6)

- GRIDGEN2D algebraic methods.
  - Standard TFI with computational LaGrange BF
  - Standard TFI with arclength based LaGrange BF
  - Ortho TFI with computational Hermite BF
  - Polar TFI
  - Re-distribution methods.
  - Parametric methods to fit the grid to the database.

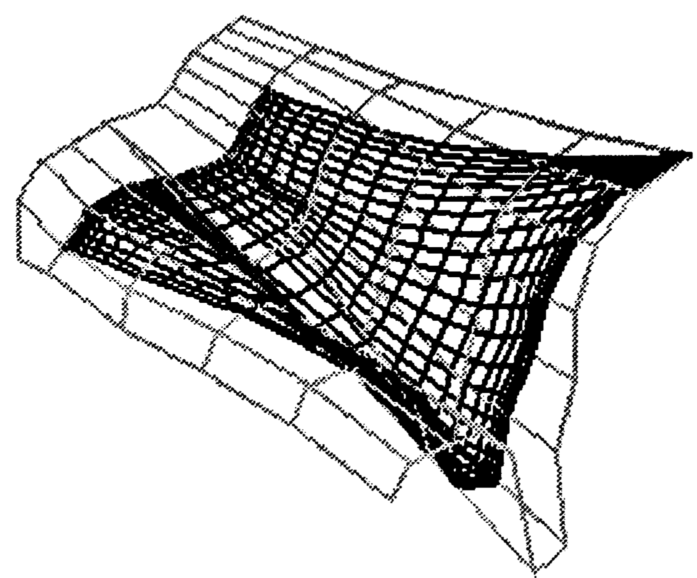

MDA Engineering, Inc.
Arlington, TX

GRIDGEN2D (Version 6)

- GRIDGEN2D's elliptic PDE methods.
  - Poisson's Equation on 3D surfaces solved using pointwise SOR with Ehrlich's optimal relaxation factor.
  - Six hybrid control function formulations.
  - Five solver types.
  - Five edge BC types

GRIDGEN2D (Version 6)

- GRIDGEN2D elliptic PDE methods cont'.

  - Hybrid control functions combine background and foreground control functions.
  - Background control functions tend to influence interior grid points, e.g. LaPlace, Thomas and Middlecoff, or Fixed Grid.
  - Foreground control functions tend to influence grid points points near the edges, e.g. Sorenson.
  - (b) Thomas and Middlecoff
  - (c) Sorenson
  - (d) Thomas and Middlecoff plus Sorenson

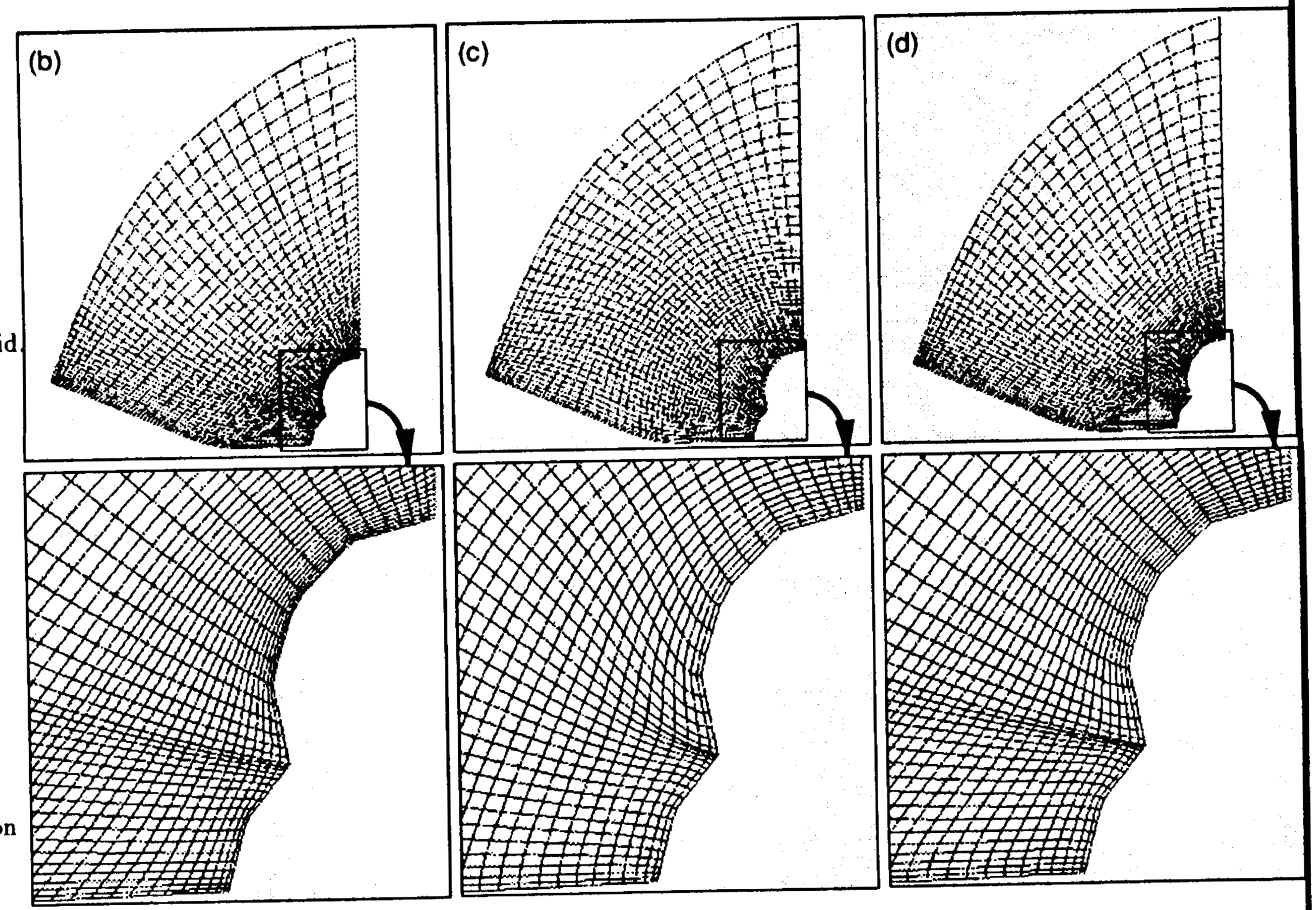

MDA Engineering, Inc.
Arlington, TX

GRIDGEN2D (Version 6)

- GRIDGEN2D elliptic PDE methods cont'.
  - Three conventional solvers:
    - Solve for x, y and leave z as is.
    - Solve for x, y, z.
    - Solve for x, y and interpolate z from the database.
  - Two parametric solvers:
    - Solve for x, y, z in terms of the current surface shape.
    - Solve for x, y, z in terms of a database network.

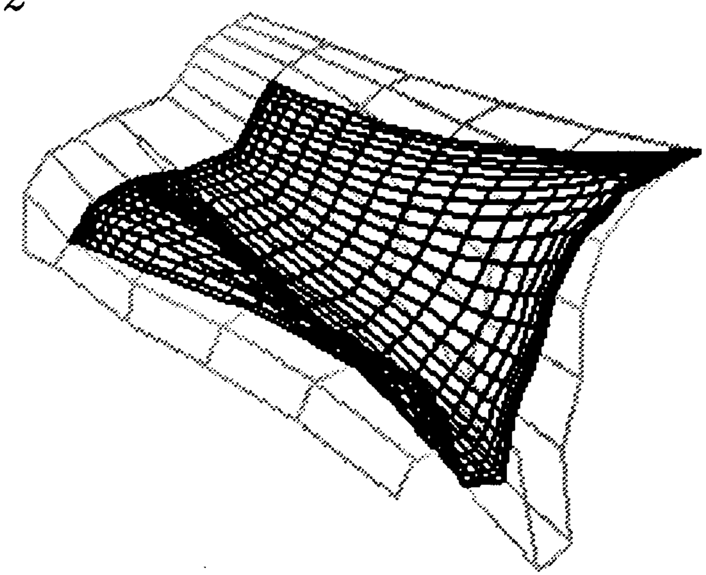

GRIDGEN2D (Version 6)

- GRIDGEN2D tools
  - A face may be divided into subfaces.
    - ∗ This allows the shape of and distribution of points on grid lines on the face interior to be explicitly set by the user.
  - 8600 lines of help text may be accessed via a browser.
  - There is a utility to graphically move any point.

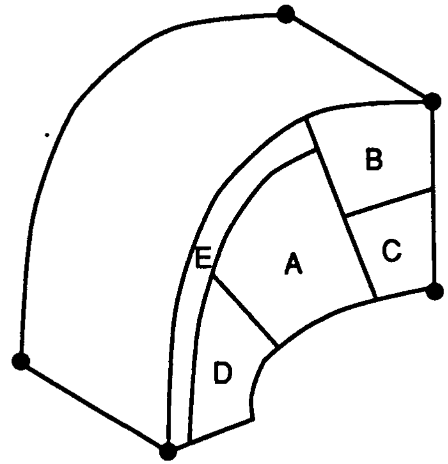

C-7

GRIDGEN3D and GRIDVUE3D (Version 6)

- GRIDGEN3D is a batch code written for a Cray X/MP running the UNICOS operating system
- It may easily be modified for other UNIX hardware.
- Algebraic methods include standard TFI with computational or arclength based LaGrange blending functions.
- Elliptic PDE methods solve the 3D Poisson equations using pointwise SOR with optimal relaxation factors.
- LaPlace, Thomas and Middlecoff, Fixed Grid, or Sorenson control functions are available.
- GRIDVUE3D is used to visualize volume grids written in either GRIDGEN or PLOT3D format.

MDA Engineering, Inc.
Arlington, TX

OUTLINE

- Overview of the GRIDGEN System
- Review of current GRIDGEN capabilities (Version 6)
- Summary of GRIDGEN enhancements (Version 8)
- Continuing GRIDGEN improvement
- Conclusions

MDA Engineering, Inc.
Arlington, TX

Summary of GRIDGEN enhancements (Version 8)

- Double precision
- Add edge point grid generation to GRIDBLOCK.
  - New connector shapes: Cubic on surface and read from file.
  - New distribution function: Monotonic Quadratic Rational Spline (MQRS), allows a smooth variation of grid point spacing along the connector with explicit control over grid point locations on the interior.
  - Improved editing capability: shape or number of points can be changed and point distribution is updated automatically.

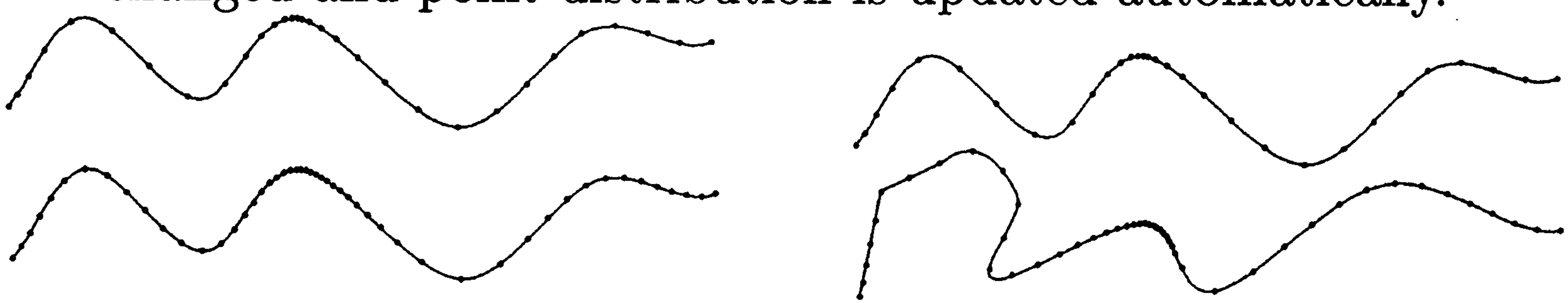

Summary of GRIDGEN enhancements (Version 8)

- Add the domain entity to GRIDBLOCK.
  - Connectors grouped into surfaces called domains. Then domains are grouped into blocks.
  - A domain may be a whole face or only a subface.
  - Point to point interblock connections will be determined *automatically.*
  - Flow BCs will be set by graphically picking the domain; no more typing indices.
  - Algebraic surface grid generation will be performed automatically; the GRIDGEN2D workload is drastically reduced.
  - Changes in number of points on a single connector will be propagated semi-automatically throughout the grid.

MDA Engineering, Inc.
Arlington, TX

Summary of GRIDGEN enhancements (Version 8)

- Add the domain entity to GRIDBLOCK cont'.
  - A domains is an entity between the connector and block entities in the GRIDBLOCK hierarchy.
  - They may represent a region of a single flow solver BC or an interblock connection.
  - The user creates a domain by interactively picking the individual connectors in a closed loop.
  - Domains must be computationally rectangular.

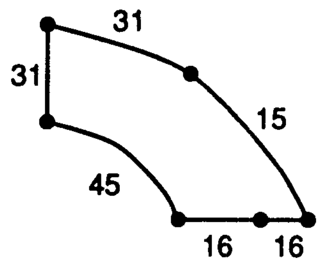

This domain maps into a 45x31 region.

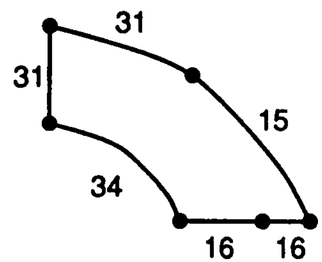

This domain does not map into a rectangular region.

MDA Engineering, Inc.
Arlington, TX

Summary of GRIDGEN enhancements (Version 8)

- Add the domain entity to GRIDBLOCK cont'.
  - Blocks are now defined by six faces, rather than twelve edges.
  - Faces are defined by at least one domain.
  - Blocks and faces are checked for a consistent number of points during construction.
  - An example of a face consisting of four non-unique domains.

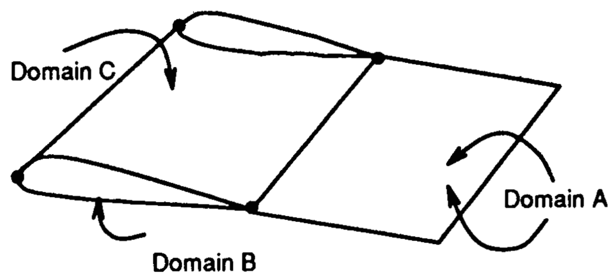

MDA Engineering, Inc.
Arlington, TX

Summary of GRIDGEN enhancements (Version 8)

- Change Number of Points Utility
  - Low level changes to an existing grid will be propagated semi-automatically throughout the entire blocking system.
  - Rather than edit a journal file, the code will do most of the work and prompt the user for any changes.
  - After a change in the number of points on the indicated connector, the code would ask the user to apportion the new points across the affected connectors.

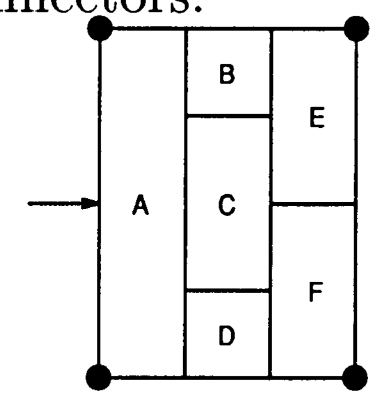

MDA Engineering, Inc.
Arlington, TX

Summary of GRIDGEN enhancements (Version 8)

- GRIDGEN3D upgrades.
  - Hybrid control functions added for improved grid quality.
  - Background CF Φ_b: control on interior of block, e.g. LaPlace, Thomas & Middlecoff
  - Foreground CF Φ_f: control near faces, e.g. Sorenson
  - Hybrid = Background + Foreground
    * Compute Φ_b on block interior, Φ_f on faces.
    * Calculate $\Phi_\Delta = \Phi_f - \Phi_b$ on faces.
    * Interpolate Φ_Δ from faces into interior using exponentially decaying blending functions.
    * Sum $\Phi = \Phi_\Delta + \Phi_b$

MDA Engineering, Inc.
Arlington, TX

Summary of GRIDGEN enhancements (Version 8)

- GRIDGEN3D upgrades.
  - Grid sequencing added: faster convergence rate in the PDE solver.
  - Robustness improved: one sided differencing based on the sign of the control function.
  - Efficiency improved: I/O of temporary files changed to reduce overhead.
  - Grid quality: several quality measures are written to a file for visualization using PLOT3D or FAST.

MDA Engineering, Inc.
Arlington, TX

Summary of GRIDGEN enhancements (Version 8)

- GRIDGEN2D Customization.
  - Goal: reduce the effort required to use GRIDGEN2D.
  - Method: eliminate seldom-used buttons and text prompts.
  - Benefit: fewer keystrokes, less confusion.
  - Implementation: verbosity setting and preferencing.
    * Terse verbosity hides obscure prompts from the user (meant for novices).
    * Preferencing allows the user to pre-select certain options such as control function type (meant for experts).
- Double precision GRIDGEN2D.

MDA Engineering, Inc.
Arlington, TX

Summary of GRIDGEN enhancements (Version 8)

- Standardized higher order surface models (databases).
- PATRAN Neutral File.
  - Bicubics.
- DT-IGES, a simplified form of the IGES standard.
  - Parametric surface.
  - Rational B-spline surface.
  - Implementation will use the Navy David Taylor Research Center DT_NURBS Library of surface geometry routines.

OUTLINE

- Overview of the GRIDGEN System
- Review of current GRIDGEN capabilities (Version 6)
- Summary of GRIDGEN enhancements (Version 8)
- Continuing GRIDGEN improvement
- Conclusions

MDA Engineering, Inc.
Arlington, TX

Continuing GRIDGEN improvement

- Merge GRIDBLOCK and GRIDGEN2D.
  - Less user confusion (What do I do in which code?)
  - Improved usability through a single GRIDBLOCK style GUI.
  - More maintainability through elimination of duplicate functionality.
- Support higher order surface definitions (databases) in standard file formats (e.g., NASA-IGES).
- Increase user base by porting to other hardware.

MDA Engineering, Inc.
Arlington, TX

Continuing GRIDGEN improvement

- Develop an interactive GRIDGEN3D.
  - Interactivity will improve user control over volume grid generation in the same manner as for surface grid generation.
  - Perform grid generation locally or remotely.
- Incorporate unstructured grid generation techniques.
  - Most of the existing GRIDGEN tools can be generalized for use with unstructured techniques.
  - Users will gain more capabilities within a familiar GUI.

MDA Engineering, Inc.
Arlington, TX

575

OUTLINE

- Overview of the GRIDGEN System
- Review of current GRIDGEN capabilities (Version 6)
- Summary of GRIDGEN enhancements (Version 8)
- Continuing GRIDGEN improvement
- Conclusions

MDA Engineering, Inc.
Arlington, TX

Conclusions

- GRIDGEN currently provides *at no cost* a practical and well-tested structured grid generation capability.
- Improvements are currently being added to the government domain version of GRIDGEN.
- GRIDGEN will remain in the government domain well into the future.
- MDA Engineering is committed to supporting GRIDGEN.

MDA Engineering, Inc.
Arlington, TX

CAGI: Computer Aided Grid Interface –A Work in Progress

By

Bharat K. Soni
Associate Professor

Tzu-Yi Yu and David Vaughn
NSF Engineering Research Center
for Computational Field Simulation
Mississippi State University

ENGINEERING RESEARCH CENTER FOR COMPUTATIONAL FIELD SIMULATION
COMPLEX GEOMETRY / COMPLEX PHYSICS

N92-32309

ABSTRACT

Pregress realized in the development of a Computer Aided Grid Interface (CAGI) software system in integrating CAD/CAM geometric system output and/or IGES files, geometry manipulations associated with grid generation and robust grid generation methodologies is presented. CAGI is being developed in a modular fashion and will offer fast, efficient and economical response to geometry/grid preparation allowing ability to upgrade basic geometry in a step–by–step fashion interactively and under permanent visual control along with minimizing the differences between the actual hardware surface descriptions and corresponding numerical analog.

The computer code GENIE (Ref. 1–3) is used as basis. The Non–Uniform Rational B–Splines (NURBS) representation of sculptured surfaces is utilized for surface grid redistribution. The computer aided analysis system, PATRAN, is adapted as a CAD/CAM system. The progress realized in NURBS surface grid generation, the development of IGES transformer, and geometry adaption using PATRAN will be presented along with their applicability to grid generation associated with rock propulsion applications.

References:

1. B. K. Soni, J. F. Thompson, M. L. Stokes, and M. H. Shih, "GENIE++, EAGLEView and TIGER: General Purpose and Special Purpose Graphically Interactive Grid Systems", AIAA-92-0071, *AIAA 30th Aerospace Sciences Meeting,* Reno, NV, January 1992.

2. B. K. Soni, "Geometry Processing Associated with Complex Configurations in Computational Fluid Dynamics", *Second SIAM Conference on Geometric Design*, Tempe, AZ, November 1991.

3. B. K. Soni, "GENIE: Generation of Computational Grids for Internal–External Flow Configurations", *Proceedings of the Second International Conference of Numerical Grid Generation in Computational Fluid Dynamics*, Miami, FL, December 1988, edited by S. Sengupta, J. Hauser, P. R. Eiseman and J. F. Thompson, Pineridge Press, P. 915–924.

4. David Vaughn, "The Graphically Interactive PATRAN Structured Grid Interface (GIPSI)", student paper to be presented at the *Southeastern Conference on Theoretical and Applied Mechanics*, Nashville, TN, April 12–14, 1992.

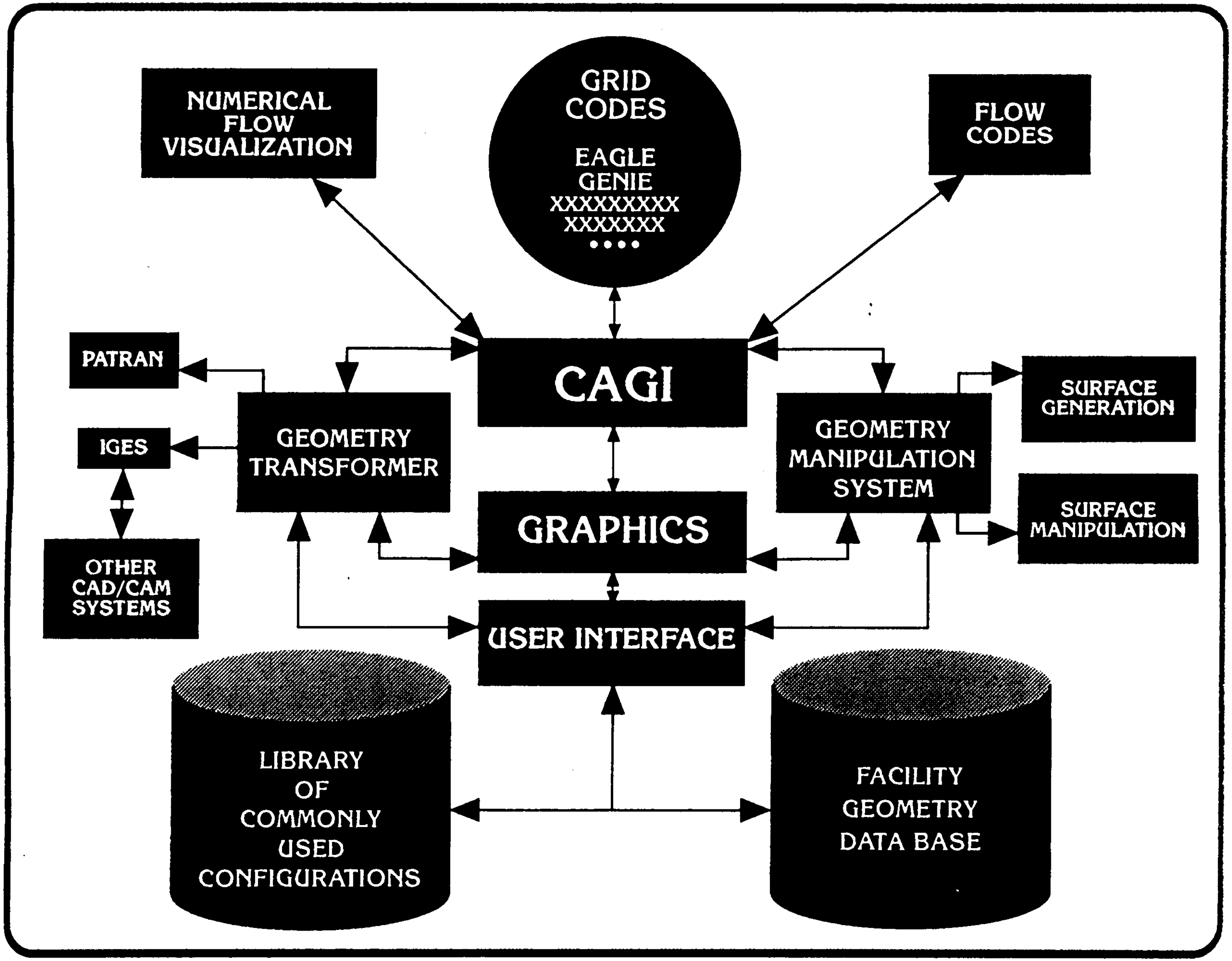
NUMERICAL FLOW VISUALIZATION
GRID CODES
EAGLE
GENIE
XXXXXXXXX
XXXXXXX
• • • •
FLOW CODES
PATRAN
IGES
OTHER CAD/CAM SYSTEMS
GEOMETRY TRANSFORMER
CAGI
GRAPHICS
USER INTERFACE
GEOMETRY MANIPULATION SYSTEM
SURFACE GENERATION
SURFACE MANIPULATION
LIBRARY OF COMMONLY USED CONFIGURATIONS
FACILITY GEOMETRY DATA BASE

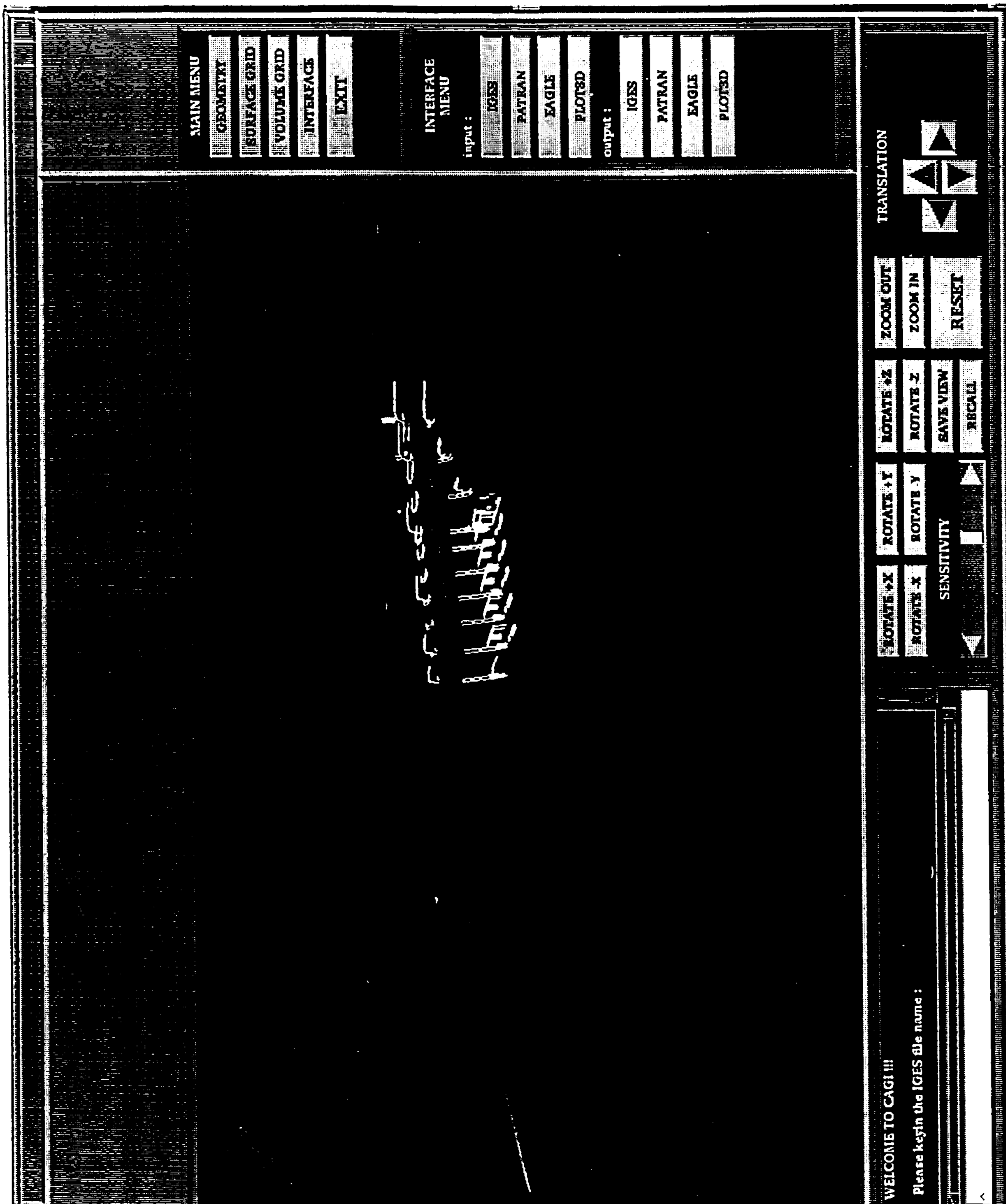
MAIN MENU
GEOMETRY
SURFACE GRID
VOLUME GRID
INTERFACE
EXIT
INTERFACE MENU
input :
IGES
PATRAN
EAGLE
PLOT3D
output :
IGES
PATRAN
EAGLE
PLOT3D
TRANSLATION
ZOOM OUT
ZOOM IN
RESET
ROTATE +X
ROTATE -X
ROTATE +Y
ROTATE -Y
ROTATE +Z
ROTATE -Z
SAVE VIEW
RECALL
SENSITIVITY
WELCOME TO CAGI !!!
Please keyin the IGES file name :

GEOMETRY DEFINITIONS

- ✲ Analytic
- ✲ Drawings
- ✲ Discretized Points
- ✲ Combo (Combination of AboveThree)
- ✲ CAD/CAM Output
- ✲ I G E S
- ✲ CAD Output ⟵ MASAJ Software ⟶ Surface Data
- ✲ Scale Model

SCULPTURED SURFACES

APPLICATION - CRITERIA

- ✲ Fits Given Information
- ✲ Smoothness
- ✲ Shape Fidelity
- ✲ Parametric Representation
- ✲ Local vs Global Schemes
- ✲ Interactive Design
- ✲ Interactive Viewing

NURB Curves

A NURB curve c(u) is a piecewise rational curve of the form

$$c(u) = \sum_{i=0}^{m} w_i d_i N_{i,k}(u) \Big/ \sum_{i=0}^{m} w_i N_{i,k}(u)\,, \quad u \in \left[u_{k-1}, u_{m+1}\right]$$

defined by

- an order k (k equalling the *degree* of the polynomials -1),
- a set of 3D control points, $\{d_0, \ldots, d_m\}$,
- a set of real weights, $\{\omega_0, \ldots, \omega_m\}$,

NURB Curves cont'd

- a set of real knots $\left\{u_0,\ldots,u_{m+k} \mid u_l \leq u_{l+1},\ l = 0\ldots(m+k-1)\right\}$,
- B-spline basis functions $N_{l,k}(u),\ u \in \left[u_l,\ u_{l+k}\right],\ l = 0\ldots m,$ where

$$N_{l,k}(u) = \frac{u - u_l}{u_{l+k-1} - u_l} N_{l,k-1}(u) + \frac{u_{l+k} - u}{u_{l+k} - u_{l+1}} N_{l+1,k-1}(u)$$

$$N_{l,1} = \begin{cases} 1, & u_l \leq u < u_{l+1}; \\ 0, & \text{otherwise.} \end{cases} \qquad l = 0\ldots m,$$

- and curve segments $c_l(u),\ u \in \left[u_l,\ u_{l+1}\right],\ l = (k-1)\ldots m.$

NURB Surfaces

$$x(u, v) = \frac{\sum_{j=0}^{n} \sum_{i=0}^{m} \omega_{i,j} d_{i,j} N_{i,k}(u) N_{j,l}(v)}{\sum_{j=0}^{n} \sum_{i=0}^{m} \omega_{i,j} N_{i,k}(u) N_{j,l}(v)}, \quad u \in \left[u_{k-1}, u_{m+1}\right], \; v \in \left[v_{l-1}, v_{n+1}\right],$$

defined by

- two orders k and l (equalling the *degree* of the polynomials -1)
- a set of 3*D* control points $\left\{d_{0,0}, \ldots, d_{m,n}\right\}$
- a set of real weights $\left\{\omega_{0,0}, \ldots, \omega_{m,n}\right\}$,

NURB Surfaces cont'd

- a set of real u-knots $\left\{u_0,\ldots,u_{m+k} \mid u_l \leq u_{l+1},\ l = 0\ldots(m+k-1)\right\}$,
- a set of real v-knots $\left\{v_0,\ldots,v_{n+l} \mid v_j \leq v_{j+1}, j = 0\ldots(n+l-1)\right\}$,
- B-spline basis functions $N_{l,k}(u),\ u \in \left[u_l,\ u_{l+k}\right],\ l = 0\ldots m,$

  $N_{l,k}(u)$ defined as for the curve case,
- B-spline basis functions $N_{j,l}(v),\ v \in \left[v_j,\ v_{j+l}\right], j = 0\ldots n,$

  $N_{j,l}(v)$ defined as for the cure case, and
- surface segments $x_{l,j}(u,v),\ u \in \left[u_l,\ u_{l+1}\right],\ l = (k-1)\ldots m,$

  $v \in \left[v_j,\ v_{j+1}\right],\ j = (l-1)\ldots n.$

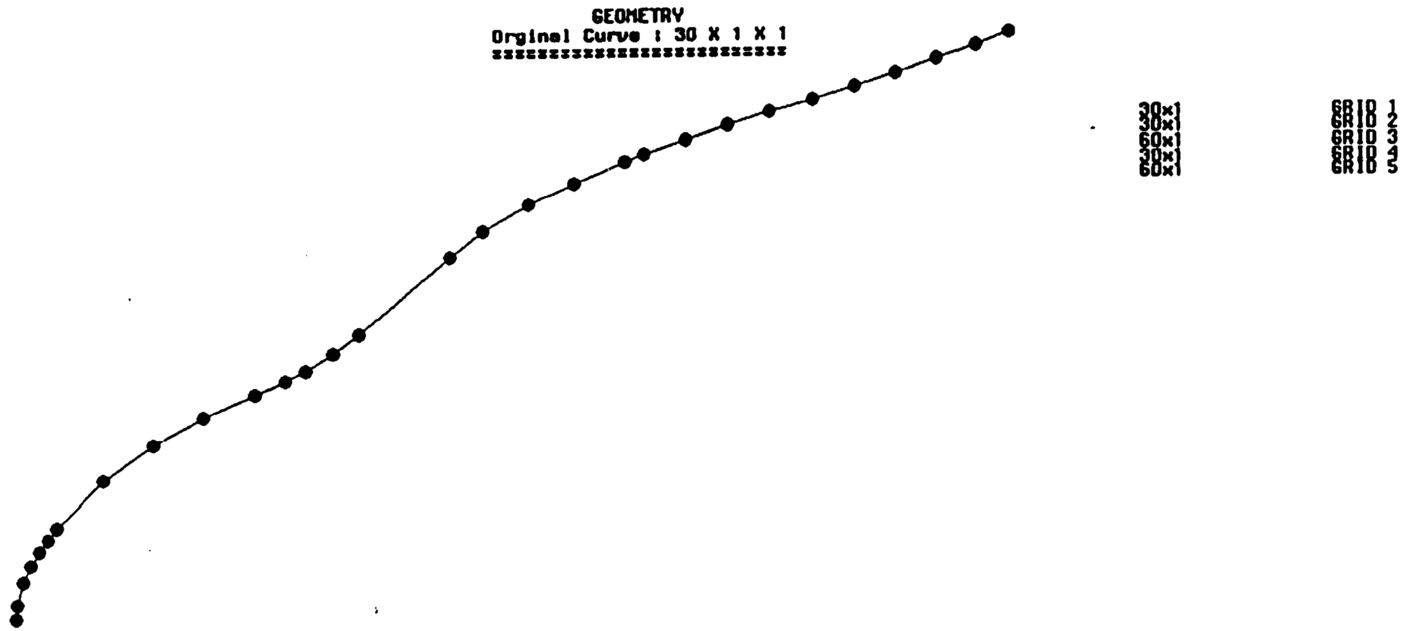
GEOMETRY
Orginal Curve : 30 X 1 X 1
30x1 GRID 1
30x1 GRID 2
60x1 GRID 3
30x1 GRID 4
60x1 GRID 5

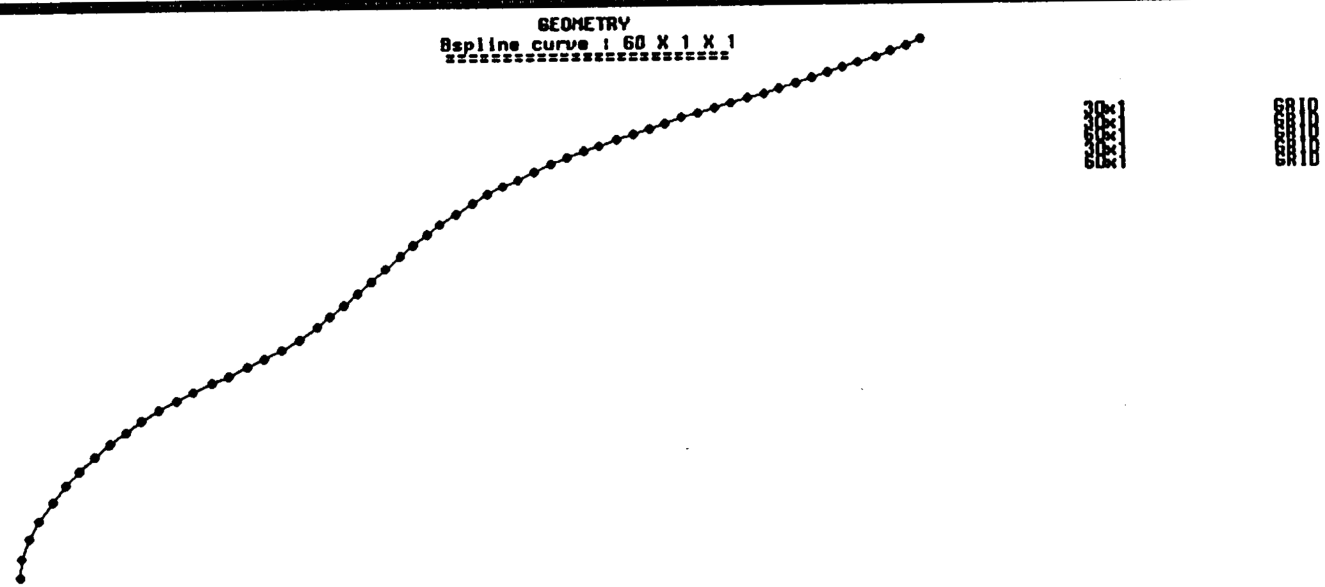
GEOMETRY
Bspline curve : 60 X 1 X 1
30x1 GRID 1
30x1 GRID 2
60x1 GRID 3
30x1 GRID 4
60x1 GRID 5

GEOMETRY
Orgainal 3D surface : 30 X 50 X 1
================================

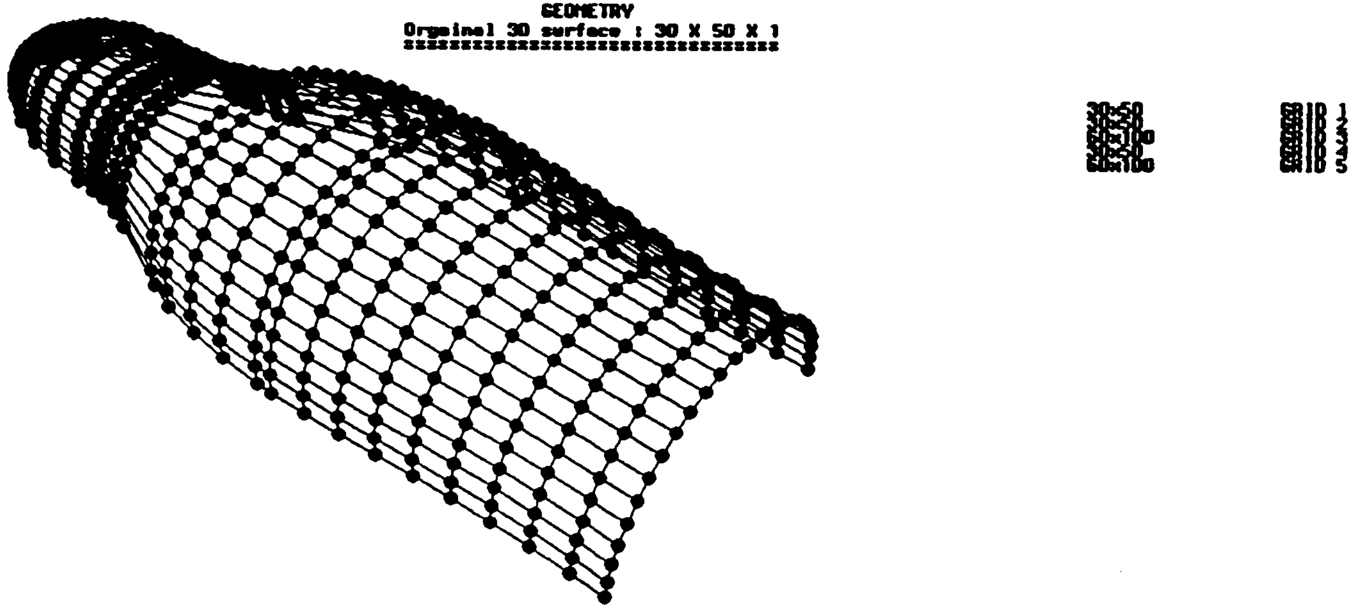

GEOMETRY
Bspline Surface : 60 X 100 X 1
==============================

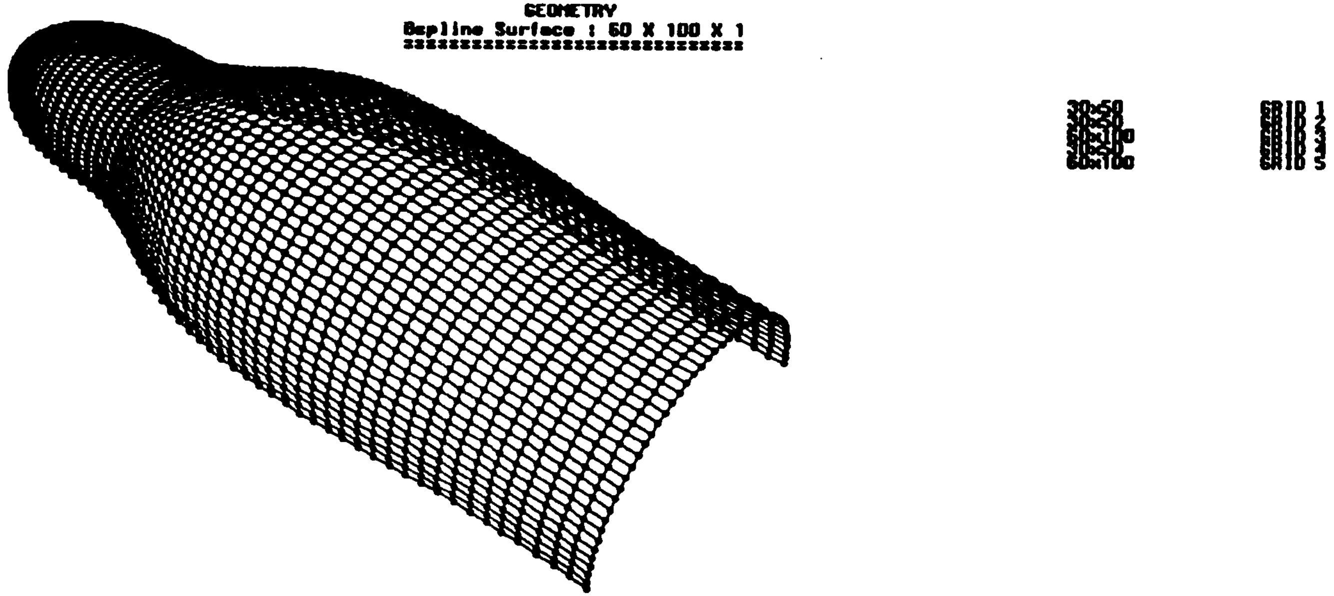

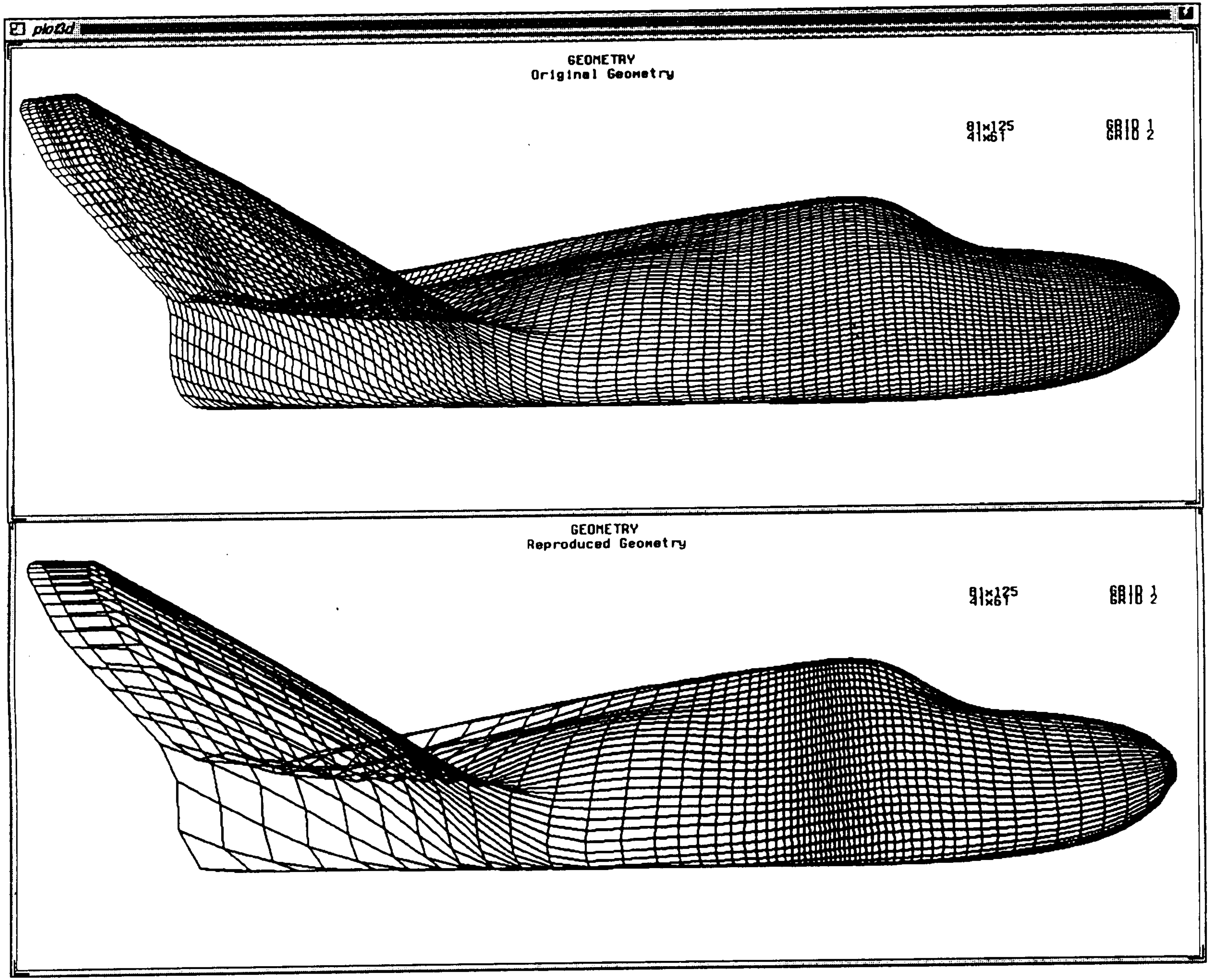
plot3d
GEOMETRY
Original Geometry
81x125
41x61
GRID 1
GRID 2
GEOMETRY
Reproduced Geometry
81x125
41x61
GRID 1
GRID 2

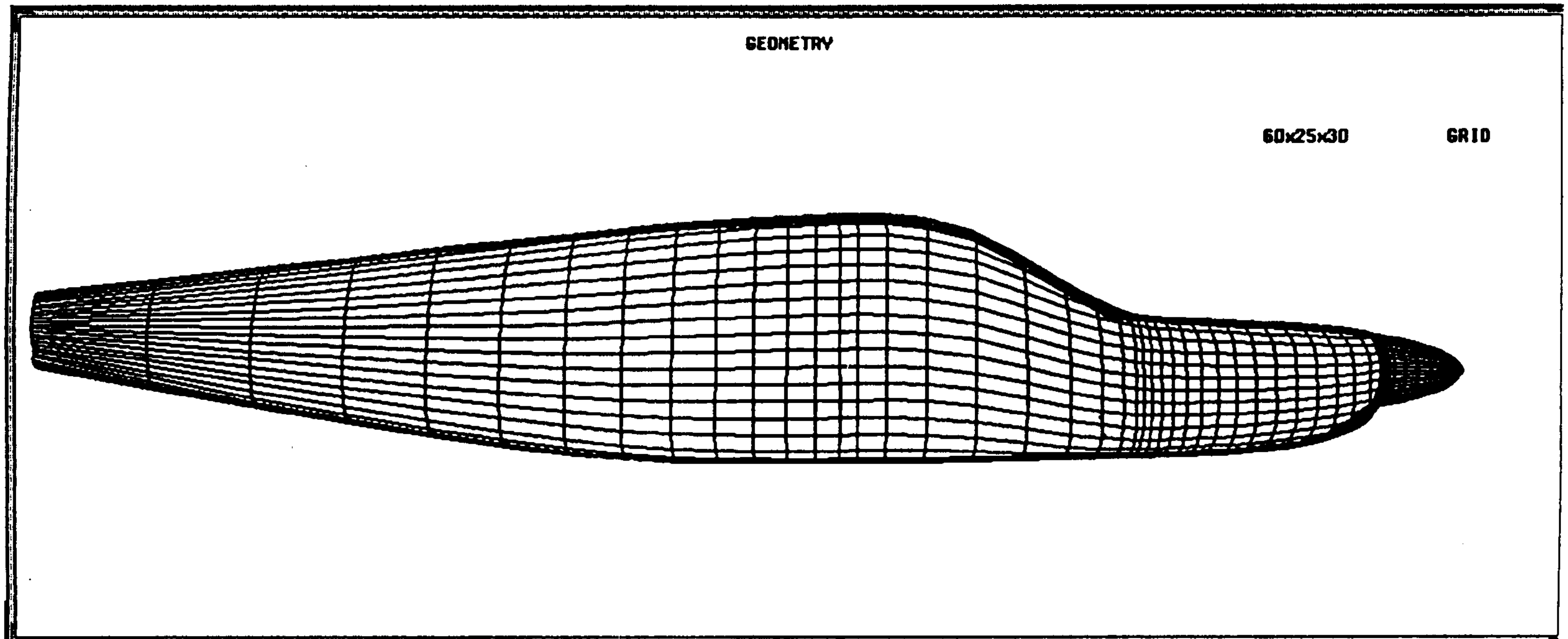
GEOMETRY
60x25x30
GRID

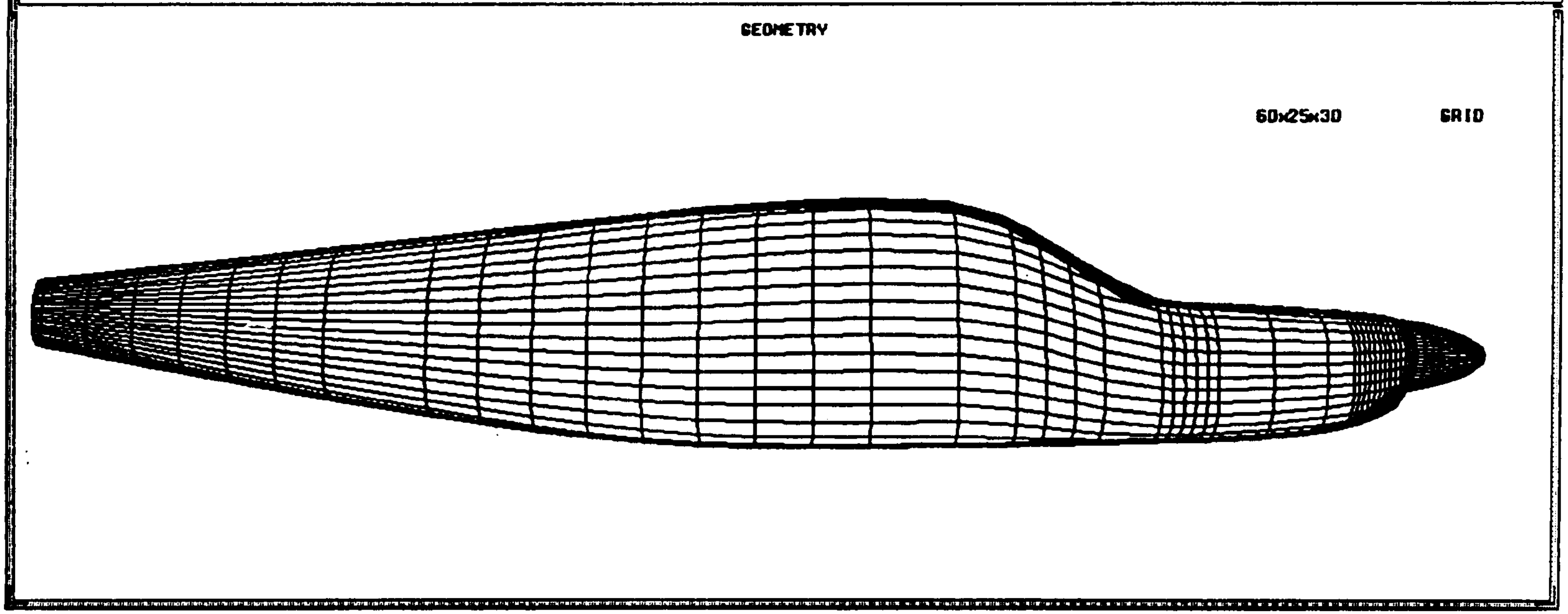
GEOMETRY
60x25x30
GRID

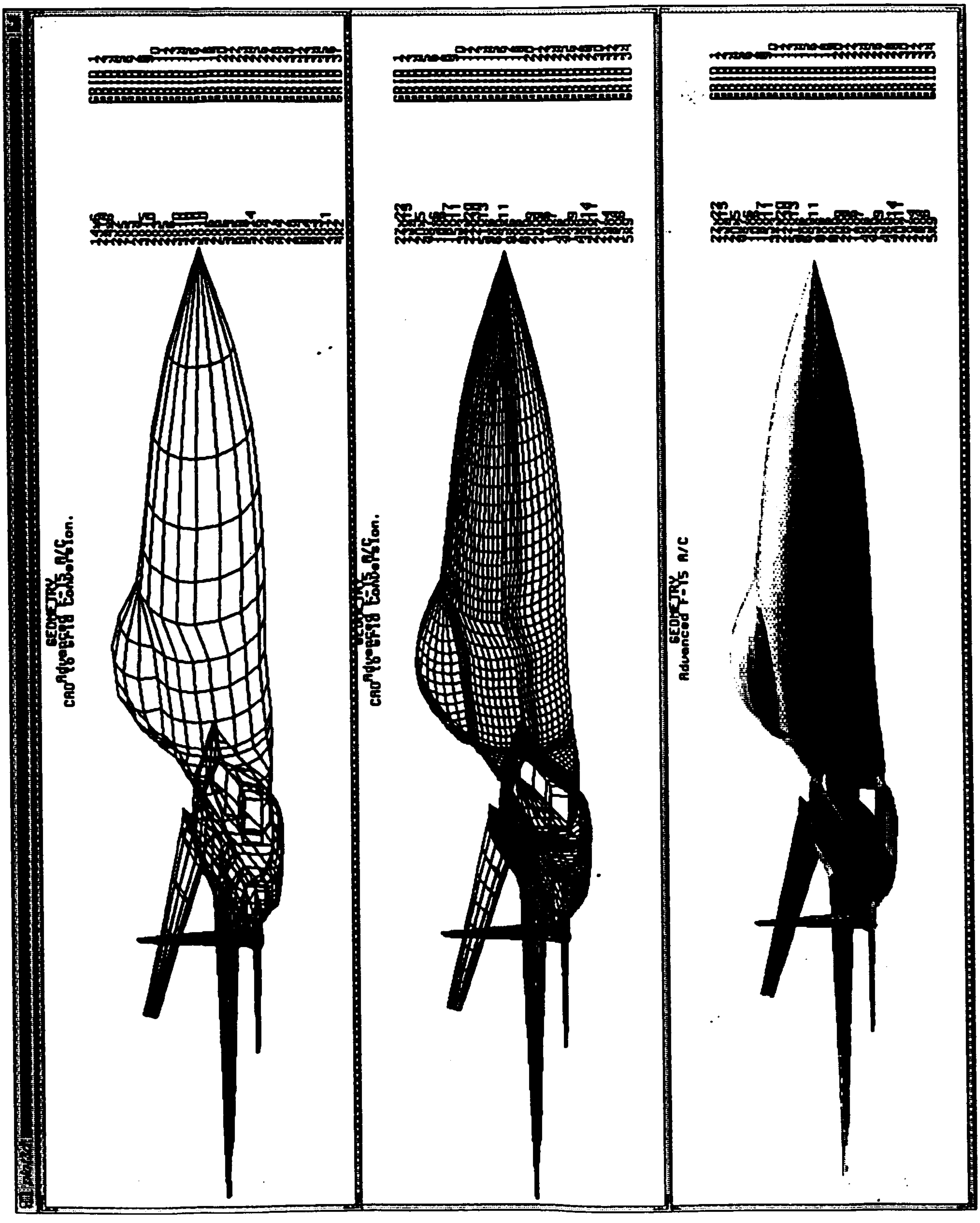
GEOMETRY
Advanced F-15 A/C
CAD to Grid Conversion.
GEOMETRY
Advanced F-15 A/C
CAD to Grid Conversion.
GEOMETRY
Advanced F-15 A/C

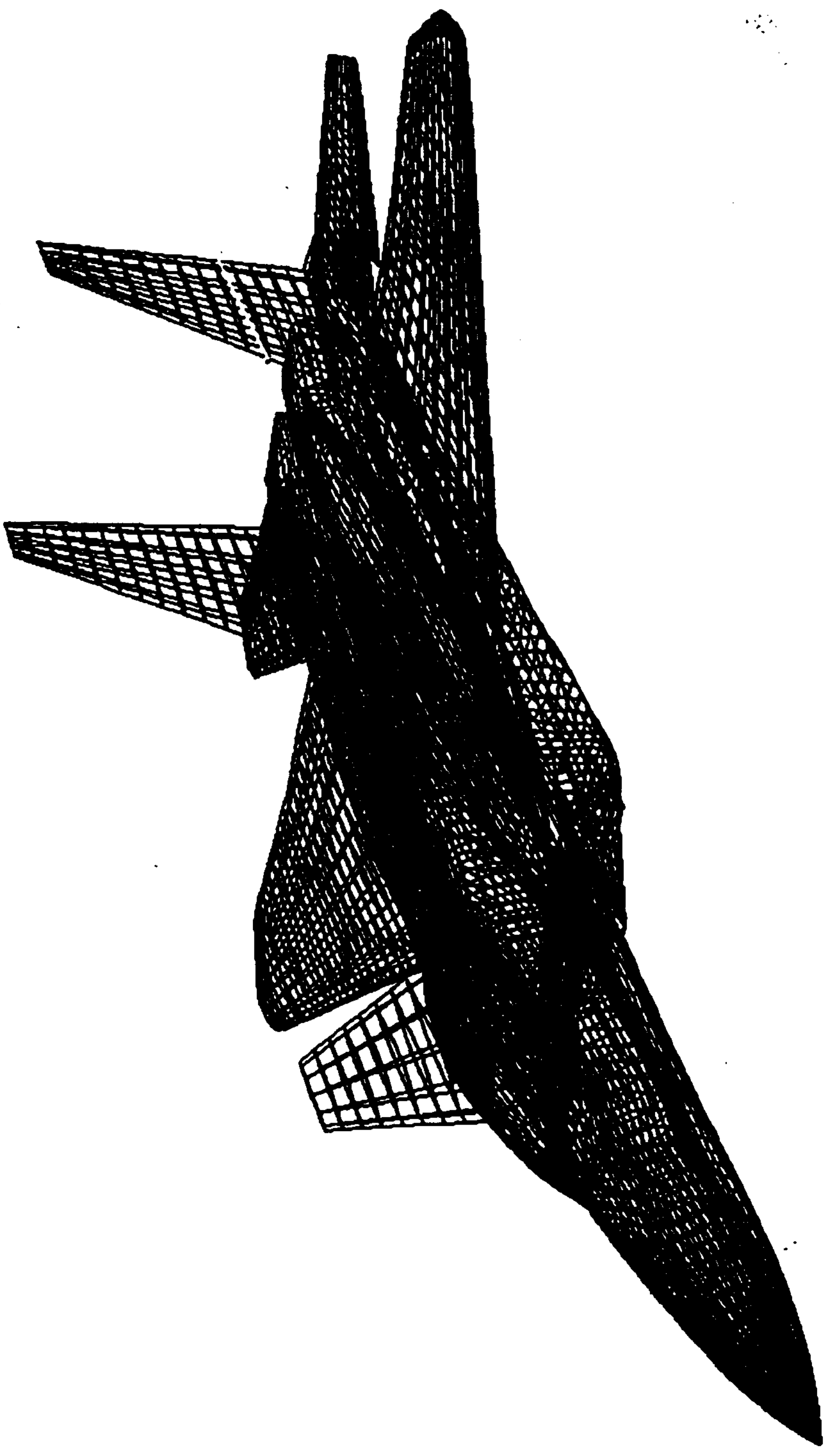

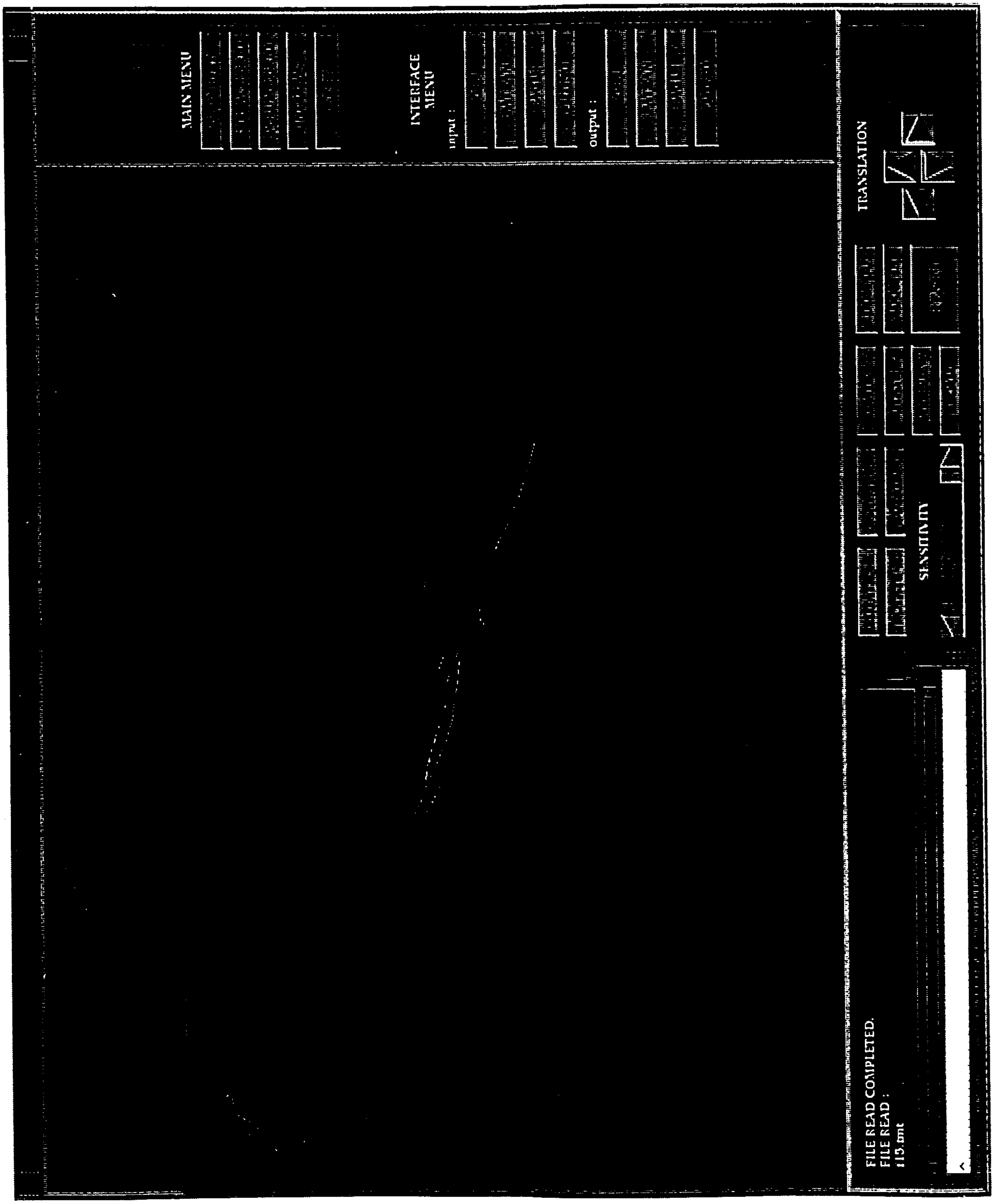
MAIN MENU
INTERFACE MENU
input :
output :
TRANSLATION
SENSITIVITY
FILE READ COMPLETED.
FILE READ :

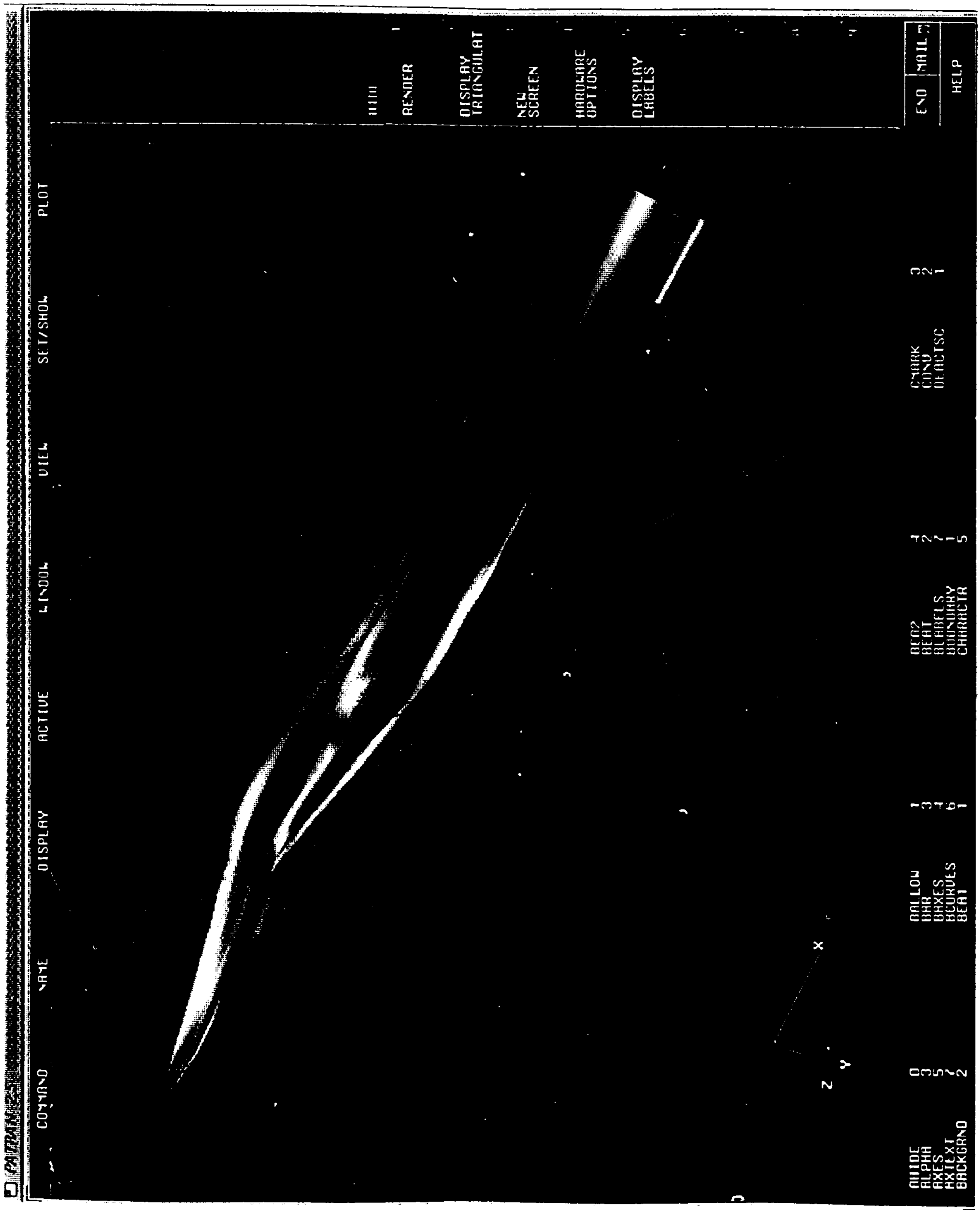

COMMAND
NAME
DISPLAY
ACTIVE
WINDOW
VIEW
SET/SHOW
PLOT
RENDER
DISPLAY TRIANGULAT
NEW SCREEN
HARDWARE OPTIONS
DISPLAY LABELS
END
HELP

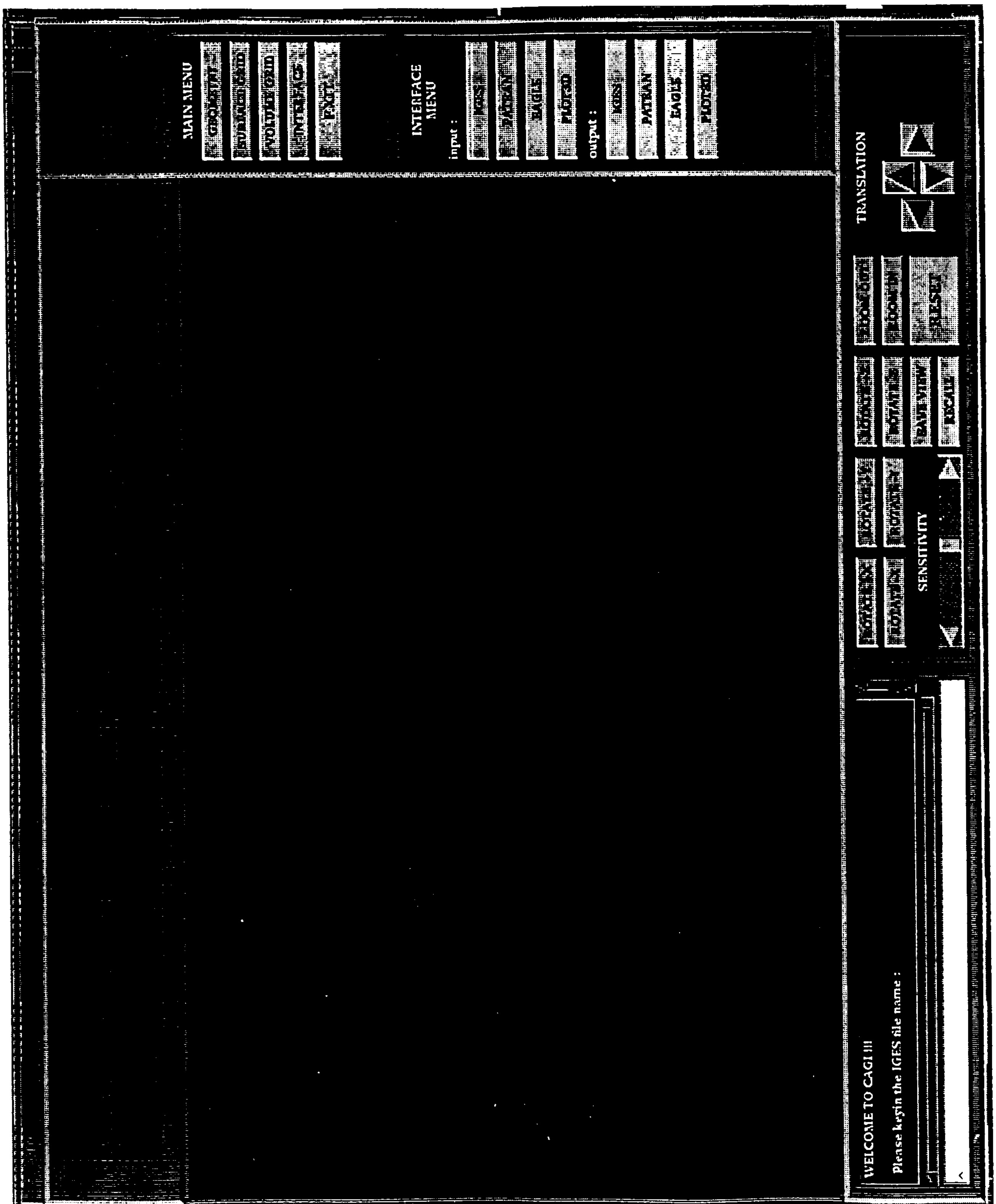
MAIN MENU
INTERFACE MENU
input :
PATRAN
EAGLE
PLOT3D
output :
PATRAN
EAGLE
PLOT3D
TRANSLATION
SENSITIVITY
WELCOME TO CAGI !!!
Please keyin the IGES file name :

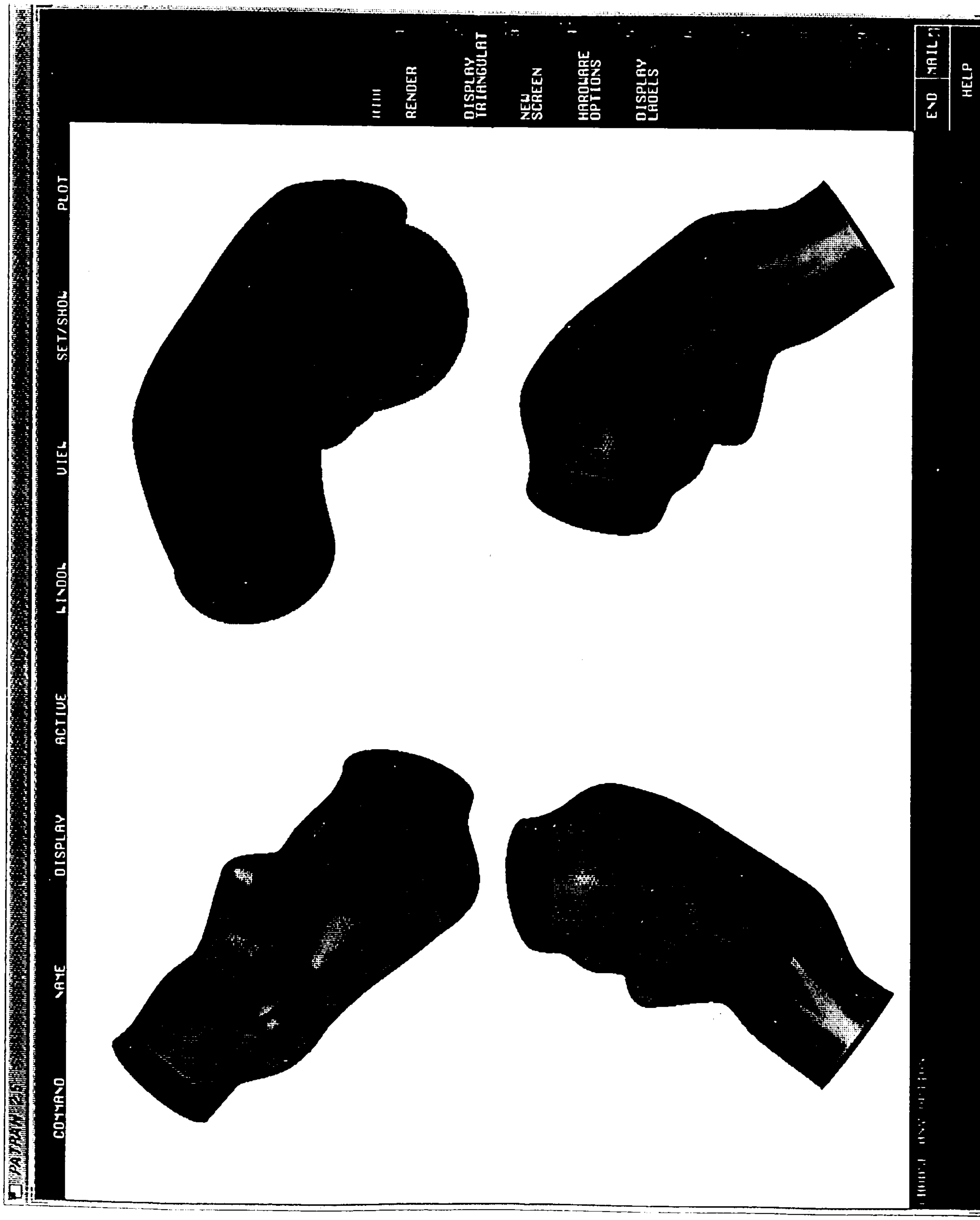
COMMAND
NAME
DISPLAY
ACTIVE
WINDOW
VIEW
SET/SHOW
PLOT
RENDER
DISPLAY TRIANGULAT
NEW SCREEN
HARDWARE OPTIONS
DISPLAY LABELS
END
HELP

GIPSI

Graphically Interactive PATRAN Structured Grid Interface

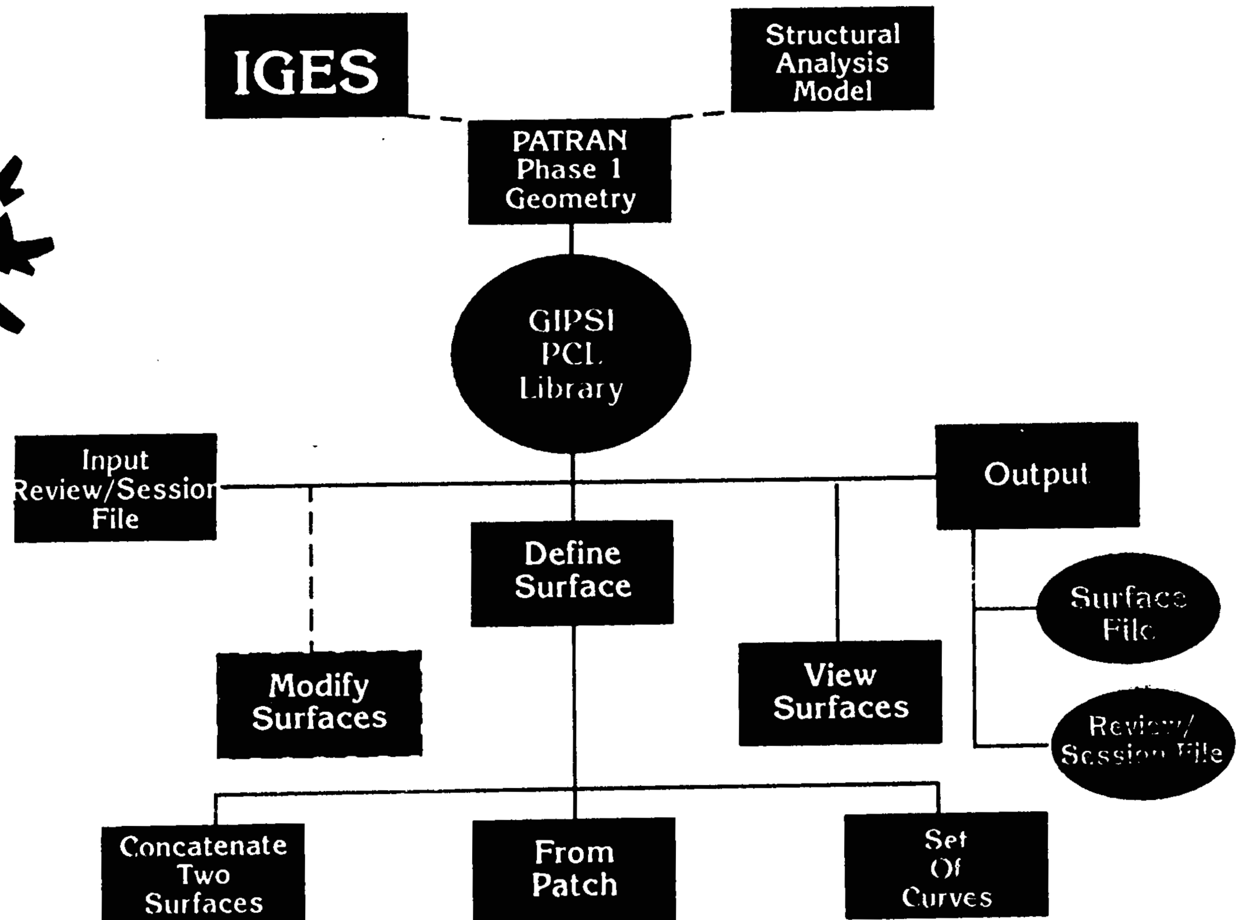

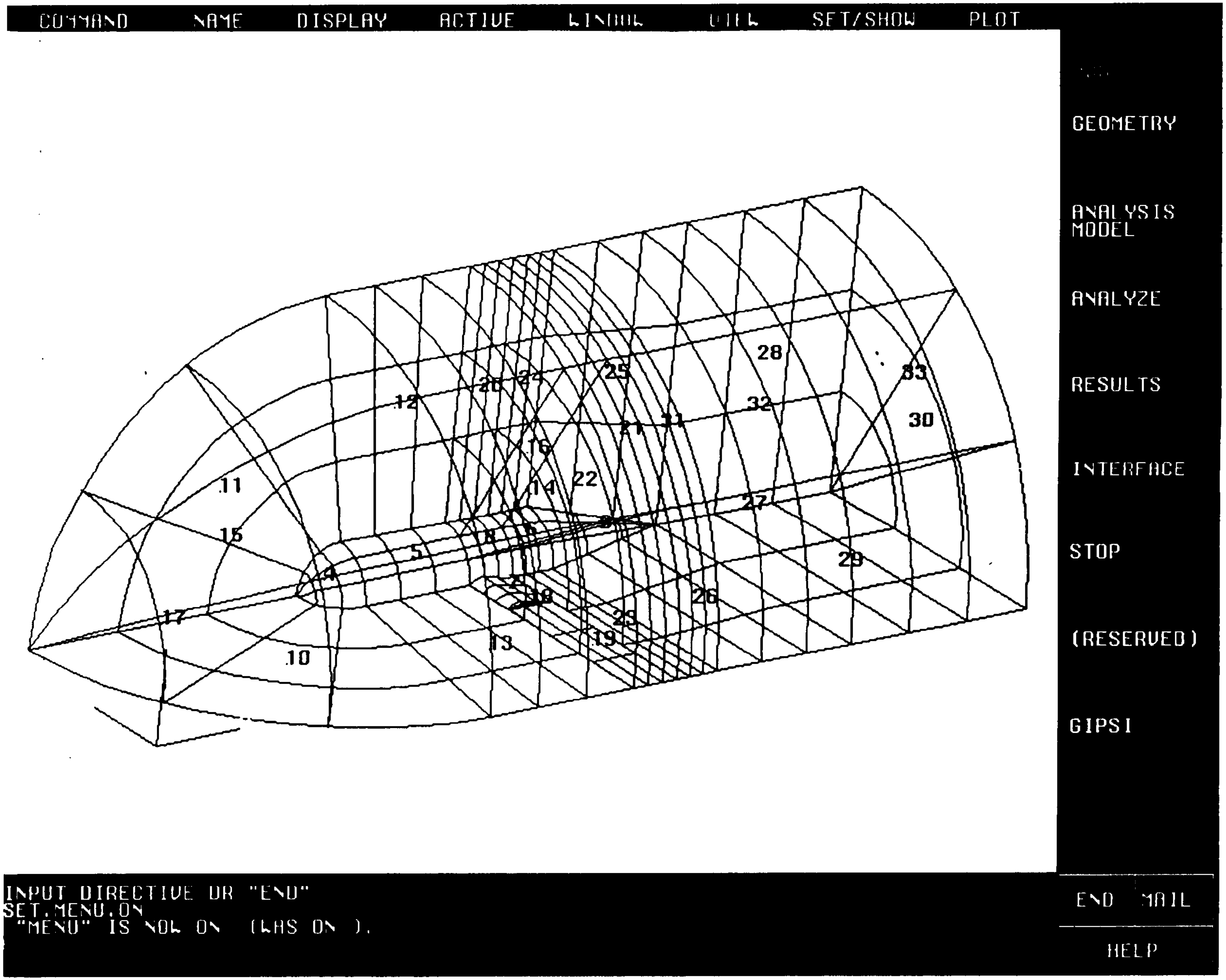
COMMAND
NAME
DISPLAY
ACTIVE
WINDOW
VIEW
SET/SHOW
PLOT
GEOMETRY
ANALYSIS
MODEL
ANALYZE
RESULTS
INTERFACE
STOP
(RESERVED)
GIPSI
END MAIL
HELP
INPUT DIRECTIVE OR "END"
SET.MENU.ON
"MENU" IS NOW ON (WAS ON).

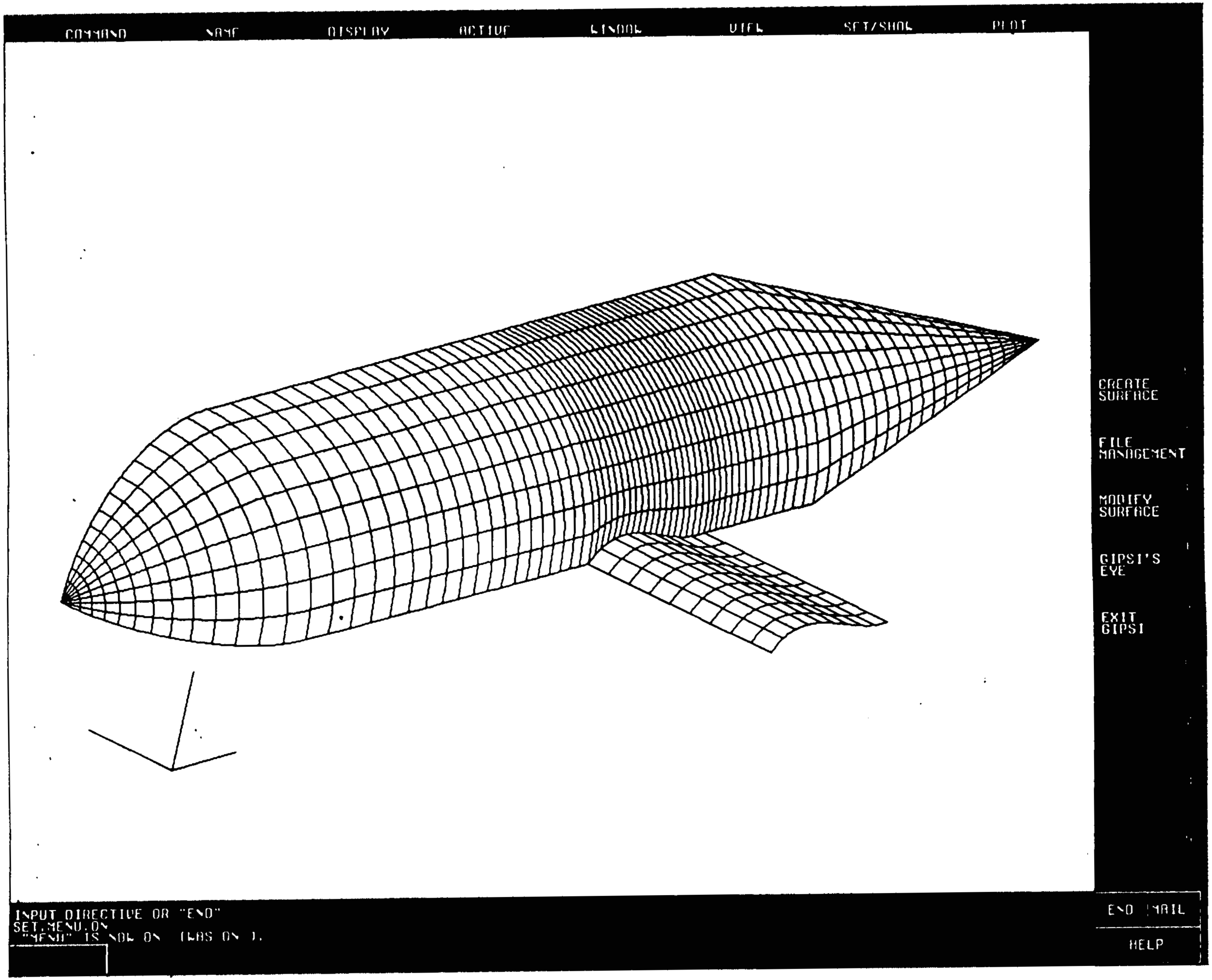

COMMAND
NAME
DISPLAY
ACTIVE
WINDOW
VIEW
SET/SHOW
PLOT
CREATE SURFACE
FILE MANAGEMENT
MODIFY SURFACE
GIPSI'S EYE
EXIT GIPSI
END MAIL
HELP
INPUT DIRECTIVE OR "END"
SET,MENU,ON
"MENU" IS NOW ON (WAS ON).

IGES Entitles: (IGES V.5.0)

Circular Arc (type 100)
Composite Curve (type 102)
Conic Arc (type 104)

- Parabola (form 1)
- Ellipse (form 2)
- Hyperbola (form 3)
- General Equation (form 0)

Copious Data

- Center line (form 20 - 21)
- Section (form 31 - 38)
- Witness line (form 40)

Plane (type 108)
Line (type 110)
Parametric Spline Curve (type 112)
Parametric Spline Surface (type 114)
Point (type 116)
Ruled Surface (type 118)

- Equal Relative Arc Length (form 0)
- Equal Relative Parametric Value (form 1)

Surface of Revolution (type 120)
Tabulated Cylinder (type 122)
Transformation Matrix (type 124)

- Orthogonal Matrix (det = 1) (form 0)
  right handed system
- Orthogonal Matrix (det = -1) (form 1)
  left handed system

IGES Entitles: (IGES V.5.0) cont.

Rational B–Spline Curve (type 126)

- General Parameters (form 0)
- Line (form 1)
- Circular Arc (form 2)
- Elliptical Arc (form 3)
- Parabolic Arc (form 4)
- Hyperbolic Arc (form 5)

Rational B–Spline Surface (type 128)

- General (form 0)
- Plane (form 1)
- Right Circular Cylinder (form 2)
- Cone (form 3)
- Sphere (form 4)
- Torus (form 5)
- Surface of Revolution (form 6)
- Tabulated Cylinder (form 7)
- Ruled Surface (form 8)
- General Quadric Surface (form 9)

IGES Entitles: (IGES V.5.0) cont.

Rational B–Spline CurveOffset Curve	(type 130)
Offset Surface	(type 140)
Boundary Entity	(type 141)
(set of curves lying on surface)	
Curve on a Parametric Surface	(type 142)
Boundary Surface	(type 143)
Trimmed Parametric Surface	(type 144)
User Defined Surface Data Form	(type 5001)

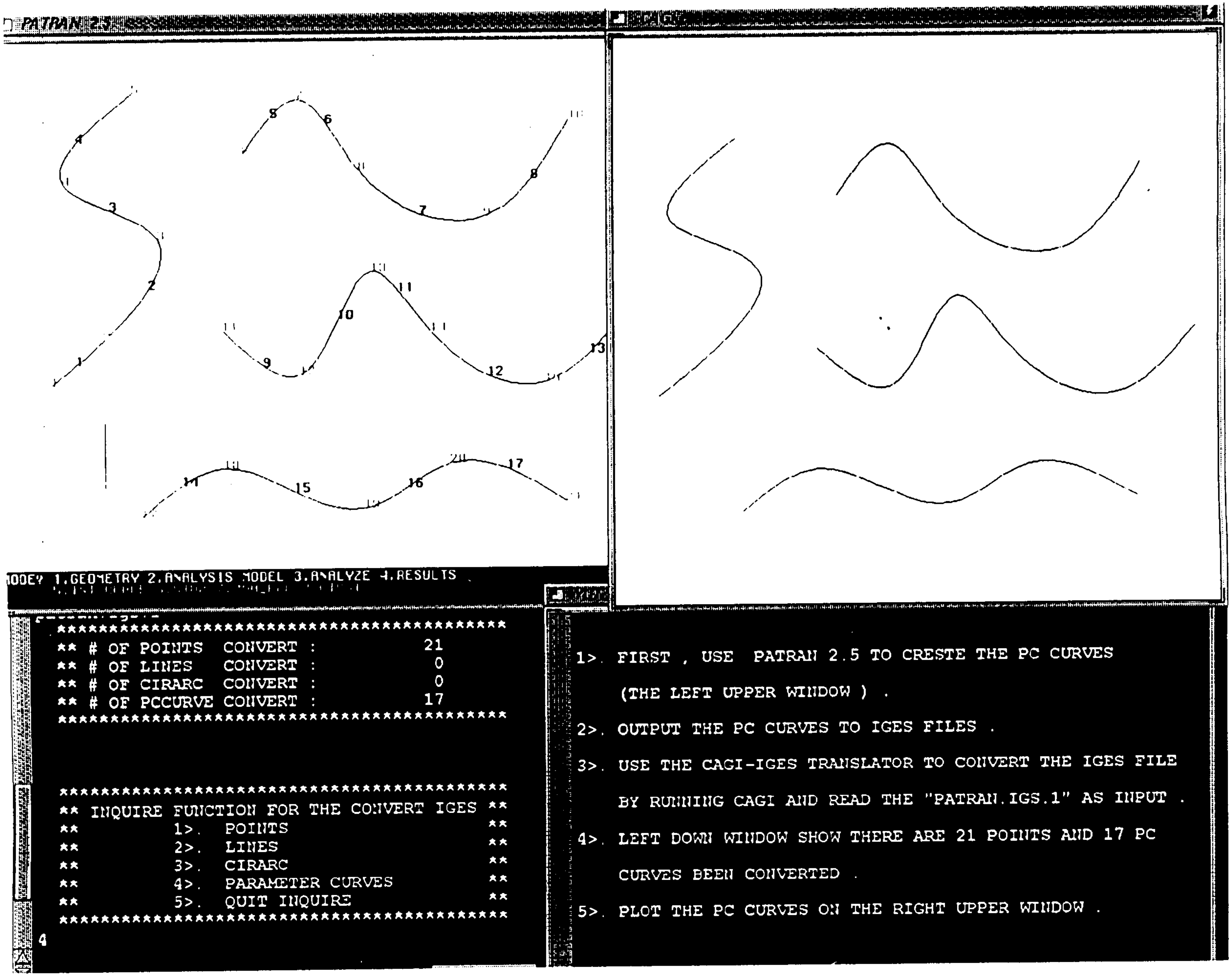
PATRAN 2.5
MODE? 1.GEOMETRY 2.ANALYSIS MODEL 3.ANALYZE 4.RESULTS
****
** # OF POINTS CONVERT : 21
** # OF LINES CONVERT : 0
** # OF CIRARC CONVERT : 0
** # OF PCCURVE CONVERT : 17
****
****
** INQUIRE FUNCTION FOR THE CONVERT IGES **
** 1>. POINTS **
** 2>. LINES **
** 3>. CIRARC **
** 4>. PARAMETER CURVES **
** 5>. QUIT INQUIRE **
****
4
1>. FIRST , USE PATRAN 2.5 TO CRESTE THE PC CURVES
(THE LEFT UPPER WINDOW) .
2>. OUTPUT THE PC CURVES TO IGES FILES .
3>. USE THE CAGI-IGES TRANSLATOR TO CONVERT THE IGES FILE
BY RUNNING CAGI AND READ THE "PATRAN.IGS.1" AS INPUT .
4>. LEFT DOWN WINDOW SHOW THERE ARE 21 POINTS AND 17 PC
CURVES BEEN CONVERTED .
5>. PLOT THE PC CURVES ON THE RIGHT UPPER WINDOW .

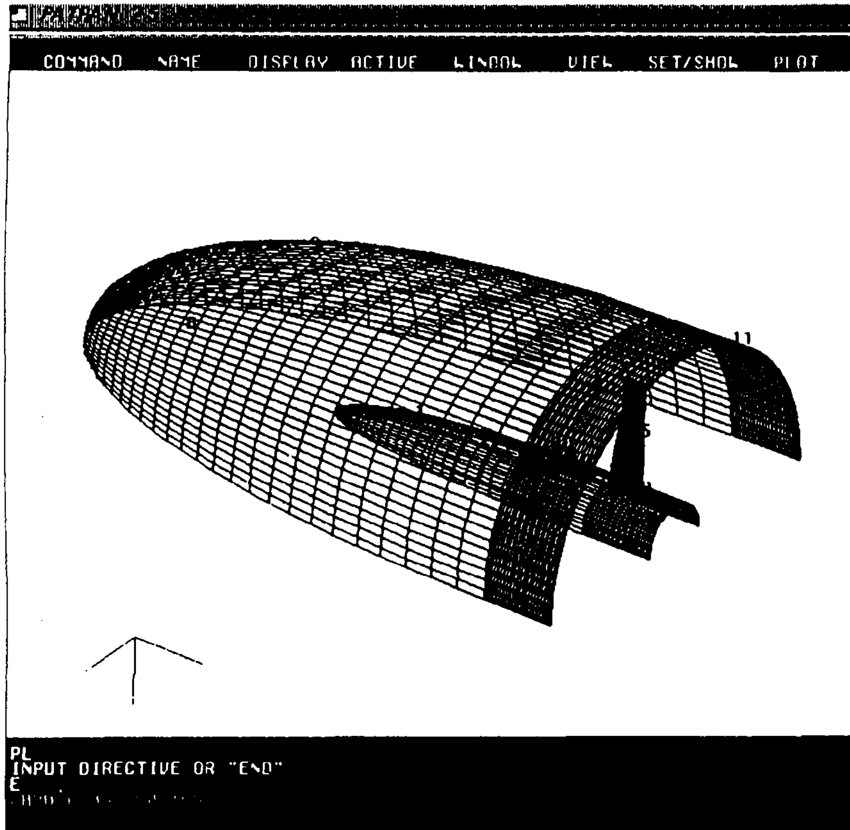

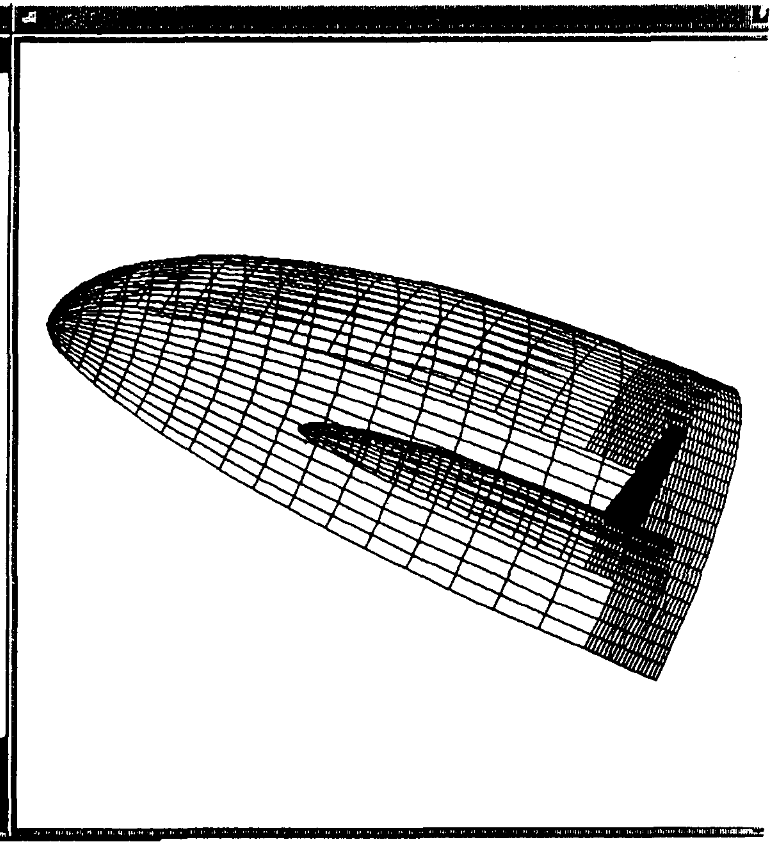

```
indy:yu 21 > cagi

  PLEASE KEYIN THE IGES FILE NEME ....
bodywing.igs
  ******************************************
  ** # OF POINTS   CONVERT :           19
  ** # OF LINES    CONVERT :            6
  ** # OF CIRARC   CONVERT :            0
  ** # OF PCCURVE  CONVERT :            6
  ** # OF PC SUR   CONVERT :           10
  ** # OF BODY OF ROV.     :            0
  ** # OF CONIC ARC        :            0
  ******************************************



  ******************************************
  ** INQUIRE FUNCTION FOR THE CONVERT IGES **
  **          1>.  POINTS                  **
```

```
1>. FIRST , USE  PATRAN 2.5 TO CREATE THE PC SURFACE

    (THE LEFT UPPER WINDOW ) .

2>. TRANSLATE THE PARAMETER SURFACES TO IGES FILES .

3>. USE THE CAGI-IGES TRANSLATOR TO CONVERT THE IGES FILE

    BY RUNNING CAGI AND READ THE "BODYWING.IGS" AS INPUT

4>. LEFT DOWN WINDOW SHOW THERE ARE 19 POINTS AND  6 PC

    CURVES 10 SURFACE AND 6 LINES BEEN CONVERTED .

5>. PLOT THE PC SURFACE ON THE RIGHT UPPER WINDOW .
```

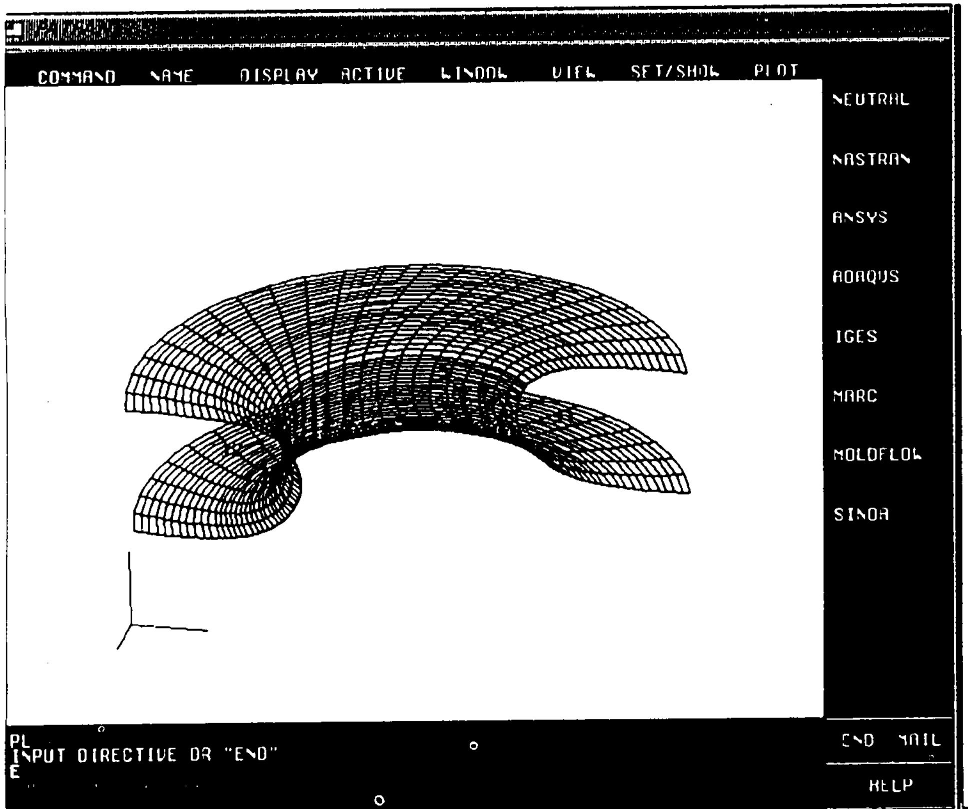

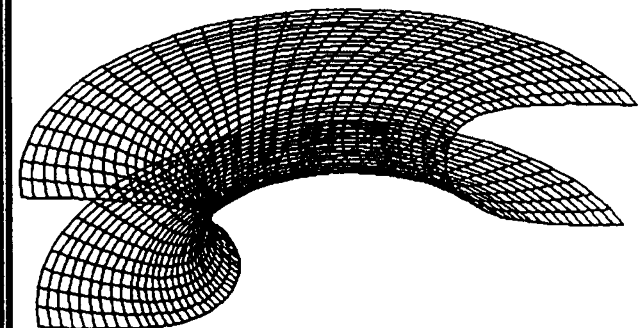

```
indy:yu 39 > cd ..
indy:yu 40 > cagi

  PLEASE KEYIN THE IGES FILE NEME ....
bodrov.igs
  ******************************************
  ** # OF POINTS  CONVERT :           0
  ** # OF LINES   CONVERT :           1
  ** # OF CIRARC  CONVERT :           0
  ** # OF PCCURVE CONVERT :           6
  ** # OF PC SUR  CONVERT :           0
  ** # OF BODY OF ROV.    :           6
  ** # OF CONIC ARC       :           0
  ******************************************


  ******************************************
  ** INQUIRE FUNCTION FOR THE CONVERT IGES **
```

1>. USE PATRAN TO READ THE IGES FILES WHICH CONTAIN TEH BODY OF REV. ENTITY 120 AND PLOT BY PATRAN .

2>. USE THE CAGI-IGES TRANSLATOR TO CONVERT THE IGES FILE BY RUNNING CAGI AND READ THE "BODROV.IGS" AS INPUT .

3>. LEFT DOWN WINDOW SHOW THERE ARE 12 BODY OF REV. ENTITIES (SURFACES) BEEN CONVERTED .

4>. PLOT THE SURFACES ON THE RIGHT UPPER WINDOW .

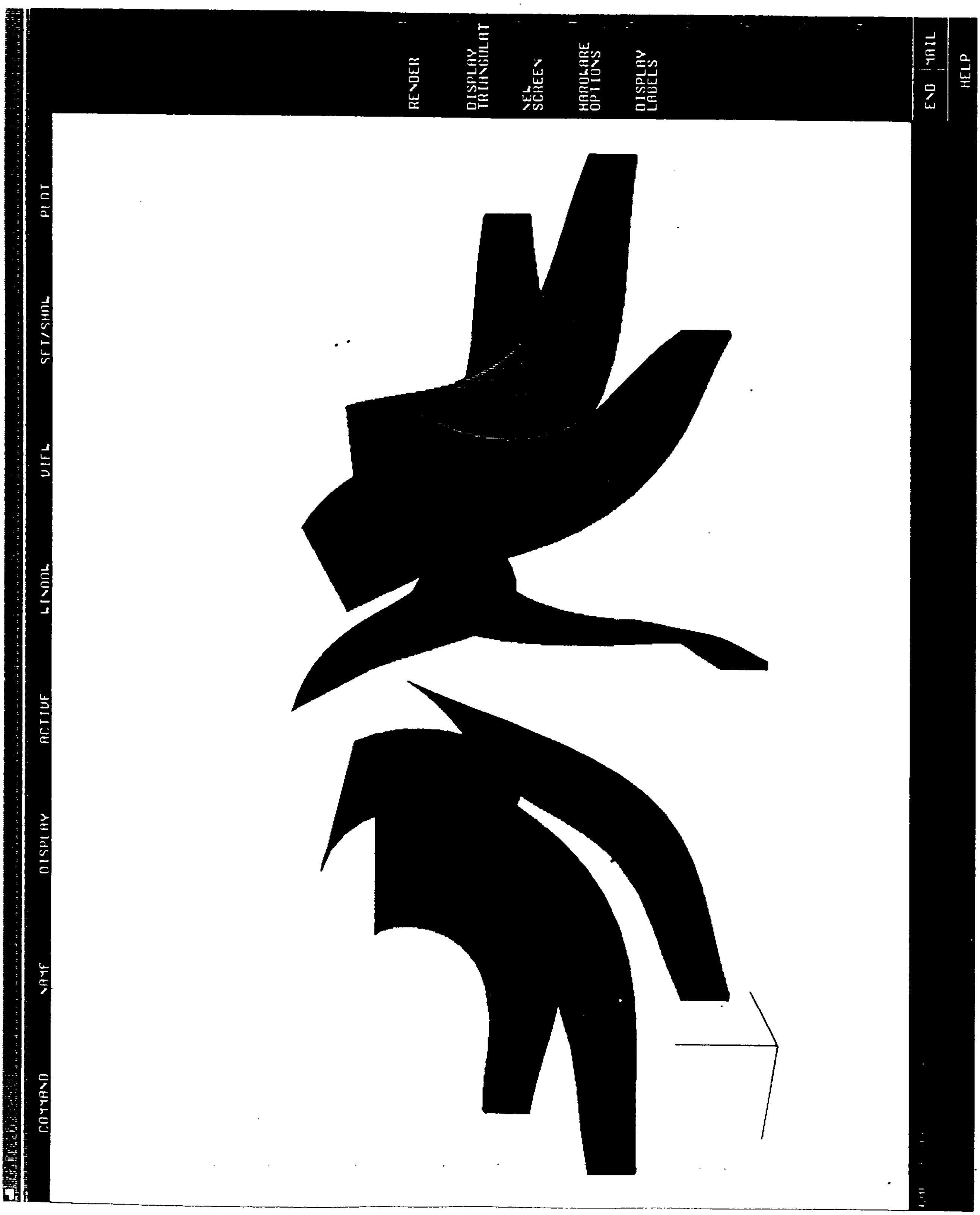
COMMAND
NAME
DISPLAY
ACTIVE
WINDOW
VIEW
SET/SHOW
PLOT
RENDER
DISPLAY TRIANGULAT
NEW SCREEN
HARDWARE OPTIONS
DISPLAY LABELS
END
MAIL
HELP

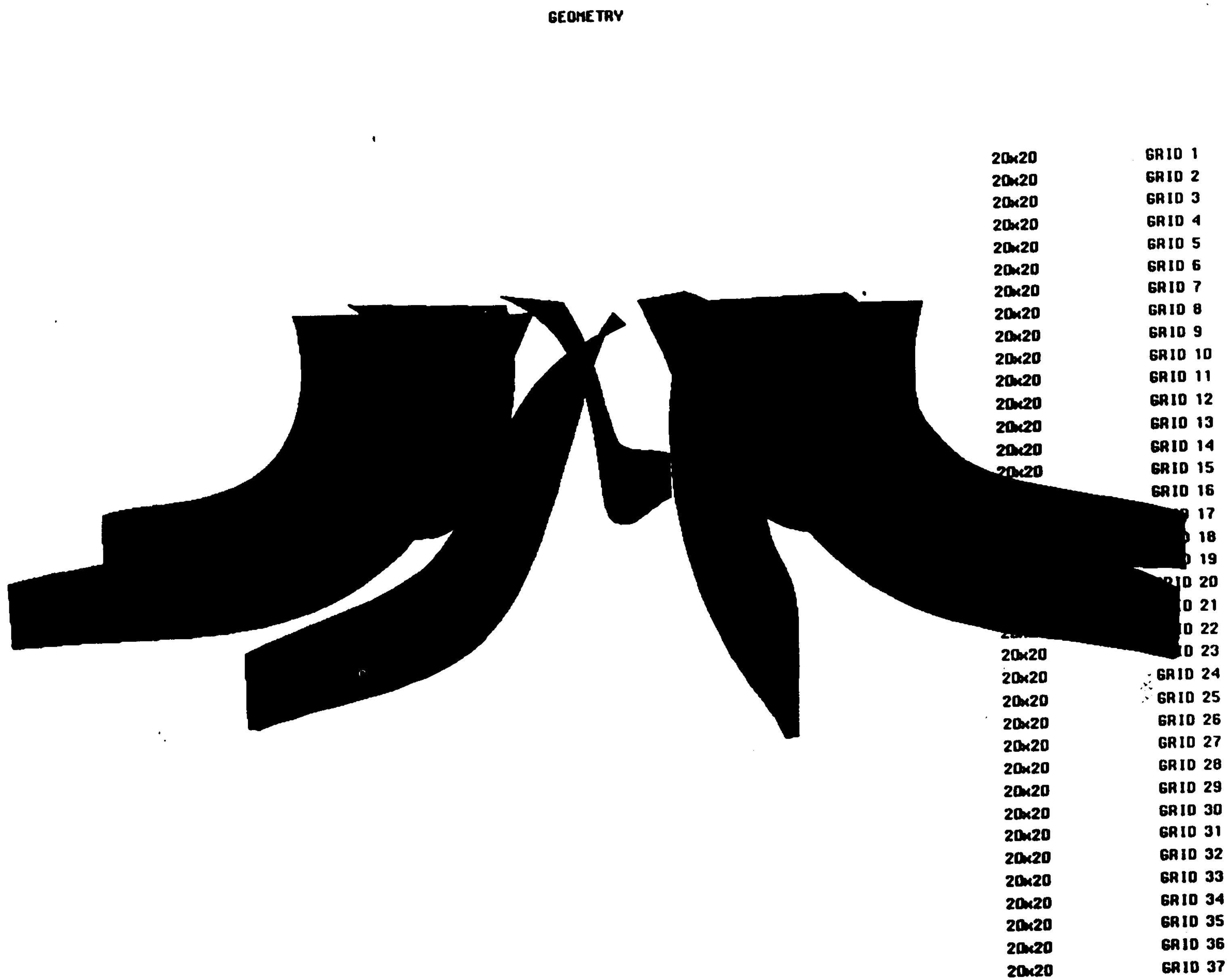
GEOMETRY
20x20 GRID 1
20x20 GRID 2
20x20 GRID 3
20x20 GRID 4
20x20 GRID 5
20x20 GRID 6
20x20 GRID 7
20x20 GRID 8
20x20 GRID 9
20x20 GRID 10
20x20 GRID 11
20x20 GRID 12
20x20 GRID 13
20x20 GRID 14
20x20 GRID 15
GRID 16
17
18
19
ID 20
D 21
D 22
20x20 D 23
20x20 GRID 24
20x20 GRID 25
20x20 GRID 26
20x20 GRID 27
20x20 GRID 28
20x20 GRID 29
20x20 GRID 30
20x20 GRID 31
20x20 GRID 32
20x20 GRID 33
20x20 GRID 34
20x20 GRID 35
20x20 GRID 36
20x20 GRID 37

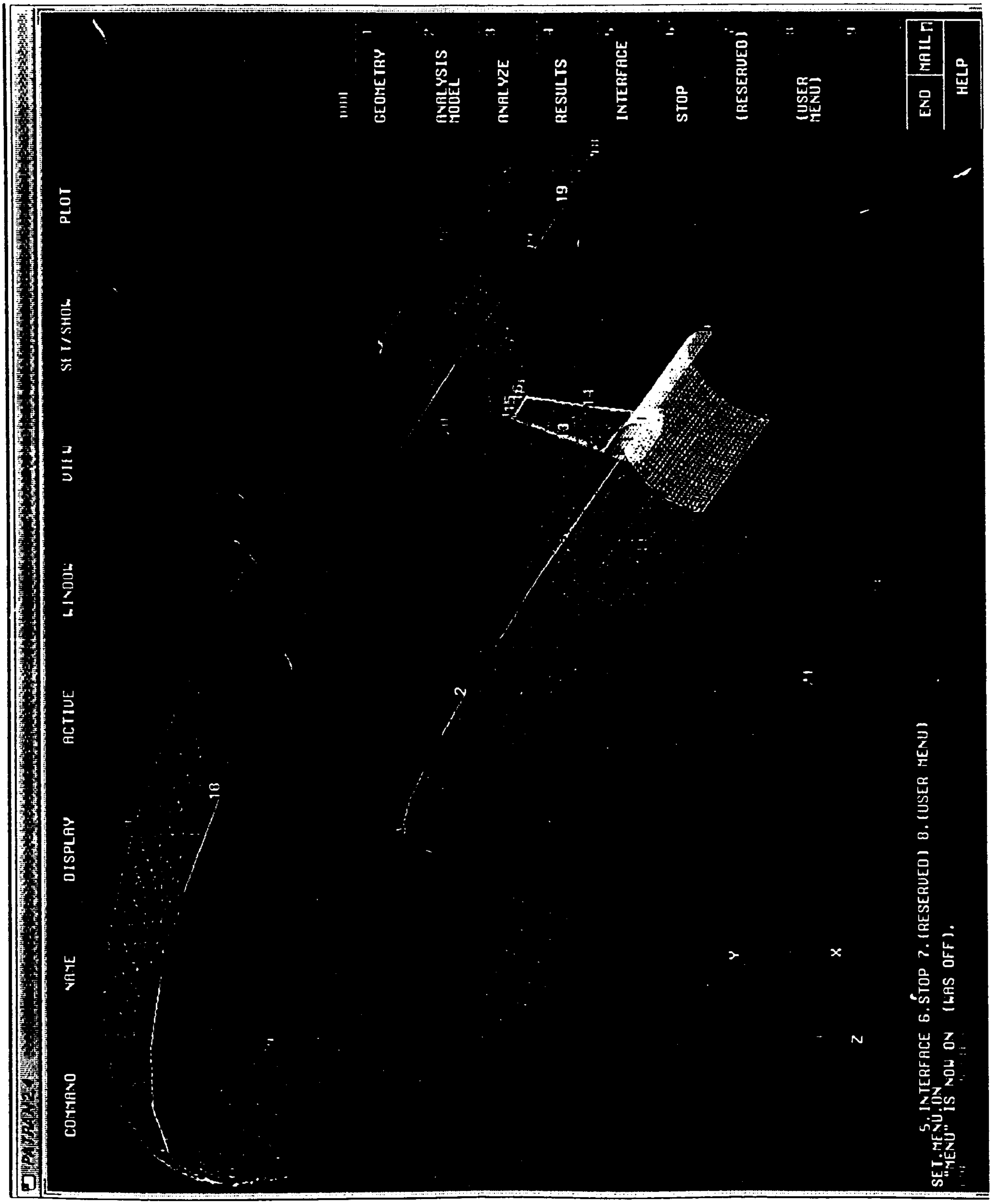
COMMAND
NAME
DISPLAY
ACTIVE
WINDOW
VIEW
SET/SHOW
PLOT
GEOMETRY
ANALYSIS MODEL
ANALYZE
RESULTS
INTERFACE
STOP
(RESERVED)
(USER MENU)
END
MAIL
HELP
5. INTERFACE 6. STOP 7. (RESERVED) 8. (USER MENU)
SET.MENU.ON
"MENU" IS NOW ON (WAS OFF).

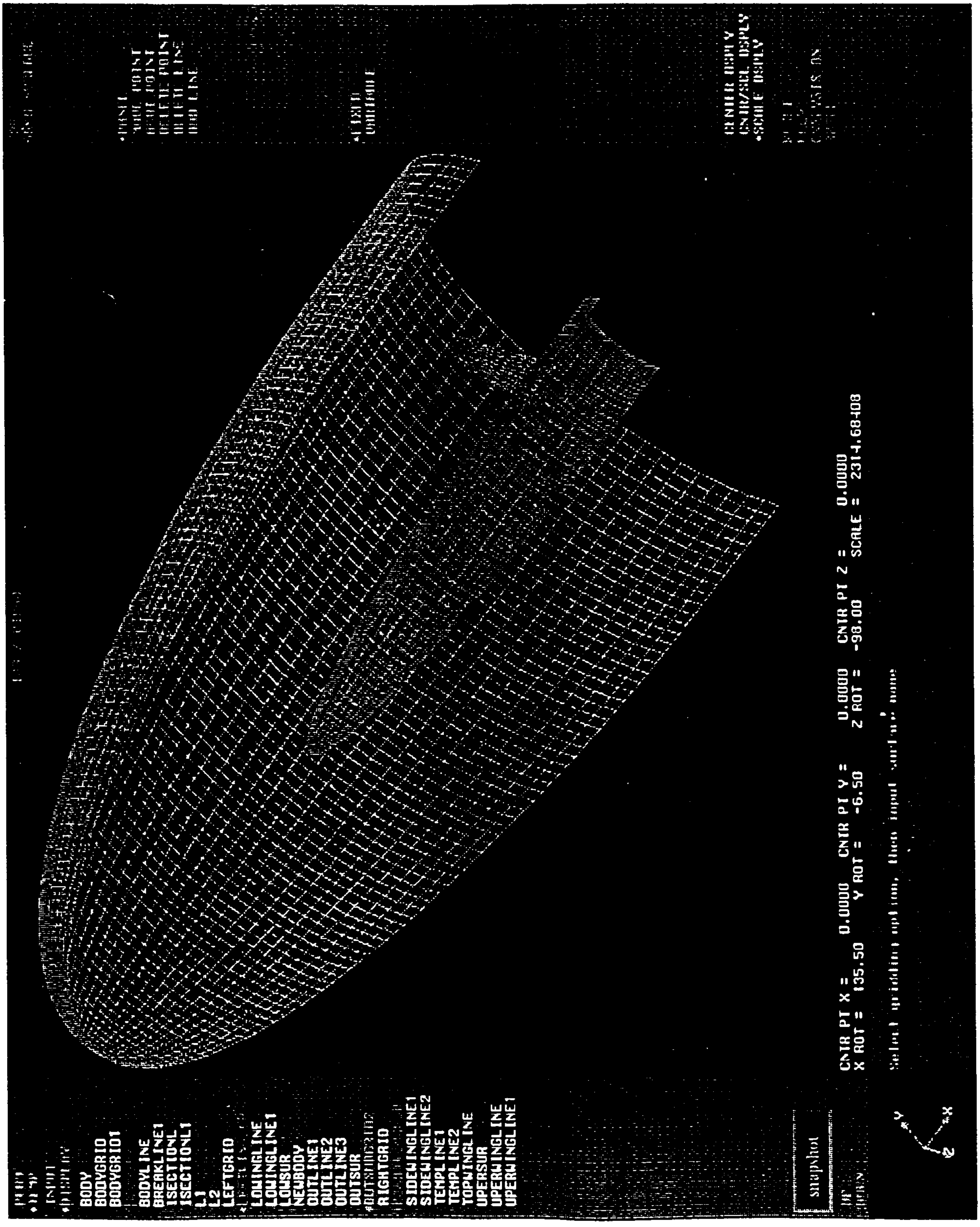
BODY
BODYGRID
BODYGRID1
BODYLINE
BREAKLINE1
ISECTIONL
ISECTIONL1
L1
L2
LEFTGRID
LOWINGLINE
LOWINGLINE1
LOWSUR
NEWBODY
OUTLINE1
OUTLINE2
OUTLINE3
OUTSUR
RIGHTGRID
SIDEWINGLINE1
SIDEWINGLINE2
TEMPLINE1
TEMPLINE2
TOPWINGLINE
UPERSUR
UPERWINGLINE
UPERWINGLINE1
CENTER DSPLY
CNTR/SCL DSPLY
SCALE DSPLY
snapshot
CNTR PT X = 0.0000 CNTR PT Y = 0.0000 CNTR PT Z = 0.0000
X ROT = 135.50 Y ROT = -6.50 Z ROT = -98.00 SCALE = 2314.68408

```
2DFOIL.IGES                                                          S0000001
,,16HPATCAD IGES FILE,10Hpatran.igs,                                 G0000001
20HPDA/PATRAN, Rel 2.4 ,3H4.0,,,,,,,1.0, 1,4HINCH,                   G0000002
,,13H910313.235011,,,,,6,0;                                          G0000003
     116       1       2       2       0       0       0        000000000D0000001
     116       0       0       1       0       0       0POINT           1D0000002
     116       2       2       2       0       0       0        000000000D0000003
     116       0       0       1       0       0       0POINT           2D0000004
     116       3       2       2       0       0       0        000000000D0000005
     116       0       0       1       0       0       0POINT           3D0000006
     116       4       2       2       0       0       0        000000000D0000007
     116       0       0       1       0       0       0POINT           4D0000008
     116       5       2       2       0       0       0        000000000D0000009
     116       0       0       1       0       0       0POINT           5D0000010
     116       6       2       2       0       0       0        000000000D0000011
     116       0       0       1       0       0       0POINT           6D0000012
     116       7       2       2       0       0       0        000000000D0000013
     116       0       0       1       0       0       0POINT           7D0000014
     116       8       2       2       0       0       0        000000000D0000015
     116       0       0       1       0       0       0POINT           8D0000016
     110       9       2       1       0       0       0        000000000D0000017
     110       0       0       2       0       0       0LINE            1D0000018
     124      11       2       1       0       0       0        000010000D0000019
     124       0       0       4       0       0       0MATRIX          2D0000020
     100      15       2       1       0       0      19        000000000D0000021
     100       0       0       3       0       0       0CIRC ARC        2D0000022
     110      18       2       1       0       0       0        000000000D0000023
     110       0       0       2       0       0       0LINE            3D0000024
     110      20       2       1       0       0       0        000000000D0000025
     110       0       0       2       0       0       0LINE            4D0000026
     110      22       2       1       0       0       0        000000000D0000027
     110       0       0       2       0       0       0LINE            5D0000028
     110      24       2       1       0       0       0        000000000D0000029
     110       0       0       2       0       0       0LINE            6D0000030
     124      26       2       1       0       0       0        000010000D0000031
     124       0       0       4       0       0       0MATRIX          8D0000032
     100      30       2       1       0       0      31        000000000D0000033
     100       0       0       3       0       0       0CIRC ARC        8D0000034
     110      33       2       1       0       0       0        000000000D0000035
     110       0       0       2       0       0       0LINE            9D0000036
     114      35       2       1       0       0       0        000000000D0000037
     114       0       0      20       0       0       0SPLSRF          1D0000038
     114      55       2       1       0       0       0        000000000D0000039
     114       0       0      20       0       0       0SPLSRF          2D0000040
     114      75       2       1       0       0       0        000000000D0000041
     114       0       0      20       0       0       0SPLSRF          6D0000042
116, 0.000000000E+00, 0.000000000E+00, 0.000000000E+00;                1P0000001
116, -10.0000000    , 0.000000000E+00, 0.000000000E+00;                3P0000002
116, 0.000000000E+00,  10.0000000    , 0.000000000E+00;                5P0000003
116,  10.0000000    ,  10.0000000    , 0.000000000E+00;                7P0000004
116,  20.0000000    ,  10.0000000    , 0.000000000E+00;                9P0000005
116,  20.0000000    , 0.000000000E+00, 0.000000000E+00;               11P0000006
116,  10.0000000    , 0.000000000E+00, 0.000000000E+00;               13P0000007
116,  1.00000000    ,  1.00000000    , 0.000000000E+00;               15P0000008
110, -10.0000000    , 0.000000000E+00, 0.000000000E+00,               17P0000009
 0.000000000E+00, 0.000000000E+00, 0.000000000E+00;                   17P0000010
124, -1.00000000    , 0.000000000E+00, 0.000000000E+00,               19P0000011
 0.000000000E+00, 0.000000000E+00,  1.00000000    ,                   19P0000012
 0.000000000E+00, 0.000000000E+00, 0.000000000E+00,                   19P0000013
 0.000000000E+00, -1.00000000    , 0.000000000E+00;                   19P0000014
100, 0.000000000E+00, 0.000000000E+00, 0.000000000E+00,               21P0000015
  10.0000000    , 0.000000000E+00, 0.000000000E+00,                   21P0000016
  10.0000000    ;                                                     21P0000017
110, 0.000000000E+00,  10.0000000    , 0.000000000E+00,               23P0000018
```

```
$'point', point=   2, r1=-10.00000    ,0.0000000e+00,0.0000000e+00 $
$'point', point=   3, r1=0.0000000e+00, 10.00000    ,0.0000000e+00 $
$'point', point=   4, r1= 10.00000    , 10.00000    ,0.0000000e+00 $
$'point', point=   5, r1= 20.00000    , 10.00000    ,0.0000000e+00 $
$'point', point=   6, r1= 20.00000    ,0.0000000e+00,0.0000000e+00 $
$'point', point=   7, r1= 10.00000    ,0.0000000e+00,0.0000000e+00 $
$'point', point=   8, r1= 1.000000    , 1.000000    ,0.0000000e+00 $
$'line', points= 10, r1=-10.00000    ,0.0000000e+00,0.0000000e+00,
 r2=0.0000000e+00,0.0000000e+00,0.0000000e+00, coreout=  1 $
$'conicur', type='circle',points=20, angle=   0.00,  90.00,radius= 10.00,
 coreout=   2$
$'trans',corein=   2, r1=  0.00,  0.00,  0.00,r2=  0.00,  0.00,  0.00,
 cosines=-1.0, 0.0, 0.0, 0.0, 1.0, 0.0, 0.0, 0.0,-1.0,coreout=   2$
$'line', points= 10, r1=0.0000000e+00, 10.00000    ,0.0000000e+00,
 r2= 10.00000    , 10.00000    ,0.0000000e+00, coreout=  3 $
$'line', points= 10, r1= 10.00000    , 10.00000    ,0.0000000e+00,
 r2= 20.00000    , 10.00000    ,0.0000000e+00, coreout=  4 $
$'line', points= 10, r1= 20.00000    ,0.0000000e+00,0.0000000e+00,
 r2= 20.00000    , 10.00000    ,0.0000000e+00, coreout=  5 $
$'line', points= 10, r1= 10.00000    ,0.0000000e+00,0.0000000e+00,
 r2= 20.00000    ,0.0000000e+00,0.0000000e+00, coreout=  6 $
$'conicur', type='circle',points=20, angle=   0.00,  90.00,radius=  1.00,
 coreout=   7$
$'trans',corein=   7, r1= -1.00,  0.00,  0.00,r2=  0.00,  0.00,  0.00,
 cosines=-1.0, 0.0, 0.0, 0.0, 1.0, 0.0, 0.0, 0.0,-1.0,coreout=   7$
$'line', points= 10, r1= 1.000000    , 1.000000    ,0.0000000e+00,
 r2= 10.00000    ,0.0000000e+00,0.0000000e+00, coreout=  8 $
$'combine',corein=1,-8,form='plot3d',fileout=4$
$'end'$
```

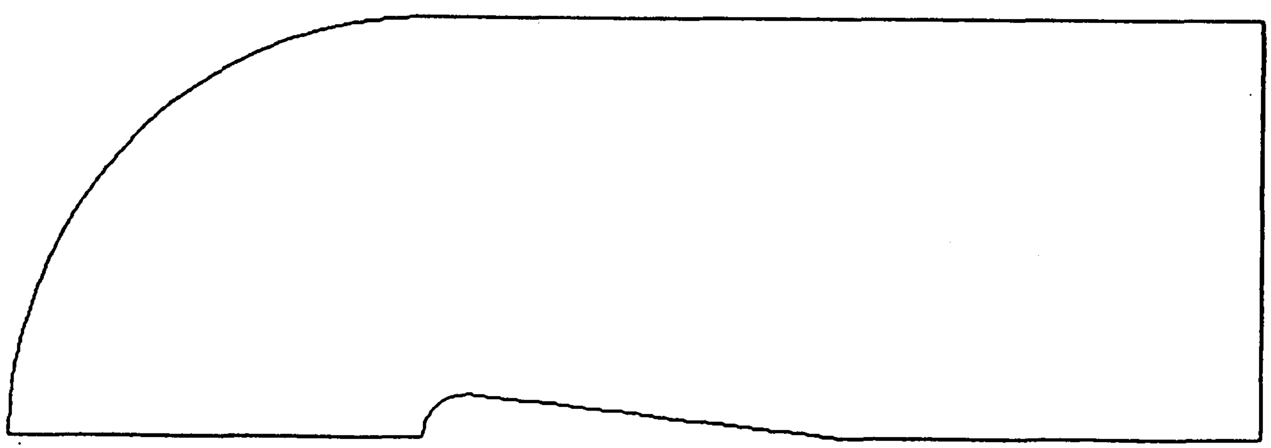

GENIE++

- Simple Minded
- Portable
- Modular
- Journal File Execution Control
- FORTRAN & C
- Extensive Error Checking
- Easy Customization
- (+) Genie Shortcomings
  - Spacings
  - Geometry/Grid Manipulations
  - On Line Storage
  - B Spline - NURBS Applications
  - Geometry Interface
  - Interactive Visualization

N92-32303

USING ADAPTIVE GRID IN MODELING ROCKET NOZZLE FLOW

By Alan S. Chow * and Kang-Ren Jin**

*NASA/Performance Analysis Branch, Marshall Space Flight Center, AL 35812.

**Department of Civil Engineering, Mississippi State University, Mississippi State, MS 39762.

ABSTRACT

The mechanical behavior of a rocket motor internal flow field results in a system of nonlinear partial differential equations which cannot be solved analytically. However, this system of equations called the Navier-Stokes equations can be solved numerically. The accuracy and the convergence of the solution of the system of equations will depend largely on how precisely the sharp gradients in the domain of interest can be resolved. With the advances in computer technology, more sophisticated algorithms are available to improve the accuracy and convergence of the solutions. An adaptive grid generation is one of the schemes which can be incorporated into the algorithm to enhance the capability of numerical modeling. It is equivalent to putting intelligence into the algorithm to optimize the use of computer memory. With this scheme, the finite difference domain of the flow field called the grid does neither have to be very fine nor strategically placed at the location of sharp gradients. The grid is self adapting as the solution evolves. This scheme significantly improve the methodology of solving flow problems in rocket nozzle by taking the refinement part of grid generation out of the hands of computational fluid dynamics (CFD) specialists and place it into the computer algorithm itself.

PRECEDING PAGE BLANK NOT FILMED

MSFC
GEORGE C. MARSHALL
SPACE FLIGHT CENTER
HUNTSVILLE, ALABAMA

NASA
NATIONAL AERONAUTICS
AND
SPACE ADMINISTRATION

Using Adaptive Grid in Modeling Rocket Nozzle Flow

by
Alan S. Chow
&
Kang-Ren Jin

April 29, 1992

619

OBJECTIVE

- To develope a user-friendly solution-adaptive grid generator that will simplify grid generation process so that a 'perfect' grid can be generated everytime without the intervention of CFD experts.

$$\frac{\partial \mathbf{U}}{\partial t} + \frac{\partial \mathbf{E}}{\partial x} + \frac{\partial \mathbf{F}}{\partial y} + \frac{\partial \mathbf{G}}{\partial z} = 0$$

$$\mathbf{U} = \begin{bmatrix} \rho \\ \rho u \\ \rho v \\ \rho w \\ E_t \end{bmatrix} \qquad \mathbf{E} = \begin{bmatrix} \rho u \\ \rho u^2 + p - \tau_{xx} \\ \rho u v - \tau_{xy} \\ \rho u w - \tau_{xz} \\ (E_t + p)u - u\tau_{xx} - v\tau_{xy} - w\tau_{xz} + q_x \end{bmatrix}$$

$$\mathbf{F} = \begin{bmatrix} \rho v \\ \rho u v - \tau_{xy} \\ \rho v^2 + p - \tau_{yy} \\ \rho v w - \tau_{yz} \\ (E_t + p)v - u\tau_{xy} - v\tau_{yy} - w\tau_{yz} + q_y \end{bmatrix} \qquad \mathbf{G} = \begin{bmatrix} \rho w \\ \rho u w - \tau_{xz} \\ \rho v w - \tau_{yz} \\ \rho w^2 + p - \tau_{zz} \\ (E_t + p)w - u\tau_{xz} - v\tau_{yz} - w\tau_{zz} + q_z \end{bmatrix}$$

$$\frac{\partial S}{\partial t} + \frac{\partial F_j}{\partial X_j} = \frac{1}{Re}\frac{\partial G_j}{\partial X_j}$$

where S is a vector containing the conservation variables,

$$S = \begin{bmatrix} \rho \\ \rho u_j \\ E \end{bmatrix}$$

The F_j vectors represent the inviscid flux vectors,

$$F_j = \begin{bmatrix} \rho u_j \\ \rho u_i u_j + P_g \delta_{ij} \\ (E + P_g) u_j \end{bmatrix}$$

and G_j vectors are the viscous flux vectors

$$G_j = \begin{bmatrix} 0 \\ \tau_{ij} \\ u_k \tau_{jk} - q_j \end{bmatrix}$$

$$\xi_j = \xi_j(X_j, t)$$

$$\frac{\partial \hat{S}}{\partial t} + \frac{\partial \hat{F}_j}{\partial \xi_j} = \frac{1}{Re}\frac{\partial \hat{G}_j}{\partial \xi_j}$$

$$\hat{S} = \frac{1}{J} S$$

$$\hat{F}_j = \frac{1}{J}\left(\frac{\partial \xi_j}{\partial t} S + \frac{\partial \xi_j}{\partial X_k} F_k\right)$$

$$\hat{G}_j = \frac{1}{J}\frac{\partial \xi_j}{\partial X_k} G_k$$

GRID GENERATION METHODS

- Complex variables (Conformal Mapping)
- Algebraic
- Partial Differential Equations (PDE)
  - -Elliptic
  - -Hyperbolic

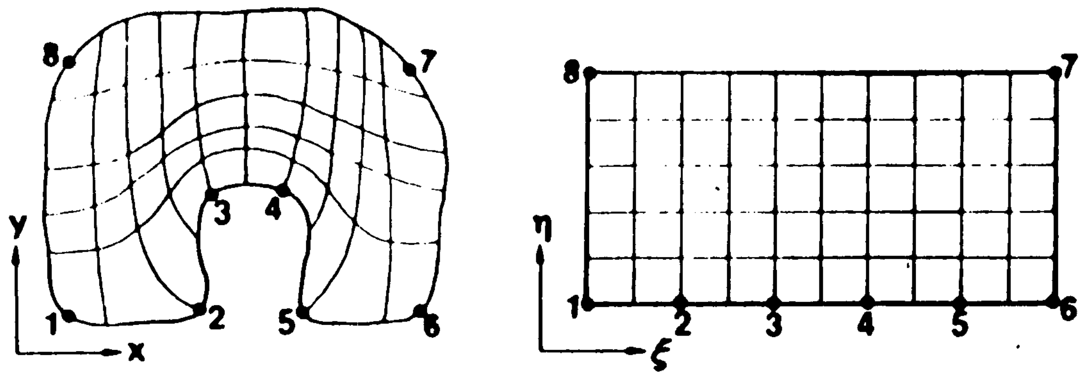

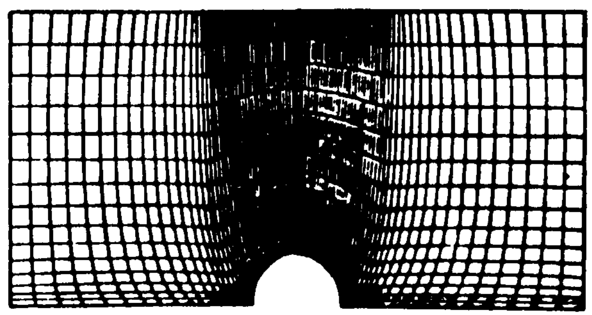

$$\nabla^2 \xi^i = P^i \qquad (i = 1, 2)$$

$$\xi_{xx} + \xi_{yy} = P$$

$$\eta_{xx} + \eta_{yy} = Q$$

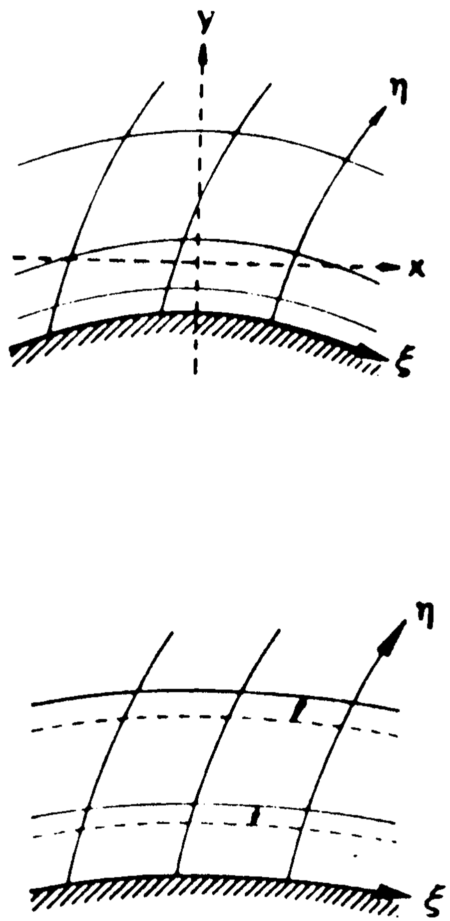

Q < 0

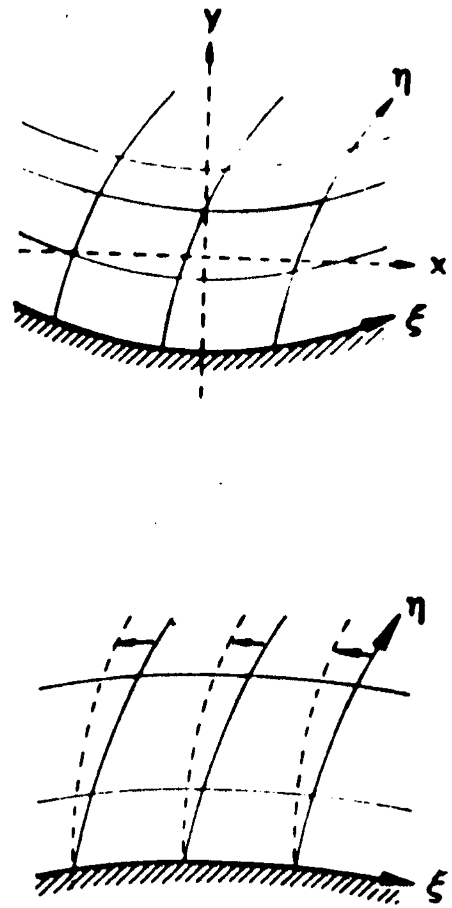

P < 0

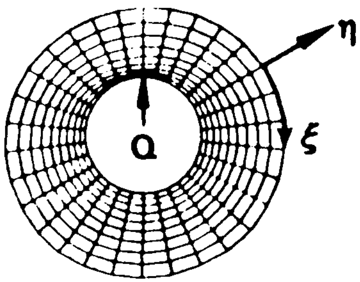
η
ξ
Q

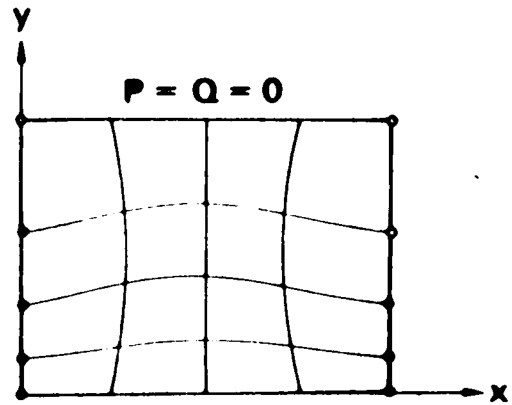
y
P = Q = 0
x

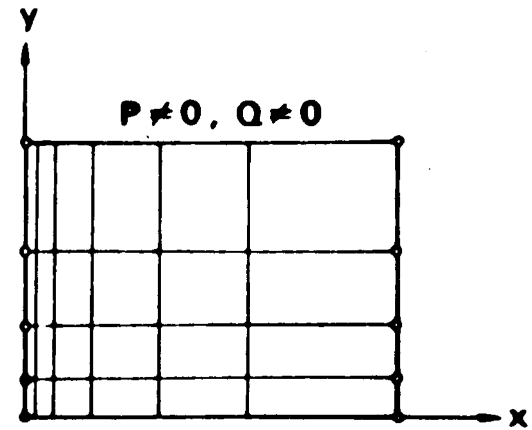
y
P ≠ 0, Q ≠ 0
x

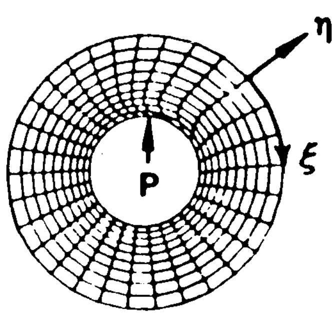
η
ξ
P

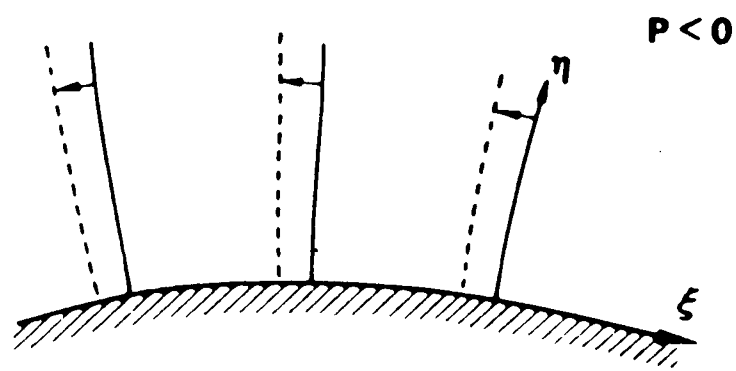
P < 0
η
ξ

$$P(\xi,\eta) = -\sum_{i=1}^{N} a_i \operatorname{sign}(\xi - \xi_i) \exp(-c_i|\xi-\xi_i|)$$

$$- \sum_{i=1}^{M} b_i \operatorname{sign}(\xi - \xi_i) \exp(-d_i[(\xi-\xi_i)^2+(\eta-\eta_i)^2]^{1/2})$$

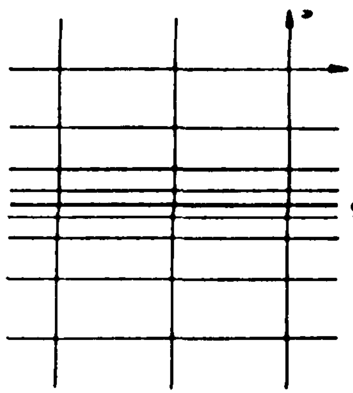

$\xi=\xi_i$ Attraction line

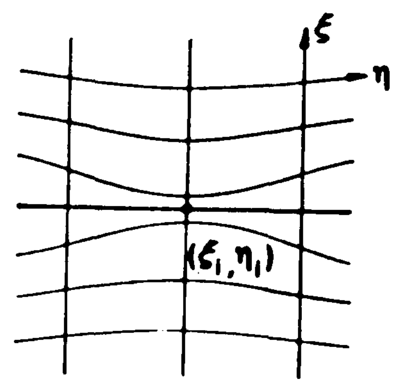

Attraction point

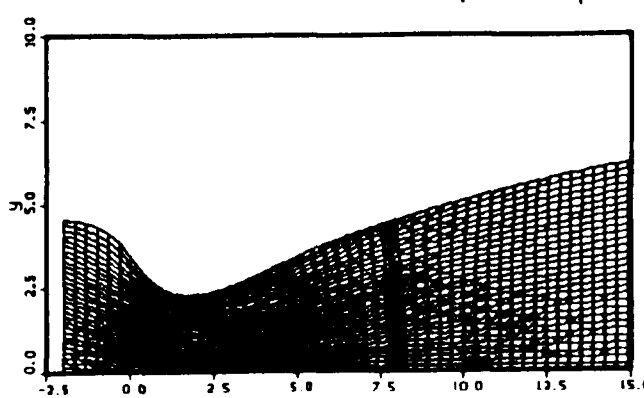

$$W(x)x_\xi = constant$$

W(x) : weight function
x(ξ): point distribution

$$x_{\xi\xi}W + x_\xi W_\xi = 0$$

$$x_{\xi\xi} + P\,x_\xi = 0$$

$$P = -\frac{x_{\xi\xi}}{x_\xi} = \frac{W_\xi}{W}$$

$$P_i = \frac{W_{\xi^i}}{W} \qquad (i = 1, 2, 3)$$

$$W = 1 + |\underline{\nabla} p|$$

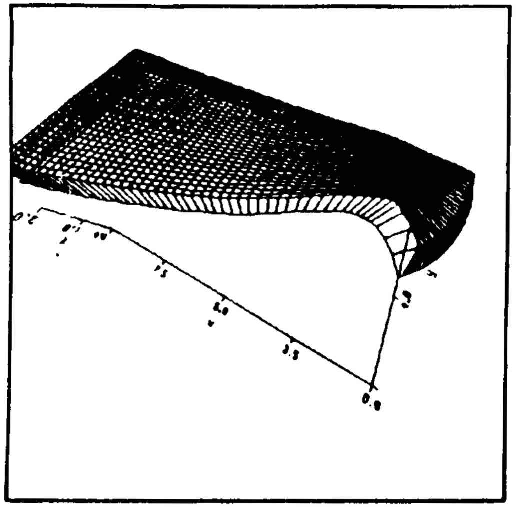

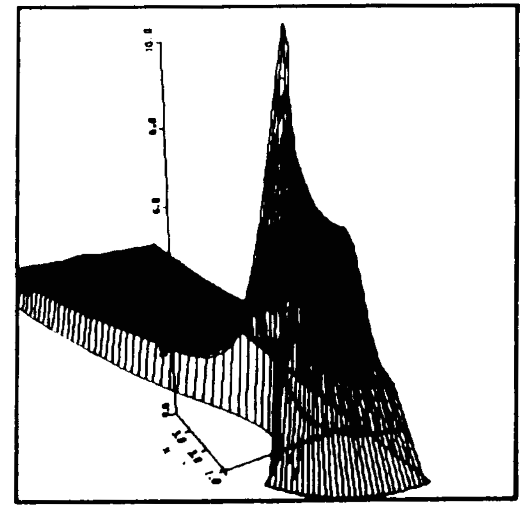

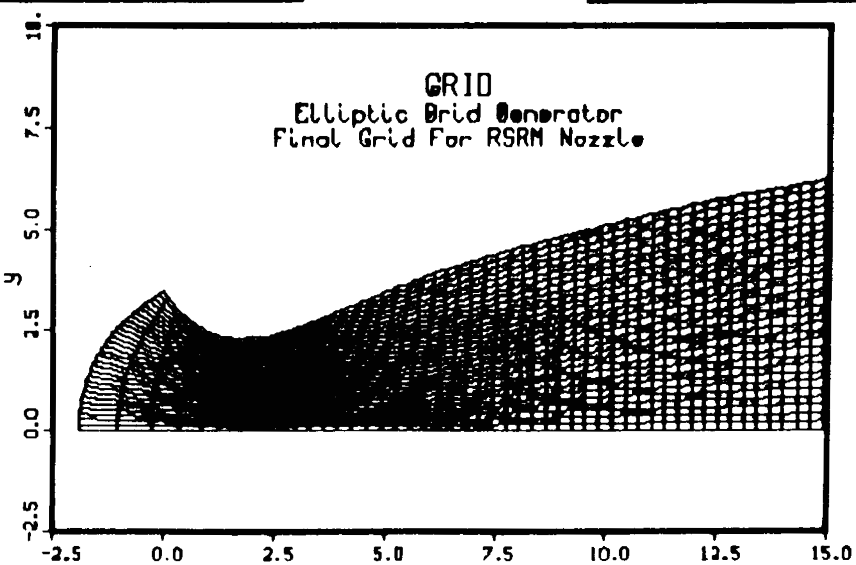

GRID
Elliptic Grid Generator
Final Grid For RSRM Nozzle
y
-2.5
0.0
2.5
5.0
7.5
10.
-2.5
0.0
2.5
5.0
7.5
10.0
12.5
15.0

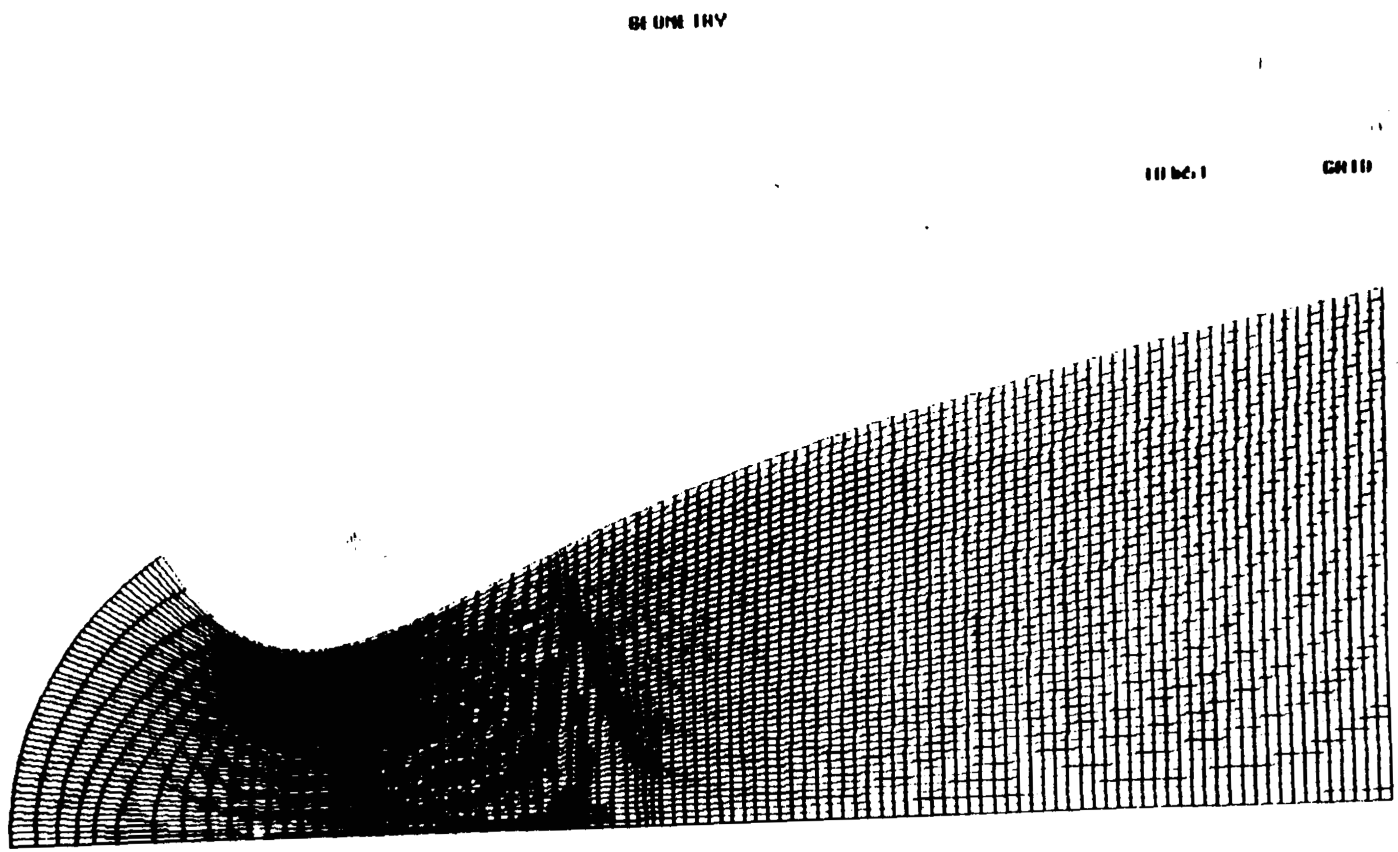

The Adaptive Grid at Time Step = 500 for Inviscid Flow.

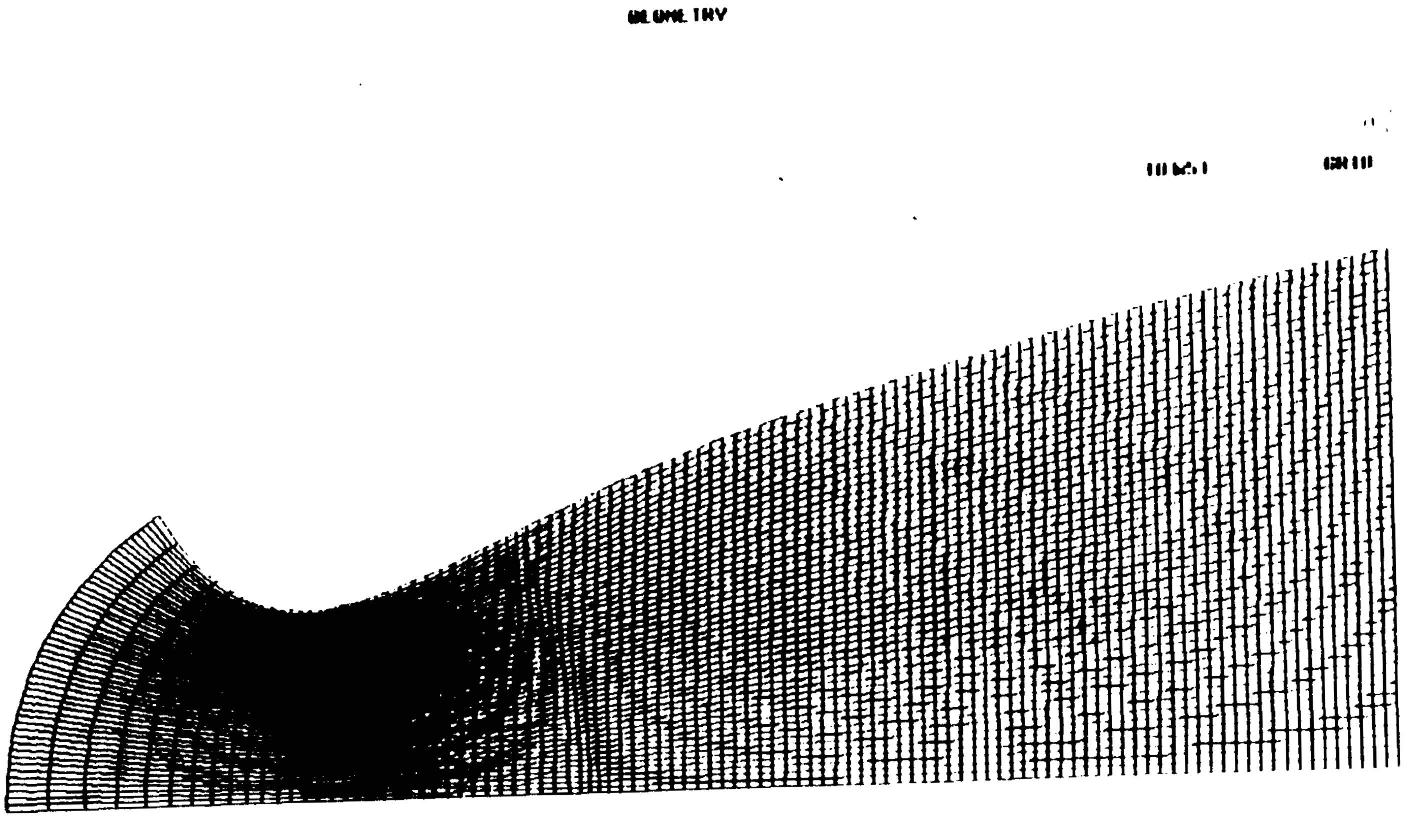

The Adaptive Grid at Time Step = 1000 for Inviscid Flow.

MSFC
GEORGE C. MARSHALL
SPACE FLIGHT CENTER
HUNTSVILLE, ALABAMA

NASA
NATIONAL AERONAUTICS
AND
SPACE ADMINISTRATION

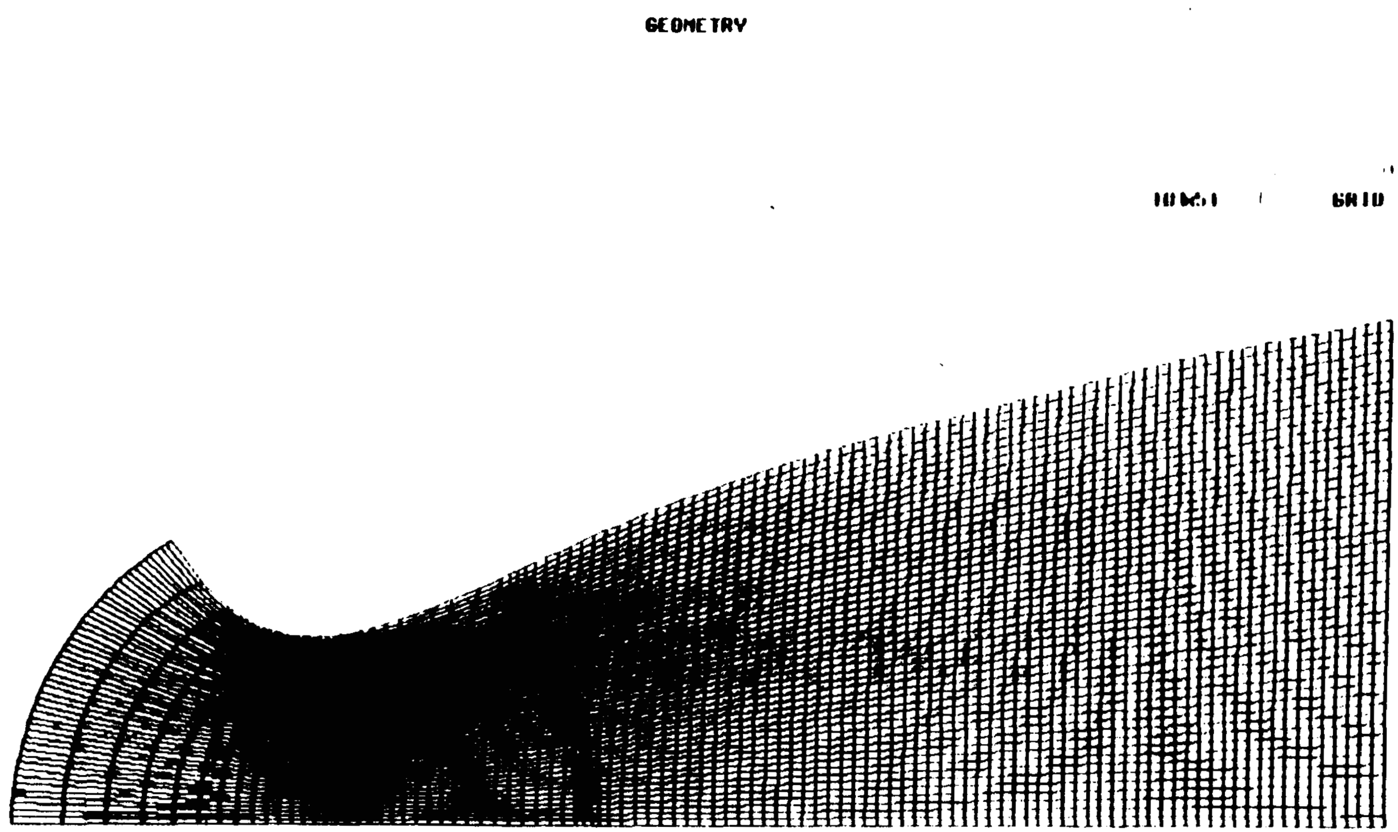

The Adaptive Grid at Time Step = 2000 for Inviscod Flow.

630

WEIGHT FUNCTION

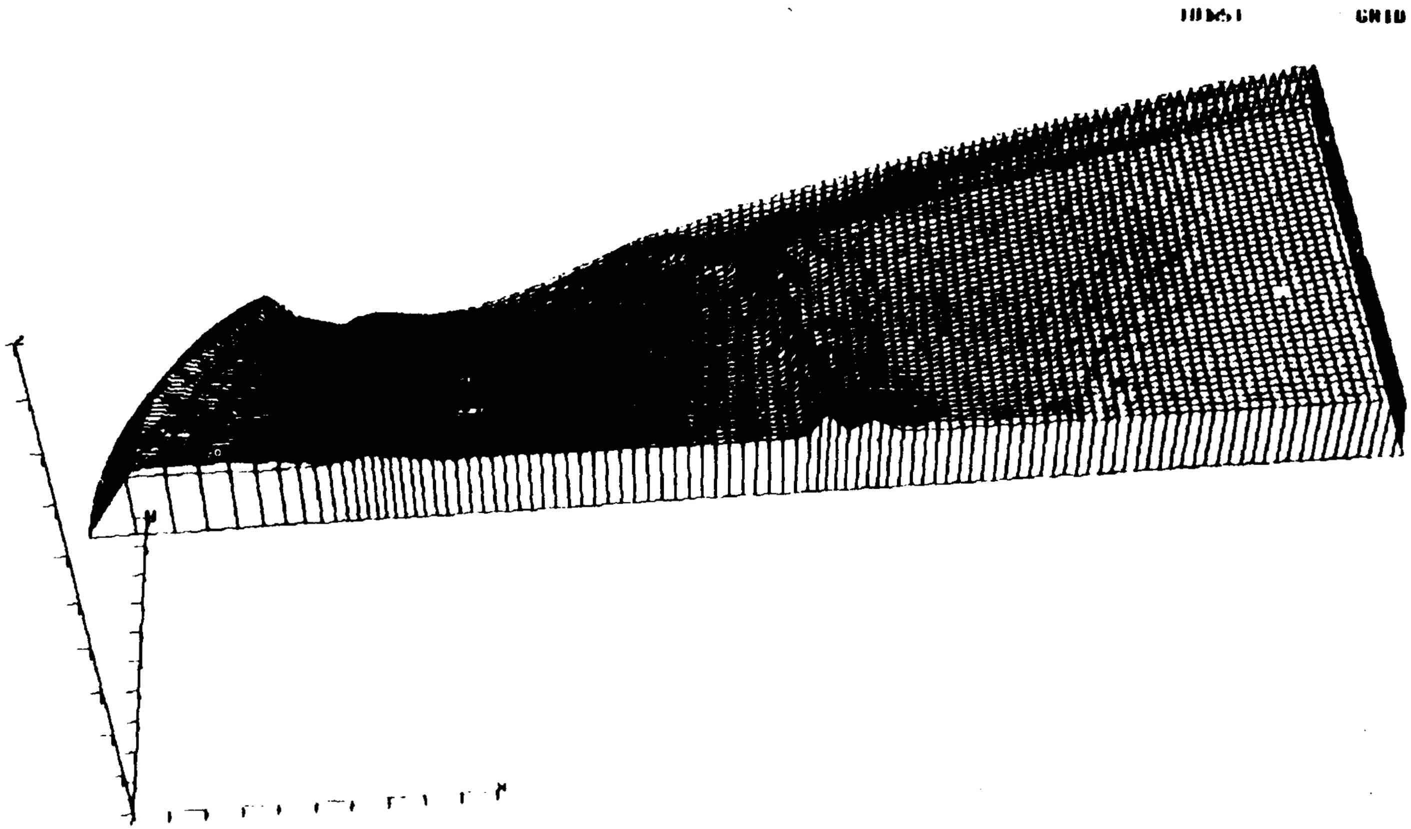

The Weight Function Distribution at Time Step = 300 for Viscous Flow.

MSFC
GEORGE C. MARSHALL
SPACE FLIGHT CENTER
HUNTSVILLE, ALABAMA

NASA
NATIONAL AERONAUTICS
AND
SPACE ADMINISTRATION

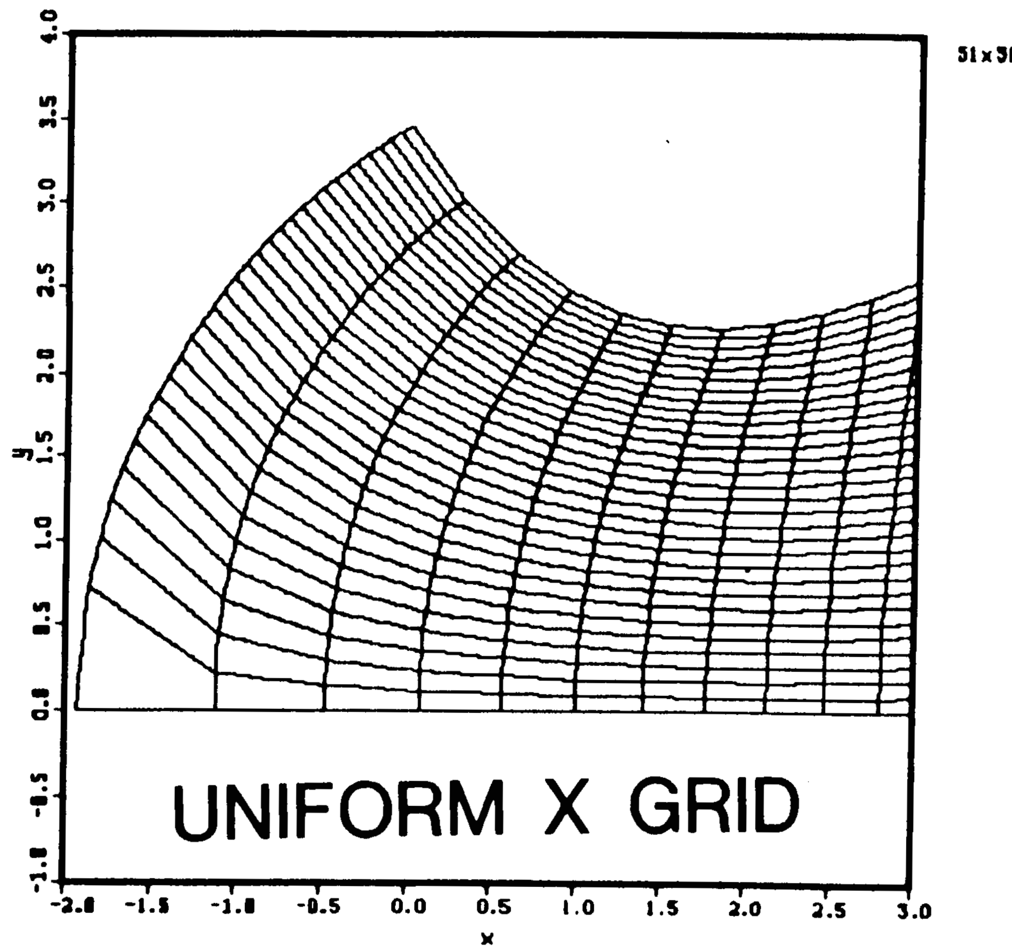

PRESSURE

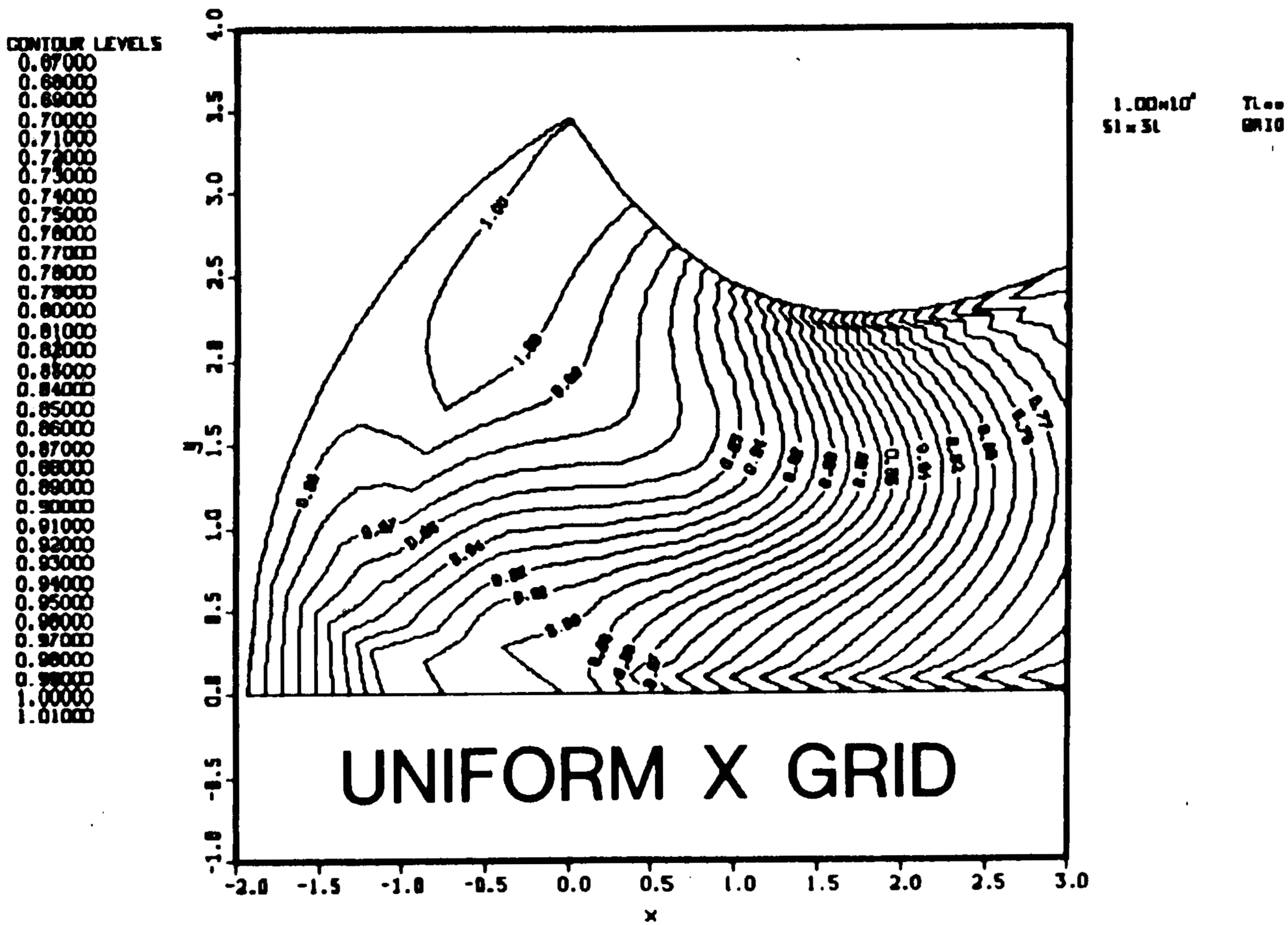
CONTOUR LEVELS
0.67000
0.68000
0.69000
0.70000
0.71000
0.72000
0.73000
0.74000
0.75000
0.76000
0.77000
0.78000
0.79000
0.80000
0.81000
0.82000
0.83000
0.84000
0.85000
0.86000
0.87000
0.88000
0.89000
0.90000
0.91000
0.92000
0.93000
0.94000
0.95000
0.96000
0.97000
0.98000
0.99000
1.00000
1.01000
UNIFORM X GRID
x
y
-2.0
-1.5
-1.0
-0.5
0.0
0.5
1.0
1.5
2.0
2.5
3.0
4.0
3.5
3.0
2.5
2.0
1.5
1.0
0.5
0.0
-0.5
-1.0

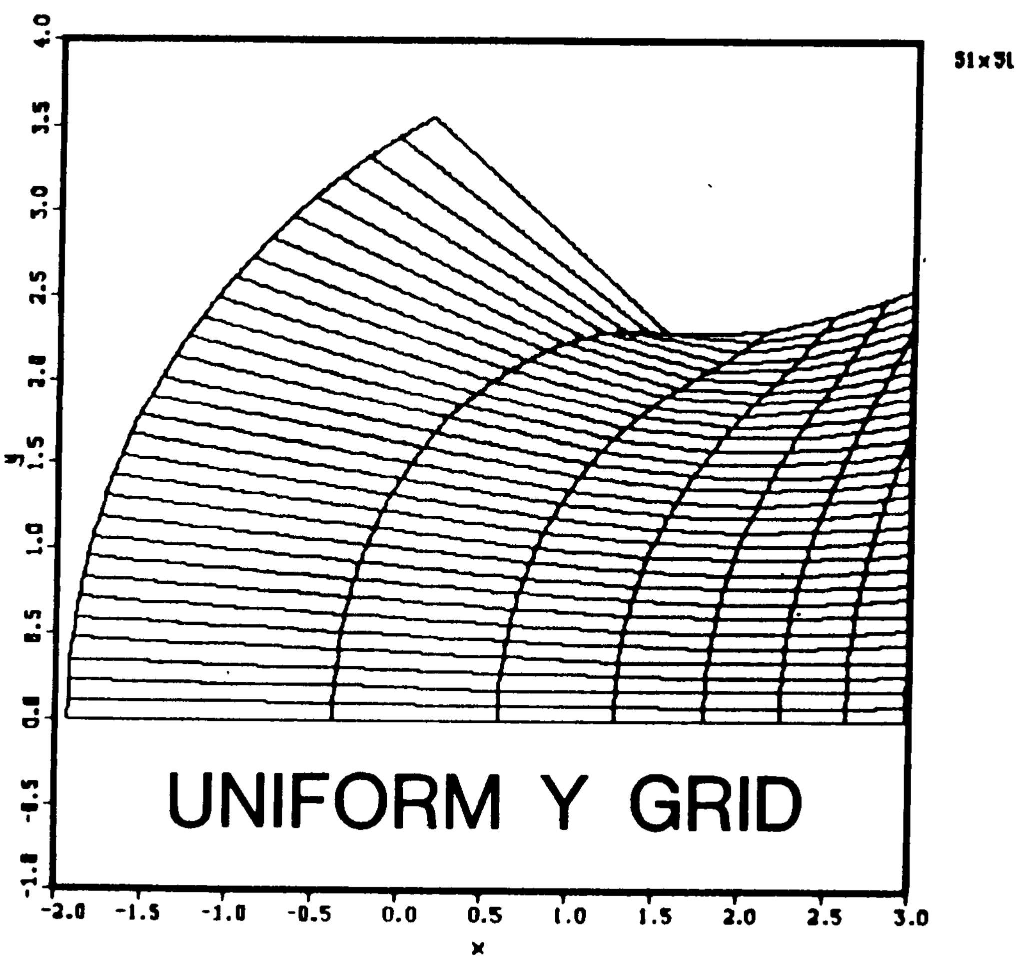
51x51
y
x
-2.0
-1.5
-1.0
-0.5
0.0
0.5
1.0
1.5
2.0
2.5
3.0
4.0
3.5
3.0
2.5
2.0
1.5
1.0
0.5
0.0
-0.5
-1.0
UNIFORM Y GRID

PRESSURE

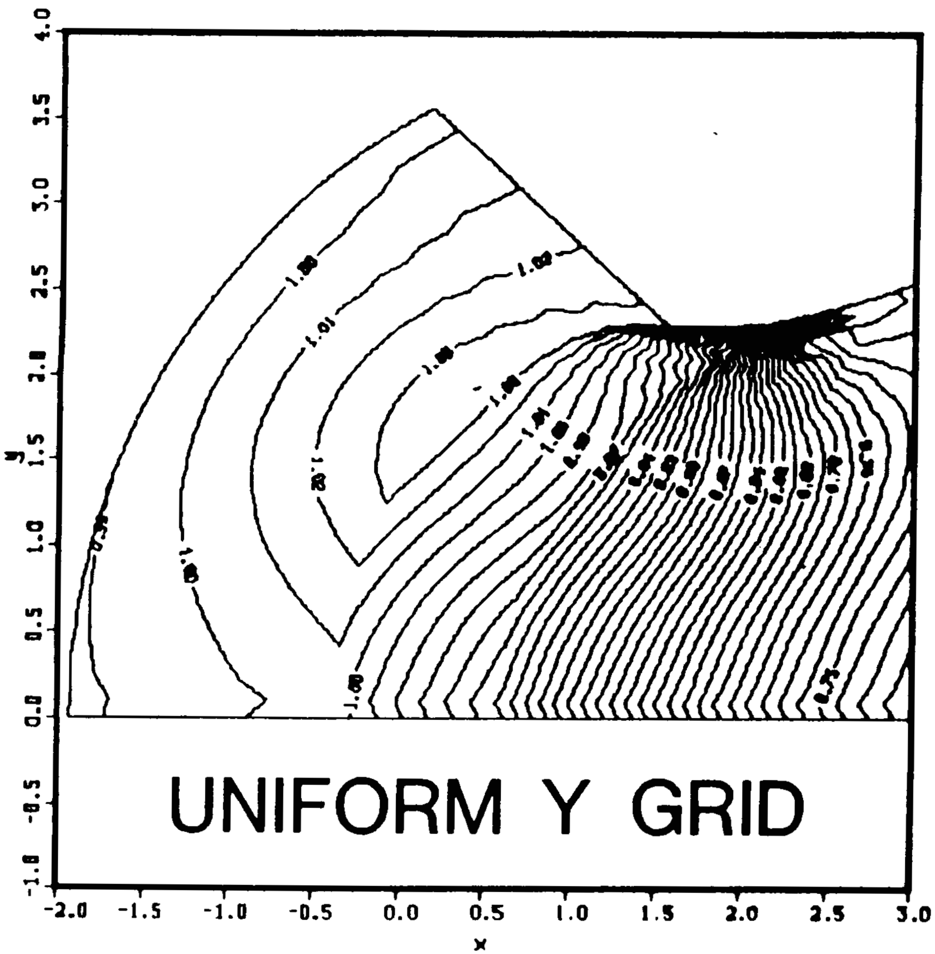
UNIFORM Y GRID
-2.0 -1.5 -1.0 -0.5 0.0 0.5 1.0 1.5 2.0 2.5 3.0
x
-1.0 -0.5 0.0 0.5 1.0 1.5 2.0 2.5 3.0 3.5 4.0
y

MSFC

GEORGE C. MARSHALL
SPACE FLIGHT CENTER
HUNTSVILLE, ALABAMA

NASA

NATIONAL AERONAUTICS
AND
SPACE ADMINISTRATION

PRESSURE

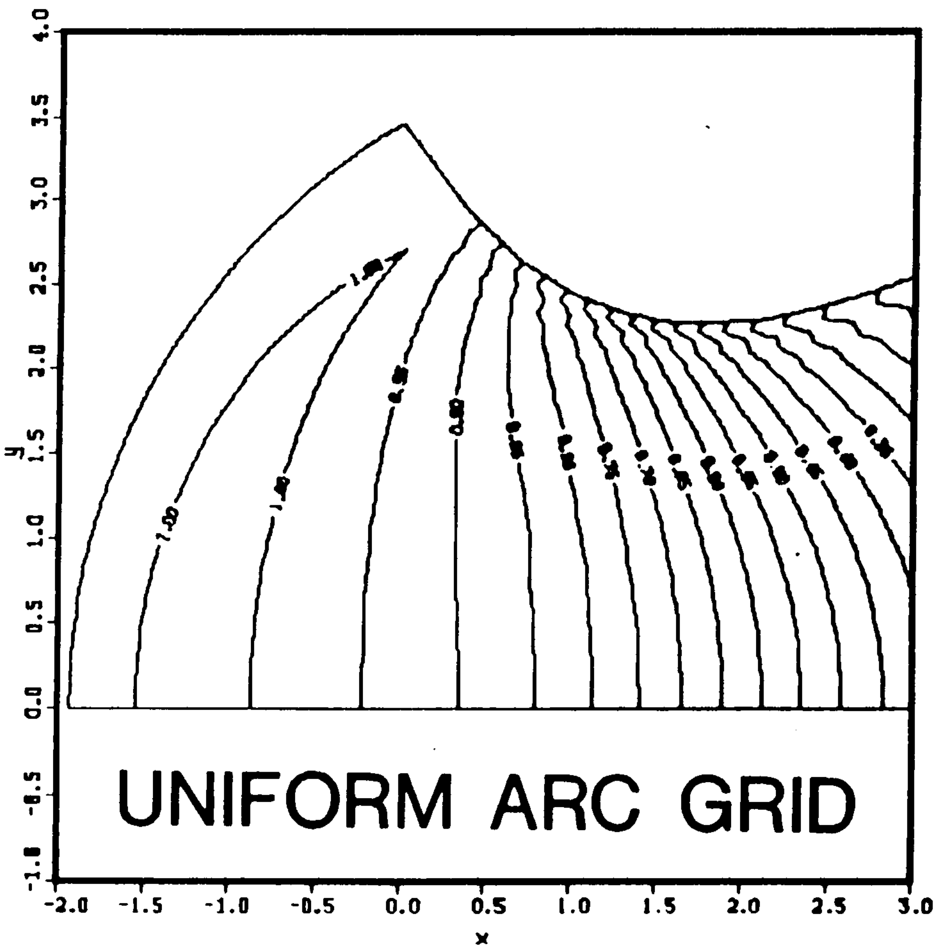

MSFC
GEORGE C. MARSHALL
SPACE FLIGHT CENTER
HUNTSVILLE, ALABAMA

NASA
NATIONAL AERONAUTICS
AND
SPACE ADMINISTRATION

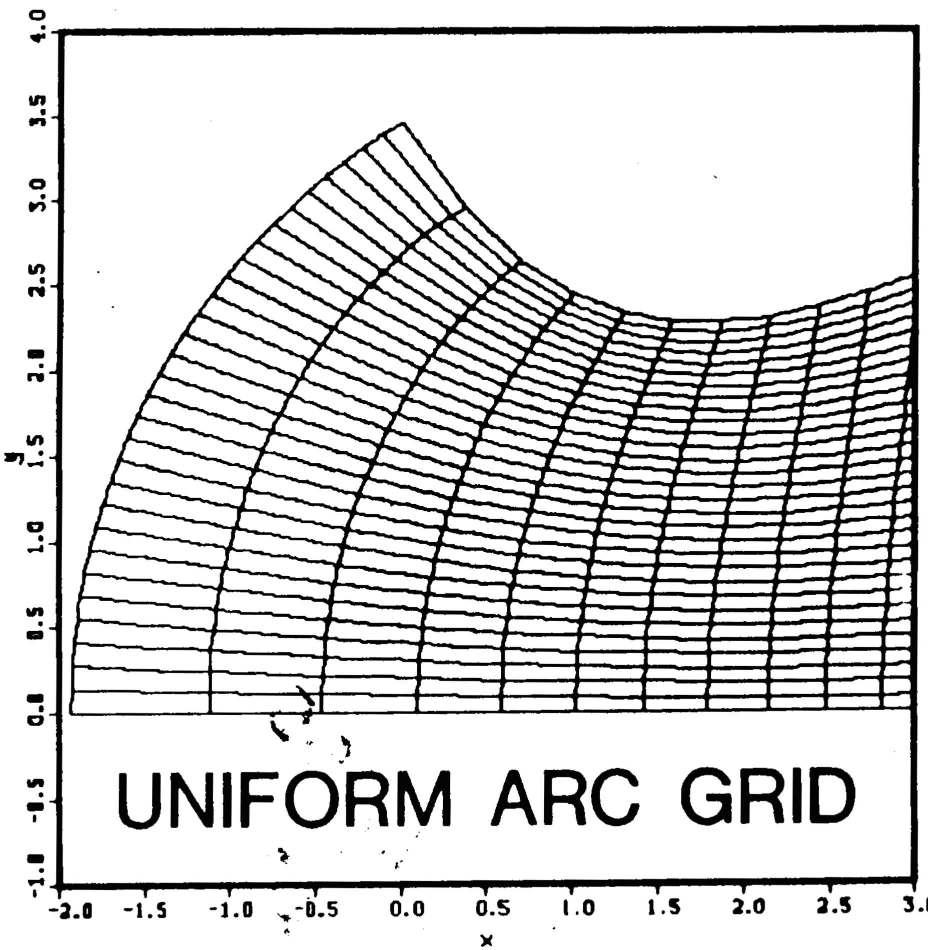

UNIFORM ARC GRID

MSFC
GEORGE C. MARSHALL
SPACE FLIGHT CENTER
HUNTSVILLE, ALABAMA

NASA
NATIONAL AERONAUTICS
AND
SPACE ADMINISTRATION

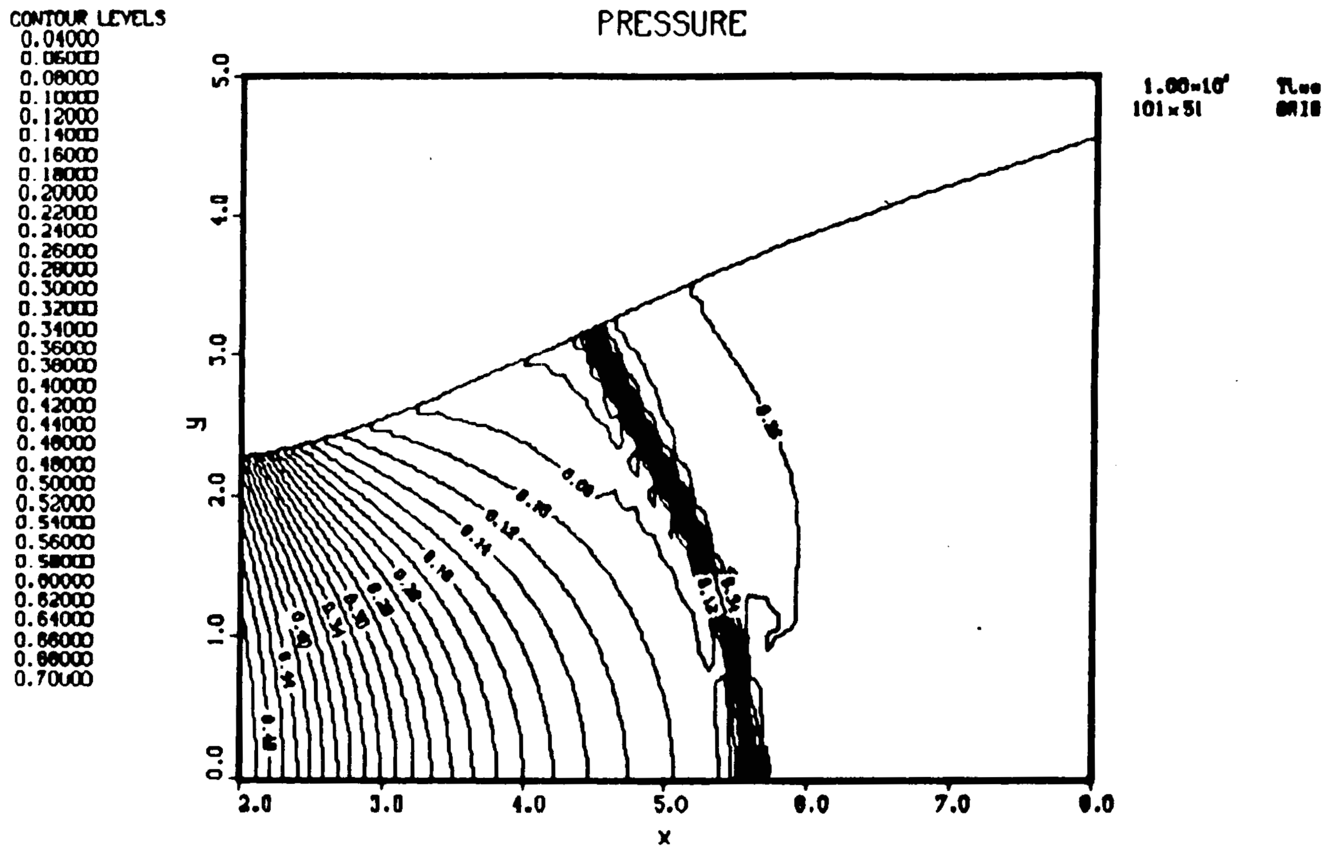

INVISCID NOZZLE FLOW

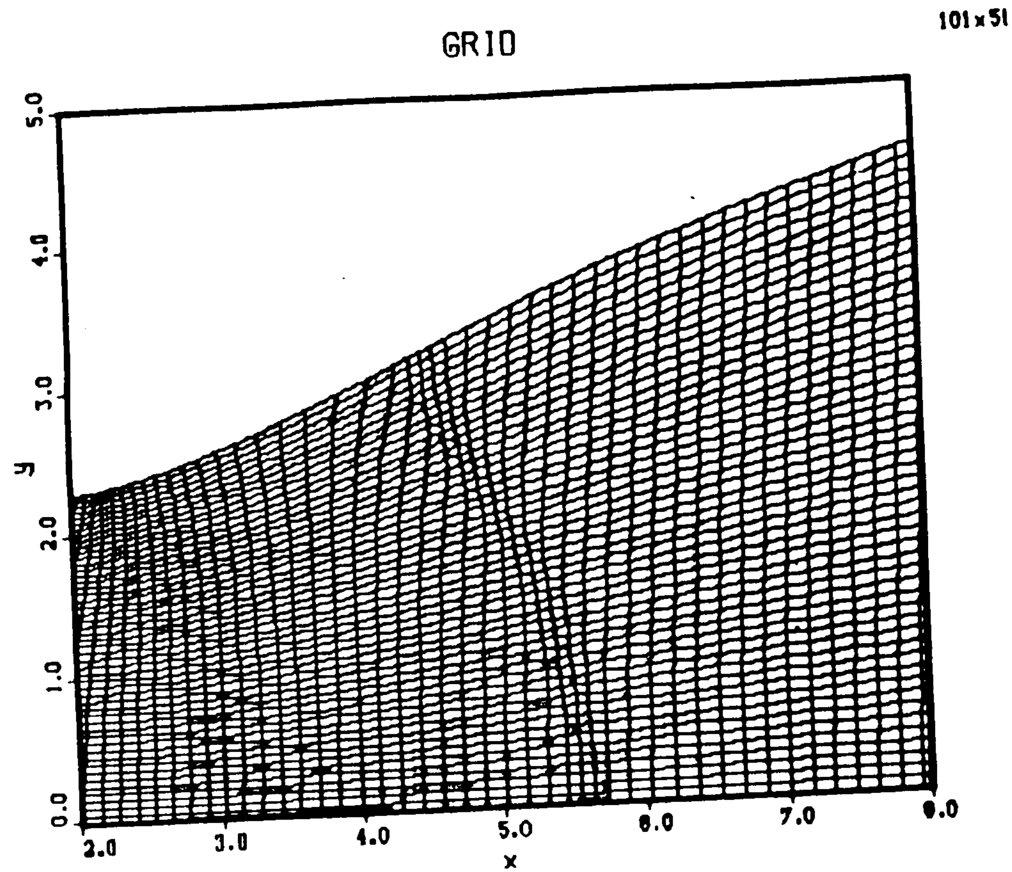

INVISCID NOZZLE FLOW

MSFC

GEORGE C. MARSHALL
SPACE FLIGHT CENTER
HUNTSVILLE, ALABAMA

NASA

NATIONAL AERONAUTICS
AND
SPACE ADMINISTRATION

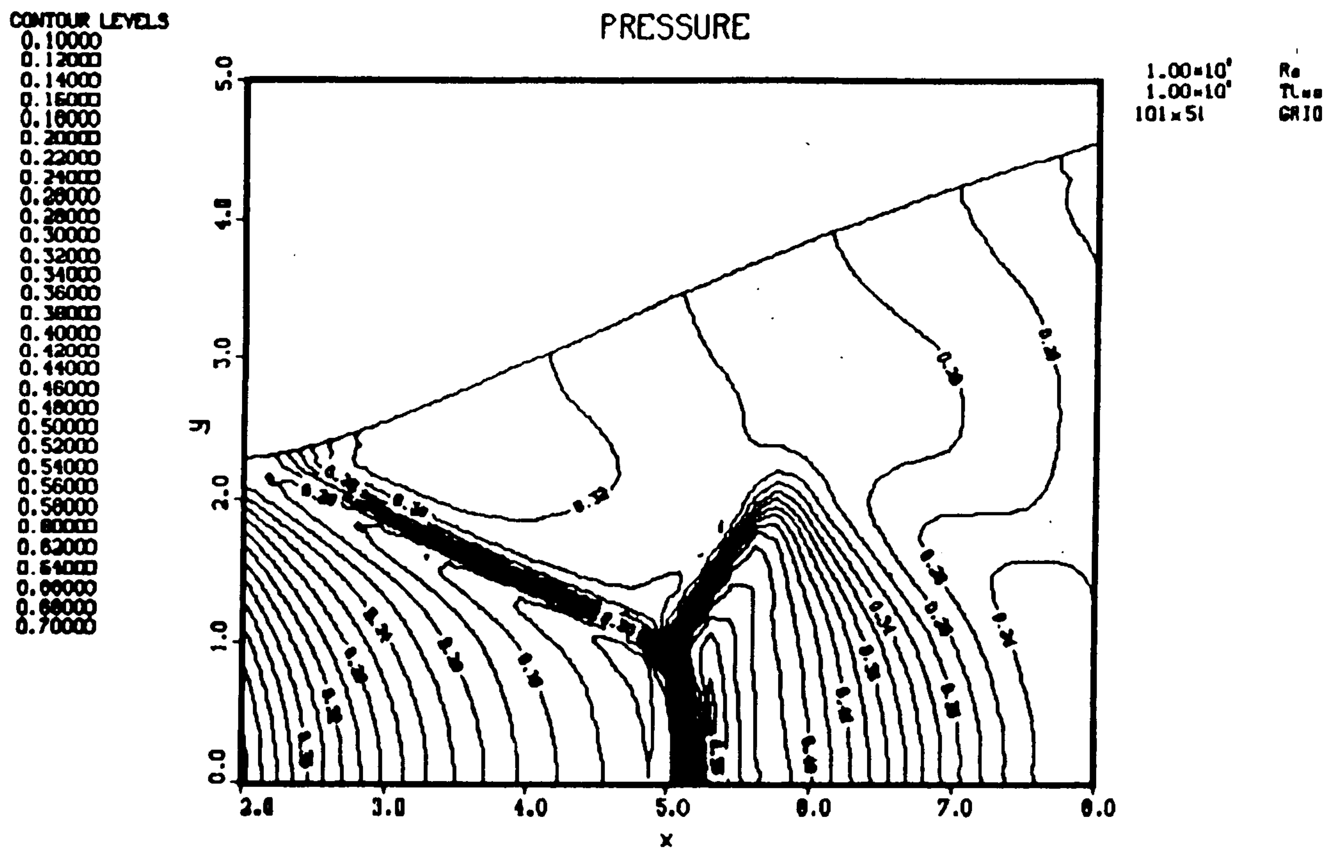

VISCOUS NOZZLE FLOW

MSFC
GEORGE C. MARSHALL
SPACE FLIGHT CENTER
HUNTSVILLE, ALABAMA

NASA
NATIONAL AERONAUTICS
AND
SPACE ADMINISTRATION

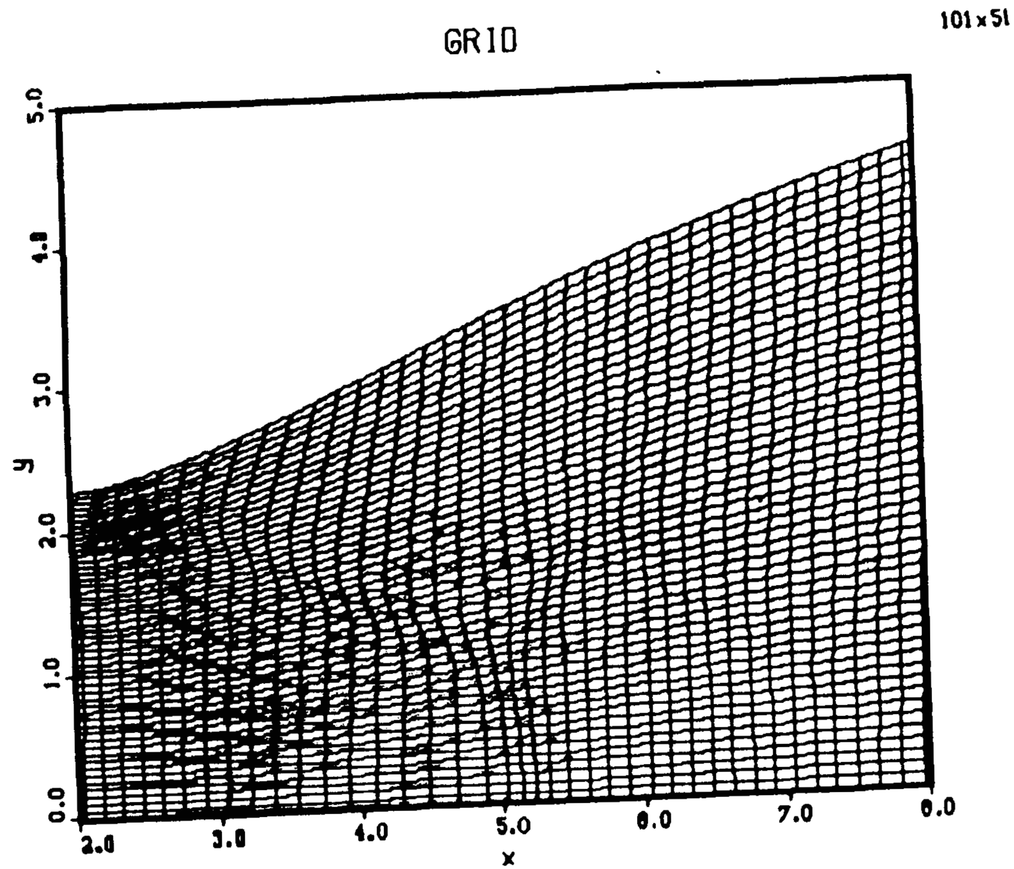

640

VISCOUS NOZZLE FLOW

WEIGHT FUNCTION

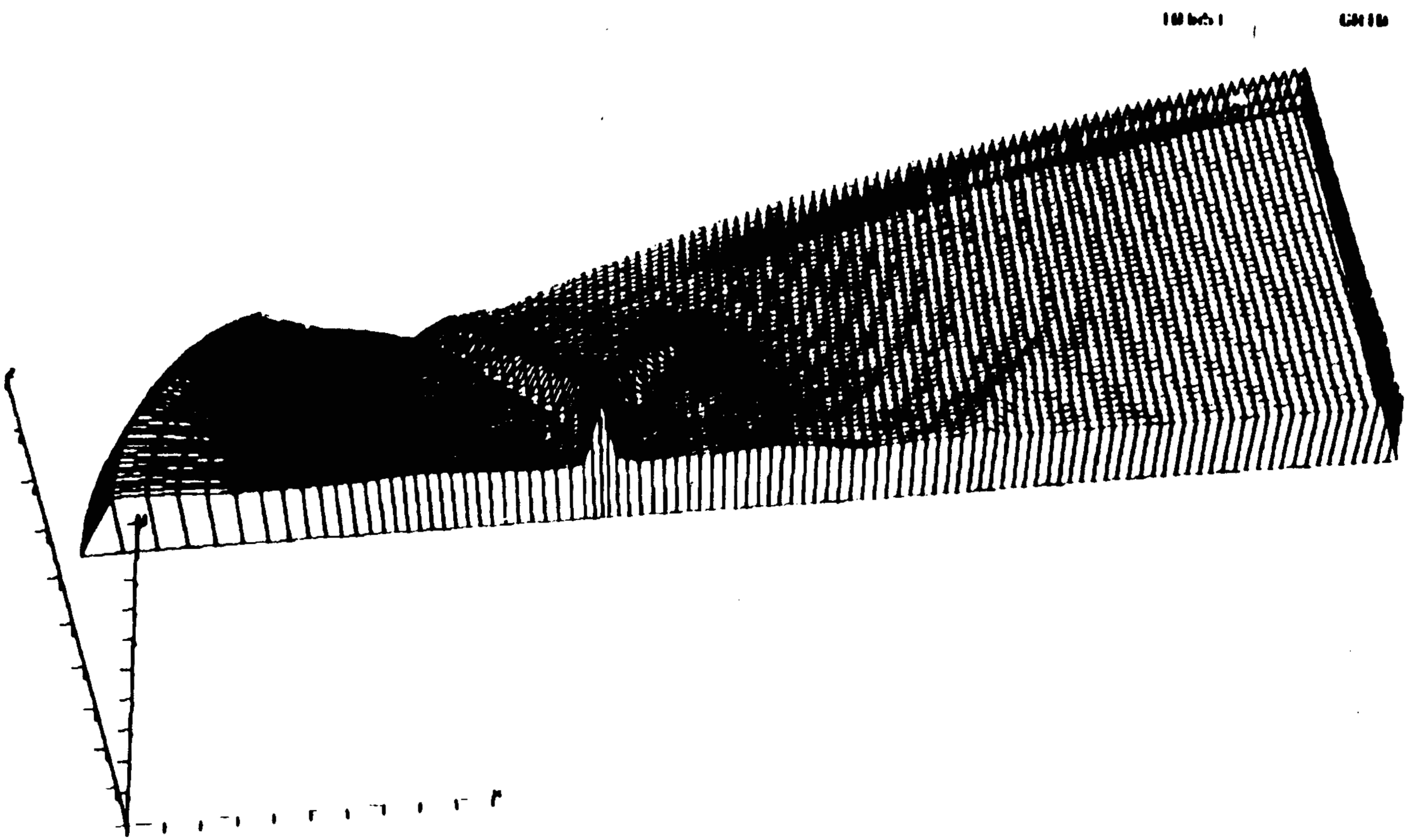

The Weight Function Distribution at Time Step = 5500 for Viscous Flow.

MSFC
GEORGE C. MARSHALL
SPACE FLIGHT CENTER
HUNTSVILLE, ALABAMA

NASA
NATIONAL AERONAUTICS
AND
SPACE ADMINISTRATION

642

GEOMETRY

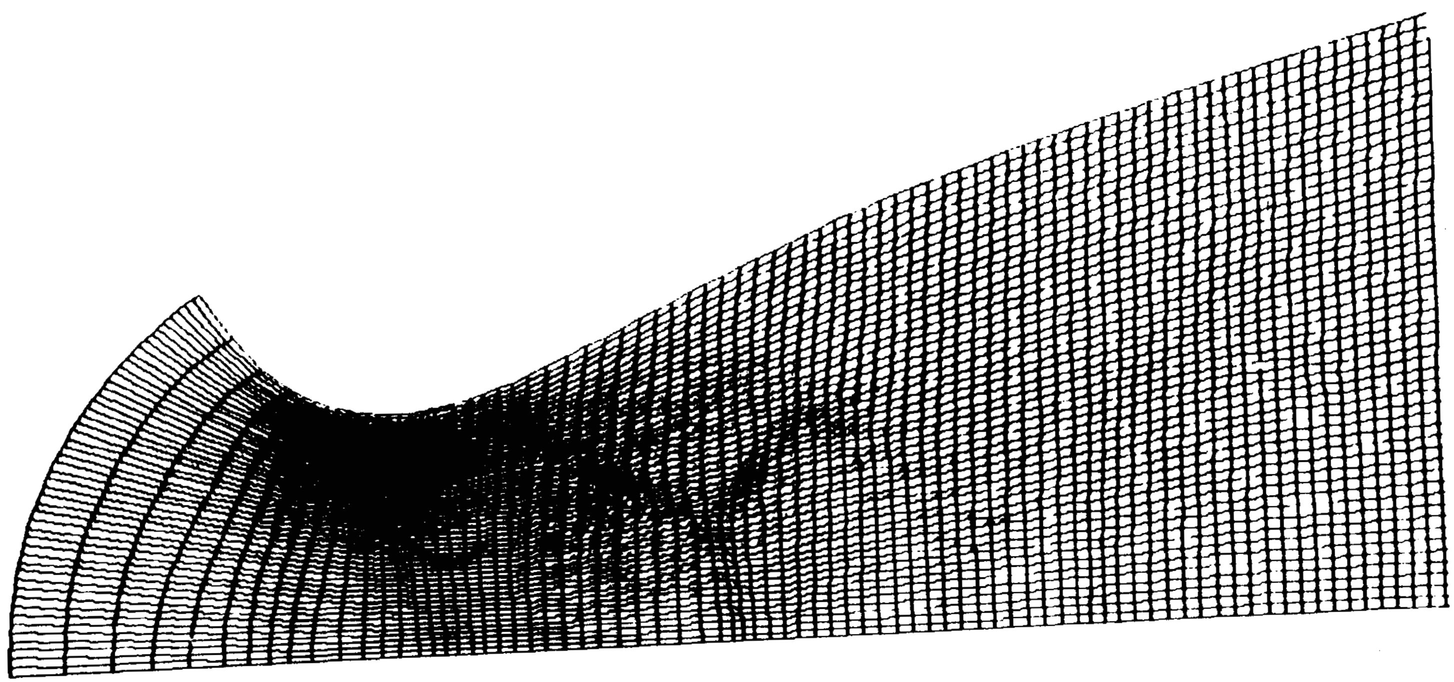

The Adaptive Grid at Time Step = 500 for Viscous Flow.

WEIGHT FUNCTION

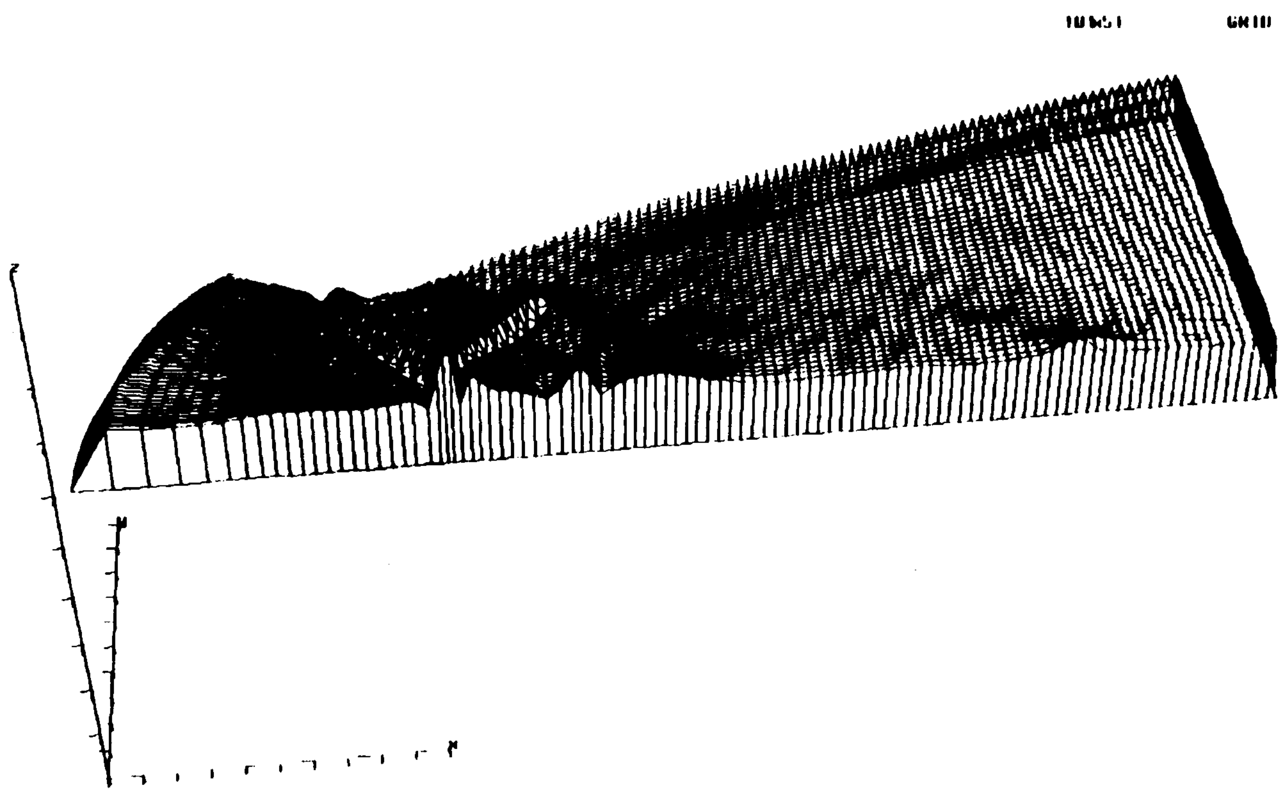

The Weight Function Distribution at Time Step = 1000 for Viscous Flow.

644

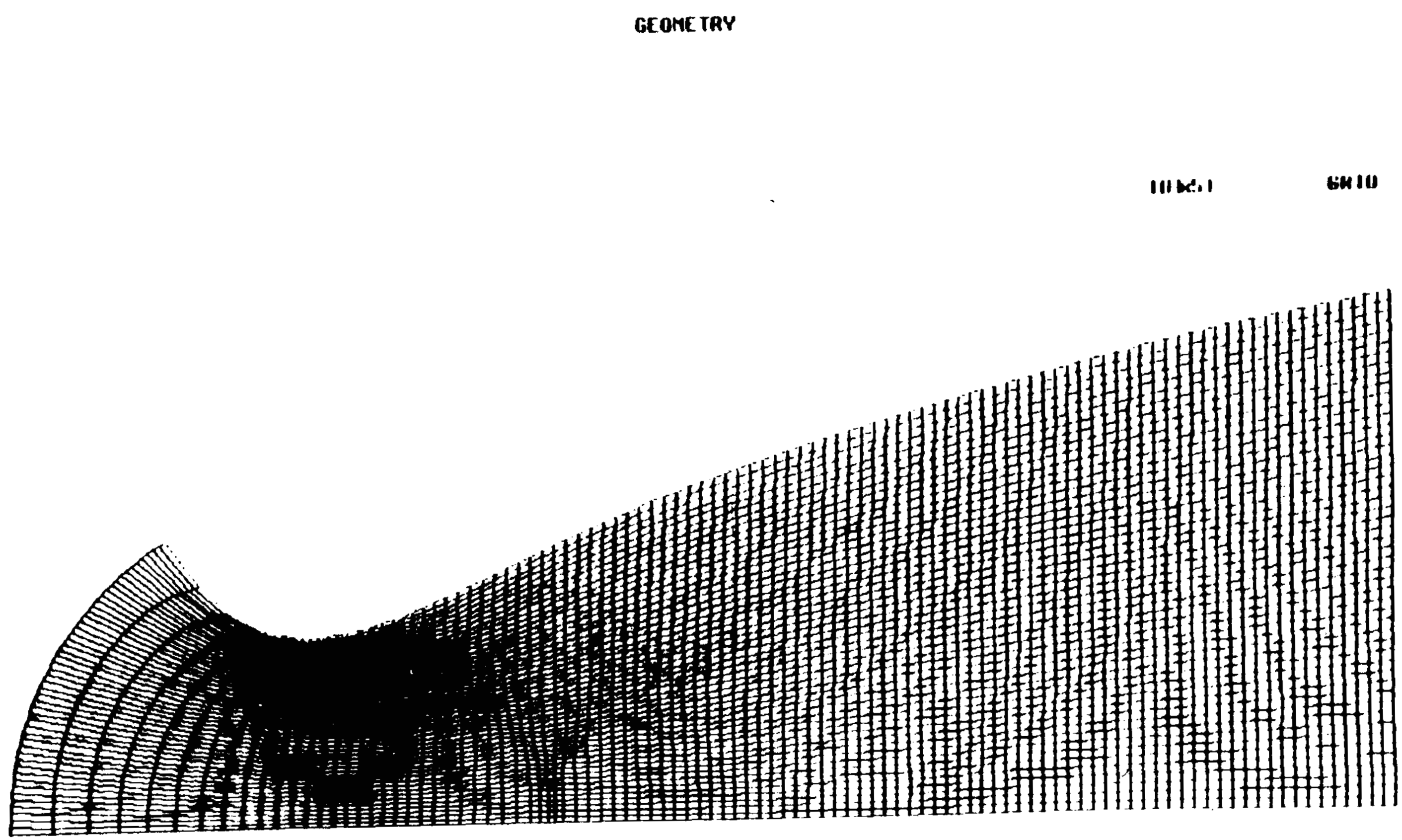

The Adaptive Grid at Time Step = 5500 for Viscous Flow.

CONCLUSIONS & RECOMMENDATIONS

- ✓ 2-D Solution-Adaptive Grid Generator has been completed and demostrated.
- ✓ It simplifies grid generation and makes better use of computer and human resources.
- ✓ Should be verified on various CFD codes to ensure robustness.
- ✓ Continue development in 3-D and Time-accurate Solution-Adaptive Grid Generator.

N92-32304

Abstract for the Tenth CFD Working Group Meeting:

Complex Three-Dimensional Internal Flows in the ASRM and RSRM Aft End Segments

Presented By: Dr. Edward J. Reske
Dr. Dana F. Billings
Ms. Joni W. Cornelison

Results from computational fluid dynamic analyses for complex three-dimensional internal flows in the Advanced Solid Rocket Motor (ASRM) and Redesigned Solid Rocket Motor (RSRM) are presented. In particular, a parametric study for the case of a gimballed nozzle in these motors at various burn times and gimbal angles is presented. The resultant pressure fields are used to determine the location of the center of pressure and hinge moments due to the interal flow for these geometries.

PRECEDING PAGE BLANK NOT FILMED

George C. Marshall Space Flight Center
Structures and Dynamics Laboratory
Computational Fluid Dynamics Branch

NASA

COMPLEX THREE-DIMENSIONAL FLOWS IN THE ASRM AND RSRM AFT END SEGMENTS

CFD BRANCH, ED32

Ed Reske

Dana Billings

Joni Cornelison

ASRM AFT END ANALYSIS

- Objective
  - Characterize flow environment in aft end of ASRM
- Purpose
  - Hinge moments due to internal flow for a gimballed nozzle
  - Nozzle performance
  - Heat transfer for insulation sizing
- Approach
  - Axisymmetric analyses
    - -- CMINT (48K and 24K grid points)
    - -- FDNS (14K grid points)
  - Three-dimensional gimballed nozzle analysis
    - -- FDNS3D (14K X 26 planes = 366K grid points)
- Results
  - Axisymmetric analysis complete
  - 3-D gimballed nozzle analyses nearing completion

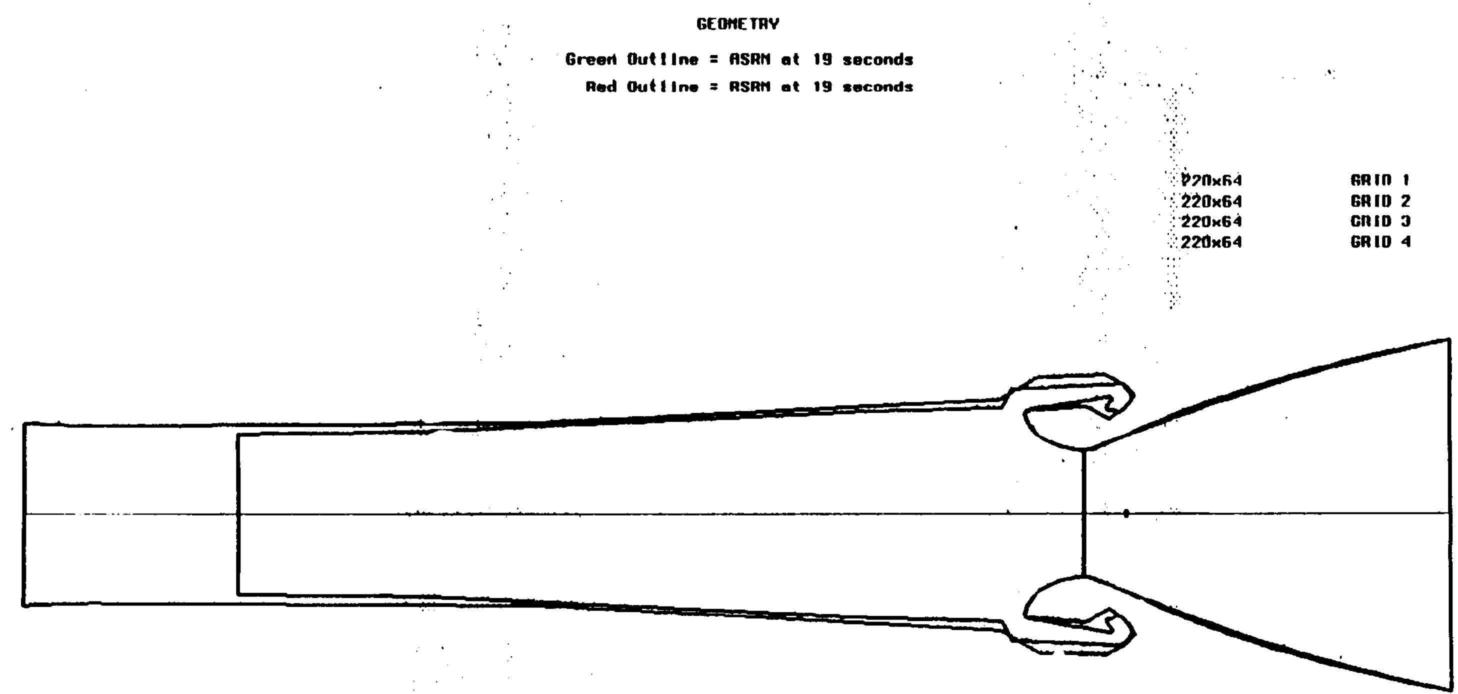
GEOMETRY
Green Outline = ASRM at 19 seconds
Red Outline = ASRM at 19 seconds
220x64 GRID 1
220x64 GRID 2
220x64 GRID 3
220x64 GRID 4

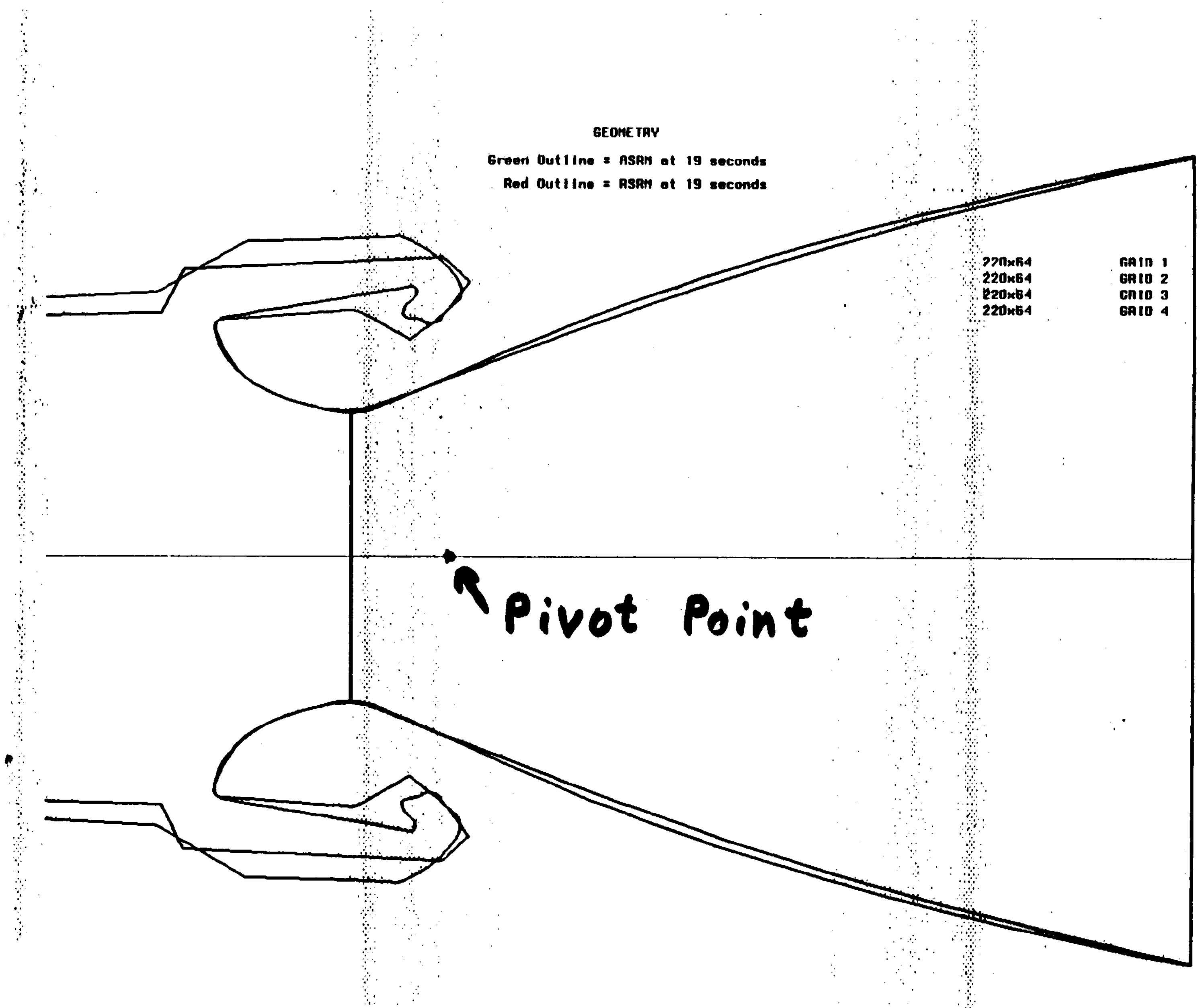

GEOMETRY
Green Outline = ASRM at 19 seconds
Red Outline = ASRM at 19 seconds
220x64 GRID 1
220x64 GRID 2
220x64 GRID 3
220x64 GRID 4
Pivot Point

GEOMETRY

ASRM two-dimensional, axisymmetric grid at 115 second burn time: 3/24/92

220x64 GRID

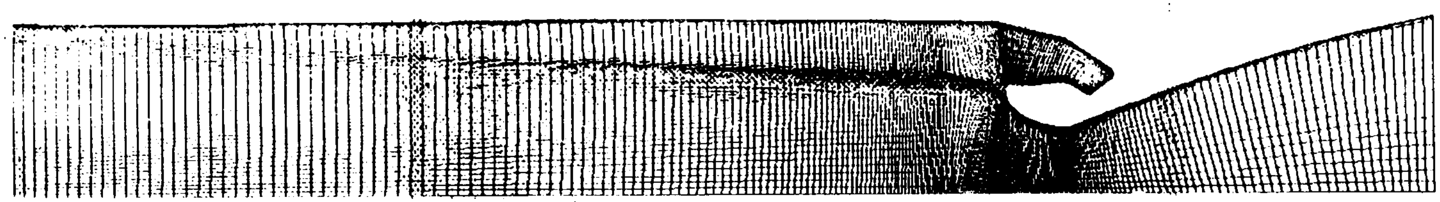

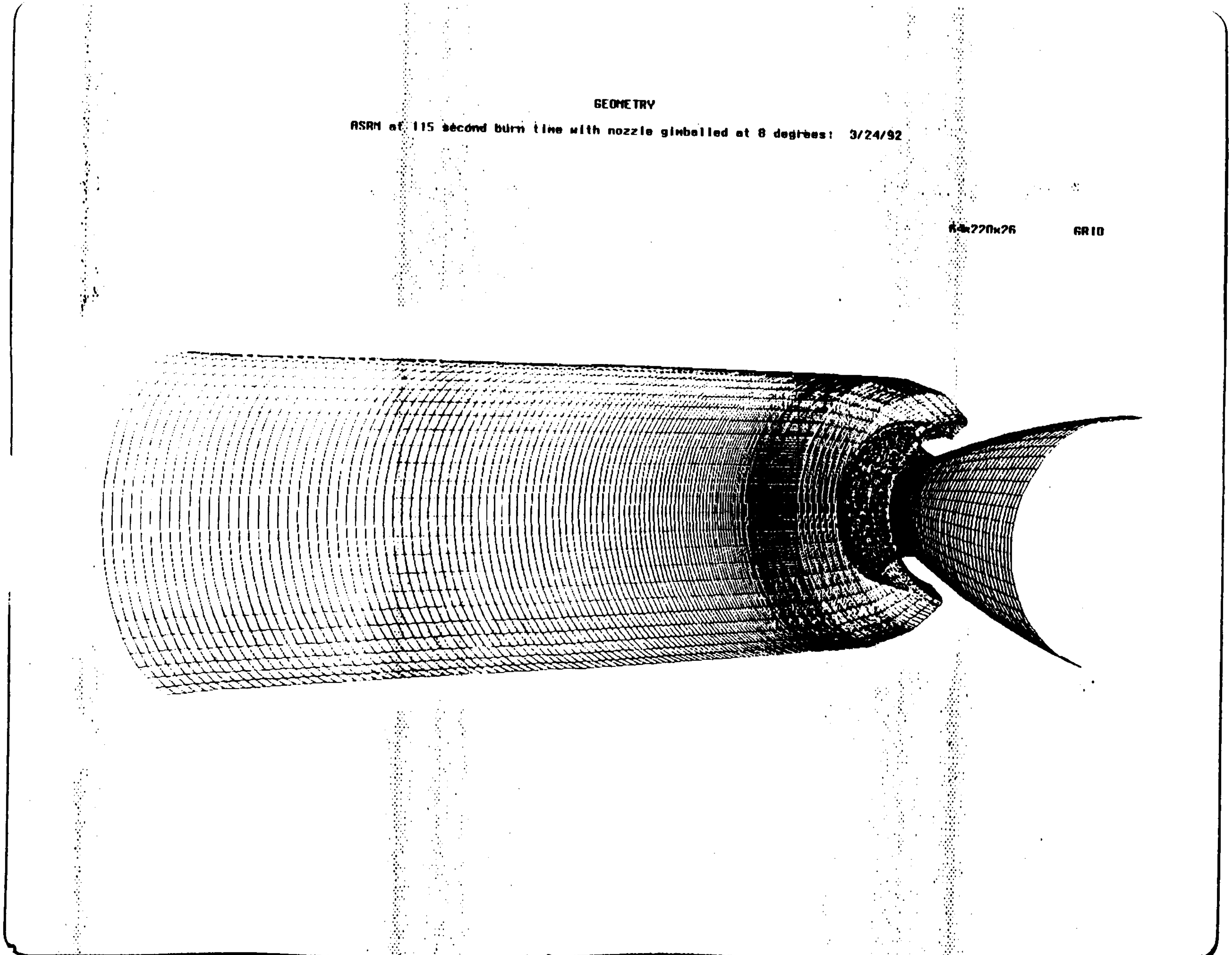
GEOMETRY
ASRM at 115 second burn time with nozzle gimballed at 8 degrees: 3/24/92
64x220x26
GRID

George C. Marshall Space Flight Center
Structures and Dynamics Laboratory
Computational Fluid Dynamics Branch

HINGE MOMENTS AND LOADS

MOTOR	BURN TIME sec.	GIMBAL ANGLE deg.	HINGE MOMENT in.-lb.	NORMAL LOAD lb.	AXIAL LOAD lb.	CENTER OF PRESSURE wrt pivot in.	CENTER OF PRESSURE wrt throat in.
ASRM	19	4	627 K	39.6 K	2.52 M	-15.9	+1.7
ASRM	19	8	1.28 M	80.8 K	2.51 M	-16.0	+1.6
RSRM	19	4	730 K	49.5 K	3.18 M	-14.7	+2.9
ASRM	115	4	150 K	6.9 K	1.25 M	-21.7	-4.1
ASRM	115	8	546 K	12.8 K	1.25 M	-42.6	-25.0
RSRM	114	4	165 K	14.7 K	0.96 M	-11.2	+6.4

Note: All the above hinge moments are non-restoring torques. The axial load acts along the axis of symmetry of the nozzle, and the normal load acts in the direction perpendicular to this axis, with both components acting in a direction away from the motor. The center of pressure is determined by finding a point on the nozzle axis of symmetry where the torque vanishes. A negative value indicates that it is upstream of the reference point, whereas a positive value indicates that it is downstream of the reference point.

PARTICLE TRACES

RSRM with nozzle gimballed at 4 degrees.

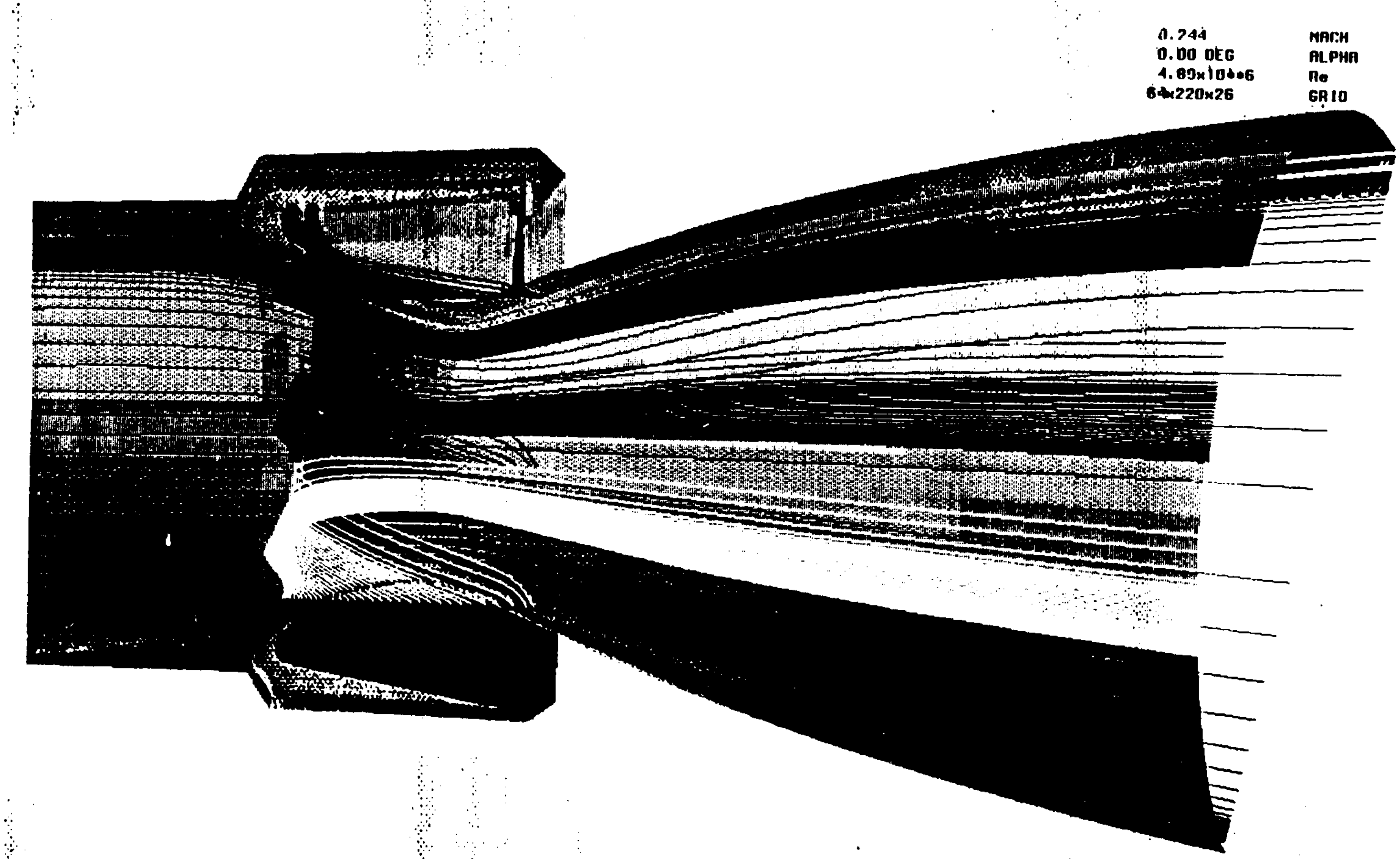

Space Administration

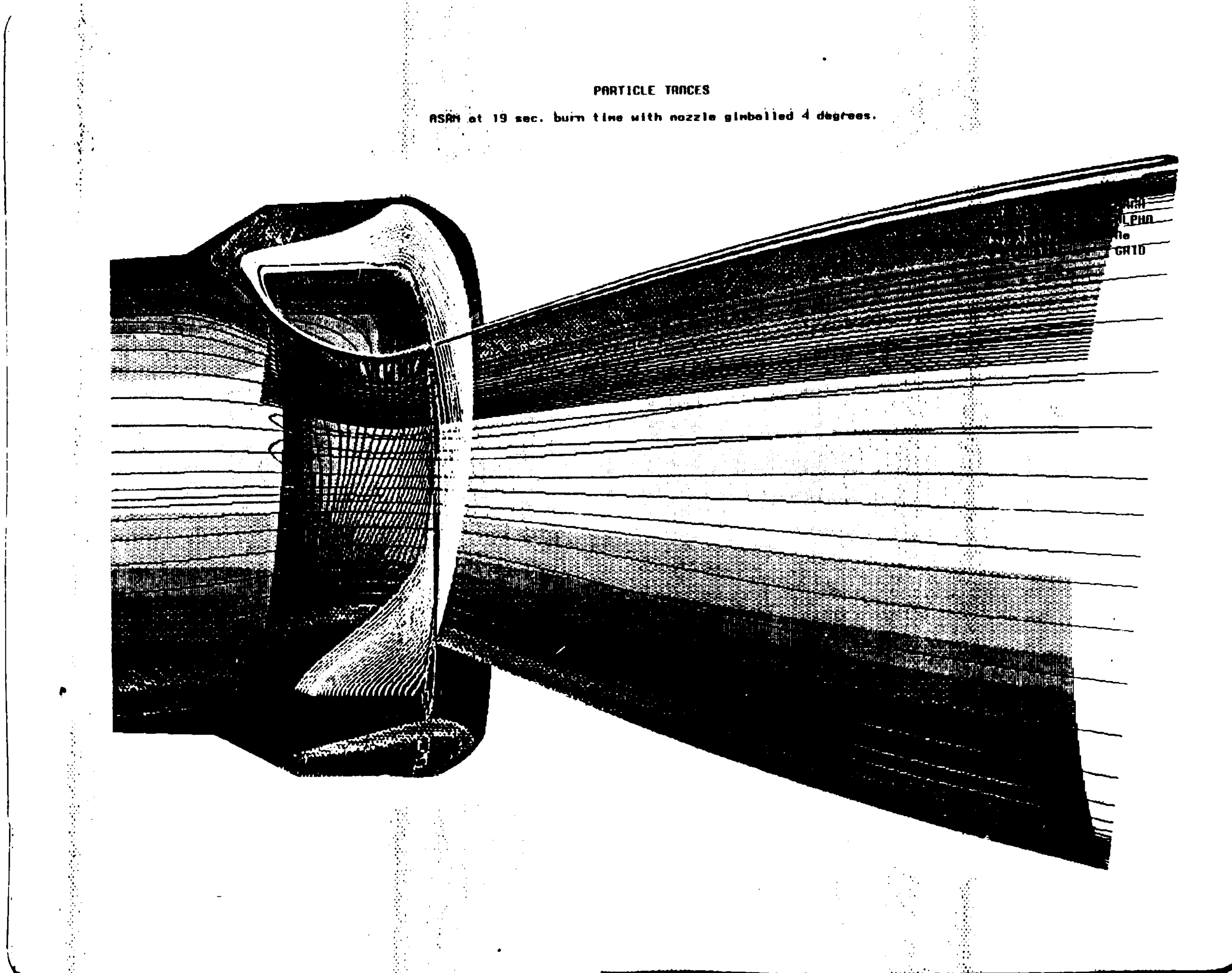

656

PARTICLE TRACES

ASRM with nozzle gimballed at 4 degrees.

0.244 MACH
0.00 DEG ALPHA
4.89x10**6 Re
64x220x26 GRID

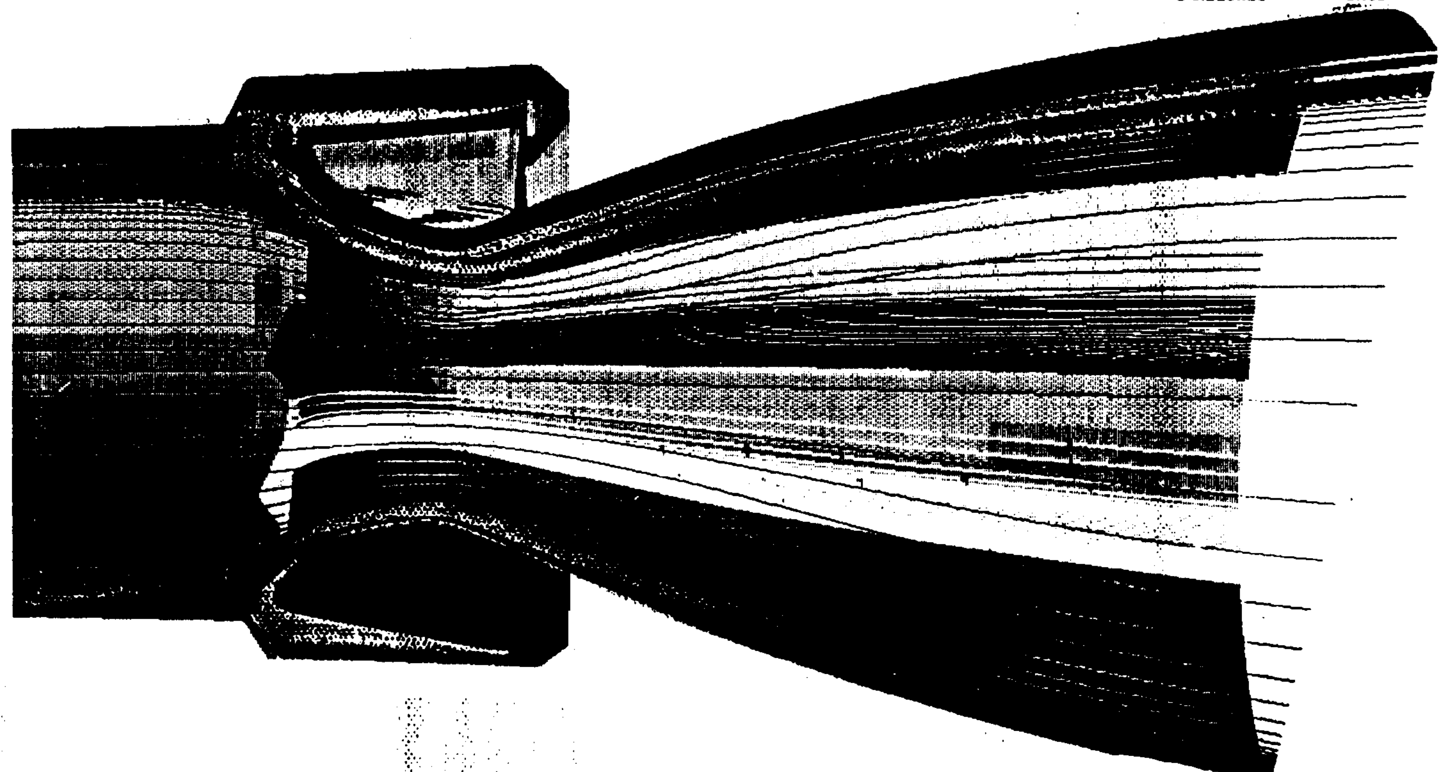

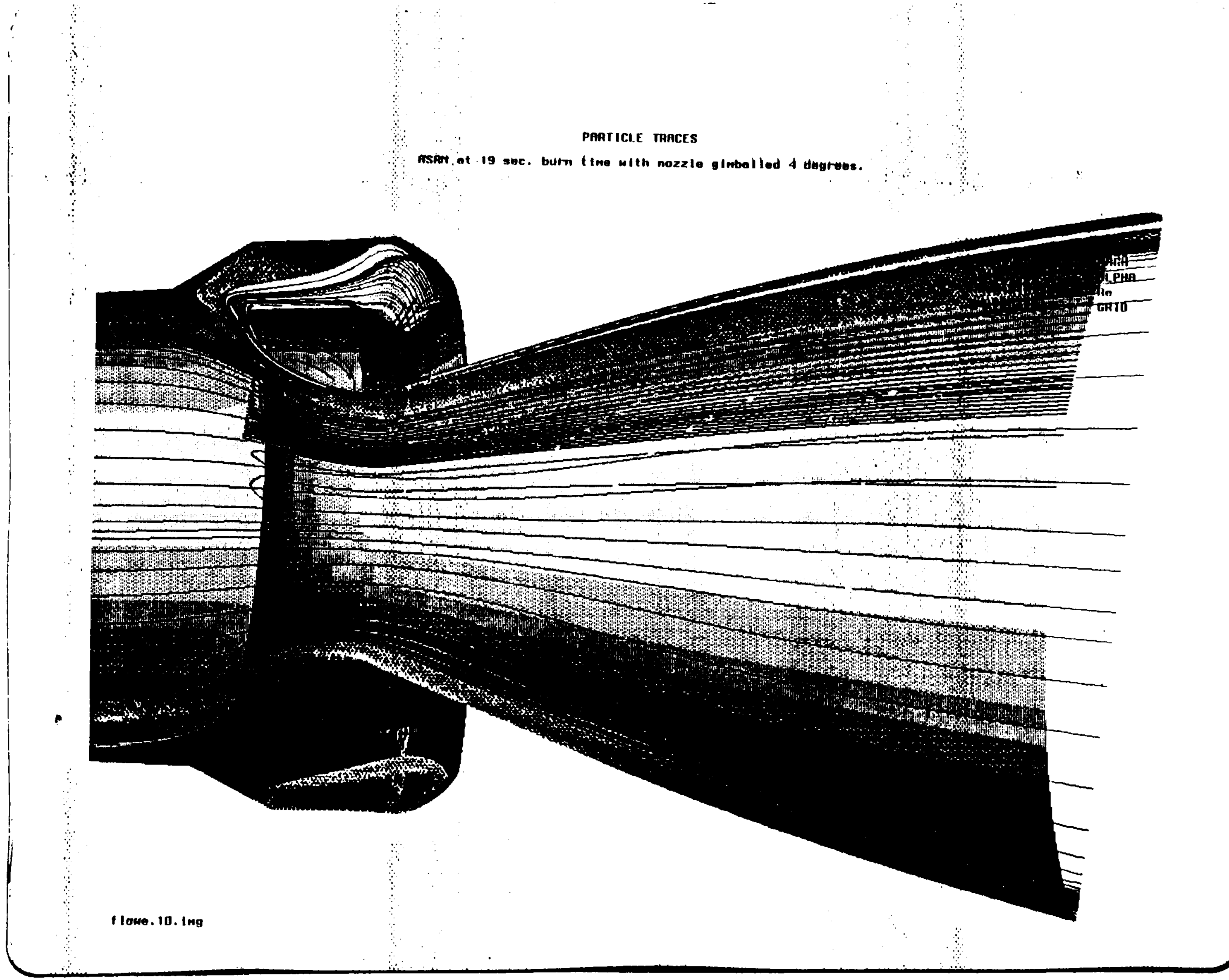
PARTICLE TRACES
ASRM at 19 sec. burn time with nozzle gimballed 4 degrees.
flowe.10.img

PARTICLE TRACES

ASRM with nozzle gimballed at 4 degrees.

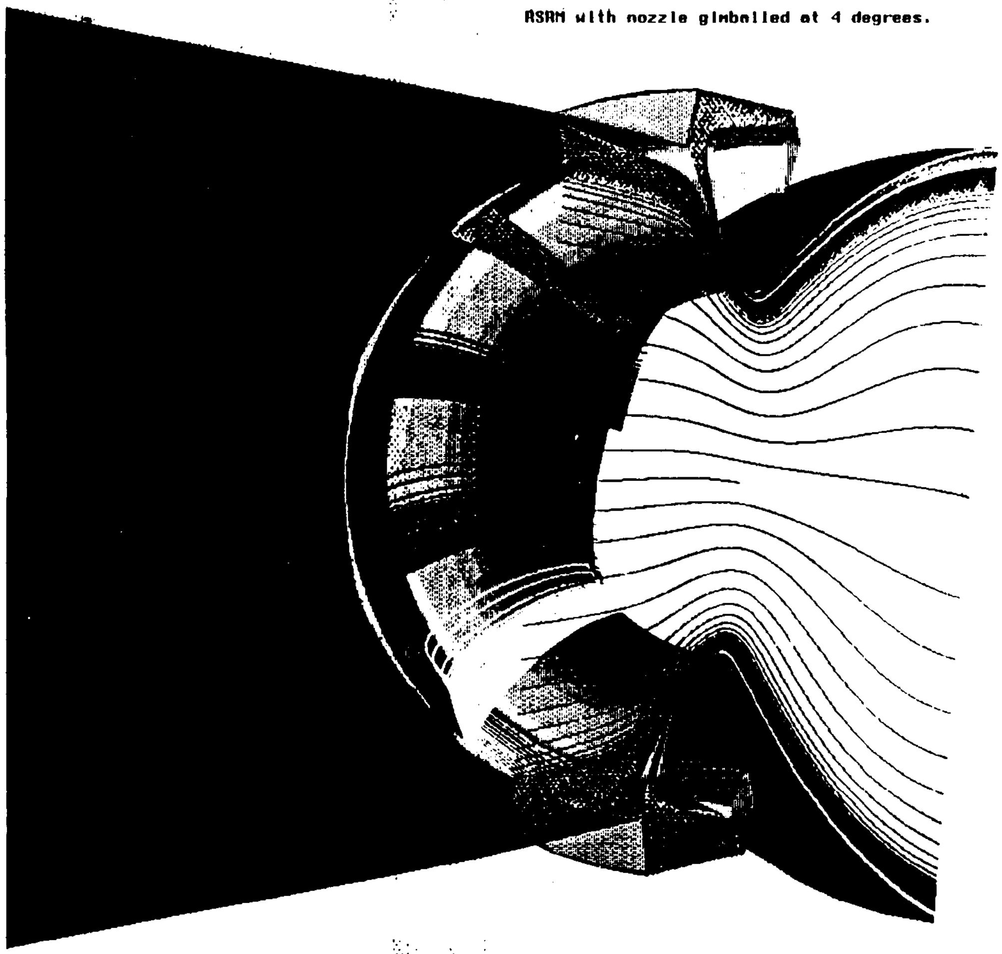

0.244	MACH
0.00 DEG	ALPHA
4.89x10**6	Re
64x220x26	GRID

flowd.16.img

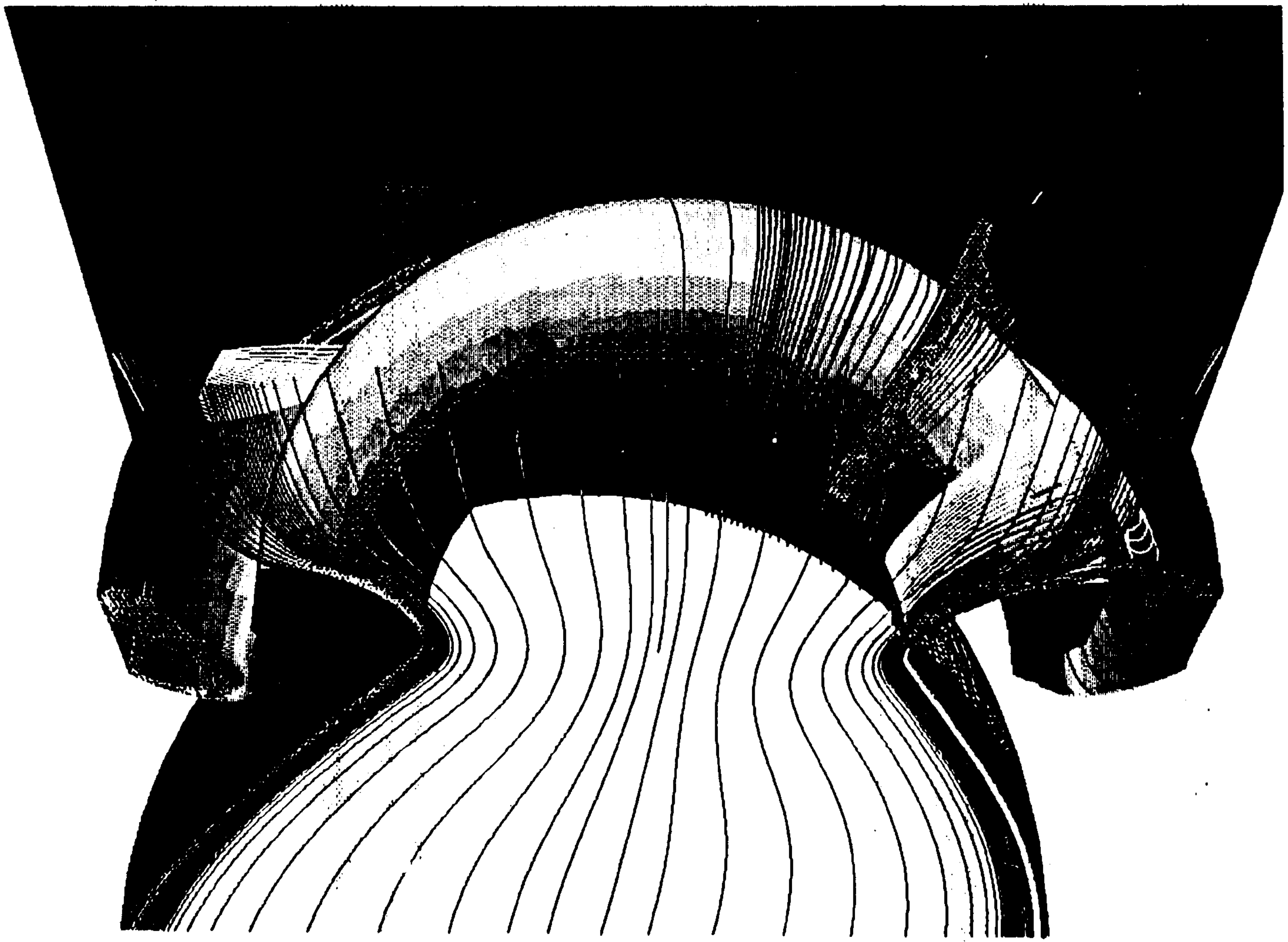
flowe.11.img

A simple model for calculating the hinge moment about a pivot point that is shifted relative to the nominal location:

$$T_z = T_{pz} + y F_N - x F_A$$

where, using a body-fixed coordinate system,

T_z = torque about the new pivot point;

T_{pz} = torque about the nominal pivot point;

y = axial displacement of the new pivot point;

x = normal displacement of the new pivot point;

F_N = normal load;

F_A = axial load.

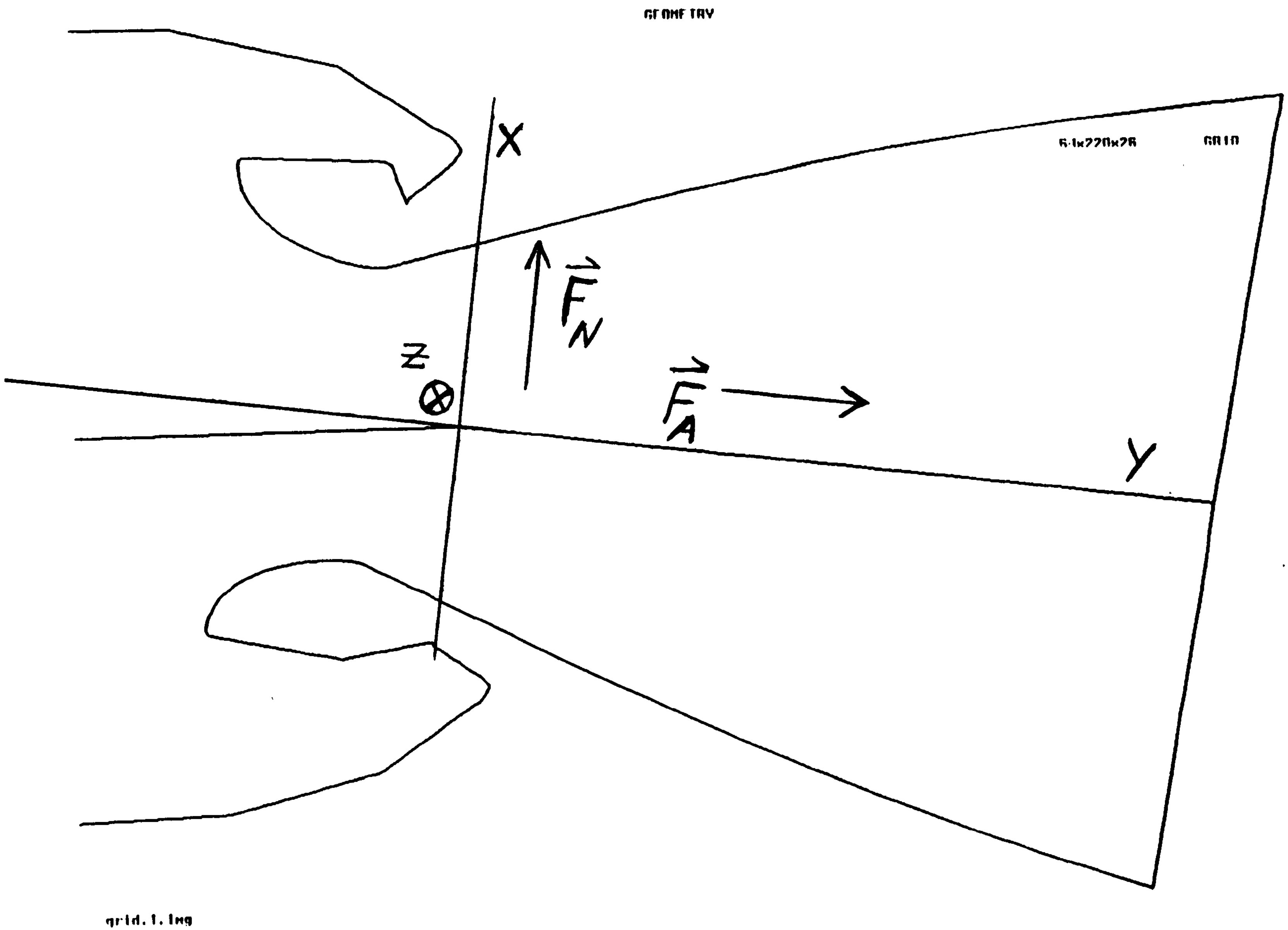
GEOMETRY
64x220x26
GRID
X
$\vec{F}_N$
Z
$\vec{F}_A$
Y
grid.1.img

N92-32305

An Analysis of the Flow Field in the Region of the ASRM Field Joints

Richard A. Dill, ERC Incorporated
Harold R. Whitesides, ERC Incorporated

Abstract

The flow field in the region of a solid rocket motor field joint is very important since fluid dynamic and mechanical propellant stresses can couple to cause a motor failure at a joint. This paper presents an examination of the flow field in the region of the ASRM field joints. The analyses were performed as a first step in assessing the design of the ASRM forward and aft field joints in order to assure the proper operation of the motor prior to further development or test firing.

The analyses discussed are a first step in the process of a full analysis of the ASRM field joints. The first step involves the analysis of both the forward and aft motor field joints at the 0 and 19 second motor burn back times. The zero second burn back time has the potential for causing the greatest possible fluid dynamic induced stresses at the joints. This is because the port flow Mach number and dynamic pressure decrease as the motor burns, thus reducing the stresses at the joints. Initial analyses have also been performed on the inhibitor stub left protruding into the port flow field at the field joint caused by propellant burn back at the 19 second burn back time. The analyses discussed are for non-deformed propellant grains. Analyses of the field joints deformed from cure shrinkage, thermal cool down and gravity loading will be included at a later time. Also a coupled fluid dynamic/mechanical stress analysis will be performed in conjunction with NASA/MSFC mechanical stress analysts in order to assess any adverse dynamic mechanical effects of the flow field on the propellant grain shape.

The analyses presented in this paper have been performed by employing a two-dimensional axi-symmetric assumption. Fluent/BFC, a three dimensional full Navier-Stokes flow field code, has been used to make the numerical calculations. This code utilizes a staggered grid formulation along with the SIMPLER numerical algorithm. Wall functions are used to determine the character of the laminar sub-layer flow and a standard $\kappa-\varepsilon$ turbulence model is used to close the fluid dynamic equations.

The analyses performed to this date verify that the ASRM field joint design operates properly. The fluid dynamic stresses at the field joints are small due to the inherent design of the field joints. A problem observed in some other solid rocket motors is that large fluid dynamic stresses are generated at the motor joint on the downstream propellant grain due to forward facing step geometries. The design of the ASRM field joints are such that this is not a problem as shown by the analyses. Also, the analyses of the inhibitor stub left protruding into the port flow from normal propellant burn back show that more information is necessary to complete these analyses. These analyses were performed as parametric analyses in relation to the height of the inhibitor stub left protruding into the motor port. A better estimate of the amount of the inhibitor stub remaining at later burn times must be determined since the height which the inhibitor stub protrudes into the port flow drastically affects the fluid dynamic induced stresses on the propellant grain at the field joints.

AN ANALYSIS OF THE FLOW FIELD IN THE REGION OF THE ASRM FIELD JOINTS

Richard A. Dill and R. Harold Whitesides
ERC, Inc.

Tenth Annual CFD Working Group Meeting

Session 7

NASA/MSFC

April 29, 1992

OBJECTIVES

1) DETERMINE SLOT/PORT FLOW INTERACTIONS FOR ASRM FWD AND AFT FIELD JOINT DESIGNS

2) PERFORM PRELIMINARY CFD ANALYSES OF INITIAL GRAIN CONFIGURATIONS AT THE FORWARD AND AFT FIELD JOINTS TO DETERMINE PROPELLANT GRAIN PRESSURE LOADS AND IDENTIFY POTENTIAL EARLY DESIGN PROBLEMS

ERC, Inc. 4/29/92

CFD METHODOLOGY

- GOVERNING EQUATIONS ARE THE 3-D ENSEMBLE-AVERAGED NAVIER STOKES EQUATIONS IN CONSERVATION FORM
- CLOSURE OF THE EQUATIONS BY THE STANDARD TWO-EQUATION $\kappa-\varepsilon$ MODEL OF TURBULENCE
- WALL FUNCTIONS USED TO DETERMINE NEAR WALL GRADIENTS
- DISCRETIZATION METHOD
    - GOVERNING EQUATIONS ARE WRITTEN IN COMPONENT FORM USING CONTRAVARIANT VELOCITY COMPONENTS
    - THIS ALLOWS THE USE OF A BOUNDARY FITTED CURVILINEAR COORDINATE SYSTEM
    - NUMERICAL METHOD IS FINITE VOLUME BASED
    - STAGGERED GRID STORAGE SYSTEM IS USED
    - CONVECTION AND DIFFUSION FLUXES ARE APPROXIMATED USING A POWER-LAW SCHEME
    - TIME DERIVATIVES ARE CALCULATED USING A FULLY IMPLICIT FIRST ORDER SCHEME
- PRESSURE-VELOCITY COUPLING IS ACCOMPLISHED BY USING THE SIMPLER ALGORITHM
- SOLVER USES LINEARIZED BLOCK IMPLICIT SCHEME

ERC, Inc. 4/29/92

THE ASRM

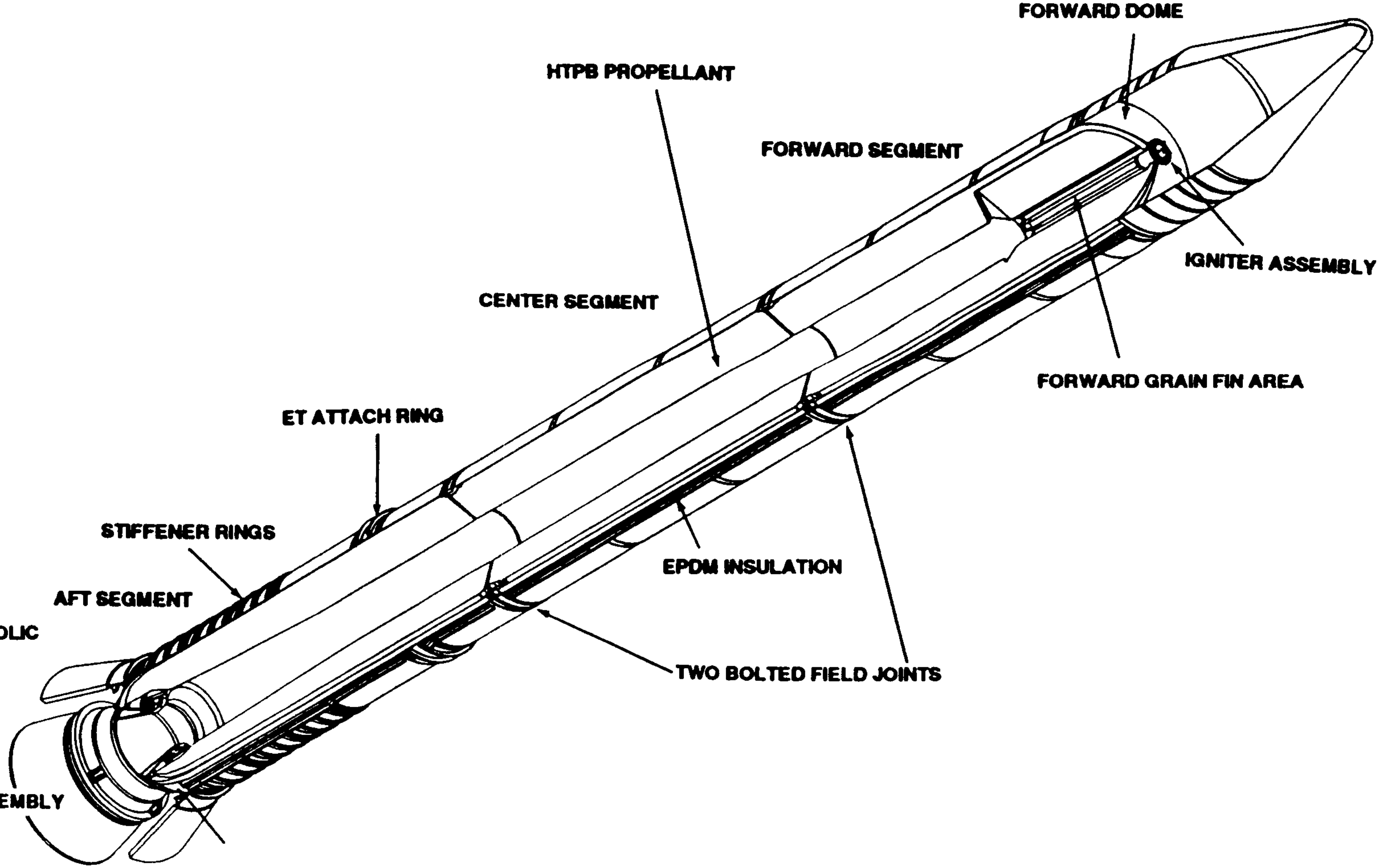
FORWARD DOME
HTPB PROPELLANT
FORWARD SEGMENT
IGNITER ASSEMBLY
CENTER SEGMENT
FORWARD GRAIN FIN AREA
ET ATTACH RING
STIFFENER RINGS
EPDM INSULATION
AFT SEGMENT
• CARBON PHENOLIC EXIT CONE
• D6AC HOUSING
TWO BOLTED FIELD JOINTS
NOZZLE ASSEMBLY

OVERVIEW OF THE GENERAL SLOT GEOMETRY

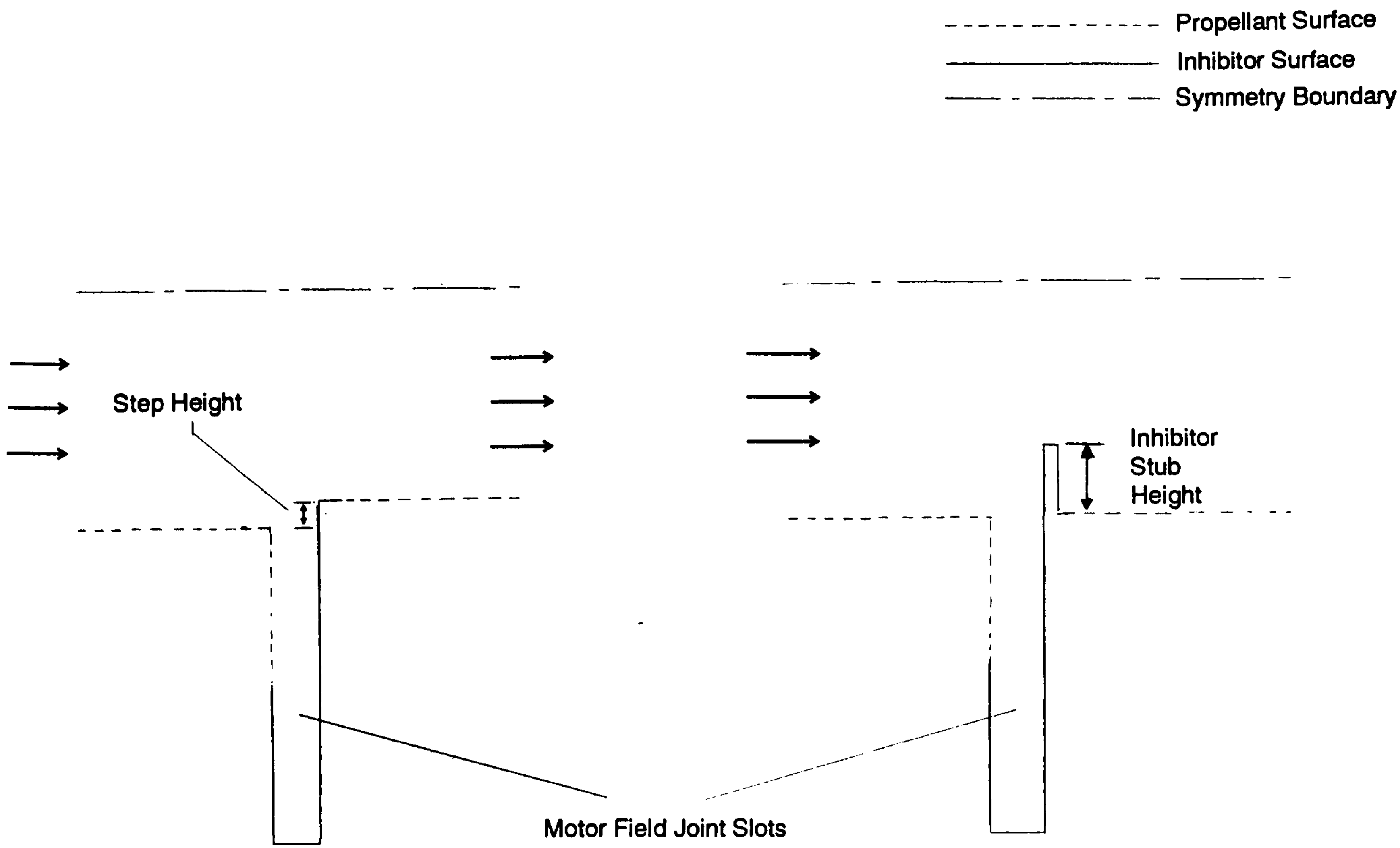

ASRM FIELD JOINT CONFIGURATIONS ANALYZED

- 0 SECOND BURN TIME MOTOR CONFIGURATION
  - FORWARD SLOT
  - AFT SLOT
- 19 SECOND BURN TIME MOTOR CONFIGURATION
  - FORWARD SLOT
    INHIBITOR STUB HEIGHT, 3.9 INCHES
    INHIBITOR STUB HEIGHT, 0 INCHES
  - AFT SLOT
    INHIBITOR STUB HEIGHT, 3.9 INCHES
    INHIBITOR STUB HEIGHT, 0 INCHES

ERC, Inc. 4/29/92

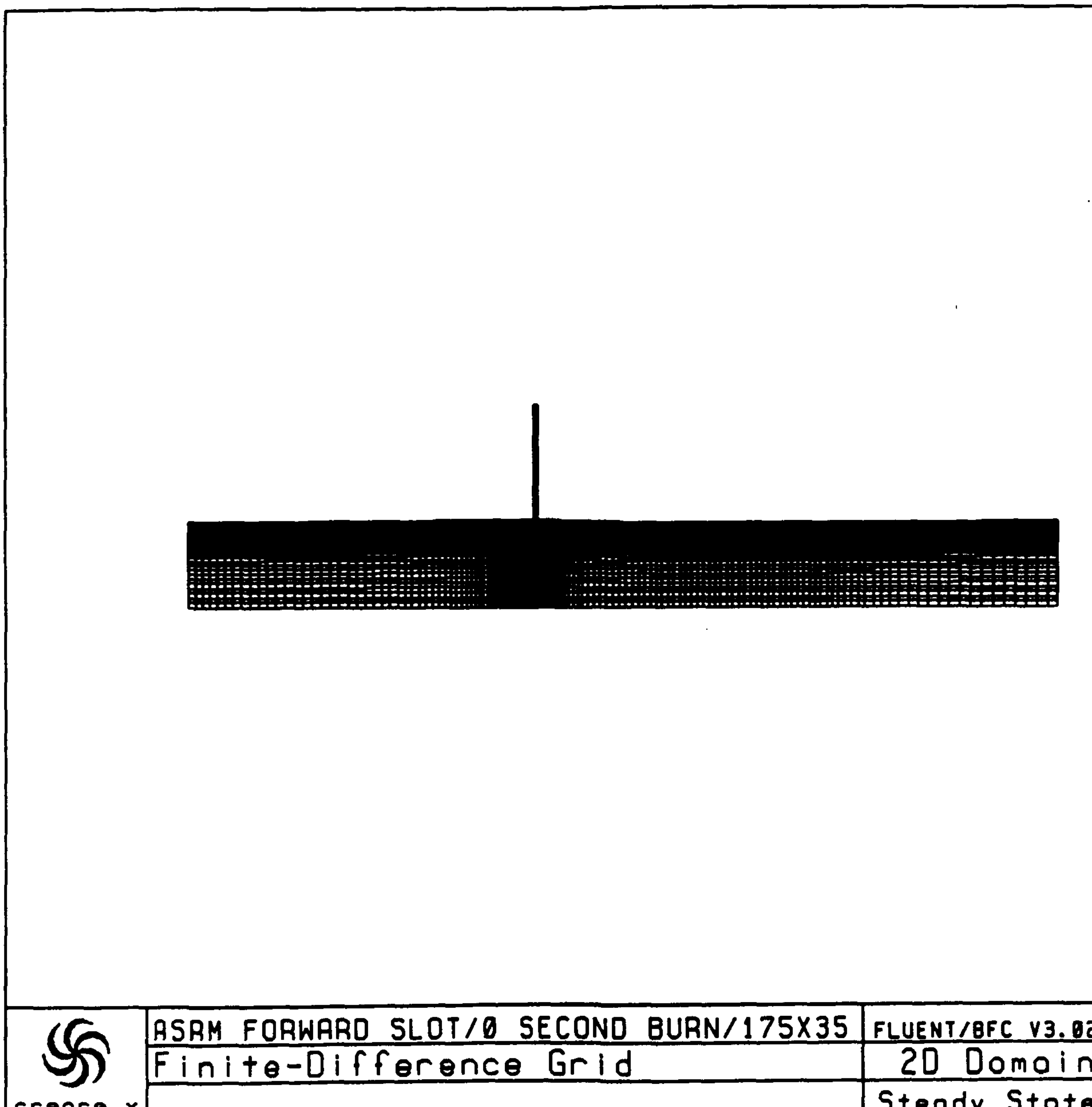
ASRM FORWARD SLOT/0 SECOND BURN/175X35
FLUENT/BFC V3.02
Finite-Difference Grid
2D Domain
creare.x
Steady State

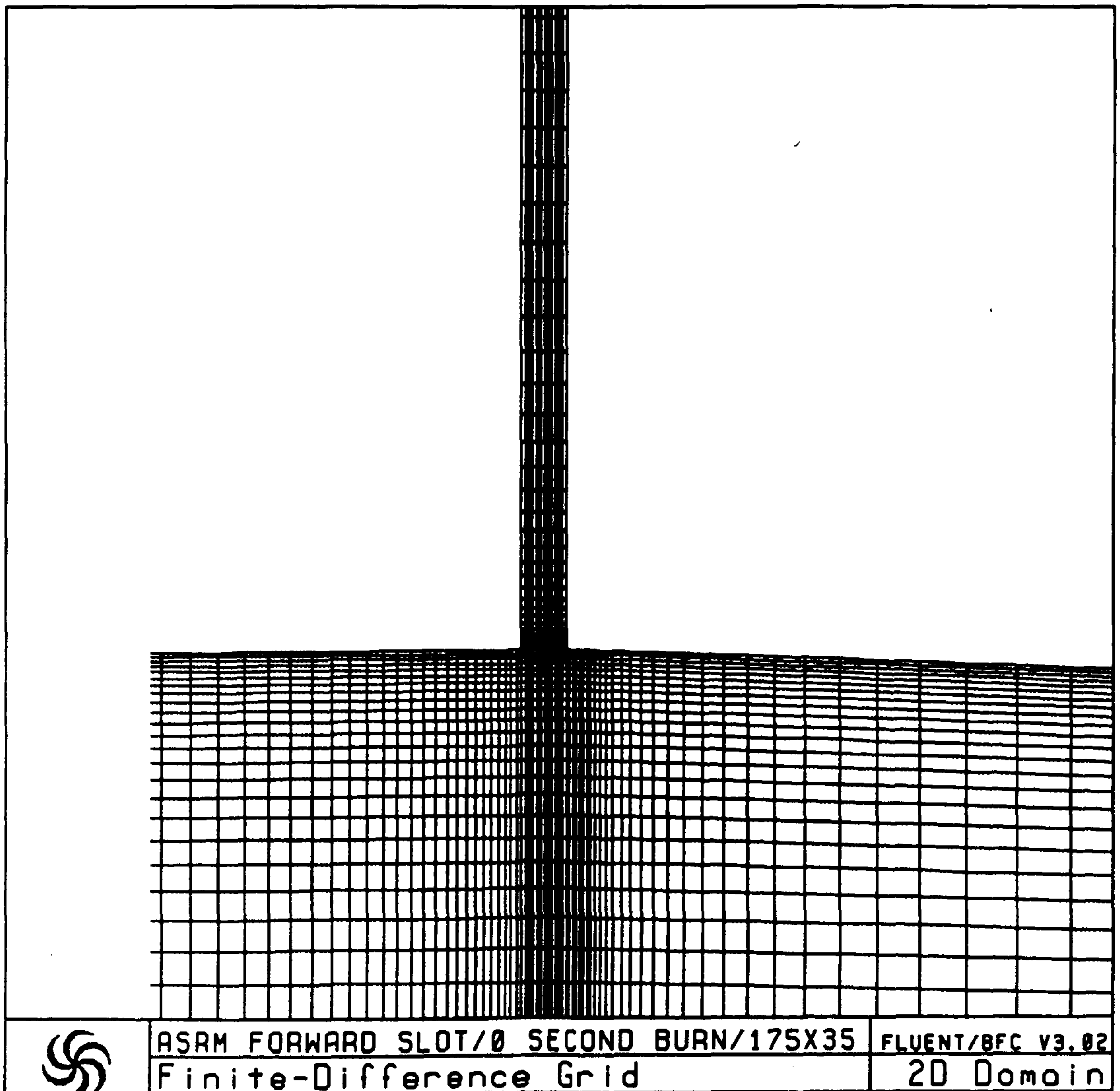

ASRM FORWARD SLOT/0 SECOND BURN/175X35
FLUENT/BFC V3.02
Finite-Difference Grid
2D Domain
Steady State
creare.x

ASRM MOTOR FIELD JOINT BOUNDARY CONDITIONS
0 SECOND BURN TIME CONFIGURATION

AFT SLOT

INLET STATIC PRESSURE	:	821.9 psia
AVERAGE PORT VELOCITY	:	177.5 ft/s
STAGNATION TEMPERATURE AT THE INLET	:	6345 °R
RATIO OF SPECIFIC HEATS	:	1.128
PROPELLANT INJECTION VELOCITY	:	13.467 ft/s
MOLECULAR WEIGHT	:	29.489
MASS FLOW RATE (INLET)	:	8682 lbm/s
CFD CALCULATED MASS FLOW RATE (INLET)	:	8562 lbm/s

FORWARD SLOT

INLET STATIC PRESSURE	:	855.9 psia
AVERAGE PORT VELOCITY	:	877.5 ft/s
STAGNATION TEMPERATURE AT THE INLET	:	6345 °R
RATIO OF SPECIFIC HEATS	:	1.128
PROPELLANT INJECTION VELOCITY	:	9.9837 ft/s
MOLECULAR WEIGHT	:	29.489
MASS FLOW RATE (INLET)	:	6178 lbm/s
CFD CALCULATED MASS FLOW RATE (INLET)	:	6103 .bm/s

ERC, Inc. 4/29/92

ASRM Fwd Slot Undeformed Grain Port Pressures On the Surface and at the Motor Centerline

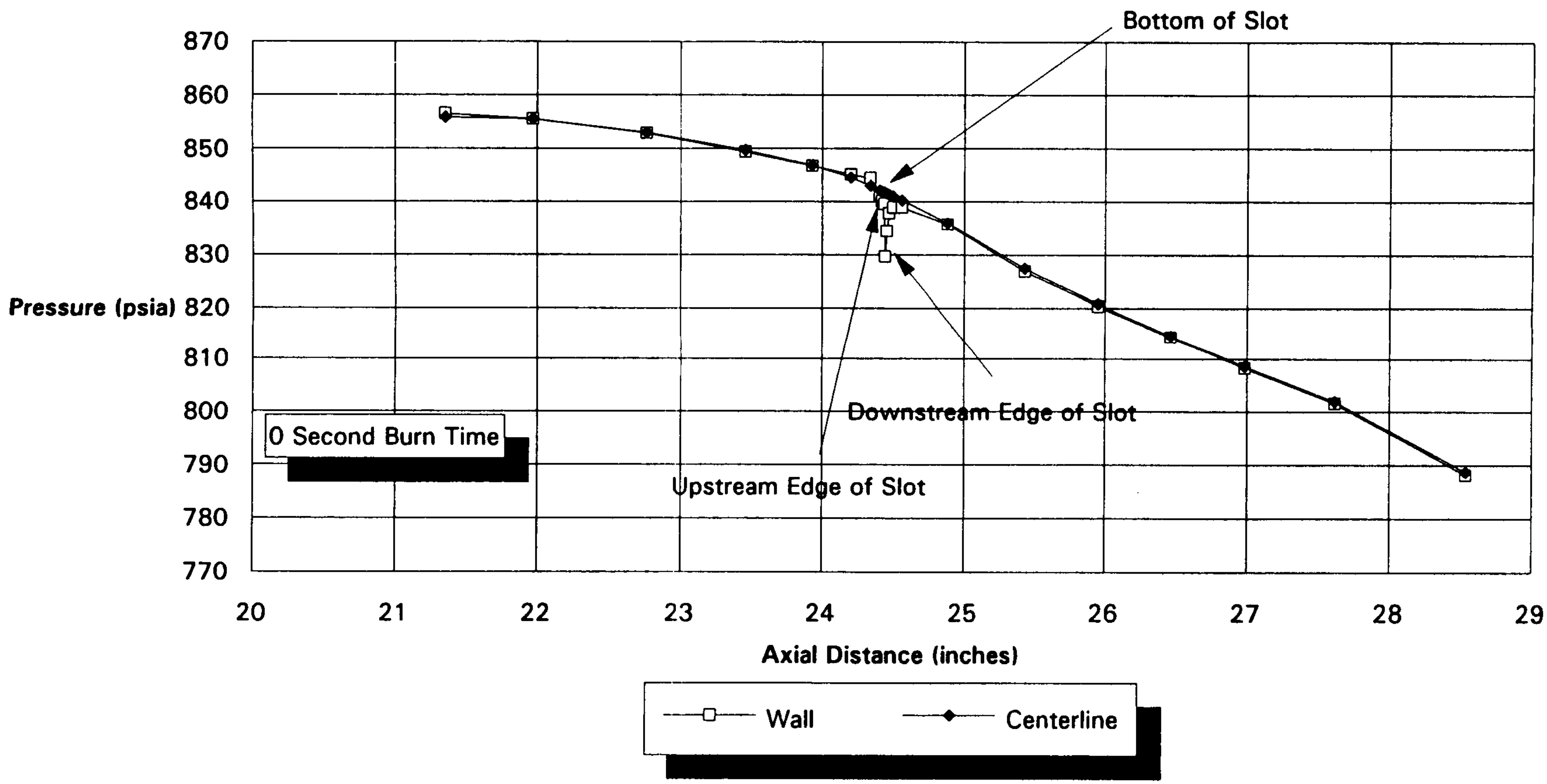

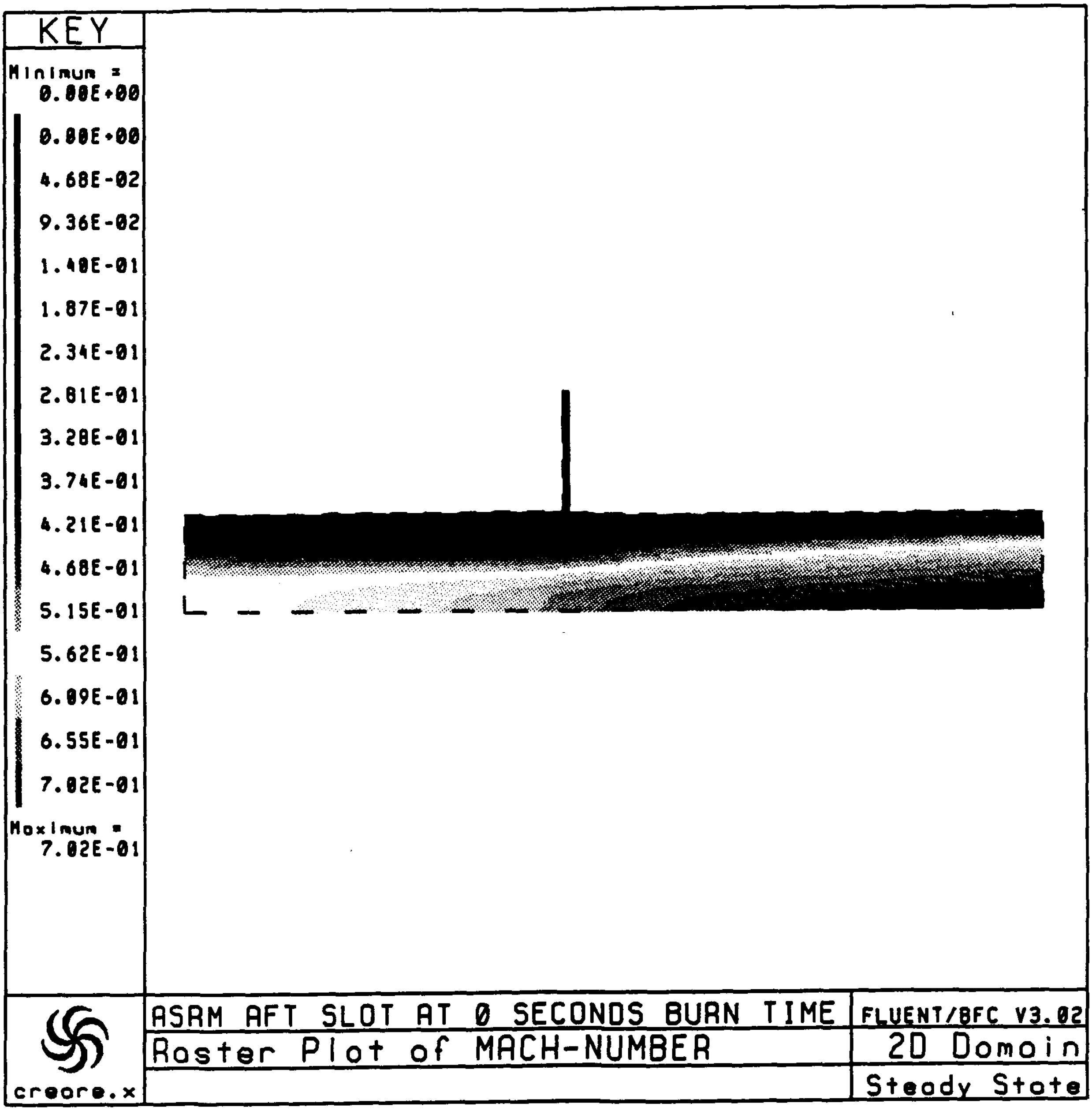
KEY
Minimum =
0.00E+00
0.00E+00
4.68E-02
9.36E-02
1.40E-01
1.87E-01
2.34E-01
2.81E-01
3.28E-01
3.74E-01
4.21E-01
4.68E-01
5.15E-01
5.62E-01
6.09E-01
6.55E-01
7.02E-01
Maximum =
7.02E-01
creare.x
ASRM AFT SLOT AT 0 SECONDS BURN TIME
Raster Plot of MACH-NUMBER
FLUENT/BFC V3.02
2D Domain
Steady State

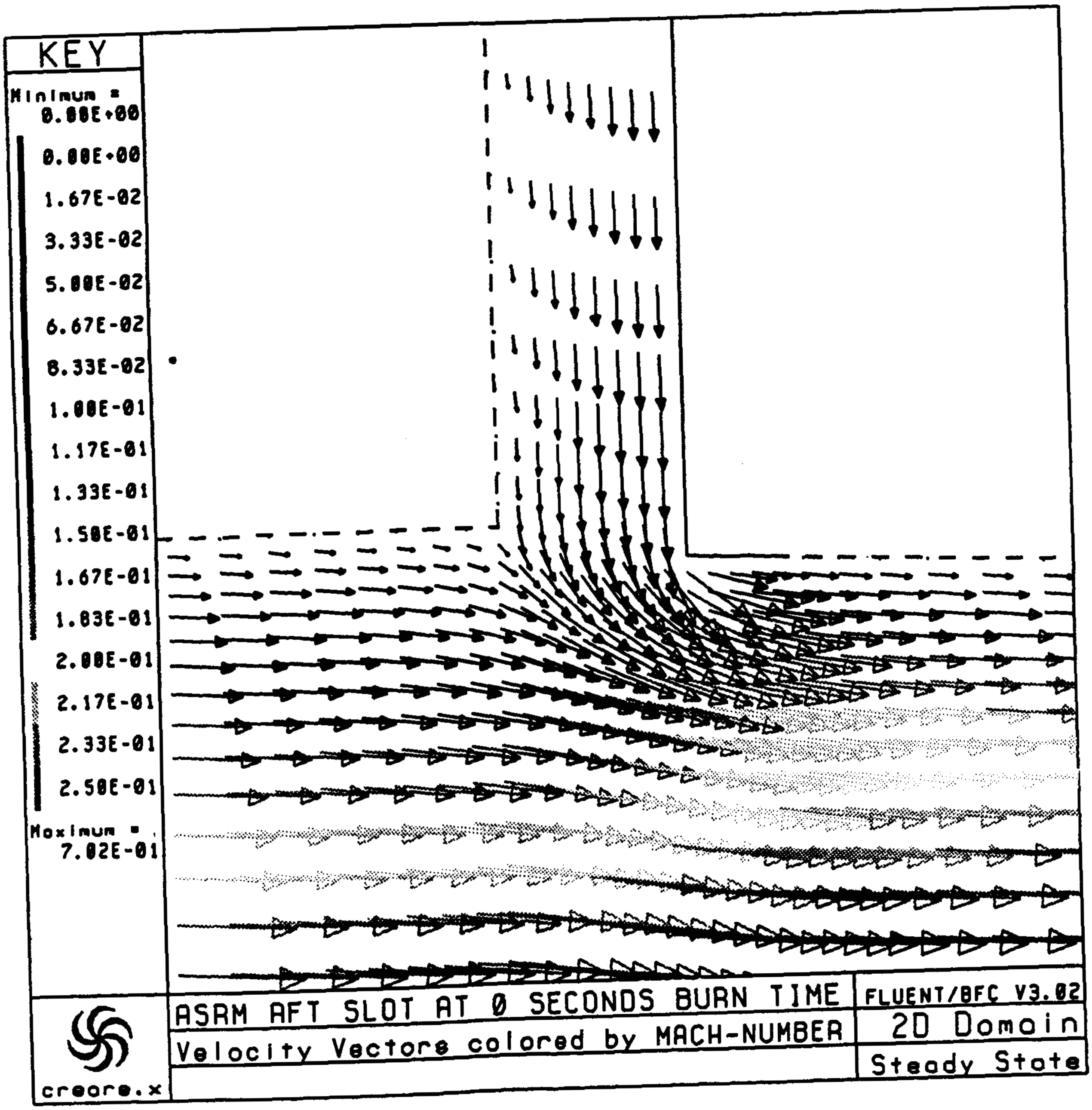

KEY
Minimum =
0.00E+00
0.00E+00
1.67E-02
3.33E-02
5.00E-02
6.67E-02
8.33E-02
1.00E-01
1.17E-01
1.33E-01
1.50E-01
1.67E-01
1.83E-01
2.00E-01
2.17E-01
2.33E-01
2.50E-01
Maximum =
7.02E-01
creare.x
ASRM AFT SLOT AT 0 SECONDS BURN TIME
Velocity Vectors colored by MACH-NUMBER
FLUENT/BFC V3.02
2D Domain
Steady State

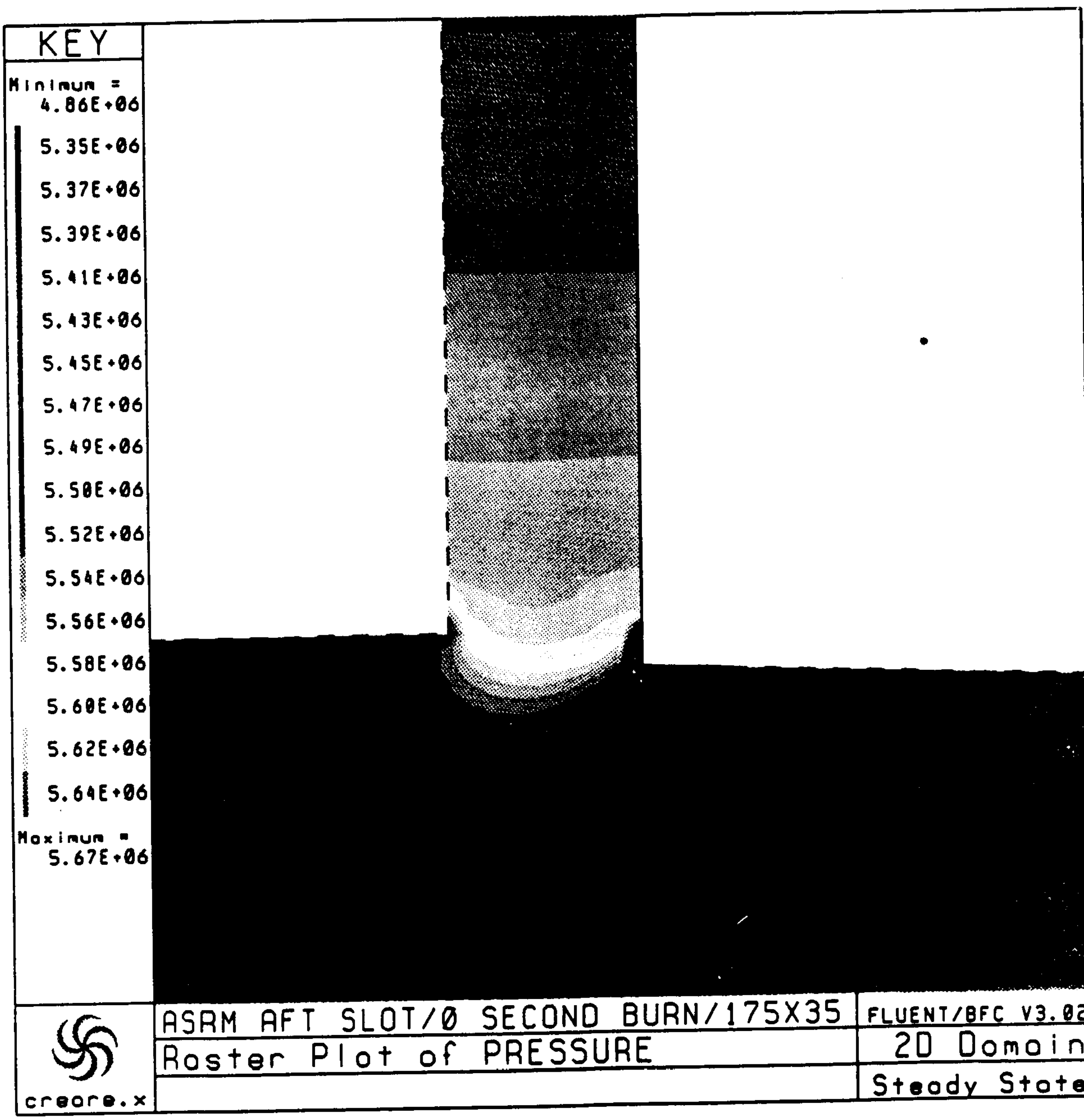
KEY
Minimum =
4.86E+06
5.35E+06
5.37E+06
5.39E+06
5.41E+06
5.43E+06
5.45E+06
5.47E+06
5.49E+06
5.50E+06
5.52E+06
5.54E+06
5.56E+06
5.58E+06
5.60E+06
5.62E+06
5.64E+06
Maximum =
5.67E+06
creare.x
ASRM AFT SLOT/0 SECOND BURN/175X35
Raster Plot of PRESSURE
FLUENT/BFC V3.02
2D Domain
Steady State

ASRM Aft Slot Undeformed Grain Port Pressures On the Surface and at the Motor Centerline

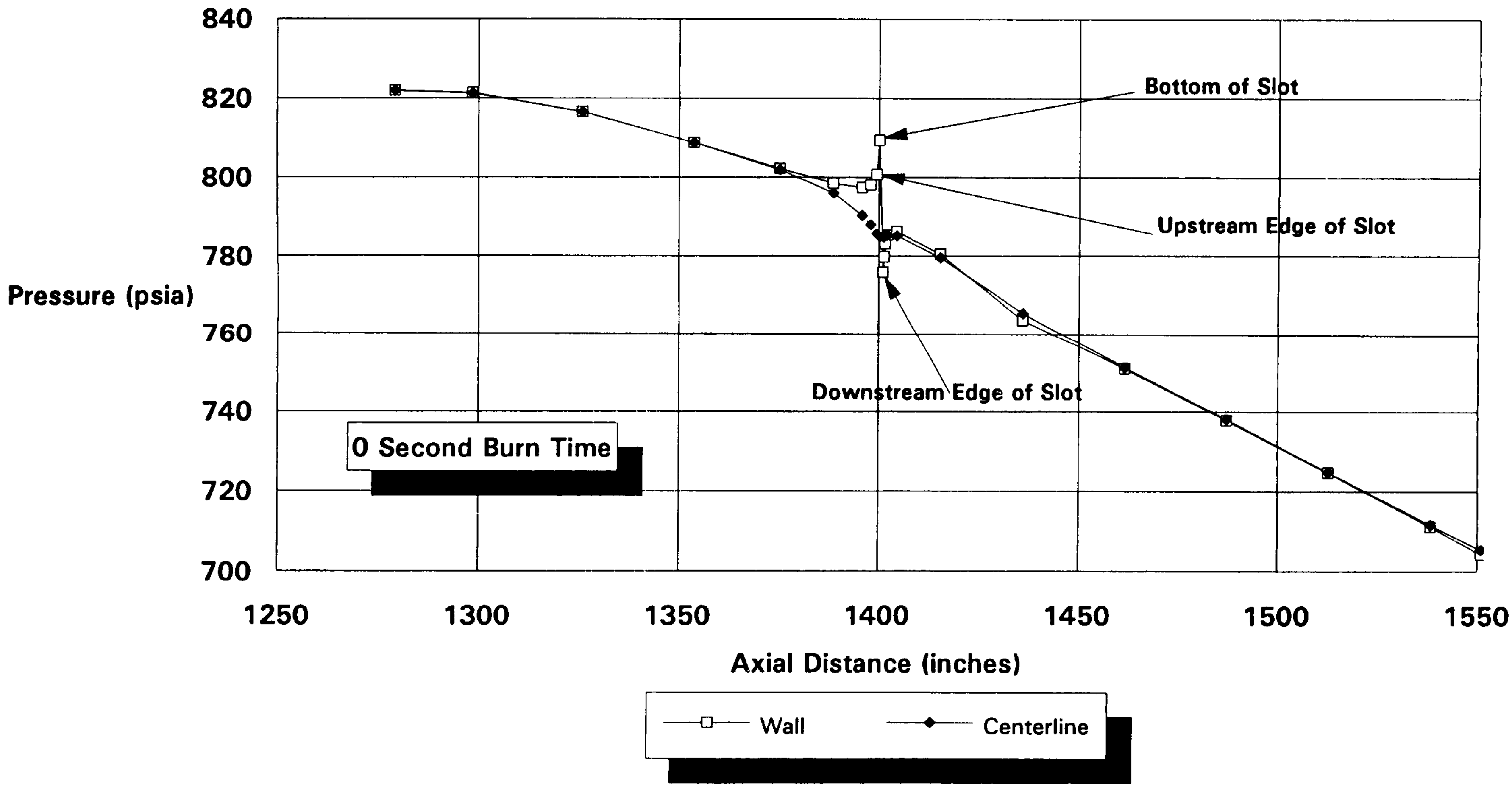

ASRM MOTOR FIELD JOINT BOUNDARY CONDITIONS
19 SECOND BURN TIME CONFIGURATION

AFT SLOT

INLET STATIC PRESSURE	:	861.3 psia
AVERAGE PORT VELOCITY	:	746.25 ft/s
STAGNATION TEMPERATURE AT THE INLET	:	6317.6 °R
RATIO OF SPECIFIC HEATS	:	1.128
PROPELLANT INJECTION VELOCITY	:	10.135 ft/s
MOLECULAR WEIGHT	:	29.295
MASS FLOW RATE (INLET)	:	8846 lbm/s
CFD CALCULATED MASS FLOW RATE (INLET)	:	8824 lbm/s

FORWARD SLOT

INLET STATIC PRESSURE	:	886.0 psia
AVERAGE PORT VELOCITY	:	521.2 ft/s
STAGNATION TEMPERATURE AT THE INLET	:	6317.6 °R
RATIO OF SPECIFIC HEATS	:	1.128
PROPELLANT INJECTION VELOCITY	:	9.956 ft/s
MOLECULAR WEIGHT	:	29.295
MASS FLOW RATE (INLET)	:	5963 lbm/s
CFD CALCULATED MASS FLOW RATE (INLET)	:	5944 .bm/s

ERC, Inc. 4/29/92

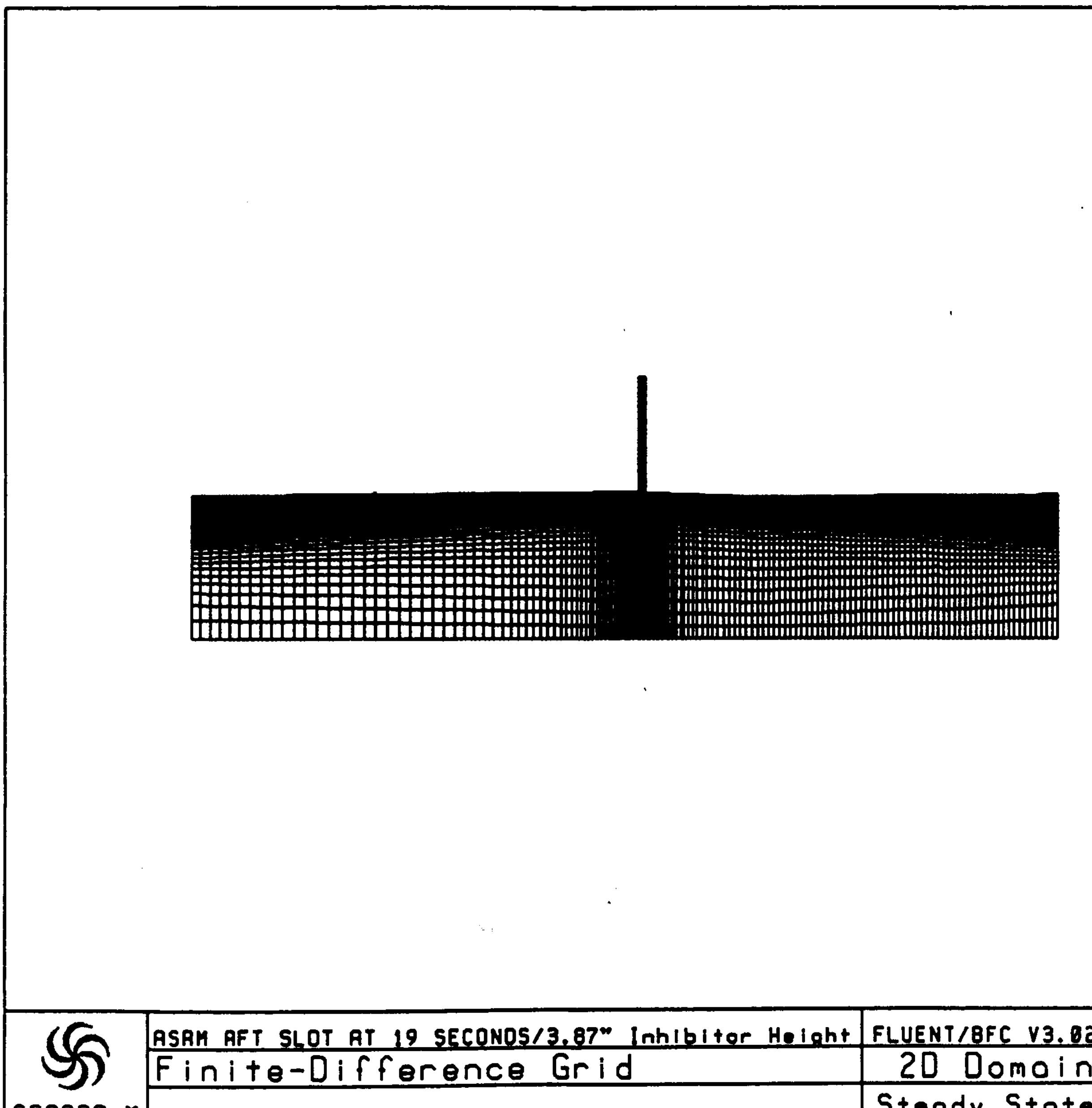

creare.x
ASRM AFT SLOT AT 19 SECONDS/3.87" Inhibitor Height
Finite-Difference Grid
FLUENT/BFC V3.02
2D Domain
Steady State

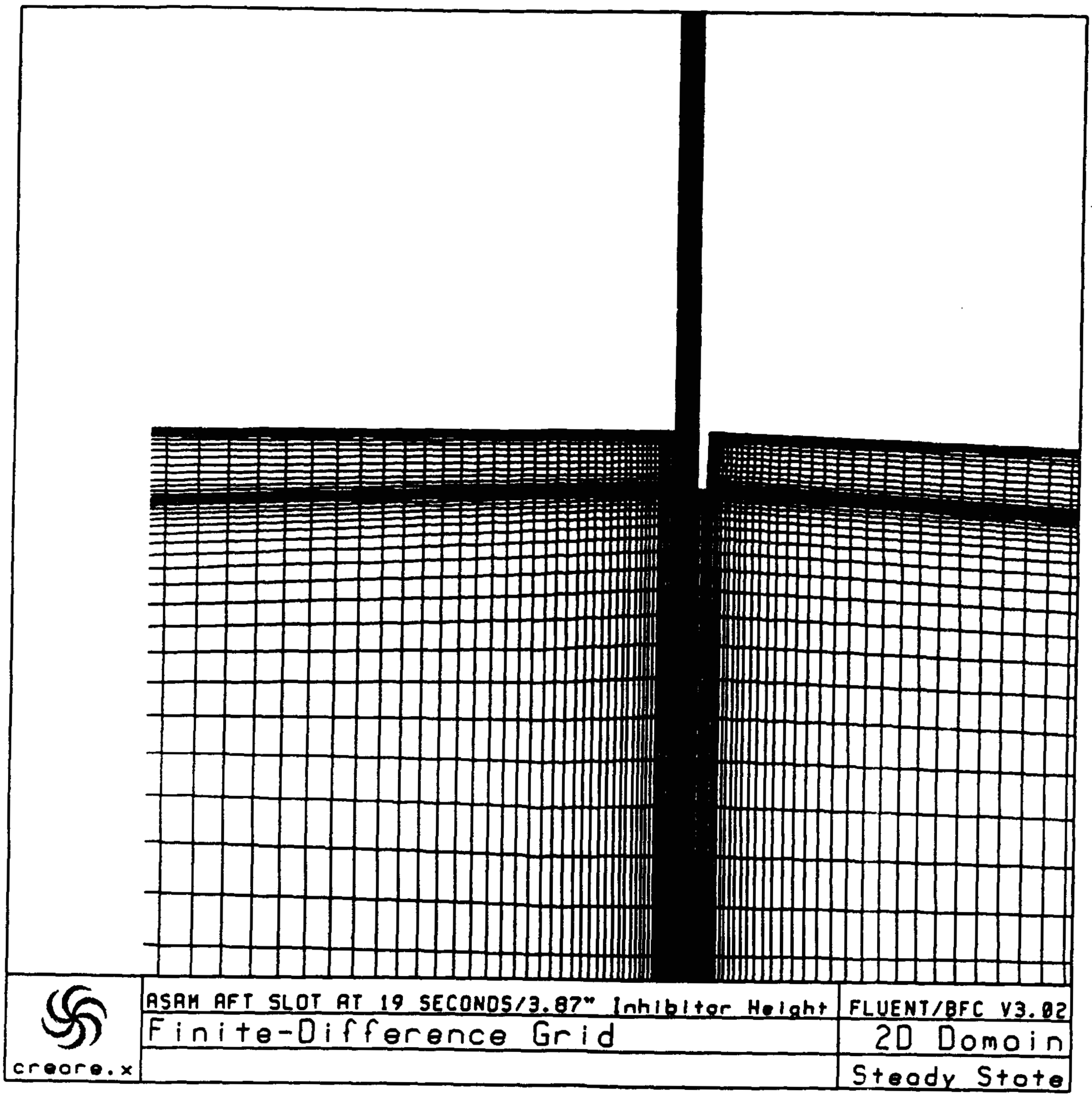
ASAM AFT SLOT AT 19 SECONDS/3.87" Inhibitor Height
Finite-Difference Grid
creare.x
FLUENT/BFC V3.02
2D Domain
Steady State

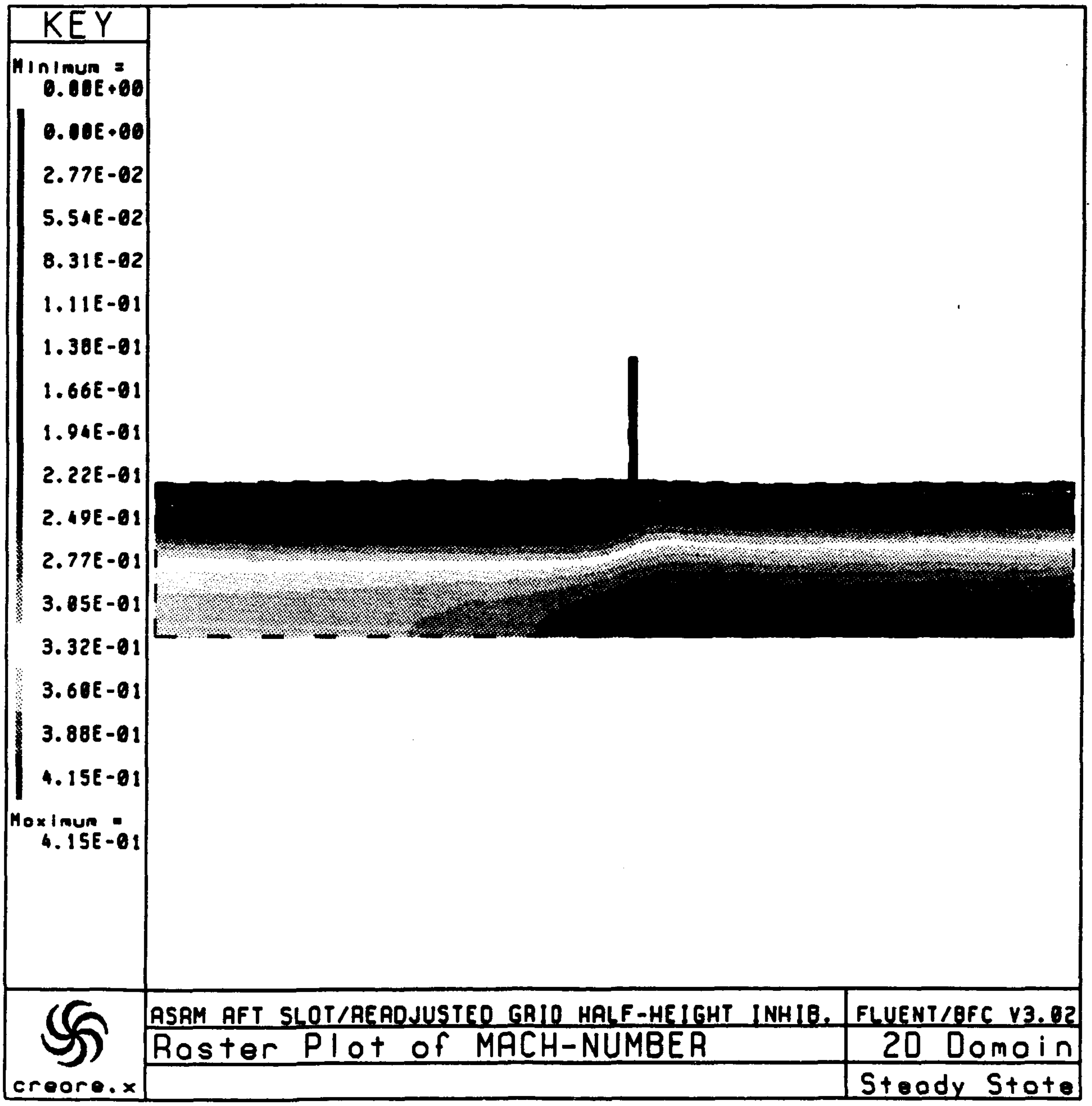
KEY
Minimum =
0.00E+00
0.00E+00
2.77E-02
5.54E-02
8.31E-02
1.11E-01
1.38E-01
1.66E-01
1.94E-01
2.22E-01
2.49E-01
2.77E-01
3.05E-01
3.32E-01
3.60E-01
3.88E-01
4.15E-01
Maximum =
4.15E-01
creare.x
ASAM AFT SLOT/READJUSTED GRID HALF-HEIGHT INHIB.
FLUENT/BFC V3.02
Raster Plot of MACH-NUMBER
2D Domain
Steady State

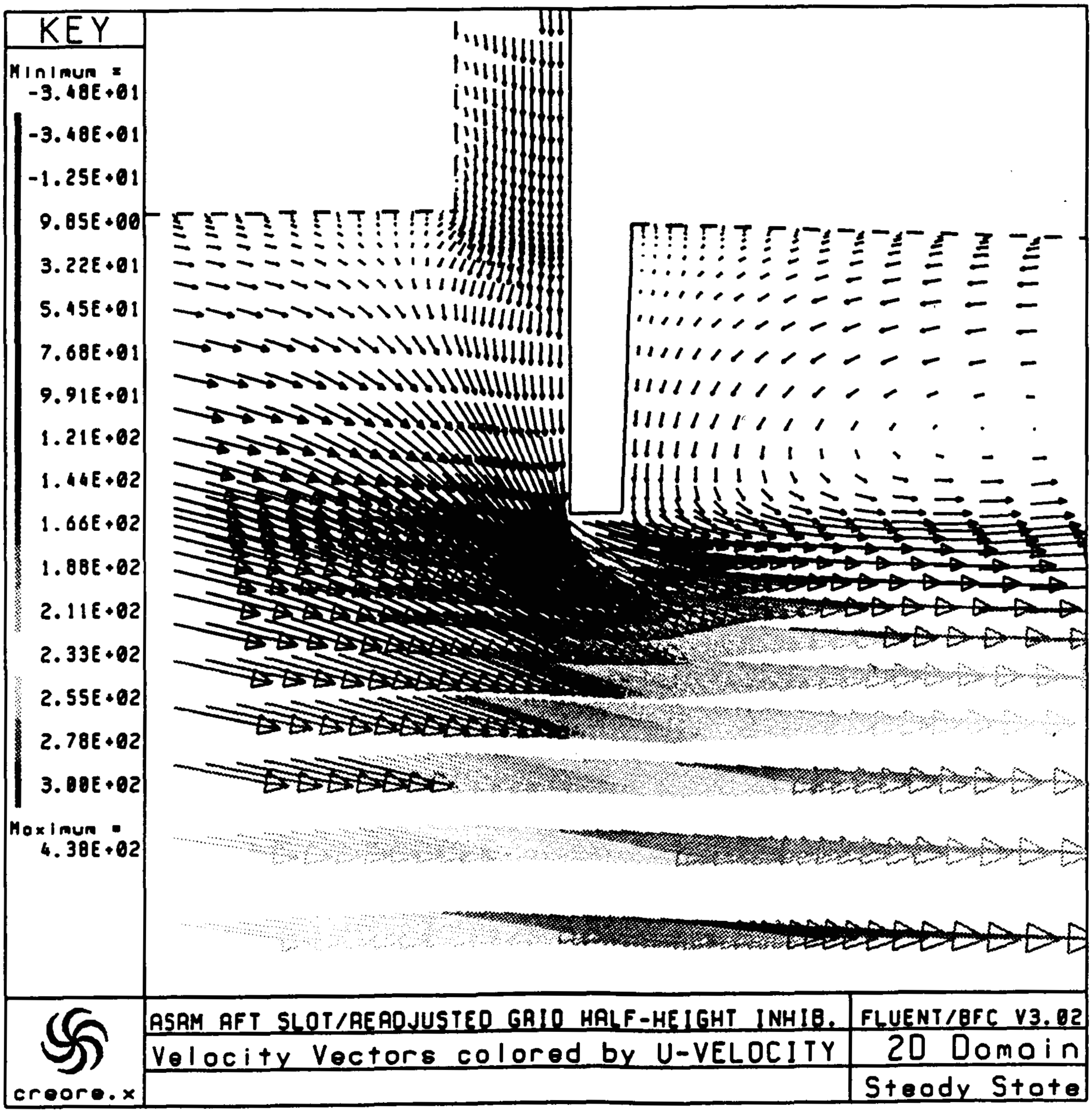
KEY
Minimum =
-3.48E+01
-3.48E+01
-1.25E+01
9.85E+00
3.22E+01
5.45E+01
7.68E+01
9.91E+01
1.21E+02
1.44E+02
1.66E+02
1.88E+02
2.11E+02
2.33E+02
2.55E+02
2.78E+02
3.00E+02
Maximum =
4.38E+02
creare.x
ASRM AFT SLOT/READJUSTED GRID HALF-HEIGHT INHIB.
Velocity Vectors colored by U-VELOCITY
FLUENT/BFC V3.02
2D Domain
Steady State

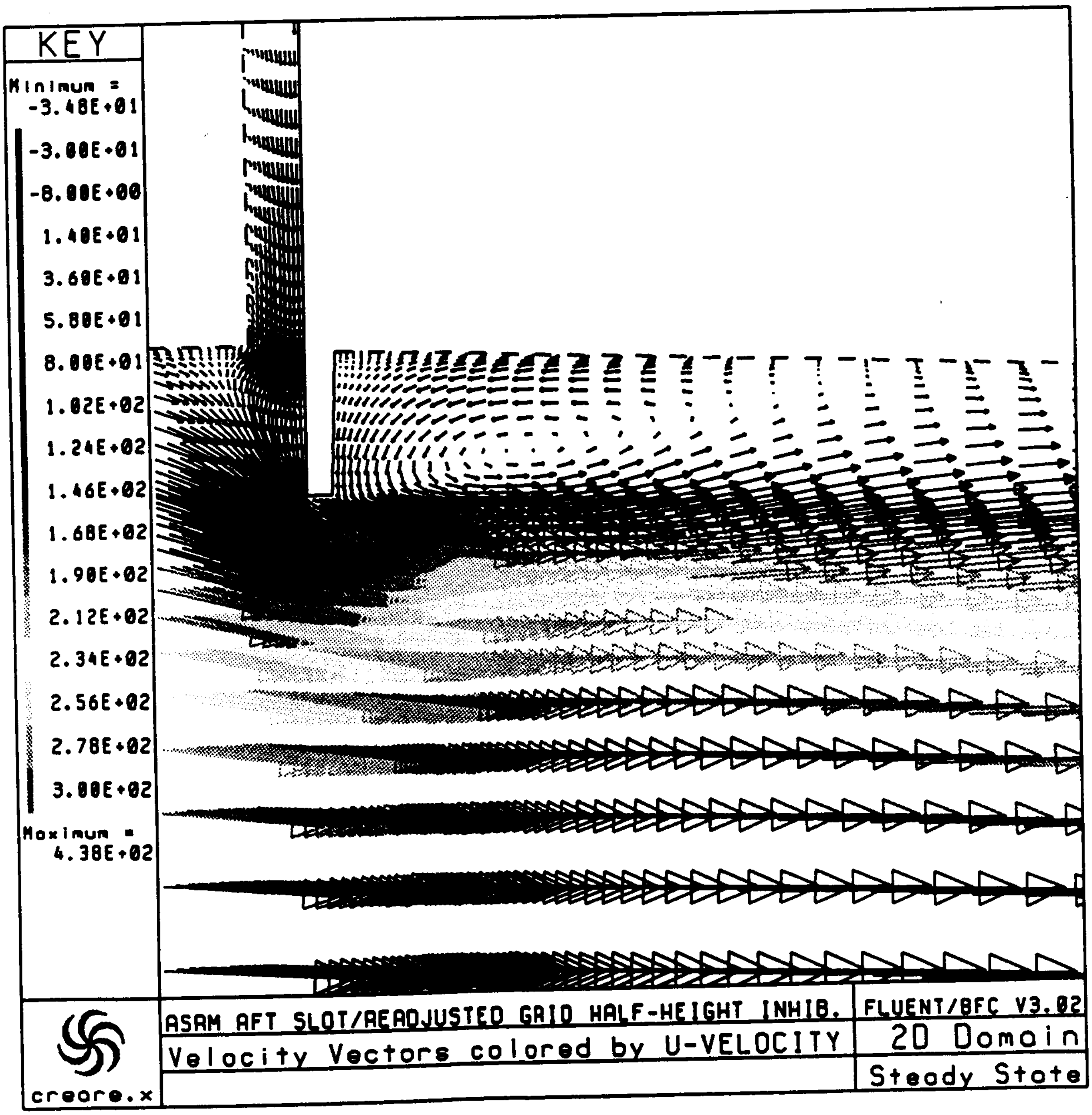
KEY
Minimum =
-3.48E+01
-3.00E+01
-8.00E+00
1.40E+01
3.60E+01
5.80E+01
8.00E+01
1.02E+02
1.24E+02
1.46E+02
1.68E+02
1.90E+02
2.12E+02
2.34E+02
2.56E+02
2.78E+02
3.00E+02
Maximum =
4.38E+02
ASRM AFT SLOT/READJUSTED GRID HALF-HEIGHT INHIB.
Velocity Vectors colored by U-VELOCITY
FLUENT/BFC V3.02
2D Domain
Steady State
creare.x

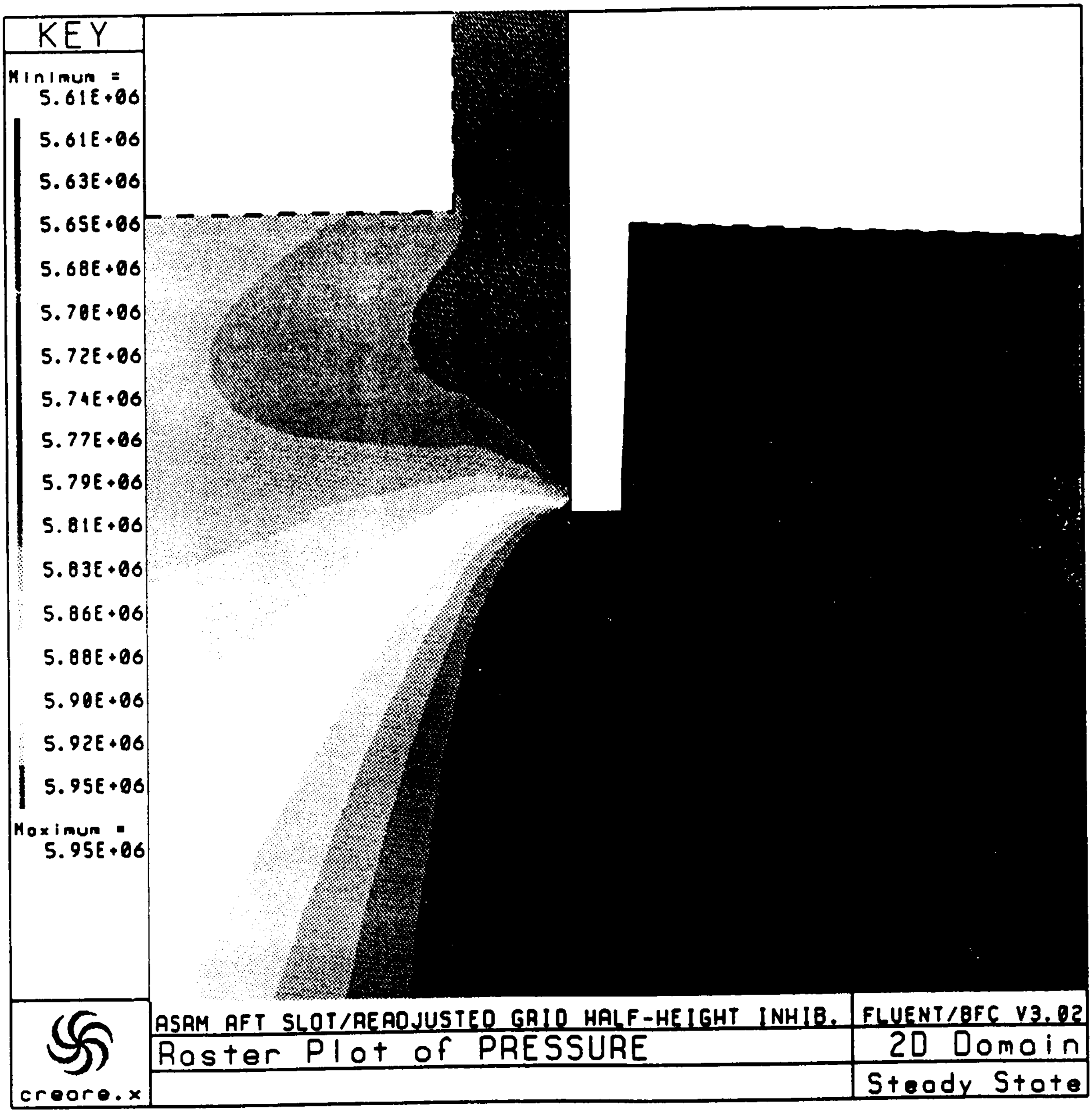
KEY
Minimum =
5.61E+06
5.61E+06
5.63E+06
5.65E+06
5.68E+06
5.70E+06
5.72E+06
5.74E+06
5.77E+06
5.79E+06
5.81E+06
5.83E+06
5.86E+06
5.88E+06
5.90E+06
5.92E+06
5.95E+06
Maximum =
5.95E+06
creare.x
ASRM AFT SLOT/READJUSTED GRID HALF-HEIGHT INHIB.
FLUENT/BFC V3.02
Raster Plot of PRESSURE
2D Domain
Steady State

ASRM Fwd Slot Undeformed Grain Port Pressures On the Surface and at the Motor Centerline

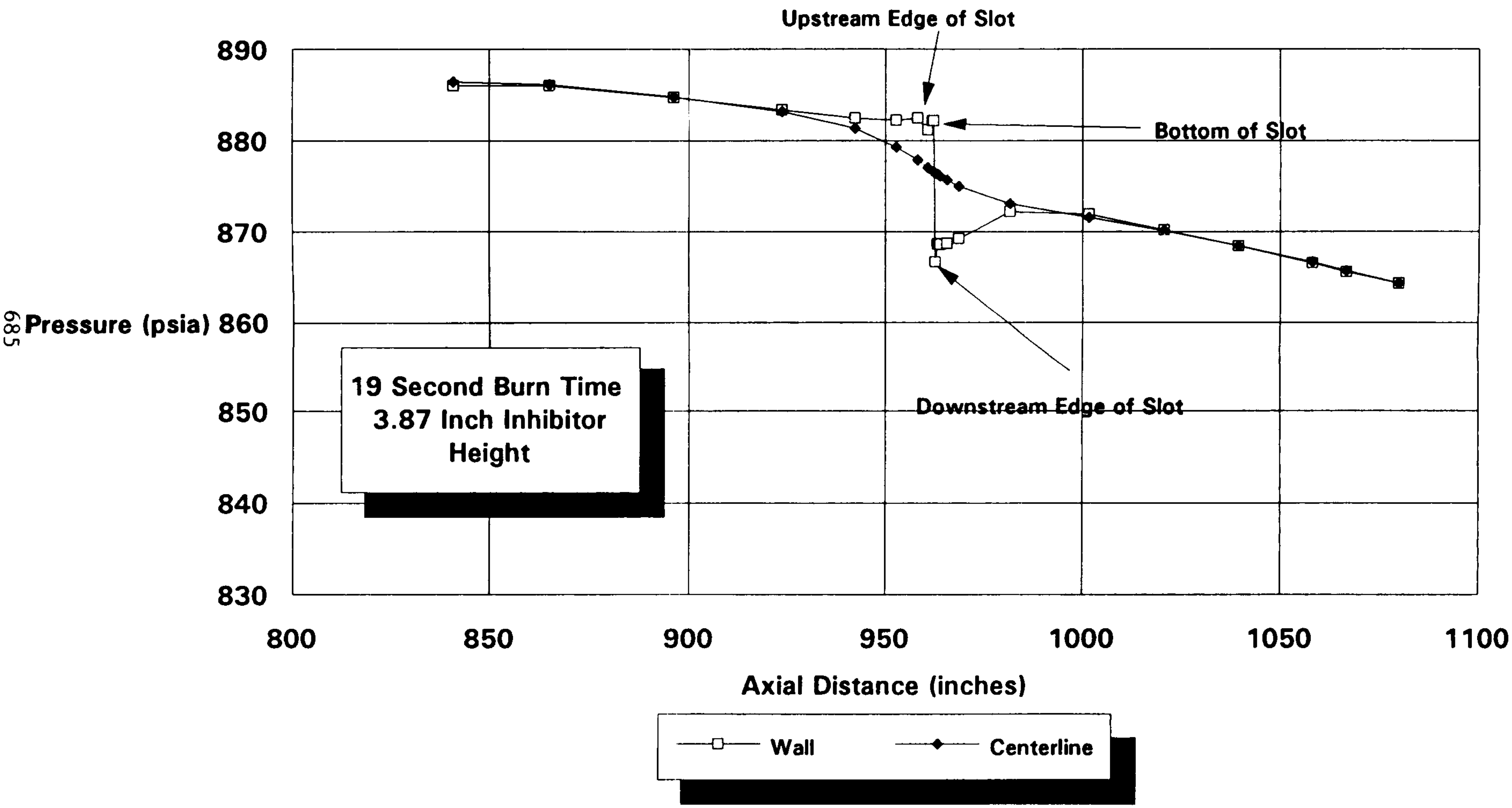

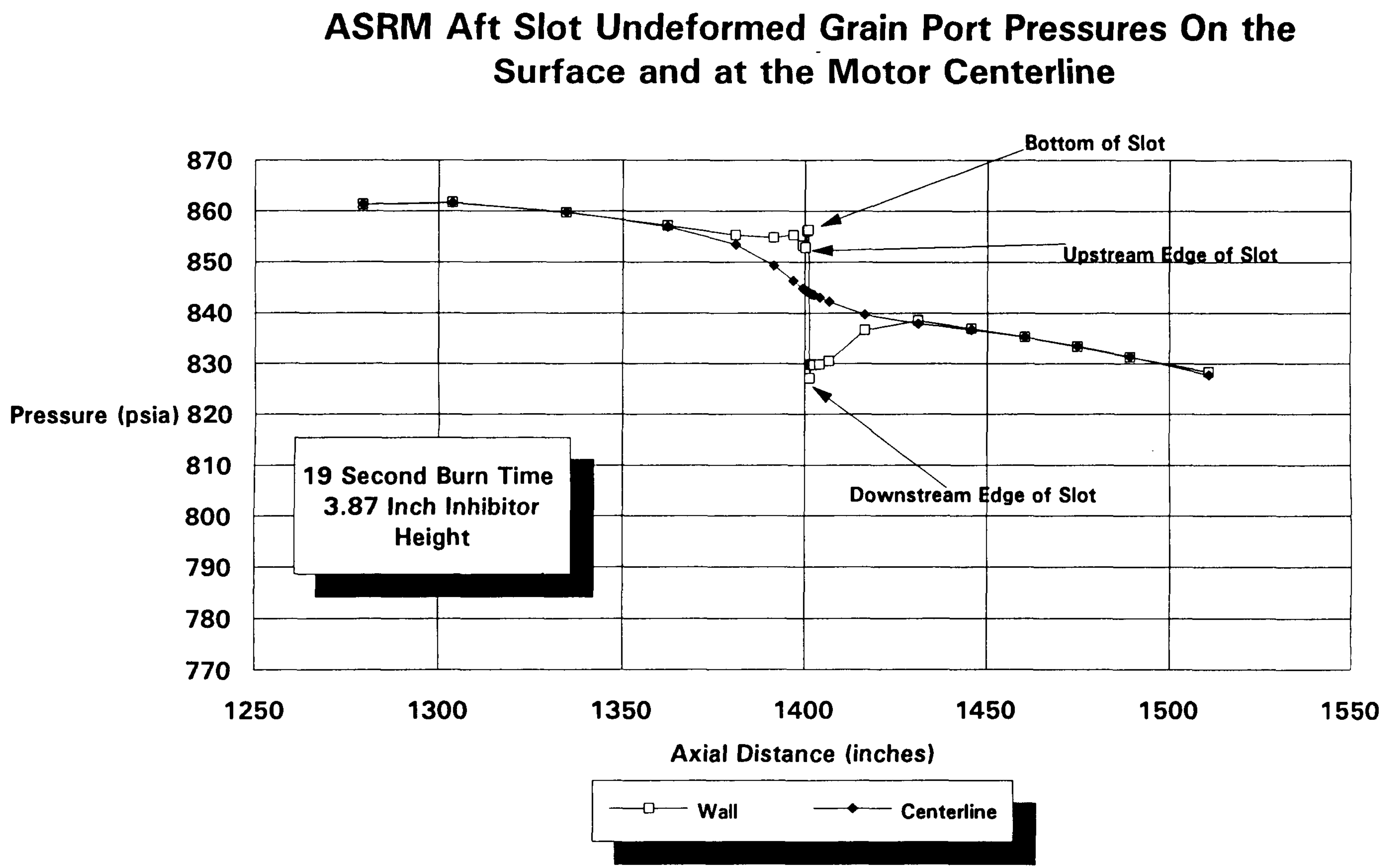
ASRM Aft Slot Undeformed Grain Port Pressures On the Surface and at the Motor Centerline
Bottom of Slot
Upstream Edge of Slot
Downstream Edge of Slot
19 Second Burn Time
3.87 Inch Inhibitor
Height
Pressure (psia)
870
860
850
840
830
820
810
800
790
780
770
1250
1300
1350
1400
1450
1500
1550
Axial Distance (inches)
Wall
Centerline

989

ASRM Aft Slot Undeformed Grain Port Pressures On the Surface and at the Motor Cenerline

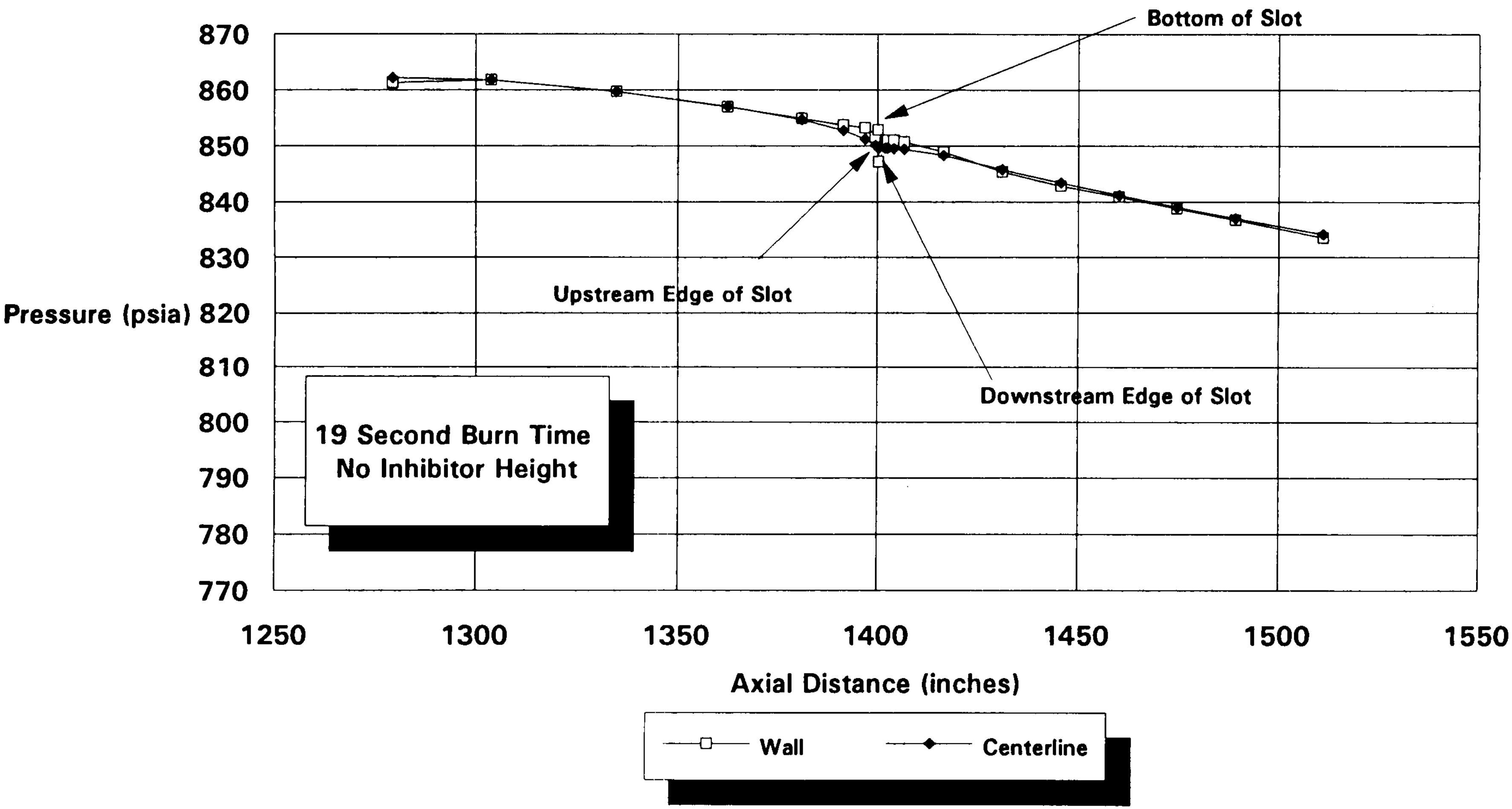

CONCLUSIONS

1) CFD ANALYSES HAVE BEEN COMPLETED FOR THE AFT AND FORWARD SLOTS AT 0 AND 19 SECOND BURN TIMES.

2) THE PRESSURE LOADS AT 0 SECOND BURN TIME ARE SMALL.

3) THE PRESSURE LOADS ON THE PROPELLANT GRAIN AT THE MOTOR JOINTS AT 19 SECONDS BURN TIME IS SIGNIFICANTLY AFFECTED BY THE INHIBITOR HEIGHT AND ORIENTATION.

4) THE SLOT REGION ANALYSES ARE BEING EXTENDED TO INCLUDE ACTUAL DEFORMED GRAIN AND ERODED INHIBITOR GEOMETRIES.

5) INTERACTIVE CFD/STRUCTURAL ANALYSES ARE REQUIRED TO PROVIDE REALISTIC ASSESSMENT OF THE SLOT/PORT FLOW INTERACTIONS AND RESULTING PROPELLANT LOADS.

ERC, Inc. 4/29/92

N92-32306

Effect of Including Variable Gas Properties and Entrained Particles in the Flow Analysis of the ASRM Nozzle

Curtis D. Clayton, Ph.D.
Aerojet ASRM Division
Iuka, Mississippi

ABSTRACT

CFD analyses of solid rocket motors typically use constant fluid properties throughout the flow domain. While this may be an acceptable approximation inside the motor chamber, it is probably not a good approach for the expansion that occurs in the nozzle.

As the flow expands from 900 psi chamber pressure, the temperature decreases by 35%, viscosity and thermal conductivity are reduced by similar amounts (25%), and the specific heat (C_p) and specific heat ratio (γ) change by 4% and 1%, respectively. While the change in γ appears to be small, its effect is significant because of its use as an exponent in the isentropic expansion equations.

The objective of this study is to determine the effect of using constant gas properties for the analysis of the ASRM nozzle and to gain more understanding concerning those types of analysis which might require this additional complexity.

Kinetics data for viscosity, thermal conductivity, specific heat (C_p), and specific heat ratio (γ) are extracted from the Solid Propellant Rocket Motor Performance Prediction Computer Program (SPP) and tabulated as a function of temperature. These tables are added to the Aerovisc CFD code in place of the constant gas property values.

The results of a CFD analysis of the ASRM 48" motor with constant gas properties will be compared with an analysis which uses variable gas properties. Mach number, surface pressure,and torque plots will be presented. A full scale ASRM analysis using SPP with and without particle flow will also be presented.

ASRM
LOCKHEED • AEROJET • RUST

1992 WORKSHOP FOR COMPUTATIONAL FLUID DYNAMICS APPLICATIONS IN ROCKET MOTORS

Effect of Including Variable Gas Properties and Entrained Particles in the Flow Analysis of the ASRM Nozzle

Curtis D. Clayton, Ph.D.

APRIL 28 -30, 1992

Overview

- CFD analyses frequently assume that the fluid behaves as an ideal gas with constant properties.
- Combustion gases in solid rocket motors are not ideal.
  - Chemical and phase changes
  - Entrained particles in the flow
  - Extreme temperature changes effect gas properties
- This study compares several analyses with and without these effects to determine their impact on the results.

ASRM
LOCKHEED • AEROJET • RUST

Variable Gas Properties

- Performed Aerovisc CFD analysis of 48" motor with a scaled ASRM nozzle.
- Case 1 was run with constant gas properties typical of chamber conditions.
- Case 2 used local temperatures to determine:
  - Specific heats - Cp and Cv
  - Viscosity, μ
  - Thermal heat transfer coefficient, K
- Values were obtained from the SPP kinetics module.

Variation of Cp with Temperature

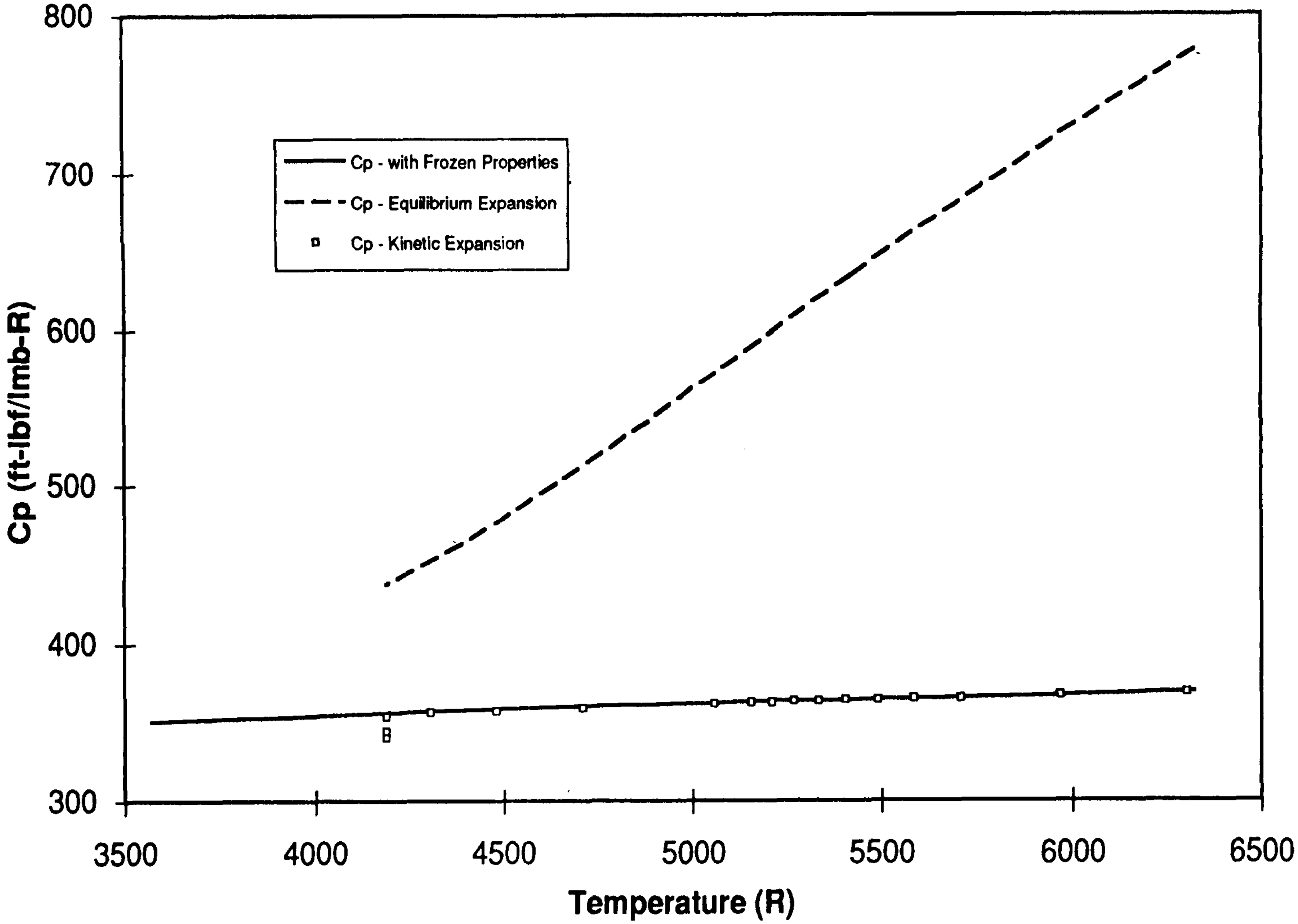

Effect of Temperature Changes on Thermodynamic Properties

Property	Change for 2000 R Temperature Change (4000-6000 R)
Cp	3.5 %
Cv	3.6 %
Conductivity	33 %
Viscosity	27 %

ASRM
LOCKHEED · AEROJET · RUST

Nozzle Exit Plane

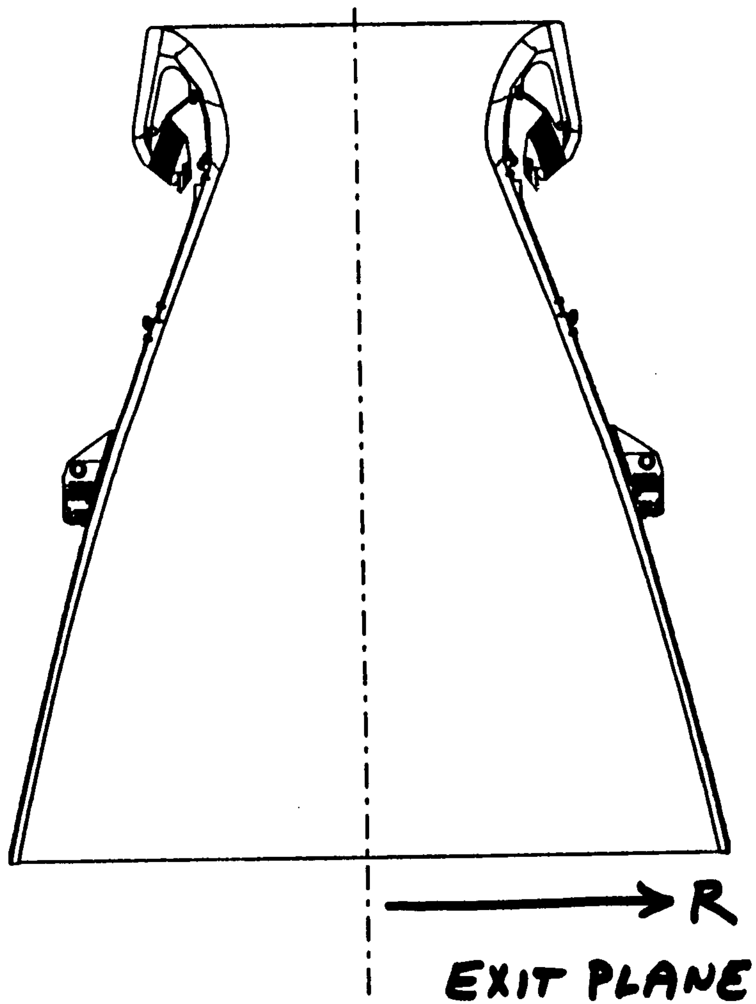

LOCKHEED • AEROJET • RUST

48" Motor Nozzle Exit Plane
Mach Number

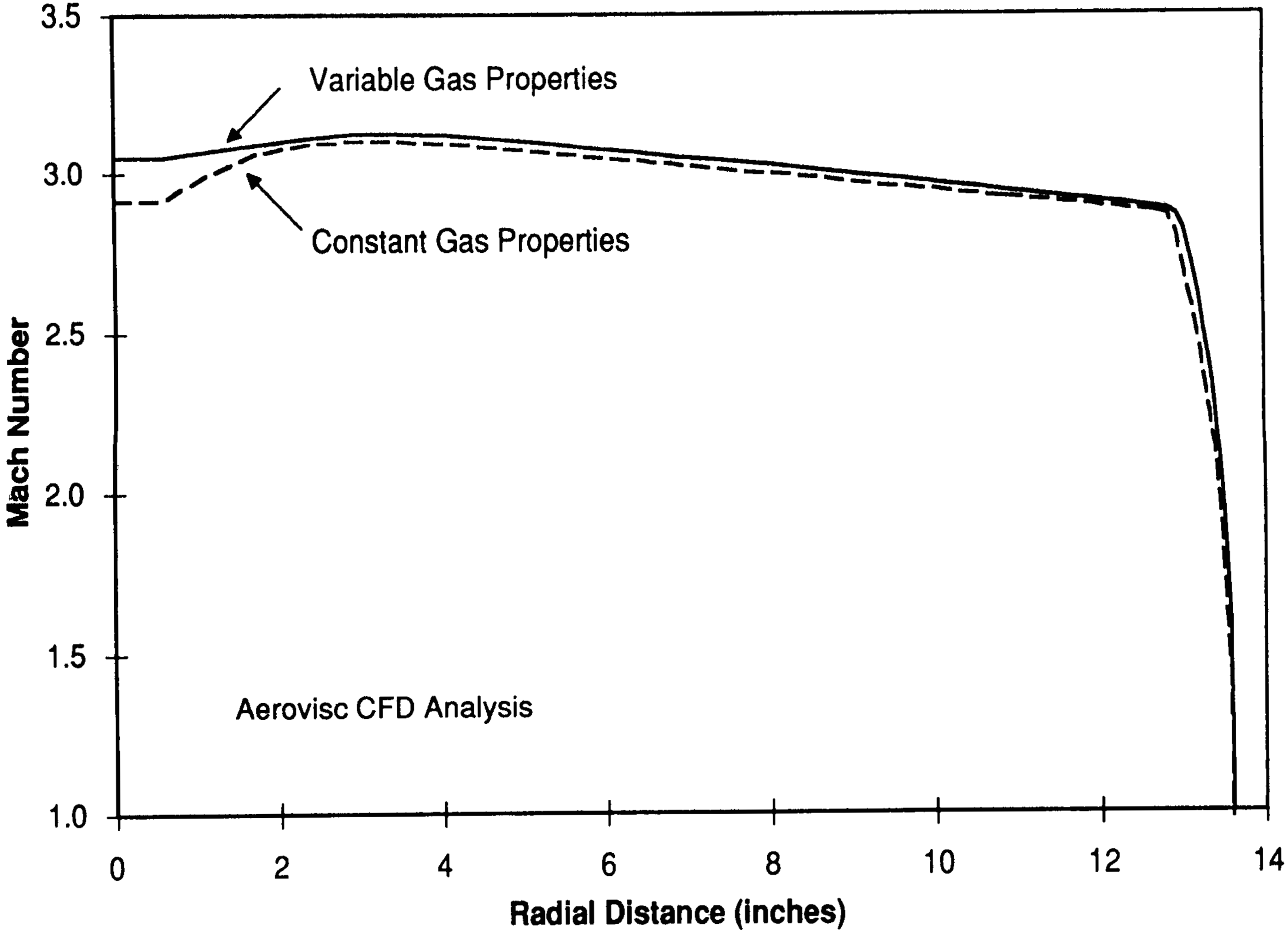

ASRM
LOCKHEED • AEROJET • RUST

Nozzle Wall Profile

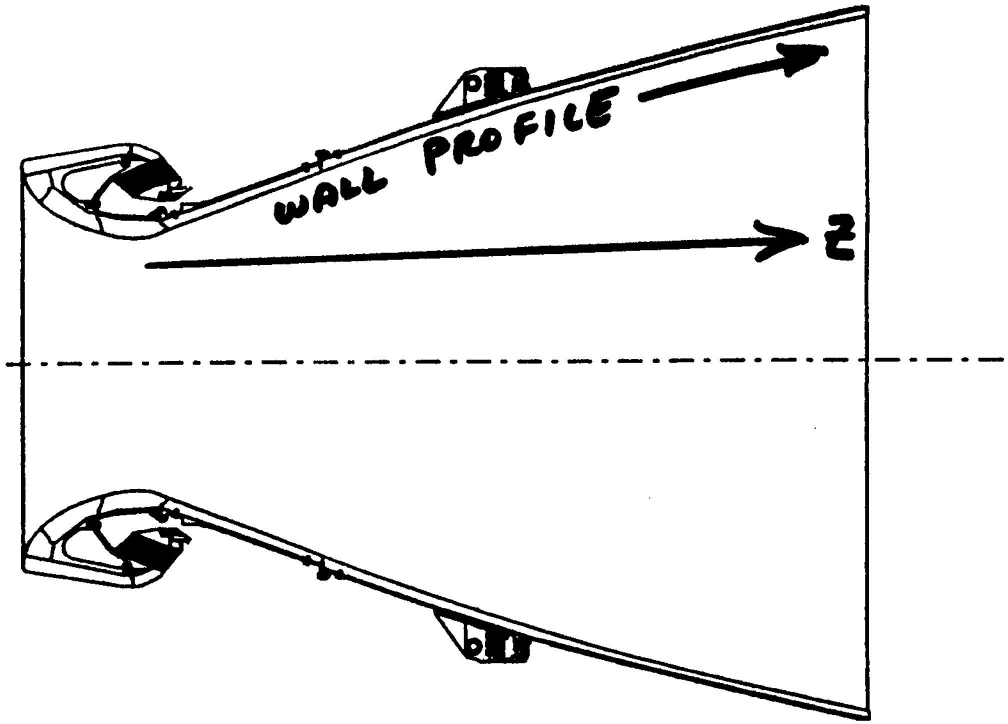

LOCKHEED • AEROJET • RUST

48" Motor Nozzle Pressure Profile Along Wall

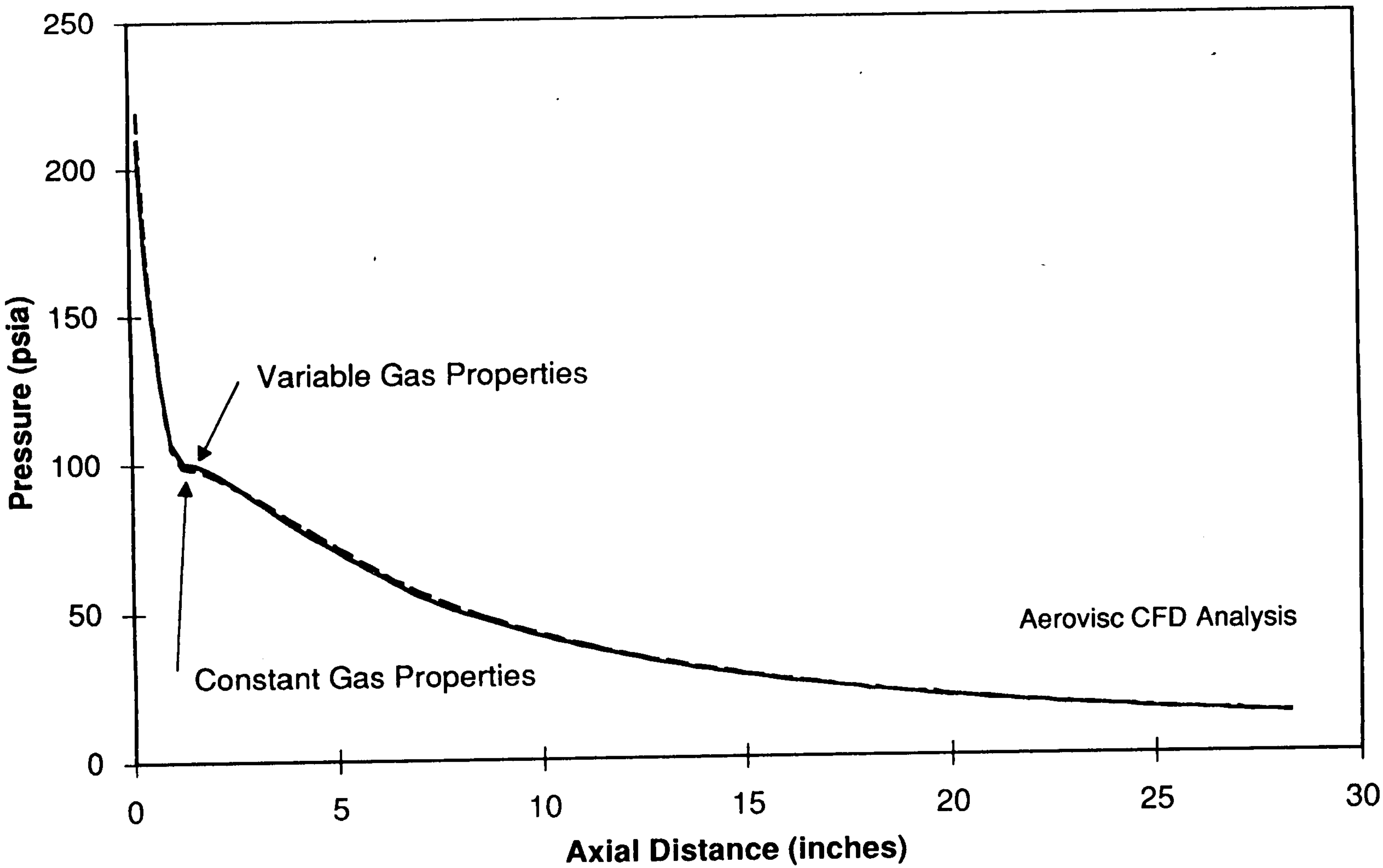

Effect of Pressure Differences

- Fictitious torque created by applying different pressure profiles to different halves of the nozzle.
- Net torque 2.32 K in-lbf
  - 1.3% of torque due to variable properties
  - 342 K in-lbf if scaled to ASRM
- This would be a significant error if it were present in the gimbaled nozzle analysis.

ASRM
LOCKHEED • AEROJET • RUST

1992 Workshop for CFD Applications in Rocket Motors

48" Motor Nozzle Torque

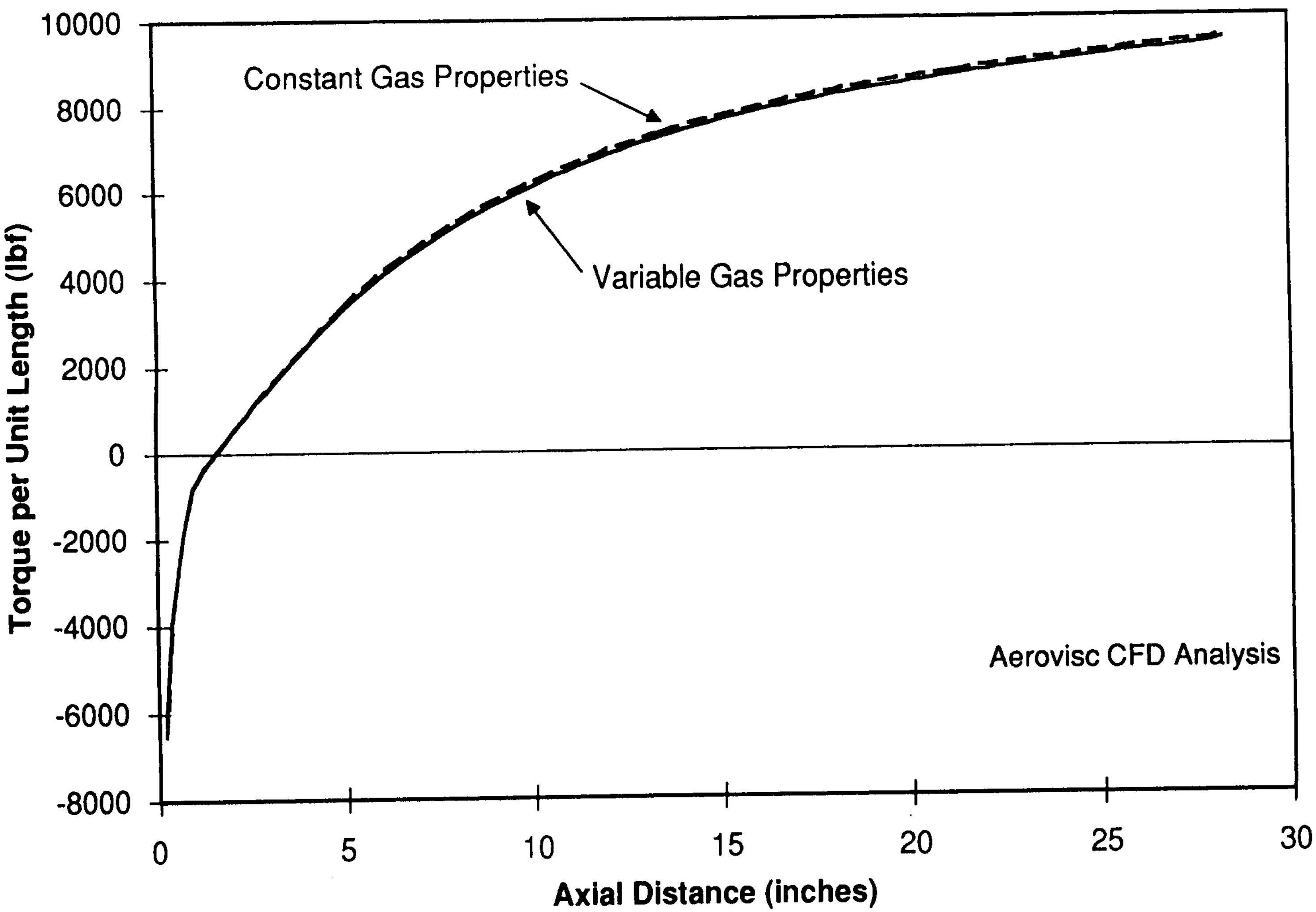

LOCKHEED • AEROJET • RUST

Entrained Particle Flow

- Compared SPP analysis with and without particles in full scale ASRM.
- SPP - Solid Rocket Motor Performance Program
  - Industry standard for motor performance
  - Inviscid, axisymmetric, real gas flow
  - Method of Characteristics
- Three particle groups with diameters of 6.3μ, 11.7μ, and 21.8μ.

LOCKHEED • AEROJET • RUST

48" Motor Nozzle Exit Plane
Mach Number

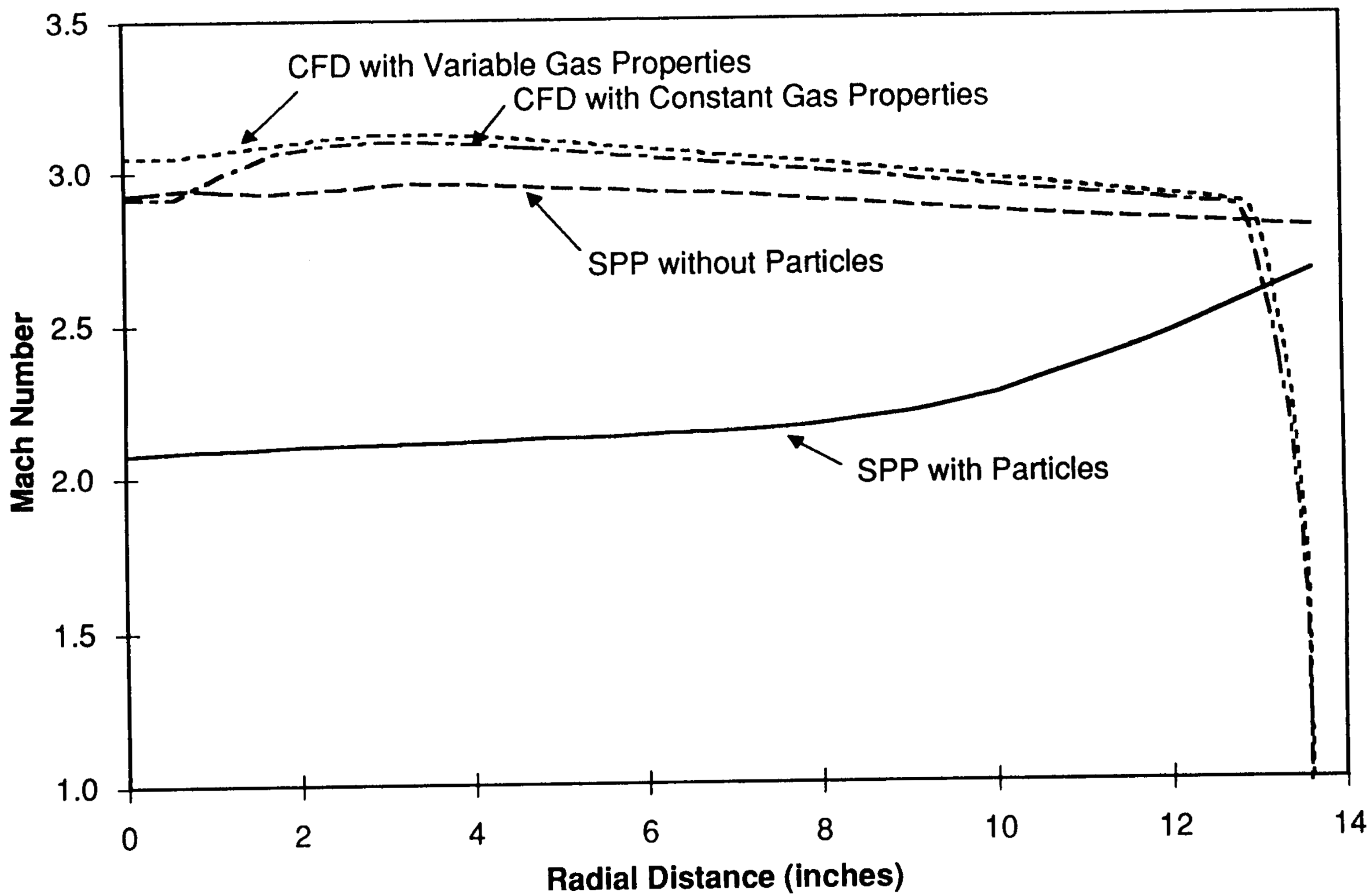

Effect of Particles on Wall Pressure in Full Scale ASRM Nozzle

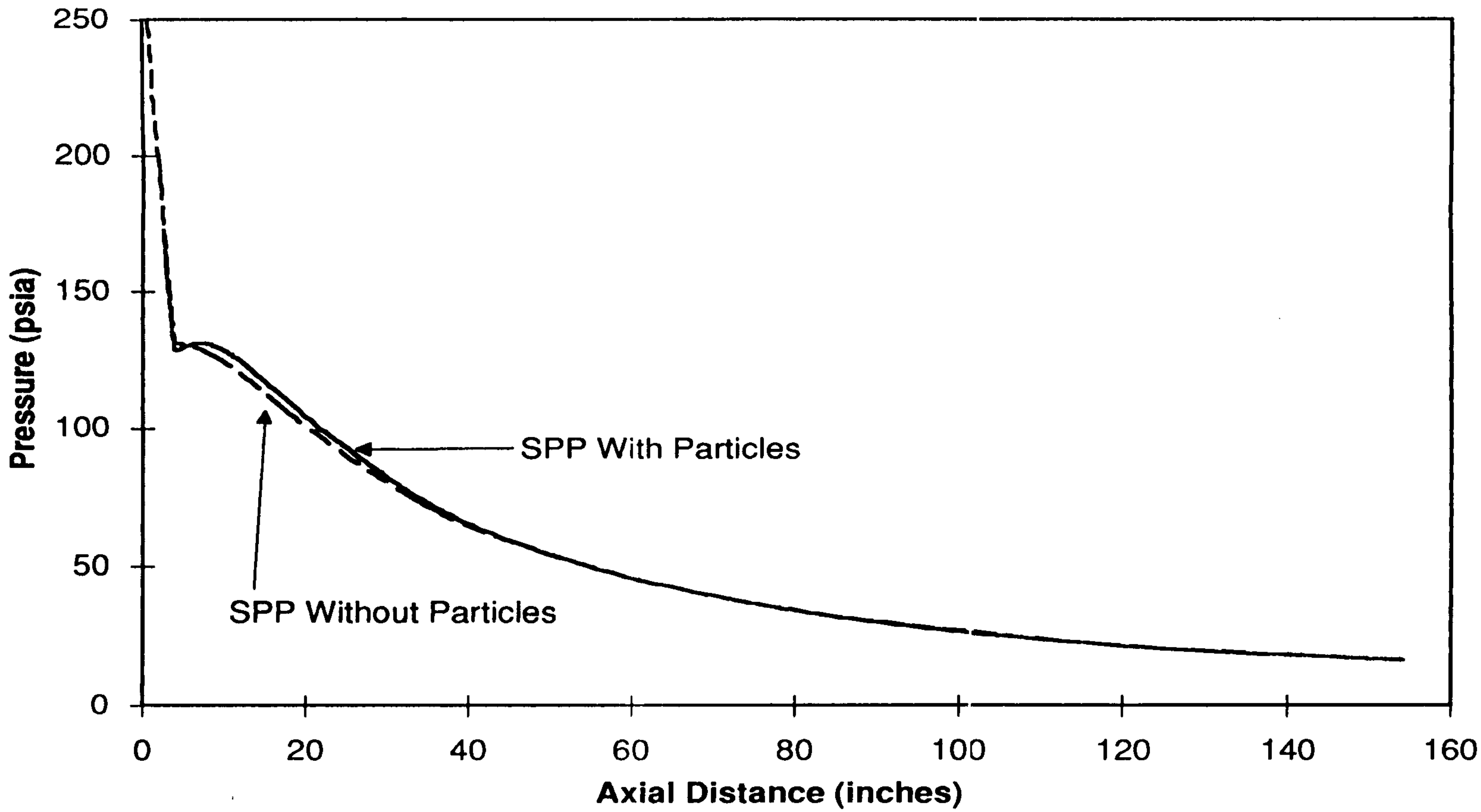

LOCKHEED • AEROJET • RUST

Effect of Particles on Torque in Full Scale ASRM Nozzle

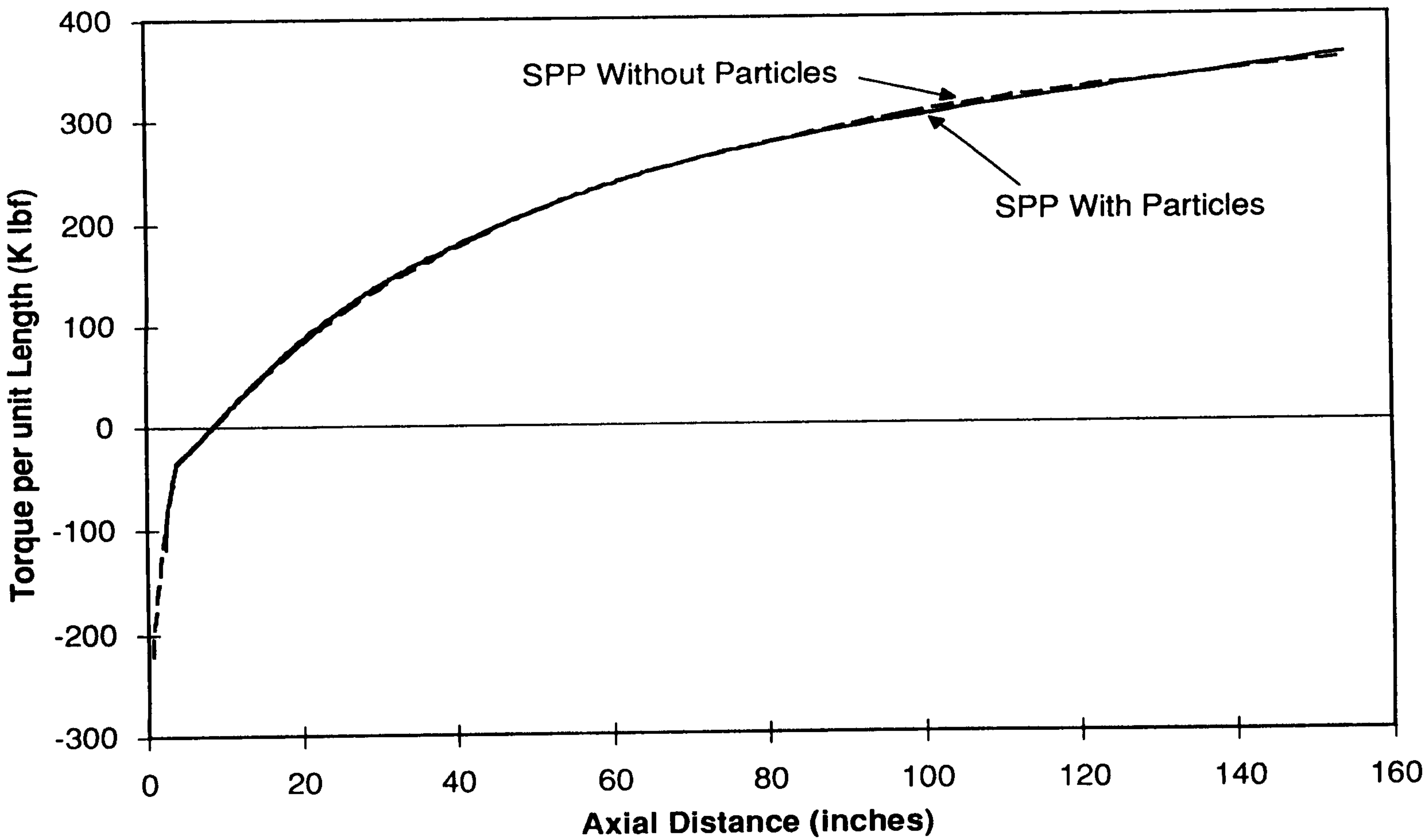

Effect of Pressure Differences

- Fictitious torque created by applying different pressure profiles to different halves of the nozzle.
- Net torque 142 K in-lbf
  - 0.39% of torque due to particles
  - Net torque would have been greater if pressure profiles had not crossed
- This would be a significant error if it were present in the gimbaled nozzle analysis.

1992 Workshop for CFD Applications in Rocket Motors

Torque Differences With and Without Particles

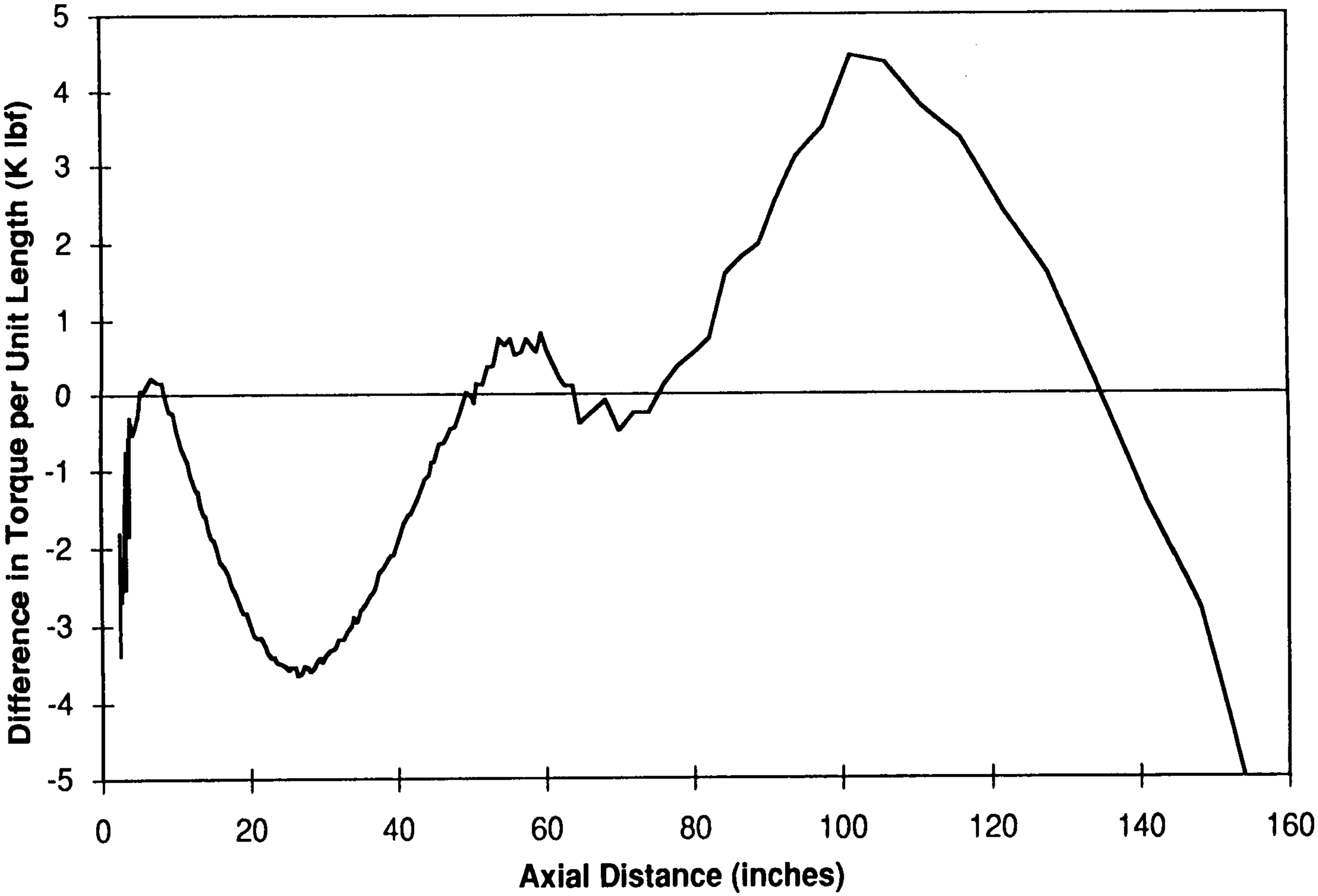

Flow Field Effects

- Particles slow the flow along the center line.
  - 33% mass fraction
  - Less actual gas per unit volume to expand
  - Velocity difference adds to drag
- Using an effective R does not correct for these problems because the particles are not uniformly distributed.
- When the nozzle is gimbaled the low-flow, particle entrained region comes closer to the wall.

ASRM
LOCKHEED • AEROJET • RUST

ASRM Nozzle Exit Plane
Mach Number

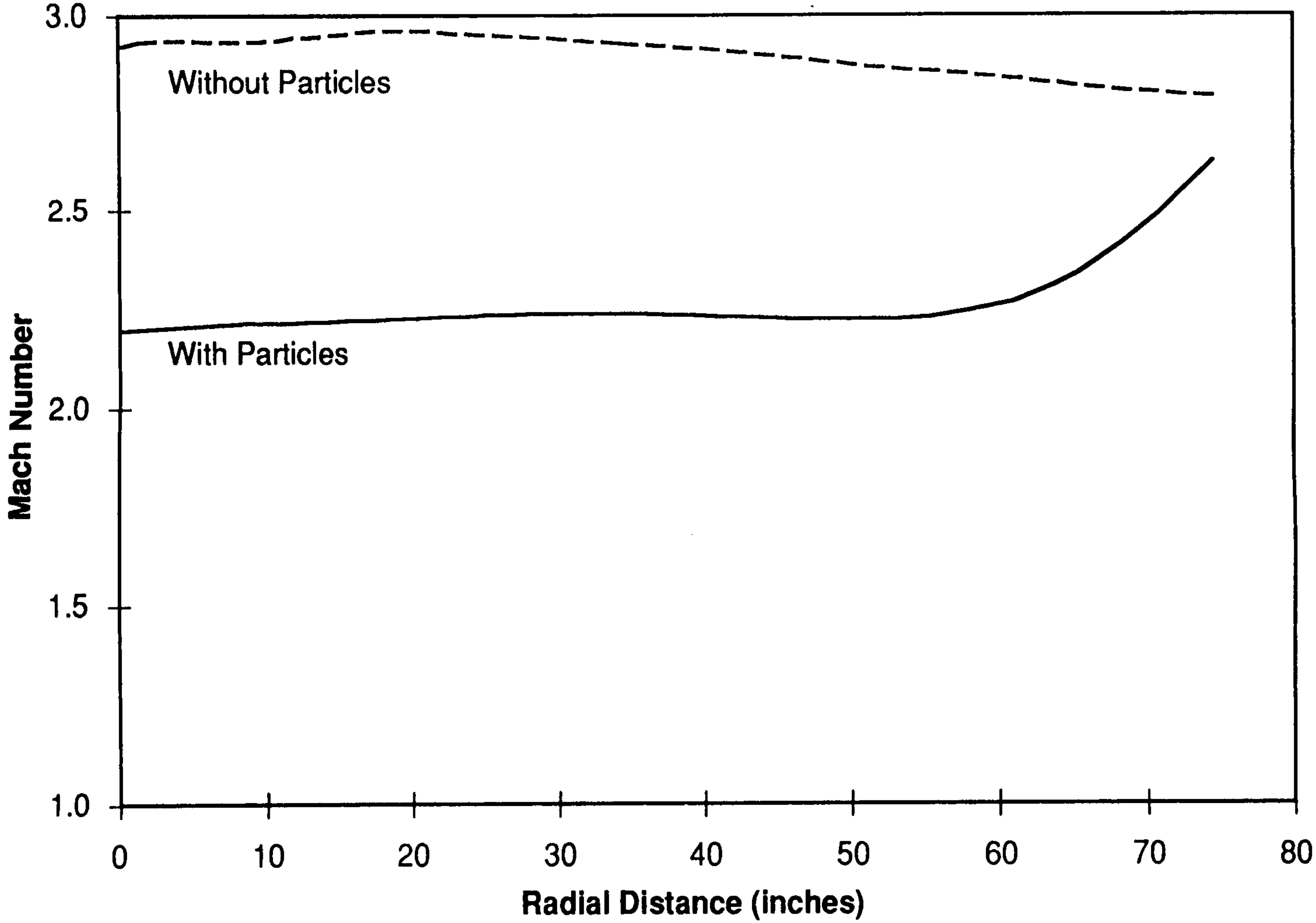

LOCKHEED • AEROJET • RUST

ASRM Nozzle

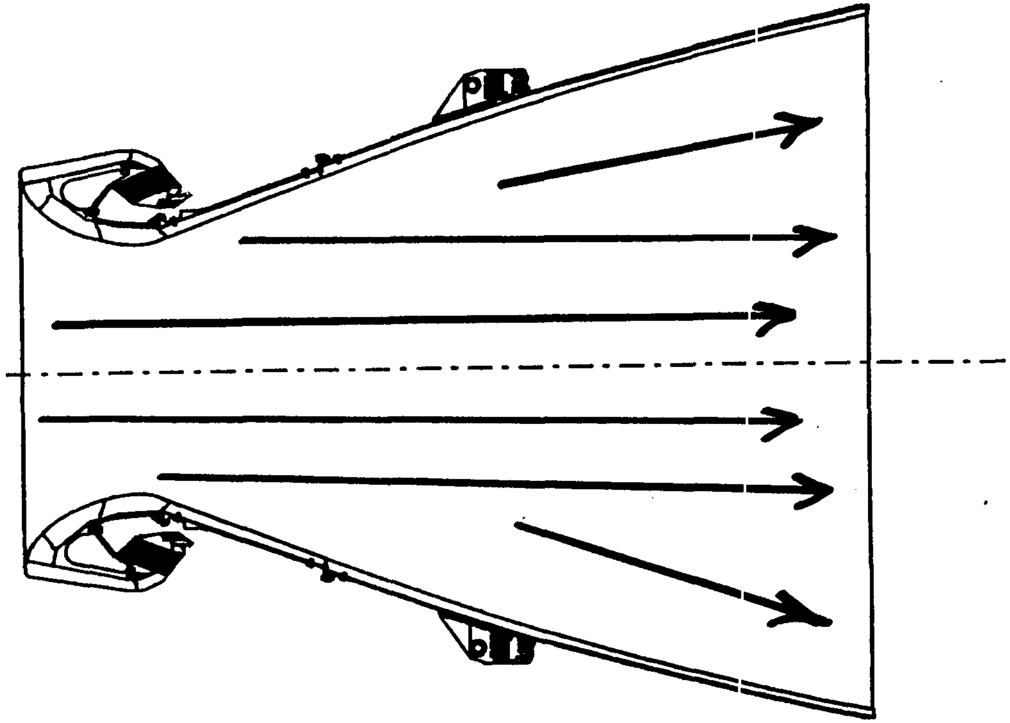

- Particle laden flow retards velocity in center.
- Flow along wall is nearly equal to non-particle values.

ASRM Gimbaled Nozzle

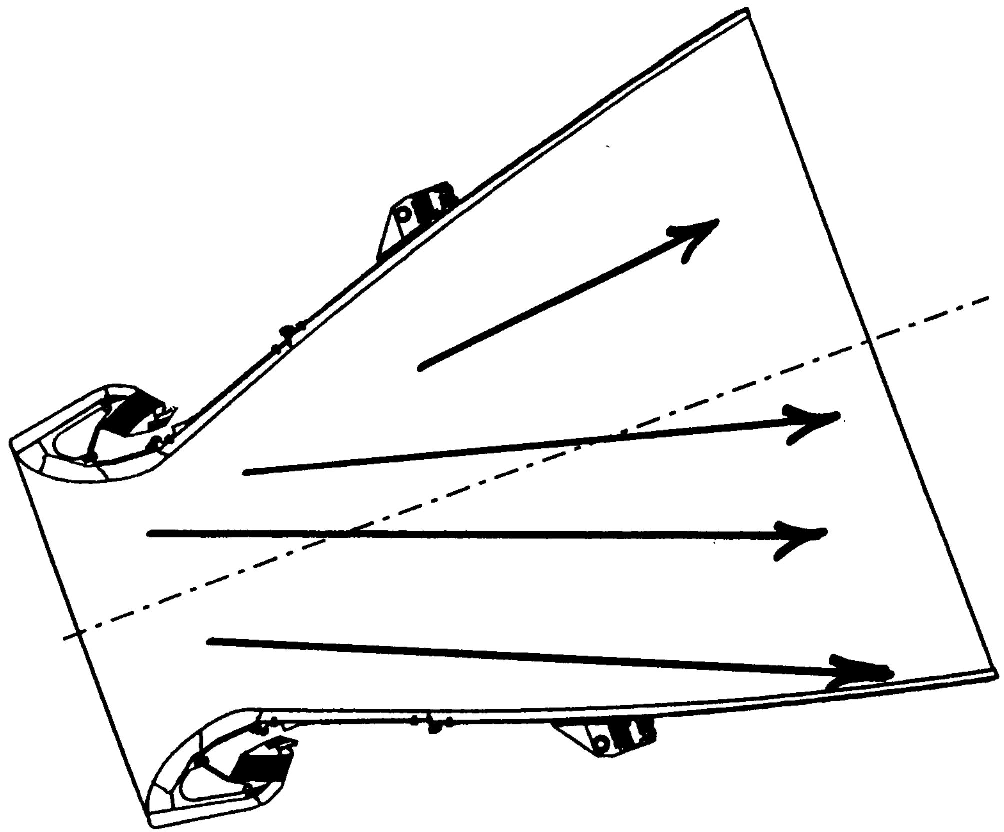

- Particles influence flow near nozzle wall.
- Flow decreases along lower wall; increases on upper wall.

Summary

- Actual gas properties and characteristics do effect the flow field.
  - Especially compressible flows
- Particles have a significant impact on the flow field.
- Torque calculations magnify these effects.

N92-32307

A TWO-PHASE RESTRICTED EQUILIBRIUM MODEL FOR COMBUSTION OF METALIZED SOLID PROPELLANTS†

J. S. Sabnis*, F. J. de Jong and H. J. Gibeling
Scientific Research Associates, Inc.
Glastonbury, Connecticut

ABSTRACT

An Eulerian-Lagrangian two-phase approach has been adopted to model the multi-phase reacting internal flow in a solid rocket with a metalized propellant. An Eulerian description has been used to analyze the motion of the continuous phase which includes the gas as well as the small (micron-sized) particulates, while a Lagrangian description is used for the analysis of the discrete phase which consists of the larger particulates in the motor chamber. The particulates consist of Al and Al_2O_3 such that the particulate composition is 100% Al at injection from the propellant surface with Al_2O_3 fraction increasing due to combustion along the particle trajectory. An empirical model is used to compute the combustion rate for agglomerates while the continuous phase chemistry is treated using chemical equilibrium. The computer code was used to simulate the reacting flow in a solid rocket motor with an AP/HTPB/Al propellant. The computed results show the existence of an extended combustion zone in the chamber rather than a thin reaction region. The presence of the extended combustion zone results in the chamber flow field and chemical being far from isothermal (as would be predicted by a surface combustion assumption). The temperature in the chamber increases from about 2600 K at the propellant surface to about 3350 K in the core. Similarly the chemical composition and the density of the propellant gas also show spatially non-uniform distribution in the chamber. The analysis developed under the present effort provides a more sophisticated tool for solid rocket internal flow predictions than is presently available, and can be useful in studying apparent anomalies and improving the simple correlations currently in use. The code can be used in the analysis of combustion efficiency, thermal load in the internal insulation, plume radiation, etc.

† This work was supported by Phillips Laboratory, Edwards AFB, under Contract F04611-86-C-0096

* Currently at United Technologies Research Center, East Hartford, CT

PRECEDING PAGE BLANK NOT FILMED

OBJECTIVE

DEVELOPMENT OF A PREDICTIVE TOOL FOR REACTING MULTI-PHASE FLOW IN SOLID ROCKETS WITH METALIZED PROPELLANTS

MOTIVATION

- MOTOR PERFORMANCE AND DESIGN
  - STABILITY ANALYSIS
  - EROSIVE BURNING MODELING
- NOZZLE PERFORMANCE PREDICTON
- INSULATOR DESIGN

Scientific Research Associates

PREVIOUS ANALYSES

- POTENTIAL FLOW MODELS
- ROTATIONAL INVISCID FLOW MODEL
  - INADEQUATE WHEN VISCOUS EFFECTS BECOME SIGNIFICANT
- INVISCID FLOW MODELS COUPLED WITH ITERATIVE BOUNDARY LAYER CORRECTIONS
  - REQUIRE DIVISION OF FLOW INTO INVISCID CORE AND BOUNDARY LAYER
- NAVIER-STOKES ANALYSES
- TWO-PHASE NAVIER-STOKES ANALYSES

Scientific Research Associates

COMBUSTION OF ALUMINUM DROPLET

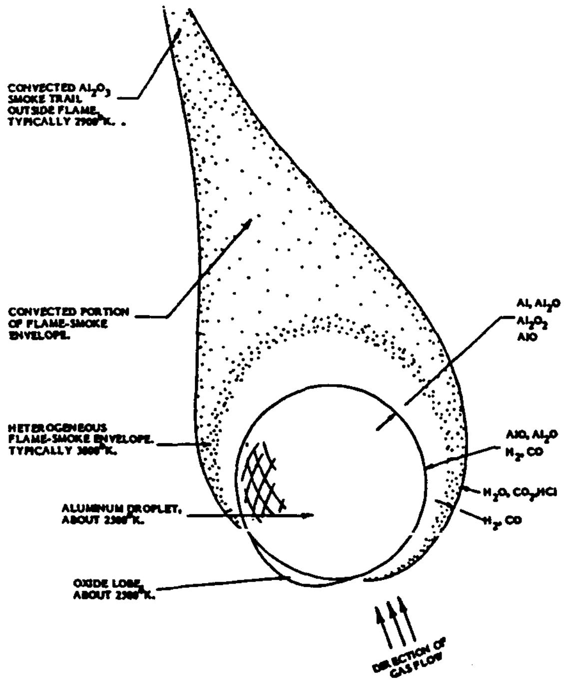

Scientific Research Associates

CHARACTERISTICS OF METALIZED SOLID PROPELLANT COMBUSTION

- MULTI-PHASE REACTING FLOW WITH POLY-DISPERSED PARTICLES WHICH UNDERGO CHANGES IN SIZE, TEMPERATURE AND COMPOSITION
- DISPARATE TIME SCALES ASSOCIATED WITH THE DROPLET COMBUSTION AND THE GAS PHASE CHEMISTRY
- SPATIAL VARIATION OF GAS COMPOSITION DUE TO
  - SPECIES TRANSPORT
  - COMBUSTION OF ALUMINUM DROPLETS
  - CHANGE OF THERMODYNAMIC STATE
- GAS COMPOSITION DETERMINES MIXTURE MOLECULAR WEIGHT, SPECIFIC HEAT ETC.

Scientific Research Associates

TWO PHASE REACTING FLOW MODEL FOR SOLID ROCKET INTERNAL FLOWS

- CONTINUOUS PHASE CONSISTING OF PRODUCTS OF COMBUSTION FROM AP, BINDER AND REACTED ALUMINUM.
- DISCRETE PHASE CONSISTING OF DROPLETS CONTAINING UNREACTED ALUMINUM AND Al_2O_3 CAPS.
- KINETIC TIME SCALES FOR CONTINUOUS PHASE REACTIONS SIGNIFICANTLY SMALLER THAN FLUID DYNAMIC TIME SCALES. HENCE CHEMICAL EQUILIBRIUM ASSUMED FOR CONTINUOUS PHASE ANALYSIS.
- COMBUSTION OF ALUMINUM DROPLET LIMITED BY AVAILABILITY OF OXIDIZING SPECIES AT THE DROPLET. HENCE MASS TRANSPORT CONTROLLED COMBUSTION OF ALUMINUM DROPLET ASSUMED.
- AN EULERIAN-LAGRANGIAN ANALYSIS ADOPTED TO SIMULATE THE MULTI-PHASE REACTING FLOW.

Scientific Research Associates

CONTINUOUS PHASE ANALYSIS

- CONTINUITY EQUATION

$$\frac{\partial(\alpha\rho)}{\partial t} + \nabla\cdot(\alpha\rho U) = m_v$$

- MOMENTUM EQUATION

$$\frac{\partial(\alpha\rho U)}{\partial t} + \nabla\cdot(\alpha\rho UU) = \nabla(\alpha p) + \nabla\cdot\alpha\tau + m_v U_p + F_D$$

- ENERGY EQUATION

$$\frac{\partial(\alpha\rho h)}{\partial t} + \nabla\cdot(\alpha\rho Uh) = \alpha\frac{Dp}{Dt} + \alpha\phi + \nabla\cdot q + q_v - U_R\cdot F_D + m_v\left(h_v + \frac{1}{2}U_R\cdot U_R\right)$$

Scientific Research Associates

CONTINUOUS PHASE ENERGY EQUATION

MIXTURE ENTHALPY

$$h = \sum_{i=1}^{n} Y_i^s h_i$$

$$h_i = h_i^0 + \sum_{j=1}^{5} a_{ij} T^j$$

HEAT FLUX VECTOR

$$q = \kappa \nabla T - \sum_{i=1}^{n} h_i \rho D \nabla Y_i^S$$

IF TURBULENT AND LAMINAR LEWIS NUMBERS ARE ASSUMED TO BE UNITY, THIS CAN BE SIMPLIFIED TO

$$q = -\left(\frac{\mu_\ell}{Pr_\ell} + \frac{\mu_T}{Pr_T} \right) \nabla h$$

Scientific Research Associates

CONTINUOUS PHASE MASS TRANSPORT ANALYSIS

$$\frac{\partial \left(\rho Y_i^s \right)}{\partial t} + \nabla \cdot \left(\rho U Y_i^s \right) = \nabla \cdot \left(\rho D_i \nabla Y_i^s \right) + w_i + m_{v_i}$$

NOTES:

1. $\sum_{i=1}^{n} w_i = 0$

2. $m_{v_i} \equiv 0$ FOR $i > 2$ ($i = 1 \Rightarrow Al$; $i = 2 \Rightarrow Al_2O_3$)

DEFINE

α_{ki} = MASSFRACTION OF ELEMENT k IN SPECIES

$Y_k = \sum_{i=1}^{n} \alpha_{ki} Y_i^s$ = MASS FRACTION OF ELEMENT k IN GAS

$\alpha_{k1} \equiv \alpha_{k2} \equiv 0$ FOR $k > 2$ ($k = 1 \Rightarrow Al$; $k = 2 \Rightarrow O$)

ASSUME

$D_i = D$; $i = 1,2,\ldots n$

Scientific Research Associates

CONTINUOUS PHASE MASS TRANSPORT ANALYSIS (cont'd)

$$\frac{\partial(\rho Y_k)}{\partial t} + \nabla\cdot(\rho U Y_k) = \nabla\cdot(\rho D \nabla Y_k) + \sum_{l=1}^{n} \alpha_{kl} m_{v_l}$$

BOUNDARY CONDITIONS

- PROPELLANT SURFACE: Y_k SPECIFIED BY PROPELLANT COMPOSITION
- INERT SURFACE: $\frac{\partial Y_k}{\partial n} = 0$
- IF PROPELLANT COMPOSITION IS UNIFORM THEN ELEMENTAL TRANSPORT EQUATIONS FOR k = 3, ..., ℓ ARE PROPORTIONAL TO EACH OTHER AND NEED NOT BE SOLVED!
- IF $m_{v1} \propto m_{v2}$ THEN ELEMENTAL TRANSPORT EQUATIONS FOR Al AND O ARE PROPORTIONAL AND ONLY ONE NEEDS TO BE SOLVED.

Scientific Research Associates

CONTINUOUS PHASE CHEMISTRY ANALYSIS

- ELEMENTAL MASS FRACTIONS AND TWO STATE VARIABLES DEFINE THE THERMODYNAMIC STATE.
- COMPUTE SPECIES MASS FRACTIONS USING SUITABLE CURVE FITS OBTAINED FROM EQUILBRIUM CODE.
- COMPUTE TEMPERATURE FROM MIXTURE COMPOSITION AND ENTHALPY USING POLYNOMIAL COEFFICIENTS (ITERATION REQUIRED).
- COMPUTE MIXTURE MOLECULAR WEIGHT AND SPECIFIC HEAT.

Scientific Research Associates

DISCRETE PHASE ANALYSIS

- COMPUTATIONAL PARTICLES USED TO REPRESENT COLLECTION OF DROPLETS CONTAINING ALUMINUM AND ALUMINUM OXIDE
- DISTRIBUTION OF PARTICLES IN THE DOMAIN COMPUTED USING LAGRANGIAN ANALYSIS IN COORDINATE SPACE
- SOURCE TERMS FOR EULERIAN ANALYSIS COMPUTED FROM THE COMBUSTION RATE, DRAG FORCE AND HEAT TRANSFER FOR THE PARTICLES

Scientific Research Associates

DISCRETE PHASE ANALYSIS

- EQUATION OF MOTION FOR PARTICLE

$$F_P = m\ddot{X}_P$$

$$\dot{X}_P = \int_{t_0}^{t} \frac{F_P}{m} d\tau + \dot{X}_P\Big|_{t_0}$$

- COORDINATE TRANSFORMATION

$$y^i = y^i(x_1, x_2, x_3)$$

$$\dot{Y}_P = J\dot{X}_P \quad \text{where } J = \left[\frac{\partial y^i}{\partial x_j}\right]$$

- INTEGRATION YIELDS

$$\Delta Y_P = \frac{1}{2}\Delta t^2 J\frac{F_P}{m} + \Delta t\dot{X}_P\Big|_{t_0}$$

Scientific Research Associates

DISCRETE PHASE DROPLET COMBUSTION MODEL

- IDEALIZED ANALYSIS DIFFUSION CONTROLLED COMBUSTION OF DROPLET WITH SURFACE REACTION YIELDS

$$\dot{m}_b = 2\pi D_p \rho D \ln(1+\chi Y_{0,\infty})$$

WHERE

χ = STOICHIOMETRIC FUEL TO OXIDIZER MASS RATI

$Y_{0,\infty}$ = MASS FRACTION OF OXIDIZER IN FAR FIEL

- FOR MASS TRANSPORT CONTROLLED COMBUSTION OF ALUMINUM DROPLET CALCULATE BURNING RATE FROM

$$\dot{m}_{Al} = \frac{\pi}{2} \rho_{Al} \frac{k}{n} D_p^{3-n}$$

- REDUCES TO RESULTS OF THE IDEALIZED ANALYSIS FOR n=2 AND APPROPRIATE EXPRESSION FOR k.

Scientific Research Associates

DISCRETE PHASE DROPLET COMBUSTION MODEL (Cont'd)

- REDUCES TO HERMSEN MODEL WITH

$$n = 1.8$$
$$k = 8.3314 \times 10^{-5} \cdot A_k^{0.9} \cdot p_c^{0.27} \cdot R_k$$
$$R_k = 2.7$$
$$A_k = 100 \sum_i X_i \quad ; i = CO_2, H_2O, O_2, OH, O$$

- CAN ACCOUNT FOR EFFECTS OF FORCED CONVECTION, DROPLET-DROPLET INTERACTION, VARIATION OF OXIDIZER CONCENTRATION ALONG TRAJECTORY ETC. ON BURNING RATE WITH REDUCED EMPIRICISM.

FOR EXAMPLE

$$k \propto 1 + 0.24\ Re^{1/2} Sc^{1/3}$$
$$k \propto f\left(\sum_{i=1}^{n} \chi_i Y_i^s\right)$$

IN GENERAL

$$k = k(D, Sh, \alpha, \chi_i, Y_i^s)$$

Scientific Research Associates

APPLICATION CASE STUDY

- GEOMETRY

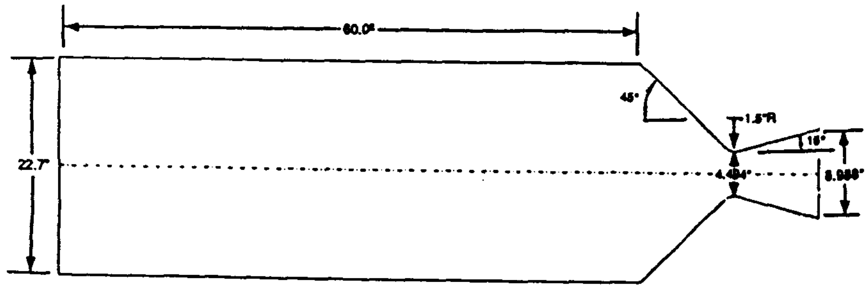

- PROPELLANT DATA

COMPOSITON

AP	71.0%
BINDER (HTPB)	14.0%
Al	15.0%
DENSITY	1794.6 kg/m^3 (112.0 lbm/ft^3)
BURN RATE	9.0678 x 10^{-3} m/s (0.357 in/s)

Scientific Research Associates

APPLICATION CASE STUDY(Continued)

CASE I - SURFACE COMBUSTION SIMULATION

- ALL ALUMINUM ASSUMED TO BURN AT PROPELLANT SURFACE
  - FLAME TEMPERATURE = 3435 K
- 20% Al_2O_3 ASSUMED TO BE IN CAPS
  - GAS PHASE ELEMENTAL ALUMINUM MASS FRACTION GIVEN BY (0.8 x 0.15) / (1 - 0.2 x 0.15 x 102 / 54) = 0.1272

CASE II - DISTRIBUTED COMBUSTION SIMULATION

- ALL ALUMUNUM INJECTED AS DROPLETS IN DISCRETE PHASE
  - FLAME TEMPERATURE = 2592.5 K
- LOG-NORMAL SIZE DISTRIBUTION WITH MEAN DIAMETER = 150μm AND LOG_{10} STANDARD DEVIATION = 0.2
- PARTICLES ASSUMED TO RETAIN 20% OF REACTED ALUMINUM IN FORM OF Al_2O_3 CAPS

Scientific Research Associates

COMPUTATIONAL DOMAIN AND GRID

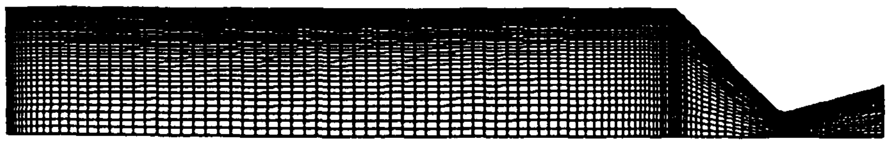

Scientific
Research
Associates

PRESSURE CONTOURS
($P_{max} = 6.6$ MPa, $P_{min} = 0.4$ MPa, $\Delta P = 0.2$ MPa)

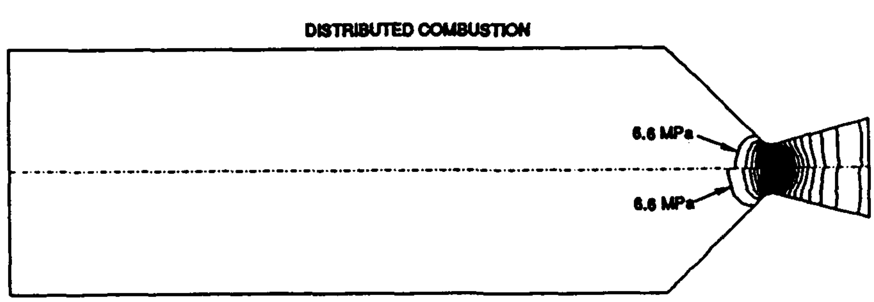

Scientific
Research
Associates

TEMPERATURE CONTOURS
(T_{max} = 3750K, T_{min} = 2350K, ΔT = 100 K)

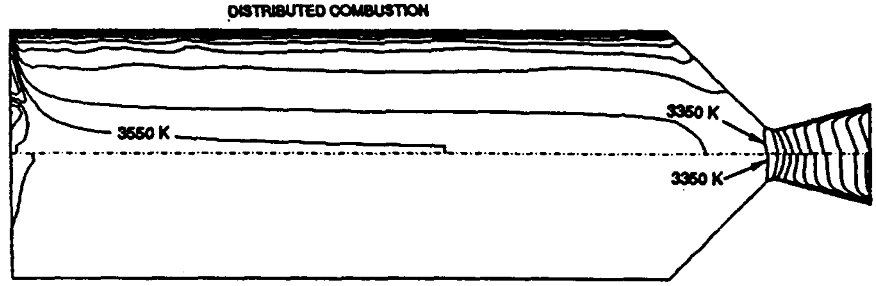

Scientific Research Associates

DENSITY CONTOURS
(ρ_{max}= 7.7kg/m^3, ρ_{min} = 0.3kg/m^3, $\Delta\rho$ = 0.2kg/m^3)

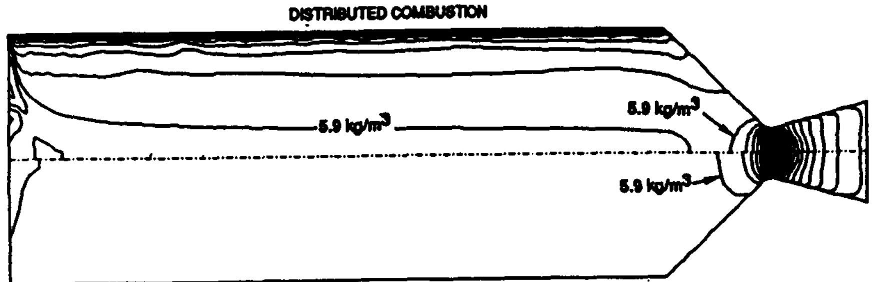

Scientific Research Associates

ALUMINUM MASS FRACTION CONTOURS
(Y_{max} = 17.0%, Y_{min} = 0.0%, ΔY = 1.0%)

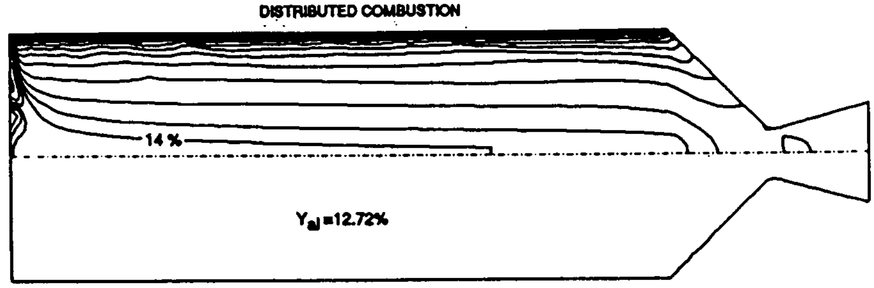

Scientific Research Associates

SUMMARY

- A TWO-PHASE DISTRIBUTED COMBUSTION MODEL DEVELOPED TO SIMULATE COMBUSTION OF METALIZED SOLID PROPELLANTS
- CALCULATED RESULTS SHOW EXISTENCE OF AN EXTENDED COMBUSTION REGION IN THE MOTOR CHAMBER
  - SIGNIFICANT SPATIAL VARIATION IN TEMPERATURE, COMPOSITION AND DENSITY IN THE CHAMBER
- EXPERIMENTAL DATA NEEDED FOR INITIAL PARTICLE SIZE DISTRIBUTION AND FRACTION OF METAL THAT BURNS AT SURFACE FOR FURTHER CODE VALIDATION
- CODE CAN BE EFFECTIVELY USED IN PARAMETRIC STUDIES AT PRESENT
- PRESENT APPROACH CAN BE READILY MODIFIED TO STUDY EFFECTS SUCH AS RADIATION AND PARTICLE SIZE CHANGES DUE TO BREAKUP AND COALESCENCE

Scientific Research Associates

*U.S. GOVERNMENT PRINTING OFFICE: 1992-627-150/60004

REPORT DOCUMENTATION PAGE

Form Approved
OMB No. 0704-0188

Public reporting burden for this collection of information is estimated to average 1 hour per response, including the time for reviewing instructions, searching existing data sources, gathering and maintaining the data needed, and completing and reviewing the collection of information. Send comments regarding this burden estimate or any other aspect of this collection of information, including suggestions for reducing this burden, to Washington Headquarters Services, Directorate for Information Operations and Reports, 1215 Jefferson Davis Highway, Suite 1204, Arlington, VA 22202-4302, and to the Office of Management and Budget, Paperwork Reduction Project (0704-0188), Washington, DC 20503.

1. AGENCY USE ONLY *(Leave blank)*

2. REPORT DATE
July 1992

3. REPORT TYPE AND DATES COVERED
Conference Publication

4. TITLE AND SUBTITLE
Tenth Workshop for Computational Fluid Dynamic Applications in Rocket Propulsion

5. FUNDING NUMBERS

6. AUTHOR(S)
R.W. Williams, Compiler

7. PERFORMING ORGANIZATION NAME(S) AND ADDRESS(ES)
George C. Marshall Space Flight Center
Marshall Space Flight Center, Alabama 35812

8. PERFORMING ORGANIZATION REPORT NUMBER
M-693

9. SPONSORING/MONITORING AGENCY NAME(S) AND ADDRESS(ES)
National Aeronautics and Space Administration
Washington, DC 20546

10. SPONSORING/MONITORING AGENCY REPORT NUMBER
NASA CP-3163, Part 1

11. SUPPLEMENTARY NOTES
Prepared by Structures and Dynamics Laboratory, Science and Engineering Directorate

12a. DISTRIBUTION/AVAILABILITY STATEMENT
Subject Category: 34
Unclassified—Unlimited

12b. DISTRIBUTION CODE

13. ABSTRACT *(Maximum 200 words)*

Conference publication includes 59 abstracts and presentations and three invited presentations given at the Tenth Workshop for Computational Fluid Dynamic Applications in Rocket Propulsion held at George C. Marshall Space Flight Center, April 28–30, 1992. The purpose of the workshop is to discuss experimental and computational fluid dynamic activities in rocket propulsion. The workshop is an open meeting for government, industry, and academia. A broad number of topics are discussed including computational fluid dynamic methodology, liquid and solid rocket propulsion, turbomachinery, combustion, heat transfer, and grid generation.

14. SUBJECT TERMS
Computational Fluid Dynamics, Rocket Propulsion, Liquid Rocket, Solid Rocket, Turbopump, Turbomachinery, Combustion, Methodology, Impeller, Inducer, Heat Transfer, Grid Generation, Nozzle, Plume, Spray, Injector

15. NUMBER OF PAGES
736

16. PRICE CODE
A99

17. SECURITY CLASSIFICATION OF REPORT
Unclassified

18. SECURITY CLASSIFICATION OF THIS PAGE
Unclassified

19. SECURITY CLASSIFICATION OF ABSTRACT
Unclassified

20. LIMITATION OF ABSTRACT
Unlimited